Probabilistic Quantification of the Effects of Soil-Shallow Foundation-Structure Interaction on Seismic Structural Response

A THESIS
SUBMITTED TO THE UNIVERSITY OF CANTERBURY
IN PARTIAL FULFILMENT OF THE REQUIRMENTS
FOR THE DEGREE OF DOCTOR OF PHILOSOPHY

By
Masoud Moghaddasi
June 2012

Department of Civil and Natural Resources Engineering
College of Engineering
University of Canterbury
Christchurch, New Zealand

This Thesis Is Dedicated to

My Great Mother and My Lovely Wife

Abstract

Previous earthquakes demonstrated destructive effects of soil-structure interaction on structural response. For example, in the 1970 Gediz earthquake in Turkey, part of a factory was demolished in a town 135 km from the epicentre, while no other buildings in the town were damaged. Subsequent investigations revealed that the fundamental period of vibration of the factory was approximately equal to that of the underlying soil. This alignment provided a resonance effect and led to collapse of the structure. Another dramatic example took place in Adapazari, during the 1999 Kocaeli earthquake where several foundations failed due to either bearing capacity exceedance or foundation uplifting, consequently, damaging the structure. Finally, the Christchurch 2012 earthquakes have shown that significant nonlinear action in the soil and soil-foundation interface can be expected due to high levels of seismic excitation and spectral acceleration. This nonlinearity, in turn, significantly influenced the response of the structure interacting with the soil-foundation underneath.

Extensive research over more than 35 years has focused on the subject of seismic soil-structure interaction. However, since the response of soil-structure systems to seismic forces is extremely complex, burdened by uncertainties in system parameters and variability in ground motions, the role of soil-structure interaction on the structural response is still controversial. Conventional design procedures suggest that soil-structure interaction effects on the structural response can be conservatively ignored. However, more recent studies show that soil-structure interaction can be either beneficial or detrimental, depending on the soil-structure-earthquake scenarios considered.

In view of the above mentioned issues, this research aims to utilise a comprehensive and systematic probabilistic methodology, as the most rational way, to quantify the effects of soil-structure interaction on the structural response considering both aleatory and epistemic uncertainties. The goal is achieved by examining the response of established

rheological single-degree-of-freedom systems located on shallow-foundation and excited by ground motions with different spectral characteristics. In this regard, four main phases are followed.

First, the effects of seismic soil-structure interaction on the response of structures with linear behaviour are investigated using a robust stochastic approach. Herein, the soil-foundation interface is modelled by an equivalent linear cone model. This phase is mainly considered to examine the influence of soil-structure interaction on the approach that has been adopted in the building codes for developing design spectrum and defining the seismic forces acting on the structure. Second, the effects of structural nonlinearity on the role of soil-structure interaction in modifying seismic structural response are studied. The same stochastic approach as phase 1 is followed, while three different types of structural force-deflection behaviour are examined. Third, a systematic fashion is carried out to look for any possible correlation between soil, structural, and system parameters and the degree of soil-structure interaction effects on the structural response. An attempt is made to identify the key parameters whose variation significantly affects the structural response. In addition, it is tried to define the critical range of variation of parameters of consequent. Finally, the impact of soil-foundation interface nonlinearity on the soil-structure interaction analysis is examined. In this regard, a newly developed macro-element covering both material and geometrical soil-foundation interface nonlinearity is implemented in a finite-element program Raumoko 3D. This model is then used in an extensive probabilistic simulation to compare the effects of linear and nonlinear soil-structure interaction on the structural response.

This research is concluded by reviewing the current design guidelines incorporating soil-structure interaction effects in their design procedures. A discussion is then followed on the inadequacies of current procedures based on the outcomes of this study.

Acknowledgment

I am thankful to all people, who have supported me during my years of post-graduate studies. Without their help, contributions and funding I would not be able to complete my studies.

I firstly wish to acknowledge my supervisors including Associate Professor. S. Pampanin, Professor M. Cubrinovski, Professor A. Carr, and Professor J.G. Chase. They constantly supported and encouraged me during my studies, and also patiently worked through difficult problems with me. Each of them has provided a significant and unique contribution which I am greatly indebted for. I also would like to specially thank Dr. A. Pecker and Dr. C.T. Chatzigogos for their support and technical contribution provided for part of my studies.

In addition, I would like to acknowledge financial support provided to me by the University of Canterbury, Department of Civil and Natural Resources Engineering and New Zealand Society for Earthquake Engineering. Without their support, this thesis and the variety of opportunities I have experienced would not be completed.

This thesis and my professional development have also greatly benefited from interactions with many individuals. My post-graduate colleagues who supported me extensively throughout my studies, in particular: Umut Akguzel, Dion Mariot, Vinod Sadashiva, Javad Arefi and numerous others. My colleagues in Aurecon who provided me a unique opportunity and a great environment to finish my studies while I was working, specially: John Finnegan, Sean Gledhill and Sam Jones. My friends: Bahjat Harach and David Gilmore who reviewed part of this thesis.

Finally, I am immensely appreciative of the support provided by my wife, mother, father and brother during my entire time at university.

Table of Contents

List of Figures

List of Tables

CHAPTER

1. Introduction and Scope of the Research

Introduction. When a structure is exposed to seismic forces, the response of the structure is affected by the response of the foundation and the surrounding soil underneath. Therefore, in an accurate dynamic analysis and, consequently, in an effective design procedure, it is important to consider the effects of interaction between the soil and structure. Seismic soil-structure interaction has been the topic of many studies for the last 35 years. However, since determining the dynamic response of a soil-structure system to seismic forces is a complicated nonlinear procedure, there are still some misconceptions about the effect of foundation flexibility on the response of structure. This research aims to comprehensively and systematically quantify the influence of foundation flexibility on seismic structural response considering both variability in soil-structure system parameters and uncertainty in input ground motions.

1.1 Research Motivation

In the existing literature with regard to the effects of soil-structure interaction on the structural response, there are two major issues needing further more comprehensive investigation: (i) clarification of the beneficial or detrimental role of soil-structure interaction; and (ii) the influence of structural and soil-foundation interface nonlinearity on soil-structure interaction effects.

Beneficial/detrimental role of soil-structure interaction: the dynamic properties of a structure fixed at the base, such as mode shapes, periods of vibration and damping, may be significantly modified by the presence of foundation flexibility. In this context, a soil-structure system has most notably a longer fundamental period than the

corresponding fixed-base structure, as well as a modified (usually increased) level of damping. With this in mind, today's seismic codes concluded that consideration of soil-structure interaction results invariably in lower acceleration and stresses in the structure and its foundation. A beneficial effect compared to the fixed-base case. This presumption is made because design codes use idealised smooth design spectra that have constant acceleration up to a certain period and a monotonically decreasing branch thereafter. Therefore, a longer period and increased damping automatically lead to lower design forces. Supposedly, conservative simplification through ignoring soil-structure interaction would thus presumably result in an improved safety margin.

However, this simple assumption is not always true. There is documented evidence in numerous case histories [1, 2] that the perceived beneficial role of soil-structure interaction is an oversimplification that may lead to an unsafe design for both the structure and foundation. More specifically, it may not always be beneficial effect. Many factors might be influencing this controversy between the code assumptions and the results observed in the real events.

The most important deviation from the assumption made in the typical code approach is shown in Figure 1-1 [3]. It shows the response spectra of four earthquake records: Brancea (Bucharest) 1997, Michoacán (Mexico City) 1985, Kobe (Fukiai, Takatori) 1995, where recorded spectra attain their maximum at periods exceeding 1.0 s.

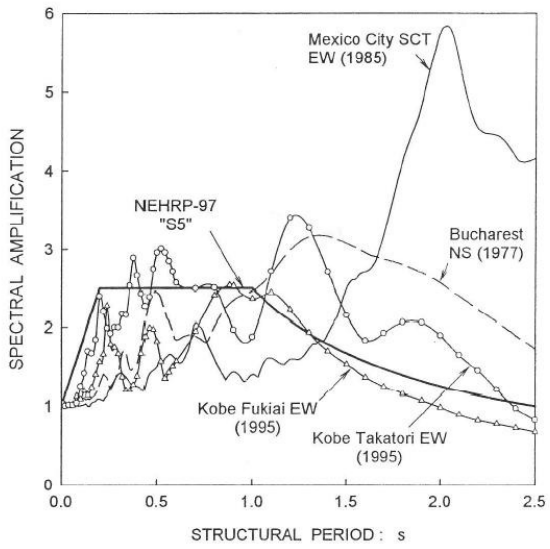

Figure 1-1. Comparison of typical seismic design spectrum to actual earthquake spectra [3].

Thus, in these cases, the increase in the fundamental period due to soil-structure interaction may actually result in an increased structural response, which contradicts the expectation created by conventional design spectra. Hence, the conventional assumption regarding beneficial role of soil-structure interaction could be dramatically wrong in similar situations.

The other issue that has to be highlighted is that code provisions on soil-structure interaction effects are based on an equivalent static method without considering extensive time-history analysis or dynamic reasoning. In contrast, it should be noted that soil-structure interaction is a complex nonlinear dynamic problem that is significantly influenced by dynamic phenomena, such as resonance and de-resonance of different interacting parts. In addition, analysing this complex problem and making a final statement get more challenging when the impact of uncertainties in the system's parameters and randomness in the input ground motion are considered.

*The influence of structural and soil-foundation interface nonlinearity***:** seismic accelerograms recorded in the last 20 years, and especially during the Northridge 1994, Kobe 1995, Kocaeli 1999 and Christchurch 2010-2011 earthquakes, have shown that very high ground acceleration levels can be experienced. In such cases, significant nonlinear response might be expected in the soil stratum, soil-foundation interface and structural elements [4, 5]. However, most studies and simplified methodologies used to investigate soil-structure interaction effects either do not consider nonlinearities occurring in the soil, soil-foundation interface and structure, or selectively addresses some of them. Therefore, the conclusions made regarding the effects of soil-structure interaction on the structural response might not be applicable for the scenarios with high levels of system nonlinearity.

Considering the above mentioned concerns and challenges, this research project aims to *"comprehensively and systematically reinvestigate the effects of soil-structure interaction on seismic structural response to assess the benefits and risks".*

1.2 Objectives and Scope of the Research

The objective of this research is achieved through carrying out four main tasks:

Task 1) **Quantify** the effects of seismic soil-structure interaction on the response of structures with linear behaviour.

This task is the first step in understanding the effects of foundation flexibility in the dynamic response of structures. It investigates the response of a single-degree-of-freedom system to develop a conceptual understanding and a benchmark reference for the effects of structural nonlinearity. In this context, an established rheological soil-shallow foundation-structure system is investigated. In this system: (i) the structure is modelled by a single-degree-of-freedom mass-spring-dashpot model with 5% equivalent viscous damping ratio and a linear force-displacement relationship; and (ii) the soil-foundation part is represented by an equivalent linear cone model [6, 7]. Since uncertainties arising from structural and geotechnical properties of a soil-structure system, as well as ground motion characteristics, play an important role in the performance prediction of the system, a comprehensive probabilistic approach using suites of ground motions is utilized.

A superior basic understanding of the effects of soil-structure interaction is achieved that can be used as a reference point and an insight for subsequent tasks.

Task 2) **Investigate** the effects of structural nonlinearity on the role of soil-structure interaction in modifying seismic structural response.

As mentioned, it is critical to reinvestigate the soil-structure interaction effects when structural nonlinearity occurs. In this regard, the same probabilistic methodology defined for task 1 is implemented again. The only difference is the structural force-deflection behaviour used. Three different hysteretic types are selected to represent the cyclic force-deflection behaviour of the structure, including: (i) Takeda, (ii) bilinear elasto-plastic and (iii) Takeda with negative post-yield stiffness. The Takeda model is selected to represent a new designed concrete-framed structure for investigating

structural nonlinearity on soil-structure interaction effects. A bilinear elasto-plastic model is chosen to represent the behaviour of a new designed steel-framed structure. Finally, the Takeda with negative post-yield stiffness model is used to approximate the response of a structure with either significant second-order ($P-\Delta$) or strength degradation effects.

The results yield comprehensive insights regarding the effects of soil-structure interaction in typical scenarios when the foundation is expected to behave linearly. They can also be used in performance-based or probabilistic-based design procedures including soil-structure interaction effects.

Task 3) **Examine** the possible correlation between soil, structural and system parameters, and the degree of soil-structure interaction effects on the structural response.

After quantifying the effects of soil-structure interaction on the structural response, it is important to identify any correlation and dependency between those effects and soil, structural and system parameters. Using a robust statistical approach, the key parameters whose variation significantly affects the structural response are identified, and the critical range of variation of these parameters resulting in a detrimental soil-structure interaction effects (i.e. scenarios with amplified structural response) are also outlined.

Task 4) **Scrutinize** the impact of soil-foundation interface nonlinearity on the soil-structure interaction analysis.

The final step is to investigate the effects of soil-foundation nonlinearity on all previous results. A newly developed soil-foundation interface macro-element accounting for both geometrical and material nonlinearity [8] is used. This element is implemented in a yielding single-degree-of-freedom system with Takeda type hysteretic behaviour. A set of nonlinear time-history analyses using this system systematically compares soil-structure interaction effects for linear and nonlinear base flexibility conditions.

Finally, it should be noted that, respecting the scope of this study, the outcomes presented are limited to the single-degree-of-freedom structural systems attached to a simple rheological soil-shallow foundation model. Thus, some extra modelling uncertainty is also introduced. In addition, the outcomes do not consider extreme conditions such as those imposed by very soft (liquefiable) soils. Nevertheless, the overall approach is designed to provide input and guidance to performance-based design methods and standards. Hence, these assumptions and approach are fit for that purpose.

1.3 Organization and Thesis Overview

Chapter 2 presents the fundamental aspects of seismic soil-structure interaction analysis to give a reader an idea about the concepts and terminologies used later on in this thesis. In addition, it reviews the existing literature has been carried out to investigate the effects of foundation flexibility on structural response.

Chapter 3 highlights the importance of uncertainty and randomness consideration in performance prediction of soil-structure systems. It also presents the relevant literature and scrutinises the potential for any further study.

Chapter 4 focuses on reviewing some basics of probability theory to facilitate understanding of the analysis presented in the following chapters. It also briefly explains the Monte Carlo simulation, a stochastic process for complex systems, which is implemented in this research.

Chapter 5 introduces the soil-structure model used for the stochastic analysis presented in Chapters 7, 8 and 9. **Chapter 6** describes the probabilistic methodology adopted to investigate the soil-structure interaction effects on structural response. It explains how the models with random parameters are generated and how the input ground motions are selected. The outcomes of this chapter are used as the basis for the results presented in Chapters 7, 8 and 9.

Chapter 7 presents the results of analysis defined in Tasks 1. It demonstrates probabilistically how soil-structure interaction modifies structural response. It should be

noted that structural part of the models considered in this chapter are assumed to behave linearly. **Chapter 8** investigates the role of structural nonlinearity on the soil-structure interaction effects, as defined in Task 2. Specifically, the comprehensive methodology introduced in Chapter 7 for quantification of soil-structure interaction effects is reused for structures with nonlinear behaviour, and the results are compared with that has been presented before.

Chapter 9 focuses on defining a coherent correlation and dependency between the soil-structure interaction effects observed in Chapter 8 and the soil, structural and system parameters, as defined in Task 3. It presents the key parameters whose variation are influential, and also identifies the critical range of variation of these parameters.

Chapter 10 describes how soil-foundation interface nonlinearity can be simply integrated into soil-structure interaction analysis. It presents the fundamental formulation of a newly developed macro-element taking into account both geometrical and material nonlinearity. **Chapter 11** shows how this model has been implemented in the finite-element program Raumoko 3D to make the future planned analysis possible. Following this implementation, **Chapter 12** attempts to investigate the sensitivity of the foundation response to the parameters of macro-element. It provides a decent insight on how to choose and tune these parameters in a probabilistic analysis.

Utilizing the knowhow and capability provided through Chapters 10, 11 and 12, **Chapter 13** presents the effects of nonlinearity at soil-foundation interface on soil-structure interaction analysis, as defined in Task 4. It uses a probabilistic approach and compares the results of four types of soil-structure models with different base fixity configurations. The conditions considered are: (i) fixed-base; (ii) linear flexible-base; (ii) nonlinear flexible-base without uplift; and (iv) nonlinear flexible-base with uplift.

Finally, **Chapter 14** reviews the current design guidelines focusing on how soil-structure interaction effects are incorporated in their design procedures. It also attempts to present the inadequacies existing in the procedures introduced based on the outcomes of this thesis.

References

[1] E. E. R. Institute, "1999 Kocaeli, Turkey," *Earthquake Reconnaissance Report,* vol. Special Issue of Earthquake Spectra, 2001.

[2] M. Cubrinovski*, et al.*, "Geotechnical aspects of the 22 February 2011 Christchurch earthquake," *Bulletin of the New Zealand Society of Earthquake Engineering,* vol. 44, pp. 205-226, 2011.

[3] G. Mylonakis and G. Gazetas, "Seismic soil-structure interaction: beneficial or detrimental?," *Journal of Earthquake Engineering,* vol. 4, pp. 277-301, Jul 2000.

[4] G. Gazetas and M. Apostolou, "Nonlinear soil-structure interaction: foundation uplifting and soil yielding," presented at the Proceedings Third UJNR Workshop on Soil-Structure Interaction, Menlo Park, California, USA, 2004.

[5] A. Pecker and C. T. Chatzigogos, "Non linear soil structure interaction: impact on the seismic response of structures," presented at the 14th European Conference on Earthquake Engineering, Ohrid, Republic of Macedonia, 2010.

[6] J. P. Wolf, *Foundation Vibration Analysis Using Simple Physical Models*. Englewood Cliffs, N.J.: Prentice-Hall, 1994.

[7] H. B. Seed and I. M. Idriss, "Soil moduli and damping factors for dynamic response analysis," Earthquake Engineering Research Centre Report EERC 7010, 1970.

[8] C. T. Chatzigogos*, et al.*, "Macroelement modeling of shallow foundations," *Soil Dynamics and Earthquake Engineering,* vol. 29, pp. 765-781, 2009.

CHAPTER

2. Fundamentals of Seismic Soil-Structure Interaction Analysis

Abstract. The purpose of this chapter is to first review the fundamentals of seismic soil-structure interaction analysis. It then briefly introduces the existing methods that have been specifically developed for soil-structure interaction analysis. Finally, it presents a review of the literature regarding the interaction effects on the structural response.

2.1 Problem Definition

The main objective of soil-structure interaction analysis considering seismic forces is to determine the dynamic response of a complex system composed of three linked and interacting elements: (i) the soil stratum beneath and surrounding the foundation; (ii) the foundation; and (iii) the structure [1, 2]. In this consideration, instead of applying a seismic force directly to the structure assumed to be fixed at the base, an incident excitation modified by the coupled dynamic behaviour of the soil-foundation interface and the structure has to be considered. In particular, the force or displacement cannot be directly specified in every point of the structure following the standard dynamic structural analysis approach. This is because the motion of the structure depends on the forces acting on it, and the forces, in turn, are affected by the soil and soil-foundation interface properties and response, which are not considered if a fixed-base assumption is used.

The interaction between the soil, foundation, and structure simultaneously integrates two primary physical phenomena: (i) kinematic interaction that is the inability of the foundation to follow the free-field motion, and (ii) inertial interaction that is the influence of the foundation-structure's dynamic response on the movement of supporting soil [3-10]. In the following subsections, these two main phenomena are described in detail.

2.1.1 Kinematic Interaction

The stiff foundation on the surface of, or embedded in, a soil stratum does not follow the free-field motions in horizontal or vertical directions, even if it has no mass. This phenomenon is recognized as kinematic interaction resulting from the contribution of two mechanisms:

1) *Displacement averaging*: the rigidity of a massless foundation, as a kinematic constraint, prevents it from following the exact horizontal and vertical varying components of the free-field motion and results in developing an incoherent motion. As illustrated in Figure 2-1, displacement averaging results in an averaged motion within the footprint area of the foundation base, regardless of the actual component of free-field motion.

2) *Wave scattering*: corners and asperities of the foundation cause the seismic waves to be scattered from the foundation.

The effects of kinematic interaction may be described by a complex-valued transfer function relating the free-field motion with the resulting foundation input motion [11-15]. However, if a shallow foundation is subjected to vertically propagating S-waves, the effect of kinematic interaction would no longer exist [15].

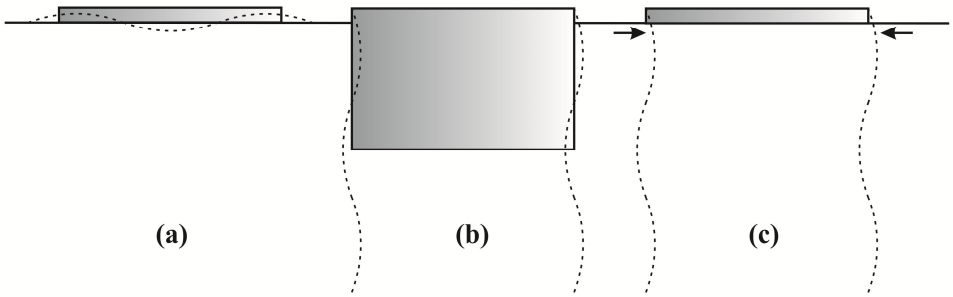

Figure 2-1. Kinematic interaction due to displacement averaging: (a) the flexural stiffness of a shallow foundation prevents it from following the vertical component of the free-field displacement; (b) the rigidity of a block foundation prevents it from following the horizontal component of the free-field displacement; and (c) the axial stiffness of a shallow foundation prevents the immediate underlying soil from deforming incoherently [3].

2.1.2 Inertial Interaction

Inertial interaction exists when the considered mass of the structure and foundation responds dynamically to the earthquake excitation and causes inertia forces (D'Alembert forces) in the foundation-structure system. The induced inertia forces give rise to base shear and moment, which, in turn, cause foundation displacements relative to the free-field and thus imperfect tracking of the free-field input motion.

2.2 Methods of Analysis

To analyse the soil-structure interacting systems numerically, an interaction surface is considered between the structure and the semi-infinite soil stratum. The unbounded soil domain extending to infinity and located outside this surface is then neglected, while its features are represented by the force and displacement associated with the interaction surface. The location of the interaction surface can be selected arbitrarily, which may result in two possible methodologies for performing soil-structure interaction analysis: (i) the direct method; and (ii) the substructure method.

If the interaction surface coincides with an artificial boundary presenting the entire soil domain considered in the model, the approach is called the "direct method". If the interaction surface is assumed to be identical to the soil-foundation interface, then the

approach is defined as the "substructure method". Figure 2-2 shows both definitions schematically.

Regardless of the method selected for soil-structure interaction analysis, the soil domain located outside the interaction surface and extending to infinity is assumed to remain elastic. However, this assumption can be adjusted to cover soil nonlinearity. In this context, soil material properties have to be selected so as to be compatible with the averaged shear strain reached during an earthquake. The averaged shear strain (or degraded shear strain) is defined by using an iterative procedure in which the response of a linear system is computed first and the corresponding soil properties are modified afterwards based on the computed response until a desired convergence is attained, a process used in equivalent linear analysis [16, 17].

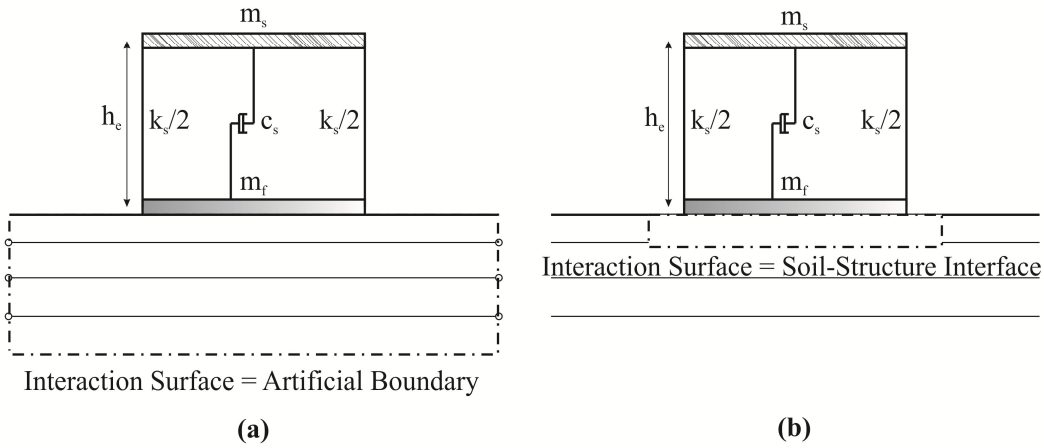

Figure 2-2. Methodologies for soil-structure interaction analysis: (a) the direct method in which the interaction surface coincides with an artificial boundary presenting the entire soil domain considered in the model; (b) the substructure method in which the interaction surface is identical to the generalized soil-structure interface.

2.2.1 Direct Method

In the direct method, illustrated in Figure 2-3, the entire soil-structure system is included in the same model and analysed in a single step. In addition, an artificial boundary has to be introduced representing the missing soil located in the exterior of the interaction surface. This boundary represents the stiffness of the soil up to infinity and avoids reflections of outward moving waves from the boundary. As an excitation to the system, the seismic free-field input motions $\{\ddot{u}_{FF}\}$ is specified along the artificial

boundary, and the displacement response of the interacting system $\{u\}$ is computed from the equations of motion defined:

$$[M^*]\{\ddot{u}\} + [C^*]\{\dot{u}\} + [K^*]\{u\} = -[M^*]\{\ddot{u}_{FF}\} \tag{2.1}$$

where $[M^*]$, $[C^*]$ and $[K^*]$ are mass, damping and stiffness matrices respectively.

In this method, because the entire soil domain and structure is integrated in the same model, consideration of actual nonlinear behaviour of the soil is possible. However, when a direct method is used for soil-structure interaction analysis, the results are quite sensitive to the parameters of the constitutive soil model, and the analysis is thus computationally expensive.

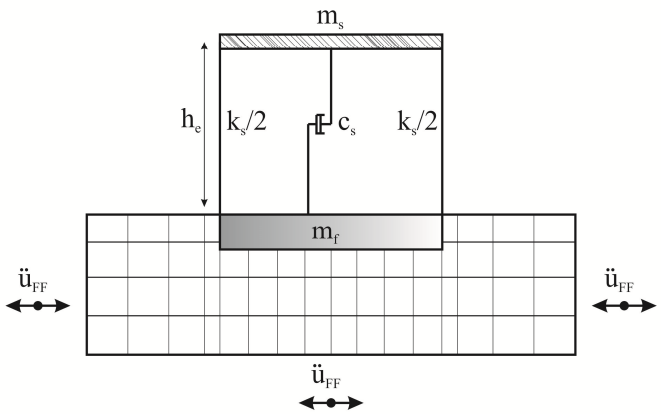

Figure 2-3. Soil-structure interaction analysis using direct method: the entire soil-structure system is included in the same model and analysed in a single step.

2.2.2 Substructure Method

In the substructure method, the soil-foundation interface and the structure are represented as two independent mathematical models or substructures. The superposition concept is then utilized to combine their dynamic response and define the response of the soil-structure system. This decomposition breaks down the interaction problem into its primary causes: kinematic and inertial interaction, as shown in Figure 2-4.

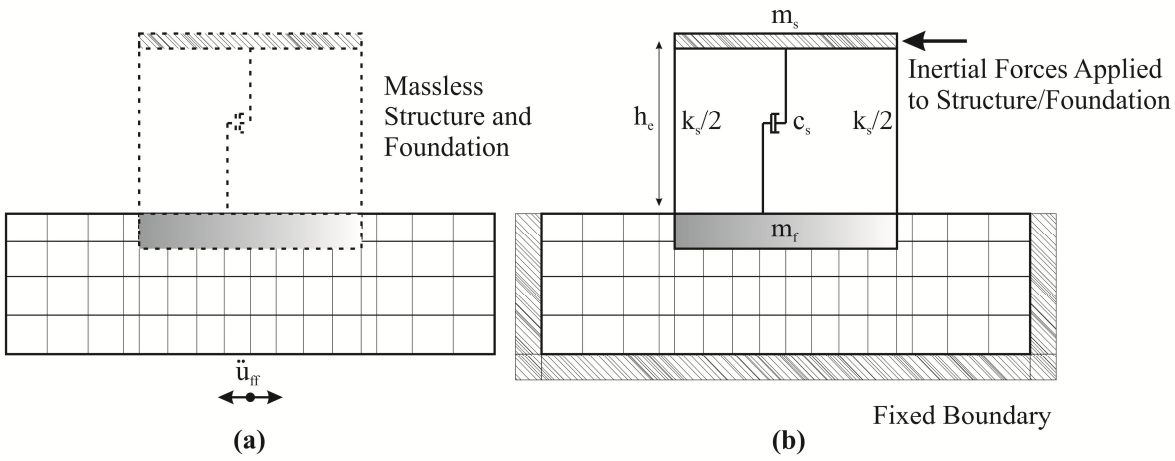

Figure 2-4**.** Soil-structure interaction analysis using the substructure method, the interaction problem is broken down into its primary causes: (a) kinematic; (b) and inertial interaction.

The displacement response of the system is defined as the sum of kinematic interaction displacement $\{u_{KI}\}$ and inertial interaction displacement $\{u_{II}\}$:

$$\{u\} = \{u_{KI}\} + \{u_{II}\} \tag{2.2}$$

To calculate kinematic interaction displacement, the soil-structure system is subjected to the free-field motion, while considering no mass for the foundation and the structure. The equation of motion representing kinematic interaction is defined:

$$[M_{soil}]\{\ddot{u}_{KI}\} + [C^*]\{\dot{u}_{KI}\} + [K^*]\{u_{KI}\} = -[M_{soil}]\{\ddot{u}_{FF}\} \tag{2.3}$$

where $[M_{soil}]$ is the mass matrix of the system assuming no mass for the foundation and the structure. The resulting $\{u_{KI}\}$ from solving Equation (2.3) is then used to define the inertial loading, $-[M_{structure}]\{\ddot{u}_{KI} + \ddot{u}_{FF}\}$, required for the inertial interaction analysis. The principal equation of motion for the inertial interaction is defined:

$$[M^*]\{\ddot{u}_{II}\} + [C^*]\{\dot{u}_{II}\} + [K^*]\{u_{II}\} = -[M_{structure}]\{\ddot{u}_{KI} + \ddot{u}_{FF}\} \tag{2.4}$$

where $[M_{structure}]$ is the mass matrix representing the mass for the foundation and structure. It should be noted that the inertial loading is merely applied to the structure, and not to the soil.

To solve Equation (2.4), the soil can be modelled with: (i) finite elements; or (ii) equivalently with a stiffness matrix condensing all degrees of freedom of the entire soil medium into the degrees of freedom located at the interaction surface. The condensed stiffness matrix describes the stiffness and damping characteristics of the soil at the exterior of the interaction surface.

For a rigid foundation, the condensed stiffness matrix can be represented with a 6×6 matrix providing the rigid body motion of the foundation. The adopted 6×6 matrix is called an impedance function and conceptually replaces the soil medium by a set of equivalent springs and dashpots. The coefficients of this assemblage depend on the soil properties, soil layering and foundation geometry. Implementing the impedance function in the stiffness matrix is contained within Equation (2.4). This equation may be viewed as the equation of motion of a structure that is supported by a set of equivalent springs and dashpots and subjected to foundation input motion (FIM) that has the kinematic soil-structure interaction included.

In summary, using the substructure method, the soil-structure interaction problem can be solved using the three following steps:

1) The evaluation of foundation input motion considering a massless rigid foundation that is subjected to the design seismic motion. The resulted motion represents the effects of kinematic interaction and depends on the stiffness and geometry of the soil and foundation.

2) The determination of soil-foundation impedance function.

3) The calculation of the dynamic response of a system including the structure and foundation impedances to the foundation input motion.

Figure 2-5 shows this process schematically. The most important advantage of the substructure method is its flexibility. Specifically, each separated substructure is allowed to be analysed by the best-suited computational technique. In addition, in the substructure method, the local soil nonlinearity that occurs beneath the soil-foundation interface, including geometrical and material nonlinearity, can simply be covered. This nonlinearity can be integrated in the analysis by defining the interaction surface so that it locates the structure and the finite soil region with nonlinear behaviour inside the interior part.

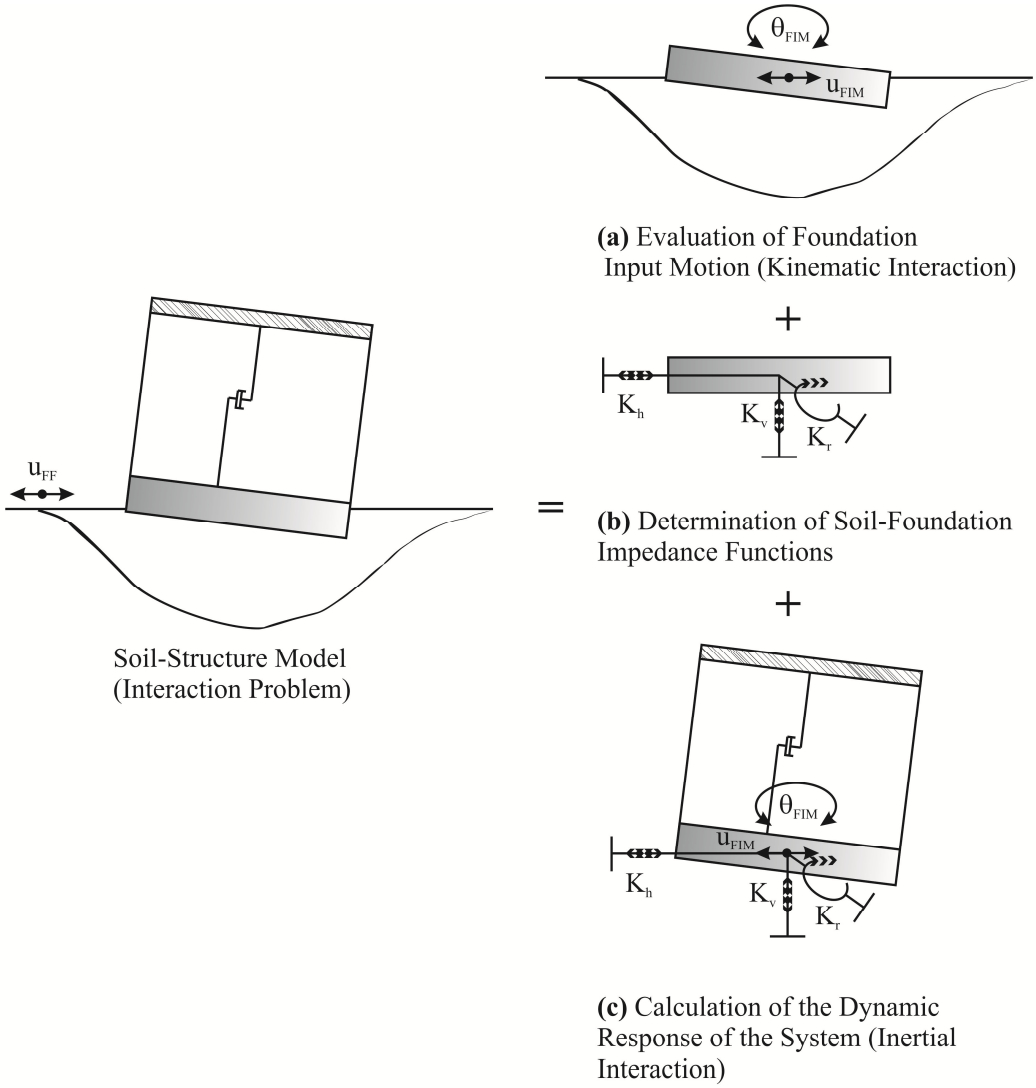

Figure 2-5. Substructure method for soil-structure interaction analysis using the concept of impedance function: (a) evaluation of foundation input motion; (b) determination of soil-foundation impedance function; (c) calculation of the dynamic response of the representative soil-structure interacting system.

2.3 Soil-Foundation Impedance Functions

As explained in Section 2.2.2, an important step in inertial soil-structure interaction analysis, using the substructure method, is to determine the impedance function representing the stiffness and damping characteristics of the soil-foundation interface. The Impedance function is expressed mathematically by a matrix that relates the generated forces by the structure at the soil-foundation interface to the displacements and rotations of the foundation relative to the free-field. In the most general case, to define the impedance function, six degrees of freedom have to be considered for each grid point of the soil-foundation interface. However, when a rigid foundation is assumed, there are only six degrees of freedom, in total, each corresponding to one mode of foundation vibration. The vibration modes considered are the three rigid translational displacements along the x, y, z axes and three rigid rotations around the same axes.

For each mode, the soil can be replaced by a dynamic spring with coefficient K and by a dashpot with damping coefficient C. This concept is illustrated in Figure 2-6 representing a foundation located on a spring and a dashpot.

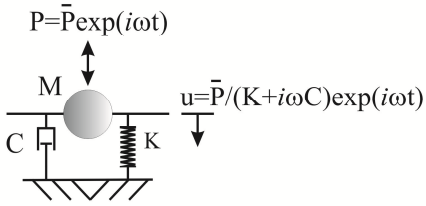

Figure 2-6. For each mode of foundation vibration, soil at foundation interface can be replaced by a spring with coefficient K and by a dashpot with viscous damping coefficient C.

For a harmonic input force $P(t) = \bar{P}\exp(i\omega t)$ with amplitude $\bar{P}$ and frequency ω, the foundation experiences a harmonic steady-state displacement $u(t)$, which has the same frequency ω and can be expressed [1]:

$$u(t) = \bar{u}\exp(i\omega t) \tag{2.5}$$

The harmonic force and the displacement are related by a complex value in the frequency domain, denoted dynamic impedance function, $\overline{K}(\omega)$, and defined:

$$\overline{K}(\omega) = \frac{\bar{P}}{\bar{u}} = K(\omega) + i\omega C(\omega) \tag{2.6}$$

The real and imaginary components of $\overline{K}(\omega)$ are both functions of the frequency ω. The real part, denoted dynamic stiffness, reflects the stiffness and inertia of the supporting soil, and its dependency on frequency is solely attributed to the influence of frequency on inertia. In this context, it should be noted that soil stiffness properties are essentially frequency independent. The imaginary part, on the other hand, represents the energy dissipation in the system generated as a result of the wave propagation away from the foundation (radiation damping). As evident from Equation (2.6), damping is responsible for the phase difference between the excitation $P(t)$ and the response $u(t)$.

The definition in Equation (2.6) can be applied for all modes of foundation vibration and, consequently, the coefficients of impedance function in the vertical, longitudinal, perpendicular, rocking and torsional directions will be defined. In embedded foundations and piles, horizontal forces along the x and y axes cause rotations around the y and x axes respectively, in addition to the induced translational displacement. Therefore, cross-coupling horizontal-rocking coefficients also exist in the impedance matrix. However, these off-diagonal terms are usually negligible for the case of shallow foundations [1].

Note that the dynamic impedance functions of a foundation are affected by geometric and stratification factors such as: (i) the foundation shape (circular, strip, rectangular, and arbitrary); (ii) the type of soil profile (deep uniform, multi-layer, and shallow stratum on rock); and (iii) the embedment (surface foundation, embedded foundation, and pile foundation). Over the years, several attempts have been made to construct impedance functions capable of explaining the complex interaction and force-displacement relationship at the soil-foundation interface. The two most utilized

methods are based on either: (i) elastic half-space theory; or (ii) simple physical cone models [18-44].

An analytical solution for a vertically excited rigid circular disk resting on an elastic half-space was first developed by Reissner [18] assuming a uniform stress distribution under the footing. Later, many other researchers extended this work for different modes of vibration and stress distribution [19-21]. These complicated mathematical solutions were then summarized/simplified by Gazetas and co-workers into simple formulas and charts [22-24]. In these works, the dynamic impedances of both surface and embedded foundations excited in various modes of vibration were presented.

Most of these studies assumed that the soil stratum is homogeneous and elastic. However, this assumption is not always true in reality. In this context, the effects of layering and non-homogeneity were studied by other researchers [25-31].

Alongside these efforts, Ehlers [32] was the first to introduce a truncated semi-infinite cone model to formulate the force-displacement relationship of a foundation resting on the surface of a half-space moving in translational direction. The same concept was applied by Meek and Veletsos [33] for rotational motion and by Veletsos and Nair [34] for torsional motion. The attraction of the cone model has been that it presents the dynamic stiffness of the soil-foundation interface by a simple discrete-element model consisting of a spring and a dashpot (also a mass moment of inertia with its own internal degree of freedom for rotational motion) with frequency-independent coefficients.

Because of these studies being frequency-independent and thus simpler to use, this approach has been used much more in practical applications. In this context, attempts were made to more accurately define the coefficients of the discrete-element model using curve fitting techniques and matching the results of rigorous solutions with that of simplified solution [35-38].

The concept of cone model was further extended by the extensive work of Wolf and co-workers [39-42]. They finally summarized the details of using the cone model in foundation vibration analysis in [43]. Recently, the validity of the cone model to

represent the dynamic response of machine foundations on layered soil has also been experimentally proven [44].

2.4 Basic Studies in Soil-Structure Interaction Effects on Seismic Structural Response

Despite the extensive research over the last 40 years, there are still some controversies regarding the role of soil-structure interaction (SSI) on the structural response to the seismic forces. Traditionally, it has been considered that incorporating foundation flexibility into dynamic analysis reduces seismic structural demands, and thus, disregarding SSI effects on the structural response leads to a conservative design and hence an improved safety margin. For example, the seismic code FEMA 450-Section 5.6 [45] states:

> *"The use of soil-structure interaction effects will decrease the design values of the base shear, lateral forces, and overturning moments."*

However, there is evidence from numerous case histories that the assumption of a beneficial role of SSI is an over simplification that may result in an unsafe design for the structure and the foundation [46-50]. Considering this dissimilarity, it is important to explore by what means different studies lead to such diverse and contrasting interpretations about the effects of SSI on structural response.

The response of a single-storey and a multi-storey structure located on a flexible foundation was studied by Jennings and Bielak [51]. As a result, simplified approximate formulas were developed to represent the modified natural frequency and damping ratio of the system, as well as the input excitation. They showed that the interaction tends to decrease all resonant frequencies, but that the effects are more significant for the fundamental vibration mode of multi-storey structures and are more pronounced for rocking motion than for translational motion. Finally, it was concluded that SSI effects on the structural response might be either beneficial or detrimental, and the decrease or increase in the response highly depends on the parameters of the system.

Following this work, Veletsos and Meek [52] investigated the effects of SSI on the dynamic response of a linear single-degree-of-freedom system. They assumed that the structure is supported at the surface of a homogeneous, elastic half-space and is excited at its base. The ground motions adopted in their study were presumed to be either a harmonic motion (a relatively simple pulse-type excitation) or a recorded earthquake motion. In this study, a comprehensive spectral analysis was performed for a range of the parameters defining the problem. The results were then used to assess the accuracy of a simple method of analysis in which the actual soil-structure system can be represented by an equivalent fixed-base oscillator with the modified period and damping. They then concluded that the interaction between soil and structure reduces the resonance frequency of the structure and modifies its effective damping. As a result of these modifications, SSI may cause a reduction or an amplification in the maximum deformation of the structure. They also introduced the three most important parameters controlling the interaction phenomenon: (i) the wave parameter, a measure of the relative stiffness of the foundation and the structure; (ii) the height to radius ratio (aspect ratio) of the system; and (iii) the ratio of the natural frequency of the fixed-base system to the frequency of the design spectrum.

Using the same approach presented by Veletsos and Meek [52], Veletsos and Nair [53] studied the effects of SSI on the response of a single-degree-of-freedom structure with linear behaviour located on a viscoelastic soil stratum. Two forms of viscoelastic action were considered in this study: (i) the standard Voigt model; and (ii) the constant hysteretic model. The outcomes were also used to assess the accuracy of a simple approximation method of analysis introduced, in which the system is represented by a viscously damped simple oscillator. This study concluded that for accurate determination of the structural response, it is essential to consider the effects of energy dissipation by hysteretic action in the soil. The principle effect of this additional energy dissipation is to reduce the deformation of the structure. They also emphasized that the foundation damping contributed by radiation and by hysteretic action in the soil is not directly additive to the structural damping. Consequently, the overall damping of the system may be increased or decreased compared to the initial damping of the fixed-base structure.

In the same period of time, an approximate analytical approach based on modal analysis was presented by Novak [54]. This approach made it possible to consider SSI effects in the dynamic structural analysis for external excitation, such as wind and earthquake. Novak concluded that the modification in modal damping of the system due to considering SSI generally increases with the order of the mode and the softness of the soil. In addition, for a particular soil-structure condition, the effects of SSI highly depend on the stiffness of the structure and the nature of the external excitation, and, in most scenarios, SSI tends to reduce the structural response to dynamic loads.

Novak also studied the effects of SSI on the structural damping [55]. It was concluded that the structural damping is always reduced by foundation flexibility, but this loss is usually less than that replaced by foundation damping.

The steady-state response of structure with a bilinear hysteretic behaviour supported on the surface of a viscoelastic half-space was studied by Bielak [56]. The method of equivalent linearization was used to solve the equations of motion, and simplified approximate formulas were obtained for the fundamental resonant frequency of the system and for an effective critical damping ratio. Numerical results in this study indicated that for structures with nonlinear hysteretic behaviour, foundation flexibility may lead to larger displacements than would occur if the base was rigid. Clearly, this behaviour differs from what has generally been considered for linear systems, for which SSI reduces the response of a fixed-base system.

Ciampoli and Pinto [57] tried to assess the importance of SSI effects on the dynamic response of bridge piers responding in the inelastic range. A simplified structural configuration, a vertical cantilever carrying a mass at the top and attached to a shallow foundation, was used in a parametric study. In this regard, realistic cases of bridge piers and soil-foundation interfaces were covered, where the principal parameter investigated was the maximum required ductility in the critical region of the structure. The results indicated that although in most cases SSI produces an increase in the maximum displacement, this effect is not significant. In addition, the inelastic demand in terms of curvature remains essentially unaffected, even showing a tendency to decrease. The stability of these conclusions was confirmed against extreme scenarios of very soft soil conditions and high levels of seismic excitation.

Recorded data was also used to evaluate the effects of SSI on the seismic structural response. Using system identification techniques and the recorded data for 77 strong motion data sets at 57 building sites, Stewart et al. [5, 8, 58] concluded that kinematic interaction effects on the input earthquake motion to the structure at the foundation level is relatively modest, whereas, inertial interaction effects on the structural response might be significant. They observed that the response of some structures in terms of fundamental natural period and effective damping might be dominated by SSI effects. However, there are scenarios in which structures can undergo negligible SSI effects. They also recognized that the structure-to-soil stiffness ratio is the most important parameter influencing SSI effects, and that the other parameters, such as structural aspect ratio, foundation embedment, type, shape, and flexibility, are in the second order of importance.

The role of SSI in the seismic response of structures was re-explored by Gazetas and Mylonakis [46, 47, 59]. It was emphasized that in certain seismic and soil environments, SSI may result in detrimental effects on the structural response. This finding is clearly in contradiction to the prevailing view implemented in current seismic design codes [45, 60-62].

In particular, they highlighted that the controversy is caused because of the way in which seismic forces are calculated in the design codes. Specifically, design codes use an idealized smooth design spectrum with a constant acceleration up to a certain period and a decreasing branch thereafter. Using this spectrum and considering that SSI increases the fundamental period and the effective damping of the system, it has been simply concluded that SSI always decreases seismic structural demands. Gazetas and Mylonakis [46, 47, 59] finally concluded that the current structural engineering view of the always beneficial role of SSI is an oversimplification and might result in an unsafe design.

An evaluation of SSI effects on the response of soil-structure interacting systems considering both kinematic and inertial interaction, and structural yielding, was also made by Aviles and Perez-Rocha [63]. A nonlinear replacement oscillator characterized by the effective ductility, period, and damping was developed and used for the analysis. The results indicated that the combined effects of foundation flexibility and structural

yielding are beneficial for slender structures with natural period somewhat longer than the site period, and are quite detrimental for the structures with natural period shorter than the site period. They also stated that there is no evidence whether elastic or yielding systems are most influenced by interaction.

Aviles and Perez-Rocha [64] used the same nonlinear replacement oscillator to investigate the influence of foundation flexibility on strength-reduction and displacement-modification factors. It was found that the use of factors derived for the fixed-base condition may lead to strength and displacement demands that are considerably different from those developed in structures with flexible foundation. Hence, it reinforces the impact of design codes on interpretation of the effects of SSI.

The effect of foundation flexibility on the demand reduction factor was also investigated by Ghannad and Jahankhah [65] using a parametric study. The adopted model was an elasto-plastic single-degree-of-freedom system laying on a homogeneous half-space, and the selected earthquake motions were chosen to characterize the recorded motions at rock, alluvium, and soft soil conditions. It was concluded that SSI reduces the strength reduction factors, especially for the case of buildings located on soft soils. Hence, using the derived values for fixed-base systems may result in non-conservative design forces.

SSI effects on peak structural responses were also investigated through rigorous dimensional analysis [66, 67]. Structures with linear and bilinear behaviour supported on shallow foundations with horizontal and rocking degrees of freedom were considered. In addition, it was assumed that the soil-structure system is subjected to near-fault ground motions. Results of numerical simulations showed that SSI effects on the structural response depend highly on the structure-to-pulse frequency ratio, foundation-to-structure stiffness ratio, damping coefficient of foundation impedance, foundation rocking, and the development of nonlinearity in the structure. Furthermore, different ranges of parameters were identified for which SSI effects can be negligible or significant. Another important conclusion was that the structures with bilinear behaviour may experience more significant SSI effects than structures with linear behaviour in certain frequency ranges.

In addition to the studies that investigate the SSI effects on seismic structural demands, there is research dealing with damage analysis of structures considering foundation flexibility. A parametric study was conducted by Rodriguez and Montes [68] to understand the effects of SSI on the damage of soil-structure interacting systems. It indicates that in most cases of inelastic response, SSI is not significant. Hence, a similar procedure used for the fixed-base structures can be applied to assess the induced seismic damage in structures supported on flexible foundations.

In contrast, Aviles and Perez-Rocha [69] showed that when the structural period is less than the predominant period of the site, seismic strength and energy demands increase due to foundation flexibility, and these effects tend to increase with the decrease of ductility. It was also mentioned that for the lower ductility, the strength including damage can increase more than 100% depending on the period ratio. Similar conclusions were made by Nakhaei and Ghanad [70] through investigating the SSI effects on the Park and Ang Damage Index. In particular, on an extensive parametric study using a nonlinear single-degree-of-freedom system located on a homogeneous viscoelastic half-space, it was concluded that the damage index increases due to SSI effects when structural period is below the threshold limit that is directly related to the predominant period of the ground motion. This effect is also more pronounced for the short period structures. It was also indicated that increasing the aspect ratio of the structure increases this effect.

Considering all these somewhat contradictory findings, further studies are needed to rigorously evaluate the SSI effects on seismic structural responses while accounting for various system and input scenarios. Furthermore, a robust quantification of these effects is required to calibrate and possibly modify the current design procedures incorporating SSI effects.

2.5 Summary

Fundamentals of soil-structure interaction analysis were introduced in this chapter. Specifically, the two primary physical phenomena that occur simultaneously in the interaction process, the kinematic interaction and the inertial interaction, were

described. Also, the methods developed to solve the complex soil-structure interaction problem, direct and substructure method, were briefly explained. In addition to the above, a comprehensive review of the existing literature regarding the soil-structure interaction effects on structural response was presented.

References

[1] J. P. Wolf, *Dynamic Soil-Structure Interaction*. Englewood Cliffs, N.J.: Prentice Hall, 1985.

[2] J. P. Wolf, *Soil-Structure-Interaction Analysis in Time Domain*. Englewood Cliffs, N.J.: Prentice-Hall, 1988.

[3] S. L. Kramer, *Geotechnical Earthquake Engineering*. Upper Saddle River, N.J.: Prentice Hall, 1996.

[4] W. D. L. Finn, "State-of-the-art of geotechnical earthquake engineering practice," *Soil Dynamics and Earthquake Engineering,* vol. 20, pp. 1-15, 2000.

[5] J. P. Stewart*, et al.*, "Seismic soil-structure interaction in buildings. I: analytical methods," *Journal of Geotechnical and Geoenvironmental Engineering,* vol. 125, pp. 26-37, Jan 1999.

[6] G. Mylonakis*, et al.*, "Footings under seismic loading: analysis and design issues with emphasis on bridge foundations," *Soil Dynamics and Earthquake Engineering,* vol. 26, pp. 824-853, 2006.

[7] R. W. Clough and J. Penzien, *Dynamics of structures*, 2nd ed. N.Y.: McGraw-Hill, 1993.

[8] J. P. Stewart*, et al.*, "Seismic soil-structure interaction in buildings. II: Empirical findings," *Journal of Geotechnical and Geoenvironmental Engineering,* vol. 125, pp. 38-48, 1999.

[9] A. Gomez-Masso, "Seismic soil-structure interaction by the superposition method," *Nuclear Engineering and Design,* vol. 78, pp. 37-52, 1984.

[10] E. Kausel*, et al.*, "Spring method for embedded foundations," *Nuclear Engineering and Design,* vol. 48, pp. 377-392, 1978.

[11] A. S. Veletsos and A. M. Prasad, "Seismic interaction of structures and soils: stochastic approach," *Journal of Structural Engineering,* vol. 115, pp. 935-956, 1989.

[12] A. S. Veletsos, "Dynamics of structure-foundation systems," in *Structural and Geotechnical Mechanics*, ed Englewood Cliffs, N.J.: Prentice-Hall Inc., 1977, pp. 333-361.

[13] F. Elsabee and J. P. Morray, "Dynamic behaviour of embedded foundations," Department of Civil Engineering, MIT, Cambridge, Mass.1977.

[14] A. Mita and J. E. Luco, "Dynamic response of a square foundation embedded in an elastic half-space," *Soil Dynamics and Earthquake Engineering,* vol. 8, pp. 54-67, 1989.

[15] S. Kim and J. P. Stewart, "Kinematic soil-structure interaction from strong motion recordings," *Journal of Geotechnical and Geoenvironmental Engineering,* vol. 129, pp. 323-335, 2003.

[16] H. B. Seed and I. M. Idriss, "Soil moduli and damping factors for dynamic response analysis," Earthquake Engineering Research Centre Report EERC 7010, 1970.

[17] G. A. Ordonez, "SHAKE2000, A Computer Program for the 1-D Analysis of Geotechnical Earthquake Engineering Problems," ed. Berkeley: University of California, 2011.

[18] E. Reissner, "Sattion are axialsymmetricle druch eine elastischen halb raues," *Ingenieur Archive,* vol. 7, pp. 381-396, 1936.

[19] P. M. Quinlan, "The elastic theory of soil dynamics," *ASTM-SPT No. 156,* pp. 3-34, 1936.

[20] F. E. Richart*, et al.*, *Vibrations of soils and foundations*. Englewood Cliffs, N.J.: Printice-Hall, 1970.

[21] J. E. Luco and R. A. Westmann, "Dynamic response of circular footings," *Journal of Engineeirng Mechanics,* vol. 97, pp. p 1381-95, 1971.

[22] G. Gazetas, "Analysis of machine foundation vibrations: state of the art," *Soil Dynamics and Earthquake Engineering,* vol. 2, pp. 2-42, 1983.

[23] G. Gazetas, "Formulas and charts for impedances of surface and embedded foundations," *Journal of geotechnical engineering,* vol. 117, pp. 1363-1381, 1991.

[24] R. Dobry and G. Gazetas, "Dynamic response of arbitrarily shaped foundations," *Journal of Geotechnical Engineering-ASCE,* vol. 112, pp. 109-135, 1986.

[25] G. B. Warburton, "Forced vibration of a body on an elastic stratum," *Journal of Applied Mechanics - Transactions of the ASME,* vol. 1957, pp. 55-58, 1957.

[26] G. C. Gazetas and J. M. Roesset, "Forced vibration of strip footings on layered soils," presented at the Proceedings of the National Structural Engineering Conference, Madison, WI, USA, 1976.

[27] J. E. Luco, "Impedance functions for rigid foundation on a layered medium," *Nuclear Engineering and Design,* vol. 31, pp. 204-217, 1974.

[28] E. Kausel*, et al.*, "Dynamic analysis of footings on layered media " *Journal of Engineeirng Mechanics,* vol. 101, pp. 679-693, 1975.

[29] J. L. Tassoulas and E. Kausel, "Elements for the numerical analysis of wave motion in layered strata," *International Journal of Numerical Methods in Engineering,* vol. 19, pp. 1005-1032, 1983.

[30] H. L. Wong and J. E. Luco, "Tables of impedance functions for square foundations on layered media," *International Journal of Soil Dynamics and Earthquake Engineering,* vol. 4, pp. 64-81, 1985.

[31] R. J. Apsel and J. E. Luco, "Impedance functions for foundations embeded in a layered medium: an integral eq. approach," *Earthquake Engineering & Structural Dynamics,* vol. 15, pp. 213-231, 1987.

[32] G. Ehlers, "The effect of soil flexibility on vibrating systems," *Beton Eisen,* vol. 41, pp. 197-203, 1942.

[33] J. W. Meek and A. S. Veletsos, "Simple models for foundation in lateral and rocking motions," presented at the Proceeding of Fifth World Congress on Earthquake Engineering, Rome, 1974.

[34] A. S. Veletsos and V. D. Nair, "Response of torsionally excited foundations," *Journal of Geotechnical Engineering Division-ASCE,* vol. 100, pp. 476-482, 1974.

[35] F. C. P. De Barros and J. E. Luco, "Discrete models for vertical vibrations of surface and embedded foundations," *Earthquake Engineering and Structural Dynamics,* vol. 19, pp. 289-303, 1990.

[36] A. S. Veletsos and B. Verbic, "Vibration of viscoelastic foundations," *Earthquake Engineering and Structural Dynamics,* vol. 2, pp. 87-102, 1973.

[37] J. P. Wolf and D. R. Somaini, "Approximate dynamic model of embedded foundation in time domain," *Earthquake Engineering and Structural Dynamics,* vol. 14, pp. 683-703, 1986.

[38] A. S. Veletsos and Y. T. Wei, "Lateral and rocking vibration of footings," *Journal of Soil Mechanics and Foundation Division-ASCE,* vol. 97, p. 1227, 1971.

[39] J. W. Meek and J. P. Wolf, "Cone models for soil layer on rigid rock," *Journal of Geotechnical Engineering Division ASCE,* vol. 118, pp. 686-703, 1992.

[40] J. W. Meek and J. P. Wolf, "Cone models for an embeded foundation," *Journal of Geotechnical Engineering Division ASCE,* vol. 120, pp. 60-80, 1994.

[41] J. P. Wolf and J. W. Meek, "Cone models for a soil layer on flexible rock half-space," *Earthquake Engineering and Structural Dynamics,* vol. 22, pp. 185-193, 1993.

[42] J. P. Wolf and J. W. Meek, "Dynamic stiffness of foundation on or embedded in layered soil using cone frustums," *Earthquake Engineering and Structural Dynamics,* vol. 23, pp. 1079-1095, 1994.

[43] J. P. Wolf, *Foundation Vibration Analysis Using Simple Physical Models*. Englewood Cliffs, N.J.: Prentice-Hall, 1994.

[44] P. K. Pradhan*, et al.*, "Dynamic response of machine foundation on layered soil: cone model versus experiments " *Geothecnical and Geological Engineering* vol. 26, pp. 453-468, 2008.

[45] FEMA-450, "NEHRP recommended provisions for seismic regulations for new buildings and other structures," ed. Washington, D.C.: Building Seismic Safety Council, 2003.

[46] G. Gazetas and G. Mylonakis, "Seismic soil-structure interaction: new evidence and emerging issues," in *Geotechnical Earthquake Engineeirng and Soil Dynamics 3: Proceedings of Speciality Conference*, ed N.Y.: ASCE, 1998.

[47] G. Mylonakis and G. Gazetas, "Seismic soil-structure interaction: beneficial or detrimental?," *Journal of Earthquake Engineering,* vol. 4, pp. 277-301, Jul 2000.

[48] G. Mylonakis*, et al.*, "The role of soil in the collapse of 18 piers of Hanshin expressway in the Kobe earthquake," *Earthquake Engineering and Structural Dynamics,* vol. 35, pp. 547-575, 2006.

[49] D. Resendiz and J. M. Roesset, "Soil-structure interaction in Mexico City during the 1985 earthquake," in *The Mexico Earthquakes - 1985*, M. A. Cassaro and E. M. Romero, Eds., ed: ASCE, 1987, pp. 193-203.

[50] J. Avilés and L. E. Pérez-Rocha, "Site effects and soil-structure interaction in the valley of Mexico," *Soil Dynamics and Earthquake Engineering,* vol. 17, pp. 29-39, 1998.

[51] P. C. Jennings and J. Bielak, "Dynamics of building-soil interaction," *Bulletin of the Seismological Society of America,* vol. 63, pp. 9-48, 1973.

[52] A. S. Veletsos and J. W. Meek, "Dynamic behaviour of building-foundation systems," *Earthquake Engineering and Structural Dynamics,* vol. 3, pp. 121-138, 1974.

[53] A. S. Veletsos and V. D. Nair, "Seismic interaction of structures on hysteretic foundations," *Journal of Structural Engineering,* vol. 101, pp. 109-129, 1975.

[54] M. Novak, "Effect of soil on structural response to wind and earthquake," *Earthquake Engineering and Structural Dynamics,* vol. 3, pp. 79-96, 1974.

[55] M. Novak and L. El Hifnawy, "Damping of structures due to soil-structure interaction," *Journal of Wind Engineering and Industrial Aerodynamics,* vol. 11, pp. 295-306, 1983.

[56] J. Bielak, "Dynamic response of non-linear building-foundation systems," *Earthquake Engineering & Structural Dynamics,* vol. 6, pp. 17-30, 1978.

[57] M. Ciampoli and P. E. Pinto, "Effects of soil-structure interaction on inelastic seismic response of bridge piers," *Journal of Structural Engineering,* vol. 121, pp. 806-814, 1995.

[58] J. P. Stewart and G. L. Fenves, "System identification for evaluating soil-structure interaction effects in buildings from strong motion recordings," *Earthquake Engineering and Structural Dynamics,* vol. 27, pp. 869-885, Aug 1998.

[59] G. Gazetas and G. Mylonakis, "Soil-structure interaction effects on elastic and inelastic structures," presented at the Fourth International Conference on Recent Advances in Geotechnical Earthquake Engineering and Soil Dynamics, San Diego, California, 2001.

[60] ATC-40, "Seismic evaluation and retrofit of concrete buildings," ed: Applied Technology Concil, 1996.

[61] ASCE-7, "Minimum design loads for buildings and other structures," ed: Amarican Society of Civil Engineers, 1998.

[62] FEMA-440, "Improvement of nonlinear static seismic analysis procedures," ed. Redwood City, California: Applied Technology Council, 2005.

[63] J. Avilés and L. E. Pérez-Rocha, "Soil-structure interaction in yielding systems," *Earthquake Engineering and Structural Dynamics,* vol. 32, pp. 1749-1771, 2003.

[64] J. Aviles and L. E. Perez-Rocha, "Influence of foundation flexibility on Rμ and Cμ," *Journal of Structural Engineeirng,* vol. 131, pp. 221-230, 2005.

[65] M. A. Ghannad and H. Jahankhah, "Site-dependent strength reduction factor for soil-structure systems," *Soil Dynamics and Earthquake Engineering,* vol. 27, pp. 99-110, 2007.

[66] J. Zhang and Y. Tang, "Evaluating soil-structure interaction effects using dimensional analysis," presented at the The 14th Worl Conference on Earthquake Engineering, Beijing, China, 2008.

[67] J. Zhang and Y. Tang, "Dimensional analysis of structures with translating and rocking foundations under near-fault ground motions," *Soil Dynamics and Earthquake Engineering,* vol. 29, pp. 1330-1346, 2009.

[68] M. E. Rodriguez and R. Montes, "Seismic response and damage analysis of buildings supported on flexible soils," *Earthquake Engineering aand Structural Dynamics,* vol. 29, pp. 647-665, 2000.

[69] J. Aviles and L. E. Perez-Rocha, "Damage analysis of structures on elastic foundation," *Journal of Structural Engineeirng,* vol. 133, pp. 1453-1461, 2007.

[70] M. Nakhaei and M. A. Ghannad, "The effect of soil-structure interaction on damage index of buildings," *Engineering Structures,* vol. 30, pp. 1491-1499, 2008.

CHAPTER

3. Introduction to Seismic Soil-Structure Interaction Analysis using Stochastic Approach

Abstract. The purpose of this chapter is to emphasize the importance of considering uncertainties in the seismic analysis of soil-structure systems. It also reviews the existing literature about the stochastic soil-structure interaction studies.

3.1 Stochastic Response of Soil-Structure Systems

As briefly described in the preceding chapters, prediction of soil-structure systems response to seismic forces requires accurate modelling of the geotechnical and structural components of the system, as well as selecting a proper input ground motion. Geotechnical and structural properties of the soil-structure systems can be described using deterministic and/or probabilistic approaches. If deterministic models are used, parameters of interest are typically described by using specific descriptors. However, if probabilistic models are considered, parameters have to be described with statistical descriptors or probability distribution functions.

Uncertainties arising from geotechnical and structural properties, as well as input ground motion characteristics, play an important role in the performance prediction of the seismically excited structures [1]. The effects of uncertainty are even more

pronounced if structural systems with foundation flexibility are considered [2-5]. Therefore, a comprehensive investigation of soil-structure interaction effects requires a stochastic approach. The primary goal of this approach is to estimate the response of a system using statistical measures such as means, variances, and probabilities associated with specific outcomes.

However, the stochastic response of a complex system (such as a soil-structure system) to earthquake excitation cannot be obtained by a closed-form analytical method, since the response is nonlinear and depends on the hysteretic behaviour of the system. Thus, the principle of superposition cannot be employed [6]. In these circumstances, numerical simulation techniques are ideal as they are simple and lead directly to results. The main disadvantage of numerical simulation is that they do not give an understanding of how the response or probabilities will change with changes in system or input parameters. In other words, if the system or the input is changed, the simulation must be repeated to determine the effect on response statistics and probabilities.

3.2 Sources of Uncertainty in Soil-Structure Interaction Analysis

Uncertainty exists as a state of nature and is represented with a non-negative probability of at least two possible values. This uncertainty can be categorized as either aleatory or epistemic uncertainty. Aleatory uncertainty represents the natural randomness of the properties of a model and/or the inputs to the model, while epistemic uncertainty results from the lack of information or shortcoming in measurement or calculations. Epistemic uncertainty can be divided into three groups: (i) statistical; (ii) measurement-related; and (iii) model-related. Statistical uncertainty is due to limited information, such as a limited number of observations. Measurement uncertainty is due to imperfection of an instrument. Finally, model uncertainty is due to idealization in the physical formulation of the problem. It is important to note that aleatory uncertainty is inherent to the variable or the input and cannot be reduced by collecting additional information or data. However, epistemic uncertainty can be reduced or even eliminated by acquisition of additional data or improvements in measurement procedures.

In soil-structure interaction analysis, both types of uncertainty may play a crucial role in estimation of structural responses. The aleatory uncertainty has to be considered

because of inherent uncertainties in the complex ground conditions. The epistemic uncertainty has to be considered because of the randomness or lack of knowledge of considered model parameters.

3.2.1 Characterization of Geotechnical Variability

Geotechnical variability is very complex and arises from three main sources of uncertainty: (i) inherent variability; (ii) measurement error; and (iii) transformation error [7-10]. Inherent soil variability is modelled as a random field in which all soil properties differ vertically and horizontally. This type of variability can be precisely described by the coefficient of variation and scale of fluctuation. Details are not discussed here, but can be found elsewhere [7, 11-15]. Measurement error, introducing some additional variability into the soil data, is directly extracted from field measurements using a simple additive probabilistic model or is determined from a comparative laboratory testing program. There are some simple models in the literature that account for this type of soil variability [7, 16]. Uncertainty due to transformation models are introduced when geotechnical measurements are applied to a design procedure. This additional degree of uncertainty is then a result of the transformation models not being exact, and having generally been defined by empirical data fitting. To quantify this type of uncertainty, probabilistic models can be utilized. Some examples are available in literature [8].

Since soil properties are uncertain, they can be simply described as random variables. Typical probability distribution functions can be used, such as uniform distribution, normal distribution or lognormal distribution [12, 17-19], whichever is the most appropriate. A uniform distribution is used for parameters with an equal range of values that may occur. For the other parameters a normal or lognormal distribution function can be selected to represent their uncertainty depending on the skewness of the data observed.

Reliability analysis has shown that uncertainty and variability of different soil properties may significantly affect the result of geotechnical analyses [11, 13, 16, 20-25]. It is therefore important to adequately quantify these uncertainties and to carefully evaluate their effects. However, it has to be noted that taking account of the effects of uncertainty

involving measurement and transformation errors is much easier than characterising the effects of uncertainty due to inherent soil variability.

3.2.2 Randomness in Structural Parameters

In a stochastic analysis to establish the validity of the result and make a general conclusion of the study, a wide range of structural cases have to be considered. The most meaningful structural features that should be considered are: (i) number of degrees of freedom; (ii) natural periods, generally the first natural period; (iii) structural type; (iv) force-displacement or hysteretic relationship; and (v) target ductility. For each of these factors a wide range of values has to be considered to increase the limit of acceptance of the results, as well as to cover all realistic scenarios or realizations.

3.2.3 Uncertainty in Input Ground Motion

The seismic response of structures and soil-structure interacting systems are strongly dependent on the input ground motion and on the detailed features of its spectrum [26, 27]. In addition, since the ground motions and their characteristics are inherently random, using only one time-history to obtain the response of the structures is not enough. Therefore, an appropriate measure of structural response, especially nonlinear response, requires the use of a suite of realistic time-histories having phase and response spectral peaks and troughs that are appropriate for the magnitude (M), distance (R) and site conditions of the considered region. Note that due to using a suite of records, a proper statistical sample of the existing variability in the phase and spectra of the input ground motion will be obtained.

In this context, the number of records required for nonlinear structural analysis to obtain an estimate of the median response with a factor of X (e.g., ± 0.1) with 95% confidence can be defined from the equation introduced by Shome et al. [26]:

$$n = 4\,\delta^2/X^2 \tag{3.1}$$

where δ is the dispersion in the measured data, or more precisely the standard deviation of the natural logarithms of the data.

3.3 Review of the Effects of Uncertainty in Seismic Soil-Structure Interaction Studies

The effects of uncertain soil-foundation properties on the response variability of soil-structure systems was studied by Jin et al. [3]. In this context, a non-classical modal analysis implementing Gaussian quadrature integration was used in the frequency domain. Specifically, the structural response of the interacting system was described as a superposition of the results of uncoupled single-degree-of-freedom systems. In this formulation, to model the uncertainty of system parameters, an additional random function was introduced in the modal equations. The introduced process was followed by a few numerical examples of multi-degree-of-freedom soil-structure systems. It was thus concluded that the main effect of uncertain soil properties on the response of soil-structure systems is to alter the magnitudes of modal response close to the system resonance frequencies, rather than to shift the resonant frequencies. In addition, it was stated that when the uncertainty of soil-foundation properties is not negligible, there may be a significant variation of the transfer functions of modal response. This variation can then cause significant uncertainty in the spectral density of the structural response at frequencies close to the system resonant frequencies.

Following this work and using a similar formulation, Lutes et al. [4] studied the effects of structural and soil uncertainty on the response variability of soil-structure systems. Based on the numerical examples of multi-degree-of-freedom interacting systems presented, it was found that when the parameter uncertainty is large, significant variation/uncertainty about the spectral density of the structural response occur for frequencies close to system resonant frequencies. In addition, it was shown that the effects of soil uncertainty is more pronounced for the lower frequency resonance peaks of taller structures, while the effects of structural uncertainty is more significant for the higher frequency resonance peaks of shorter structures.

It is important to note that both studies were only focused on presentation of the trends, rather than quantifying the effects of system uncertainty on the structural responses. In addition, they used a modal analysis in the frequency-domain which can only be used to investigate the response of structures with linear behaviour. In other words, nonlinear time-history effects were not covered in these studies. Finally, because only four

parameters of the soil-structure system were considered as uncertain variables in the numerical examples presented, the analyses were not through enough and comprehensive.

In addition to these mathematical investigations, which both ignore structural nonlinearity and time-history effects, some more realistic scenarios have been investigated. A group of reinforced concrete structures with different numbers of storeys and bays, designed for earthquake resistance, were studied by Barcena and Esteva [2] to investigate the influence of soil-structure interaction on the structural response to seismic forces. These systems were assumed to be located on soft soil and subjected to a set of artificial ground motions representing the maximum probable earthquake to occur at the considered sites. It was concluded that for the near resonance condition, the effects of soil-structure interaction on the ductility demand mainly depends on the radiation damping. This damping, on the other hand, was stated to be strongly correlated with structural aspect ratio (building height/width ratio). Consequently, it was concluded that for structures with aspect ratio greater than 1.4, soil-structure interaction effects increase the global and inter-storey drift demands, while for structures with aspect ratio less than 1.4, it decreases the ductility demands. For the cases when the fundamental period of structure has values very different from that of the ground motion, it was concluded that soil-structure interaction results in a reduction of the ductility demand for all aspect ratios.

Barcena and Esteva [2] also studied the effects of soil-structure interaction on the reliability index as a function of seismic coefficient. This coefficient is defined as the ratio between the base shear and seismic intensity. The result of their study was that the reliability functions are very similar for systems on rigid or flexible foundation.

The effects of uncertainty in soil parameters on the seismic response of low-rise steel buildings supported by shallow foundations was investigated by Prishati [28]. In this study, a set of 20 ground motions representing a 10% in 50 years hazard level was considered as an input. In addition, the basic soil parameters that control the strength and stiffness of the foundation system were assumed to vary as uncertain parameters. Three major response parameters were assessed, specifically the peak base moment, base shear and inter-storey drift. It was found that uncertainty in soil parameters may

result in significant response variability of the structures. Furthermore, friction angle was recognised as the most influential soil parameter in the observed response variability, and this variability was more pronounced in the case of peak base moment and base shear. Another important conclusion made in this study was that the degree of response variability that is seen in a nonlinear soil-structure model cannot be seen in a linear model. However, this study only considered two representative steel frame buildings and thus the effects of structural uncertainty were not covered.

Finally, in a recent study by Tang and Zhang [25], the effects of uncertainty and variability associated with ground motions on the seismic demands of soil-foundation-shear wall interacting system was investigated. It was found that soil-structure interaction generally reduces the damage probability of the shear wall, especially when soil nonlinearity is considered. In addition, it was suggested that damage in foundation and surrounding soil have to be considered if a precise investigation of damage probability of shear wall buildings is required.

Looking at the studies performed in the past, it can be concluded that proper understanding and characterization of various sources of uncertainty play an important role in the performance prediction of soil-structure systems. In this regard, both geotechnical and structural parameter uncertainties were considered in this study, and time-history analyses were carried out using numbers of input ground motions to cover the inherent uncertainty involved in the ground motion. In this context, the effects of uncertainties on the structural response variability were investigated for structures with linear and nonlinear behaviour to demonstrate the role of structural nonlinearity on the soil-structure interaction effects. To be comprehensive, this role was studied for structures with different hysteretic behaviour. The following chapters will present the methodology adopted and the results achieved.

3.4 Summary

In this chapter, the importance of uncertainty in soil-structure interaction analysis was described. Specifically, the role of variability in geotechnical and structural parameters

as well as uncertainty in input ground motion has been explained. Finally, the relevant literature to the stochastic soil-structure interaction analysis was reviewed.

References

[1] S. S. F. Mehanny and A. S. Ayou, "Variability in inelastic displacement demands: Uncertainty in system parameters versus randomness in ground records," *Engineering Structures,* vol. 30, pp. 1002-1013, Apr 2008.

[2] A. Barcena and L. Esteva, "Influence of dynamic soil-structure interaction on the nonlinear response and seismic reliability of multistorey systems," *Earthquake Engineering & Structural Dynamics,* vol. 36, pp. 327-346, Mar 2007.

[3] S. Jin*, et al.*, "Response variability for a structure with soil-structure interactions and uncertain soil properties," *Probabilistic Engineering Mechanics,* vol. 15, pp. 175-183, 2000.

[4] L. D. Lutes*, et al.*, "Response variability of an SSI system with uncertain structural and soil properties," *Engineering Structures,* vol. 22, pp. 605-620, 2000.

[5] P. Raychowdhury, "Effect of soil parameter uncertainty on seismic demand of low-rise steel buildings on dense silty sand," *Soil Dynamics and Earthquake Engineering,* vol. 29, pp. 1367-1378, 2009.

[6] R. W. Clough and J. Penzien, *Dynamics of structures*, 2nd ed. N.Y.: McGraw-Hill, 1993.

[7] K. Phoon and F. H. Kulhawy, "Characterization of geotechnical variability," *Candaian Geotechnical Journal,* vol. 36, pp. 612-624, 1999.

[8] K. Phoon and F. H. Kulhawy, "Evaluation of geotechnical property variability," *Canadian Geotechinical Journal,* vol. 36, pp. 625-639, 1999.

[9] A. L. Jones*, et al.*, "Estimation of Uncertainty in Geotechnical Properties for Performance-Based Earthquake Engineering," University of California, Berkeley2002.

[10] G. D. Manolis, "Stochastic soil dynamics," *Soil Dynamics and Earthquake Engineering,* vol. 22, pp. 3-15, 2002.

[11] J. T. Christian, "Reliability methods for stability of existing slopes," in *Uncertainty in geologic environment, from theory to practice*, 1996.

[12] K. C. Foye*, et al.*, "Assessment of variable uncertainties for reliability-based design of foundations," *ASCE Journal of Geotechnical and Geoenvironmental Engineering,* vol. 132, pp. 1197-1207, 2006.

[13] U. J. Na*, et al.*, "Effects of special variation of soil properties on seismic performance of port structures," *Soil Dynamics and Earthquake Engineering,* vol. 29, pp. 537-545, 2009.

[14] M. J. Spry and F. H. Kulhawy, "Reliability-based foundation design for transmission line structures: geotechnical site characterization strategy " Electric Power Research Institute, Palo Alto1988.

[15] S. Lacasse and F. Nadim, "Uncertainty in characterising soil properties," in *Uncertainty in the geological environment, from theory to practice*, 1996.

[16] U. J. Na*, et al.*, "Probabilistic assessment for seismic performance of port structures," *Soil Dynamics and Earthquake Engineering,* vol. 28, pp. 147-158, 2008.

[17] P. Lumb, "The variability of natural soils," *Canadian Geotechinical Journal,* vol. 3, pp. 74-97, 1996.

[18] P. Lumb, "Safety factors and probability distribution of soil strength," *Canadian Geotechinical Journal,* vol. 7, pp. 225-241, 1970.

[19] S. Lacasse and F. Nadim, "Uncertainties in characterising soil properties," *Geotechnical Special Publication,* vol. 58, pp. 49-75, 1996.

[20] S. Lacasse and F. Nadim, "Reliability issues and future challenges in geotechnical engineering for offshore structures," presented at the 7th International Conference on Behaviour of Offshore Structures, MIT, Massachuset, USA, 1994.

[21] F. Nadim*, et al.*, "Probabilistic foundation stability analysis: mobilized friction angle vs available shear strength approach," in *Structural Safety and Reliability*, Balkema, Rotterdam, Netherland, 1994, pp. 2001-2008.

[22] F. H. Kulhawy and K. K. Phoon, "Observations on geotechnical reliability-based design development in North America," presented at the Proceedings of the International Workshop on Foundation Design Codes and Soil Investigation in View of International Harmonization and Performance Based Design, Kamakura, Japan, 2002.

[23] T. F. Wolff*, et al.*, "Reliability assessment of dike and levee embankments," in *Uncertainty in the geologic environment, from theory to practice*, 1996.

[24] S. Koutsourelakis*, et al.*, "Risk assessment of an interacting structure-soil system due to liquefaction," *Earthquake Engineering & Structural Dynamics,* vol. 31, pp. 851-879, 2002.

[25] Y. Tang and J. Zhang, "Probabilistic seismic demand analysis of a slender RC shear wall considering soil-structure interaction effects," *Engineering Structures,* vol. 33, pp. 218-229, 2011.

[26] N. Shome*, et al.*, "Earthquakes, records, and nonlinear responses," *Earthquake Spectra,* vol. 14, pp. 469-500, 1998.

[27] "HAZUS-MH Version 1.1," ed. Washington D.C.: Federal Emergency Management Agency and U.S. Army Corps of Engineers, 2005, p. FEMA's software program for estimating potential losses from disasters (technical manual)

[28] R. Prishati, "Effect of soil parameter uncertainty on seismic demand of low-rise steel buildings on dense silty sand," *Soil Dynamics and Earthquake Engineering,* vol. 29, pp. 1367-1378, 2009.

CHAPTER 4. Fundamental Aspects of Probability Theory

Abstract. This chapter contains a brief overview of some fundamental aspects of probability theory to facilitate understanding of the analysis presented in the following chapters. The concepts and terminologies reviewed are: (i) probability space; (ii) random variable; (iii) probability distributions; (iv) measures of spread; and (v) some special probability distributions. The interested reader is also referred to the introductory textbooks on probability, such as [1-4], for more details. In addition, this chapter introduces Monte Carlo simulation, a stochastic process that can be used in analysing complex systems with uncertainty.

4.1 Probability Space

A probability space is a mathematical representation of a real-world situation or experiment consisting of states that occur randomly. This space consists of three parts:

1) An outcome space Ω, which is the set of all possible outcomes.

2) A collection of events ϑ, where each event is a set containing zero or more outcomes.

3) A procedure for assigning probabilities to specific events, which is a function from events to probability levels.

An outcome is the result of a single execution of a representative model or experiment. In real situations, individual outcomes are not usually of much interest. Thus, a

collection of outcomes is used that is called an event. When the events are defined, there is a need to specify each event's likelihood of happening, or the relative frequencies of occurrence of that event. This specification is done by using the probability mass function or the probability density function. Generally, two types of probability space exist: (i) discrete space; (ii) continuous space.

1) Discrete space is comprised of finite and countable sample points. In this type of space, probabilities can be ascribed to points of Ω by the probability mass functions $p(\vartheta)$. In a discrete space:

$$p(\vartheta) \geq 0 \text{ for all } \vartheta \in \Omega, \text{and } \sum_{\vartheta \in \Omega} p(\vartheta) = 1.0 \tag{4.1}$$

2) Continuous space is consisted of infinite and uncountable numbers of sample points. In this type of space, probabilities are assigned to intervals instead of points and probabilities are defined by density functions $f_X(x)$. In a continuous space:

$$f_X(x) \geq 0 \text{ for all } x \in \Omega, \text{and } \int_{\Omega} f_X(x) = 1.0 \tag{4.2}$$

It is important to note that most structural and geotechnical phenomena occur in uncountable probability space, because they are continuous quantities and cannot be specified only at specific points.

4.1.1 Random Variable

A random variable is a function $Z(x)$ that associates the outcomes from probability space to numbers, which are typically real values. In other words, a random variable is a numerical description of the outcome of an experiment. In this regard, the possible values of a random variable might represent the possible outcomes of a yet-to-be-performed experiment, or the potential values of a quantity whose already existing value is uncertain. Considering the definition presented for random variables, the function $\{Z(x) \leq x_i\}$ is then recognised as an event for any value of x_i.

Depending on the outcome space expected for an experiment, the random variables can be classified as either discrete, where a random variable takes on values from discrete probability space, or continuous, where a random variable takes on values from continuous probability space.

4.1.2 Probability Distributions

A probability distribution is a function that describes the probability of a random variable taking certain values. This function can be defined in two different ways:

1) It can be assigned to every point of a discrete or continuous outcome space. When the function is assigned to a discrete outcome space, it gives the probability that a discrete random variable is exactly equal to some particular value. The function, in this case, is called probability mass function (pmf) and denoted as $p_X(x)$. When the function is assigned to a continuous outcome space, the probability of a random variable falling within a particular region is given by the integral of this function over the region. The function, in this case, is called probability density function (pdf) and is denoted as $f_X(x)$. Probability distribution functions have the following properties:

For discrete outcome space:

$$p_X(x) \geq 0 \tag{4.3}$$

$$\sum_{X\in\Omega} p_X(x) = 1.0 \tag{4.4}$$

$$P[X] = \sum_{X\in\Omega} p_X(x) \tag{4.5}$$

For continuous outcome space:

$$f_X(x) \geq 0 \tag{4.6}$$

$$\int_{-\infty}^{+\infty} f_X(x) = 1.0 \tag{4.7}$$

$$P[a \leq x \leq b] = \int_a^b f_X(x)dx \tag{4.8}$$

It is important to note that for a continuous outcome space, the probability of any single value is zero. Examples of probability mass function and probability density function are shown in Figure 4-1 and Figure 4-2 respectively.

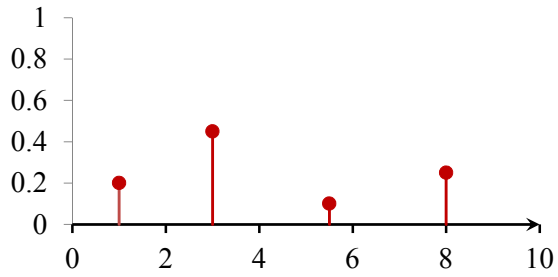

Figure 4-1. An example of probability mass function.

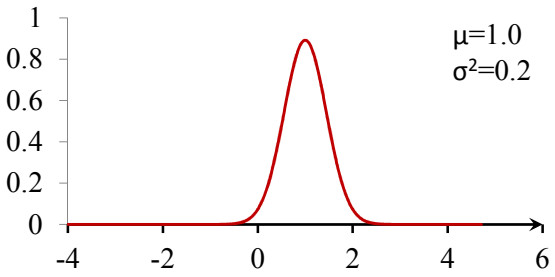

Figure 4-2. An example of probability density function (normal distribution).

2) It can also be defined by the probability of a random variable taking on values that are not larger than a given value. In this case, it is called cumulative distribution function (CDF) and is denoted as $F_X(x)$ where,

$$F_X(x) = P(X \leq x) \tag{4.9}$$

Note that cumulative distribution function can be defined for both cases of discrete and continuous outcome space. Cumulative distribution functions have the following properties:

$$0 \leq F_X(x) \leq 1 \tag{4.10}$$

$$F_X(-\infty) = 0 \text{ and } F_X(\infty) = 1 \tag{4.11}$$

$$P_X(a \leq X \leq b) = F_X(b) - F_X(a) \text{ for } a < b \tag{4.12}$$

An example of cumulative distribution function is shown in Figure 4-3.

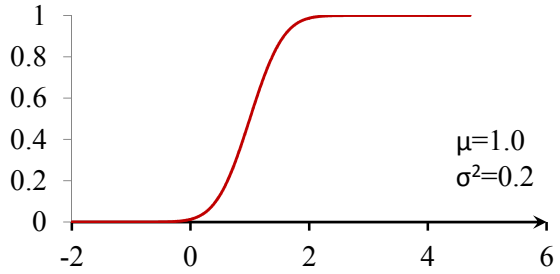

Figure 4-3. An example of cumulative distribution function (related to the normal distribution in Figure 4-2).

4.1.3 Measures of Spread

To capture important information about a data set or distribution and consequently quantify the existing variation, simple statistical measures such as the mean, median, mode, standard deviation, total range and interquartile range are used. These measurements capture the central tendency and variation of the data.

4.1.3.1 Mean

The mean value describes the central tendency in a data set or distribution, and has two related meanings: the arithmetic mean or the expected value of a random variable. The arithmetic mean is defined for a data set, as the sum of all values divided by the number of values. For example, considering a set of numbers $x_1, x_2, \ldots, x_n$, the mean is defined:

$$\mu = \frac{\sum_{i=1}^{n} x_i}{n} \tag{4.13}$$

The expected value of a random variable is a number representing the weighted average of all possible values that this random variable can take. The weights used in computing the expected value correspond to the probabilities in case of a discrete random variable, or densities in case of a continuous random variable. The expected value of a random variable X is given by:

$$E(X) = \sum_{i=1}^{n} x_i p(x_i) \text{ when } X \text{ is discrete} \tag{4.14}$$

$$E(X) = \int_{-\infty}^{+\infty} x f_X(x) \text{ when } X \text{ is continuous} \tag{4.15}$$

It is important to note that the mean is often quoted along with the standard deviation and is not necessarily the same as the middle value (median), or the most likely (mode), especially if the distribution is skewed.

4.1.3.2 Median

The median is the numerical value at which half the population is below and half is above. The median of a finite list of numbers can be found by arranging all the observations from lowest value to highest value and picking the middle one. If there is an even number of observations, then there is no single middle value and the median is defined as the mean of the two middle values. For any probability distribution, the median m has to satisfy the inequalities:

$$P_X(x \leq m) \geq \tfrac{1}{2} \text{ and } P_X(x \geq m) \leq \tfrac{1}{2} \tag{4.16}$$

$$\int_{-\infty}^{m} f_X(x) \geq \tfrac{1}{2} \text{ and } \int_{m}^{\infty} f_X(x) \leq \tfrac{1}{2} \tag{4.17}$$

The median can be used as a measure of location when a distribution is skewed or when one requires reduced importance to be attached to outliers, as they represent unrealistic measurements. A disadvantage of the median is the difficulty of handling it theoretically, which is a common issue with any non-parametric studies.

4.1.3.3 Mode

The mode is the most likely value (occurs most frequently) of a set of values or a probability distribution. Therefore, the mode for a discrete probability distribution is the value at which the probability mass function takes its maximum value, and the mode for a continuous probability distribution is the value at which the probability density function attains its maximum value. Figure 4-4 shows two examples.

The mode is in general different from the mean and median, and may be very different for strongly skewed distributions. It is also important to note that the mode is not necessarily a unique value, since the same maximum frequency may be attained at different values.

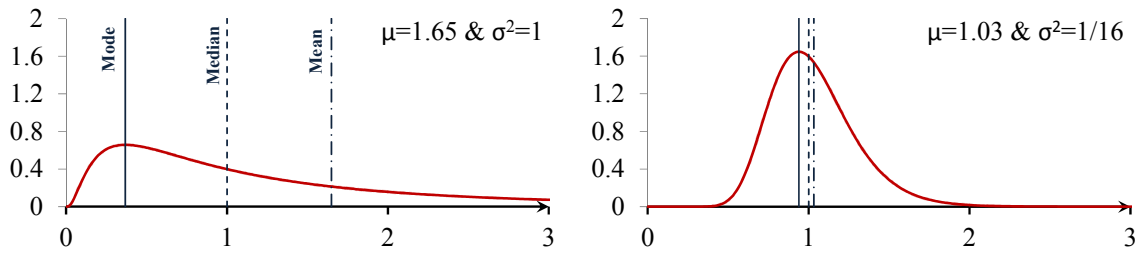

(a) (b)

Figure 4-4. Comparison of mean, median and mode of two log-normal distributions with different skewness.

4.1.3.4 Standard deviation

The standard deviation is a widely used measurement of variability or diversity in a set of values or probability distribution. It principally shows how much variation or dispersion exist around the mean or expected value. A low standard deviation indicates that the data points tend to be very close to the mean, whereas high standard deviation indicates that the data are spread out over a large range of values. Figure 4-5 and Figure 4-6 show how the variation in a data set, either being discreet or continuous, can be represented by the defined standard deviation.

For normal distribution, standard deviation can be used as a measure of confidence in any conclusion made based on statistical results. However, it is very important to note that standard deviation is invalid if the distribution is not normal or Gaussian.

Letting X be a random variable, the standard deviation is defined:

$$\sigma = \sqrt{\frac{1}{N}\sum_{i=1}^{N}(x_i - \mu)^2} \text{ when X is discrete} \tag{4.18}$$

where N is the total number of data points.

$$\sigma = \sqrt{\int_X (x-\mu)^2 p(x)dx} \text{ when X is continuous} \tag{4.19}$$

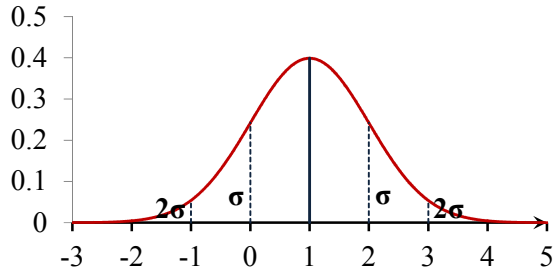

Figure 4-5. A plot of a normal distribution while each band has a width of one standard deviation.

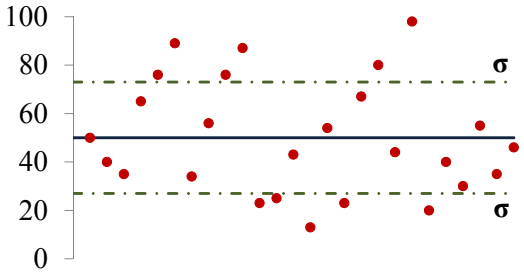

Figure 4-6. A data set with a mean of 50 and a standard deviation of 23.

4.1.3.5 Total range

The total range is the length of the interval that contains all the data. It is calculated by subtracting the smallest observation (sample minimum) from the greatest (sample maximum) and provides an indication of statistical dispersion. Since it only depends on two of the observations, it is a poor and weak measure of dispersion except when the sample size is large.

4.1.3.6 Interquartile range (IQR)

The interquartile range (IQR) is a non-parametric measure of statistical dispersion equals the difference between the third (75^{th} percentile) and first (25^{th} percentile) quartiles:

$$IQR = Q_3 - Q_1 \tag{4.20}$$

Unlike total range, the interquartile range is a robust statistic having breakdown points at 25%. It is thus often preferred to the total range. Figure 4-7 shows the interquartile range of a lognormal distribution along with its probability density function and cumulative distribution function.

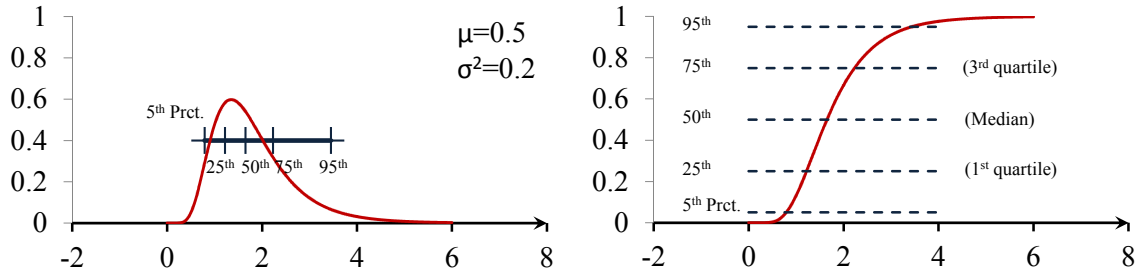

(a) (b)

Figure 4-7. Interquartile range with: (a) a lognormal probability density function; (b) a lognormal cumulative distribution function.

The IQR is used to build boxplots, simple graphical representations of a non-Gaussian probability distribution. In this type of presentation, the median is the corresponding measure of central tendency.

4.1.3.7 Boxplot presentation

Boxplot presentation is a convenient way of graphically presenting groups of numerical data through their five-number summaries: (i) the smallest observation (sample minimum); (ii) the lower quartile (Q1); (iii) the median (Q2); (iv) the upper quartile (Q3); and (v) largest observation (sample maximum). A boxplot thus indicates which observations can be considered outliers.

Boxplots are non-parametric and thus display differences between populations without making any assumptions of the underlying statistical distribution. The spacing between the different parts of the box indicates the degree of dispersion and skewness in the data, and thus identifies outliers.

4.1.4 Special Probability Distributions

The most relevant probability distributions used in this study (uniform, exponential, normal and lognormal distributions) are briefly introduced in this section. The focus is only on their properties, rather than their derivation. The interested reader is also referred to [1-4].

4.1.4.1 Uniform distribution

If a random variable is equally likely to take on any value within an interval, it is uniformly distributed. This distribution is defined by two parameters, a and b, which are the minimum and maximum values of the considered interval. The uniform distribution is often denoted $U(a,b)$. The probability density function of the continuous uniform distribution is defined:

$$f(x) = \begin{cases} \frac{1}{b-a} & \text{for } a \le x \le b \\ 0 & \text{for } x < a \text{ or } x > b \end{cases} \tag{4.21}$$

The probability density function can also be written in terms of mean μ and variance σ^2:

$$f_X(x) = \begin{cases} \frac{1}{2\sqrt{3}\sigma} & \text{for } -\sqrt{3}\sigma \le x-\mu \le \sqrt{3}\sigma \\ 0 & \text{otherwise} \end{cases} \tag{4.22}$$

The cumulative distribution function of a uniformly distributed variable is defined:

$$F_X(x) = \begin{cases} 0 & \text{for } x < a \\ \frac{x-a}{b-a} & \text{for } a \le x \le b \\ 1 & \text{for } x \ge b \end{cases} \tag{4.23}$$

The pdf and CDF of the uniform distribution are illustrated in Figure 4-8 and the other properties of this distribution are presented in Table 4-1.

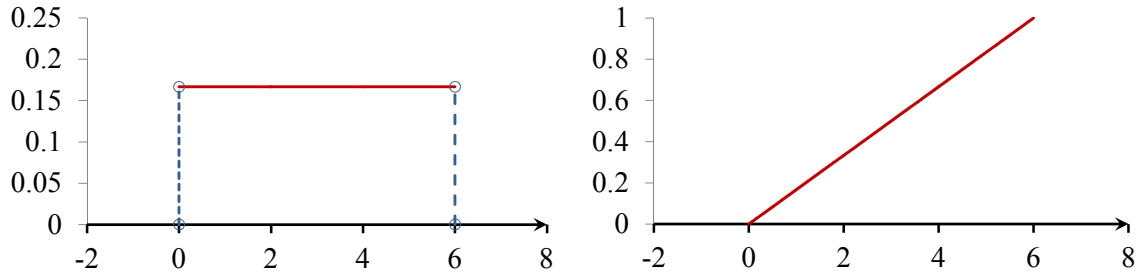

(a) (b)

Figure 4-8. Uniform distribution: (a) probability density function; (b) cumulative distribution function.

4.1.4.2 Exponential distribution

The exponential distribution is used to model situations where certain events occur with a constant probability per unit length. For example, it can be used to describe the time between events in a Poisson process, which is a process in which events occur continuously and independently at a constant average rate. The probability density function and the cumulative distribution function of an exponential distribution are defined:

$$f_X(x;\lambda) = \begin{cases} \lambda e^{-\lambda x} & \text{for } x \geq 0 \\ 0 & \text{for } x < 0 \end{cases} \tag{4.24}$$

$$F_X(x;\lambda) = \begin{cases} 1 - e^{-\lambda x} & \text{for } x \geq 0 \\ 0 & \text{for } x < 0 \end{cases} \tag{4.25}$$

The pdf and CDF of the uniform distribution are illustrated in Figure 4-9 and the other properties of this distribution are presented in Table 4-1.

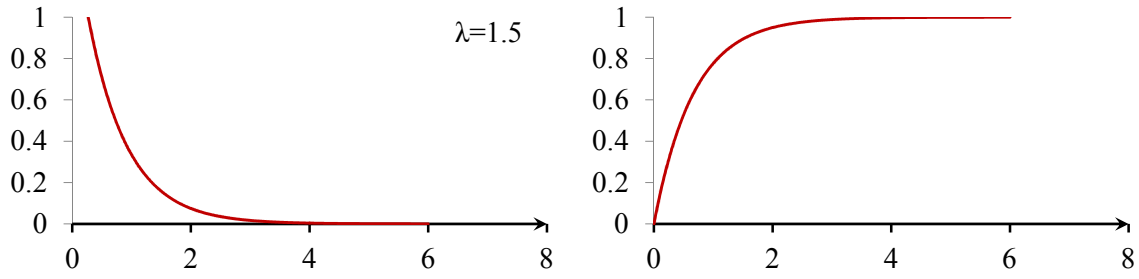

(a) (b)

Figure 4-9. Exponential distribution: (a) probability density function; (b) cumulative distribution function.

4.1.4.3 Normal distribution

The normal or Gaussian distribution is often used as a first approximation to describe real-valued random variables that tend to cluster around a single mean value. The normal distribution arises as the outcome of the central limit theorem, which states that under mild conditions the sum of a large number of random variables is distributed approximately normally.

Note that a normally-distributed variable has a symmetric distribution about its mean. Therefore, quantities that are distributed with some skew may be better described by other distributions, such as the lognormal distribution.

The simplest case of a normal distribution is known as the standard normal distribution, described by the probability density function:

$$\phi(x) = \frac{1}{\sqrt{2\pi}} e^{-\frac{1}{2}x^2} \tag{4.26}$$

The standard normal distribution has a mean of zero and a standard deviation of unity. If any other values of the mean μ and standard deviation σ are expected, the normal distribution, in a more general case, is expressed:

$$f_X(x; \mu, \sigma^2) = \frac{1}{\sqrt{2\pi\sigma^2}} e^{-\frac{(x-\mu)^2}{2\sigma^2}} = \frac{1}{\sigma}\phi\left(\frac{x-\mu}{\sigma}\right) \tag{4.27}$$

The normal distribution can also be denoted by $N(\mu, \sigma^2)$. The cumulative distribution function of a normal variable is given by:

$$F_X(x; \mu, \sigma^2) = \Phi\left(\frac{x-\mu}{\sigma}\right) \tag{4.28}$$

where $\Phi = \frac{1}{\sqrt{2\pi}} \int_{-\infty}^{x} e^{-t^2/2} dt$. The pdf and CDF of the standard normal distribution are illustrated in Figure 4-10 and the other properties of this distribution are presented in Table 4-1.

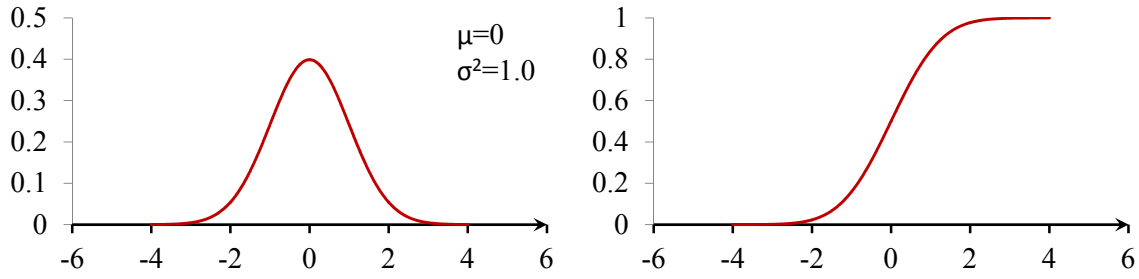

(a) (b)

Figure 4-10. Standard normal distribution: (a) probability density function; (b) cumulative distribution function.

4.1.4.4 Lognormal distribution

The lognormal distribution is a probability distribution of a random variable whose logarithm is normally distributed. If X is a random variable with a normal distribution, then $Y = exp(X)$ has a lognormal distribution. Likewise, if Y is lognormally distributed, then $X = log(Y)$ is normally distributed.

A variable might be modelled as lognormal if it can be thought of as the multiplicative product of many independent random variables each of which is positive. Hence, many structural response quantities are lognormal. The probability density function of a lognormal distribution is defined:

$$f_X(x;\mu,\sigma) = \frac{1}{x\sigma\sqrt{2\pi}} e^{-\frac{(lnx-\mu)^2}{2\sigma^2}} \tag{4.29}$$

The cumulative distribution function of a lognormal variable is then defined:

$$F_X(x;\mu,\sigma) = \Phi(\frac{lnx-\mu}{\sigma}) \tag{4.30}$$

The pdf and CDF of the standard normal distribution are illustrated in Figure 4-11 and the other properties of this distribution are presented in Table 4-1.

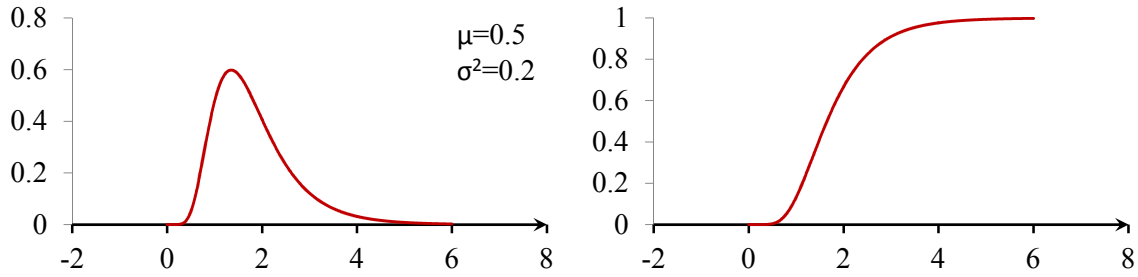

(a) (b)

Figure 4-11. Lognormal distribution: (a) probability density function; (b) cumulative distribution function.

Table 4-1. Properties of the considered probability distributions.

Property	Uniform	Exponential	Normal	Lognormal
Mean	$\frac{1}{2}(a+b)$	λ^{-1}	μ	$e^{\mu+\sigma^2/2}$
Median	$\frac{1}{2}(a+b)$	$\lambda^{-1}Ln2$	μ	e^{μ}
Mode	Any value in $[a,b]$	0	μ	$e^{\mu-\sigma^2}$
Variance	$\frac{1}{12}(b-a)^2$	λ^{-2}	σ^2	$(e^{\sigma^2}-1)e^{2\mu+\sigma^2}$
Skewness	0	2	0	$(e^{\sigma^2}+2)\sqrt{e^{\sigma^2}-1}$

4.2 Monte Carlo Simulation

Monte Carlo simulation is useful for obtaining numerical solutions for complicated problems that are hard to be solved by closed-form techniques or for which the number of variables or uncertainty is large. It is a process in which values of a property are drawn from a given data set (randomly or pseudo-randomly) multiple times to produce a series of realizations. Each realization corresponds to a probable representation of the underlying reality from the considered data set. These multiple realizations are then used as an input to simulation analysis to provide an understanding of the probability of a given outcome situation occurring. In this research, for example, the Monte Carlo

simulation was used to quantify the effects of soil-structure interaction on the seismic structural response. The implementation of the Monte Carlo method, generally involves [5, 6]:

1) Selection of a model/procedure that provides a deterministic solution to a problem of interest.

2) Selection of the input parameters that need to be modelled probabilistically.

3) Selection of probability distributions for the random parameters and generation of the values required for the analysis.

4) Repeated determination of the output using the deterministic model and randomly selected values.

5) Determination of relevant statistics for the outputs of interest to quantify performance.

The main question to be answered when a Monte Carlo simulation is run is "how many realizations should be performed to estimate an expected probability of a specific outcome with an acceptable accuracy?" The number of Monte Carlo trials required depends on the expected probability of a specific outcome and the desired level of confidence. As expected, the number of trials increases when the expected probability of a specific outcome becomes smaller or the level of confidence increases.

The number of required Monte Carlo trials can be estimated from [6]:

$$n = \hat{p}\hat{q}\left(\frac{z_{\alpha/2}}{e}\right)^2 \tag{4.31}$$

where $\hat{p}$ is the probability of a specific outcome, $\hat{q} = 1 - \hat{p}$, e is the maximum error on $\hat{p}$ at confidence $1 - \alpha$ and $z_{\alpha/2}$ is the point on the standard normal distribution satisfying $P[Z > z_{\alpha/2}] = \alpha/2$. As an example, if a Civil Engineering work has a target

failure probability ($\hat{p}_f = \hat{p}$) of $1/1000$ with the maximum accepted error on $\hat{p}_f$ of 0.0001, then the required number of realizations at confidence level of 90% will be:

$$n = (1/1000)(1 - 1/1000)(\frac{1.645}{0.0001})^2 = 270{,}332 \tag{4.32}$$

As can be seen from the above calculation, estimating some probabilities in this range of accuracy requires a very large number of realizations. However, such large numbers of realizations may not be practical. One possible solution, when a large number of realizations is impractical, is to perform as many realizations as possible, form a histogram of the response and fit a distribution to the histogram [6]. The fitted distribution is then used to predict any expected probability of a specific outcome. To produce a reasonably accurate histogram, while still being practical, the required number of Monte Carlo trials is in the order of thousands [5]. Hence, only a few thousands realizations may be required to obtain robust statistical measures based on high resolution distribution of the random input variables.

4.3 Summary

Fundamental aspects of probability theory required for better understanding of the results and discussions presented in the following chapters were reviewed. In addition, the Monte Carlo simulation, a comprehensive statistical approach suitable for complex problems that is also used in this research, was introduced.

References

[1] G. A. Fenton and D. V. Griffiths, *Risk Assessment in Geotechnical Engineering*. New York: John Wiley & Sons Inc., 2008.

[2] A. H.-S. Ang and W. H. Tang, *Probability Concepts in Engineering Planning and Design*. New York: John Wiley & Sons, Inc., 1975.

[3] D. G. Kelly, *Introduction to Probability*: Macmillan Publishing Company, 1994.

[4] W. Mendenhall and R. Beaver, *Introduction to Probability and Statistics*: PWS-Kent Publishing Company, 1991.

[5] A. L. Jones*, et al.*, "Estimation of Uncertainty in Geotechnical Properties for Performance-Based Earthquake Engineering," University of California, Berkeley2002.

[6] S. Lacasse and F. Nadim, "Uncertainty in characterising soil properties," in *Uncertainty in the geological environment, from theory to practice*, 1996.

CHAPTER 5. Soil-Structure Model for Adopted Stochastic Seismic Soil-Structure Interaction Analysis

Abstract. This chapter introduces the soil-structure model using physical cone model as the soil-foundation interface that is adopted for the stochastic analyses in this research. The model fundamentals are reviewed first and the specifications of each part of the model are explained later. Finally, the numerical model used for the time-history simulations is described and its validation is presented.

5.1 Specifications of the Soil-Structure Model

To quantitatively investigate how the response of a structure on a flexible foundation differs from the response of the same structure when fixed at the base, a fairly simple soil-structure model appropriate for dynamic time-history analysis can be used. This model, shown in Figure 5-1, is comprised of an either elastic or nonlinear (yielding) viscously damped single-degree-of-freedom structure resting on the surface of a viscoelastic half-space. For simplicity, without losing accuracy, the mass of the foundation and the mass moment of inertia of the structure can be neglected [1]. This model represents three global degrees of freedom: (i) horizontal translation of the structure relative to the foundation; (ii) horizontal translation of the foundation relative to the free-field ground; and (iii) rotation of the foundation in the plane of motion.

However, this dynamic model only shows two modes of motion which are: (i) swaying; and (ii) rocking.

It is important to note that the application of this model is restricted to the inertial interaction analysis only, which is the focus of this research, and it can be used to investigate: (i) the influence of the increased flexibility of the system due to presence of the soil; and (ii) the influence of the modified system damping that results from the combination of radiation and hysteretic soil damping with structural initial damping. In addition, it is worth mentioning that the effects of foundation embedment, soil layering, and soil-foundation interface nonlinearity are not covered in this model.

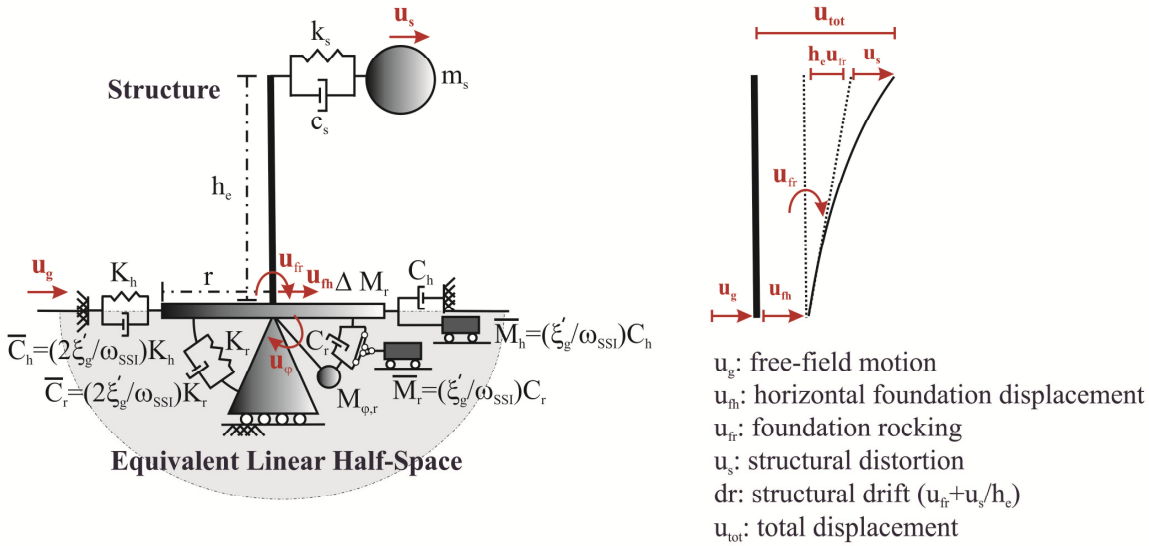

Figure 5-1. Soil-structure model for horizontal and rocking motions.

5.2 Modelling the Structure

In this model of the soil-structure system, the structure is modelled as a single-degree-of-freedom system that may be a representative of a single-storey building, a bridge pier or the fundamental mode of vibration of a multi-storey building, while responding in the fixed-base condition. This single-degree-of-freedom system is modelled by a mass indicating the structural mass which is participating in the fundamental mode of vibration m_s, a static spring representing the structural lateral stiffness k_s and a dashpot signifying the structural viscous damping c_s. It is then connected with a rigid element having the height of h_e to a rigid foundation that is bounded to the soil surface. Herein,

h_e is considered as the distance from the base of the structure to the centroid of the inertial loads. The fixed-base natural frequency of the considered structure is defined:

$$\omega_s = \sqrt{\frac{(k_s)_i}{m_s}} \tag{5.1}$$

where $(k_s)_i$ is the initial structural lateral stiffness. The coefficient of equivalent structural viscous damping in the model is defined:

$$c_s = 2\xi_s\sqrt{(k_s)_i m_s} \tag{5.2}$$

Note that ξ_s is the structural damping ratio and conventionally has been assumed to be 5%. Finally, it should be noted that the model does not include the second-order ($P-\Delta$) effects.

In the model, alternative force-displacement relationship of the structure may be investigated simply by assigning different hysteretic rules to the spring element of the model. Four different hysteretic rules were selected for this research: (i) linear; (ii) Takeda (TK); (iii) bilinear elasto-plastic (EP); and (iv) Takeda with negative post-yield stiffness (TKN). These hysteretic force-displacement relationships are shown in Figure 5-2.

The Linear rule was used to develop a conceptual understanding of soil-structure interaction effects on seismic structural response, and also to investigate the preconception in seismic design codes with regard to soil-structure interaction. The TK rule was selected to represent the behaviour of a newly designed concrete-framed structure, and to be used as a benchmark reference for investigating the effects of structural nonlinearity on soil-structure interaction effects. The EP and TK model were chosen to compare the effects of structural nonlinearity when different hysteretic scenarios are utilized. More specifically, the EP rule represents the behaviour of a newly designed steel-framed structure, and the TKN rule approximates the response of a structure with either significant second order ($P-\Delta$) or strength degradation effects.

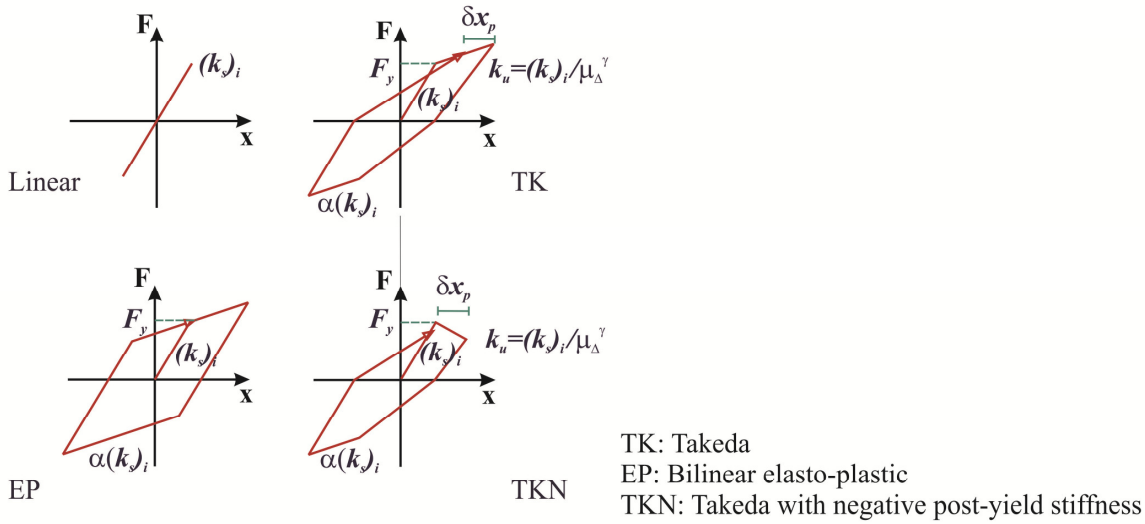

Figure 5-2. Hysteretic force-displacement relationships representing structural response.

5.3 Modelling the Soil-Foundation Interface

The restraining action of the soil-foundation interface is modelled by a discrete-element including horizontal and rocking equivalent linear springs and viscous dashpots with frequency-independent coefficients. To define the parameters of this interface element, the simple physical cone model has been used. The concept and formulation of the cone model is explained in the following sections.

5.3.1 Physical Cone Model for Soil-Foundation Interface

A rigid shallow-foundation with an equivalent radius r sitting on a homogeneous soil half-space can be modelled as a truncated semi-infinite cone for each component of foundation motion [2-7]. This model includes the soil, which begins at the bottom surface of the foundation, extends downward to infinity, and is located within the geometry of the truncated cone. The soil located outside the truncated cone is disregarded.

For each component of foundation motion, translational (horizontal or vertical) and rotational (rocking or torsional), the truncated semi-infinite cone is defined by its aspect ratio z_0/r, in which z_0 is the apex height and r is the foundation radius. The appropriate value of z_0/r depends on the nature of the foundation deformation represented by the

cone. Figure 5-3 illustrates the cone model concept and shows that if a load is applied on the foundation, the stress at each depth is distributed on an area limited to the surface of a cone. Clearly, this area increases with depth and, consequently, less stress is expected to be distributed per unit area with increasing depth.

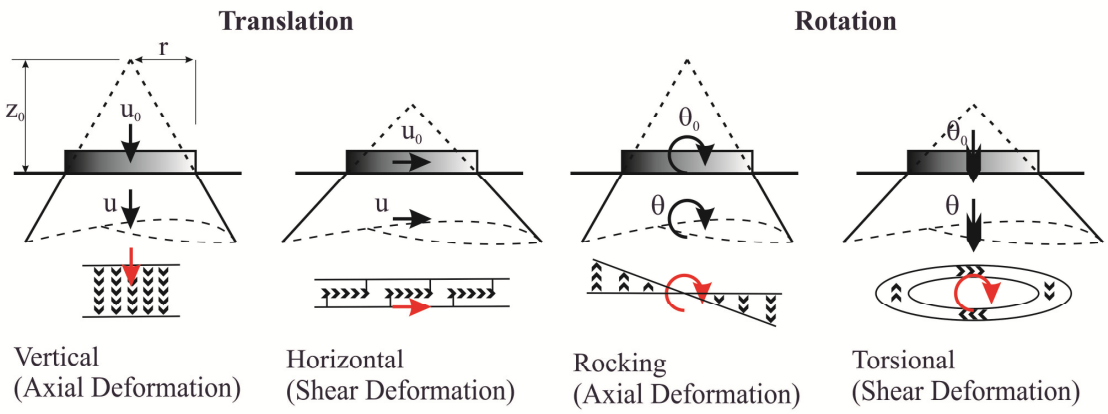

Figure 5-3. The concept of cone model for various degrees of freedom of the foundation with corresponding apex ratio, wave propagation velocity and distortion [2].

To define the soil-foundation interface cone model, the following approximations must be considered:

1) The foundation is a rigid mass-less disk with an area A and moment of inertia about the axis of rotation I.

2) The soil underneath the foundation is a homogeneous, isotropic, linearly elastic and semi-infinite medium with mass density ρ.

3) The wave propagation velocity in the cone depends on the nature of the foundation deformation. The appropriate velocity for the horizontal and tortional motion is the soil shear wave velocity V_s, and for the vertical and rocking motion is the dilatational (or P) wave velocity V_p.

4) The stress-strain relationship is specified by two independent elastic constants. These two parameters can be either the soil shear modulus G and Poisson's ratio υ, or soil shear wave velocity V_s and dilatational wave velocity V_p, for example. Note that these parameters are interrelated as defined:

$$V_s = \sqrt{\frac{G}{\rho}} = \sqrt{\frac{E}{2\rho}\frac{1-2\upsilon}{1-\upsilon}} \tag{5.3}$$

$$V_p = \sqrt{\frac{E}{\rho}} = \sqrt{\frac{2G}{2}\frac{1-\upsilon}{1-2\upsilon}} \tag{5.4}$$

5.3.2 Cone Aspect Ratio

For each degree of freedom, the aspect ratio of the cone z_0/r can be defined by equating the static-stiffness coefficient, derived from wave propagation theory [2], and the well-known closed-form solutions for a rigid disk foundation on an elastic half-space [8, 9], some of which are shown in Table 5-1. This approach ensures that cone opening angle, depending on the aspect ratio, is selected such that the behaviour of the rigid disk foundation on the half-space and the cone coincide in the low frequency limit or static case.

Table 5-1: Static-stiffness of a rigid disk foundation resting on the surface of an elastic half-space.

Horizontal	Vertical	Rocking	Torsion
$\frac{8Gr}{2-\upsilon}$	$\frac{4Gr}{1-\upsilon}$	$\frac{8Gr^3}{3(1-\upsilon)}$	$\frac{16Gr^3}{3}$

5.3.2.1 Determination of static-stiffness coefficients of the cone model

Translational cone: determination of the vertical static-stiffness coefficient of the cone model K_v relating the imposed vertical force on the foundation N_0 and the corresponding displacement at the foundation level u_0 is examined first, as shown in Figure 5-4(a). It is assumed that the area of the rigid disk foundation is $A = \pi r^2$ and the area of the cone at depth z is $A_z = (z/z_0)^2 A$, where z is measured from the apex. If an infinitesimal element of the cone at depth z is considered, static equilibrium of that element is defined:

$$-N + \left(N + N_{,z}dz\right) = 0 \tag{5.5}$$

where N is the axial force resulted from the axial displacement u, and $N_{,z}$ represents the first derivative of N with respect to z. Substituting N from the force-displacement relationship, $N = EA_z u_{,z} = (\frac{EA}{z_0^2})z^2 u_{,z}$, yields:

$$u_{,zz} + \frac{2}{z}u_{,z} = (zu)_{,zz} = 0 \tag{5.6}$$

where $u_{,zz}$ is the second derivative of u with respect to z. For this differential equation, the boundary conditions (BCs) at the foundation level ($z = z_0$) and infinity ($z = \infty$) are defined:

$$u(z = z_0) = u_0 \tag{5.7}$$

$$u(z = \infty) = 0 \tag{5.8}$$

Enforcing the BCs in Equation (5.6) yields:

$$u = \frac{z_0}{z}u_0 \tag{5.9}$$

I.e., the displacement at any depth is proportional to u_0 by the ratio of $\frac{z_0}{z}$. Knowing the solution for the defined displacement field u, the value of N_0 at the foundation level ($z = z_0$) is calculated:

$$N_0 = -N(z = z_0) = -EAu_{,z}(z = z_0) = \frac{EA}{z_0}u_0 \tag{5.10}$$

Equation (5-10) means that the static-stiffness coefficient of the translational cone in vertical motion is defined:

$$K_v = \frac{EA}{z_0} \tag{5.11}$$

If the translational cone in horizontal motion is considered, the analogous derivation considering displacement perpendicular to the cone's axis u can be used and, as a result, the horizontal static-stiffness is defined:

$$K_h = \frac{GA}{z_0} \tag{5.12}$$

The expressions in Equations (5.11) and (5.12) can be unified as $K = \rho V^2 A/z_0$ by introducing a general wave propagation velocity V, where $V = V_p$ for the vertical motion and $V = V_s$ for the horizontal motion.

Rotational cone: the rocking static-stiffness coefficient of the cone model K_r is derived by relating the rocking of the foundation θ_0 to the imposed moment M_0, as shown in Figure 5-4(b). It is assumed that the moment of inertia of the rigid disk foundation is $I = (\pi/4)r^4$ and the moment of inertia of the cone at depth z is $I_z = (z/z_0)^4 I$, where z is measured from the apex. Static equilibrium of the infinitesimal element is defined:

$$-M + (M + M_{,z}dz) = 0 \tag{5.13}$$

where M is the bending moment resulting from the rocking θ, and $M_{,z}$ represents the first derivative of M with respect to z. Substituting M from the moment-rotation relationship, $M = EI\theta_{,z} = \left(\frac{EI}{z_0^4}\right) z^4 \theta_{,z}$, into Equation (4.13) yields the differential equation:

$$\theta_{,zz} + \frac{4}{z}\theta_{,z} = 0 \tag{5.14}$$

where $\theta_{,zz}$ is the second derivative of u with respect to z. The BCs in this case are defined:

$$\theta(z = z_0) = \theta_0 \tag{5.15}$$

$$\theta(z = \infty) = 0 \tag{5.16}$$

Enforcing BCs leads to the following solution:

$$\theta = (\frac{z_0}{z})^3 \theta_0 \tag{5.17}$$

Using the moment-rotation relationship at the foundation level gives:

$$M_0 = -M(z = z_0) = -EI\theta_{,z}(z = z_0) \tag{5.18}$$

Substituting the solution for rocking into Equation (5.18) yields:

$$M_0 = \frac{3EI}{z_0}\theta_0 \tag{5.19}$$

This equation can be used to define the rocking static-stiffness coefficient of the rotational cone:

$$K_r = \frac{3EI}{z_0} \tag{5.20}$$

Considering twisting around the cone's axis, the analogous derivation for rotational cone in torsional motion can be created. As a result, torsional static-stiffness is defined:

$$K_t = \frac{3GI}{z_0} \tag{5.21}$$

Expressions introduced in Equations (5.20) and (5.21) can be unified as $K_\theta = 3\rho V^2 I/z_0$ by introducing a general wave propagation velocity V, where $V = V_p$ for the rocking motion and $V = V_s$ for torsional motion.

Figure 5-4. Truncated semi-infinite cone with static and dynamic equilibrium of infinitesimal element: (a) translational cone with nomenclature for vertical motion and, (b) rotational cone with nomenclature for rocking motion [2].

5.3.2.2 Determination of equivalent radius

The most straightforward approach to define the equivalent radius of the foundation with an arbitrary shape consists of equating the area A or the moment of inertia I of the basement to the corresponding value of the circular disk for translational or rotational cone, respectively. This approach yields:

$$r_v = r_h = \sqrt{\frac{A}{\pi}} \tag{5.22}$$

$$r_\theta = \sqrt[4]{\frac{4I}{\pi}} \tag{5.23}$$

$$r_t = \sqrt[4]{\frac{2I}{\pi}} \tag{5.24}$$

5.3.2.3 Calculation of aspect ratio for each degree of freedom

The aspect ratio z_0/r of cones presenting different components of foundation motion are shown in Table 5-2. These ratios depend, with the exception of torsional motion, on Poisson's ratio υ. Note that vertical and rocking cones for which dilatational waves govern are slender ($z_0/r > 1$), whereas horizontal and torsional cones for which shear waves dominate are more squat ($z_0/r < 1$).

It is also important to note that for vertical and rocking motions, V in principal equals V_p. However, it has to be limited to the value of $2V_s$ for nearly incompressible soils with the υ ranging between $1/3$ and $1/2$. Details of this aspect of the model are discussed in Section 5.3.4.

Table 5-2. Aspect ratio for each degree-of-freedom of foundation.

Horizontal	Vertical	Rocking	Torsion
$\frac{\pi}{8}(2-\upsilon)$	$\frac{\pi}{4}(1-\upsilon)(\frac{V}{V_s})^2$	$\frac{9\pi}{32}(1-\upsilon)(\frac{V}{V_s})^2$	$\frac{9\pi}{32}$

5.3.3 Dynamic-Stiffness Coefficient for High-Frequency Excitation

Translational cone: by taking the inertial force into account, the dynamic equilibrium for vertical motion of an infinitesimal element can be formulated:

$$-N + \left(N + N_{,z}dz\right) - \rho A_z dz\ddot{u} = 0 \tag{5.25}$$

where the term $\rho A_z dz\ddot{u}$ represents the inertial load. Substituting N from the force-displacement relationship, $N = EA_z u_{,z} = (\frac{EA}{z_0^2})z^2 u_{,z}$, into Equation (5.25) yields the one dimensional wave equation:

$$(zu)_{,zz} - \frac{(z\ddot{u})}{{V_p}^2} = 0 \tag{5.26}$$

For loading applied to the rigid disk foundation, only waves propagating in the positive z-direction will exist, and thus no wave return in the semi-infinite media is expected. Therefore, the solution of Equation (5.26) is defined:

$$zu = z_0 f(t - \frac{z - z_0}{V_p}) \tag{5.27}$$

The corresponding BC at the foundation level is defined:

$$u(z = z_0) = u_0 \tag{5.28}$$

Enforcing this BC into the Equation (5.28) results in the displacement field u defined:

$$u = \frac{z_0}{z} u_0(t - \frac{z - z_0}{V_p}) \tag{5.29}$$

Considering the defined displacement field and the governing force-displacement relationship, the applied force at the foundation level N_0 is defined:

$$N_0 = -N(z = z_0) = -EAu_{0,z} = \frac{EA}{z_0} u_0 + \rho V_p A \dot{u}_0 \tag{5.30}$$

Equation (5-30) can be reformulated:

$$N_0 = K_v u_0 + C_v \dot{u}_0 \tag{5.31}$$

This relationship gives the impression that N_0 is a representative of the combined effect of a spring and a dashpot with the coefficients defined:

$$K_v = \frac{EA}{z_0} = \frac{\rho {V_p}^2 A}{z_0} \tag{5.32}$$

$$C_v = \rho V_p A \tag{5.33}$$

If a translational cone in horizontal motion is considered, a similar formulation is derived with the only difference being that V_p has to be replaced by V_s. Consequently, Equations (5.32) and (5.33) can be unified defining $K = \rho V^2 A / z_0$ and $C = \rho V A$, where $V = V_s$ for horizontal motion and $V = V_p$ for vertical motion. Note that the simple form of the interaction force-displacement relationship presented in Equation (5.31) is valid for both low-frequency and high-frequency dynamic cases. In this equation, the spring force is dominant for low-frequency limits and the damping force governs the high-frequency limits.

Rotational cone: dynamic equilibrium of the infinitesimal element in the cone for rocking motion is defined:

$$-M + \left(M + M_{,z}dz\right) - \rho I_z dz\ddot{\theta} = 0 \tag{5.34}$$

Substituting M from the moment-rotation relationship, $M = EI_z\theta_{,z} = (\frac{EI}{z_0^4})z^4\theta_{,z}$, into Equation (5.34) results in the differential equation:

$$\theta_{,zz} + \frac{4}{z}\theta_{,z} - \frac{\ddot{\theta}}{{V_p}^2} = 0 \tag{5.35}$$

The solution of Equation (5.35) for harmonic excitation with the rocking acceleration defined as $\ddot{\theta}(\omega) = -\omega^2\theta(\omega)$ is defined:

$$\theta(\omega) = \theta_0(\omega)(\frac{z}{z_0})^2 e^{-i\frac{\omega}{c}(z-z_0)} \tag{5.36}$$

Considering the moment-rotation relationship, $M_0(\omega) = -EI\theta_0(\omega)_{,z}$, and the derivative of rocking motion from Equation (5.36), the applied moment at the foundation level is defined:

$$M_0(\omega) = (\frac{2\rho V_p^2 I}{z_0} + i\omega V_p I)\theta_0(\omega) \tag{5.37}$$

This formula illustrates that the moment at the foundation level can be interpreted as the combined effects of a spring and a dashpot having coefficients defined:

$$K_r = \frac{2\rho V_p^2 I}{z_0} \tag{5.38}$$

$$C_r = \rho V_p I \tag{5.39}$$

If a rotational cone in torsional motion is considered, a similar formulation is derived with the only difference being that V_p has to be replaced by V_s. Equations (5.38) and (5.39) are thus unified defining $K_\theta = 2\rho V^2 I/z_0$ and $C_\theta = \rho V A$, where $V = V_s$ for rocking motion and $V = V_p$ for torsional motion.

5.3.4 Modification for Nearly Incompressible Soil

For the vertical and rocking degrees of freedom, P-waves will dominate the behaviour of the cone and consequently, V_p should be used as the appropriate wave velocity. However, V_p tends to infinity for υ approaching 0.5, in the definition of V_p defined:

$$V_p = \sqrt{\frac{E}{\rho}} = \sqrt{2\frac{G}{\rho}\frac{1-\upsilon}{1-2\upsilon}} \tag{5.40}$$

Use of V_p for higher values of υ results in apparently anomalous behaviour for the cone and overestimates the radiational damping characterized by C [2]. Thus, it is necessary to develop ways to circumvent these difficulties because the range of incompressible soil is important in engineering practice. As an example, the saturated soil analysed as a single-phase medium has the Poisson's ratio of 0.5 as the water filling the pores is nearly incompressible. Even if entrained air is taken into account, the value of υ will not be smaller than 0.45.

Based on the rigorous solution for the dynamic stiffness of a rigid disk for all frequencies [2], two essential modifications are suggested for the vertical and rocking motions of nearly incompressible soil with Poisson's ratio between 0.33 and 0.5.

1) *Modification in wave velocity:* the appropriate wave velocity dominating the radiation damping is selected as twice the shear wave velocity instead of being the dilatation wave velocity. Therefore:

$$V = \begin{cases} V = V_p & if\ \upsilon \le 0.33 \\ V = 2V_s & if\ 0.33 \le \upsilon \le 0.5 \end{cases} \tag{5.41}$$

2) *Implementation of a trapped mass:* a trapped mass increasing linearly with the Poisson's ratio is introduced. It corresponds to trapped soil beneath the disk foundation that moves as a rigid body in phase with the disk. A trapped mass for vertical motion is defined:

$$\Delta M_v = \mu_v \rho r^3 \tag{5.42}$$

where $\mu_v = 2.4\pi(\upsilon - \frac{1}{3})$. For rocking motion the trapped mass moment of inertia is defined:

$$\Delta M_{\mathrm{r}} = \mu_r \rho r^5 \tag{5.43}$$

where $\mu_r = 0.3\pi(\upsilon - \frac{1}{3})$. According to these formulas, the inclusion of trapped mass begins at $\upsilon = 0.33$ and increases linearly with Poisson's ratio.

5.3.5 Dynamic-Stiffness Coefficient of Rotational Cone in Time Domain

It has been shown [2] that the dynamic-stiffness coefficient of a rotational cone in the time domain is more complex than that presented in Section 0. The relationship between interaction moment M_0 and rotation θ_0 at foundation level is defined:

$$M_0(t) = K_\theta \theta_0(t) + C_\theta \dot{\theta}_0(t) + \Delta M_\theta \ddot{\theta}_0(t) - \int_0^t h_1(t-\tau) C_\theta \dot{\theta}_0(\tau) d\tau \tag{5.44}$$

where $K_\theta = 3\rho V^2 I / z_0$, $C_\theta = \rho V I$, and $\Delta M_\theta = \mu \rho r^5$. The first three terms in Equation (5.44) represent the portion of moment due to the current values of rotation $\theta_0(t)$, rotational velocity $\dot{\theta}_0$(t) and rotational acceleration $\ddot{\theta}_0(t)$. The last term is a convolution integral with the rotational velocity $\dot{\theta}_0$(t) and involves the unit-impulse response function $h_1(t-\tau)$. This result depends on all the previous values of the rotational velocity and may be regarded as the system's memory.

To incorporate the convolution part of the soil-foundation rotational stiffness into the corresponding cone model, two simple physical models have been proposed. These models are shown in Figure 5-5 and discussed in the following:

1) *Spring-dashpot model with negative coefficients:* the node representing the foundation is connected to a rigid support by a rotational spring with the static-stiffness coefficient K_θ in parallel to a rotational dashpot with the high-frequency limit of the radiation damping C_θ. An additional internal rotational degree of freedom φ is introduced, which is connected by a rotational spring with the coefficient of $-K_\theta/3$ to the rigid disk foundation and by a rotational dashpot with the coefficient $-C_\theta$ to the rigid support, as seen in Figure 5-5(a).

2) *Monkey tail model:* negative coefficients can be avoided by using a model that consists of a mass-dashpot interconnection resembling a monkey tail, as seen in Figure 5-5(b). The rigid disk foundation is attached by a rotational spring with the coefficient K_θ to a rigid support. Again, an additional internal rotational degree of freedom φ with its own mass moment of inertia $M_\varphi = \rho z_0 I$ is introduced. This additional mass is connected to the rigid disk foundation by a rotational dashpot with the coefficient C_θ.

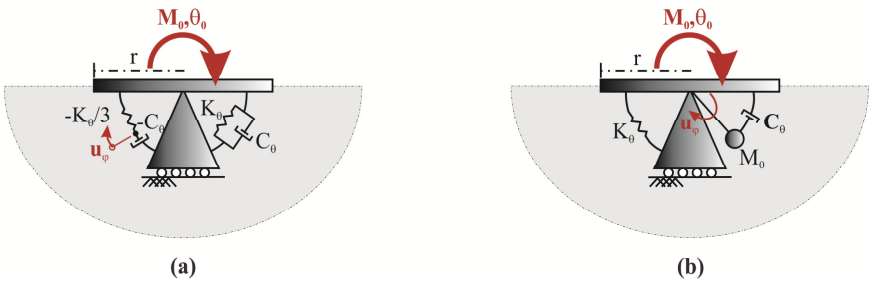

Figure 5-5. Cone model for rotational (rocking and torsional) motion: (a) spring-dashpot model with negative coefficients; (b) monkey-tail model [2].

5.3.6 Soil Material Damping

The resulting cone model is formulated under the assumption that soil is a perfectly linear material that dissipates energy only by radiation of waves towards infinity. However, the second important source of energy dissipation has to be considered is

material damping, which is also called hysteretic loss of energy. Material damping involves a frictional loss of energy, and as shown by experimental works, is independent of frequency. This type of damping can also be included in the cone model utilizing a simple modification in the elastic constants [2].

For the case of harmonic loading, material damping can be introduced into the elastic solution by using the so-called Correspondence Principle. Based on this principle, the damped solution incorporating an energy loss per cycle is obtained from the multiplication of all elastic constants by the complex factor of $(1 + 2i\xi_g)$. In other words:

$$G \rightarrow G(1 + 2i\xi_g) \tag{5.45}$$

$$E \rightarrow E(1 + 2i\xi_g) \tag{5.46}$$

where ξ_g is the soil material damping ratio. Applying the modifications introduced in Equations (5.45) and (5.46) into the coefficients of the cone model means that the amplitudes of the forces in springs and dashpots for unit-distortional motion have to be modified:

$$\rho V^2 \rightarrow \rho V^2(1 + 2i\xi_g) \tag{5.47}$$

$$i\omega\rho V \rightarrow i\omega\rho V(1 + 2i\xi_g) \tag{5.48}$$

where V corresponds to the appropriate wave propagation velocity for the predominant motion.

To adopt these modifications for a time-domain solution of the cone model, a solution with frequency-independent coefficients, the concept of Voigt type material damping introduced in viscoelasticity has to be applied [10]. In this regard, it is presumed that ξ_g is linearly proportional to the excitation frequency ω, although the experimental studies verify that the damping ratio is frequency-independent. Value of ξ_g is defined:

$$\xi_g = \xi'_g \frac{\omega}{\omega_{SSI}} \tag{5.49}$$

where ω_{SSI} is assumed to be the effective frequency of the soil-structure interacting system [11, 12], and ξ'_g is the soil material damping ratio at ω_{SSI}. Equations (5.47) and (5.48) can then be reformulated:

$$\rho V^2 \rightarrow \rho V^2 (1 + i\omega \frac{2\xi'_g}{\omega_{SSI}}) \tag{5.50}$$

$$i\omega\rho V \rightarrow \rho V (i\omega - \omega^2 \frac{\xi'_g}{\omega_{SSI}}) \tag{5.51}$$

On the right-hand sides of these expressions various powers of $i\omega$ appear: $(i\omega)^0 = 1.0$, $(i\omega)^1 = i\omega$, and $(i\omega)^2 = i\omega^2$. For harmonic motion it is well known that:

1) Terms of the dynamic stiffness coefficients not multiplied by a power $i\omega$ correspond to springs.

2) Terms involving $i\omega$ correspond to dashpots.

3) Terms containing $-\omega^2$ correspond to masses or inertial terms.

Equations. (5.50) and (5.51) have a simple physical interpretation as shown in Figure 5-6. According to Equation (5.50), each original elastic spring K is augmented by an additional parallel connected dashpot $\bar{C} = (\frac{2\xi'_g}{\omega_{SSI}})K$ and results in the force $P = \frac{2\xi'_g}{\omega_{SSI}} K(\dot{u}_0 - \dot{u}_1)$. From Equation (5.51), each original elastic dashpot C is augmented by an additional parallel connected mass (also called pully-mass) $\bar{M} = (\frac{\xi'_g}{\omega_{SSI}})C$ and results into the force $P = \frac{\xi'_g}{\omega_{SSI}} C(\ddot{u}_0 - \ddot{u}_1)$.

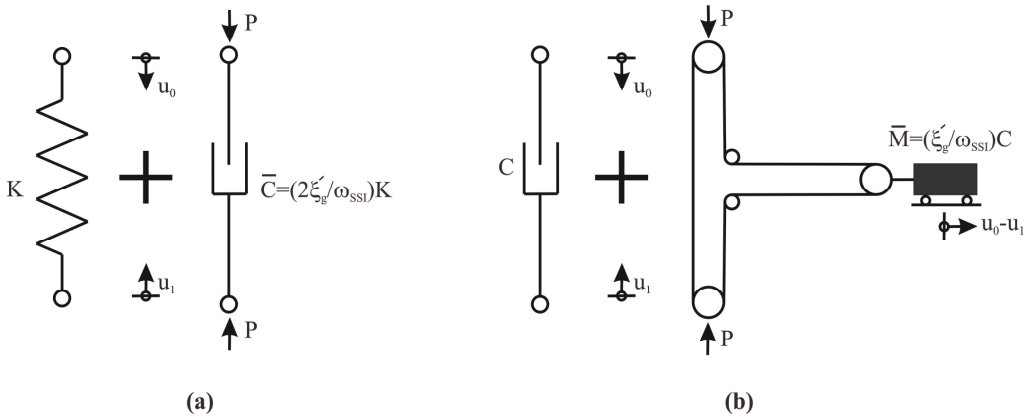

Figure 5-6. Augmenting elements to represent Voigt type material damping: (a) original spring with augmenting dashpot; (b) original dashpot with augmenting pulley mass.

The necessary modifications in the cone model are illustrated in Figure 5-7. It is important to note that:

1) The pulley mass is unnecessary if the original dashpot is fixed at the far end. In this case, the mass can be directly attached to the disk foundation.

2) The inclusion of viscoelasticity augments only the original elastic springs and dashpots. In other words, if the model includes a mass, such as the monkey tail mass, this mass will not be modified.

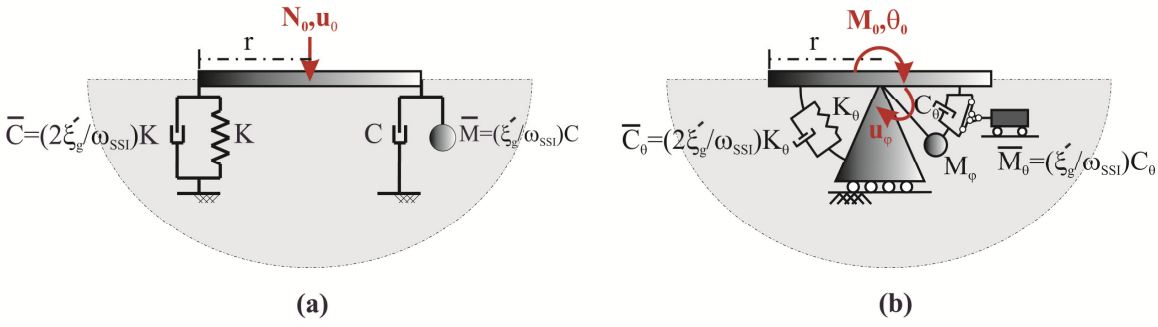

Figure 5-7. Inclusion of soil material damping into cone model for: (a) translational motion; (b) rotational motion.

5.3.7 Properties of Cone Model in Summary

The properties of the cone model representing the soil-foundation interface are summarized in Table 5-3. It is worth noting that all coefficients are frequency

independent. Therefore, the model can be directly used in structural dynamic programs working in the time domain.

Table 5-3. Properties of cone model for a rigid disk foundation on the surface of a homogeneous half-space.

<table>
<tr><th colspan="2">Motion</th><th>Stiffness</th><th>Viscous damper</th><th>Added mass</th></tr>
<tr><td rowspan="2">Vertical</td><td>$\upsilon \le \frac{1}{3}$</td><td rowspan="2">$K_v = \frac{4Gr}{1-\upsilon}$</td><td>$C_v = \rho V_p A$</td><td>–</td></tr>
<tr><td>$\frac{1}{3} \le \upsilon \le \frac{1}{2}$</td><td>$C_v = \rho(2V_s)A$</td><td>$\Delta M_v = 2.4(\upsilon - \frac{1}{3})\rho A r$</td></tr>
<tr><td colspan="2">Horizontal</td><td>$K_h = \frac{8Gr}{2-\upsilon}$</td><td>$C_h = \rho V_s A$</td><td>–</td></tr>
<tr><td rowspan="4">Rocking</td><td>$\upsilon \le \frac{1}{3}$</td><td rowspan="2">$K_r = \frac{8Gr^3}{3(1-\upsilon)}$</td><td>$C_r = \rho V_p I_r$</td><td>–</td></tr>
<tr><td>$\frac{1}{3} \le \upsilon \le \frac{1}{2}$</td><td>$C_r = \rho(2V_s)I_r$</td><td>$\Delta M_r = 1.2(\upsilon - \frac{1}{3})\rho I_r r$</td></tr>
<tr><td colspan="4">Internal mass moment of inertia</td></tr>
<tr><td>$\upsilon \le \frac{1}{3}$</td><td colspan="3">$M_{\varphi,r} = \frac{9\pi}{32}\rho I_r r(1-\upsilon)(\frac{V_p}{V_s})^2$</td></tr>
<tr><td></td><td>$\frac{1}{3} \le \upsilon \le \frac{1}{2}$</td><td colspan="3">$M_{\varphi,r} = \frac{9\pi}{8}\rho I_r r(1-\upsilon)$</td></tr>
<tr><td colspan="2" rowspan="3">Torsion</td><td>$K_t = \frac{16Gr^3}{3}$</td><td>$C_t = \rho V_s I_t$</td><td>–</td></tr>
<tr><td colspan="3">Internal mass moment of inertia</td></tr>
<tr><td colspan="3">$M_{\varphi,t} = \frac{9\pi}{8}\rho I_t r(1-\upsilon)$</td></tr>
<tr><td colspan="2" rowspan="3">Material damping</td><td colspan="3">Additional parallel connected element ($i = \upsilon, h, r, or\ t$)</td></tr>
<tr><td colspan="2">Viscous damping to stiffness K_i</td><td>Inertial mass to damping C_i</td></tr>
<tr><td colspan="2">$\overline{C_i} = (\frac{2\xi_g'}{\omega_{SSI}})K_i$</td><td>$\overline{M_i} = (\frac{\xi_g'}{\omega_{SSI}})C_i$</td></tr>
</table>

The parameters utilized in this table are defined:

1) ρ, υ, V_s, V_p and G: soil mass density, Poisson's ratio, soil shear wave velocity, soil longitudinal wave velocity and soil shear wave modulus.

2) ξ_g' and ω_{SSI}: soil material damping and effective frequency soil-structure interacting system.

3) r, A, I_r and I_t: equivalent radius of the foundation, area of the foundation ($A = \pi r^2$), mass moment of inertia for rocking motion ($I_r = \pi r^4/4$) and mass moment of inertia for torsional motion ($I_t = \pi r^4/2$).

For the purpose of this research, only translational and rocking motions of foundation are considered. It is because the vertical response of the foundation is independent from its horizontal response and rocking for the equivalent linear soil-foundation interface models, and also because no vertical ground motion is considered as an input in this study.

Therefore, a condensed version of the cone model was included in the considered soil-structure model. This interface model is shown in Figure 5-8.

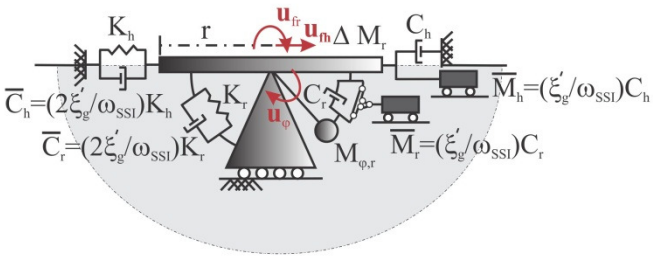

Figure 5-8. Soil-foundation interface model using cone model.

5.4 Incorporating Soil Nonlinearity into the Cone Model

The nonlinearity in stress-strain behaviour of soil can be expressed by two parameters:

1) Degrading shear modulus G with an increase in the shear strain amplitude.
2) Increase in the damping ratio ξ_g with an increases in the shear strain amplitude.

Soil nonlinearity in the analysis can be taken into account in several ways [13]. First, the stress-strain behaviour of soil can be modelled using detailed elastoplasticity models. This approach requires many input parameters, which have to be determined by elaborate laboratory testing. Even though this approach is comprehensive, it is very time consuming and is not practical for simplified analysis. The second method, which is much simpler and more practical, is the equivalent linear method [14]. Although there are many limitations for the application of this method, it has been widely used because

of its simplicity and because it provides a reasonable representation of soil behaviour for small to moderately large shear strains [15].

The equivalent linear method is based on approximating the nonlinear stress-strain behaviour of soil by a secant stiffness G_{sec} and an equivalent damping ξ_{eq} (i.e. the damping that is related to the area of hysteresis) that are compatible with the strain in the soil induced by the ground shaking. This approach is schematically illustrated in Figure 5-9.

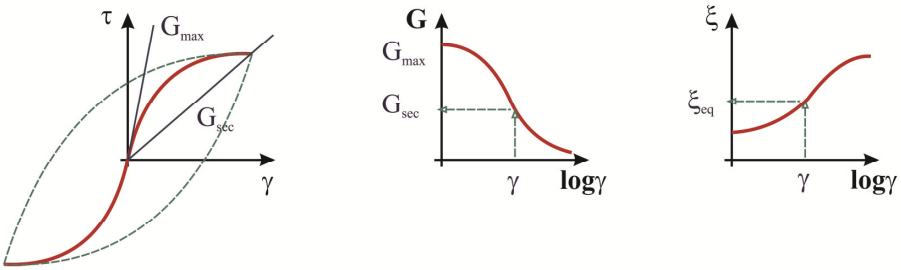

Figure 5-9. Equivalent linear idealization of nonlinear soil behaviour: (a) shear stress-strain behaviour; (b) secant modulus vs. shear strain; and (c) equivalent damping vs. shear strain.

As shown in this figure, to use the equivalent linear method, three types of data are required along with the shear strain amplitude:

1) Shear modulus at small strain G_{max}
2) Shear modulus reduction curves
3) Damping ratio variation curves

Having these data defined for the soil under investigation, the nonlinear stress-strain curve and corresponding hysteretic damping are represented by G_{sec} and ξ_{eq} at a given shear strain level, γ. There have been many curves introduced in literature presenting the shear modulus reduction and damping ratio variation. One example from the many can be found in Vucetic and Dobry [16].

By introducing G_{sec}, or respective shear wave velocity, $V_{sec} = (G_{sec}/\rho)^{1/2}$ and corresponding ξ_{eq} in the cone model defined in Table 5-3, stiffness degradation and

additional damping due to soil nonlinearity can be simply covered. In this context, it is important to note that although the real soil behaviour under cyclic loading is much more complicated than what is expressed by G_{sec} and ξ_{eq}, the dynamic response of the ground can be captured appropriately by these parameters [13].

However, there are some shortcomings when equivalent linear method is used to represent soil nonlinearity. These are: (i) inability to consider irrecoverable deformation; (ii) the assumption that soil stiffness and damping are constant through the time-history of shaking.

5.5 Defining the Dynamic Equations of Motion

The equations of motion of the soil-structure model for horizontal and rocking motions capture the key aspects of the dynamic interaction between the structure and the soil. Consider the adopted model is forced by uniform ground acceleration $\ddot{u}_g(t)$ in the horizontal direction that is resulting from vertically propagating body waves. Since the model only represents a shallow foundation, the kinematic interaction is zero and only inertial interaction needs to be considered [2, 17]. The input ground acceleration, consequently, causes foundation forces to develop at the interface between the basement of the structure and the soil half-space, forcing the basement to translate and rock.

To define the dynamic equations of motion, the substructure method explained in Chapter 2 has to be followed. Specifically, the global system is divided into two substructures including: (i) the structure as substructure No.1; and (ii) the soil-foundation as substructure No. 2. Note that the total horizontal foundation displacement $u_{fh,tot}(t)$ equals the free-field ground displacement $u_g(t)$ plus the added displacement caused by inertial soil-structure interaction $u_{fh}(t)$. Thus, $u_{fh,tot}(t)$ is defined:

$$u_{fh,tot}(t) = u_g(t) + u_{fh}(t) \tag{5.52}$$

On the other hand, foundation rocking $u_{fr}(t)$ is only caused by inertial soil-structure interaction since no free-filed motion is being considered in rocking direction.

Considering the foundation motions, the total displacement of the structure $u_{tot}(t)$ is then expressed:

$$u_{tot}(t) = u_g(t) + u_{fh}(t) + h_e u_{fr}(t) + u_s(t) \tag{5.53}$$

where $u_s(t)$ is the horizontal translation of the structure relative to the foundation, and h_e is the structural effective height.

Since the soil-structure model considered has three global degrees of freedom and one internal degree of freedom, four equations of motion are needed to completely define dynamic equilibrium. First, the mass of the structure m_s is isolated to obtain the equation of motion for substructure No.1:

$$m_s\left[\ddot{u}_g(t) + \ddot{u}_{fh}(t) + h_e\ddot{u}_{fr}(t) + \ddot{u}_s(t)\right] + c_s\dot{u}_s(t) + k_s u_s(t) = 0 \tag{5.54}$$

Equation (5.54) can be reformatted:

$$m_s\ddot{u}_s(t) + m_s\ddot{u}_{fh}(t) + (h_e m_s)\ddot{u}_{fr}(t) + c_s\dot{u}_s(t) + k_s u_s(t) = -m_s\ddot{u}_g(t) \tag{5.55}$$

Next, the entire substructure No.1 is isolated from the elastic half-space to get the substructure horizontal force equilibrium:

$$m_s\left[\ddot{u}_g(t) + \ddot{u}_{fh}(t) + h_e\ddot{u}_{fr}(t) + \ddot{u}_s(t)\right] + \left(\frac{\xi_g'}{\omega_{SSI}}C_h\right)\left[\dot{u}_g(t) + \dot{u}_{fh}(t)\right] + \left(C_h + \frac{2\xi_g'}{\omega_{SSI}}K_h\right)\dot{u}_{fh}(t) + K_h u_{fh}(t) = 0 \tag{5.56}$$

Rearranging this equation yields:

$$m_s\ddot{u}_s(t) + (m_s + \frac{\xi_g'}{\omega_{SSI}}C_h)\ddot{u}_{fh}(t) + (h_e m_s)\ddot{u}_{fr}(t) +$$
$$+\left(C_h + \frac{2\xi_g'}{\omega_{SSI}}K_h\right)\dot{u}_{fh}(t) + K_h u_{fh}(t) = -(m_s + \frac{\xi_g'}{\omega_{SSI}}C_{fh})\ddot{u}_g(t) \quad (5.57)$$

Then, if the moments about the centroidal axis of the basement are summed for substructure No.1, the third equation of motion is derived:

$$(h_e m_s)\left[\ddot{u}_g(t) + \ddot{u}_{fh}(t) + h_e\ddot{u}_{fr}(t) + \ddot{u}_s(t)\right] + \Delta M_r\ddot{u}_{fr}(t) +$$
$$K_r u_{f\theta}(t) + \left(\frac{2\xi_g'}{\omega_{SSI}}K_r\right)\dot{u}_{fr}(t) - C_r\left[\dot{u}_\varphi(t) - \dot{u}_{fr}(t)\right] -$$
$$-\left(\frac{\xi_g'}{\omega_{SSI}}C_r\right)\left[\ddot{u}_\varphi(t) - \ddot{u}_{f\theta}(t)\right] = 0 \quad (5.58)$$

Equation (5.55) can be also expressed:

$$(h_e m_s)\ddot{u}_s(t) + (h_e m_s)\ddot{u}_{fh}(t) + \left(h_e^2 m_s + \Delta M_r + \frac{\xi_g'}{\omega_{SSI}}C_r\right)\ddot{u}_{fr}(t) -$$
$$-\left(\frac{\xi_g'}{\omega_{SSI}}C_r\right)\ddot{u}_\varphi(t) + \left(C_r + \frac{2\xi_g'}{\omega_{SSI}}K_r\right)\dot{u}_{fr}(t) - C_r\dot{u}_\varphi(t) + K_r u_{fr}(t) =$$
$$-(h_e m_s)\ddot{u}_g(t) \quad (5.59)$$

Finally, if the internal soil-foundation mass (monkey-tail mass) is isolated, the resulting equation of motion is defined:

$$M_\varphi\ddot{u}_\varphi(t) + C_r\left[\dot{u}_\varphi(t) - \dot{u}_{fr}(t)\right] + \left(\frac{\xi_g'}{\omega_{SSI}}c_{fr}\right)\left[\ddot{u}_\varphi(t) - \ddot{u}_{fr}(t)\right] = 0 \quad (5.60)$$

And in the rearranged form, it is written:

$$-\left(\frac{\xi_g'}{\omega_{SSI}}c_{fr}\right)\ddot{u}_{fr}(t) + \left[M_\varphi + \frac{\xi_g'}{\omega_{SSI}}C_r\right]\ddot{u}_\varphi(t) - C_r\dot{u}_{fr}(t) + C_r\dot{u}_\varphi(t) = 0 \quad (5.61)$$

Equations (5.54)-(5.61) can be combined and written in a matrix form:

$$[M^*]\{\ddot{u}(t)\} + [C^*]\{\dot{u}(t)\} + [K^*]\{u(t)\} = \{F^*\} \tag{5.62}$$

where $[M^*], [C^*]$ and $[K^*]$ are the mass, damping and stiffness matrices, respectively, and $\{F^*\}$ is a force vector. They are defined:

$$[M^*] = \begin{bmatrix} m_s & m_s & h_e m_s & 0 \\ m_s & \left(m_s + \frac{\xi_g'}{\omega_{SSI}} C_r\right) & h_e m_s & 0 \\ h_e m_s & h_e m_s & \left(h_e^2 m_s + \Delta M_r + \frac{\xi_g'}{\omega_{SSI}} C_r\right) & -\frac{\xi_g'}{\omega_{SSI}} C_r \\ 0 & 0 & -\frac{\xi_g'}{\omega_{SSI}} C_r & \left(M_\varphi + \frac{\xi_g'}{\omega_{SSI}} C_r\right) \end{bmatrix} \tag{5.63a}$$

$$[C^*] = \begin{bmatrix} c_s & 0 & 0 & 0 \\ 0 & \left(C_h + \frac{2\xi_g'}{\omega_{SSI}} K_h\right) & 0 & 0 \\ 0 & 0 & \left(C_r + \frac{2\xi_g'}{\omega_{SSI}} K_r\right) & -C_r \\ 0 & 0 & -C_r & C_r \end{bmatrix} \tag{5.63b}$$

$$[K^*] = \begin{bmatrix} k_s & 0 & 0 & 0 \\ 0 & K_h & 0 & 0 \\ 0 & 0 & K_r & 0 \\ 0 & 0 & 0 & 0 \end{bmatrix} \tag{5.63c}$$

$$\{F^*\} = -\begin{Bmatrix} m_s \\ m_s + \frac{\xi_g'}{\omega_{SSI}} C_h \\ h_e m_s \\ 0 \end{Bmatrix} \ddot{u}_g(t) \tag{5.63d}$$

$$\{u(t)\} = \begin{Bmatrix} u_s \\ u_{fh} \\ u_{fr} \\ u_\varphi \end{Bmatrix} \tag{5.63e}$$

5.6 Forming the Numerical Soil-Structure Model in Ruaumoko 2D

To perform the intended simulations of this study, the considered soil-structure interacting model was implemented in the finite-element program "Ruaumoko 2D" [18] which is designed to carry out nonlinear dynamic time-history analysis of structures subjected to earthquake and other dynamic excitations. In these simulations, the Newmark constant average acceleration method was used to solve the dynamic equations of motion. The masses of the model were specified by either nodal masses or rotational inertia. These individual masses were then combined together to form the mass matrix in the lumped mass matrix format. No specific damping model taking into account the contribution of the mass and stiffness matrices for the structure was used. Instead, the damping in the system was captured by dashpots having appropriate coefficients. This approach is reasonable, since current damping models are not able to properly address the soil-foundation damping, as well as its combination with the structural damping. Finally, the enforced earthquake motion was assumed to act only in the horizontal direction.

In the full model generated (Figure 5-1), five nodes were defined: three nodes for the soil-foundation element and two nodes for the structural part of the model. These nodes were then connected with seven elements comprising:

1) A spring representing the stiffness of the structure
2) A dashpot representing the damping of the structure
3) A combined spring representing the stiffness of the soil-foundation interface
4) A combined dashpot representing the damping of the soil-foundation interface
5) A dashpot representing the damping for the soil-foundation interface
6) A dummy spring used for stability purpose
7) An inertia mass used to represent soil material damping

5.7 Initial Validation of Numerical Model

To provide a basic first order validation of the Ruaumoko 2D results, one sample scenario was considered. Its results were compared with the same model codified in MATLAB [19]. Note that this validation was performed only for models with structural linear behaviour. However, it is evident that if the considered model works for a linear case, it will work for the nonlinear one in which only structural stiffness changes after the yielding point. The codified model in MATLAB was based on solving the dynamic equations of motion of the considered soil-structure system (Equation 5.63). The sample scenario has the specifications shown in Table 5-4.

Table 5-4. Specifications of the sample soil-structure model.

Parameter	**Value**
Soil Parameters	
V_s: Soil shear wave velocity (degraded)	105 m/s
ρ: Soil mass density	1.8 t/m^3
υ: Poisson's ratio	0.44
ξ_g': Soil material damping ratio	21 %
Structural Parameters	
r: Foundation radius	4.2 m
h_e: Structural effective height	11 m
m_s: Structural mass	180 t
k_s: Structural initial stiffness	7095 kN/m
ξ_s: Structural damping ratio	5 %

The comparison between the results from Ruaumoko 2D and MATLAB are presented in Figure 5-10. In this comparison, two measures of foundation response and four measures of structural response have been considered, including: (i) horizontal foundation displacement u_{fh}; (ii) foundation rocking u_{fr}; (iii) structural distortion u_s; (iv) structural drift dr; (v) total displacement u_{tot}; and (vi) structural acceleration a_s.
In this context, structural distortion is the horizontal displacement of the structure relative to the foundation that measures the deformation transmitted to the structural part of the model. Structural drift is the summation of foundation rocking and structural

distortion normalized by the effective height, $dr = u_{fr} + u_s/h_e$, that causes second-order ($P-\Delta$) effects. Total displacement is the displacement measured at the roof level including foundation caused lateral structural displacement and structural distortion, $u_{tot} = u_{fh} + h_e u_{fr} + u_s$, that causes the pounding between adjacent structures. Finally, structural acceleration is the total acceleration of the structural mass, $a_s = \ddot{u}_{fh} + h_e \ddot{u}_{fr} + \ddot{u}_s$, which is related to the base shear force.

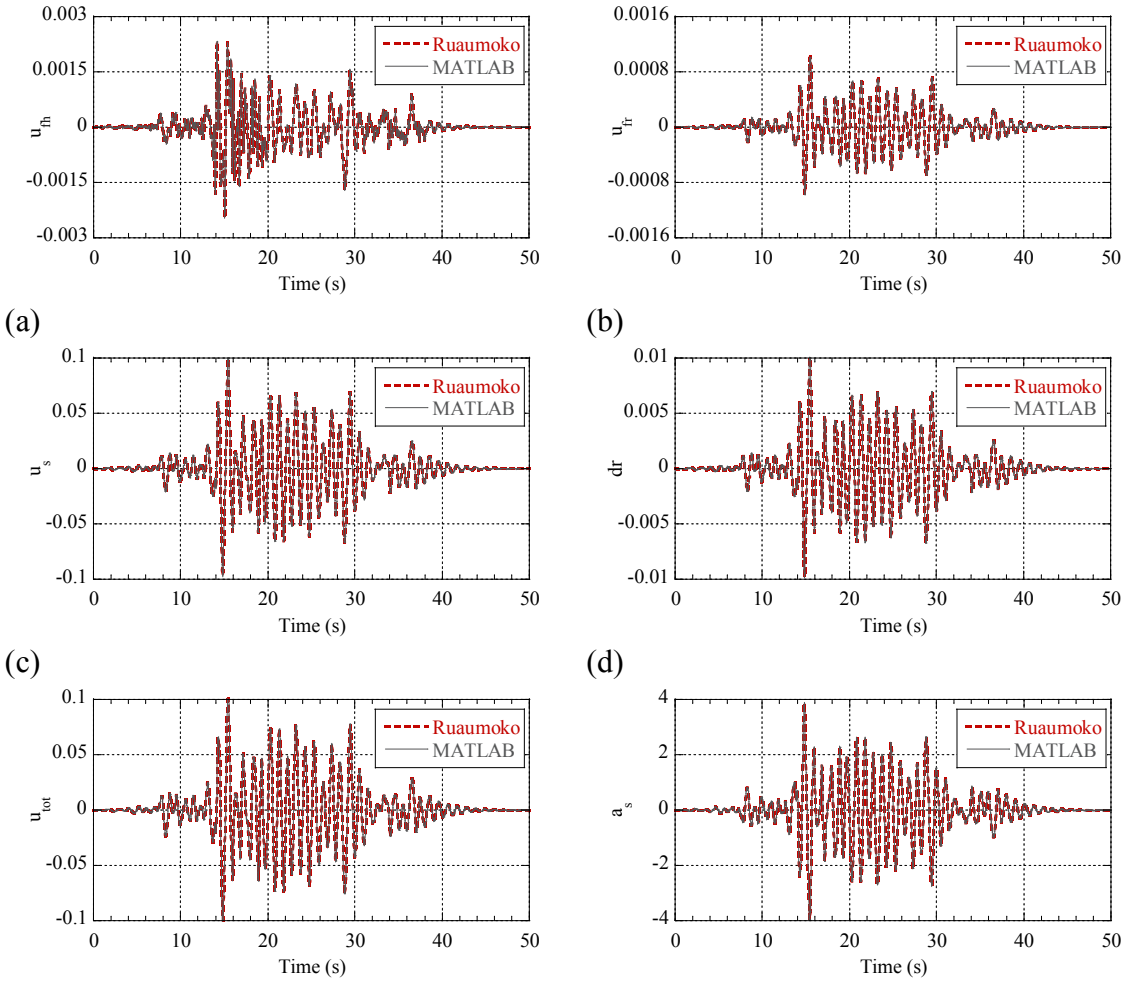

Figure 5-10. Comparison between the results from Ruaumoko 2D and MATLAB models: (a) foundation horizontal displacement; (b) foundation rocking; (c) structural distortion; (d) structural drift; (e) total displacement; (f) structural acceleration.

Figure 5-10 clearly indicates a very good agreement between the Ruaumoko 2D model and MATLAB model. Average errors were less than 2% over all six response parameters considered. Thus, it is concluded that the generated model in Ruaumoko 2D works as expected.

5.8 Summary

Details of the soil-structure model used for the purpose of analyses in Chapters 7, 8 and 9 were explained in this chapter. In the adopted model, soil-foundation interface is represented by a physical cone model. The concept and fundamental formulations of this model were then described in detail. Finally, based on an example presented, the soil-structure model built in finite-element program Ruaumoko 2D was validated using the same model codified in MATLAB. The satisfactory agreement observed between the results from Ruaumoko 2D model and those from MATLAB model suggests that the adopted model can be reliably used in future analysis.

References

[1] J. Bielak, "Dynamic response of non-linear building-foundation systems," *Earthquake Engineering & Structural Dynamics,* vol. 6, pp. 17-30, 1978.

[2] J. P. Wolf, *Foundation Vibration Analysis Using Simple Physical Models*. Englewood Cliffs, N.J.: Prentice-Hall, 1994.

[3] C. Zhang and J. P. Wolf, Eds., *Dynamic Soil-Structure Interaction*. Amesterdam, The Netherlands: Elsevier Science B.V., 1998, p.^pp. Pages.

[4] G. Ehlers, "The effect of soil flexibility on vibrating systems," *Beton Eisen,* vol. 41, pp. 197-203, 1942.

[5] J. W. Meek and A. S. Veletsos, "Simple models for foundation in lateral and rocking motions," presented at the Proceeding of Fifth World Congress on Earthquake Engineering, Rome, 1974.

[6] J. P. Wolf, *Dynamic Soil-Structure Interaction*. Englewood Cliffs, N.J.: Prentice Hall, 1985.

[7] J. P. Wolf, *Soil-Structure-Interaction Analysis in Time Domain*. Englewood Cliffs, N.J.: Prentice-Hall, 1988.

[8] G. Gazetas, "Formulas and charts for impedances of surface and embedded foundations," *Journal of geotechnical engineering,* vol. 117, pp. 1363-1381, 1991.

[9] A. Pais and E. Kausel, "Approximate formulas for dynamic stiffnesses of rigid foundations," *International Journal of Soil Dynamics and Earthquake Engineering,* vol. 7, pp. 213-227, 1988.

[10] M. A. Meyers and K. K. Chawala, *Mechanical Behaviour of Materials*. Englewood Cliffs, N.J.: Prentice Hall, Inc, 1999.

[11] M. Nakhaei and M. A. Ghannad, "The effect of soil-structure interaction on damage index of buildings," *Engineering Structures,* vol. 30, pp. 1491-1499, 2008.

[12] J. P. Stewart*, et al.*, "Seismic soil-structure interaction in buildings. I: analytical methods," *Journal of Geotechnical and Geoenvironmental Engineering,* vol. 125, pp. 26-37, Jan 1999.

[13] I. Towhata, *Geotechnical Earthquake Engineering*: Springer, 2008.

[14] H. B. Seed and I. M. Idriss, "Soil moduli and damping factors for dynamic response analysis," Earthquake Engineering Research Centre Report EERC 7010, 1970.

[15] G. A. Ordonez, "SHAKE2000, A Computer Program for the 1-D Analysis of Geotechnical Earthquake Engineering Problems," ed. Berkeley: University of California, 2011.

[16] M. Vucetic and R. Dobry, "Effect of soil plasticity on cyclic response," *Journal of Geotechnical Engineeing-ASCE,* vol. 117, pp. 89-107, 1991.

[17] S. L. Kramer, *Geotechnical Earthquake Engineering*. Upper Saddle River, N.J.: Prentice Hall, 1996.

[18] A. Carr, "Ruaumoko 2D, Nonlinear FEM Computer Program," ed. New Zealand: University of Canterbury, 2009.

[19] MathWorks, "MATLAB - The Language Of Technical Computing," ed, 2008.

CHAPTER 6. Developed Probabilistic Methodology for Seismic Soil-Structure Interaction Analysis

Abstract. This chapter introduces the probabilistic methodology used to investigate the effects of soil-structure interaction on the structural response. More specifically, the systematic approach adopted to cover the uncertainty and variability in the soil and structural parameters, as well as in the input ground motions is presented. Specifically, it explains the Monte Carlo method and approach used to vary soil and structural parameters within realistic ranges to generate a large number of analytical models. The suites of input ground motions used for the time-history simulations are also presented and their selection criteria are discussed.

6.1 Motivation and Framework

In this research, the primary interest is to provide the "best estimate" of the effects of soil-structure interaction on the structural response using spectral approach. In this case, the existing uncertainties in model parameters and ground motion characteristics that could result in a wide range of responses were taken into account and a large number of linear and nonlinear dynamic analyses were performed. Using a range of summary statistics of the results, the "best estimate" of the soil-structure interaction effects is presented by the median values and dispersion of results. Dispersion is presented by both the interquartile range (IQR) and by the coefficient of variation (i.e. standard

deviation divided by the mean). Note that a good estimate of dispersion is needed in many practical cases, for example, when the 84^{th} percentile demand is required for a design procedure or when a probabilistic or performance-based design methods need to be developed from the results specifying explicit levels of confidence or exceedance.

The approach adopted was to systematically compute the seismic response for a wide range of realistic soil-structure models when subjected to various input ground motions spanning a wide range of realistic scenarios. A robust Monte-Carlo simulation was used to generate models through a random selection procedure that is outlined:

1) Seventeen group of models were defined to cover a relevant period range in the design response spectrum. In this regard, predominant periods of $0.2, 0.3, \dots 1.8$ s were adopted for fixed-base superstructures with total height of $3 - 30$ m satisfying the period-height relationship introduced in the New Zealand Standard [1].

2) For each of these seventeen groups with a specific predominant period, one thousand soil-structure models constrained to conform to the specified period and produce realistic models were randomly generated. The relatively large number of one thousand models was chosen to: (i) give the best fit and full representation to the statistical distribution of the randomly selected parameters; and (ii) increase the confidence level of the Monte Carlo simulation to the exact solution.

6.2 Generation of Models with Randomly Selected Parameters

Soil-structure models with randomly selected parameters for each group of models with a specific predominant fixed-base period ($T_{FB} = 0.2, 0.3, \dots 1.8$ s) were generated following two steps. First, one thousand random values were defined for each soil parameter included in the soil-foundation interface element. Second, for each set of predefined soil parameters (1000 in total) the relevant structural parameters were randomly defined. The selection procedure and the limitations for each parameter used

were to ensure only realistic combinations are included as described in detail in the following sections.

6.2.1 Selection of Soil Parameters

As explained in Chapter 5, a discrete-element model composed of springs, dashpots and masses with frequency-independent coefficients was used to represent the soil-foundation interface. All the coefficients of this model are defined by specifying the basic parameters of the specific soil, including: (i) initial soil shear wave velocity $(V_s)_0$; (ii) shear wave velocity degradation ratio $(V_s)_{sec}/(V_s)_0$; (iii) soil mass density ρ; (iv) Poisson's ratio υ; and (v) equivalent soil material damping at the effective period of the interacting system ξ_g'. From these parameters, $(V_s)_0$, $(V_s)_{sec}/(V_s)_0$, ρ and υ were assumed to be independent random variables with a uniform distribution, while ξ_g' was determined by considering a linear correlation between the defined degradation ratio and the expected damping ratio.

The assumption of the independence between the first four soil parameters is supported by the literature in the characterization of geotechnical variability [2-7]. In addition, the selection of a uniform distribution for soil parameters is reasonable given that the geological conditions considered are all equally likely to occur, and no specific geological condition was considered.

In addition, it is important to acknowledge that various soil types were concurrently considered in the analysis, such as sands, gravels, clays and silty soils. For such diversity of soil types there is no significant correlation between the soil parameters such as υ and V_s, υ and ρ, or ρ and V_s (one may find correlation between ρ and V_s for a given soil type, e.g. sands, but this would not be the case if sands, clays and gravels are concurrently considered) especially if one has in mind that a degraded shear wave velocity (stiffness) was employed in the analyses as explained below.

In the analyses, a degraded shear wave velocity and corresponding damping were employed incorporating the effects on stiffness and damping associated with soil nonlinearity and level of induced shear strains in the soil. Clearly, the degraded shear wave velocity depends on the level of the earthquake excitation and induced strain

response in the soil. In other words, for any given set of reasonable values for υ and ρ, a degraded shear wave velocity could be assumed depending on the adopted initial shear wave velocity and level of degradation. For this reason, no correlation between υ and V_s, or ρ and V_s was employed. The only correlation that matters is that between the shear strain and stiffness degradation, as well as between the shear strain and soil damping, and those were rigorously accounted for.

6.2.1.1 Initial soil shear wave velocity selection

It was assumed that the initial soil shear wave velocity $(V_s)_0$ varies randomly in the range of 80-360 m/s with uniform distribution representing soft to relatively stiff soil (soil type C with $V_s = 180 - 360$ m/s and soil type D with $V_s < 180$ m/s based on USGS geomatrix soil categorization).

6.2.1.2 Shear wave velocity degradation ratio selection

Shear wave velocity degradation ratio $(V_s)_{sec}/(V_s)_0$ was selected from the range of 0.15-0.7. This degradation range results from using a representative shear wave velocity reduction curve for sand [8] and assuming the range of 0.1-1% for induced shear strain in the soil due to the ground motion. The shear strain range was selected as a representative ground response, considering the fact that the ground motions employed have magnitudes between 6.2 and 7.6, and a source-to-site distances of less than 40 km. In this approach, a given degradation of $(V_s)_0$ could be interpreted as being associated with different strain levels or soil types, and thus different amplitudes of the seismic motion.

6.2.1.3 Degraded shear wave velocity selection

After defining the values of shear wave velocity degradation ratio, the degraded shear wave velocity $(V_s)_{sec}$ was calculated by multiplying the initial shear wave velocity and the corresponding degradation ratio. Multiplying the two later uniform distributions will result in a non-uniform distribution for the degraded shear wave velocity.

6.2.1.4 Soil mass density selection

Considering soil type C and D condition, soil mass density varies within the range of 1.6-1.9 (t/m^3) [9, 10]. It was assumed that the density values are uniformly distributed in this range, and thus is equally likely.

6.2.1.5 Soil shear modulus selection

Soil degraded shear modulus G_{sec} was calculated utilising the relationship between the shear modulus, shear wave velocity $(V_s)_{sec}$ and soil mass density ρ, defined:

$$G_{sec} = \rho(V_s)_{sec}^2 \tag{6.1}$$

In this way, for each specific scenario of ρ and $(V_s)_{sec}$, a value of G_{sec} is defined. Note that G_{sec} has a non-uniform distribution as it results from multiplication of a uniform distribution by a non-uniform one.

6.2.1.6 Poisson's ratio selection

Poisson's ratio υ for soil type C and D was selected from the variation range of 0.3-0.45, using a uniform distribution [9, 10].

6.2.1.7 Soil material damping selection

Soil material damping at the effective period of the soil-structure interacting ξ_g' was defined from a representative damping curve for sand corresponding to the shear wave velocity reduction curve used and increased with the shear strain [8]. A linear link was established between the level of degradation in shear wave velocity and hysteretic damping in the soil to yield 10%-25% damping ratios for degradation ratios of 0.7-0.15, respectively. The relationship used for this calculation is defined:

$$\frac{25-\xi_g'}{25-10} = \frac{(V_s)_{sec}/(V_s)_0-0.15}{0.7-0.15} \tag{6.2}$$

In this way, for each specific scenario of $(V_s)_{sec}/(V_s)_0$, a value of ξ_g' is defined.

6.2.1.8 Generated distribution for soil parameters

As an example, the generated distributions of soil parameters considered for the group of models with $T_{FB} = 1.0$ s and 1000 total parameter value sets are shown in Figure 6-1. Clearly, the resulted distributions for $(V_s)_0$, $(V_s)_{sec}/(V_s)_0$, ρ, υ and ξ'_g match the initially assumed uniform distribution.

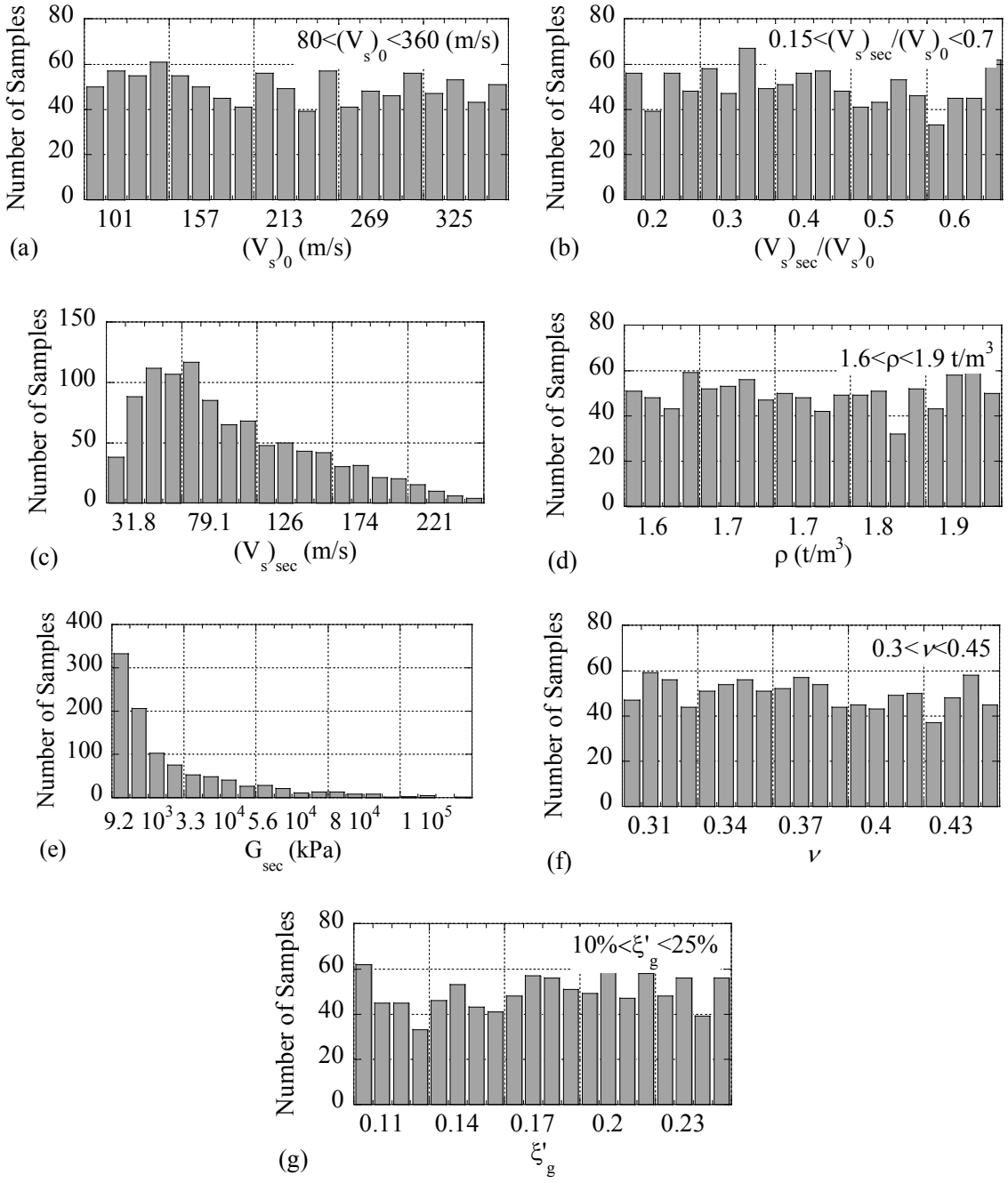

Figure 6-1. Distribution of: (a) initial soil shear wave velocity; (b) shear wave velocity degradation ratio; (c) degraded soil shear wave velocity; (d) soil mass density (e) soil shear modulus; (f) Poisson's ratio and (g) soil material damping for group of models with T_{FB}=1.0 s and 1000 total parameter value sets.

6.2.2 Selection of Structural Parameters

To define random variables for the structural part of the model, structural effective height h_e, foundation radius r, and structural mass m_s were chosen as the primary random variables. Structural stiffness k_s and damping c_s were then calculated using the selected values of these random variables and a relevant deterministic formula. To ensure realistic soil-structure models, the selection of the structural parameters was constrained by commonly accepted relationships for either the structure or for the global soil-structure model.

6.2.2.1 Structural effective height (height of inertial load) selection

It is common in seismic design codes to define the predominant period of structures using empirical formulas, such as period-height relationships that are functions of structural total height and dependent on the lateral load resisting system. This type of relationship can be rearranged and used to define the structural effective height, which is the centre of inertial load given the predominant structural period. Considering the New Zealand Standard [1] and different lateral load resisting systems, the period-height relationship is defined:

$$0.063{h_n}^{0.75} \leq T_{FB} \leq 0.14{h_n}^{0.75} \tag{6.3}$$

where h_n is the total height of the structure and T_{FB} is the predominant period of a fixed-base system. Rearranging Equation (6.3) and assuming that the centre of inertial load is located at $2/3$ of the structural total height, the structural effective height h_e is defined:

$$10{T_{FB}}^{0.75} \leq h_e \leq 27{T_{FB}}^{0.75} \tag{6.4}$$

In this study, only structures having the total height of $3-30$ m, and thus an effective height of $2-20$ m, have been considered. Therefore, Equation (6.4) is modified:

$$Max(2, 10{T_{FB}}^{0.75}) \leq h_e \leq Min(20, 27{T_{FB}}^{0.75}) \tag{6.5}$$

The range of h_e values depending on different predominant periods of the structure is defined in Table 6-1 and is also shown in Figure 6-2. Note that while they are selected randomly, h_e and T_{FB} are linked by an established deterministic formula. Considering the period and height limitations in Table 6-1, h_e was defined using a uniform distribution for each group of models with a specific predominant period.

Table 6-1. The ranges of variation for h_e.

T_{FB} (s)	h_e (m)
0.2 ... 0.32	$2 \dots 26.8T_{FB}^{1.33}$
0.32 ... 0.8	$9.1T_{FB}^{1.33} \dots 26.8T_{FB}^{1.33}$
0.8 ... 1.8	$9.1T_{FB}^{1.33} \dots 20$

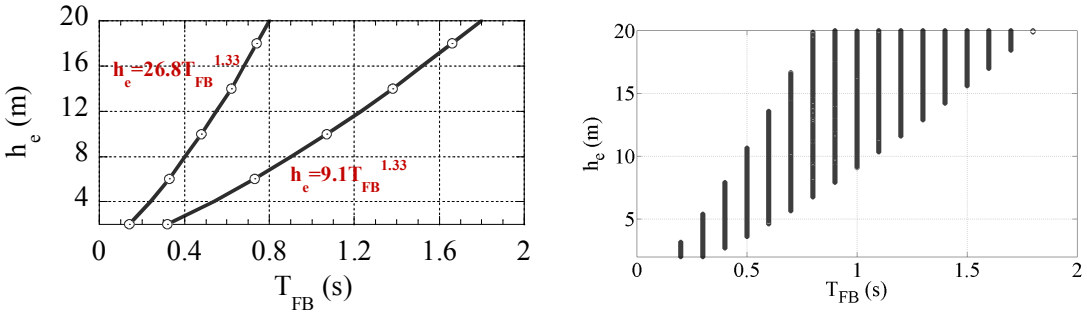

(a) (b)

Figure 6-2. The ranges of variation for h_e: (a) considered limitations; (b) generated models.

6.2.2.2 Foundation radius

Foundation radius r was uniformly selected from the ranges defined in Table 6-2 and shown in Figure 6-3. These limits were chosen assuming that the building aspect ratio h_e/r varies between 1 and 4, and r is limited to the range of $2-12$ m, covering structures having $1-3$ bays with a length of $4-8$ m each. Following this procedure ensures that r and h_e are inter-correlated by a deterministic limitation.

Table 6-2. Variation ranges for r.

h_e (m)	r (m)
2 ... 8	2 ... h_e
8 ... 12	$(h_e/4)$ ... h_e
12 ... 20	$(h_e/4)$ ... 12

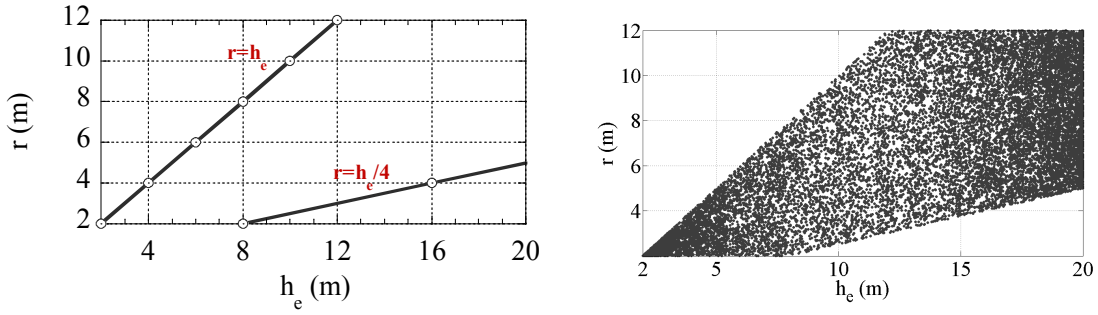

(a) (b)

Figure 6-3. Variation ranges for r: (a) considered limitations; (b) generated models.

6.2.2.3 Structural mass selection

Structure–to-soil mass ratio $\bar{m}$ was used to compute the structural mass m_s. This ratio is defined:

$$\bar{m} = \frac{m_s}{\rho r^2 h_e} \tag{6.6}$$

Thus, m_s is linked to the structural effective height, foundation radius, and soil density for a specific model.

A uniform distribution was considered for $\bar{m}$ within the range $0.4 - 0.6$, representing conventional building structures [11], and the predefined values for ρ, r and h_e were implemented in Equation (6.5) to define m_s for each model. It is important to note that the value of m_s defined is intrinsically correlated with ρ, r and h_e. These dependencies are illustrated in Figure 6-4.

6.2.2.4 Structural initial stiffness selection

Following the estimation of m_s, structural initial stiffness $(k_s)_i$ was computed directly using:

$$(k_s)_i = \frac{4\pi^2}{T_{FB}^2} m_s \tag{6.7}$$

The dependency between $(k_s)_i$ and m_s is shown in Figure 6-4.

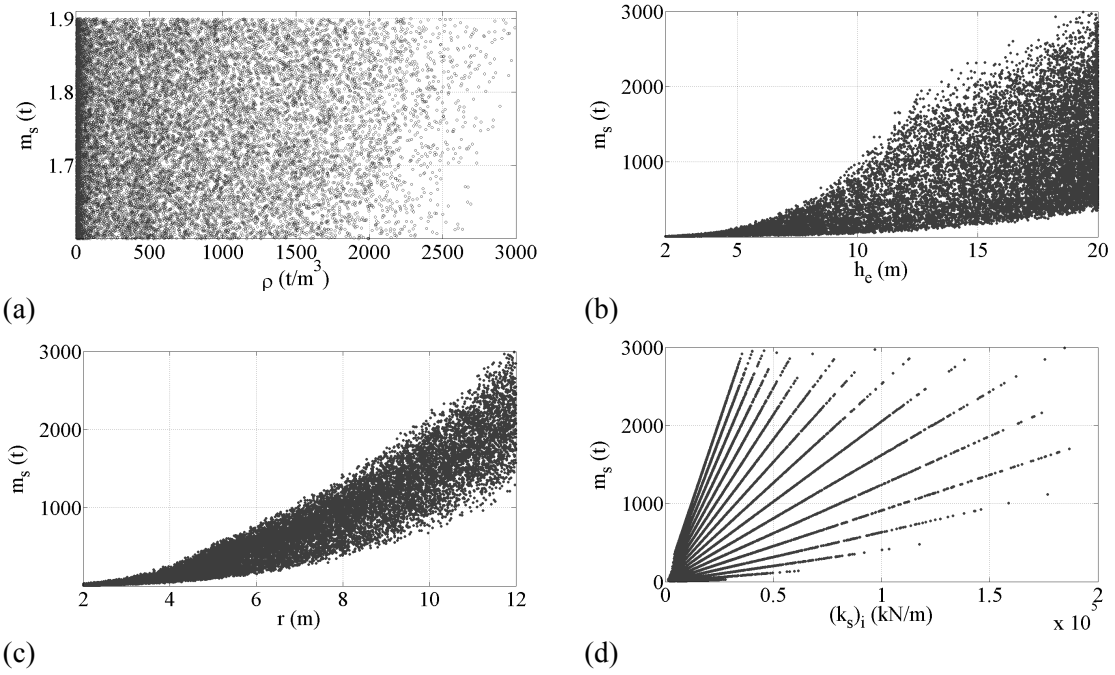

Figure 6-4. Dependency and correlation between m_s and: (a) ρ; (b) r; (c) h_e; and (d) $(k_s)_i$.

6.2.2.5 Structural yield strength selection

To present the hysteretic force-displacement behaviour of the structure, the linear branch of the structural stiffness was considered equal to $(k_s)_i$ and the yield strength f_y was defined given a displacement ductility of 6 at 2% drift. This ductility limit was selected to ensure that the structural part of all generated models responds in the nonlinear range. However, it does not mean all models reach this ductility level.

The procedure defining f_y was based on Newmark's so-called Equal Displacement Rule. This rule states that the maximum inelastic displacement of a structure can be

approximated by the elastic displacement of the same structure under the unreduced earthquake. In this context, the maximum inelastic displacement of the structure δ_d was defined assuming the maximum drift of 2% is achieved:

$$\delta_d = (2\%)h_e \tag{6.8}$$

The yield displacement was then defined using the ductility factor of 6:

$$\delta_y = \frac{\delta_d}{6} = \frac{(2\%)h_e}{6} \tag{6.9}$$

Having δ_y defined, F_y was then computed using:

$$f_y = (k_s)_i \delta_y = (\frac{2\%}{6})(k_s)_i h_e \tag{6.10}$$

The post-yielding stiffness factor α was also considered to be 0.05 or 5% of the linear branch for the TK and EP hysteretic rules, and -0.05 for TKN (ref. Chapter 5). Parameters γ and δ were selected as 0.3 and 0.2 for the TK and TKN models, where α, γ and δ are defined in Figure 5-2.

6.2.2.6 Structural damping selection

To define structural damping c_s, a constant 5% structural damping ratio was employed, and c_s was thus defined based on previously defined variables:

$$c_s = 2(0.05)\sqrt{(k_s)_i m_s} \tag{6.11}$$

6.2.2.7 Generated distribution for structural parameters

As an example, the generated distributions of structural parameters considered for the group of models with $T_{FB} = 0.2, 1.0, 1.8$ s and 1000 total parameter value sets for each group are shown in Figures 6-5, 6-6 and 6-7, respectively.

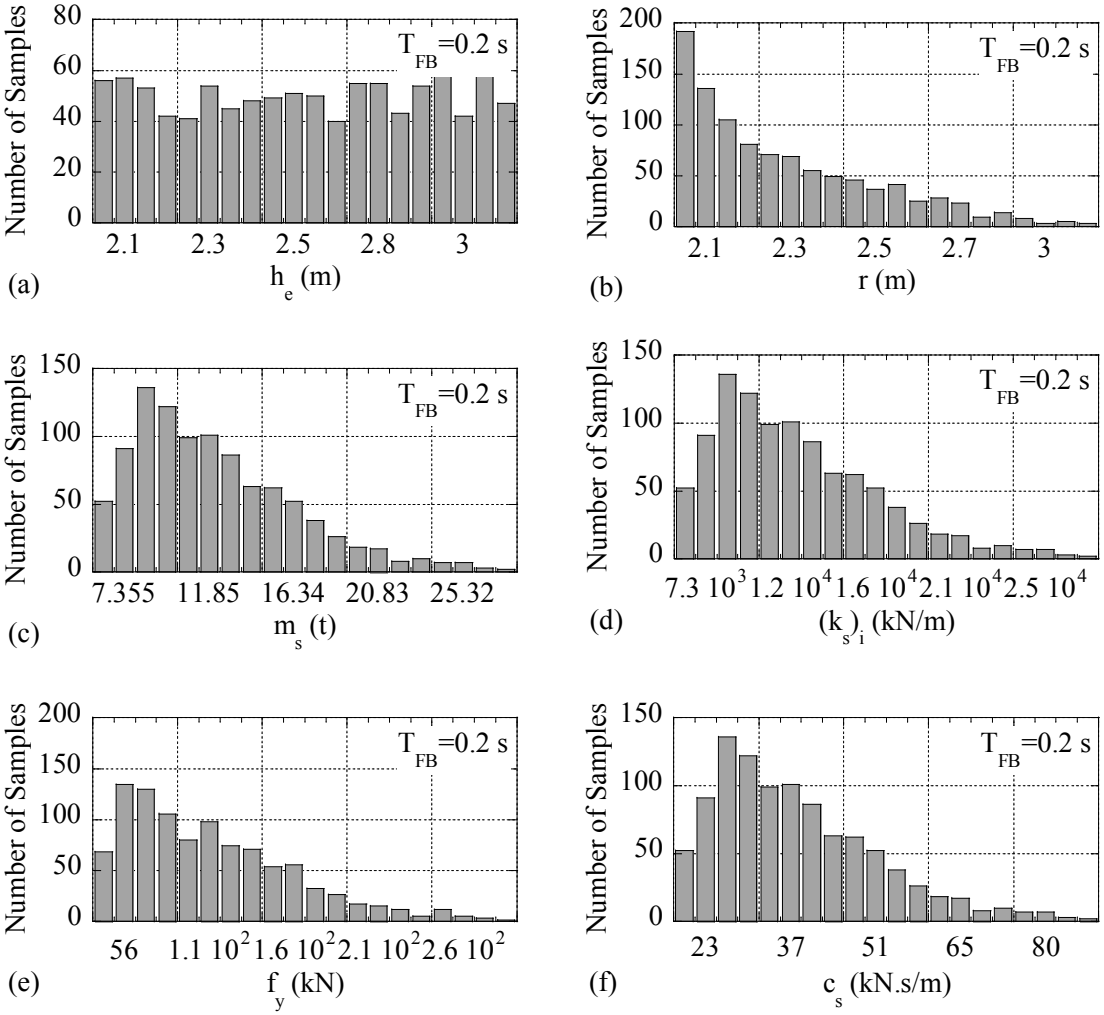

Figure 6-5. Distribution of: (a) structural effective height; (b) foundation radius; (c) structural mass; (d) structural initial stiffness; (e) structural yield strength and (f) structural damping for group of models with T_{FB}=0.2 s and 1000 total parameter value sets.

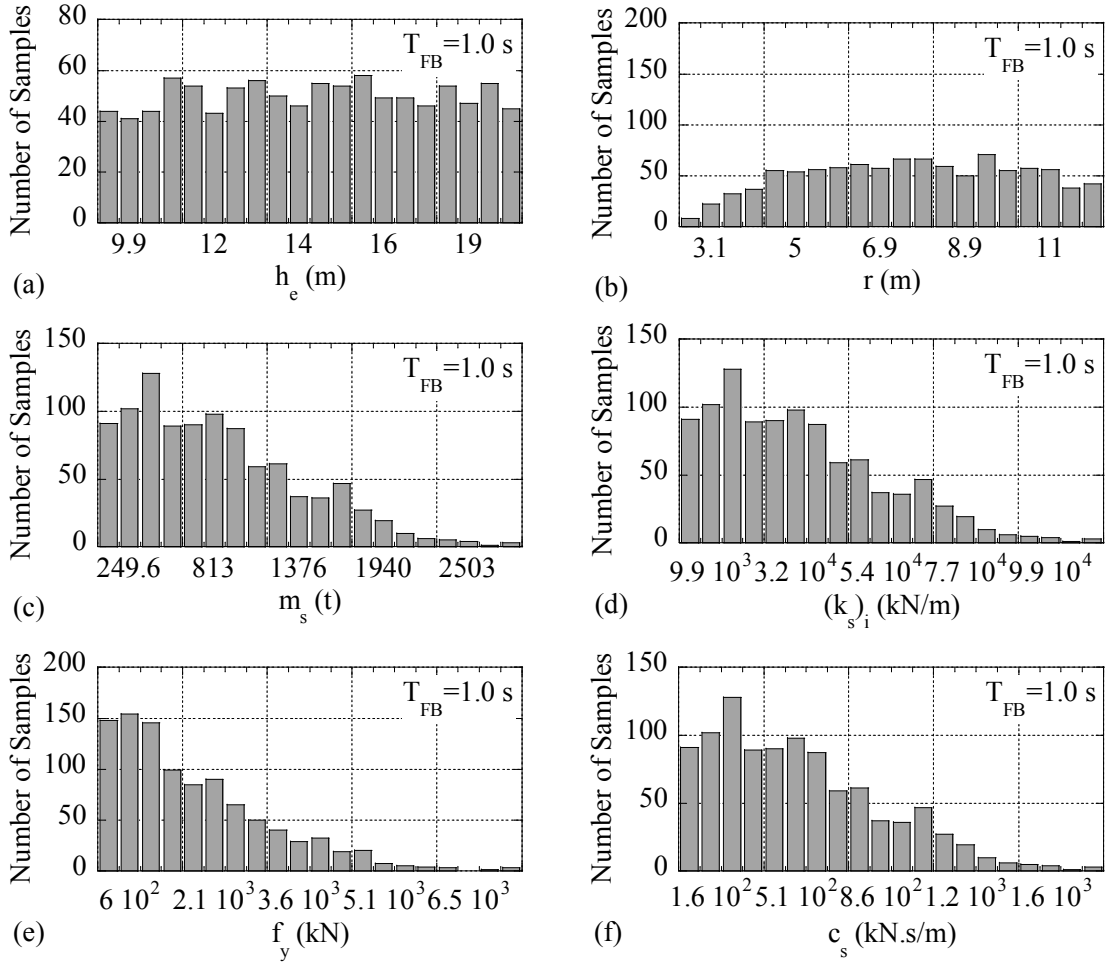

Figure 6-6. Distribution of: (a) structural effective height; (b) foundation radius; (c) structural mass; (d) structural initial stiffness; (e) structural yield strength and (f) structural damping for group of models with T_{FB}=1.0 s and 1000 total parameter value sets.

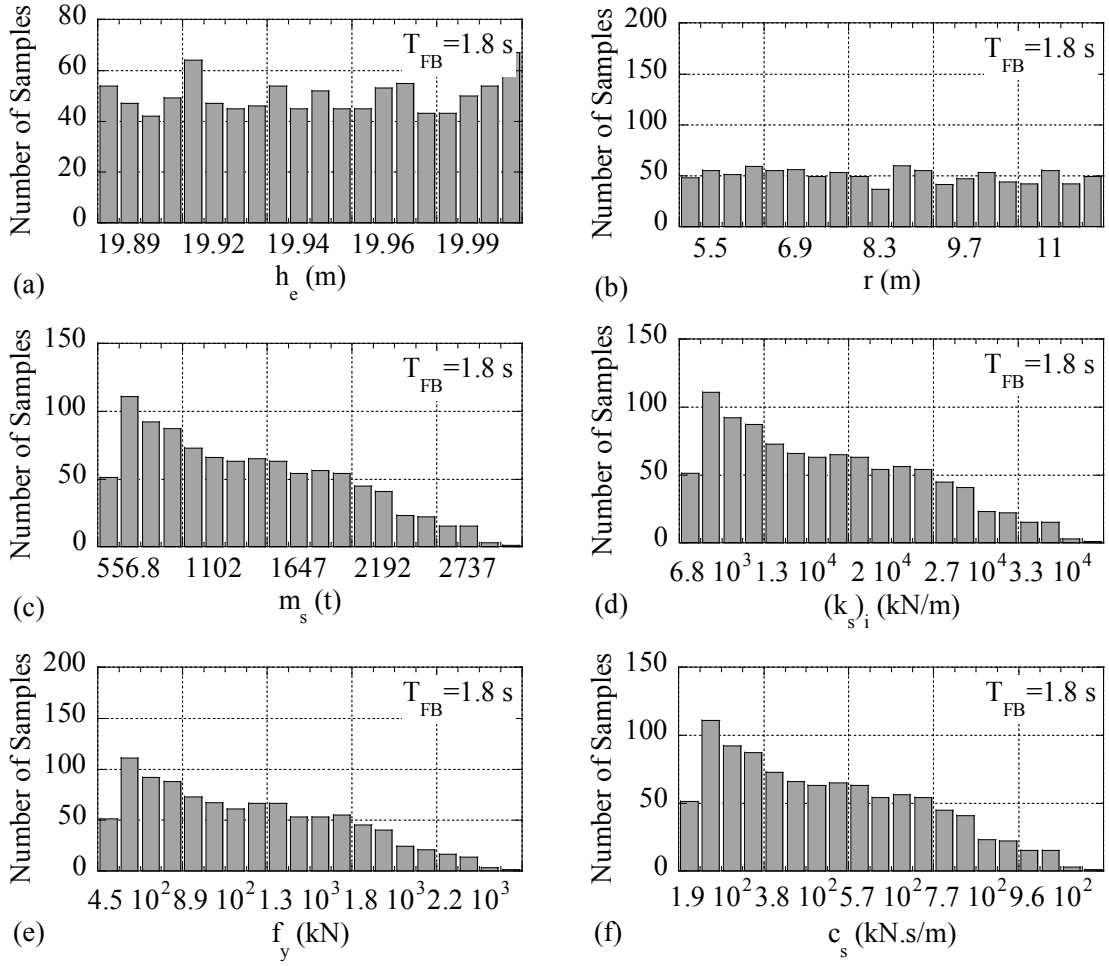

Figure 6-7. Distribution of: (a) structural effective height; (b) foundation radius; (c) structural mass; (d) structural initial stiffness; (e) structural yield strength and (f) structural damping for group of models with T_{FB}=1.8 s and 1000 total parameter value sets.

6.2.2.8 Predominant period of soil-structure system

Given all the parameters of the model, the predominant period of the soil-structure system T_{SSI} is defined:

$$T_{SSI} = T_{FB}\sqrt{1 + \frac{(k_s)_i}{K_h} + \frac{(k_s)_i h_e^2}{K_r}} \tag{6.12}$$

The relation between calculated T_{SSI} and the period of the corresponding fixed-base structure T_{FB} is a representative of the range of uncertainty/variability associated with the model parameters. This relation illustrating how the period shifts due to foundation flexibility is shown in Figure 6-8.

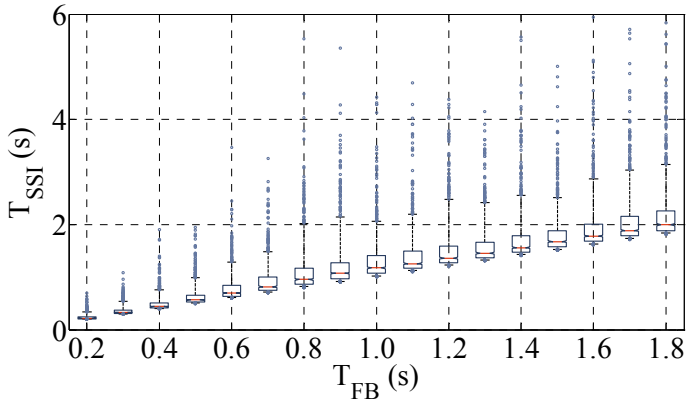

Figure 6-8. Uncertainty associated with model parameters.

6.2.3 Calculation of Soil-Foundation Element Parameters

After defining all soil parameters and foundation radius, they combined to generate the coefficients of the discrete-element representing the soil-foundation interface. The formulas used to calculate these coefficients are summarised in Table 6-3. As an example, the generated distributions of soil-foundation element parameters considered for the group of models with $T_{FB} = 0.2, 1.0$ and 1.8 s are shown in Figures 6-9, 6-10 and 6-11, respectively.

Table 6-3. Coefficients of the main parts of the soil-foundation element [Chapter 5].

Part of Soil-Foundation Element	**Formulation**
Translational stiffness	$K_h = \frac{8Gr}{2-\upsilon}$
Rocking stiffness	$K_r = \frac{8Gr^3}{3(1-\upsilon)}$
Translational damping	$C_h = \rho V_s A$
Rocking damping	$C_r = \begin{cases} \rho V_p I_r & if\ \upsilon \leq 1/3 \\ \rho(2V_s) I_r & if\ 1/3 \leq \upsilon \leq 1/2 \end{cases}$
Additional mass moment of inertia	$\Delta M_r = 1.2(\upsilon - 1/3)\rho I_r r$
Internal mass moment of inertia	$M_{\varphi,r} = \begin{cases} \frac{9\pi}{32}\rho I_r r(1-\upsilon)(\frac{V_p}{V_s})^2 & if\ \upsilon \leq 1/3 \\ \frac{9\pi}{8}\rho I_r r(1-\upsilon) & if\ 1/3 \leq \upsilon \leq 1/2 \end{cases}$

The parameters utilized in this table are defined below:

- ρ, υ, V_s, V_p and G: soil mass density, Poisson's ratio, soil shear wave velocity, soil dilatational wave velocity and soil shear wave modulus.
- ξ_g' and ω_{SSI}: soil material damping and effective frequency soil-structure interacting system.
- r, A and I_r: equivalent radius of the foundation, area of the foundation ($A = \pi r^2$) and mass moment of inertia for rocking motion ($I_r = \pi r^4/4$).

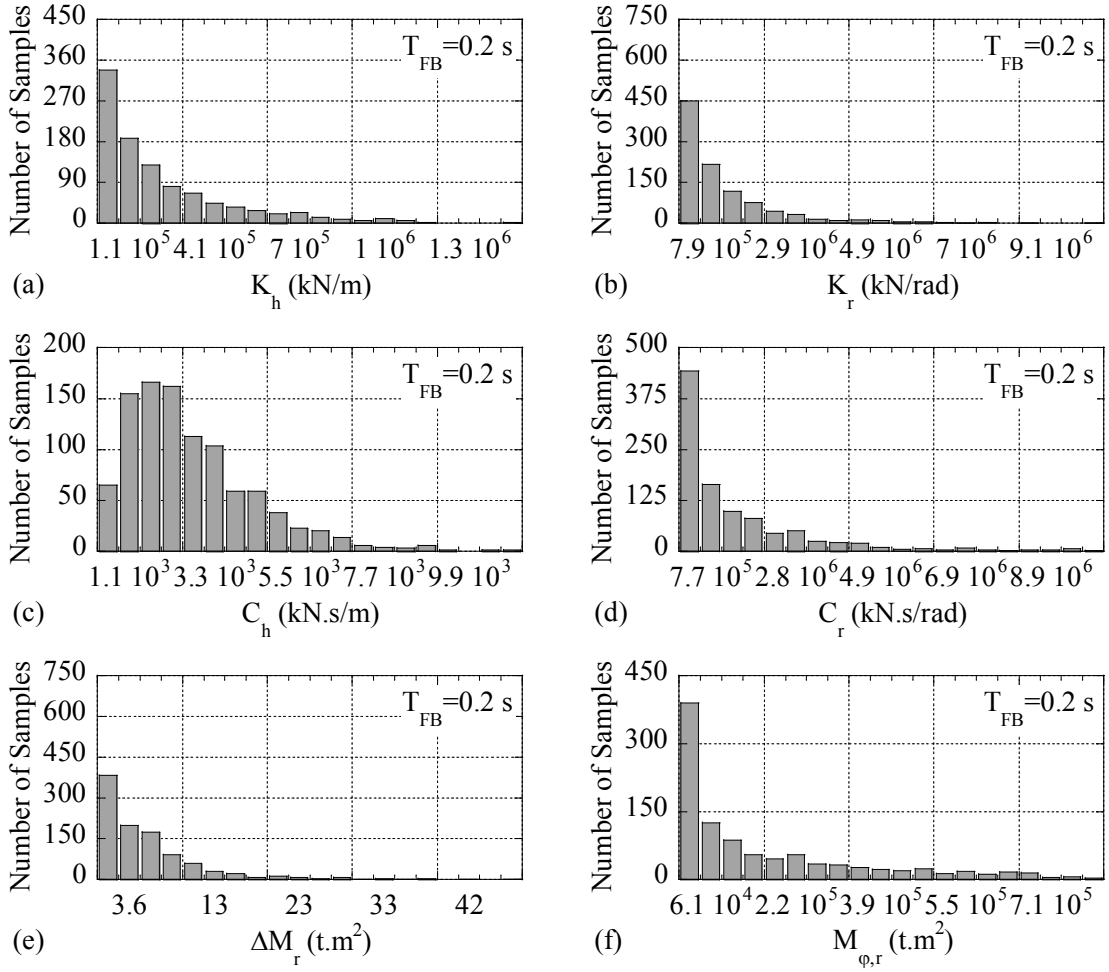

Figure 6-9. Distribution of: (a) soil-foundation translational stiffness; (b) soil-foundation rocking stiffness; (c) soil-foundation translational damping; (d) soil-foundation rocking damping; (e) additional mass moment of inertia and (f) internal mass moment of inertia for group of models with T_{FB}=0.2 s and 1000 total parameter value sets.

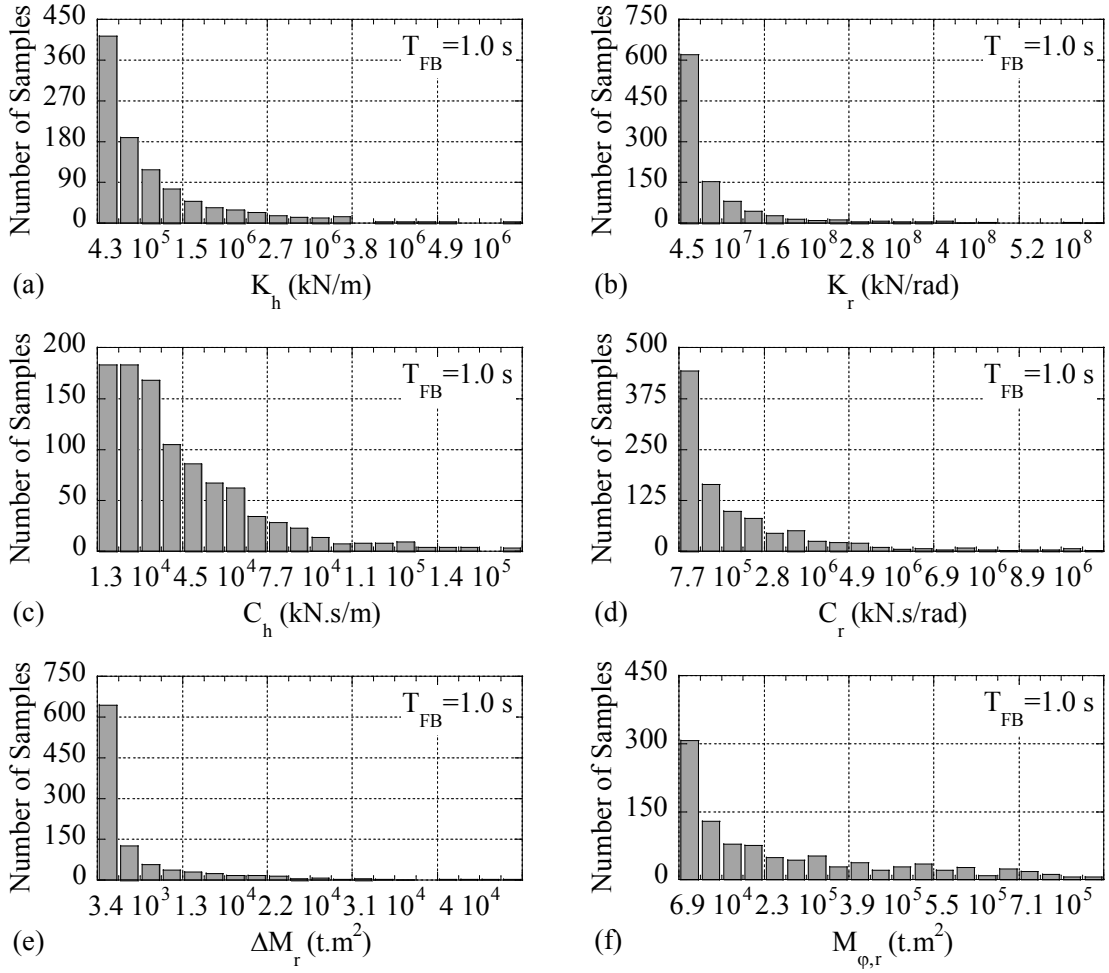

Figure 6-10. Distribution of: (a) soil-foundation translational stiffness; (b) soil-foundation rocking stiffness; (c) soil-foundation translational damping; (d) soil-foundation rocking damping; (e) additional mass moment of inertia and (f) internal mass moment of inertia for group of models with T_{FB}=1.0 s and 1000 total parameter value sets.

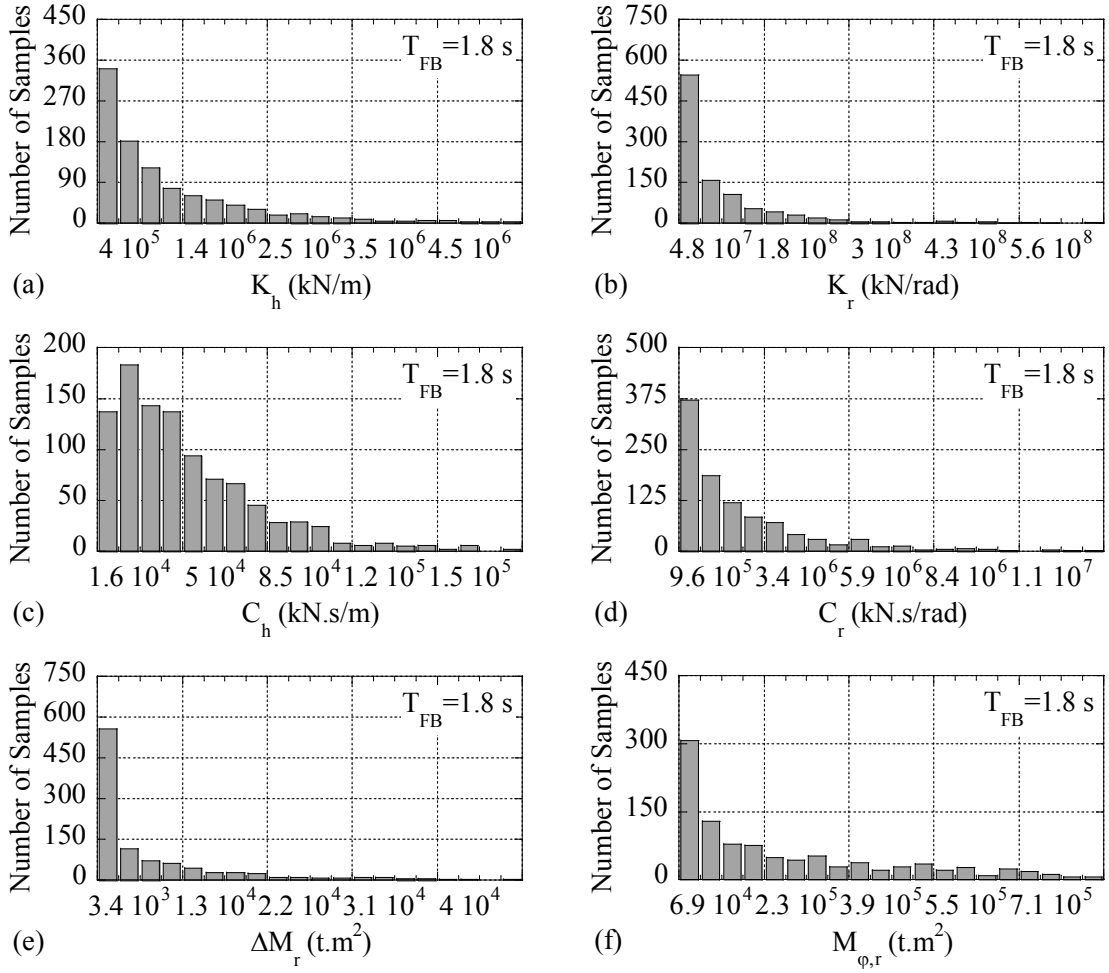

Figure 6-11. Distribution of: (a) soil-foundation translational stiffness; (b) soil-foundation rocking stiffness; (c) soil-foundation translational damping; (d) soil-foundation rocking damping; (e) additional mass moment of inertia and (f) internal mass moment of inertia for group of models with T_{FB}=1.0 s and 1000 total parameter value sets.

To get a better understanding of the distributions generated for the coefficients of the soil-foundation element, the cumulative distribution functions (CDF) of these coefficients are shown in Figure 6-12 for groups of models with $T_{FB} = 0.2, 1.0$ and1.8 s. In addition, the values derived for the example scenario with shear wave velocity $V_s = 150$ m/s, soil mass density $\rho = 1.7$ t/m^3, the Poisson's ratio $\upsilon = 0.4$ and the foundation radius $r = 7$ m are shown for comparison purposes.

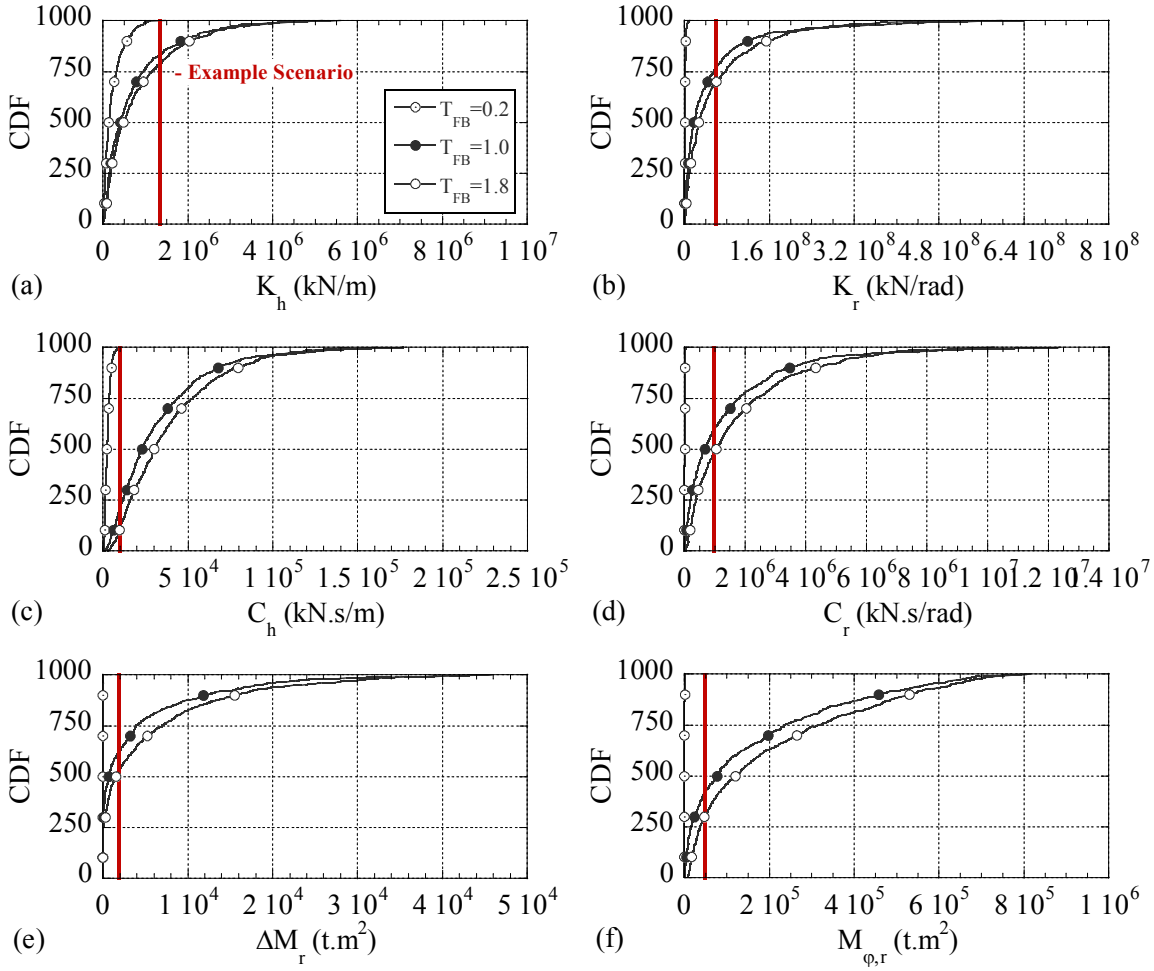

Figure 6-12. Cumulative distribution functions for the coefficients of soil-foundation element for groups of models with T_{FB}=0.2, 1.0 and 1.8 s, and 1000 total parameter value sets.

6.2.4 Summary of Model Generation

The procedures described for selection of uncertain soil and structural parameters are summarized in Table 6-4 and schematically illustrated in Figure 6-13 and. This methodology is used to generate models for the Monte Carlo analysis considering all these variables.

Table 6-4. Selection of uncertain model parameters.

Step	Parameter	Limits	Calculation
1	$(V_s)_0$: Initial shear wave velocity	80…360 m/s	-
2	$(V_s)_{sec}/(V_s)_0$:Shear wave velocity degradation ratio	0.15…0.7	-
3	ρ: Soil mass density	1.6…1.9 t/m^3	-
4	υ: Poisson's ratio	0.3…0.45	-
5	G_{sec}: Degraded shear modulus	-	$G_{sec} = \rho(V_s)_{sec}^2$
6	ξ_g': Soil material damping	-	$\frac{25-\xi_g'}{25-10} = \frac{(V_s)_{sec}/(V_s)_0 - 0.15}{0.7-0.15}$
7	h_e: Structural effective height	$\begin{cases} 2\ldots26.8(T_{FB}^{1.33}) & if\ 0.2 \le T_{FB} \le 0.32\ s \\ 9.1(T_{FB}^{1.33}) \ldots 26.8(T_{FB}^{1.33}) & if\ 0.32 \le T_{FB} \le 0.8\ s \\ 9.1(T_{FB}^{1.33}) \ldots 20 & if\ 0.8 \le T_{FB} \le 1.8\ s \end{cases}$	
8	r: Foundation radius	$\begin{cases} 2\ldots h_e & if\ 2 \le h_e \le 8\ m \\ (h_e/4) \ldots h_e & if\ 8 \le h_e \le 12\ m \\ (h_e/4) \ldots 12 & if\ 12 \le h_e \le 20\ m \end{cases}$	
9	m_s: Structural mass	$0.4(\rho r^2 h_e) \le m_{str} \le 0.6(\rho r^2 h_e)$	
10	$(k_s)_i$: Structural initial stiffness	-	$(k_s)_i = \frac{4\pi^2}{T_{FB}^2} m_s$
11	c_s: Structural damping coefficient	-	$c_s = 2(0.05)\sqrt{(k_s)_i m_s}$
12	T_{SSI}: Elastic period of the SSI system	-	$T_{SSI} = T_{FB}\sqrt{1 + \frac{(k_s)_i}{K_h} + \frac{(k_s)_i h_e^2}{K_r}}$

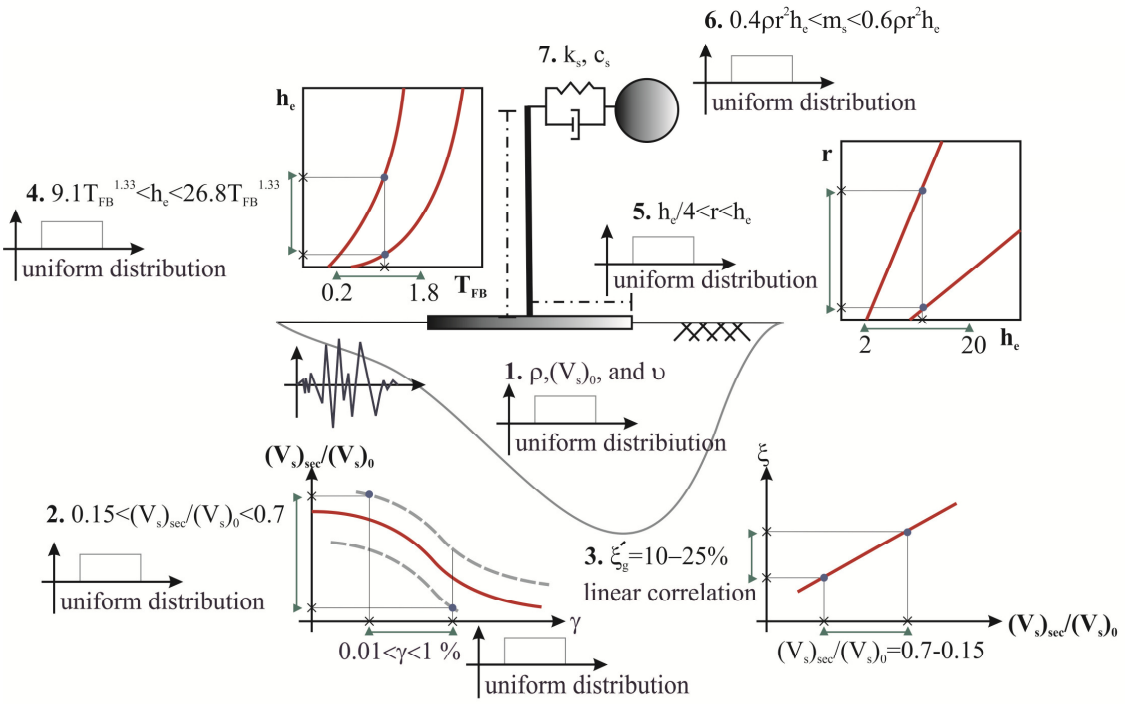

Figure 6-13. Schematic illustration for random generation of model parameters.

6.3 Selection of Input Ground Motions

To cover the uncertainties resulting from record-to-record variability, the models generated have to be subjected to a number of ground motions. The first question to be addressed in this regard is "*how many records are required in order to obtain an estimate of the median response with an acceptable level of accuracy?"* To answer this question, the simple formula introduced by Shome et al. [12] can be used:

$$n = 4\,\delta^2/X^2 \tag{6.13}$$

where n is the number of ground motions required to obtain an estimate of the median response within a factor of X with 95% confidence. In addition, δ represents the accepted dispersion in the resulting data. In this study, an estimate of the median response with a factor of $X = \pm 0.1$ with 95% confidence is targeted, while accepting the dispersion level of $\delta = 0.3$. Consequently, the number of required ground motions will be $n = 4(0.3/0.1)^2 \approx 40$.

The other essential question has to be answered is *"how exact the selection of the records has to be with regard to the magnitude-distance scenario of the region under study?"* This matter was investigated by Iervolino et al. [13], studying the nonlinear response of a set of model structures to numbers of records either selected to match a specific moderate-magnitude and distance scenario or selected arbitrarily. They found that there is no need to take great care in the selection of the records based on such factors.

Iervolino et al., specifically, also tried to answer another important question about the selection of records. "*To what extent record scaling matters in the final outcomes?*" The conclusion was that the concern over scenario-to-scenario record scaling is not justified. In specific, scaling of the records does not induce a bias in the response estimation.

Considering these statements about the selection of the records for statistical studies, two suites of ground motions were created in this research.

6.3.1 Suite 1 with 40 Records

The first suite of records was selected to represent ground motions recorded on stiff/soft soil. Specifically, soil type C with $V_s = 180 - 360$ m/s and soil type D with $V_s < 180$ m/s to a depth of 30 m based on USGS geomatrix soil classification. For this purpose, 40 ground motions were selected from earthquakes with magnitude of $6.5 - 7.5$ and source-to-site distance, which is the closest distance to the fault rupture, in the range of $15 - 40$ km. These records were screened to ensure they do not display any apparent pulse-like behaviour or near-source effects. The selected records were scaled to peak ground accelerations (PGA) within the range $0.3g - 0.8g$, assuming that nonlinear behaviour of the structure would be induced from earthquakes of such intensity. The outcome of this scaling scheme was to have 10 records with $0.3g \leq PGA \leq 0.4g$, 20 records with $0.4g \leq PGA \leq 0.6g$ and 10 records with $0.6g \leq PGA \leq 0.8g$, with all applied scaling factors in the range of $1.7 - 2.7$.

Specifications of the selected ground motions for Suite 1 including the magnitude-distance distribution graph, the un-scaled and scaled intensity levels, and the normalized elastic acceleration response spectra (5% damping), are shown in Figure 6-14. In addition, the list of the selected records with their un-scaled characteristic quantities is presented in Table 6-5.

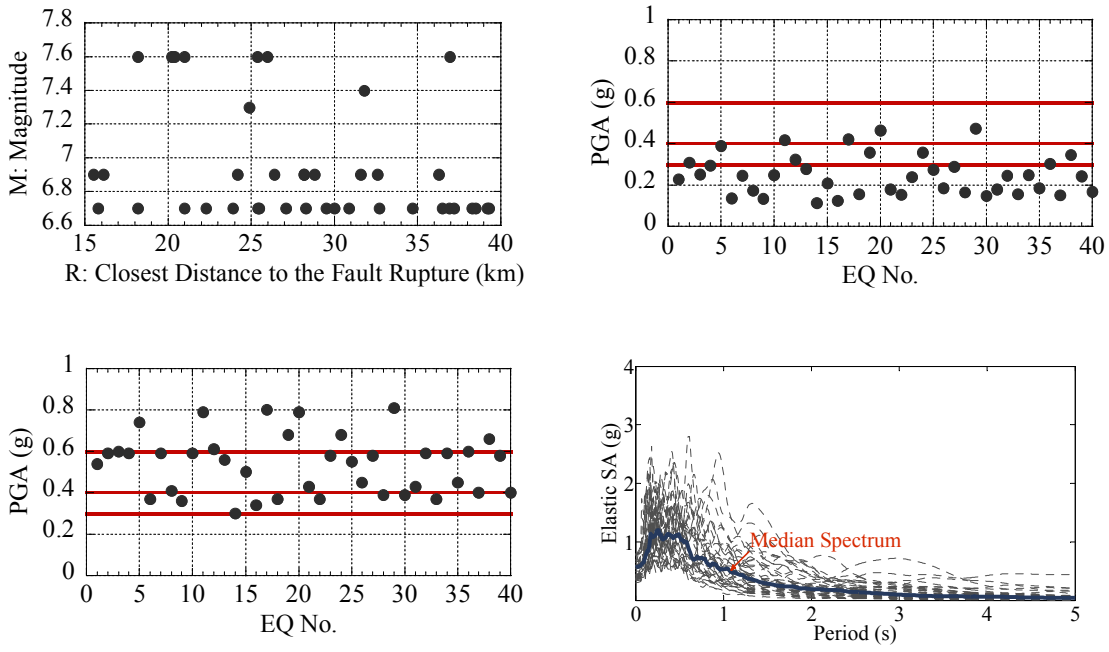

Figure 6-14. Specifications of the selected ground motions for Suite 1.

6.3.2 Suite 2 with 15 Records

The second suite of ground motions was chosen to represent records with enhanced spectral ordinates at long periods. These records do not follow the conventional design spectrum. Thus, an increase in the fundamental period due to soil-structure interaction may likely result in an increase in the structural response. They have been selected with the intention to investigate the effects of spectral ordinates on the amplification risk in structural response due to foundation flexibility effects. 6 records were selected for this purpose and then scaled with different scaling factors to result in 15 records having the peak ground acceleration (PGA) in the range of $0.3g - 0.8g$. Careful attention was paid to ensure the scaling factors were in the range of $0.3 - 3.0$. Note that the second suite of ground motions is only used for the results presented in Chapter 8-Section 6.6.

Specifications of the selected ground motions for Suite 2 are shown in Figure 6-15. The list of the selected records with their un-scaled characteristic quantities is presented in Table 6-6.

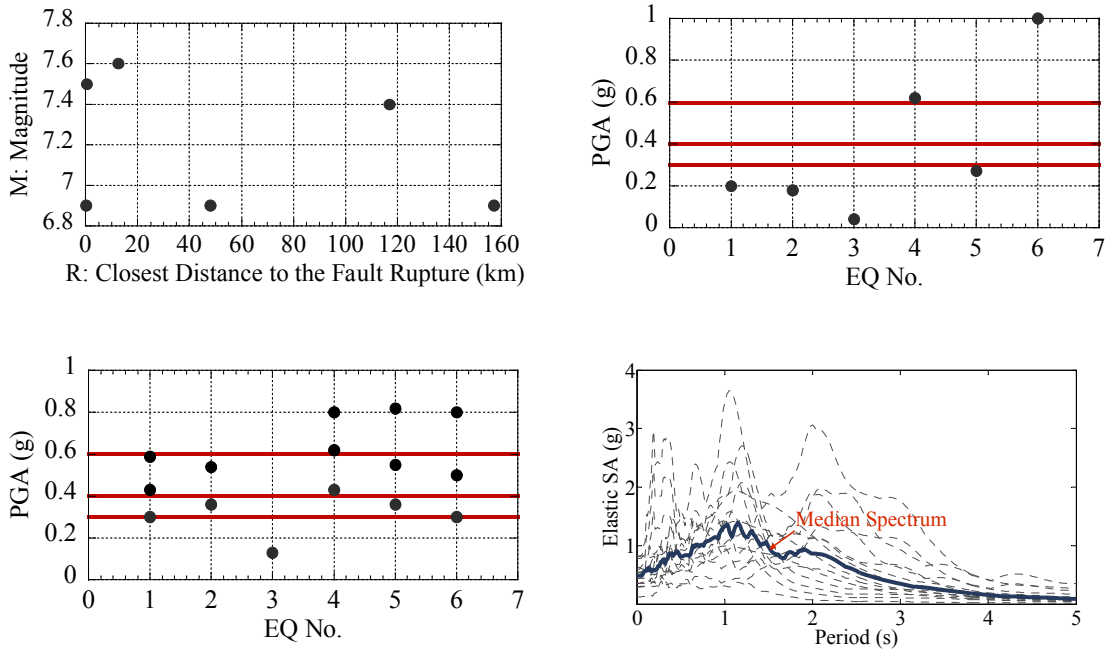

Figure 6-15. Specifications of the selected earthquake ground motions for suite 2.

Table 6-5. Selected earthquake motions for Monte Carlo simulation (Suite 1).

Record	Event	Year	Station	M[1]	Soil[2]	R[3] (km)	PGA[4] (g)	PGV[5] (cm/s)	PGD[6] (cm)	T_a[7] (s)
1			CHY010/E		C	25.4	0.23	21.9	11.1	0.27
2			CHY034/N		C	20.2	0.31	48.5	16.5	0.94
3	Chi-Chi, Taiwan	1999	CHY035/W	7.6	C	18.2	0.25	45.6	12.0	0.87
4			CHY036/W		C	20.4	0.29	38.9	21.2	0.53
5			NST/N		C	37	0.39	26.9	16.1	0.17
6	Kocaeli, Turkey	1999	Iznik/IZN090	7.4	C	31.8	0.14	28.8	17.4	1.17
7	Landers	1992	22074 Yermo Fire Station /YER270	7.3	C	24.9	0.25	51.5	43.8	0.68
8			57066 Agnews State Hospital/AGW000		C	28.2	0.17	26.0	12.6	0.26
9			57191 Halls Valley/HVR000		C	31.6	0.13	15.4	3.3	0.78
10			1028 Hollister City Hall/HCH090		C	28.2	0.25	38.5	17.8	0.82
11	Loma Prieta	1989	57382 Gilroy Array #4/G04000	6.9	C	16.1	0.42	38.8	7.1	0.44
12			57425 Gilroy Array #7/GMR090		C	24.2	0.32	16.6	3.3	0.44
13			1601 Palo Alto - SLAC Lab/SLC360		C	36.3	0.28	29.3	9.7	0.31
14			47179 Salinas - John & Work/SJW250		C	32.6	0.11	15.7	7.9	0.22
15			1695 Sunnyvale - Colton Ave/ SVL360		C	28.8	0.21	36.0	16.9	0.21
16			25282 Camarillo/CMR180		C	36.5	0.13	10.9	3.5	0.53
17			90053 Canoga Park - Topanga Can/CNP196		C	15.8	0.42	60.8	20.2	0.6
18			24575 Elizabeth Lake/ELI090		C	37.2	0.16	7.3	2.7	0.26
19			90063 Glendale - Las Palmas/GLP177		C	25.4	0.36	12.3	1.9	0.2
20	Northridge	1994	90054 LA - Centinela St/CEN155	6.7	C	30.9	0.47	19.3	3.5	0.16
21			90060 La Crescenta - New York/NYA090		C	22.3	0.18	12.5	1.1	0.46
22			90025 LA - E Vernon Ave/VER180		C	39.3	0.15	10.1	1.8	0.19
23			90034 LA - Fletcher Dr/FLE234		C	29.5	0.24	26.2	3.6	0.51
24			24303 LA - Hollywood Stor FF/HOL360		C	25.5	0.36	27.5	3.0	0.18

Table 6-5. *Continued*.

Record	Event	Year	Station	M	Soil	R (km)	PGA (g)	PGV (cm/s)	PGD (cm)	T_a (s)
25	Northridge	1994	90016 LA - N Faring Rd/FAR000	6.7	C	23.9	0.27	15.8	3.3	0.63
26			24612 LA - Pico &Sentous/PIC180		C	32.7	0.19	14.3	2.4	0.78
27			90022 LA - S Grand Ave/GR2090		C	36.9	0.29	17.9	2.4	0.29
28			90096 LA - S. Vermont Ave/VRM000		C	34.7	0.16	10.7	1.8	0.45
29			90091 LA - Saturn St/STN020		C	30	0.47	34.6	6.6	0.15
30			24055 Leona Valley #5 – Ritter/LV5000		C	38.3	0.15	14.9	2.4	0.22
31			24309 Leona Valley #6/LV6090		C	38.5	0.18	14.4	2.1	0.2
32			90095 Pasadena - N Sierra Madre/SMV180		C	39.2	0.25	12.3	1.1	0.41
33	Superstition Hills (B)	1987	5060 Brawley/B-BRA225	6.7	C	18.2	0.16	13.9	5.4	0.1
34			5061 Calipatria Fire Station/B-CAL315		C	28.3	0.25	14.6	3.1	0.16
35			5052 Plaster City/B-PLS135		C	21	0.19	20.6	5.4	0.42
36	Chi-Chi, Taiwan	1999	CHY041/W	7.6	D	26	0.3	20.4	8.6	0.26
37			TCU040/W		D	21	0.15	50.9	57.4	0.39
38	Kobe	1995	0 Kakogawa/KAK090	6.9	D	26.4	0.35	27.6	9.6	0.16
39			0 Shin-Osaka/SHI000		D	15.5	0.24	37.8	8.5	0.66
40	Superstition Hills (B)	1987	5062 Salton Sea Wildlife Refuge/B-WLF315	6.7	D	27.1	0.17	18.3	4.3	0.26

[1] Moment magnitude

[2] USGS, Geomatrix soil classification

[3] Closest distance to fault rupture

[4] Peak ground acceleration

[5] Peak ground velocity

[6] Peak ground displacement

[7] Predominant period of ground motion

Table 6-6. Selected earthquake motions for Monte Carlo simulation (Suite 2).

Record	Event	Year	Station	M	Soil	R (km)	PGA (g)	PGV (cm/s)	PGD (cm)	Ta (s)
EQ1	Bucharest	1977	Building Research Ins./NS	7.4	-	117	0.18	-	-	1.13
EQ2	Chi Chi	1999	TCU110/W	7.6	D	12.56	0.18	67.5	40.9	2.09
EQ3	Kobe	1995	Fukiai/090	6.9	D	157.2	0.04	5.3	2.0	0.57
EQ4			Takatori/090		D	0.3	0.62	120.7	32.7	0.19
EQ5	Loma Prieta	1989	Redwood City/2043	6.9	D	47.9	0.27	53.6	12.6	1.06
EQ6	Mexico City	1985	SCT1/N90W	7.5	D	0.4	0.91	58.4	58.9	2.0

6.4 Summary

This chapter reviewed the probabilistic methodology used to systematically generate soil-structure models with random parameters that were then applied in the future stochastic analyses. A wide range of soil, foundation and structural parameters were covered. However, an attempt was made to assure only realistic models are considered. In addition, the procedure followed to define the suites of ground motions presenting record-to-record variability was described.

The models and ground motions defined in this chapter were then used in time-history simulations to rigorously quantify the effects of foundation flexibility on the structural response. The results and conclusions from these simulations are presented in Chapters 7, 8 and 9.

References

[1] NZS1170.5, "Structural design actions, part 5: earthquake actions," ed. New Zealand, 2004.

[2] A. L. Jones*, et al.*, "Estimation of Uncertainty in Geotechnical Properties for Performance-Based Earthquake Engineering," University of California, Berkeley2002.

[3] K. Phoon and F. H. Kulhawy, "Characterization of geotechnical variability," *Candaian Geotechnical Journal,* vol. 36, pp. 612-624, 1999.

[4] K. Phoon and F. H. Kulhawy, "Evaluation of geotechnical property variability," *Canadian Geotechinical Journal,* vol. 36, pp. 625-639, 1999.

[5] S. Lacasse and F. Nadim, "Uncertainties in characterising soil properties," *Geotechnical Special Publication,* vol. 58, pp. 49-75, 1996.

[6] P. Lumb, "The variability of natural soils," *Canadian Geotechinical Journal,* vol. 3, pp. 74-97, 1996.

[7] P. Lumb, "Safety factors and probability distribution of soil strength," *Canadian Geotechinical Journal,* vol. 7, pp. 225-241, 1970.

[8] M. Vucetic and R. Dobry, "Effect of soil plasticity on cyclic resposne," *Journal of Geotechnical Engineeing-ASCE,* vol. 117, pp. 89-107, 1991.

[9] U. Smoltczyk, Ed., *Geotechnical Engineering Handbook*. Ernst & Sohn, 2002, p.^pp. Pages.

[10] ATC-40, "Seismic evaluation and retrofit of concrete buildings," ed: Applied Technology Concil, 1996.

[11] J. P. Stewart*, et al.*, "Seismic soil-structure interaction in buildings. I: analytical methods," *Journal of Geotechnical and Geoenvironmental Engineering,* vol. 125, pp. 26-37, Jan 1999.

[12] N. Shome*, et al.*, "Earthquakes, records, and nonlinear responses," *Earthquake Spectra,* vol. 14, pp. 469-500, 1998.

[13] I. Iervolino and C. A. Cornell, "Record Selection for Nonlinear Seismic Analysis of Structures," *Earthquake Spectra,* vol. 21, pp. 685-713, 2005.

CHAPTER

7. Stochastic Quantification of Seismic Soil-Structure Interaction I: "Structures with Linear Behaviour on Equivalent Linear Soil-Foundation Interface"

Abstract. This chapter investigates the effects of soil-structure interaction on the seismic response of structures with linear behaviour assuming an equivalent linear soil-foundation interface. Uncertainties in the model parameters and input ground motions are taken into account to quantify the risk of detrimental scenarios compared to structural fixed-base assumption, and to identify conditions under which soil-structure interaction increases the structural strength demand. In this regard, the introduced probabilistic Monte Carlo methodology is used to conduct 1.36 million time-history simulations using a wide range of realistic soil-structure models and input ground motions.

7.1 Introduction

The primary goal of seismic soil-structure interaction studies is to estimate the effects of foundation flexibility on the structural response. This objective is not straightforward since the soil-structure interaction phenomenon is a complex and coupled dynamic

problem. More complexity is expected when the consequences of uncertainties in model parameters and ground motions are considered.

Modification of the seismic response of elastic single-degree-of-freedom systems was first introduced by Jennings and Bielak [1], Veletsos and Meek [2], and Veletsos and Nair [3]. They showed that the effect of inertial interaction on the structural response can simply be investigated from the response of an equivalent single-degree-of-freedom system, also called a replacement oscillator, consisting of an increase in the fundamental period of a fixed-base structure and a change in the associated damping. Using this concept, they recognized that considering soil-structure interaction can either decrease or increase the structural response depending on system parameters and characteristics of the input ground motion. Due to simplicity of this modelling approach, it has been used in existing seismic design provisions to incorporate the effects of soil-structure interaction in design [4-7].

This use has resulted in the rudimentary conclusion that soil-structure interaction always decreases seismic structural response. The reason behind this conclusion is that current design codes use an idealized smooth design spectrum with a constant acceleration up to a certain period and a decreasing branch thereafter. Therefore, any increase in the structural period will eventually result in a decreased structural response. However, this assumption is oversimplified and unconservative in some cases.

These early studies have been followed by the question of how structural nonlinearity may change soil-structure interaction effects on the structural response. In this regard, the response of a yielding soil-structure system was examined by Veletsos and Verbic [8] and it was suggested that structural yielding decreases the effects of soil-structure interaction due to increasing system flexibility. This conclusion was then supported by Ciampoli and Pinto [9], who showed that seismic inelastic response of a single-degree-of-freedom system remains unaffected or even decreased due to foundation flexibility.

In contrast to these findings, numerical investigation by Bielak [10] indicated that for structures with nonlinear behaviour, foundation compliance may lead to a larger displacement response than a fixed-base system. Miranda and Bertero [11] also demonstrated that for ground motions recorded on soft soil, period lengthening can

result in an increase in the seismic structural response in certain frequency ranges. These latter results were supported by other studies [12, 13], highlighting the point that soil-structure interaction effects for yielding systems are as important as for elastic systems.

Hence, there is significant controversy regarding the beneficial (decreasing response) or detrimental (increasing response) role of soil-structure interaction on seismic structural response [14, 15], and this controversy has led to an important question of whether soil-structure interaction should be considered in a design procedure. To answer these questions, a more rigorous study is needed that accounts for all existing uncertainties in model parameters and input ground motions. Uncertainties arising from structural and geotechnical properties of a system, as well as ground motion characteristics, play an important role in the overall performance prediction of seismically excited structures [16]. Specifically, for example, when foundation flexibility is considered, the effect of uncertainty on structural response gets even more pronounced [17-20].

In this context, the current study presents an effort to create a comprehensive and systematic investigation of the effects of soil-structure interaction on the seismic structural response. A robust stochastic analysis using Monte Carlo simulation was conducted considering soil-shallow foundation-structure models satisfying the current design practice [7].

The structural part of the models was assumed to be either a linear or a nonlinear single-degree-of-freedom system with 5% equivalent viscous damping. The outcomes of analyses assuming structures with linear behaviour are presented here, and the results for structures with nonlinear behaviour are discussed in the next chapter. The reasons behind choosing the models with linear behaviour were: (i) to follow the approach that has been adopted in building codes for developing design spectrum and defining the seismic forces acting on the structure; and (ii) to systematically address the problem and evaluate the soil-structure interaction effects, starting with a more simple behaviour.

The soil-foundation interface was represented by an equivalent linear cone model [21] taking into account nonlinearity in the soil stress-strain behaviour via the equivalent linear approach [22]. It is acknowledged that the adopted soil-foundation element does

not cover material and geometrical nonlinearity. The results covering this issue are presented in Chapter 13. The generated soil-structure models were excited by an ensemble of ground motions recorded on stiff/soft soils to account for variability in the input motion.

Thus, the simulations employed provided sufficient means to address uncertainties in soil, structure and ground motion characteristics through a comprehensive set of time history analyses. However, respecting the scope of this study, the outcomes presented are limited to a single-degree-of-freedom system as a first step in the evaluation of soil-structure interaction effects. In addition, this study does not consider extreme conditions such as those imposed by very soft (liquefiable) soils. Nevertheless, the overall approach is designed to provide input and guidance to performance-based design methods and standards. Hence, these assumptions and approach are fit for that purpose.

7.2 The Importance of Uncertainty in Soil-Structure Interaction Studies

Figure 7-1 illustrates the consequences of uncertainty on the seismic strength demand of a soil-structure system compared to a fixed-base system. If a presumed structure when fixed at the base with a fundamental period of T_{FB} is subjected to two different ground motions, as shown in Figure 7-1(a), the demand ratio between soil-structure system with a fundamental period of T_{SSI} and fixed-base system is not the same. Depending on the characteristics of the soil-structure system and the ground motion considered, seismic demand of the soil-structure system can be either decreased or increased compared to the reference fixed-base system. The possible increase in demand is caused by an enhanced spectral ordinate of EQ 2 at longer periods. Note the records with this type of response are not necessarily rare in nature [14], and the recent 2010 Darfield and 2010 Christchurch earthquakes, in New Zealand, amply demonstrated this fact. Therefore, an increase in the fundamental period due to soil-structure interaction does not always lead to a decrease in the structural response.

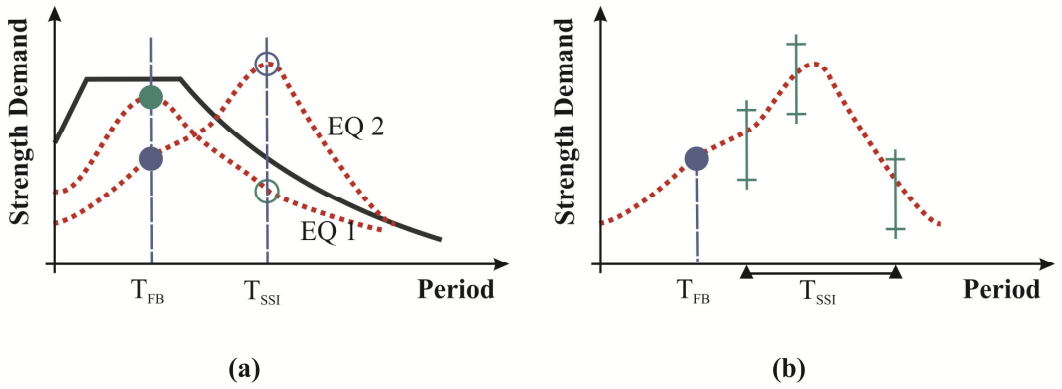

Figure 7-1. Schematic illustration of soil-structure interaction on seismic structural response: (a) the effects of uncertainty in input ground motion; and (b) the effects of uncertainty in model parameters.

In addition to this argument, significant variation in the strength demand ratio might be expected even for one ground motion with a specific spectrum shape, depending on the relative configuration of structural parameters, foundation radius and soil characteristics. This possibility is shown in Figure 7-1(b). As a result, depending on the response of the considered soil-structure system within this variation boundary, soil-structure interaction may play either a beneficial or detrimental role.

What has been presented in Figure 7-1 clearly highlights the significant role of uncertainties in quantifying the effects of soil-structure interaction on the structural response. Therefore, as mentioned previously, a rational way for re-investigating the soil-structure interaction phenomena is to make use of a stochastic approach, an approach that is gaining a growing attention in the geotechnical engineering community [23] and in some soil-structure interaction studies [18, 19, 24].

7.3 Outline of the Adopted Stochastic Procedure

For the Monte Carlo simulation used in this study, an established rheological soil-shallow foundation-structure model was considered. Consequently, a large number of linear and nonlinear time-history simulations were run over models with randomly selected parameters using an ensemble of scaled recorded ground motions. Parameters of these models were systematically defined by a random process carefully ensuring

each model analysed satisfied the requirements of realistic models and also covered a relevant period range in the design spectrum.

The periods of $0.2, 0.3 \ldots 1.8$ s were selected to represent structures with the fixed-base condition having total height of $3 - 30$ m and satisfying the period-height relationship adopted in the New Zealand Standard [25]. For each considered period T_{FB}, 1000 models were generated by assembling the randomly defined model parameters and using commonly accepted deterministic relationships between these parameters and the other required parameters. Following this procedure, a complete dataset comprised of 17 groups of models each having 1000 models (i.e. 17,000 models in total) was generated.

The number 1000 was chosen with the intention to: (i) give the best fit statistical distribution for the randomly selected parameters and (ii) increase the confidence level of the Monte-Carlo simulation compared to the exact expected solution [26]. The procedure adopted for defining the parameters was discussed in detail in Chapter 6. It also needs to be mentioned that all nonlinear time-history simulations were carried out using the finite-element program "Ruaumoko 2D" [27].

7.4 Soil-Structure System Considered

"Structure with Linear Behaviour on Equivalent Linear Soil-Foundation Interface"

The soil-structure model used for the series of analyses whose results are presented in this chapter is constituted from a single-degree-of-freedom structure with linear behaviour and a set of equivalent linear springs and dashpots representing the soil-shallow foundation interface, as shown in Figure 7-2. In this model, only horizontal and rocking motions of the foundation were considered, and, since the foundation is located on the ground surface, the horizontal and rocking degrees of freedom were modelled independently. The mass of the foundation and the mass moment of inertia of the structure were neglected [10], as a further reasonable simplification.

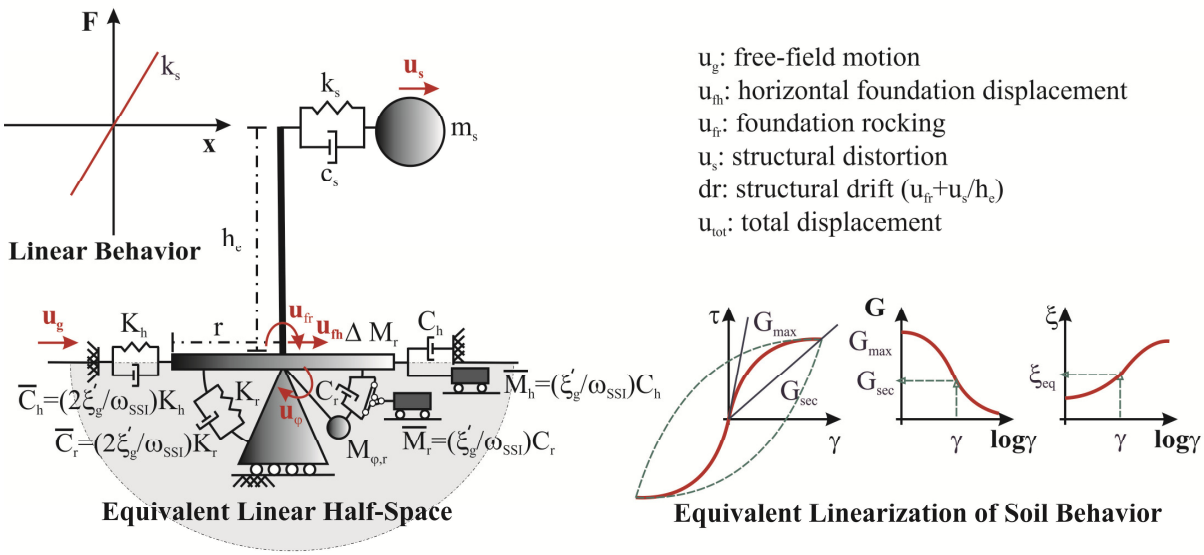

Figure 7-2. Soil-structure model considered: structure with linear behaviour on equivalent linear soil-foundation interface.

The idealized structural part of the model can be interpreted as an equivalent representation of the fundamental mode of vibration of a fixed-base multi-storey structure. This structural representation is characterized by: (i) the structural mass participating in fundamental mode of vibration m_s; (ii) the structural lateral stiffness k_s; (iii) the coefficient of relative viscous damping c_s; and (iv) the effective height considered from the foundation level to the centre of the structural mass h_e. It should be noted that this structural model does not take into account second order ($P-\Delta$) effects.

The soil-foundation element was modelled by a lumped-parameter model representing a rigid circular footing resting on the soil surface and having a perfect bond to the soil. For evaluating the dynamic soil impedances incorporating soil nonlinearity, the frequency-independent coefficients of a rheological cone model [21] were modified using the conventional equivalent linear method [22]. To avoid more complication in time-domain analysis, soil material damping was assumed to be viscous instead of hysteretic. Details about the soil-structure model can be found in Chapter 5.

7.5 Uncertainty in Model Parameters and Input Ground Motions

A brief overview of the approach used to cover the uncertainty in model parameters and input ground motions is presented here. For more detailed information the reader is referred to Chapter 6.

7.5.1 Selection of Model Parameters

The four main soil parameters defining the soil-foundation interface were assumed to be uncertain and independent, and their values were selected randomly. The parameters considered are: (i) initial soil shear wave velocity $(V_s)_0$; (ii) shear wave velocity degradation ratio $(V_s)_{sec}/(V_s)_0$, where $(V_s)_{sec}$ represents the degraded shear wave velocity; (iii) soil mass density ρ; and (iv) Poisson's ratio υ. For each of these parameters, a realistic range was defined, and 1000 uniformly distributed values were selected from that range afterwards.

In addition, structural parameters that were chosen randomly include: (i) structural effective height h_e; (ii) foundation radius r; and (iii) structural mass m_s. To achieve realistic soil-structure models, the selection of these parameters was constrained by commonly accepted relationships either for the structure or for the whole soil-structure system. Depending on the values of these generated parameters, the values for the structural lateral stiffness k_s and the coefficient of relative viscous damping c_s were then calculated.

7.5.2 Selection of Input Ground Motions

Forty different large-magnitude and moderate-distance ground motions recorded on stiff/soft soil (soil type C with $V_s = 180 - 360$ m/s and soil type D with $V_s < 180$ m/s to a depth of 30 m based on USGS soil geomatrix classification) were used as an input in the simulations. This number was chosen to reduce the variance in the response due to record-to-record variability and obtain an estimate of median response within a factor of ± 0.1 with 95% confidence [28]. The records were selected in such a way to satisfy the constrains of: (i) the magnitude in the range of $6.5 - 7.5$, (ii) the closest distance to fault rupture in the range of $15 - 40$ km and (iii) the peak ground acceleration (PGA) greater than $0.1g$. The selected records were then scaled to have reasonably distributed

PGAs within the range of $0.3g - 0.8g$, assuming that a nonlinear behaviour of the structure is caused by these levels of intensity. Respecting rigorous scaling criteria and recommendations in NZS 1170.5, all scaling factors were chosen to be less than 3.0.

7.5.3 Presentation of Response Statistics

To characterize the central tendency, the median is selected as the statistical measure because results were not necessarily Gaussian distributed. Dispersion is presented in a box and whisker plot in which the box has lines at the 25^{th} percentile (bottom line), 50^{th} percentile or median (middle line), and 75^{th} percentile (top line). Whiskers extend from each end of the box to the 5^{th} and 95^{th} percentiles, respectively. Outliers are the data with values beyond those indicated by the whiskers. This presentation easily enables direct evaluation of soil-structure interaction effects at different levels of probability.

7.6 Quantification of Foundation Response

Variation in foundation response in the horizontal and rocking directions, u_{fh} and u_{fr}, are quantified in Figure 7-3. The responses are categorized based on fundamental structural period T_{FB}, while at each reported period, the ensuing statistics resulted from $80{,}000 = 2 \times 1000 \times 40$ (i.e. # FB & SSI Models × # Random Models × # EQs) time-history simulations are presented. The format adopted in showing the results is denoted as a *"foundation response spectrum"*, from here onwards. The median values and associated dispersion are thus a function of fundamental structural period.

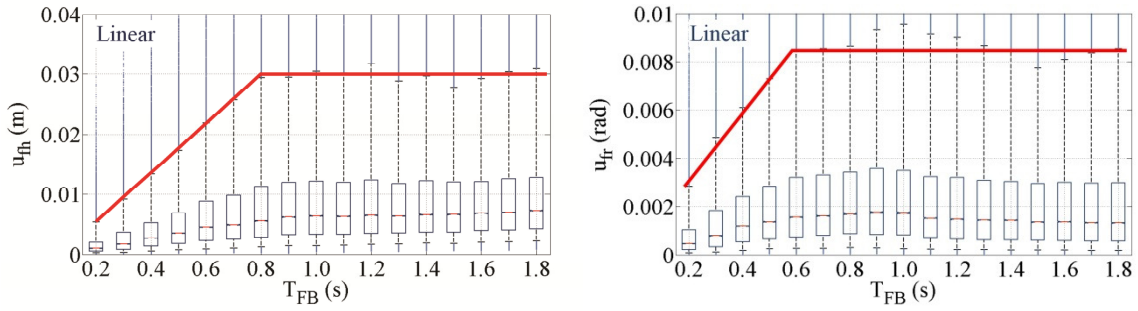

(a) (b)

Figure 7-3. Foundation response spectra for structures with linear behaviour: (a) horizontal displacement spectrum; and (b) rocking spectrum.

If horizontal foundation displacement is considered, the median values and associated dispersion increase with the fundamental structural period up to $T_{FB} = 1.0$ s and remain unchanged afterwards. This observed trend gives the impression that structures with longer periods are more probable to experience greater foundation horizontal displacement. Experiencing a greater displacement at longer periods is similar to that for a displacement response spectrum of ground motions. In other words, horizontal foundation displacement due to seismic forces follows the same logic applied to the response of structures fixed at the base.

Similar to that for horizontal foundation displacement, the median values and associated dispersion of foundation rocking increases up to $T_{FB} = 0.6$ s, remains almost unchanged up to $T_{FB} = 1.2$ s and tends to decrease slightly after this period. The trend shows that structures with the fundamental period in the range of $0.6 - 1.2$ s are more likely to be affected by large foundation rocking.

Figure 7-3 also shows that the 95^{th} percentiles are much further from the median values than the 5^{th} percentiles. Such observation signifies that foundation responses are more spread above than below the median values. It implicitly concludes that even though the likelihood of having a greater response than the median is the same as that for having a smaller response, but the difference between the maximum response experienced and the median response is very large. Therefore, to obtain a more conservative design, values corresponding to higher percentiles have to be used.

In this context, considering the 95^{th} percentiles (allowing for 5% risk of increase), the suggested foundation response spectra are shown in Figure 7-3 by solid red lines. Note that the corner periods of the introduced spectra are $T_{FB} = 0.8$ s for horizontal displacement and $T_{FB} = 0.6$ s for rocking. In addition, the spectra lines correspond to values that are $4 - 6$ times larger than the median values.

7.7 The Contribution of Foundation Response to Total Displacement

The contribution of horizontal foundation displacement and foundation rocking on total displacement at roof level u_{tot} is presented in Figure 7-4. Here, u_{fh}/u_{tot} represents the portion of horizontal foundation displacement in the expected total displacement, and $h_e u_{fr}/u_{tot}$ represents the corresponding portion of foundation rocking.

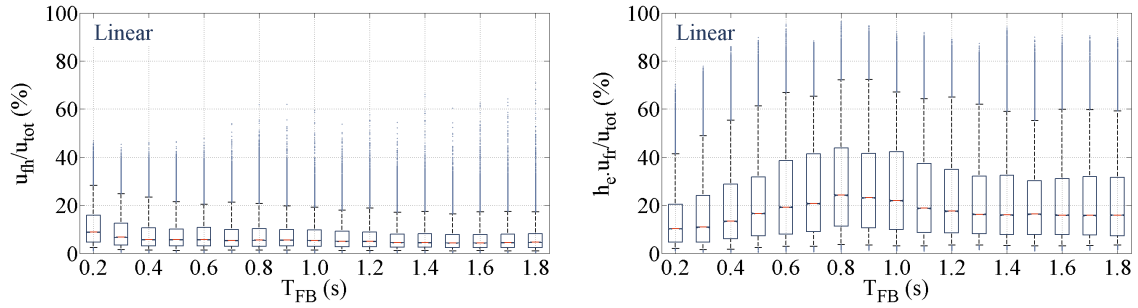

(a) (b)

Figure 7-4. The contribution of foundation response to total displacement for structures with linear behaviour: (a) contribution of horizontal displacement; and (b) contribution of rocking.

For the 5^{th}-95^{th} percentile range, considering 90% probability, structural displacement due to horizontal foundation displacement may have a contribution of $1\% - 30\%$ to the total displacement, while this contribution is $5\% - 70\%$ for structural displacement due to the foundation rocking. Obviously, the contribution percentage values depend on the fundamental structural period.

Considering the median values and the extent of variation implies that horizontal foundation displacement is more important for stiff structures ($T_{FB} < 0.6$ s), while foundation rocking is more significant for structures having periods in the range of $0.6 - 1.2$ s. It is interesting to note that although stiff structures may experience less horizontal foundation displacement, Figure 7-3(a), the contribution of this displacement to total displacement is higher compared to that for structures with longer periods. If the contribution percentage values for foundation horizontal displacement are compared with that for foundation rocking, it is readily concluded that foundation rocking, in general, plays a more important role in the total displacement than horizontal foundation displacement.

7.8 Soil-Structure Interaction Effects on Seismic Structural Response

Four measures of structural response to seismic forces were examined in this study: (i) structural distortion u_s, (ii) structural drift dr, (iii) total displacement u_{tot} and structural acceleration a_s. Structural distortion is the horizontal displacement of the structure relative to the foundation. Structural drift is the summation of foundation rocking and normalized structural distortion by the effective height ($dr = u_{f\theta} + u_s/h_e$) that causes second-order ($P-\Delta$) effects. Total displacement is the displacement measured at the roof level including lateral displacement resulted from foundation response and structural distortion ($u_{tot} = u_{fh} + h_e u_{f\theta} + u_s$) that can cause the pounding between adjacent structures. Finally, structural acceleration is the total acceleration of the structural mass ($a_s = \ddot{u}_{fh} + h_e \ddot{u}_{f\theta} + \ddot{u}_s$) that is a representative of the base shear.

To simplify presentation of the results from numerous time-history simulations, the maximum calculated responses of soil-structure models were normalized by that of the corresponding fixed-base models. This ratio is called the *"response modification factor"*. Soil-structure interaction is beneficial when this factor is less than 1.0 and is detrimental when it is greater than 1.0.

All the response modification factors are presented and discussed as a function of fundamental structural period T_{FB}. The variation in these values is presented in box and whisker plot format. This graph is called a *"response modification spectrum"* from now onward. The corresponding response modification spectra for structures with linear behaviour are illustrated in Figure 7-5.

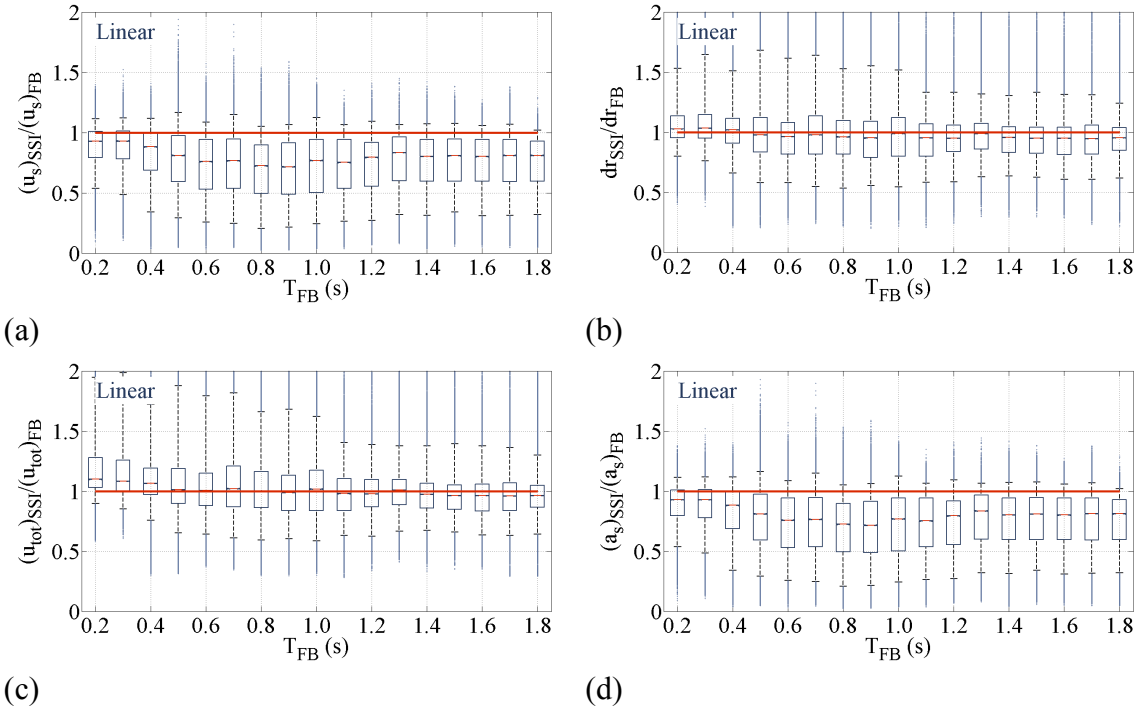

Figure 7-5. Response modification spectra for structures with linear behaviour, considering: (a) structural distortion; (b) structural drift; (c) total displacement; and (d) structural acceleration.

7.8.1 Effects on Structural Distortion

If structural distortion is considered, Figure 7-5(a), the response with a 90% probability can be either decreased up to 80% or amplified up to 20% depending on the fundamental structural period. However, the maximum probable amplification in the response, defined as the values corresponding to the 95^{th} percentiles, is independent of the fundamental structural period. However, the maximum reduction, defined as the values corresponding to the 5^{th} percentiles, increases up to $T_{FB} = 0.8$ s and decreases afterwards.

The observed trend in the maximum reduction of structural distortion can be simply explained considering the role of foundation rocking. Specifically, when the contribution of foundation rocking to the total displacement increases, more reduction in the structural distortion is expected, *ref.* Figure 7-4(b).

It is also evident in Figure 7-5(a) that structural distortion modification factor is less than 1.0 for most examined scenarios, indicating that soil-structure interaction generally reduces the structural distortion. However, there is $20\% - 30\%$ likelihood for stiff

structures ($T_{FB} < 0.6$ s) and 10% likelihood for structures with longer periods ($T_{FB} > 0.6$ s) in which soil-structure interaction may increase the structural distortion. Note these likelihoods are large enough that they cannot be ignored.

7.8.2 Effects on Structural Drift

Figure 7-5(b) shows the effects of foundation flexibility on structural drift. The structural drift modification factor for the 5^{th}-95^{th} percentile of the examined cases varies within the range of $0.5 - 1.7$ depending on the fundamental structural period. In this case, it is important to note that with $40\% - 60\%$ likelihood the response modification factor may be greater than 1.0. Considering the high values of probability and the possible level of amplification, it is concluded that soil-structure interaction effects on structural drift cannot be simply neglected.

The maximum amplification in the response decreases with an increase in fundamental structural period. This result implies that the amplification in structural drift is more important for stiffer structures ($T_{FB} < 0.6$ s). However, the maximum reduction in the response follows the same trend as observed in the case of structural distortion emphasizing the key role of foundation rocking.

7.8.3 Effects on Total Displacement

The response modification spectrum for the total displacement is shown in Figure 7-5 (c). Here, the effects of both rigid motions caused by foundation flexibility are considered. The trend is almost similar to that for structural drift, except the variation range for the 5^{th}-95^{th} percentiles has slightly higher values, $0.6 - 2.0$. The likelihood of having the total displacement modification factor greater than 1.0 is also slightly higher compared to the case of structural drift, as it is in the range of $40\% - 80\%$. This increase is not unexpected since one additional rigid body motion is included in the response. Considering the range of variation, as well as the median of the results, soil-structure interaction should always be considered in studies related to pounding effects.

7.8.4 Effects on Structural Acceleration

Finally, if structural acceleration is considered, Figure 7-5(d), similar trends and values to that of structural distortion are expected. It is only because the induced accelerations

(or forces) in a system with linear structural behaviour are directly proportional to the generated deformations.

7.9 Quantification of the Existing Dispersion in the Outcomes

The level of dispersion existing in the response modification factors resulted for each group of models was quantified in terms of the coefficient of variation COV. As a reminder, COV is the ratio of standard deviation σ to mean μ. Two alternative approaches, in addition to the COVs calculated were used to distinguish between the origin of dispersion resulting from uncertainty in: (i) model parameters (MPs); and (ii) record-to-record (RTR) variability. These approaches are shown in Figure 7-6 and are explained as:

1) *Measuring the dispersion in the structural response (X) due to uncertainty in model parameters* $COV[E(X|MP)]$. To evaluate this measurement: first, the mean of 40 response values $E(X|MP)$ resulting from 40 time-history simulations using the selected ground motions was calculated for each of the 1000 adopted models; second, the COV of these 1000 calculated mean values was evaluated.

2) *Measuring the dispersion in the structural response (X) due to record-to-record variability* $COV[E(X|RTR)]$. To calculate this measurement: first, the mean value of 1000 response values $E(X|RTR)$ resulting from 1000 time-history simulations over 1000 adopted models was calculated for each of the 40 selected ground motions; second, the COV of these 40 calculated mean values was calculated.

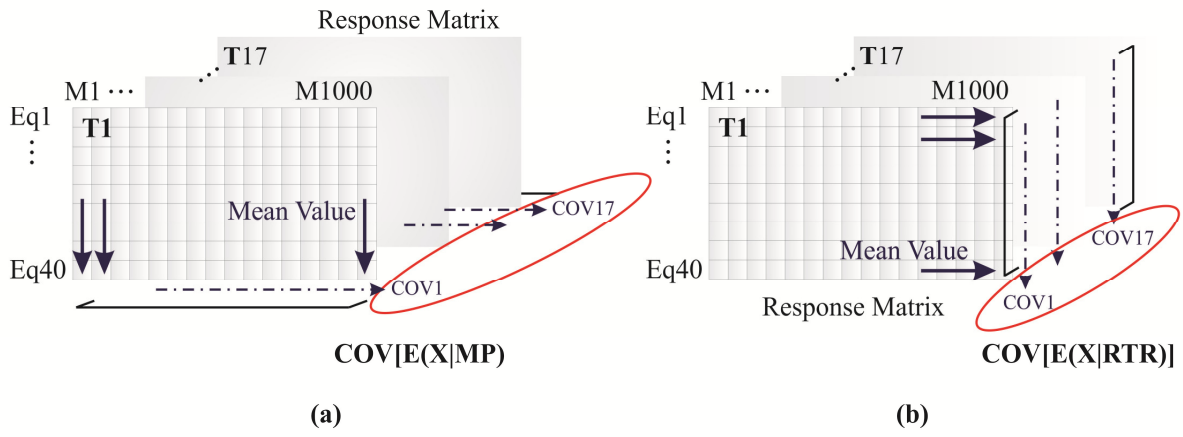

Figure 7-6. Alternative approaches to distinguish between the dispersions resulting from uncertainty in: (a) model parameters (MPs); and (ii) record-to-record (RTR) variability.

The computed COVs are shown in Figure 7-7 for all structural responses considered. Clearly, the dispersion in the resulting data is in the acceptable range (i.e. $COV < 0.4$). Therefore, the output dataset resulting from the simulations used is a reliable dataset. Hence the conclusions made based on these results are valid and robust.

If the values of $COV[E(X|MP)]$ and $COV[E(X|RTR)]$ are compared when structural distortion modification factor or structural acceleration modification factor are considered as the structural response (X), then the contribution of uncertainty in modal parameters to the existing dispersion is greater than the contribution of record-to-record variability. This result suggests that soil-structure interaction effects on structural distortion and structural acceleration are more sensitive to the modelling parameters than to the input ground motion characteristics, at least within the ground motion constraints adopted in this study.

However, if structural drift modification factor or total displacement modification factor is considered, a converse trend is observed for structures with $T_{FB} > 0.4\,s$. In this context, the contribution of uncertainty in model parameters to the existing dispersion is less than the contribution of record-to-record variability. Therefore, the soil-structure interaction effects on structural drift and total displacement are more sensitive to the input ground motion characteristics than the modelling parameters.

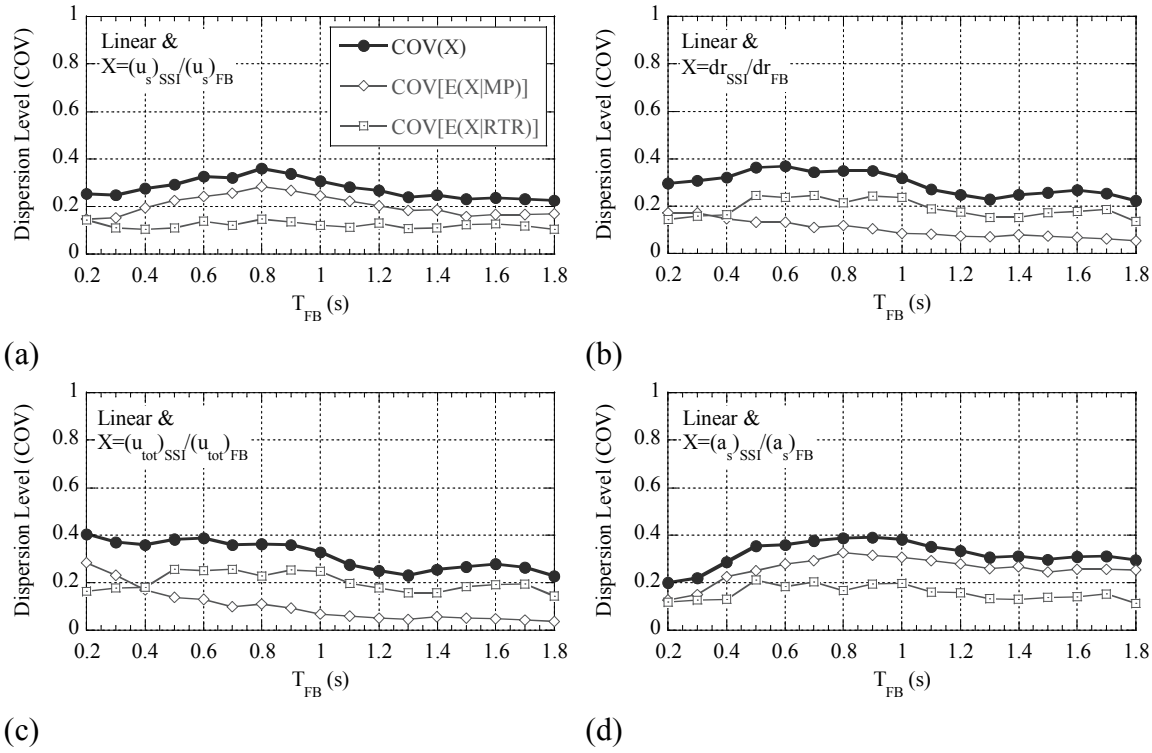

Figure 7-7. Quantification of the existing dispersion in the response modification factors considering: (a) structural distortion; (b) structural drift ; (c) total displacement ; and (d) structural acceleration.

7.10 Risk of Detrimental Soil-Structure Interaction Effects

To quantify the significance of detrimental soil-structure interaction effects on structural response, two main aspects of risk were analysed: (i) the probability of having amplification in the response of the soil-structure model as compared to the response of a fixed-base model; and (ii) the level of amplification in the structural response due to soil-structure interaction consideration. These two aspects have been referenced in terms of all considered structural responses (i.e. u_s, dr, u_{tot}, and a_s), following the previously defined spectral format and considering three amplification levels A.L.=1.0, 1.1 and 1.2.

The defined risks are shown in Figure 7-8. On the left-side, the probabilities of having amplification in structural responses are presented across all considered periods, whereas on the right-side, the corresponding values of median percentage increase (Med[P.I.])are shown.

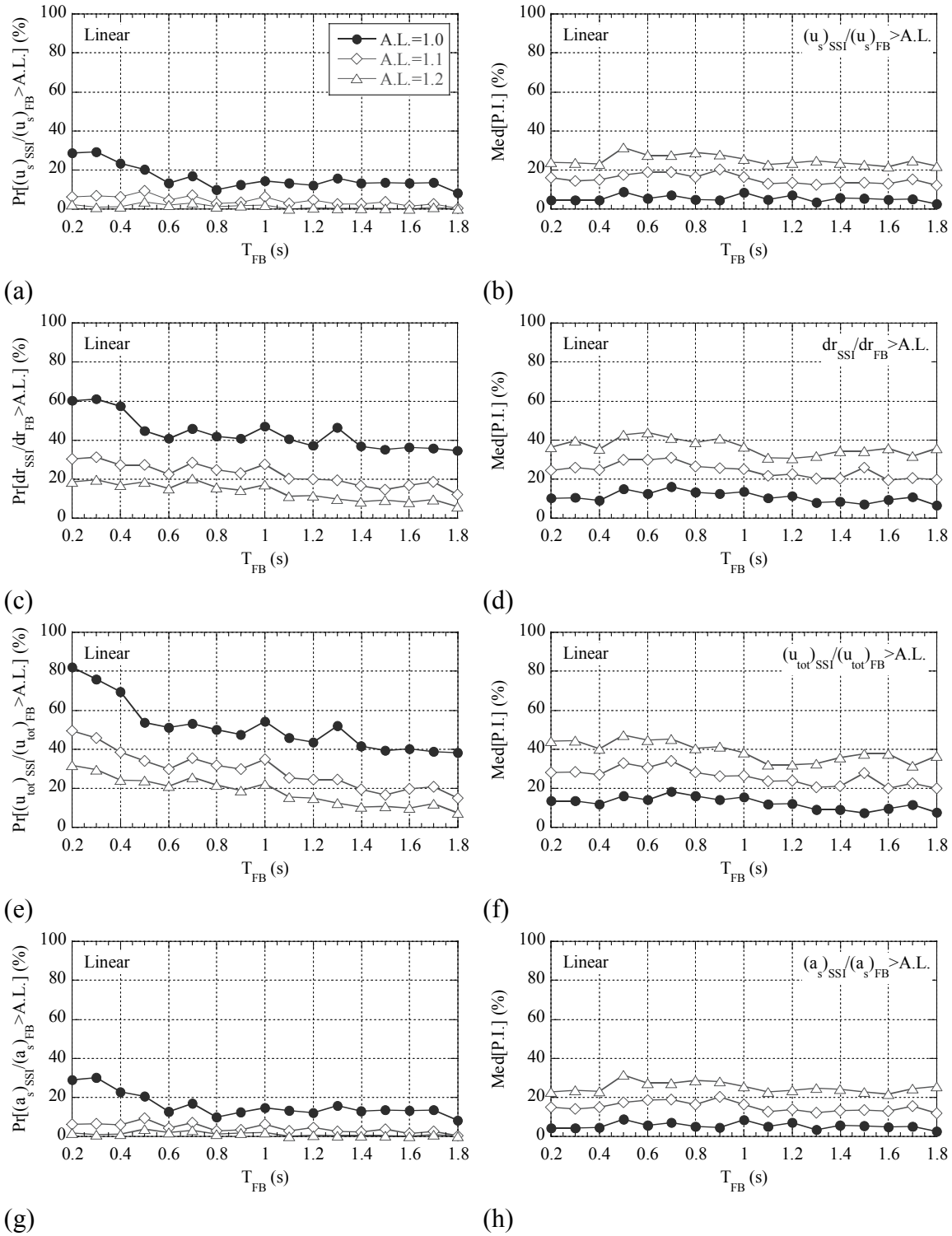

Figure 7-8. Risk spectra for structures with linear behaviour: (left) probability of amplification in the response; and (right) level of amplification in the response.

7.10.1 Amplification Risk in Structural Distortion

As illustrated in Figure 7-8(a), the probability of amplification in structural distortion is between $10\% - 30\%$ for A.L.=1.0, and it is reduced to $1\% - 10\%$ and $1\% - 5\%$ for A.L.=1.1 and 1.2, respectively. The expected median increase in the response is $5\% - 10\%$ for A.L.=1.0, $10\% - 20\%$ for A.L.=1.1, and $20\% - 30\%$ for A.L.=1.2, as shown in Figure 7-8(b). Considering the observed probabilities of amplification along with the median percentage increase values, it can be concluded that consideration of soil-structure interaction in the analysis may increase the deformation and stress within the structure. However, the total risk of having amplification in the expected response is relatively low.

7.10.2 Amplification Risk in Structural Drift

As shown in Figure 7-8(c), the probability of amplification in structural drift is $35\% - 60\%$, $10\% - 30\%$, and $5\% - 20\%$ for A.L.=1.0, 1.1 and 1.2, respectively. The corresponding median percentage increase in the response is $5\% - 15\%$ for A.L.=1.0, $20\% - 30\%$ for A.L.=1.1, and $30\% - 45\%$ for A.L.=1.2, as shown in Figure 7-8(d). Considering the probabilities of amplification in structural drift along with the median percentage increase values, it has to be emphasized again that soil-structure interaction effects cannot be simply ignored in the calculation of structural drift. Furthermore, as shown in Figure 7-5(b), there is always a possibility of encountering extreme cases where the amplification in the structural drift is almost 60%.

7.10.3 Amplification Risk in Total Displacement

Similar trends and conclusions as presented for structural drift are observed for total displacement, as shown in Figure 7-8(e)-(f). The reason for this similarity is that in both cases the rigid body rocking motion is prominent. The probabilities of amplification are $40\% - 80\%$, $15\% - 50\%$, and $10\% - 30\%$, and the corresponding median percentage increase values are $5\% - 20\%$, $20\% - 35\%$, and $30\% - 45\%$ for A.L.=1.0, 1.2, and 1.5, respectively.

7.10.4 Amplification Risk in Structural Acceleration

Since the modification in structural acceleration due to soil-structure interaction effects is similar to that of structural distortion when structure behaves linearly, analogous risk is also expected.

7.10.5 General Comments

The observed trends in Figure 7-8 also show: (i) the probability of having amplification in structural response is higher when stiff structures ($T_{FB} < 0.6\ s$) are considered, indicating that stiff structures are more likely to exhibit detrimental soil-structure interaction effects; and (ii) obviously, if higher levels of safety are required, larger amplification values in the response must be considered.

7.11 Identification of Detrimental Soil-Structure Interaction Scenarios in Terms of Structural Strength Demand

Since it is recognized that considering soil-structure interaction can cause amplification in the structural acceleration, or strength demand, contradicting the prevailing view in most conventional building design codes, it is important to identify scenarios for which this consideration will result in amplification. As already mentioned it is the combined effect of system properties and ground motion characteristics that may result in detrimental soil-structure interaction effects on structural response. This fact is demonstrated in Figure 7-9, as an example, by showing the histogram of ground motions causing amplification in structural acceleration for the set of models with $T_{FB} = 0.2, 0.6, 1.0$ and 1.8 s.

Clearly, for some ground motions the soil-structure interaction effects increase the structural response for a large number of soil-structure models, while for other ground motions the soil-structure interaction effects were either trivial or absent. It should also be noted that at lower periods, more ground motions have a larger number of soil-structure models that show increased structural acceleration. This point clarifies why the likelihood of having an amplified structural acceleration due to soil-structure interaction effects is higher for stiffer structures.

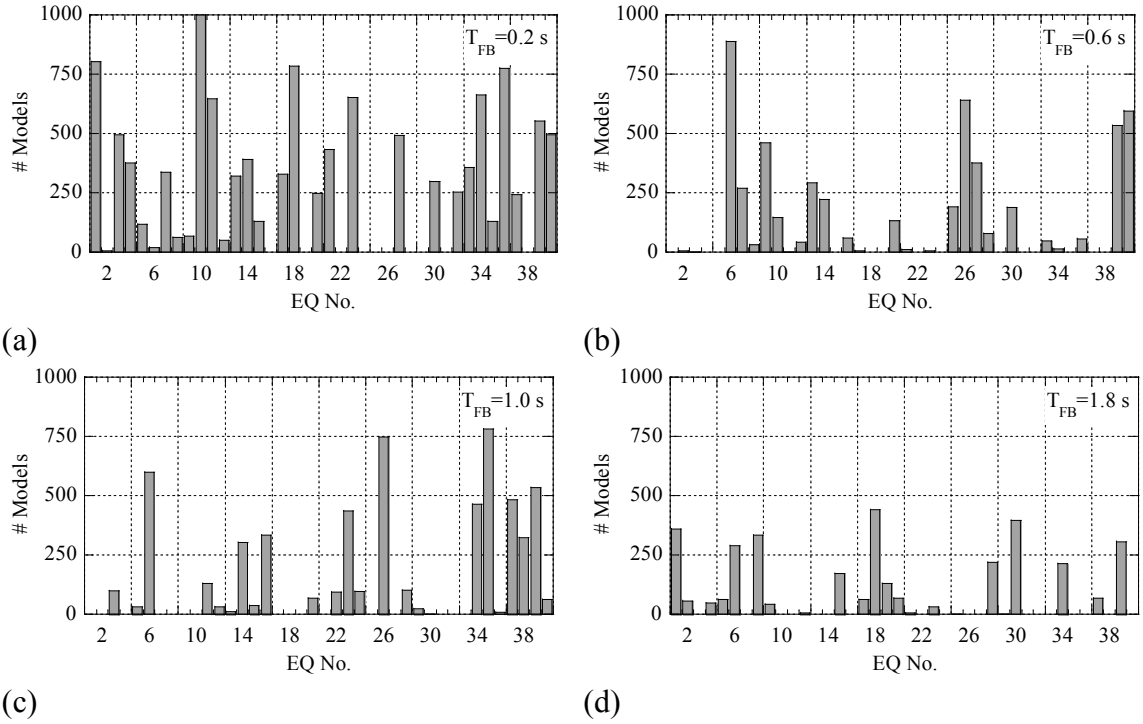

Figure 7-9. Histogram of the ground motions causing amplification in structural distortion for group of models with: (a) T_{FB}=0.2 s; (b) T_{FB} =0.6 s; (c) T_{FB} =1.0 s; and (d) T_{FB} =1.8 s.

To investigate what characteristic of the ground motion makes it produce amplification in the structural distortion, the maximum acceleration response of the soil-structure models are compared with the maximum acceleration response of the fixed-base models (acceleration response spectrum) for two types of earthquakes. In particular, one with significant detrimental effects, and a second with no detrimental effects. Figure 7-10 shows this comparison for models with $T_{FB} = 1.0$ s and for earthquakes number 23 and 2. In this figure, solid line represents the acceleration response spectrum of the considered input ground motions $(S_a)_{EQ}$, bold symbols are the computed maximum acceleration response of the fixed-base model $(a_s)_{FB}$ and open symbols are the maximum acceleration response of soil-structure models $(a_s)_{SSI}$ with $T_{FB} = 1.0$ s.

Clearly, the response pattern of the soil-structure models (points represented by open symbols) closely follows the shape of the acceleration response spectrum of the ground motions considered (solid lines). However, some deviation around the spectrum line is apparent and thus the responses could be either beyond or below the spectrum line. This trend along with the fact that system period increases due to foundation flexibility

($T_{SSI} > T_{FB}$) lead to a simple rule for identifying soil-structure interaction scenarios with detrimental effects.

Soil-structure interaction will result in detrimental effects or increase in the structural response relative to that of the fixed-base model if the response spectrum of the input ground motion has an ascending branch, Figure 7-10(a), in the range of periods slightly greater than T_{FB}. On the other hand, if the spectrum has a descending branch in this range of periods, soil-structure interaction effects will be beneficial and will cause a decrease in the structural response, Figure 7-10(b).

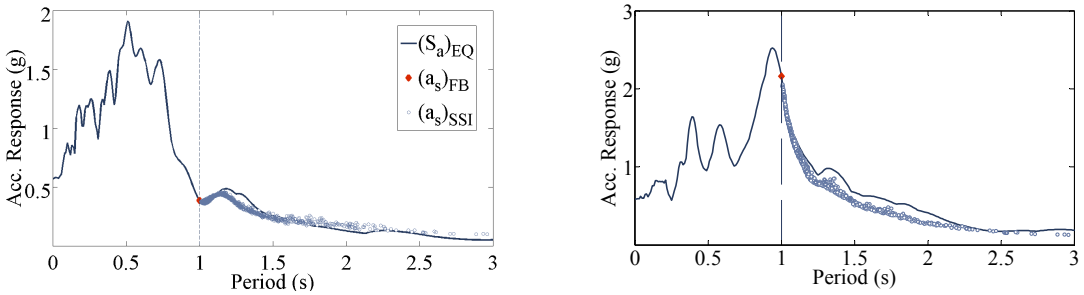

Figure 7-10. Comparison between the input acceleration response spectrum and the acceleration response of the soil-structure models considered for: (a) EQ 23 (PGA=0.24g); and (b) EQ 2 (PGA=0.31g) at T_{FB}=1.0 s.

The observed behaviour can be conceptually summarized as depicted in Figure 7-11. This figure indicates that to define whether considering soil-structure interaction is beneficial or detrimental, the response of two systems: (i) the original fixed-base system and (ii) the substitute fixed-base representation of the original soil-structure system have to be compared using the acceleration response spectrum for the input ground motion. The substitute system is defined as a fixed-base system with the same mass and stiffness as the original soil-structure system, but with a modified damping. This substitute system has also to be subjected to a modified input ground motion.

The period of the soil-structure system, which is also equals to the period of the substitute fixed-base system, is always greater than the period of the original fixed-base system ($T_{SSI} > T_{FB}$). Hence, due to this period shift, the response of the original fixed-base system $S_a(T_{FB})$ is shifted to $S_a(T_{SSI})$ on the input acceleration spectrum. In

addition, as a result of having a modified damping, the acceleration response of the substitute fixed-base system $(a_s)_{SSI}$ varies either bellow or beyond $S_a(T_{SSI})$. Based on this reasoning, if the resulting $(a_s)_{SSI}$ is greater than $S_a(T_{FB})$, then detrimental soil-structure interaction effects are expected. Clearly, depending on the characteristics of acceleration response spectrum in the region between fundamental periods of the fixed-base system and corresponding soil-structure system, soil-structure interaction may result in either beneficial or detrimental effects.

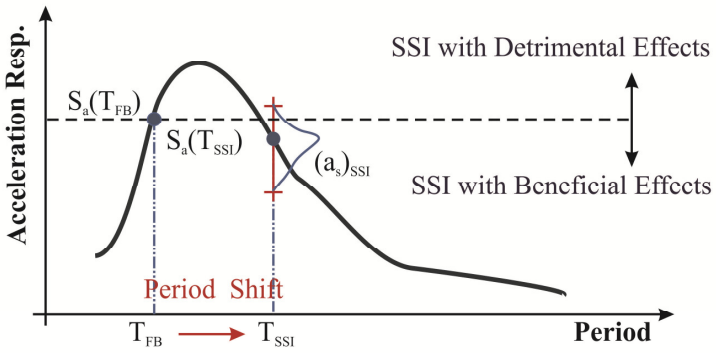

Figure 7-11. The conceptual presentation of beneficial or detrimental effects of soil-structure interaction on structural strength demand.

To quantify the variation of $(a_s)_{SSI}/S_a(T_{SSI})$, its probability of occurrence through the related variation range was evaluated. Figure 7-12 illustrates this quantification where each circle represents the probability of a certain value of $(a_s)_{SSI}/S_a(T_{SSI})$ among all the resulted values, considering one certain input ground motion and all soil-structure models. In addition, Figure 7-12 shows the median probability curve which is produced to represent the likelihood of $(a_s)_{SSI}/S_a(T_{SSI})$ for 50% of the cases and more.

Clearly, the ratio of $(a_s)_{SSI}/S_a(T_{SSI})$ varies between 0.4-1.3 and it is more likely to vary in the range of $0.8-1.0$. This observation emphasizes that soil-structure interaction may increase or decrease the structural strength demand. However, it is more likely to have a reduction in the response than an amplification. It should also be noted that the probability of having an amplification in the structural strength demand is small, but not negligible.

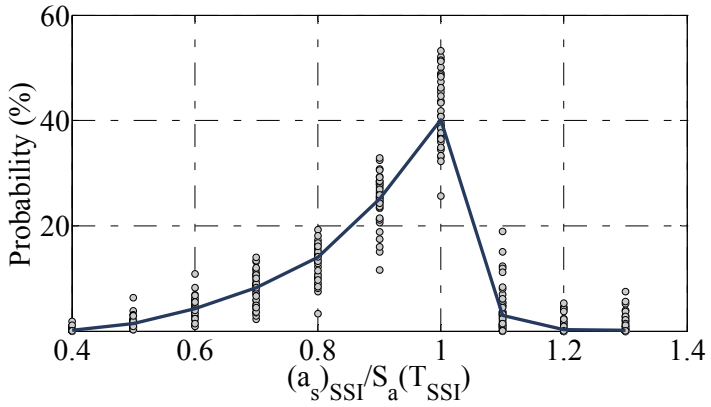

Figure 7-12. Probability of $(a_s)_{SSI}/S_a(T_{SSI})$ for all considered EQs and models.

7.12 Summary

A comprehensive Monte Carlo simulation using an established rheological soil-shallow foundation-structure model was carried out to systematically investigate the effects of soil-structure interaction on the seismic response of structures. In the analyses, the structure was represented by a linear single-degree-of-freedom system while the nonlinear stress-strain relationship of the soil was approximated by an equivalent linear model. The process of random generation of models was designed to cover a wide range of soil, foundation and structure properties and was constrained to yield realistic and representative soil-foundation-structure models. To account for variability in the input ground motion, 40 different ground motions were used as input in the time-history analyses resulting in a comprehensive set of 1.36 million simulations. The key findings from these analyses are summarized:

1) The existing uncertainty in input ground motion and variability in model parameters cause a significant variation in the foundation response. Considering the observed median values and associated dispersion results in the fact that foundations will experience larger horizontal displacement and rocking when structures with longer periods are considered. In this context, foundation response spectra, similar to that for displacement response spectra of ground motions, can be established.

2) The contribution of foundation rocking to the total displacement is more significant compared to the contribution of horizontal foundation

displacement. Furthermore, horizontal foundation displacement is more important for the case of stiffer structures, while foundation rocking plays a more significant role for structures with periods in the range of $0.6 - 1.2$ s.

3) Consideration of soil-structure interaction in dynamic analysis with linear structural behaviour may increase the structural distortion up to 20%, even though, in a median sense, a reduction is expected. Taking into account the probability of having amplification in the structural distortion, $10\% - 30\%$, along with the median percentage increase values, $5\% - 10\%$, implies the risk of having amplification in the structural distortion is relatively low. Since the structure behaves linearly, similar trends and conclusions can be also made if structural acceleration is considered.

4) The likelihood of having amplification in the structural drift rises to $40\% - 60\%$, while the likely maximum amplification might be up to 70%. The Corresponding values are more significant for total displacement. Specifically, the probability of having amplification is $45\% - 80\%$, and the maximum amplification is 100% considering the substantial probability of amplification and expected maximum response in terms of structural drift and total displacement, it is suggested the soil-structure interaction effects has to be considered in second order ($P - \Delta$) and pounding studies.

5) In general, the probability of having amplification in the structural response is higher for stiffer structures ($T_{FB} < 0.6$ s), indicating the stiff structures are more likely to exhibit detrimental soil-structure interaction effects. However, the median amplification level is effectively similar for all period ranges.

6) There is a clear link between the increase in the structural strength demand due to soil-structure interaction effects and the response spectrum characteristics of the ground motion. Detrimental soil-structure interaction effects or amplification in the structural strength demand occur for ground motions having an ascending branch in the response spectrum in the range of periods slightly greater than fundamental structural period.

References

[1] P. C. Jennings and J. Bielak, "Dynamics of building-soil interaction," *Bulletin of the Seismological Society of America,* vol. 63, pp. 9-48, 1973.

[2] A. S. Veletsos and J. W. Meek, "Dynamic behaviour of building-foundation systems," *Earthquake Engineering and Structural Dynamics,* vol. 3, pp. 121-138, 1974.

[3] A. S. Veletsos and V. D. Nair, "Seismic interaction of structures on hysteretic foundations," *Journal of Structural Engineering,* vol. 101, pp. 109-129, 1975.

[4] ASCE-7, "Minimum design loads for buildings and other structures," ed: Amarican Society of Civil Engineers, 1998.

[5] FEMA440, "Improvement of nonlinear static seismic analysis procedures," ed. Redwood City, California: Applied Technology Council, 2005.

[6] ATC, "Improvement of Nonlinear Static Seismic Analysis Procedures (FEMA 450)," ed. Washington, D.C.: Applied Technology Council, Federal Emergency Management Agency, 2005.

[7] J. P. Stewart*, et al.*, "Revisions to soil-structure interaction procedures in NEHRP design provisions," *Earthquake Spectra,* vol. 19, pp. 677-696, 2003.

[8] A. S. Veletsos and B. Verbic, "Dynamics of elastic and yielding structure-foundation systems," presented at the Proceeding of the 5th World Conference on Earthquake Engineering, Rome, Italy, 1974.

[9] M. Ciampoli and P. E. Pinto, "Effects of soil-structure interaction on inelastic seismic response of bridge piers," *Journal of Structural Engineering,* vol. 121, pp. 806-814, 1995.

[10] J. Bielak, "Dynamic response of non-linear building-foundation systems," *Earthquake Engineering & Structural Dynamics,* vol. 6, pp. 17-30, 1978.

[11] E. Miranda and V. V. Bertero, "Evaluation of strength reduction factors for earthquake-resistant design," *Earthquake Spectra,* vol. 10, pp. 357-357, 1994.

[12] J. Avilés and L. E. Pérez-Rocha, "Soil-structure interaction in yielding systems," *Earthquake Engineering and Structural Dynamics,* vol. 32, pp. 1749-1771, 2003.

[13] J. Zhang and Y. Tang, "Dimensional analysis of structures with translating and rocking foundations under near-fault ground motions," *Soil Dynamics and Earthquake Engineering,* vol. 29, pp. 1330-1346, 2009.

[14] G. Mylonakis and G. Gazetas, "Seismic soil-structure interaction: beneficial or detrimental?," *Journal of Earthquake Engineering,* vol. 4, pp. 277-301, Jul 2000.

[15] G. Gazetas and G. Mylonakis, "Seismic soil-structure interaction: new evidence and emerging issues," in *Geotechnical Earthquake Engineeirng and Soil Dynamics 3: Proceedings of Speciality Conference*, ed N.Y.: ASCE, 1998.

[16] S. S. F. Mehanny and A. S. Ayou, "Variability in inelastic displacement demands: Uncertainty in system parameters versus randomness in ground records," *Engineering Structures,* vol. 30, pp. 1002-1013, Apr 2008.

[17] A. Barcena and L. Esteva, "Influence of dynamic soil-structure interaction on the nonlinear response and seismic reliability of multistorey systems," *Earthquake Engineering & Structural Dynamics,* vol. 36, pp. 327-346, Mar 2007.

[18] S. Jin*, et al.*, "Response variability for a structure with soil-structure interactions and uncertain soil properties," *Probabilistic Engineering Mechanics,* vol. 15, pp. 175-183, 2000.

[19] L. D. Lutes*, et al.*, "Response variability of an SSI system with uncertain structural and soil properties," *Engineering Structures,* vol. 22, pp. 605-620, 2000.

[20] P. Raychowdhury, "Effect of soil parameter uncertainty on seismic demand of low-rise steel buildings on dense silty sand," *Soil Dynamics and Earthquake Engineering,* vol. 29, pp. 1367-1378, 2009.

[21] J. P. Wolf, *Foundation Vibration Analysis Using Simple Physical Models*. Englewood Cliffs, N.J.: Prentice-Hall, 1994.

[22] H. B. Seed and I. M. Idriss, "Soil moduli and damping factors for dynamic response analysis," Earthquake Engineering Research Centre Report EERC 7010, 1970.

[23] J. M. Duncan, "Factors of safety and reliability in geotechnical engineering," *Journal of Geotechnical and Geoenvironmental Engineering,* vol. 126, pp. 307-314, 2000.

[24] D. Breysse*, et al.*, "A generic approach to soil-structure interaction considering the effects of soil heterogeneity," vol. 55, ed, 2005, pp. 143-150.

[25] NZS1170.5, "Structural design actions, part 5: earthquake actions," ed. New Zealand, 2004.

[26] G. S. Fishman, *Monte Carlo: concepts, algorithms, and applications*. N.Y.: Springer, 1996.

[27] A. Carr, "Ruaumoko 2D, Nonlinear FEM Computer Program," ed. New Zealand: University of Canterbury, 2009.

[28] N. Shome*, et al.*, "Earthquakes, records, and nonlinear responses," *Earthquake Spectra,* vol. 14, pp. 469-500, 1998.

CHAPTER 8. Stochastic Quantification of Seismic Soil-Structure Interaction II: "Structures with Nonlinear Behaviour on Equivalent Linear Soil-Foundation Interface"

Abstract. This chapter presents the effects of structural nonlinearity on the role of soil-structure interaction in modifying seismic structural response. In this regard, three different types of structural force-deflection behaviour including Takeda, bilinear elasto-plastic and Takeda with negative post-yield stiffness are examined. The same stochastic methodology used in Chapter 7 is followed to enable direct comparison. Specifically, 4.08 million nonlinear time-history simulations are run using a wide range of realistic soil-structure models and input ground motions. Using the statistical outcomes, the effects of soil-structure interaction on structural response are quantified and the risk of having detrimental effects is evaluated in the context of realistic nonlinear structural response. Furthermore, an attempt is made to illustrate the importance of ground motion spectral characteristics in the risk of having amplification in the seismic structural response.

8.1 Soil-Structure System Considered

"Structure with Nonlinear Behaviour on Equivalent Linear Soil-Foundation Interface"

The soil-structure model used for the series of analyses whose results are presented in this chapter is constituted from a single-degree-of-freedom structure with nonlinear behaviour and a set of equivalent linear springs and dashpots representing the soil-shallow foundation interface, as shown in Figure 8-1. For this model, the same considerations as explained in Section 7.4 are applied. However, three different hysteretic types were selected to represent the cyclic force-deflection ($F - \delta$) behaviour of the structure, including: (i) Takeda (TK), (ii) bilinear elasto-plastic (EP) and (iii) Takeda with negative post-yield stiffness (TKN).

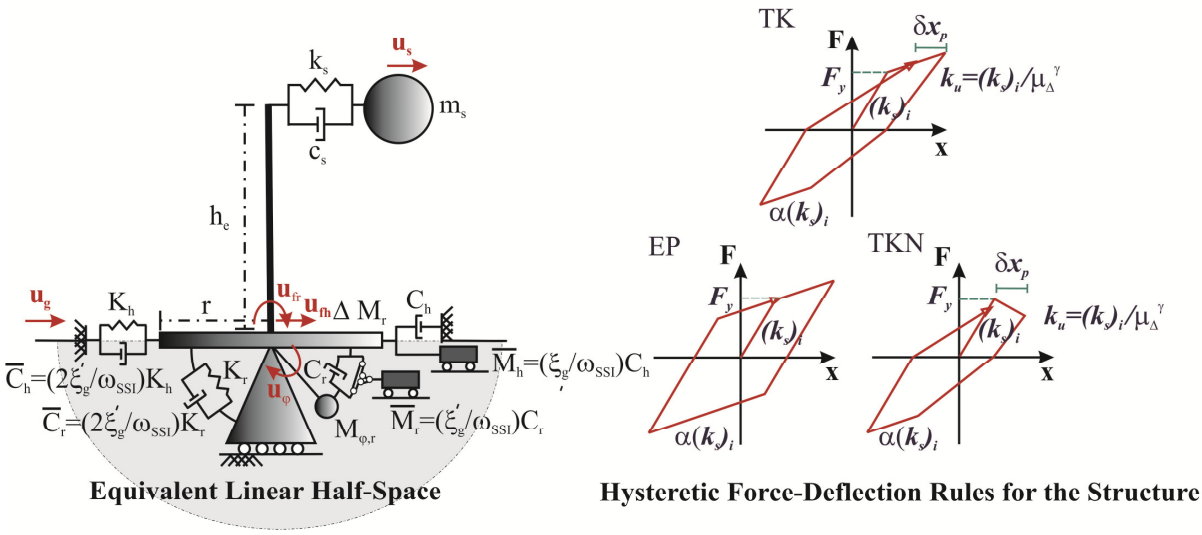

Figure 8-1. Soil-structure model considered: structure with nonlinear behaviour on equivalent linear soil-foundation interface.

The *Takeda* model was selected to represent the behaviour of a new designed concrete-framed structure, and to be used as a benchmark reference for investigating the effects of structural nonlinearity on soil-structure interaction effects. In addition, to compare the effects of structural nonlinearity when different hysteretic scenarios are utilized, the bilinear elasto-plastic and Takeda with negative post-yield stiffness models were chosen. The *bilinear elasto-plastic* model represents the behaviour of a new designed

steel-framed structure, and the *Takeda with negative post-yield stiffness* model shows the response of a structure with either significant second-order $(P-\Delta)\Delta$ or strength degradation effects.

8.2 The Effects of Structural Nonlinearity on Foundation Response

Variation in foundation response in the horizontal and rocking directions, u_{fh} and u_{fr}, are illustrated in Figure 8-2 for the structures with Takeda hysteretic behaviour. Similar trends to those seen for structures with linear behaviour in Chapter 7 are repeated. Thus, the same discussion, interpretation and conclusion apply. However, the range of periods for which the structures might be more affected by foundation rocking is changed to $0.6-1.0$ s. In addition, the shape of foundation rocking spectrum has to be modified. In this context, a decreasing trend instead of a constant line should be considered after $T_{FB}=1.0$ s.

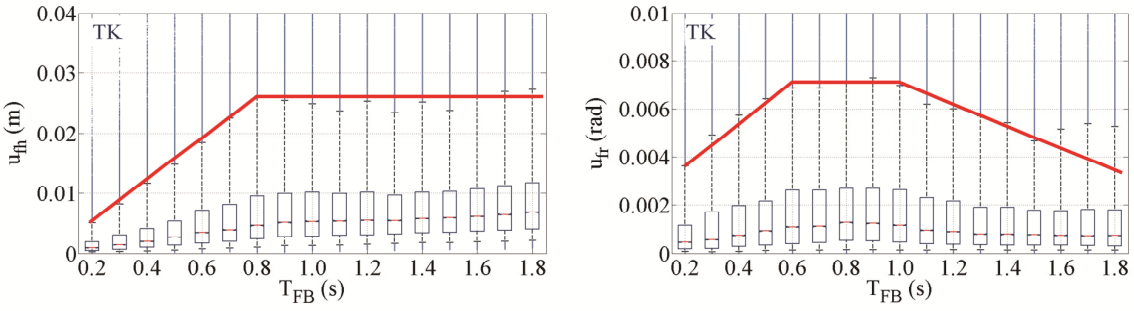

(a) (b)

Figure 8-2. Foundation response spectra for structures with Takeda hysteretic behaviour: (a) horizontal displacement spectrum; and (b) rocking spectrum.

Both foundation responses are also compared for the cases of structures with Takeda hysteretic behaviour and linear behaviour in Figure 8-3, emphasizing only the 5^{th}, 50^{th} (median) and 95^{th} percentiles. It is clear that, considering structural nonlinearity reduces the 95^{th} percentile and the median values, even though it does not have any significant effect on the 5^{th} percentile. This observation results in the fact that structural nonlinearity reduces the possible maximum foundation response and, consequently, reduces the related variation in foundation response. Figure 8-3 also shows that structural nonlinearity is more significant and pronounced for: (i) the 95^{th} percentile

instead of the median; (ii) foundation rocking instead of horizontal foundation displacement; and (iii) structures with longer fundamental periods instead of stiff structures with shorter periods.

The modification in foundation response due to structural nonlinearity has also been quantitatively investigated. In this regard, the ratio between foundation response when structure behaves nonlinearly to the response when it behaves linearly is considered. The results are shown in Figure 8-4.

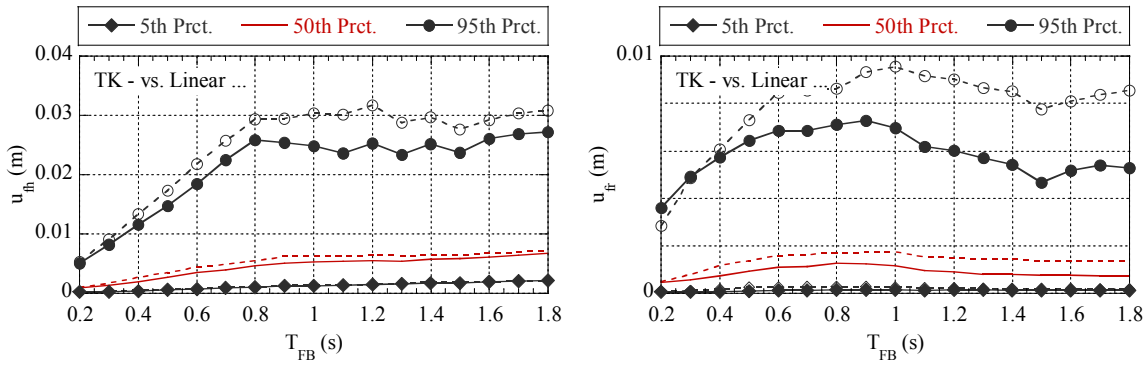

(a) (b)

Figure 8-3. The effects of structural nonlinearity on foundation response spectra at the 5th, 50th (median) and 95th percentiles: (a) horizontal displacement spectrum; and (b) rocking spectrum.

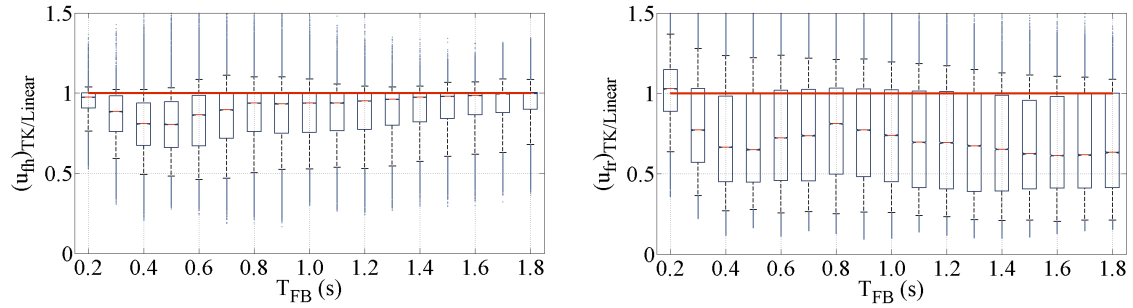

(a) (b)

Figure 8-4. The effects of structural nonlinearity on foundation response spectra: (a) horizontal displacement spectrum; and (b) rocking spectrum.

For almost 75% of the scenarios, structural nonlinearity reduces horizontal foundation displacement and this reduction with 95% confidence is limited to 50%, as shown in Figure 8-4(a). On the other hand, it is important to note that there is always up to a 25% probability that horizontal foundation displacement might be increased due to structural

nonlinearity. However, this increase is not significant and in worst case with a 95% probability can be limited to 10%. If the median values are considered, the reduction in horizontal foundation displacement changes between $0\% - 20\%$ depending on the values of fundamental structural period. Note that this reduction is more significant for systems with fundamental period ranging between $0.3 - 0.7$ s.

Considering foundation rocking, with a similar probability of 75%, structural nonlinearity reduces the foundation response, as shown in Figure 8-4(b). However, in this case, the variation range in the reduction ratio is higher, such that a reduction of 75% may also occur. At the median, the reduction ratio varies between $20\% - 40\%$ depending on the fundamental structural period. Nevertheless, it is important to note that there is up to a 25% probability that foundation rocking might be increased considering structural nonlinearity. Importantly, the resulting amplification in foundation response cannot be ignored. This amplification ranges between $10\% - 40\%$ with the tendency to increase with structural rigidity. Finally, taking into account the extent of variation in foundation response and the expected reduction at the median, it is concluded that structural nonlinearity has a more significant effect on foundation rocking than horizontal foundation displacement.

8.3 The Effects of Structural Nonlinearity on the Contribution of Foundation Response to Total Displacement

If the effects of structural nonlinearity are considered, the contribution of foundation response to total displacement follows the same trend as that for structures with linear behaviour, except that the percentage contribution is different. These values are shown in Figure 8-5.

To investigate the changes in more detail, the ratio between the percentage contribution in the case of structures with Takeda hysteretic behaviour and those with linear behaviour are calculated and presented in Figure 8-6. Clearly, by taking into account the extension of dispersion, structural nonlinearity may either decrease or increase the contribution of foundation response to total displacement. The possible reduction in the

percentage contribution has almost a 75% probability for both foundation responses, meaning there is always up to a 25% chance of having amplification in the response.

If the contribution of horizontal foundation displacement to total displacement u_{fh}/u_{tot} is considered, the maximum reduction due to structural nonlinearity is about 75% and is expected for stiffer structures, while the maximum amplification is about 50% and is expected for structures with longer fundamental periods. When foundation rocking contributes to total displacement $h_e u_{fr}/u_{tot}$, the maximum reduction due to structural nonlinearity is almost 80% and is similar through all fundamental structural periods. In contrast, the maximum amplification is about 40% and is expected for stiffer structures.

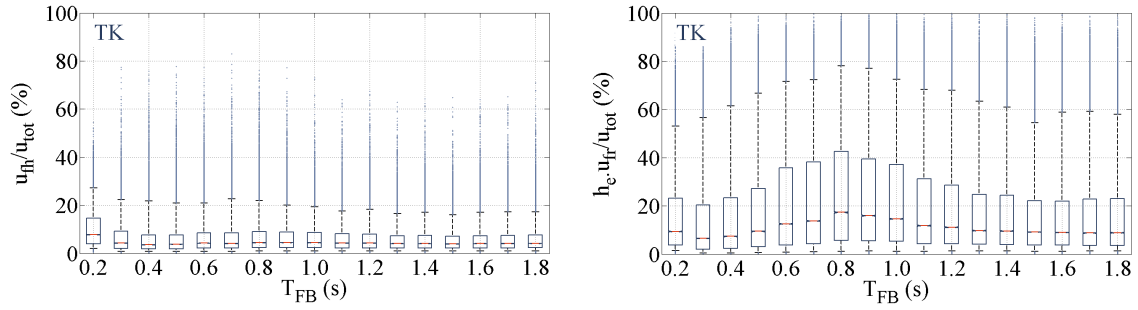

(a) (b)

Figure 8-5. The contribution of foundation response to total displacement for structures with Takeda hysteretic behaviour: (a) horizontal displacement contribution; and (b) rocking contribution.

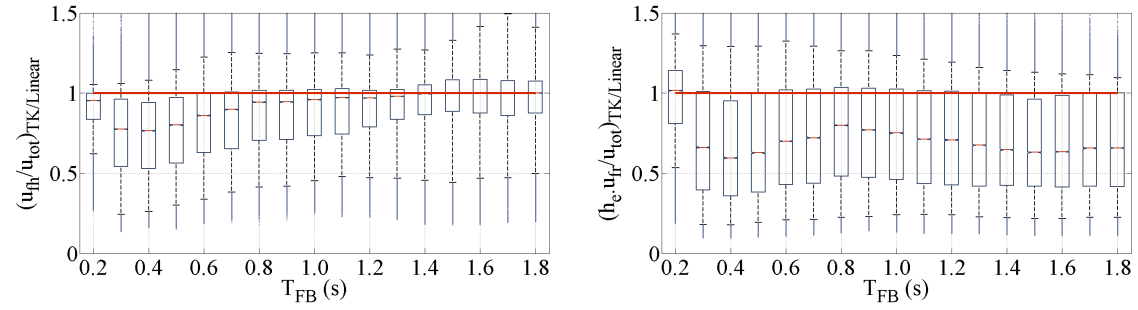

(a) (b)

Figure 8-6. The effects of structural nonlinearity on the contribution of foundation response to total displacement: (a) contribution of horizontal displacement; and (b) contribution of rocking.

8.4 The Effects of Structural Nonlinearity on the Structural Response Modification Spectra

To investigate the effects of structural nonlinearity on soil-structure interaction induced modification in structural response, Takeda hysteretic behaviour is considered. In this regard, the corresponding response modification spectra for structural distortion u_s, structural drift dr, total displacement u_{tot} and structural acceleration a_s are compared with the previous results presented for structures with linear behaviour in Chapter 7. Structural response modification spectra for structures with Takeda hysteretic behaviour are illustrated in Figure 8-7.

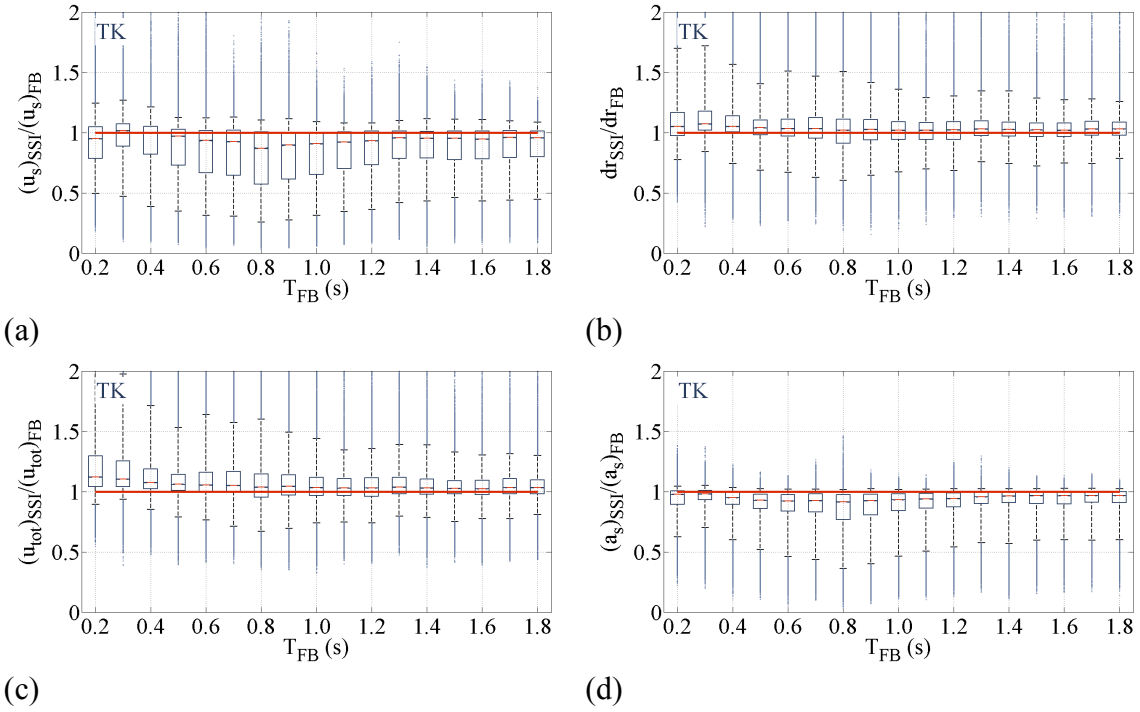

Figure 8-7. Response modification spectra for structures with Takeda hysteretic behaviour, considering: (a) structural distortion; (b) structural drift; (c) total displacement; and (d) structural acceleration.

8.4.1 Soil-Structure Interaction Effects on Structural Distortion

If structural distortion is considered, Figure 8-7(a), similar trends and values as those observed for structures with linear behaviour, Figure 7-5(a), are distinguishable. However, for the $25^{th} - 75^{th}$ percentile ranges, the response modification factors are greater if structural nonlinearity is considered.

To further investigate the changes on the variation boundaries and the median values, structural distortion modification factors at the 5^{th}, 50^{th} (median) and 95^{th} percentiles are compared for structures with Takeda hysteretic behaviour and those with linear behaviour, and the results are shown in Figure 8-8(a). It is clear that, structural nonlinearity has no significant effect on boundary lines. However, it increases the median values and also decreases the distance between the median and the 95^{th} percentiles. Such observation signifies that even though structural nonlinearity does not change the maximum reduction or maximum amplification in the structural distortion, it may increase the structural distortion modification factor in general terms by shifting the distribution.

This point is better illustrated in Figure 8-9(a) by presenting the ratio between the response modification factors for nonlinear and linear cases. It is clear that for nearly 75% of the considered scenarios, structural nonlinearity causes an increase in the structural distortion modification factor, and that this increase with a 95% probability is up to 100%. It should also be noted that for those 25% of the cases with a decrease in the response modification factor, the reduction is less than 20%. It is thus concluded that the beneficial soil-structure interaction effects on structural distortion are much less pronounced when structural nonlinearity is considered.

8.4.2 Soil-Structure Interaction Effects on Structural Drift

Modification in structural drift for structures with Takeda hysteretic behaviour and those with linear behaviour is compared next, Figure 8-7(b) vs. Figure 7-5(b). It is clear that the $25^{th} - 75^{th}$ percentile ranges become narrower indicating that structural nonlinearity decreases the dispersion around the median values, which, in turn, result in less variation in the response. It can also be stated that structural nonlinearity slightly reduces maximum reduction and maximum amplification in the structural drift, as shown in Figure 8-8(b). However, in terms of the ratio between the structural drift modification factors for nonlinear and linear cases, Figure 8-9(b), structural nonlinearity causes an increase for almost 75% of the scenarios and depending on the situation, an increase in the order of 50% may also occur.

Comparing the effects of structural nonlinearity on structural distortion and structural drift modification factors at the 95^{th}, 75^{th}, and 50^{th} (median) percentiles implies that the effects of structural nonlinearity on structural drift is not as extreme as it is for structural distortion. The reason is that an important part of structural drift is foundation rocking, which is added to the structural distortion. As shown in Figure 8-4(b), foundation rocking is reduced in many cases due to structural nonlinearity. This reduction is then able to partially cancel the amplification caused by structural distortion.

8.4.3 Soil-Structure Interaction Effects on Total Displacement

The effects of structural nonlinearity on the modification in total displacement are very similar to those discussed for structural drift, as can be seen in Figure 8-7(c), Figure 8-8(c) and Figure 8-9(c). For almost 75% of the scenarios, structural nonlinearity causes an increase in total displacement, and depending on the situation this increase may be in the order of 50%.

8.4.4 Soil-Structure Interaction Effects on Structural Acceleration

If structural acceleration is considered, in contrast to what has been observed for structures with linear behaviour, soil-structure interaction has either a beneficial role or very negligible detrimental effects, as shown in Figure 8-7(d). Consequently, it is conservative in a design procedure to ignore soil-structure interaction effects on structural acceleration (or similarly on base shear). Structural nonlinearity also reduces the maximum reduction in the structural acceleration, while it increases the median values, as shown in Figure 8-8(d).

In addition, structural nonlinearity increases the structural acceleration modification factor for almost 75% of the scenarios, and depending on the situation this increase can be up to 250%, as shown in Figure 8-9(d). High levels of increase in the structural acceleration due to structural nonlinearity imply that the current design code approach for calculation of the reduced based shear due to soil-structure interaction may be a significant oversimplification.

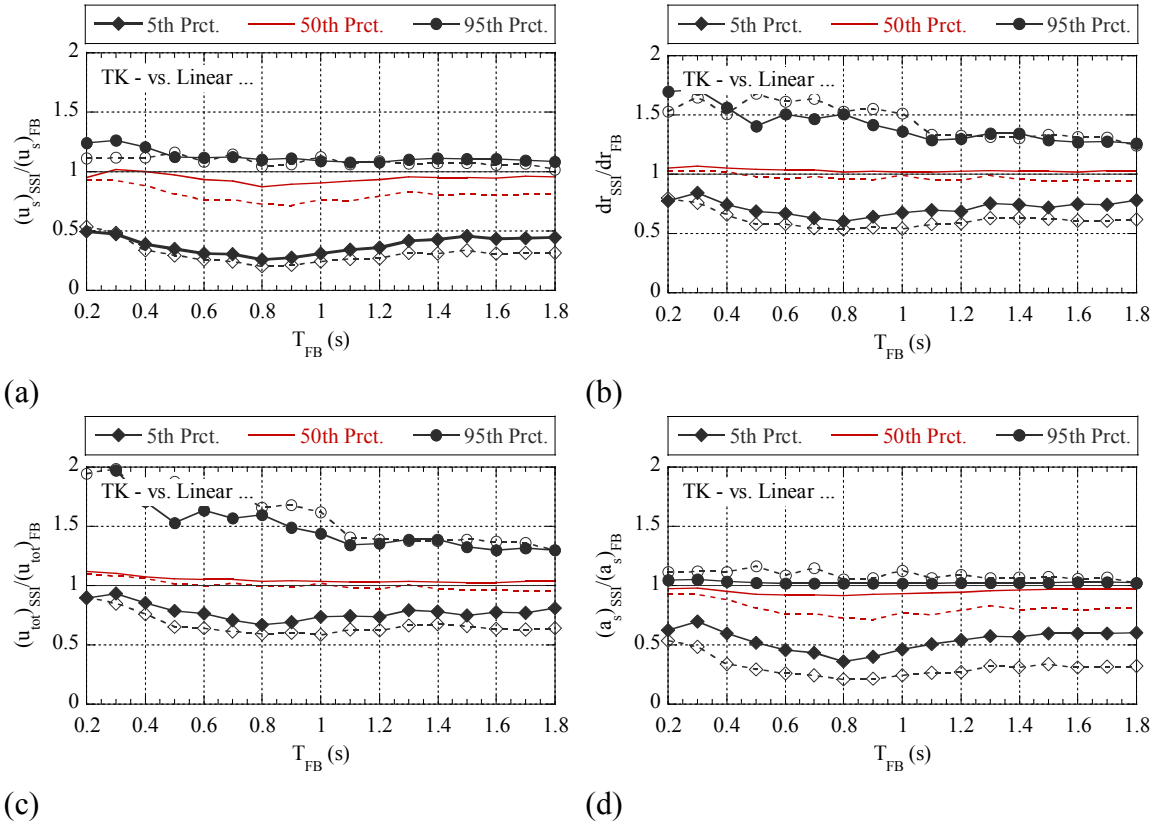

Figure 8-8. The effects of structural nonlinearity on structural response modification spectra at 5th, 50th (median) and 95th percentiles, considering: (a) structural distortion; (b) structural drift ; (c) total displacement ; and (d) structural acceleration.

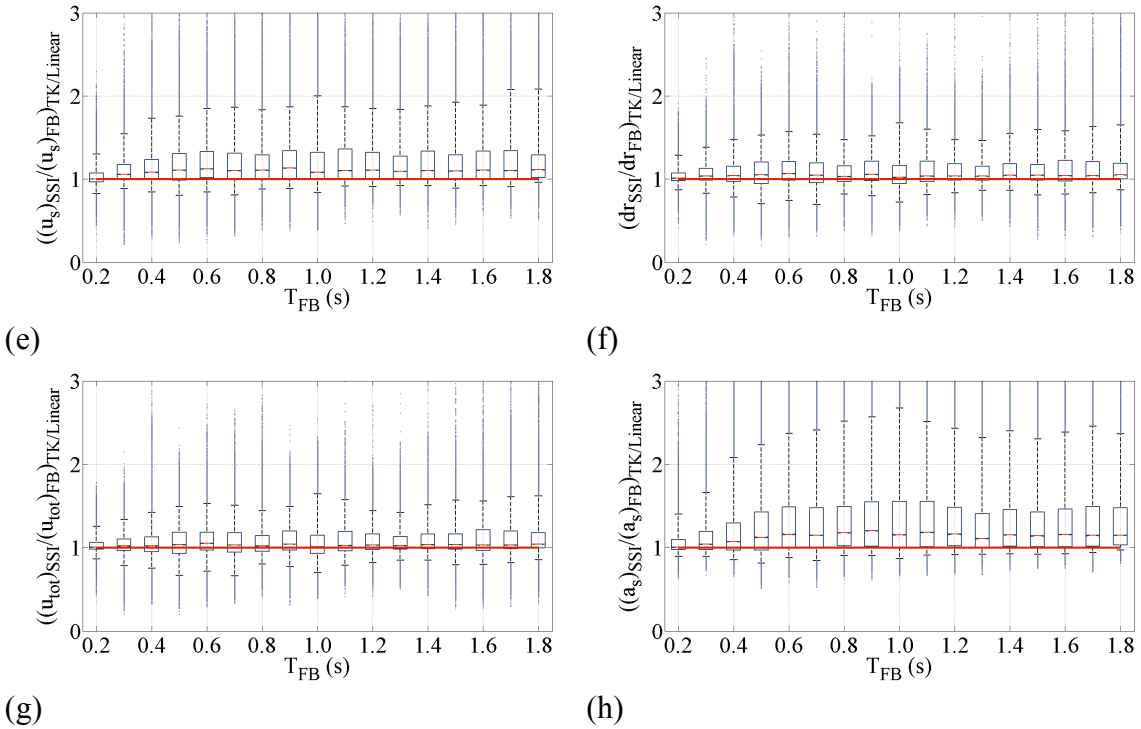

Figure 8-9. The effects of structural nonlinearity on structural response modification spectra, considering: (a) structural distortion; (b) structural drift; (c) total displacement; and (d) structural acceleration.

8.5 The Effects of Structural Hysteretic Force-Deflection Behaviour

To investigate the effects of soil-structure interaction on seismic structural response when different structural force-deflection ($F-\delta$) behaviour is considered, the response modification spectra for structures with Takeda (TK), bilinear elasto-plastic (EP) and Takeda with negative post-yield stiffness (TKN) hysteretic behaviour are compared. This comparison is presented in Figure 8-10. It shows the ratio between structural response modification factors for the cases considered.

Clearly, the median values and the values located in the 25^{th}-75^{th} percentile ranges are close to 1.0. The dispersion around median values is also limited to $\pm 20\%$ depending on the considered structural response and fundamental structural period. In addition, the modification in structural response for Takeda and Takeda with negative stiffness models is more similar than the corresponding values for the cases of Takeda and bilinear elasto-plastic.

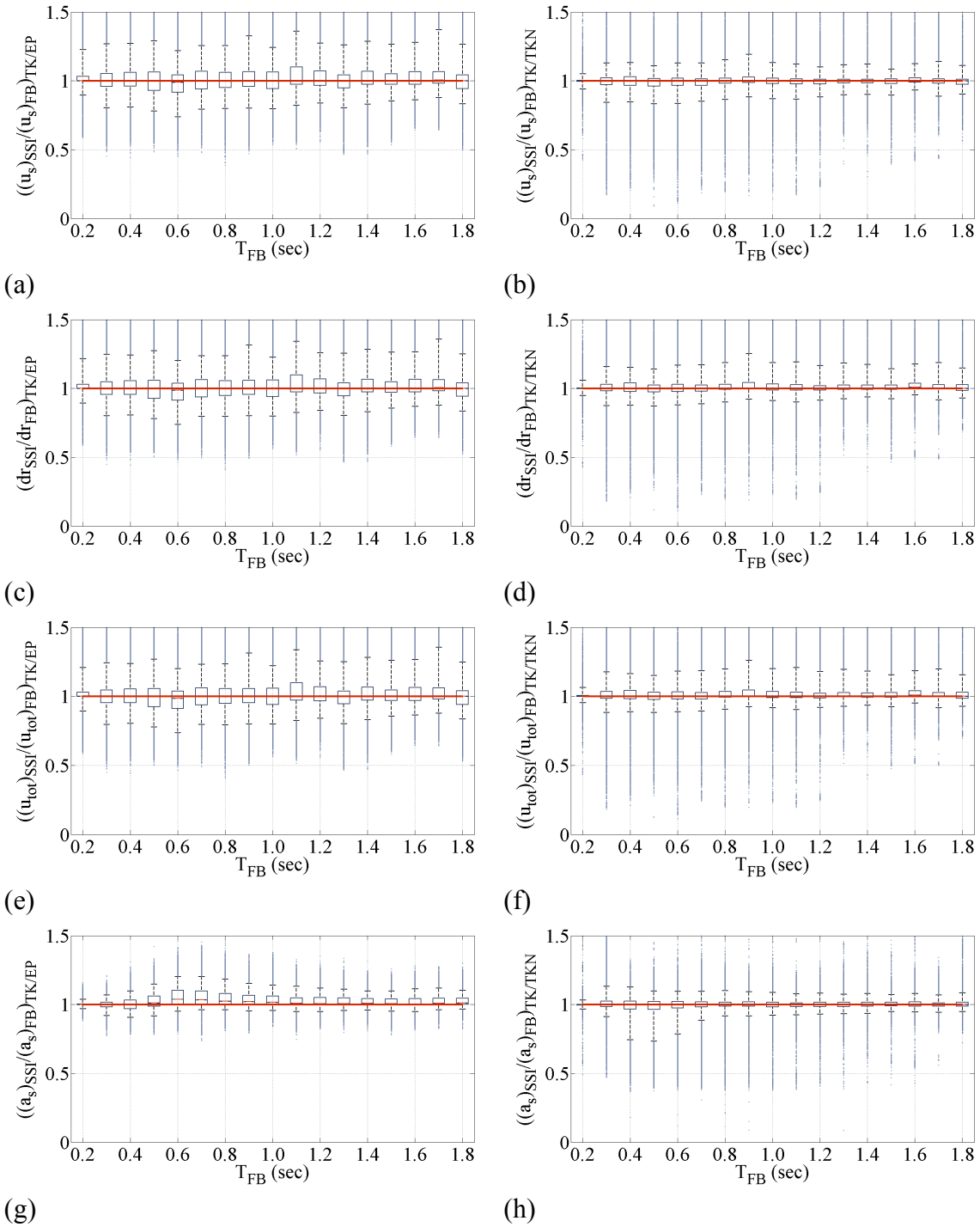

Figure 8-10. The effects of structural force-deflection behaviour on structural response modification spectra, considering: (a-b) structural distortion; (c-d) structural drift; (e-f) total displacement; and (g-h) structural acceleration.

Therefore, it can be concluded that the specific structural force-deflection behaviour does not have a significant effect on seismic structural response modification factors due to soil-structure interaction effects. In other words, even though structural nonlinearity may cause an increase in the response modification due to soil-structure interaction, this modification is independent of the type of general structural hysteretic model used in the analysis.

8.6 The Effects of Structural Nonlinearity on the Risk of Detrimental Soil-Structure Interaction Effects

The risk of detrimental soil-structure interaction effects for structures with Takeda hysteretic behaviour is shown in Figure 8-11. On the left-side, the probabilities of having amplification in structural response are presented across all considered periods, whereas on the right-side, the corresponding values of median percentage increase are shown. Comparing the values of probability of amplification and median percentage increase presented for the structures with Takeda hysteretic behaviour, Figure 8-11, and for those with linear behaviour, Figure 7-8, results in a general conclusion that structural nonlinearity increases the probability of amplification in structural response, but does not have a significant effect on median percentage increase. This conclusion is better presented in Figure 8-12, where the results for A.L.=1.0 and 1.2 are compared. Note that, in this illustration, the results for A.L.=1.1 were omitted only to make the presentation more transparent.

8.6.1 Amplification Risk in Structural Distortion

As briefly mentioned in Section 8.4 and clearly presented in Figure 8-12(a), the probability of amplification in the structural distortion due to soil-structure interaction effects are increased when structural nonlinearity is considered. The probability of amplification in the response is between $25\% - 60\%$ (instead of $10\% - 30\%$) for A.L.=1.0, and it reduces to $1\% - 10\%$ (instead of $1\% - 5\%$) for A.L.=1.2. Note that the increase in the probability values is more pronounced when A.L.=1.0 is taken into account.

However, if the median percentage increase in the response is considered, the modification due to structural nonlinearity is not that noticeable, as shown in Figure 8-12(b). The values of median percentage increase are $5\% - 10\%$ for A.L.=1.0 and $20\% - 40\%$ for A.L.=1.2.

8.6.2 Amplification Risk in Structural Drift

Similar to the results observed in the case of structural distortion, structural nonlinearity increases the probability of having amplified structural drift, as shown in Figure 8-12(c). The probabilities are $60\% - 80\%$ (instead of $35\% - 60\%$) for A.L.=1.0 and $10\% - 20\%$ (instead of $5\% - 20\%$) for A.L.=1.2. In terms of the median percentage increase, no significant change is observed due to structural nonlinearity, as shown in Figure 8-12(d). The median percentage increases are $5\% - 15\%$ for A.L.=1.0 and $30\% - 45\%$ for A.L.=1.2.

8.6.3 Amplification Risk in Total Displacement

The probability of amplification in total displacement when structural nonlinearity is considered change to $65\% - 90\%$ (instead of $40\% - 80\%$) and $10\% - 35\%$ (instead of $10\% - 30\%$) for A.L.=1.0 and 1.2, respectively. The corresponding values of median percentage increase are $5\% - 15\%$ for A.L.=1.0 and $30\% - 40\%$ for A.L.=1.2.

8.6.4 Risk of Amplification in Structural Acceleration

The quantified probability of amplification in structural acceleration is $15\% - 35\%$ for A.L.=1.0 and almost 0% for the other cases. It has to be noted that, structural nonlinearity does not have a significant effect on the probability of amplification in structural acceleration, in contrast to what has been seen for other structural responses.

Along with these probabilities, the corresponding median percentage increases are in the range of $1\% - 2\%$. Given the small values of either probability or median percentage increase, the risk of having amplification in structural acceleration is negligible when structural nonlinearity is considered.

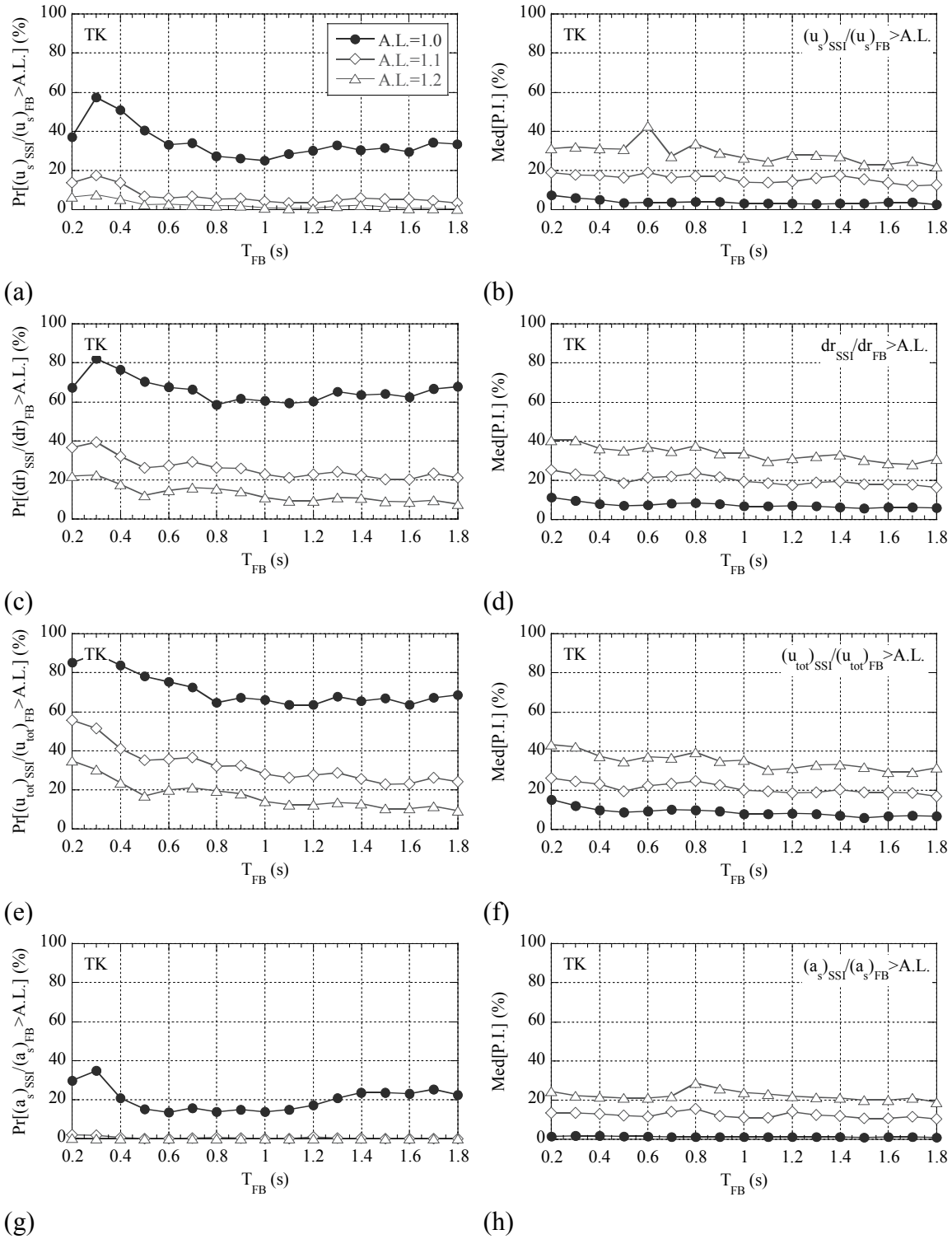

Figure 8-11. Risk spectra for structures with Takeda hysteretic behaviour: (left) probability of amplification in the response; (right) level of amplification in the response.

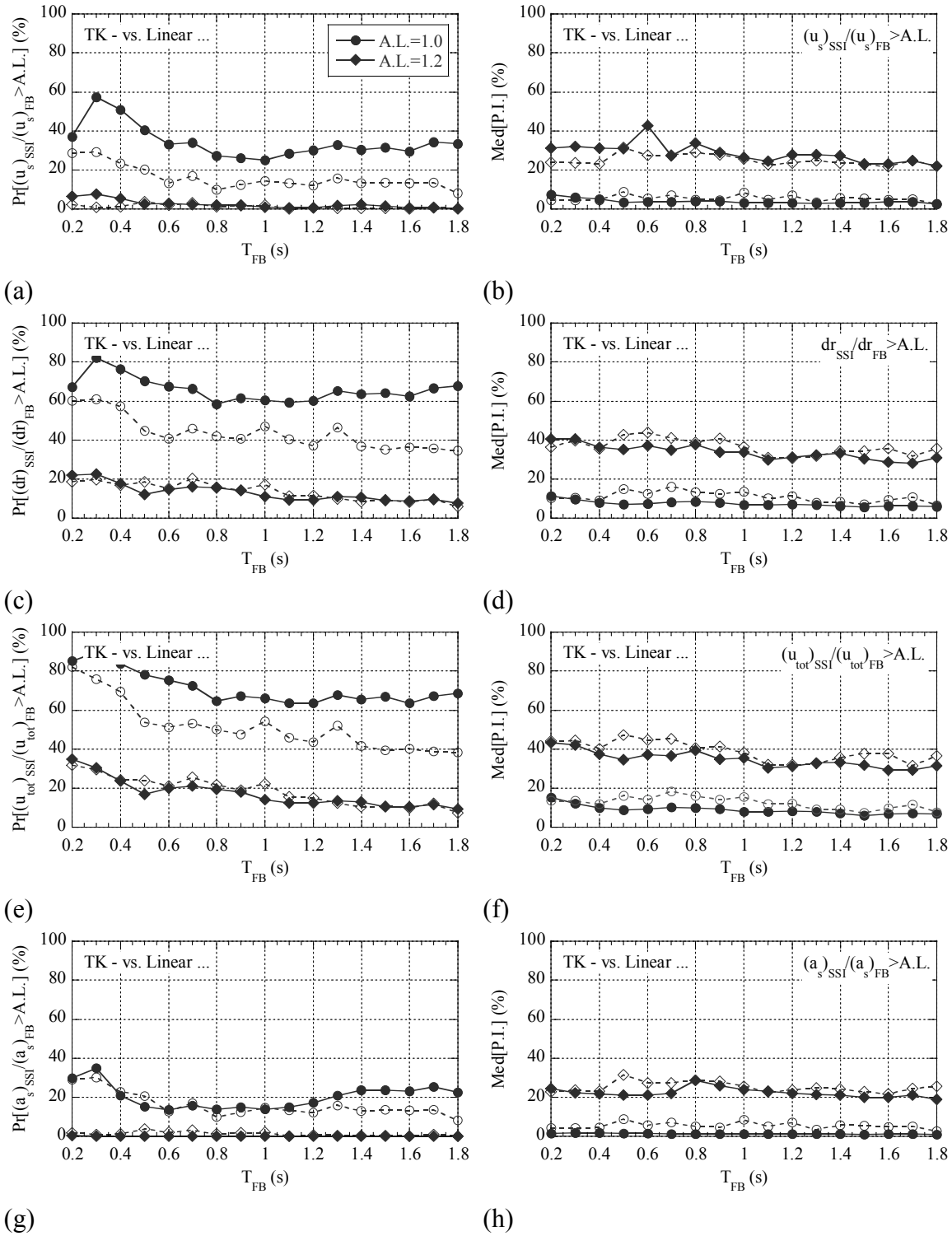

Figure 8-12. The effects of structural nonlinearity on risk spectra: (left) probability of amplification in the response; (right) level of amplification in the response.

8.7 The Risk of Detrimental Effects for Special Ground Motions

8.7.1 Selected Input Ground Motions

To investigate the effects of spectral ordinates of input ground motions on the risk of detrimental soil-structure interaction effects, a second suite of ground motions was chosen. The records in this suite were selected so that they are not following the conventional design spectrum. Instead, they have enhanced spectral ordinates at longer periods. Using these records makes it more likely to have an increase in the structural response when an increase in the fundamental period occurs due to soil-structure interaction. Six records were selected for this purpose and then scaled with different scaling factors to result in 15 records having peak ground acceleration (PGA) in the range of $0.3g - 0.8g$. Careful attention was made to have the scaling factors in the range of $0.3 - 3.0$, following the suggestion made in NZS 1170.5.

The selected ground motions were then used as an input for the nonlinear time-history simulations utilizing the previously generated models with Takeda hysteretic behaviour. The same approach adopted in Section 8.6 was followed. The comparison between the results for the new suite 2 and the original suite 1 are presented in Figure 8-13.

8.7.2 Quantification of the Risk

As shown in Figure 8-13(left), when A.L.=1.0 is considered, the probability of having amplification in structural response due to soil-structure interaction effects increases for almost all fundamental periods assumed. The level of increase in the probability of amplification clearly depends on the expected structural response and structural fundamental period. However, if a higher level of amplification is considered, such as A.L.=1.2, the increase in probability occurs only up to $T_{FB} = 1.0$ s, and a decreasing trend is observed after this value. The median percentage increase for A.L.=1.0 shows no significant difference between the results of the two suites of ground motions considered, as shown in Figure 8-13(right). However, if A.L.=1.2 is concerned, the median percentage increase is slightly higher for the second suite of ground motions up to $T_{FB} = 1.0$ s and no significant change is observed afterwards.

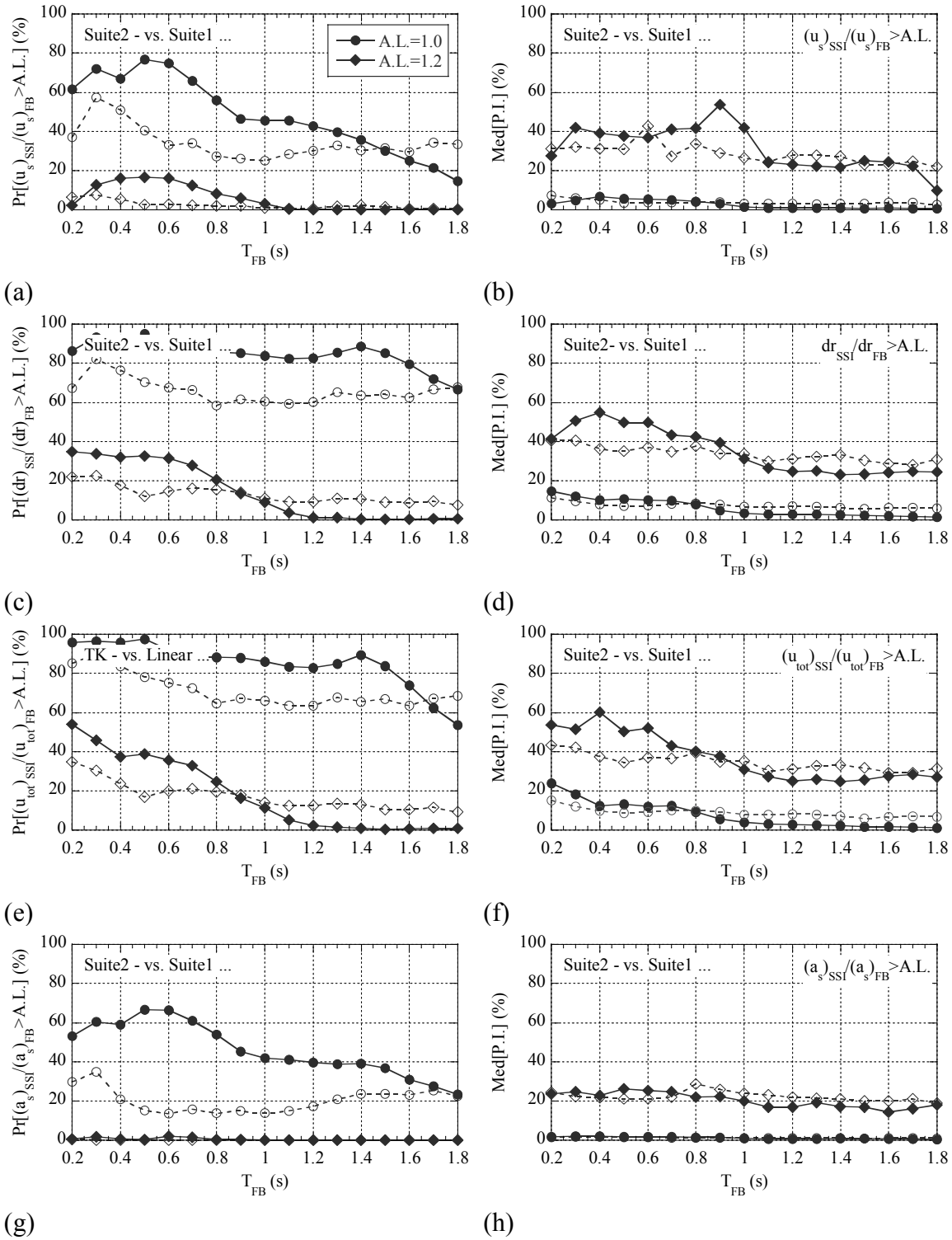

Figure 8-13. Risk spectra for structures with Takeda hysteretic behaviour considering special ground motions: (left) probability of amplification in the response; (right) level of amplification in the response.

8.8 Summary

The effects of soil-structure interaction on the seismic response of structures with nonlinear behaviour were investigated using a robust Monte-Carlo simulation. A large number of models with varying soil, foundation and structural properties were used to systematically and exhaustively examine the response of realistic soil-structure systems when subjected to earthquake excitations with different ground motion characteristics. Based on statistical analysis of the results from 4.08 million analyses, the following primary conclusions are made:

1) When structural nonlinearity is considered, foundation response will decrease and this reduction is more pronounced for foundation rocking.

2) Based on median structural response and probability of amplification in the structural response due to soil-structure interaction effects, detrimental effects of soil-structure interaction are more pronounced for structures with nonlinear behaviour. This implies that the evaluation of soil-structure interaction effects based on systems with linear behaviour is not conservative and needs to be reconsidered.

3) The specific nonlinear force-displacement behaviour of the structure does not have a significant effect on any structural response modification factors due to soil-structure interaction effects.

4) If ground motions with enhanced spectral ordinates at large periods are considered, the probability of having amplification in seismic structural response due to soil-structure interaction effects will increase. However, in terms of the median percentage increase, no significant change is expected. Note that this latter point implies a significant shift in the level of exceedance and its contribution.

5) Overall, the results presented in Chapter 7 and 8 clearly indicate increased probabilities of exceedance and levels of amplification when soil-structure interaction effects are considered compared to standard accepted fixed-base assumptions. The results are generalizable to a range of cases, guidelines and

design codes. However, it should be noted that these findings were obtained using a rudimentary, but commonly used, soil-shallow foundation-structure model.

CHAPTER

9. Sensitivity of Seismic Soil-Structure Interaction Effects to Model Parameters

Abstract. This chapter analyses 1.36 million realistic soil-structure interaction scenarios in a systematic fashion to define the correlation between soil, structural, and system parameters and interaction effects on the structural response. In the analyses, a soil-shallow foundation-structure model that satisfies design building code requirements is utilized. Specifically, the soil-foundation interface is represented by the equivalent linear cone model and the structure is characterised by a single-degree-of-freedom system with the Takeda type nonlinear hysteretic behaviour. Using a robust statistical approach, the key parameters whose variation significantly affects the structural response are identified, and the critical range of variation of these parameters resulting in a detrimental soil-structure interaction effects (i.e. scenarios with amplified structural response) is also outlined.

9.1 Introduction

It has been clearly demonstrated in Chapters 7 and 8 that the structural response of a soil-structure system to seismic forces is strongly affected by the impact of uncertainty in soil and structural parameters accompanied with the inherent randomness of the input ground motion. For the single-degree-of-freedom model assumed, it has also been shown that soil-structure interaction effects cannot be always safely ignored, given the likelihood of having amplification in the structural response due to foundation

flexibility. Thus, at least for critical scenarios, soil-structure interaction effects have to be taken into account in the seismic design procedure.

However, significant complexities and variation in the structural response make the identification of the critical scenarios a challenging task. A considerable step towards identification of these critical scenarios is to: (i) define the correlation between different parameters and the observed variation in response modification factors; and (ii) to comprehensively characterize and quantify the scenarios causing either reduction or amplification in the structural response. Thus, those scenarios causing the greatest likelihood of exceeding demand can be more precisely defined.

In this context, Veletsos and Nair [1] and Bielak [2] showed that the difference between seismically induced linear response of a fixed-base and flexible-base system is strongly affected by structural aspect ratio, soil Poison's ratio, soil hysteretic damping ratio, a dimensionless parameter expressing the relative stiffness of foundation and structure, and a dimensionless parameter representing soil-to-structure mass. Following these studies, a more comprehensive investigation was carried out by Ciampoli and Pinto [3]. They concluded that structural response of a nonlinear system does not show any systematic dependencies on the parameters regulating soil-structure interaction phenomena, and it is statistically reduced due to foundation flexibility.

Later on, Stewart, Fenves et al. [4] and Stewart, Seed et al. [5] used a comprehensive database of recorded data, and concluded that the ratio of structure-to-soil stiffness has the greatest influence on the structural response of a soil-structure system to seismic forces. In addition, it has been established that structural aspect ratio, foundation embedment, and foundation flexibility are the other parameters with significant effect on inertial interaction.

Finally, based on the framework of a dimensional analysis, Zhang and Tang [6] showed that soil-structure interaction effects are highly dependent on the structure-to-pulse frequency, foundation-to-structure stiffness ratio, and foundation damping ratio. They also presented certain limits for these controlling parameters to distinguish whether or not soil-structure interaction effects were significant.

Given the existing controversy in the previous findings and the assumed limitations in the analysis performed, it is believed that the most rational way to identify critical soil-structure interaction scenarios is to make use of a probabilistic approach. With this in mind, the results of the comprehensive probabilistic simulation presented in Chapter 8 are summarised and then used to:

1) Define the correlation and dependency between structural response modification factors and model parameters.

2) Identify the key parameters having a significant effect on the structural response.

3) Present the trend of variation of soil-structure interaction effects due to change of these parameters.

4) Quantify the critical range of variation of the parameters of consequence that causes detrimental soil-structure interaction scenarios.

This probabilistic analysis is a critically important step towards understanding and reliably characterizing the complex soil-structure problem. It also is important to note that the outcomes presented are limited to a single-degree-of-freedom system, and that the scenarios presented do not consider extreme conditions, such as those imposed by liquefiable soils or near-fault effects on the ground motion. However, the cases covered represent a significant majority of typical design cases and scenarios.

9.2 Correlation between Soil-Structure Interaction Effects and Model Parameters

To investigate the correlation between soil-structure interaction induced modification in structural response and randomly selected model parameters, the variation in the structural response modification factors, for all considered groups of models categorized based on T_{FB}, was examined as a function of:

1) Soil parameters: (i) soil mass density ρ; (ii) Poison's ratio υ; (iii) initial soil shear wave velocity $(V_s)_0$; and (iv) shear wave velocity degradation ratio $(V_s)_{sec}/(V_s)_0$.

2) Structural parameters: (i) structural effective height h_e; (ii) foundation radius r; (iii) structural mass m_s; structural aspect ratio h_e/r.

3) Soil-structure system parameters: (i) $m_s/\rho r^3$; (ii) $\delta = m_s/\rho\pi r^2 h_e$; (iii) $\sigma = (V_s)_{sec}T_{FB}/h_e$; and (iv) $\varphi = \frac{h_e}{(V_s)_{sec}T_{FB}}(h_e/r)^{0.25}$.

Note that the combined model parameters selected are based on the previous studies in literature such as [3, 4, 7], which introduce the regulating parameters in soil-structure interaction phenomenon. In this context, h_e/r represents the structural aspect ratio. This parameter is not a complete parameter in terms of describing both soil and structural characteristics. However, it is a geometric parameter of immediate engineering and design significance, as well as easily and robustly determined. Furthermore, $m_s/\rho\, r^3$ and δ are measures of structure-to-soil mass ratio, and σ is a representative of structure-to-soil stiffness ratio. Finally, the combined effect of σ and h_e/r is captured in φ, a parameter suggested by [3] to be the best suited in measuring the limit condition where soil-structure interaction effects are not worth to consider.

In the following, the possibility of having either a linear or nonlinear correlation is analysed and discussed. For presentation purposes, structural response modification factors are denoted as $(u_s)_{SSI}/(u_s)_{FB}$, dr_{SSI}/dr_{FB}, $(u_{tot})_{SSI}/(u_{tot})_{FB}$ and $(a_s)_{SSI}/(a_s)_{FB}$ representing modification in structural distortion, structural drift, total displacement, and structural acceleration due to soil-structure interaction, respectively.

9.2.1 Linear Correlations

The existing linear dependency of the structural response modification factors on the parameters considered is presented through Pearson correlation coefficient ρ. Pearson correlation coefficients are obtained by dividing the covariance of two variables by the product of their standard deviations and represent the level of correlation across a range [8]. Assuming X is the calculated structural response modification factor with mean and

standard deviation values of μ_X and σ_X, and Y is the model parameter with mean and standard deviation values of μ_Y and σ_Y, the Pearson correlation coefficient between these two random variables is defined:

$$\rho(X,Y) = \frac{COV(X,Y)}{\sigma_X \sigma_Y} = \frac{E[(X-\mu_X)(Y-\mu_Y)]}{\sigma_X \sigma_Y} \quad (14)$$

where E represents the expected value and COV means covariance.

The Pearson correlation coefficient is $+1$ in a perfectly increasing (positive) linear relationship, and -1 in the case of a perfectly decreasing (negative) linear relationship. It approaches zero when there is less of a correlation between variables. In all the other cases, it gives values between -1 and $+1$ indicating the degrees of linear dependence between the variables. If the variables are independent, the Pearson correlation coefficient is zero. However, the converse is not always true.

The Pearson correlation coefficients representing the linear dependency between structural response modification factors and the adopted soil, structural, and soil-structure system parameters are presented in Figures 9-1, 2 and 3, respectively. Note that in the spectra format presented, all considered scenarios are taken into account and categorized based on the values of fundamental structural period T_{FB}.

9.2.1.1 Correlation between soil-structure interaction effects and soil parameters

In terms of soil parameters, as shown in Figure 9-1, only initial soil shear wave velocity and shear wave velocity degradation ratio have a more pronounced linear correlation with the $(u_s)_{SSI}/(u_s)_{FB}$ and $(a_s)_{SSI}/(a_s)_{FB}$. The existence of linear correlation for the other different scenarios can almost always be ignored. In addition, the existing correlations are stronger for $(u_s)_{SSI}/(u_s)_{FB}$ compared to those for $(a_s)_{SSI}/(a_s)_{FB}$. However, note that the correlations observed are not a very strong linear correlation as the Pearson correlation coefficients are not very close to ± 1 ($\rho \sim 0.5$).

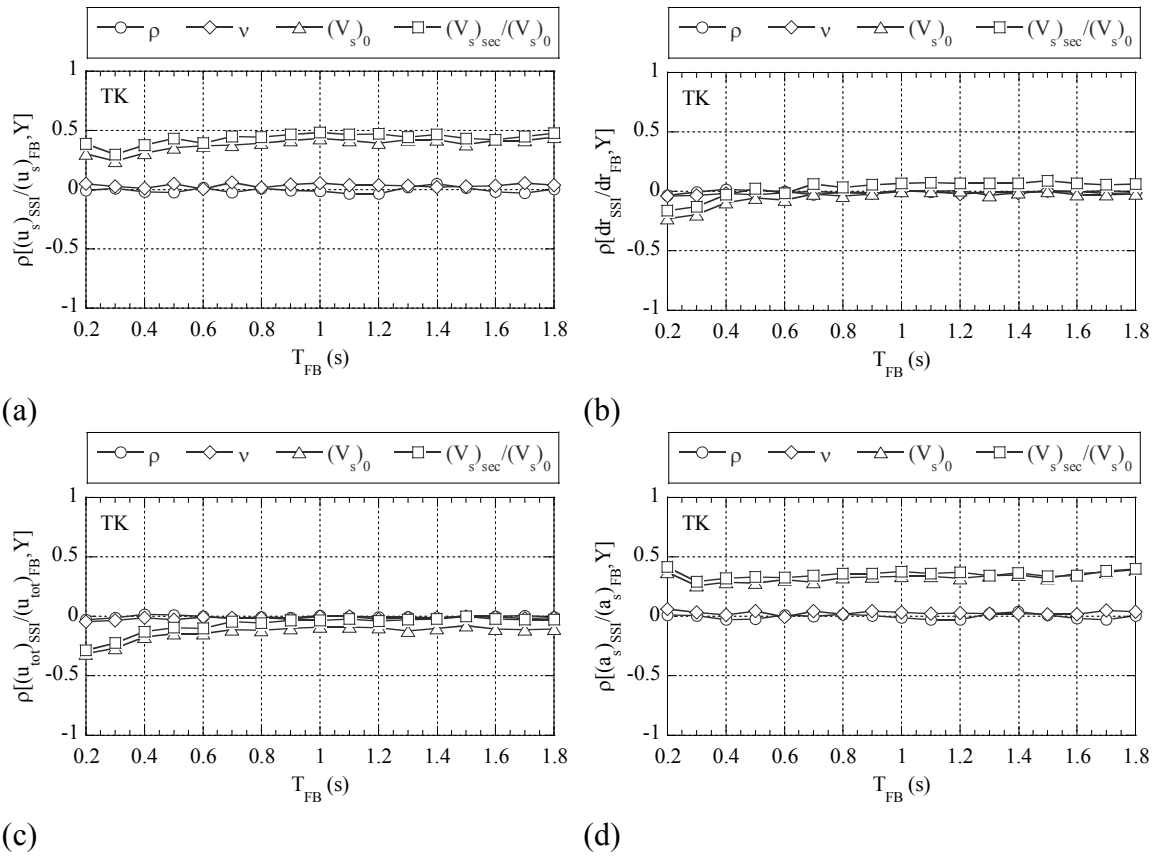

Figure 9-1. Pearson correlation coefficient spectra for structures with Takeda hysteretic behaviour, representing the correlation between soil parameters and: (a) structural distortion; (b) structural drift; (c) total displacement; (d) structural acceleration.

It should be also noted that the existing linear correlations (or Pearson correlation coefficients) are almost unchanged for all considered periods, meaning the dependency of $(u_s)_{SSI}/(u_s)_{FB}$ and $(a_s)_{SSI}/(a_s)_{FB}$ on initial soil shear wave velocity and shear wave velocity degradation ratio are independent from the fundamental structural period.

9.2.1.2 Correlation between soil-structure interaction effects and structural parameters

If the linear correlation between structural parameters and structural response modification factors are considered, no significant correlation exist as all Pearson correlation coefficients are small compared to ± 1. This result is illustrated in Figure 9-2. Therefore, no linear trend can be defined to correlate the variation in structural parameters to the modification in structural response due to soil-structure interaction effects.

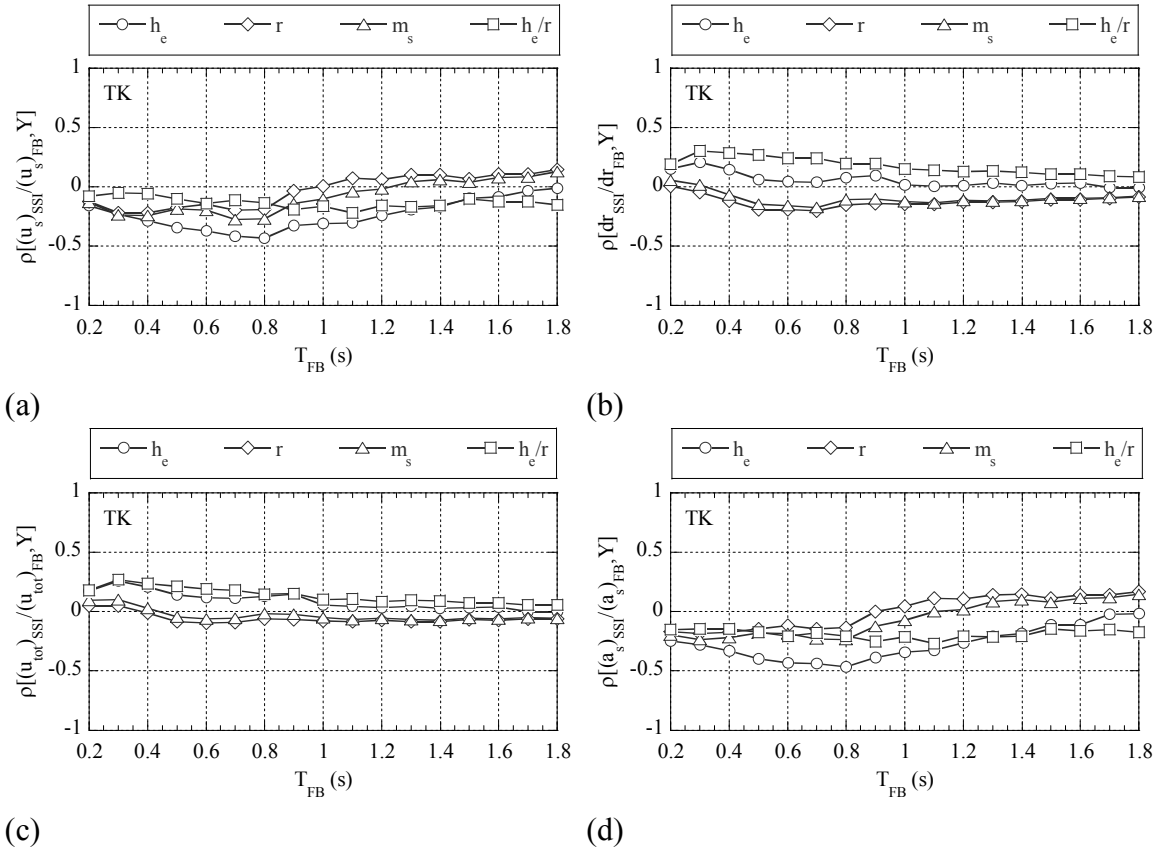

Figure 9-2. Pearson correlation coefficient spectra for structures with Takeda hysteretic behaviour, representing the correlation between structural parameters and: (a) structural distortion; (b) structural drift; (c) total displacement; (d) structural acceleration.

9.2.1.3 Correlation between soil-structure interaction effects and soil-structure system parameters

When soil-structure system parameters are taken into account, Figure 9-3, σ and φ are the only parameters that have a significant linear relationship with $(u_s)_{SSI}/(u_s)_{FB}$ and $(a_s)_{SSI}/(a_s)_{FB}$. In addition, the correlation between φ and $(u_s)_{SSI}/(u_s)_{FB}$ or $(a_s)_{SSI}/(a_s)_{FB}$ is more likely to be linear compared to that for σ, as the corresponding Pearson correlation coefficients are closer to ± 1. It is also noted that the evaluated Pearson correlation coefficients, representing the dependency of structural response modification factors to σ and φ, are independent from the periods considered. Parameters σ and φ also show a small linear correlation with dr_{SSI}/dr_{FB} and $(u_{tot})_{SSI}/(u_{tot})_{FB}$ when stiff structures ($T_{FB} \leq 0.6$ s) are considered.

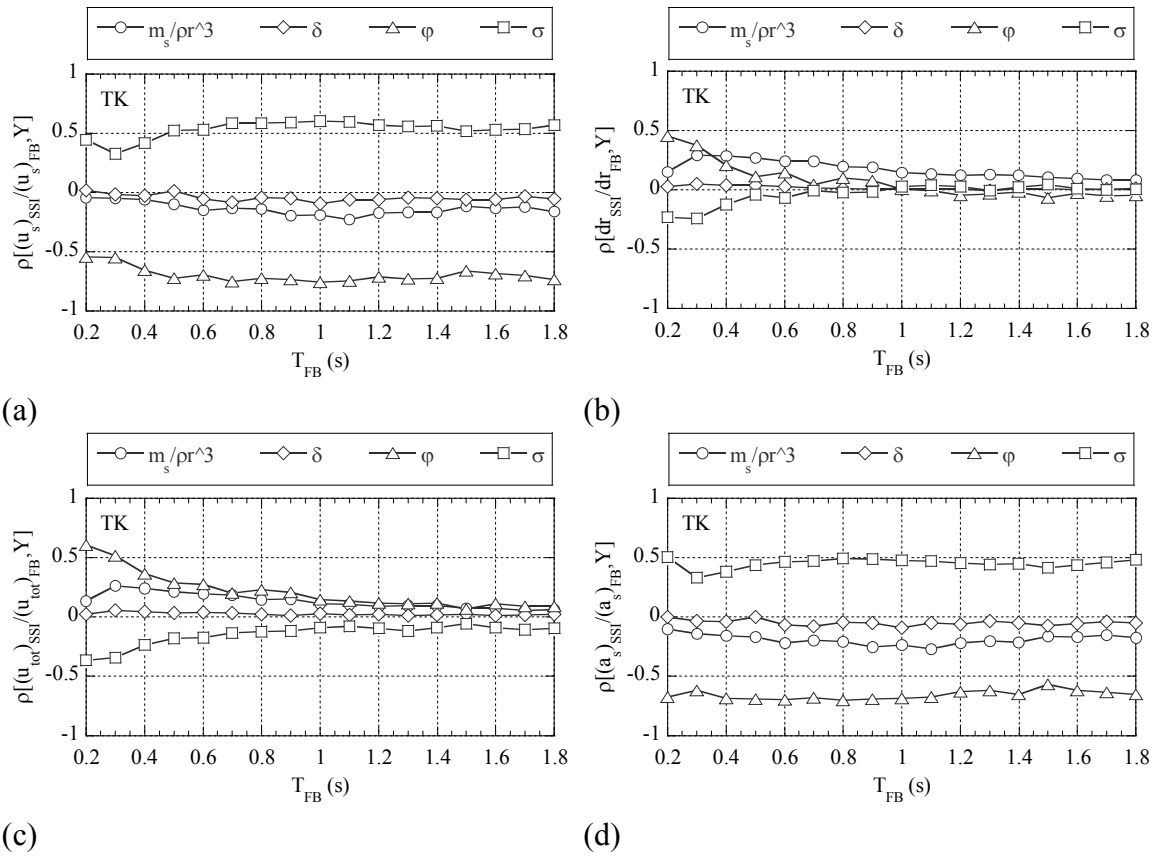

Figure 9-3. Pearson correlation coefficient spectra for structures with Takeda hysteretic behaviour, representing the correlation between soil-structure system parameters and: (a) structural distortion; (b) structural drift; (c) total displacement; (d) structural acceleration.

9.2.1.4 General comments

Finally, considering the increasing (positive) or decreasing (negative) linear relationship between structural response modification factors and soil, structural, and soil-structure system parameters, it is concluded that $(u_s)_{SSI}/(u_s)_{FB}$ and $(a_s)_{SSI}/(a_s)_{FB}$ are increased when: (i) initial soil shear wave velocity increases; (ii) smaller degradation in shear wave velocity occurs; (iii) σ increases; or (iv) φ decreases. These trends are discussed in more detail in Section 9.3.

9.2.2 Nonlinear Correlations

To examine the possibility of having a nonlinear correlation between the response modification factors and the soil, structural, and soil-structure system parameters, the graphs showing data distribution are considered. In these graphs, the response modification factors for each selected group of models with a specific period are presented based on the variation of a certain parameter. By examining all possible

scenarios, it can be seen that the measured structural response modification factors only have an obvious relationship with σ and φ. The graphs are noisy for all other cases. Therefore, parameters having no linear correlation with the response modification factors (i.e. $\rho, \upsilon, h_e, r, m_s, h_e/r$, $m_s/\rho\pi r^2 h_e$ and $m_s/\rho r^3$) also have no distinguishable nonlinear dependency. In other words, soil-structure interaction induced modification in structural response does not have a significant linear or nonlinear correlation with any of these parameters.

To avoid presenting unnecessary information, only the graphs showing the variation of $(u_s)_{SSI}/(u_s)_{FB}$ and $(u_{tot})_{SSI}/(u_{tot})_{FB}$ with σ and φ are illustrated and discussed in the following. In these graphs, the Pearson correlation coefficients previously presented are also shown to specify the existing relationship in terms of being a linear or nonlinear. The reader is referred to Appendix E for the graphs presenting the distribution of structural response based on the other adopted parameters.

Figure 9-4 illustrates the relationship between $(u_s)_{SSI}/(u_s)_{FB}$ and σ for different T_{FB} values. Clearly, there is a strong directionality in the data presented. In this context, as the Pearson correlation coefficients are small, the existing relationship can be considered as a nonlinear correlation. Equally, Figure 9-5 shows the relationship between $(u_s)_{SSI}/(u_s)_{FB}$ and φ. In this case, in addition to the strong directionality, it can be seen that the Pearson correlation coefficients are located in the range of $\rho \cong 0.5 - 0.7$. Thus, the existing dependency between $(u_s)_{SSI}/(u_s)_{FB}$ and φ is better to be assumed as a linear correlation rather than a nonlinear type. These observations are in complete agreement with that has been presented in Section 9.2.1.3.

If the relationship between $(u_{tot})_{SSI}/(u_{tot})_{FB}$ and σ is examined (Figure 9-6), it can be clearly concluded that the existing correlation between $(u_{tot})_{SSI}/(u_{tot})_{FB}$ and σ is nonlinear, respecting the small values of Pearson correlation coefficients observed. In addition, when the correlation between $(u_{tot})_{SSI}/(u_{tot})_{FB}$ and φ is considered (Figure 9-7), only a nonlinear correlation can be distinguished when $\varphi < 0.5$. Above this value, the dependency vanishes very quickly.

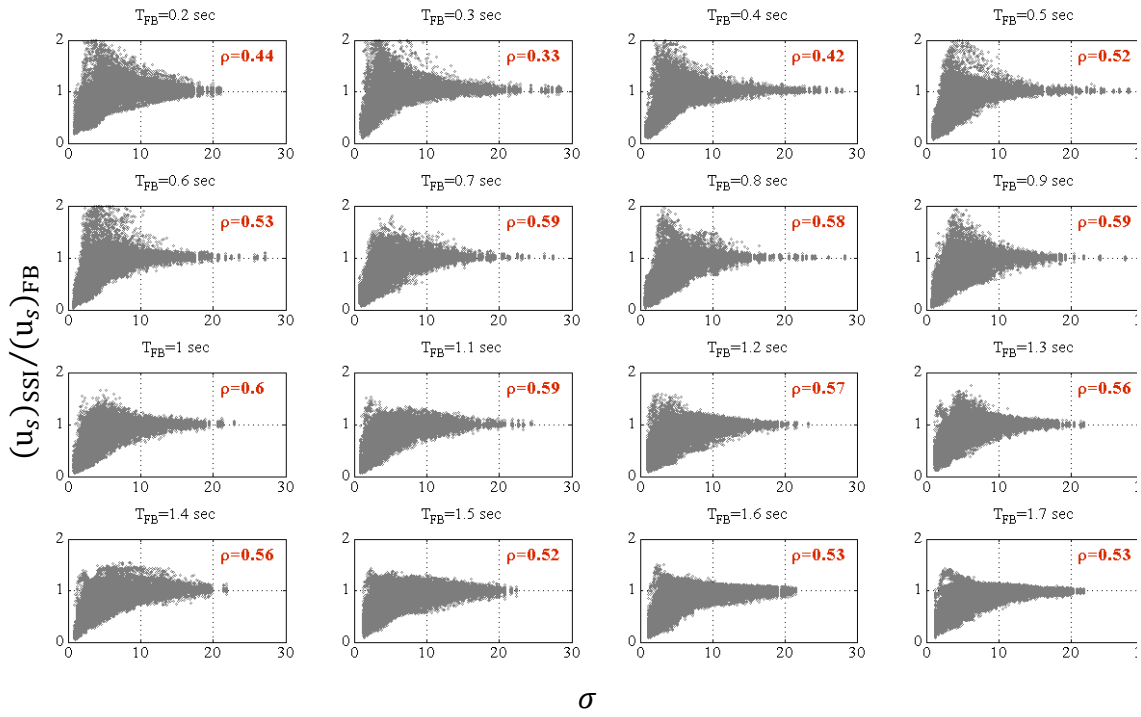

Figure 9-4. Correlation and dependency between structural distortion modification factors and $\sigma=(V_s)_{sec}T_{FB}/h_e$.

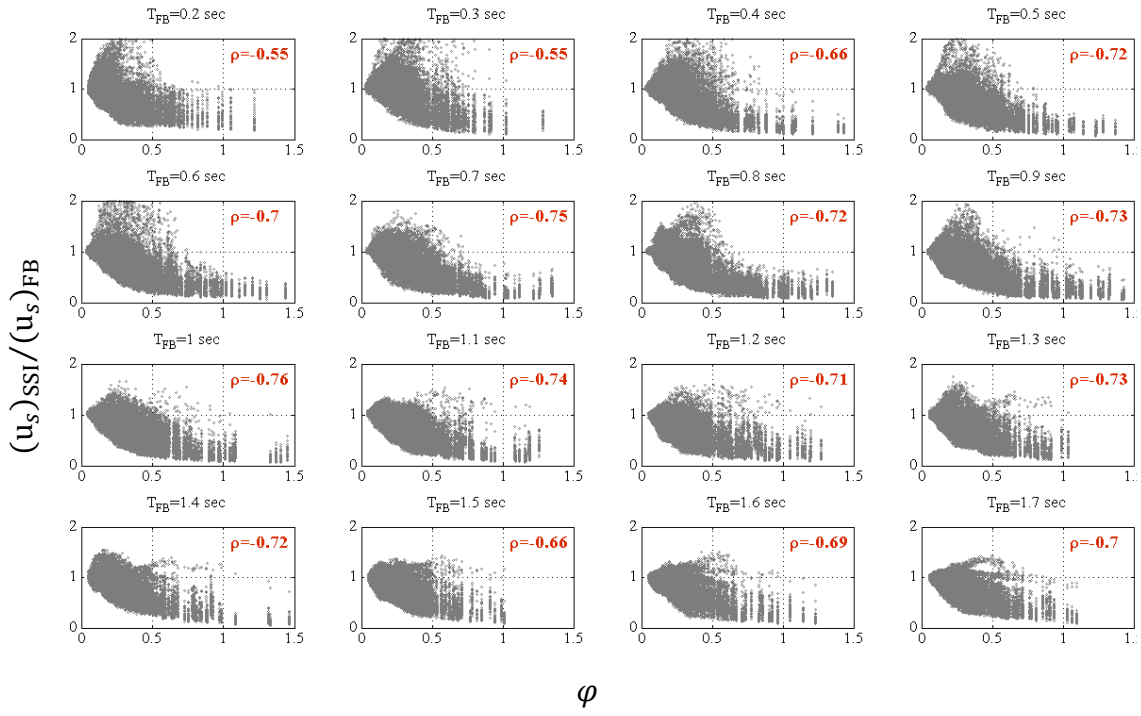

Figure 9-5. Correlation and dependency between structural distortion modification factors and $\varphi=h_e/[(V_s)_{sec}T_{FB}](h_e/r)^{0.25}$.

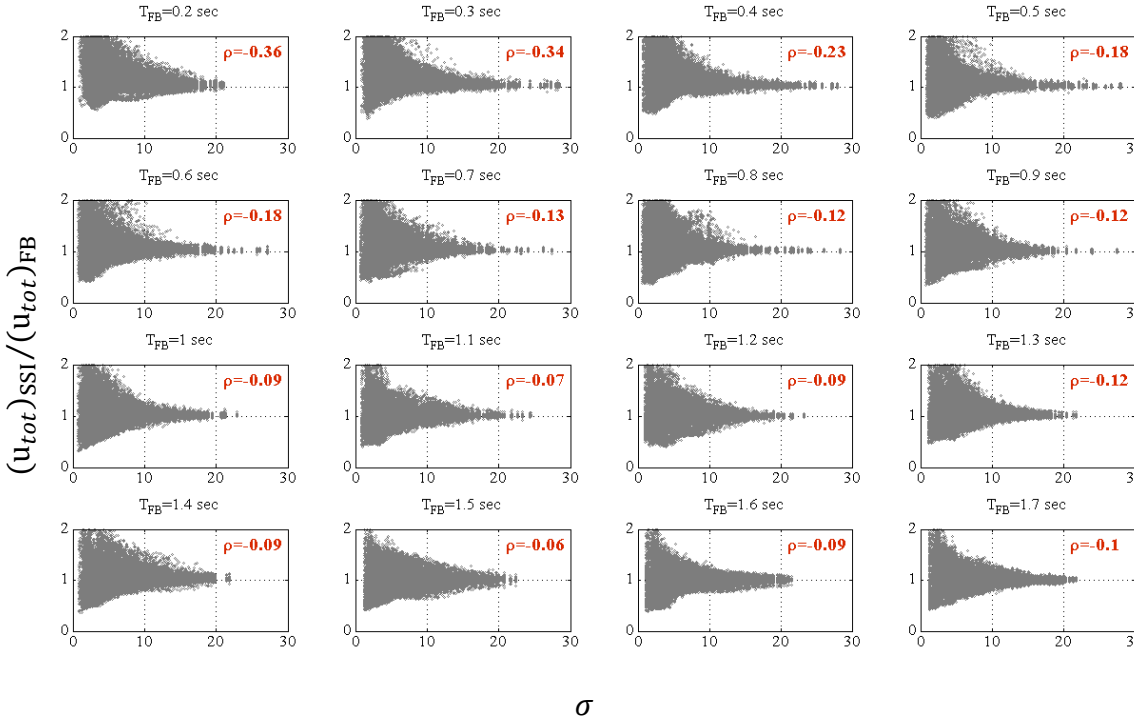

Figure 9-6. Correlation and dependency between total displacement modification factors and $\sigma=(V_s)_{sec}T_{FB}/h_e$.

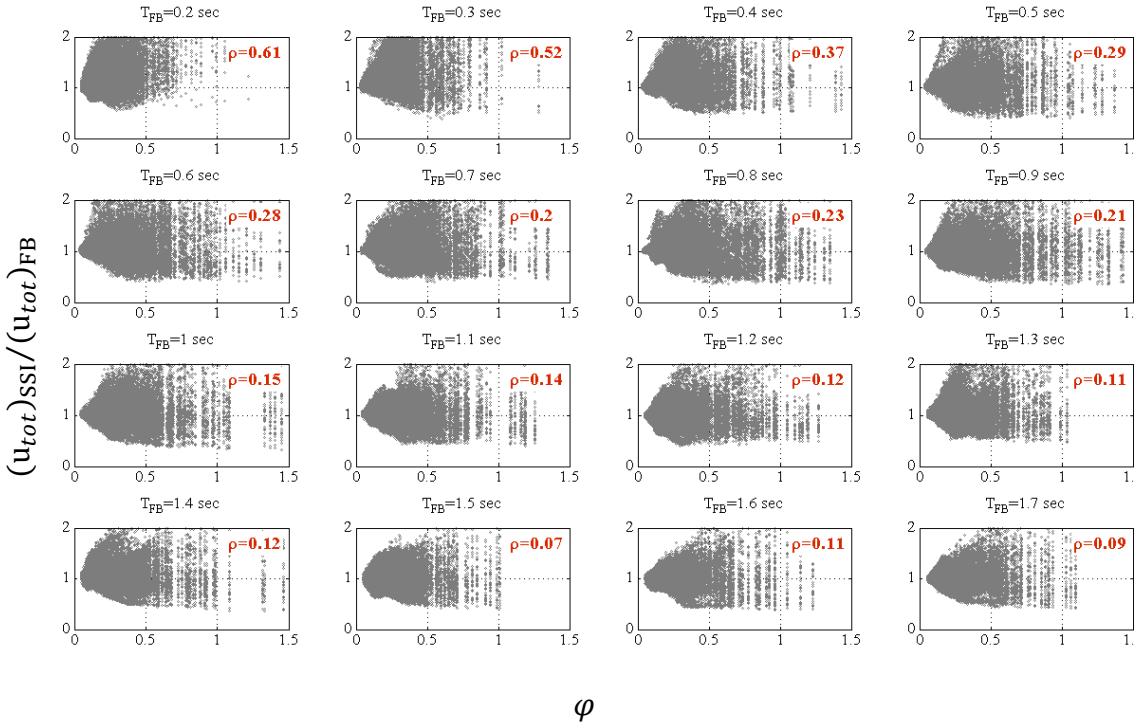

Figure 9-7. Correlation and dependency between total displacement modification factors and $\varphi=h_e/[(V_s)_{sec}T_{FB}](h_e/r)^{0.25}$.

9.2.3 Linear and Nonlinear Correlation in Summary

In summary, on the basis of the results presented for both linear and nonlinear correlations, it can be concluded that structural response modification factors due to soil-structure interaction do not show a systematic dependency on the model parameters except for: (i) initial shear wave velocity, (ii) shear wave velocity degradation ratio and system parameters of (iii) $\sigma = (V_s)_{sec} T_{FB}/h_e$ and (iv) $\varphi = \frac{h_e}{(V_s)_{sec} T_{FB}} (h_e/r)^{0.25}$.

9.3 Variation of Soil-Structure Interaction Effects with Model Parameters

To quantify the variation of structural response modification factors due to change in the model parameters of consequence, a robust statistical presentation was adopted. In this regard, all the scenarios examined are considered together, regardless of the initial grouping based on fundamental structural period. This approach is acceptable since the observed correlation between the response modification factors and initial soil shear wave velocity, shear wave velocity degradation ratio, σ and φ are not changing, but are almost the same for all considered periods. Thus, the variation of structural response modification factors due to change in the model parameters of consequence is independent of the structural fundamental period.

To carry out this quantification, the existing dependency of the response modification factors to the parameters considered were presented for the 5^{th}, 50^{th}, 75^{th}, and 95^{th} percentile lines representing different levels of likelihood. The distance between the 5^{th} and 95^{th} percentile boundary lines shows the possible variation in the response. The larger this distance, the higher the variation. The line assigned to the 50^{th} percentiles shows the central trend of the response, and the boundary lines assigned to the 75^{th}, and 95^{th} percentiles are seen as the response trend at the high levels of probability.

9.3.1 Dependency on Initial Shear Wave Velocity

The dependency of structural response modification factors on initial shear wave velocity is shown in Figure 9-8. Clearly, if smaller values of initial soil shear wave

velocity or softer soil conditions are considered, larger variation in the response modification factors are expected. This variation in terms of structural drift and total displacement could result in either large reduction or amplification in the response. However, for structural distortion and structural acceleration, this variation causes the possibility of a large reduction or only very small amplification.

This observation can be explained noting that a large foundation response is expected at softer soil conditions. As a result, a large rigid body motion accompanied with a large damping can be imposed to the soil-structure system that, in turn, is responsible for a significant amplification in structural drift and total displacement, and a significant reduction in structural distortion and structural acceleration. In addition, the scenarios with a decreased structural drift and total displacement might be correspondent to the cases where foundation imposed structural displacement is not as significant as structural distortion, which is also decreased due to soil-structure interaction effects.

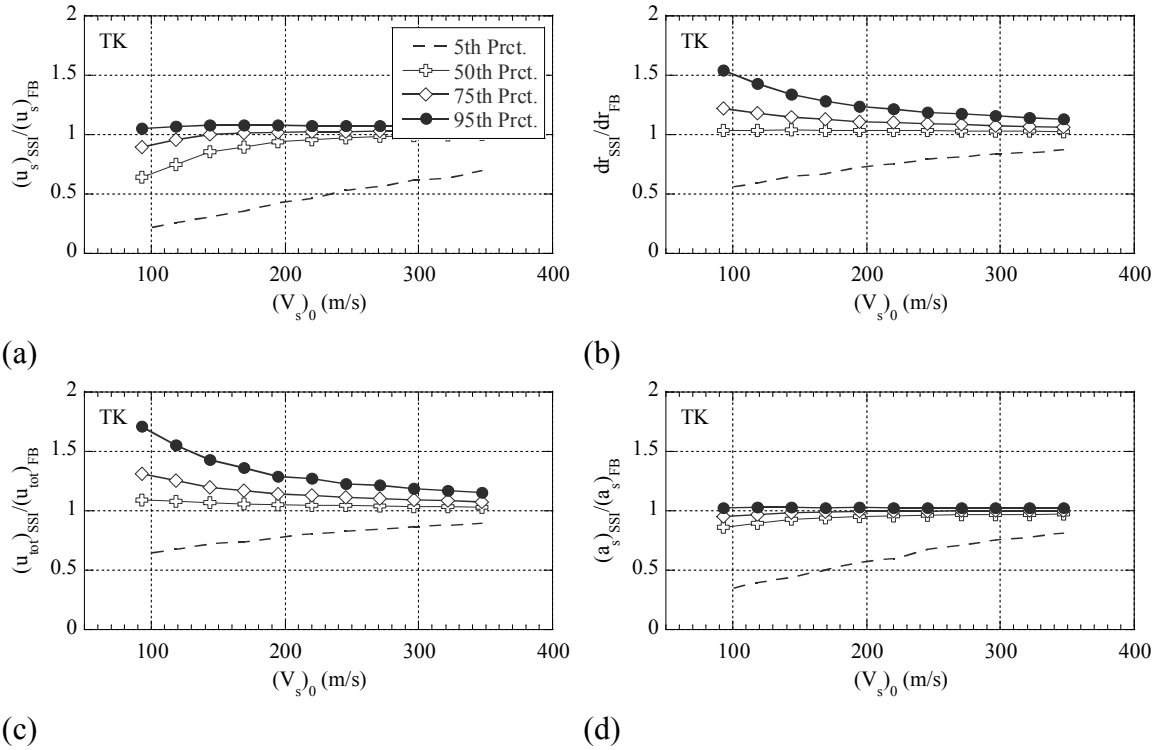

Figure 9-8. The effects of soil shear wave velocity on structural response modification factors, considering: (a) structural distortion; (b) structural drift; (c) total displacement; (d) structural acceleration.

As initial shear wave velocity increases, the variation in the response modification factors reduces significantly, such that the response modification factors approaches to 1.0. This trend is because an increase in initial shear wave velocity corresponds to the stiffer foundation condition. Consequently, soil-structure systems are forced to a more similar behaviour to that of the corresponding fixed-base systems.

In Figure 9-8, it is also shown that, at the median values, only $(u_s)_{SSI}/(u_s)_{FB}$ is strongly affected by the variation of initial shear wave velocity. In this context, when smaller values of initial shear wave velocity are considered, smaller values of $(u_s)_{SSI}/(u_s)_{FB}$ or higher reduction in structural distortion are expected. However, if higher levels of probability are considered, different interpretations appear. For $(u_s)_{SSI}/(u_s)_{FB}$ and $(a_s)_{SSI}/(a_s)_{FB}$, the 75^{th} and 95^{th} percentiles do not show a significant dependency on the change of initial shear wave velocity. It thus indicates that the maximum expected modification in structural distortion and structural acceleration is independent from initial shear wave velocity. In other words, the maximum modification in structural distortion and structural acceleration may occur for any values of initial shear wave velocity. However, different probabilities have to be considered.

When modification in structural drift and total displacement at the 75^{th} and 95^{th} percentiles is considered, an increase in initial shear wave velocity tends to sharply decrease the response modification factors. This observation indicates that foundation imposed structural response is significantly reduced due to the increase of initial shear wave velocity and, thus, the likelihood of having a large amplification in structural drift and total displacement decreases sharply.

9.3.2 Dependency on Shear Wave Velocity Degradation Ratio

The effects of shear wave velocity degradation ratio on the structural response modification factors are shown in Figure 9-9. The trends and conclusions are very similar to those indicated for the initial shear wave velocity, noting smaller degradation ratios correspond to the scenarios with smaller values of shear wave velocity or softer soil conditions. Clearly, wider variation in the structural response modification factors are expected when higher degradation in shear wave velocity occurs, i.e. when smaller degradation values are considered. This trend is justified as higher levels of degradation

will result in the more flexible foundations, as well as more added damping to the system. Consequently, the response of the soil-structure system gets more dissimilar to that of the corresponding fixed-base condition.

In this context, similar to that has been presented for initial shear wave velocity, a large reduction or amplification in structural drift and total displacement may occur, while only a large reduction or a very small amplification is expected for structural distortion and structural acceleration. Obviously, the reduction is due to the large amount of damping added to the system, and the amplification is due to the large foundation motion imposed. In addition, at the median values, only $(u_s)_{SSI}/(u_s)_{FB}$ is sensitive to the variation of shear wave velocity degradation ratio. However, at the 75^{th} and 95^{th} percentiles, only dr_{SSI}/dr_{FB} and $(u_{tot})_{SSI}/(u_{tot})_{FB}$ are significantly influenced by shear wave velocity degradation ratio. It should also be noted that the maximum expected modification in structural distortion and structural acceleration is independent from the shear wave velocity degradation ratio.

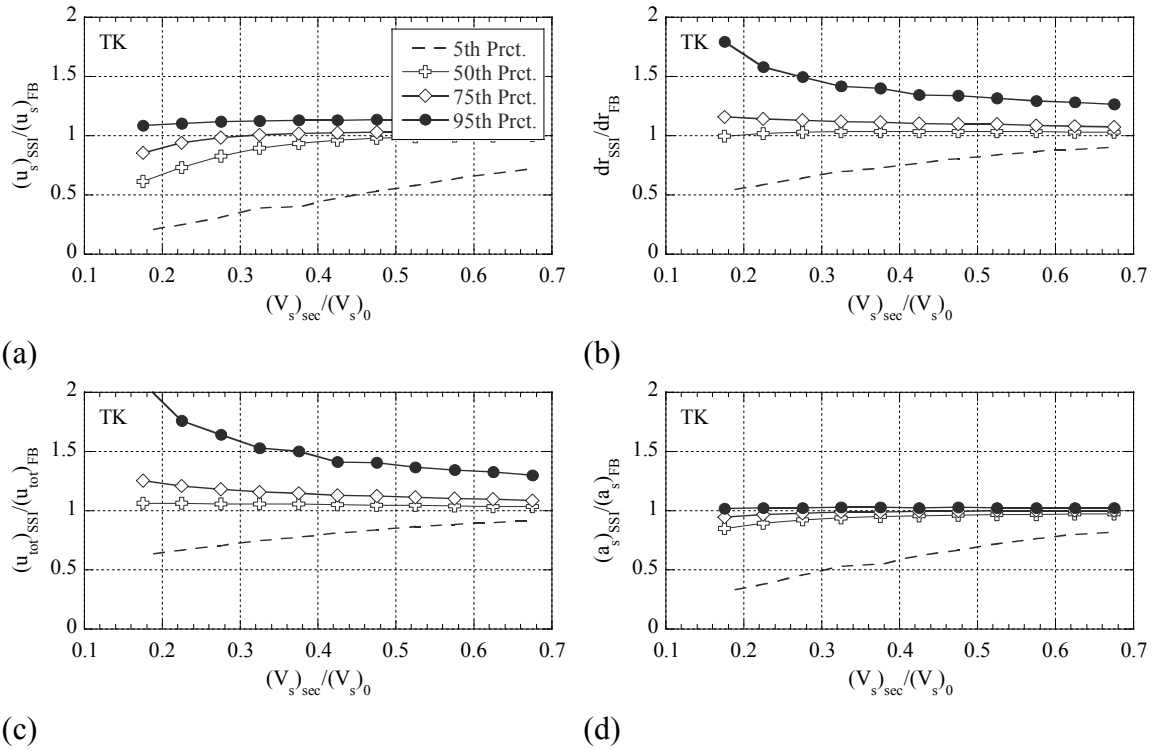

Figure 9-9. The effects of shear wave velocity degradation ratio on structural response modification factors, considering: (i) structural distortion; (b) structural drift; (iii) total displacement; (iv) structural acceleration.

9.3.3 Dependency on Parameter σ

The dependency of structural response modification factors on σ is discussed next. Note that, as defined in Section 9.2, σ combines the effects of three parameters including: (i) degraded soil shear wave velocity, (ii) fundamental structural period, and (iii) structural effective height. Since degraded shear wave velocity is directly related to initial shear wave velocity and shear wave velocity degradation ratio, σ is then highly influenced by these two parameters. Therefore, similar trends to those have been observed for initial shear wave velocity and shear wave velocity degradation ratio might be expected.

The results are presented in Figure 9-10. Clearly, the variation in the response reduces very sharply with the increase of σ, such that the variation can be practically ignored when $\sigma > 20$. In addition, since the response modification factors approach to 1.0, it can be concluded that soil-structure interaction does not have any reduction or amplification effects on the structural response after $\sigma > 20$.

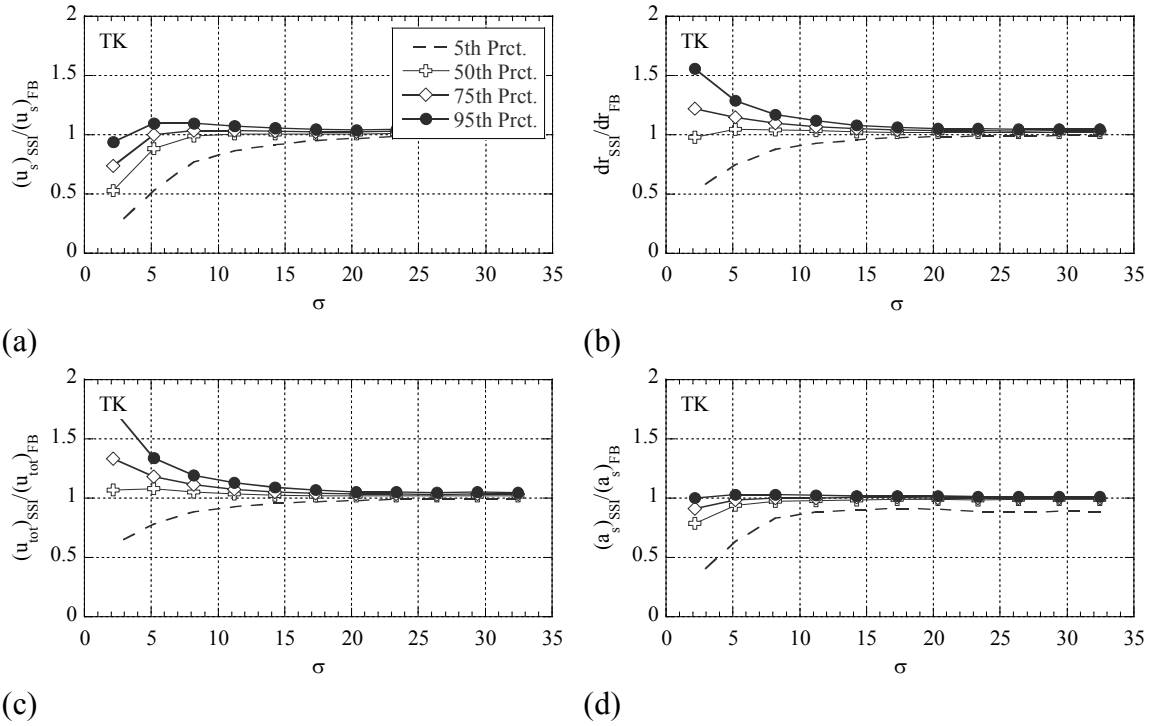

Figure 9-10. The effects of $\sigma=(V_s)_{sec}T_{FB}/h_e$ on structural response modification factors, considering: (i) structural distortion; (b) structural drift; (iii) total displacement; (iv) structural acceleration.

This observation is in complete agreement with that has been previously presented for initial shear wave velocity and shear wave velocity degradation ratio. Specifically, because smaller σ can be correspondent to the scenarios with the softer soil condition or larger shear wave velocity degradation. Smaller σ may also be related to the scenarios with smaller structural period (i.e. greater structural stiffness) or greater structural height. In both cases, foundation motion is dominant and, thus, larger variation in soil-structure interaction effects can be expected. After all, it should be noted that it is the combined effect of soil stiffness, structural period and structural height that could result in the trends observed due to the variation of σ.

For scenarios with $\sigma < 20$, if the median values are considered, only $(u_s)_{SSI}/(u_s)_{FB}$ and $(a_s)_{SSI}/(a_s)_{FB}$ are affected by the variation of σ. As a result of this dependency, smaller values of σ cause higher reduction in the response modification factors. However, if higher levels of probability are considered, $(u_s)_{SSI}/(u_s)_{FB}$ and $(a_s)_{SSI}/(a_s)_{FB}$ increase when σ increases and approach to 1.0, while dr_{SSI}/dr_{FB} and $(u_{tot})_{SSI}/(u_{tot})_{FB}$ reduce sharply to 1.0.

9.3.4 Dependency on Parameter φ

Finally, the dependency of structural response modification factors on φ is presented in this section. As defined in Section 9.2, φ is a parameter combining the effects of: (i) degraded soil shear wave velocity; (ii) fundamental structural period; (iii) structural effective height; and (iv) structural aspect ratio. Similar to σ, φ is also highly subjective to the effects of initial shear wave velocity and shear wave velocity degradation ratio, but in the reverse order.

The results for the dependency of structural response modification factors on φ are illustrated in Figure 9-11. Obviously, the response modification factors approaches to 1.0 when smaller φ is considered. However, the degree of variation increases for greater φ that, in turn, corresponds to the scenarios with smaller shear wave velocity (i.e. softer soil conditions), smaller structural period (i.e. very stiff structures), greater structural height and structural aspect ratio (i.e. very tall and narrow structures).

When φ increases, the response modification factors for $(u_s)_{SSI}/(u_s)_{FB}$ and $(a_s)_{SSI}/(a_s)_{FB}$ decrease even for large percentile values. In this regard, at the 95^{th} percentiles, the likelihood of having amplification in structural distortion and structural acceleration is negligible after $\varphi > 0.5$.

In contrast, if the dependency of dr_{SSI}/dr_{FB} and $(u_{tot})_{SSI}/(u_{tot})_{FB}$ on φ is considered, the variation in the response modification factors increases with φ. This increase results in a wide degree of variation, with the amount of amplification being greater than that of reduction. Observing a large amplification in structural drift and total displacement, but only a large reduction in structural distortion and structural acceleration can be due to the significant foundation response occurring as φ increases. Large foundation response, consequently, reduces the transmitted displacement (or force) to the structure, while it increases the structural responses including rigid body motion due to foundation flexibility.

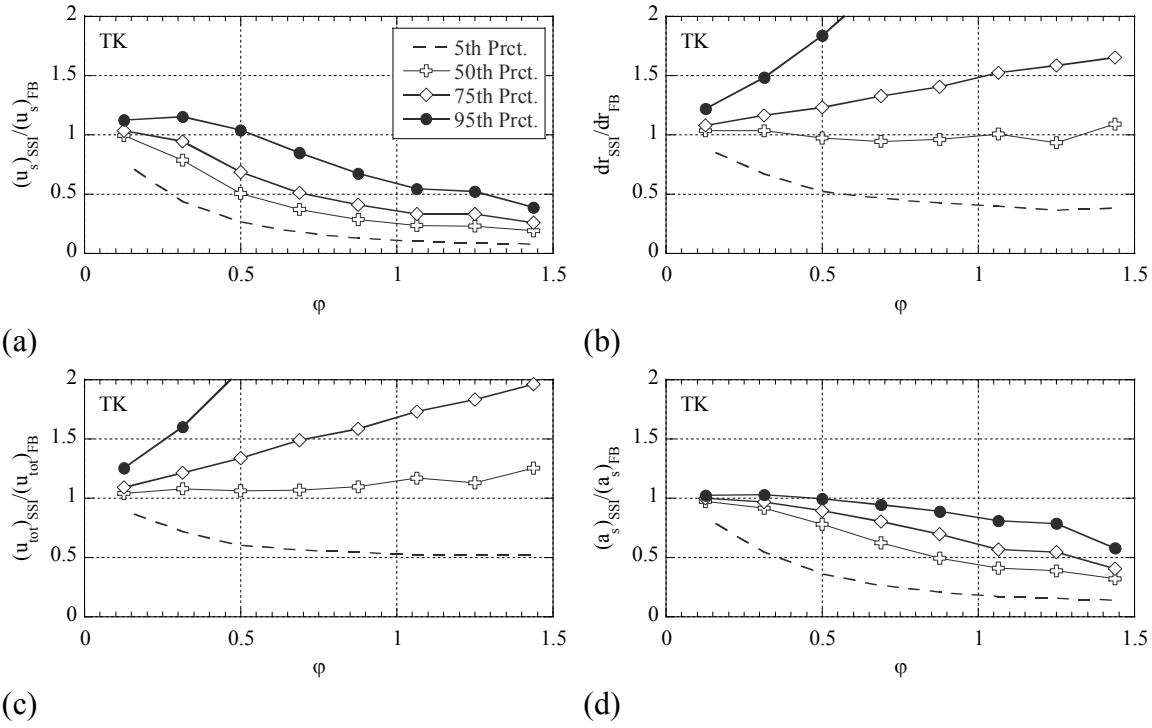

Figure 9-11. The effects of $\varphi=h_e/[(V_s)_{sec}T_{FB}](h_e/r)^{0.25}$ on structural response modification factors, considering: (i) structural distortion; (b) structural drift; (iii) total displacement; (iv) structural acceleration.

It should be also noted that scenarios with $\varphi > \sim 0.5 - 0.7$ are the unusual cases, i.e. tall and narrow or stiff structures located on very soft soils, that are considered as outliers in the response modification spectrum shown in Chapter 8. This fact is also distinguished in Figures 9-5 and 9-7 as the number of data points presented is significantly reduced when $\varphi > \sim 0.5 - 0.7$. It basically means only a small number of models generated satisfy this condition. Therefore, the results presented for $\varphi > \sim 0.5 - 0.7$ can be practically ignored.

9.4 Risk of Detrimental Soil-Structure Interaction Effects based on Model Parameters

To evaluate the risk of detrimental soil-structure interaction effects, as compared to fixed-base assumptions, on structural response due to variation in the model parameters of consequence, two main aspects of risk were analysed: (i) the probability of having amplification in the response of the soil-structure model as compared to the response of the corresponding fixed-base model; and (ii) the level of amplification in the response due to soil-structure interaction consideration. For this purpose, two amplification levels (A.L.) were taken into account: 1.1 and 1.2, and the probability of having scenarios with the response modification factors greater than each level were calculated. For the considered amplification levels, the corresponding values of median percentage increase in the response (Med[P.I.]) were also evaluated.

9.4.1 Amplification Risk due to Variation of Initial Soil Shear Wave Velocity

The risk of detrimental soil-structure interaction effects on structural response due to variation in initial shear wave velocity is presented in Figure 9-12. On the left-side, the probabilities of amplification in the structural response are presented, whereas on the right-side, the corresponding values of median percentage increase are shown.

As expected from the results presented in Section 9.3.1, the probability of amplification in the response is very small for structural distortion and is almost negligible for structural acceleration, whereas the probability of amplification in structural drift and total displacement cannot be simply neglected. It is also noted that the probability of

amplification in the response is reduced as the higher level of amplification is considered.

The probability of amplification in the response decreases when initial shear wave velocity increases. It implicitly indicates that when structures on stiffer soil conditions are considered, the probability of having detrimental soil-structure interaction effects will be less critical. If initial shear wave velocity changes from: $100 - 350$ m/s, the observed probability values at A.L.=1.1 vary from $10\% - 5\%$ for structural distortion; $40\% - 15\%$ for structural drift; and $50\% - 20\%$ for total displacement, and are almost 0% for structural acceleration. Equally, these probabilities at A.L.=1.2 are in the range of: $5\% - 1\%$ for structural distortion; $30\% - 5\%$ for structural drift; and $35\% - 5\%$ for total displacement.

If the values of median percentage increase in the response are taken into account, a reduction is also expected when initial shear wave velocity increases. Therefore, the degree of amplification in the structural response decreases similar to the probability of amplification when stiffer soil conditions are considered. The corresponding values of median percentage increase are in the range of: $20\% - 15\%$ for structural distortion; $30\% - 15\%$ for structural drift; and $30\% - 15\%$ for total displacement; and $15\% - 10\%$ for structural acceleration when A.L.=1.1 is considered. Equally, for A.L.=1.2, the values of median percentage increase are in the range of: $30\% - 25\%$ for structural distortion; $40\% - 30\%$ for structural drift; and $45\% - 30\%$ for total displacement; and $30\% - 20\%$ for structural acceleration. It should be noted that the values presented for structural acceleration are mostly related to the outliers (uncommon soil-structure scenarios) as the probability of amplification in structural acceleration is negligible. This point is also valid for the results followed in case of shear wave velocity degradation ratio, σ and φ.

9.4.2 Amplification Risk due to Variation of Shear Wave Velocity Degradation Ratio

The risk of detrimental soil-structure interaction effects on structural response due to variation in shear wave velocity degradation ratio is shown in Figure 9-13. Regardless of the values, the trends and conclusions are similar to those for initial shear wave

velocity. In this comparison, smaller degradation ratios have to be considered instead of smaller shear wave velocities.

The probabilities of amplification in the response and the corresponding values of median percentage increase decrease when shear wave velocity degradation ratio increases or smaller soil shear wave velocity degradation is considered. In this context, when shear wave velocity degradation ratio changes from $0.2 - 0.7$, the probability of amplification at A.L.=1.1 vary from: $10\% - 5\%$ for structural distortion; $35\% - 20\%$ for structural drift; and $40\% - 20\%$ for total displacement, and are almost 0% for structural acceleration. Equally, these probabilities at A.L.=1.2 are in the range of: $2\% - 1\%$ for structural distortion; $30\% - 15\%$ for structural drift; and $30\% - 15\%$ for total displacement.

The corresponding values of median percentage increase are in the range of: $20\% - 15\%$ for structural distortion; $30\% - 15\%$ for structural drift; $30\% - 20\%$ for total displacement; and $15\% - 10\%$ for structural acceleration at A.L.=1.1, and $30\% - 25\%$ for structural distortion; $40\% - 30\%$ for structural drift; $45\% - 30\%$ for total displacement; and $25\% - 20\%$ for structural acceleration at A.L.=1.2.

9.4.3 Amplification Risk due to Variation of σ

The risk of detrimental soil-structure interaction effects on structural response due to variation in σ is shown in Figure 9-14. Clearly, an increase in σ yields smaller probability values such that after $\sigma > 20$ any amplification more that 10%, and after $\sigma > 15$ any amplification more that 20% in the structural response may be practically ignored. In addition, an increase in σ is accompanied with a decrease in the values of median percentage increase. These observations once more highlight that soil-structure interaction effects are less critical for soil-structure scenarios including stiffer soil condition, greater structural period and smaller structural height.

When σ changes from $2 - 20$, the probability values at A.L.=1.1 vary from: $10\% - 0\%$ for structural distortion; $35\% - 0\%$ for structural drift; and $45\% - 0\%$ for total displacement, and are almost 0% for structural acceleration. Equally, these probabilities at A.L.=1.2 are in the range of: $5\% - 0\%$ for structural distortion; $35\% - 0\%$ for

structural drift; and $30\% - 15\%$ for total displacement. The corresponding values of median percentage increase are in the range of: $20\% - 10\%$ for structural distortion; $35\% - 10\%$ for structural drift; $35\% - 10\%$ for total displacement; and about 10% for structural acceleration at A.L.=1.1, and $35\% - 25\%$ for structural distortion; $45\% - 25\%$ for structural drift; $45\% - 20\%$ for total displacement; and about 20% for structural acceleration at A.L.=1.2.

9.4.4 Amplification Risk due to Variation of φ

Finally, Figure 9-15 illustrates the risk of detrimental soil-structure interaction effects on the structural response due to variation in φ. In this case, two different trends are seen for the probability of amplification in structural distortion and structural acceleration compared to the probability of amplification in structural drift and total displacement. The probability of amplification in structural distortion is very small and decreases as φ increases, while the probability of amplification in structural acceleration is almost negligible. In addition, an amplification in structural distortion can be practically ignored when $\varphi > 1.0$. In contrast, the probability of amplification in structural drift and total displacement increases as φ increases. The reason behind this increase is previously described in Section 9.3.4.

When φ changes from $0.1 - 1.5$, the probability values at A.L.=1.1 vary from: $8\% - 0\%$ for structural distortion; $20\% - 50\%$ for structural drift; and $25\% - 60\%$ for total displacement, and are almost 0% for structural acceleration. Equally, these probabilities at A.L.=1.2 are in the range of: $2\% - 0\%$ for structural distortion; $5\% - 45\%$ for structural drift; and $8\% - 50\%$ for total displacement.

In terms of the median percentage increase, an increasing trend exists for structural distortion, structural drift and total displacement when φ increases, whereas the values of median percentage increase for structural acceleration are almost constant for all φ values. The values of median percentage increase are in the range of: $15\% - 25\%$ for structural distortion; $15\% - 65\%$ for structural drift; $15\% - 80\%$ for total displacement; and about 15% for structural acceleration at A.L.=1.1, and $25\% - 35\%$ for structural distortion; $25\% - 90\%$ for structural drift; $25\% - 95\%$ for total displacement; and about 15% for structural acceleration at A.L.=1.2.

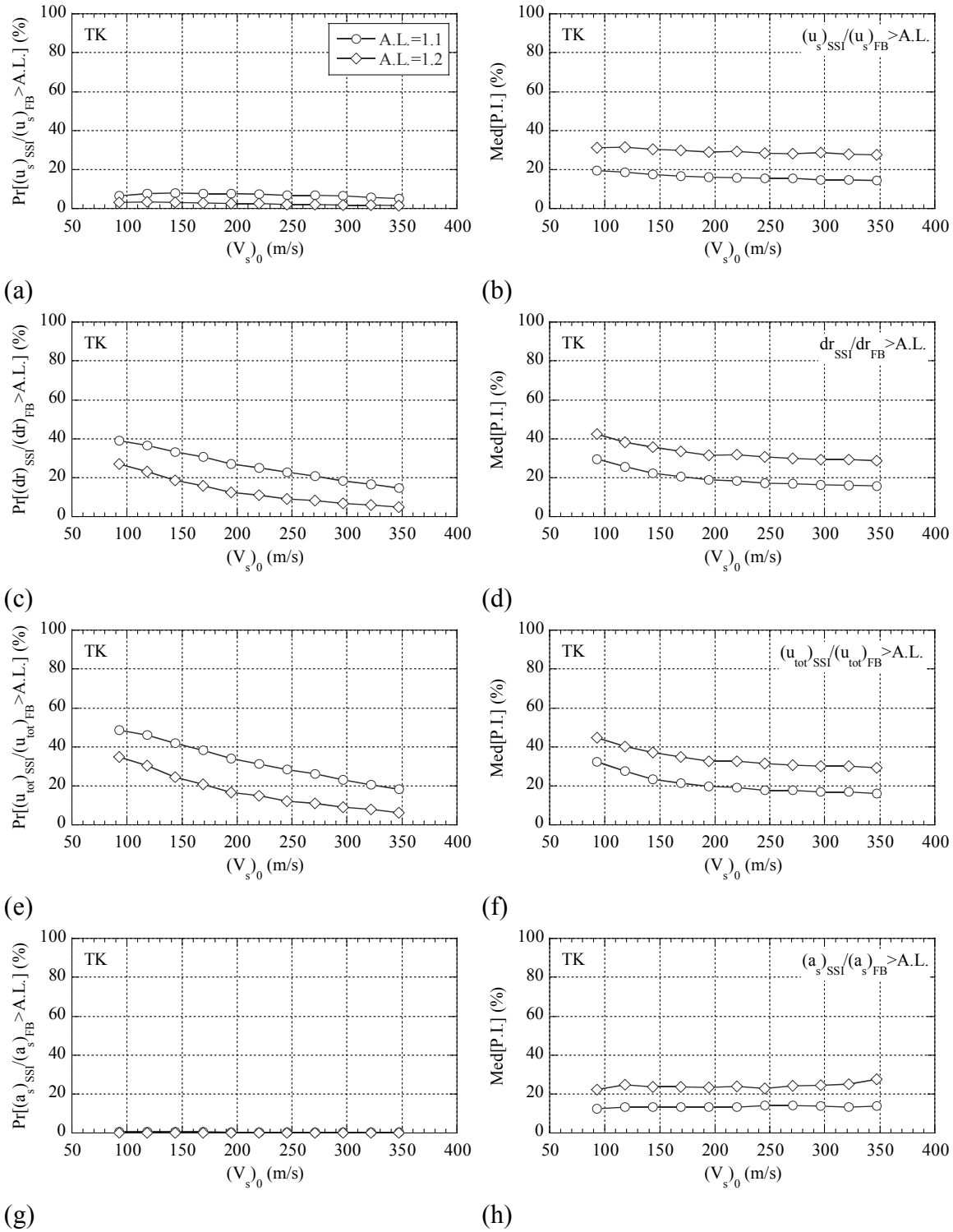

Figure 9-12. Risk of detrimental soil-structure interaction effects based on variation in initial soil shear wave velocity: (left) probability of amplification in the response; (right) level of amplification in the response.

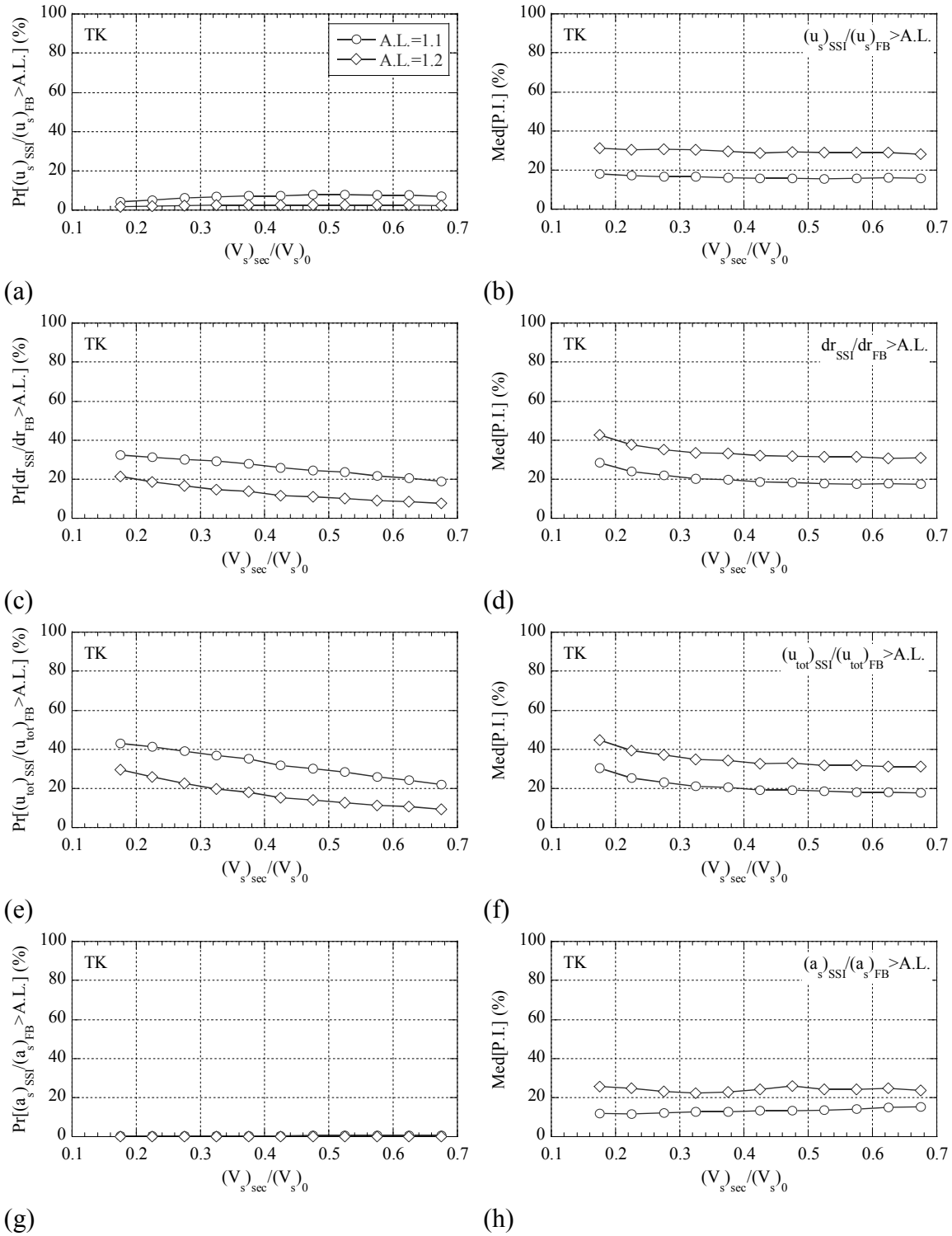

Figure 9-13. Risk of detrimental soil-structure interaction effects based on variation in shear wave velocity degradation ratio: (left) probability of amplification in the response; (right) level of amplification in the response.

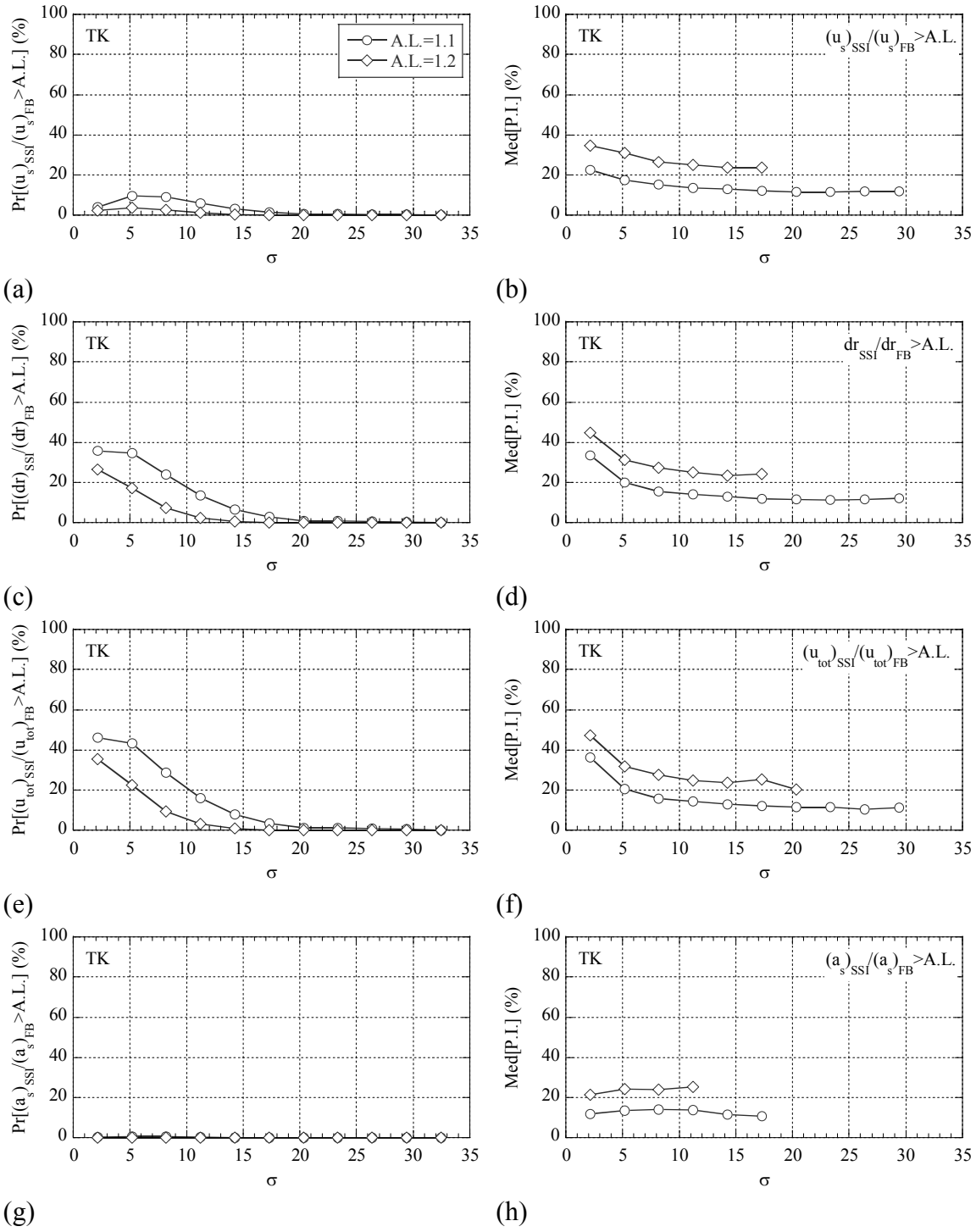

Figure 9-14. Risk of detrimental soil-structure interaction effects based on variation in $\sigma=(V_s)_{sec}T_{FB}/h_e$: (left) probability of amplification in the response; (right) level of amplification in the response.

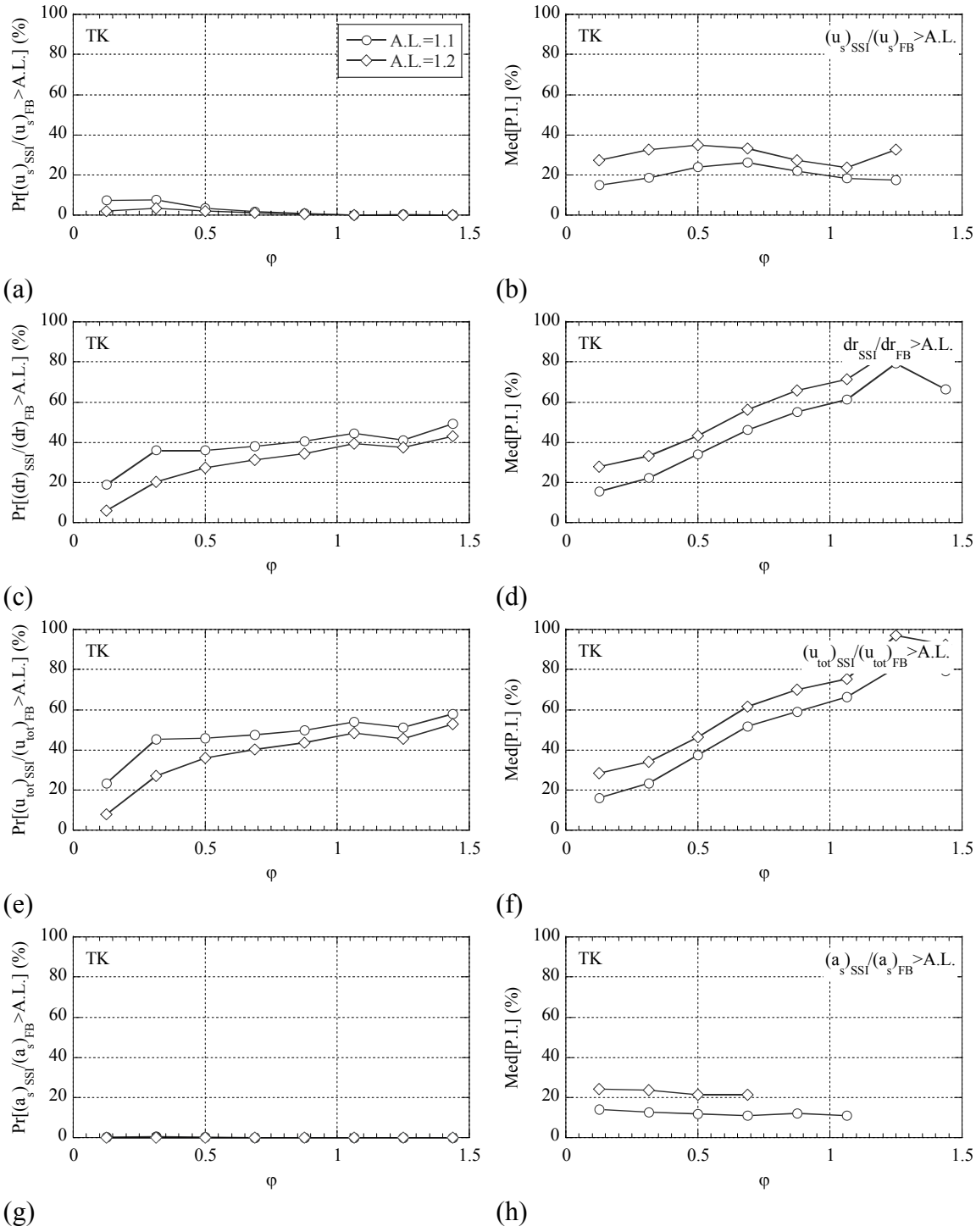

Figure 9-15. Risk of detrimental soil-structure interaction effects based on variation in $\varphi=h_e/[(V_s)_{sec}T_{FB}](h_e/r)^{0.25}$: (left) probability of amplification in the response; (right) level of amplification in the response.

9.5 Summary

A comprehensive statistical evaluation of seismic soil-structure interaction effects has been conducted using a rheological soil-shallow foundation-structure model with equivalent linear soil domain and nonlinear structural behaviour following a Takeda type hysteretic model. The key findings are summarised:

1) From all considered soil, structural, and soil-structure system parameters only initial soil shear wave velocity, shear wave velocity degradation ratio, $\sigma = (V_s)_{sec}T_{FB}/h_e$ and $\varphi = \frac{h_e}{(V_s)_{sec}T_{FB}}(h_e/r)^{0.25}$ have a pronounced correlation with structural response modification factors due to soil-structure interaction effects.

2) An increase in the values of initial soil shear wave velocity, shear wave velocity degradation ratio and σ cause a less variation in the resulted structural response modification factors. In addition, as these parameters increase, the response modification factors approach 1.0, indicating the behaviour of the soil-structure systems are more similar to the behaviour of the corresponding fixed-base system.

3) Considering the median values (the 50^{th} percentiles), an increase in the values of initial soil shear wave velocity, shear wave velocity degradation ratio and σ results in an increase in the structural distortion modification factors, while modification in structural drift, total displacement and structural acceleration are only weakly sensitive to the parameters considered.

4) The likely maximum modification in the structural distortion and structural acceleration are independent from the variation of initial soil shear wave velocity, shear wave velocity degradation ratio and σ. However, if structural drift or total displacement is considered, a sharp reduction in the maximum modification factors is observed due to an increase in the initial soil shear wave velocity, shear wave velocity degradation ratio and σ.

5) When φ increases, structural distortion modification factors and structural acceleration modification factors reduce very sharply at median and likely maximum values. In contrast, the variation in structural drift modification factors and total displacement modification factors gets more significant as φ increases. This variation mostly results in amplification in structural drift and total displacement than reduction.

6) In terms of quantification of the risk, the probability of amplification in the response is very small for structural distortion and is almost negligible for structural acceleration, whereas the probability of amplification in structural drift and total displacement cannot be simply neglected.

7) An increase in initial shear wave velocity, shear wave velocity degradation ratio and σ results in a reduction in the probability of amplification in the structural response modification factors, as well as a reduction in the values of median percentage increase. Specifically, when $\sigma > 20$, detrimental soil-structure interaction effects on the structural response can be practically ignored.

8) An increase in φ reduces the probability of amplification in structural distortion such that the amplification can be practically ignored when $\varphi > 1.0$. However, the probabilities of amplification and the corresponding values of median percentage increase for structural drift or total displacement rise when φ increases.

References

[1] A. S. Veletsos and V. D. Nair, "Seismic interaction of structures on hysteretic foundations," *Journal of Structural Engineering,* vol. 101, pp. 109-129, 1975.

[2] J. Bielak, "Dynamic behaviour of structures with embedded foundations," *Earthquake Engineering and Structural Dynamics,* vol. 3, pp. 259-174, 1975.

[3] M. Ciampoli and P. E. Pinto, "Effects of soil-structure interaction on inelastic seismic response of bridge piers," *Journal of Structural Engineering,* vol. 121, pp. 806-814, 1995.

[4] J. P. Stewart, *et al.*, "Seismic soil-structure interaction in buildings. I: analytical methods," *Journal of Geotechnical and Geoenvironmental Engineering,* vol. 125, pp. 26-37, Jan 1999.

[5] J. P. Stewart, *et al.*, "Seismic soil-structure interaction in buildings. II: empirical findings," *Journal of Geotechnical and Geoenvironmental Engineering,* vol. 125, pp. 38-48, Jan 1999.

[6] J. Zhang and Y. Tang, "Dimensional analysis of structures with translating and rocking foundations under near-fault ground motions," *Soil Dynamics and Earthquake Engineering,* vol. 29, pp. 1330-1346, 2009.

[7] J. P. Wolf, *Foundation Vibration Analysis Using Simple Physical Models*. Englewood Cliffs, N.J.: Prentice-Hall, 1994.

[8] A. S. Veletsos, "Dynamics of structure-foundation systems," in *Structural and Geotechnical Mechanics*, ed Englewood Cliffs, N.J.: Prentice-Hall Inc., 1977, pp. 333-361.

[9] S. Dowdy and S. Wearden, *Statistics for Research*: Wiley, 1983.

CHAPTER

10. Integration of Soil-Foundation Interface Nonlinearity to Seismic Soil-Structure Interaction Analysis

Abstract. This chapter reviews a new soil-foundation interface macro-element that accounts for both soil material nonlinearity and interface geometrical nonlinearity. In this context, the fundamental concept behind the model is described and the formulation is presented.

10.1 Introduction

The results presented in the preceding chapters, similar to the most studies on soil-structure interaction and current design procedures, were based on the assumption that the soil adjacent to foundation behaves as a linear or at most an equivalent linear viscoelastic material. In addition, the foundation is assumed to be fully bonded to the soil underneath. However, geotechnical investigations after the Northridge 1994, Kobe 1995, Kocaeli 1999 and Christchurch 2010-2011 earthquakes have shown that significant nonlinear action in the soil and soil-foundation interface can be expected due to high levels of seismic excitation and spectral acceleration. Basically, three types of soil-foundation interface nonlinearity might occur during substantial ground shaking:

1) Sliding at the soil-foundation interface

2) Uplifting of the foundation from the supporting soil

3) Experiencing soil material nonlinearity underneath the foundation

Figure 10-1 illustrates these possible nonlinearities. Nonlinear conditions may be assumed as an energy dissipating mechanism that potentially may result in reduced structural response. However, they can also cause foundation settlement and permanent deformations in horizontal and rocking directions that consequently affect the overall behaviour of the structure. Hence, their net impact is not clear or easily predictable.

Figure 10-1. Possible types of soil-foundation interface nonlinearity.

Therefore, it is very important to investigate the influence of soil-foundation nonlinearity on the effects of seismic soil-structure interaction. This investigation can be achieved using complex nonlinear finite-element models and analysis. However, since a large amount of analyses are required to result in a reliable conclusion, using such rigorous finite-element models is very computationally expensive and not ideal. Thus, a simpler but still reliable tool is required to efficiently evaluate the effects of soil-foundation interface nonlinearity on the response of structures. In this context, the concept of macro-element has been developed over the last decade [1-7] to facilitate this goal.

Macro-element is a single element that can be attached to the base of a structural model replacing the entire soil-foundation medium. This relatively simple element aims to reproduce all nonlinearity expected at the foundation level including soil material nonlinearity (yielding) and interface geometrical nonlinearity (uplift), using a predefined nonlinear “constitutive law” linking generalized force parameters to the

corresponding displacement parameters. These generalized forces and displacements are selected such that to be directly linked to those related to the structure supported by the foundation. Therefore, macro-element can be viewed as a practical and rigorous modelling solution to enable efficient nonlinear dynamic analysis.

For the purpose of this research, the macro-element introduced by Chatzigogos et al. [6] for shallow foundations was chosen. This model was then implemented in the finite-element program Ruaumoko 3D as part of this research.

10.2 Macro-Element for Soil-Foundation Interface

The formulation of macro-element is based on a nonlinear constitutive law written in terms of force and displacement parameters [6]. The constitutive law is comprised of a linear and nonlinear part. The linear part is defined based on the commonly used foundation dynamic impedances. The nonlinear part covers two mechanisms: (i) totally reversible and non-dissipative foundation uplift; and (ii) irreversible soil material nonlinearity. The soil material nonlinearity is described by a bounding surface hypoplastic model, while the foundation uplift is defined by a phenomenological nonlinear elastic model. These mechanisms are briefly described in the following sections, while the interested reader is referred to the original work by Chatzigogos et al. [6] for complete details.

10.2.1 Fundamental Assumptions

The concept and formulation of a perfectly rigid circular foundation with diameter D located at the ground surface (zero embedment depth) is reviewed herein. The assumption of foundation rigidity allows the foundation to be represented as a single point, while the movement of any other parts of the foundation is defined based on the location of this point. The representative point is assumed to be at the centre of foundation, where the vertical and horizontal forces, as well as moments, are presumed to be acting. Corresponding to these forces, the vertical and horizontal displacements and foundation rocking are also evaluated at this point.

In the formulation defined, the soil is assumed to behave as an undrained cohesive material due to short duration of applied seismic loads, which does not allow the soil to dissipate the generated water pressure. In this context, the soil is characterised by a Tresca strength criterion with an associated plasticity rule. In addition, the soil-foundation interface is assumed to be a no-tension interface allowing for foundation uplift or deatachment between the soil and foundation. The interface strength criteria used for this condition is thus a no-tension interface. Finally, the uplift mechanism and the plasticity mechanism are treated independently in the current presentation of formulation.

10.2.2 Loading and Deformation Space

To facilitate the presentation of this model's concept, only a planar loading comprising a vertical force N_0, a horizontal force V_0 and a moment M_0 is considered. This type of loading is a relevant condition for a 2D analysis of soil-structure systems enforced to seismic forces. The definition of the adopted planar loading along with the corresponding displacements u_{fv}, u_{fh}, and u_{fr} are shown in Figure 10-2.

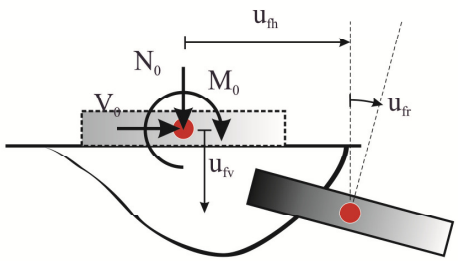

Figure 10-2. Definition of the planar loading along with the corresponding displacements.

10.2.3 Normalized Forces and Displacements

The constitutive equations of macro-element are written in terms of normalized forces and displacements. The normalization scheme used is defined:

$$\bar{Q} = \begin{pmatrix} Q_N \\ Q_V \\ Q_M \end{pmatrix} = \begin{pmatrix} N/N_{max} \\ V/N_{max} \\ M/DN_{max} \end{pmatrix} \tag{10.1}$$

$$\bar{q} = \begin{pmatrix} q_N \\ q_V \\ q_M \end{pmatrix} = \begin{pmatrix} u_{fv}/D \\ u_{fh}/D \\ u_{fr} \end{pmatrix} \tag{10.2}$$

where N_{max} is the maximum centred vertical force could be supported by the foundation in absence of any horizontal force and moment (or bearing capacity).

Considering the normalization scheme introduced, the force and displacement increments can be related to each other using a general tangent stiffness matrix $\bar{\bar{\mathfrak{R}}}$ defined:

$$\bar{\bar{\mathfrak{R}}} = \begin{bmatrix} \mathfrak{R}_v & \mathfrak{R}_{vh} & \mathfrak{R}_{vr} \\ \mathfrak{R}_{hv} & \mathfrak{R}_h & \mathfrak{R}_{hr} \\ \mathfrak{R}_{rv} & \mathfrak{R}_{rh} & \mathfrak{R}_r \end{bmatrix} = \frac{1}{N_{max}} \begin{bmatrix} D\widetilde{K}_v & D\widetilde{K}_{vh} & \widetilde{K}_{vr} \\ D\widetilde{K}_{hv} & D\widetilde{K}_h & \widetilde{K}_{hr} \\ \widetilde{K}_{rv} & \widetilde{K}_{rh} & \frac{1}{D}\widetilde{K}_r \end{bmatrix} \tag{10.3}$$

where $\widetilde{K}_{ij},\ i,j = v,h,r$ are the elements of tangent stiffness of the original soil-foundation system. Note that the final goal of the macro-element formulation is to define $\bar{\bar{\mathfrak{R}}}$ for each time step in an incremental dynamic analysis such that foundation uplift and soil material nonlinearity are properly taken into account. If $\bar{\bar{\mathfrak{R}}}$ is defined and the increment of normalized displacements $\dot{\bar{q}}$ is known, the increment of normalized forces $\dot{\bar{Q}}$ is then simply calculated:

$$\begin{pmatrix} \dot{Q}_N \\ \dot{Q}_V \\ \dot{Q}_M \end{pmatrix} = \bar{\bar{\mathfrak{R}}} \begin{pmatrix} \dot{q}_N \\ \dot{q}_V \\ \dot{q}_M \end{pmatrix} \tag{10.4}$$

Since the uplift mechanism and the plasticity mechanism are modelled separately, the normalized displacement response of the model $\bar{q}$ can be defined following a very simple rheological concept, in which the normalized displacement increment $\dot{\bar{q}}$ can be decomposed into an elastic part $\dot{\bar{q}}^{el}$ and a plastic part $\dot{\bar{q}}^{pl}$, yielding:

$$\dot{\bar{q}} = \dot{\bar{q}}^{el} + \dot{\bar{q}}^{pl} \tag{10.5}$$

This concept is also shown in Figure 10-3.

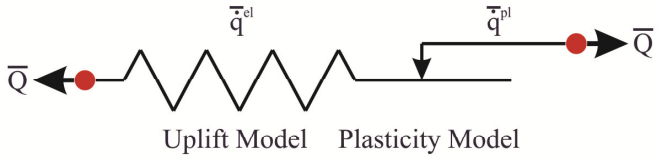

Figure 10-3. Simple rheological concept adopted in formulation of macro-element.

10.2.4 Nonlinear Elastic Mechanism for Uplift

The foundation uplift mechanism is described by a phenomenological nonlinear elastic model. Thus, the elastic response is incorporated into the model independent from any plastic soil behaviour. This approach results in a relationship linking the increment of forces with the increment of elastic displacements:

$$\dot{\bar{Q}} = \bar{\bar{\mathfrak{K}}}^{el} \dot{\bar{q}}^{el} \tag{10.6}$$

In this equation, $\bar{\bar{\mathfrak{K}}}^{el}$ is the tangent elastic stiffness matrix with elements that are functions of the elastic displacement increment, yielding:

$$\bar{\bar{\mathfrak{K}}}^{el} = f(\bar{\bar{q}}^{el}) \tag{10.7}$$

Before the initiation of foundation uplift, the elements of $\bar{\bar{\mathfrak{K}}}^{el}$ can be defined from the commonly used static foundation impedances [8]. Note that for shallow foundations located on the ground surface, only the diagonal terms need to be considered in $\bar{\bar{\mathfrak{K}}}^{el}$, as the coupling terms are almost negligible [9]. In this context, $\bar{\bar{\mathfrak{K}}}^{el}$ before foundation uplift is defined:

$$\bar{\bar{\mathfrak{R}}}^{el} = \begin{bmatrix} \mathfrak{R}_v^{st} & 0 & 0 \\ 0 & \mathfrak{R}_h^{st} & 0 \\ 0 & 0 & \mathfrak{R}_r^{st} \end{bmatrix} \tag{10.8}$$

where $\mathfrak{R}_v^{st}$, $\mathfrak{R}_h^{st}$ and $\mathfrak{R}_r^{st}$ are the normalized static foundation impedances in vertical, horizontal and rocking directions: $\mathfrak{R}_v^{st} = \frac{D}{N_{max}}\left(\frac{4Gr}{1-\nu}\right)$, $\mathfrak{R}_h^{st} = \frac{D}{N_{max}}\left(\frac{8Gr}{2-\nu}\right)$, $\mathfrak{R}_r^{st} = \frac{1}{DN_{max}}\left(\frac{8Gr^3}{3(1-\nu)}\right)$.

To define $\bar{\bar{\mathfrak{R}}}^{el}$ during foundation uplift, results from finite-element analysis of foundations rocking on elastic soil are required for calibration [4, 6, 10]. In this regard, it is first assumed that uplift is independent from the horizontal force applied on the foundation. Second, it is considered that uplift initiates when the absolute value of the moment applied on the foundation exceeds a specified limit $Q_{M,0}$. If the soil behaves elastically, $Q_{M,0}$ can be assumed to be a linear function of the applied vertical force on the foundation:

$$Q_{M,0} = \frac{Q_N}{\alpha} \tag{10.9}$$

However, as the plasticity mechanism has to be simultaneously considered, the limiting moment after which uplift initiates $Q_{M,0}$ is no longer a linear function of the applied vertical force, because the vertical stress below the foundation has to be limited to soil strength as the soil behaves plastically. In this case, an approximate formula proposed by Cremer [4] is used:

$$Q_{M,0} = \frac{Q_N}{\alpha}\exp(-\beta Q_N) \tag{10.10}$$

For both Equations (10.9) and (10.10), $\alpha = 6$ if circular foundations are taken into account. However, β is a numerical fit parameter that has to be defined from numerical analysis investigating foundation uplift on plastic soil. Cremer [4] also suggested that a variation range of $1.5 - 2.5$ can be considered for β.

In addition, three more approximations must be taken into account to completely define the elastic stiffness matrix $\bar{\bar{\mathfrak{R}}}^{el}$. These approximations are:

1) $\frac{Q_M}{Q_{M,0}} = 3 - 2(\frac{q_{M,0}^{el}}{q_M^{el}})^{0.5}$ for $|Q_M| > |Q_{M,0}|$ (10.11)

2) $\frac{\dot{q}_N^{el}}{\dot{q}_M^{el}} = -\frac{3}{4}(1 - \frac{q_{M,0}^{el}}{q_M^{el}})$ (10.12)

3) $\mathfrak{R}_v^{el}$ is assumed to be constant before and after uplift. This assumption means foundation uplift only affects the vertical force and displacement through the coupling term of $\mathfrak{R}_{rv}^{el} = \mathfrak{R}_{vr}^{el}$.

Following the assumptions and approximations introduced, the tangent elastic stiffness matrix $\bar{\bar{\mathfrak{R}}}^{el}$ is defined:

$$\bar{\bar{\mathfrak{R}}}^{el} = \begin{bmatrix} \mathfrak{R}_v^{st} & 0 & \mathfrak{R}_{vr}^{el} \\ 0 & \mathfrak{R}_h^{st} & 0 \\ \mathfrak{R}_{rv}^{el} & 0 & \mathfrak{R}_r^{el} \end{bmatrix} \tag{10.13}$$

where,

$$\mathfrak{R}_{vr}^{el} = \mathfrak{R}_{rv}^{el} = \begin{cases} 0, & |q_M^{el}| \le |q_{M,0}^{el}| \\ \frac{3}{4}(1 - \frac{q_{M,0}^{el}}{q_M^{el}})\mathfrak{R}_v^{st}, & |q_M^{el}| > |q_{M,0}^{el}| \end{cases} \tag{10.14}$$

$$\mathfrak{R}_r^{el} = \begin{cases} \mathfrak{R}_r^{st}, & |q_M^{el}| \le |q_{M,0}^{el}| \\ \left(\frac{q_{M,0}^{el}}{q_M^{el}}\right)^{3/2}\mathfrak{R}_r^{st} + \frac{9}{16}(1 - \frac{q_{M,0}^{el}}{q_M^{el}})^2\mathfrak{R}_v^{st}, & |q_M^{el}| > |q_{M,0}^{el}| \end{cases} \tag{10.15}$$

and $\mathfrak{R}_v^{st}$, $\mathfrak{R}_h^{st}$ and $\mathfrak{R}_r^{st}$ are the normalized static foundation impedances in the vertical, horizontal and rocking directions, respectively.

It should be noted that when foundation rocking q_M and, consequently, its elastic portion q_M^{el} becomes large, the maximum moment resisted by foundation (toppling moment) is obtained. Based on Equation (10.11), this moment is $Q_M = 3Q_{M,0}$ for circular foundations.

10.2.5 Plasticity Model

The soil plasticity mechanism is described by a bounding surface hypoplastic model. Specifically, an ellipsoid-type surface that is centred at the origin of a normalized force space (Q_N, Q_V and Q_M), called a bounding surface, is used to allow for a straightforward and flexible definition of plastic stiffness $\bar{\bar{\mathfrak{K}}}^{pl}$. If the state of forces applied on the foundation $\bar{Q}$ stays in the interior of this surface, a continuous plastic response is obtained. This plastic response, similar to that for classical plasticity theory, is a function of the distance between the current state of forces and its image point on the bounding surface $I(\bar{Q})$ that is defined based on a radial mapping rule. As the state of forces approaches the bounding surface, the plastic response becomes more and more pronounced with eventual plastic flow occurring when the state of forces reaches the bounding surface. This situation corresponds to a bearing capacity failure of the foundation [11].

The bounding surface $f_{BS}(\bar{Q})$ can be described by a simple approximation sufficient enough for the purpose of macro-element application:

$$f_{BS}(\bar{Q}) = Q_N^2 + (\frac{Q_V}{Q_{V,max}})^2 + (\frac{Q_M}{Q_{M,max}})^2 - 1 = 0 \tag{10.16}$$

In Equation (10.16), $Q_{V,max}$ and $Q_{M,max}$ for a circular foundation are defined [6]:

$$Q_{V,max} = \frac{c_0 A}{N_{max}} = 0.165 \tag{10.17}$$

$$Q_{M,max} = \frac{0.67 c_0 AD}{DN_{max}} = 0.11 \tag{10.18}$$

where A is the foundation area and D is the foundation diameter. The bounding surface defined for hypoplastic soil behaviour is illustrated schematically in Figure 10-4.

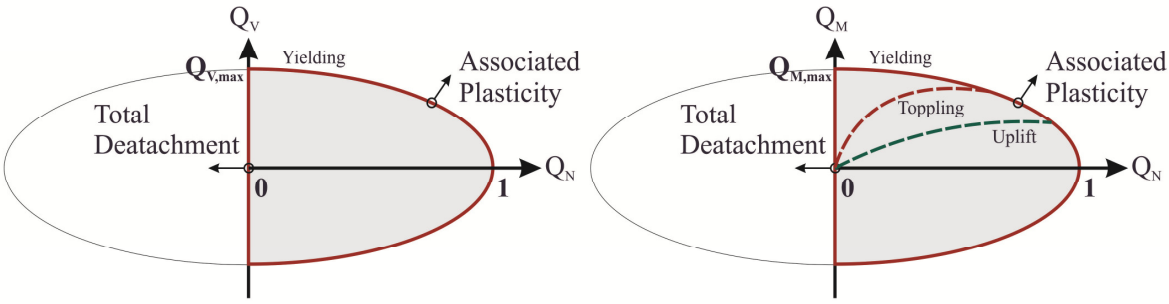

Figure 10-4. Bounding surface for hypoplastic soil behaviour incorporated in macro-element formulation.

As mentioned earlier, a simple radial mapping rule is used to define the plastic response of the macro-element in its current formulation. This rule maps every point in the interior of the bounding surface $\bar{Q}$ to an image point $I(\bar{Q})$ on the surface boundary. The image point $I(\bar{Q})$ is defined:

$$I(\bar{Q}) = \{\lambda \bar{Q} | I \in \partial f_{BS}, \lambda \geq 1.0\} \tag{10.19}$$

where ∂f_{BS} is the boundary of the bounding surface f_{BS}. The defined image point $I(\bar{Q})$ is then used to specify:

1) The situations of loading, unloading and reloading
2) The direction of plastic displacement increment $\bar{q}^{pl}$
3) The magnitude of the plastic stiffness $\bar{\bar{\Re}}^{pl}$

In this formulation, loading and reloading are treated as a plastic mechanism, while unloading is treated as an elastic mechanism. For plastic loading, the relationship between the increment of forces $\dot{\bar{Q}}$ and the increment of plastic displacements $\dot{\bar{q}}^{pl}$ is defined:

$$\dot{\bar{Q}} = \bar{\bar{\Re}}^{pl}\dot{\bar{q}}^{pl} \tag{10.20}$$

where $\bar{\bar{\Re}}^{pl}$ is the plastic stiffness matrix and its inverse $\bar{\bar{\Re}}^{pl^{-1}}$ is given by:

$$\bar{\bar{\Re}}^{pl^{-1}} = h^{-1}\bar{n}\otimes\bar{n} \tag{10.21}$$

In Equation (10.21), h is a diagonal matrix that expresses the magnitude of plastic response, and $\bar{n}$ is the unit vector normal to the bounding surface on the image point that defines the direction of the increment of plastic displacements. In the context of bounding surface hypoplasticity, h is defined as a function of the distance between the current state of forces $\bar{Q}$ and its image point $I(\bar{Q})$. This distance can be measured by the positive scalar λ defined in Equation (10.19). As suggested by Butterfield [12], h can be approximated as a logarithmic function of λ:

$$h = h(\lambda) = h_0 \ln(\lambda) \tag{10.22}$$

where h_0 in Equation (10.22) is the initial plastic stiffness matrix and has to be calibrated based on the loading test of the foundation under centred vertical loading. Basically, h_0 is defined:

$$h_0 = p_1 \begin{bmatrix} \Re_v^{st} & 0 & 0 \\ 0 & \Re_h^{st} & 0 \\ 0 & 0 & \Re_r^{st} \end{bmatrix} \tag{10.23}$$

where p_1 is a numerical parameter. For cyclic loading, the relationship between h and λ is defined:

$$h = \ln\left(\frac{\lambda^{p_2+1}}{\lambda_{min}^{p_2}}\right) h_0 \tag{10.24}$$

in this equation, λ_{min} is the minimum value of λ obtained during loading and p_2 is a numerical parameter expressing the extent of plastic response in reloading. Note that in

Equation (10.24), $\lambda = \lambda_{min}$ when virgin loading is considered, and $\lambda > \lambda_{min}$ when reloading situation is taken into account. Consequently, the foundation response is less plastic in reloading as λ/λ_{min} is always greater than 1.0. In addition, when λ is large, h is also large and, as a result, the magnitude of the increment of plastic displacements is small, meaning the response is almost elastic. However, when λ is small, $h \to 0$ and the system head to the state of plastic flow.

10.2.6 Model Parameters

A summary of the macro-element parameters for circular foundations is presented in Table 10-1. In this table, formulation required to define the model parameters and a brief description of how to define the adopted numerical values is described.

Table 10-1. Summary of the soil-foundation interface model parameters for circular foundations.

Parameter	Formulation/Description
Initial Stiffness	
1. Vertical stiffness	$K_v = \frac{4Gr}{1-\upsilon}$
2. Horizontal stiffness	$K_h = \frac{8Gr}{2-\upsilon}$
3. Rocking stiffness	$K_r = \frac{8Gr^3}{3(1-\upsilon)}$
Plasticity Parameters	
1. Maximum centred vertical force supported by foundation	$N_{max} = 6.06c_0A$
2. Maximum normalized horizontal force supported by foundation	$Q_{V,max} = \frac{c_0A}{N_{max}} = 0.165$
3. Maximum normalized moment supported by foundation	$Q_{M,max} = \frac{0.67c_0AD}{DN_{max}} = 0.11$
4. Numerical parameter expressing the extent of initial plastic stiffness	p_1: has to be calibrated based on the loading test of the foundation under centred vertical loading
5. Numerical parameter expressing the extent of stiffness degradation in reloading	p_2: has to be calibrated based on the loading-unloading-reloading test of the foundation under centred vertical loading
Uplift Parameters	
1. $\alpha = 6$	$Q_{M,0} = \pm\frac{Q_N}{\alpha}\exp(-\beta Q_N)$
2. $\beta = 2$	
3. $\xi = 0.75$	$\mathfrak{R}_{vr}^{el} = \mathfrak{R}_{rv}^{el} = \begin{cases} 0, & \lvert q_M^{el}\rvert \le \lvert q_{M,o}^{el}\rvert \\ \xi(1-\frac{q_{M,o}^{el}}{q_M^{el}})\mathfrak{R}_v^{st}, & q_M^{el}\rvert > \lvert q_{M,o}^{el}\rvert \end{cases}$
4. $\delta = 0.5$	$\mathfrak{R}_r^{el} =$
5. $\gamma = 2$	$\begin{cases} K_r, & \lvert q_M^{el}\rvert \le \lvert q_{M,o}^{el}\rvert \\ \gamma\delta\left(\frac{q_{M,o}^{el}}{q_M^{el}}\right)^{1+\delta}\mathfrak{R}_r^{st} + \xi^2(1-\frac{q_{M,o}^{el}}{q_M^{el}})^2\mathfrak{R}_v^{st}, & q_M^{el}\rvert > \lvert q_{M,o}^{el}\rvert \end{cases}$
6. $Q_M/Q_{M,0}$	$\frac{Q_M}{Q_{M,0}} = 3 - 2(\frac{q_{M,0}^{el}}{q_M^{el}})$
Radiation Damping	
1. Vertical damping	$C_v = \rho[\frac{3.4}{\pi(1-\upsilon)}V_s]A$
2. Horizontal damping	$C_h = \rho V_s A$
3. Rocking damping	$C_r = \rho[\frac{3.4}{\pi(1-\upsilon)}V_s]I_r$

The parameters utilized in this table are defined below:

- ρ, υ, V_s and G: soil mass density, Poisson's ratio, soil shear wave velocity and soil shear wave modulus.
- r, A and I_r: equivalent radius of the foundation, area of the foundation ($A = \pi r^2$), mass moment of inertia for rocking motion ($I_r = \pi r^4/4$).
- c_0: soil cohesion.

10.3 Summary

The concept and formulation of a new soil-foundation interface macro-element introduced by Chatzigogos et al. [6] was reviewed in this chapter. This model is based on a nonlinear constitutive law comprised of a linear and nonlinear part. Its nonlinear part covers both soil material nonlinearity and interface geometrical nonlinearity using a simple rheological concept. Because of its simplicity, macro-element is ideal for nonlinear dynamic analysis and, consequently, it prevents using computationally expensive finite-element models. In addition, it readily provides a sufficient precision required to investigate the nonlinear seismic soil-structure interaction on the structural response.

In the next chapter, an attempt made to implement this model in the finite-element program Ruaumoko 3D is described and the element test simulation results are presented.

References

[1] R. Nova and L. Montrasio, "Settlement of shallow foundations on sand," *Geotechnique,* vol. 41, pp. 243-256, Jun 1991.

[2] R. Paolucci, "Simplified evaluation of earthquake-induced permanent displacements of shallow foundations," *Journal of Earthquake Engineering,* vol. 1, pp. 563-579, 1997.

[3] C. Cremer*, et al.*, "Cyclic macro-element for soil-structure interaction: material and geometrical non-linearities," *International Journal for Numerical and Analytical Methods in Geomechanics,* vol. 25, pp. 1257-1284, Nov 2001.

[4] C. Cremer*, et al.*, "Modelling of nonlinear dynamic behaviour of a shallow strip foundation with macro-element," *Journal of Earthquake Engineering,* vol. 6, pp. 175-211, Apr 2002.

[5] Y. Le Pape and J. G. Sieffert, "Application of thermodynamics to the global modelling of shallow foundations on frictional material," *International Journal for Numerical and Analytical Methods in Geomechanics,* vol. 25, pp. 1377-1408, Dec 2001.

[6] C. T. Chatzigogos*, et al.*, "Macroelement modeling of shallow foundations," *Soil Dynamics and Earthquake Engineering,* vol. 29, pp. 765-781, 2009.

[7] C. T. Chatzigogos*, et al.*, "A macroelement formulation for shallow foundations on cohesive and frictional soils," *International Journal for Numerical and Analytical Methods in Geomechanics,* 2010.

[8] G. Gazetas, "Formulas and charts for impedances of surface and embedded foundations," *Journal of geotechnical engineering,* vol. 117, pp. 1363-1381, 1991.

[9] A. S. Veletsos and Y. T. Wei, "Lateral and rocking vibrations of footings," *Journal of Soil Mechanics and Foundation Division,* vol. 97, pp. 1227-1248, 2001.

[10] J. P. Wolf, *Soil-Structure-Interaction Analysis in Time Domain*. Englewood Cliffs, N.J.: Prentice-Hall, 1988.

[11] A. Pecker and C. T. Chatzigogos, "Non linear soil structure interaction: impact on the seismic response of structures," presented at the 14th European Conference on Earthquake Engineering, Ohrid, Republic of Macedonia, 2010.

[12] R. Butterfield, "A simple analysis of the load capacity of rigid footings on granular materials," *Journée de Geotechnique,* pp. 128-134, 1980.

CHAPTER

11. Implementation of Macro-Element in Finite-Element Program Ruaumoko 3D

Abstract. The macro-element introduced in the previous chapter incorporating soil material nonlinearity and interface geometrical nonlinearity is used in the rest of this research. To enable this goal possible, this element was implemented in the finite-element program Ruaumoko 3D. This chapter describes the implementation procedure. Algorithms developed for this purpose are explained first, and the element test simulation results for a comprehensive set of loading scenarios are shown afterwards.

11.1 The Algorithms for Model Implementation

The macro-element works based on an incremental displacement-control formulation. The essence of the computation flow used in Ruaumoko 3D is outlined in the flow chart of Figure 11-1. As shown in this figure, for a given increment of displacements $\bar{\dot{u}}$, the algorithm calculates the increment of forces $\bar{\dot{F}}$ and the updated tangent stiffness matrix $\bar{\bar{K}}$. The algorithm also requires: (i) the current state of forces $\bar{F}^i$; (ii) and an estimate of the increment of forces $\bar{\dot{F}}_{estimated}$ that is defined from the multiplication of the current tangent stiffness matrix by the given increment of displacements. The current state of forces is used to define the uplift initiation limit, as well as the extent of nonlinearity in

the plasticity mechanism. Equally, the estimate of increment of forces is used to distinguish between the loading, unloading and reloading scenarios. Note that all the calculations in the algorithm are made in the normalized space in terms of forces and displacements.

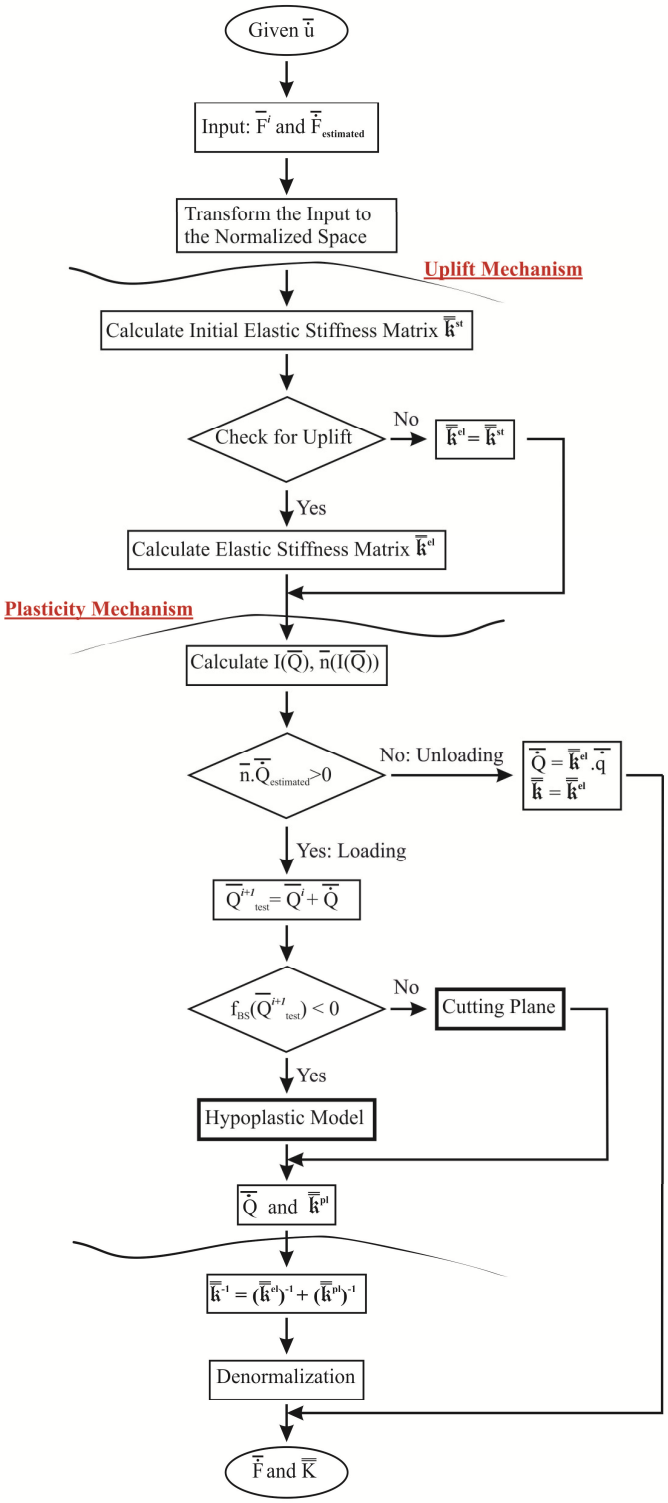

Figure 11-1. Flow chart of the computation scheme adopted for implementing the macro-element formulation in finite-element program Raumoko 3D.

The algorithm first defines the normalised tangent elastic stiffness matrix $\bar{\bar{\Re}}^{el}$, following the formulations introduced in Section 10.2.4 for the uplift mechanism. Then, it follows the formulations introduced for plasticity mechanism in Section 10.2.5 to define the normalised increment of forces $\bar{\dot{Q}}$ and the normalised tangent plastic stiffness matrix $\bar{\bar{\Re}}^{pl}$. Having defined both $\bar{\bar{\Re}}^{el}$ and $\bar{\bar{\Re}}^{pl}$, the inverse of the normalized tangent stiffness matrix $\bar{\bar{\Re}}^{-1}$ is calculated as the sum of $(\bar{\bar{\Re}}^{el})^{-1}$ and $(\bar{\bar{\Re}}^{pl})^{-1}$. Finally, following a denormalization process, the increment of forces $\bar{\dot{F}}$ and the updated tangent stiffness matrix $\bar{\bar{K}}$ are defined using the calculated values for $\bar{\dot{Q}}$ and $\bar{\bar{\Re}}$.

11.1.1 Hypoplastic Model Algorithm

The main purpose of the algorithm adopted for the Hypoplastic Model is to define the normalised increment of forces $\bar{\dot{Q}}$ and the normalised tangent plastic stiffness matrix $\bar{\bar{\Re}}^{pl}$. To achieve this goal, the simple rheological concept illustrated in Figure 10.3 for defining the macro-element response is used. Based on this concept, any increment of displacements applied to the macro-element $\bar{\dot{q}}$ can be decomposed into two incremental components: (i) increment of elastic displacements $\bar{\dot{q}}^{el}$; and (ii) increment of plastic displacements $\bar{\dot{q}}^{pl}$:

$$\bar{\dot{q}} = \bar{\dot{q}}^{el} + \bar{\dot{q}}^{pl} \tag{11.1}$$

Since the two elastic and plastic mechanisms are working in series, the generated forces for both mechanisms are the same and are similar to the total increment of forces $\bar{\dot{Q}}$. Since the increment of forces results from the multiplication of the tangent stiffness matrix by the increment of displacements, the following equation can be written:

$$\bar{\bar{\Re}}^{el}\bar{\dot{q}}^{el} = \bar{\bar{\Re}}^{pl}\bar{\dot{q}}^{pl} \tag{11.2}$$

Equation (11.2) can be rewritten:

$$\bar{\dot{q}}^{pl} = (\bar{\bar{\Re}}^{pl})^{-1}\bar{\bar{\Re}}^{el}\bar{\dot{q}}^{el} \tag{11.3}$$

Substituting the derived $\bar{\dot{q}}^{pl}$ into Equation (11.1), $\bar{\dot{q}}^{el}$ is calculated:

$$\bar{\dot{q}}^{el} = [I + (\bar{\bar{\Re}}^{pl})^{-1}\bar{\bar{\Re}}^{el}]^{-1}\bar{\dot{q}} \tag{11.4}$$

The $\bar{\dot{q}}^{el}$ defined is then used to calculate $\bar{\dot{Q}}$:

$$\bar{\dot{Q}} = \bar{\bar{\Re}}^{el}\bar{\dot{q}}^{el} \tag{11.5}$$

Now, to define the normalised tangent plastic stiffness matrix $\bar{\bar{\Re}}^{pl}$, it is only needed to use the formulation introduced in Section 10.2.5 for the updated state of normalized forces defined:

$$\bar{Q}^{i+1} = \bar{Q}^{i} + \bar{\dot{Q}} \tag{11.6}$$

11.1.2 Cutting Plane Algorithm

The Cutting Plane algorithm is developed to prevent the state of forces being outside the bounding surface. Basically, if in any case the state of forces goes beyond the bounding surface as a result of an applied increment of forces, the Cutting Plane tries to bring the forces back inside the bounding surface in the same direction as the original increment of forces following a simple scaling procedure. This procedure is shown in Figure 11-2.

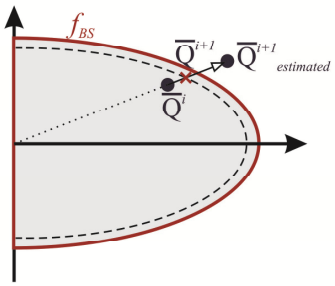

Figure 11-2. The scaling procedure used in the algorithm developed for Cutting Plane.

To describe the scaling procedure developed, $\bar{Q}^{i}$ is assumed as the current state of forces that has to be increased by the imposed increment of forces $\bar{\dot{Q}}$. As shown in

Figure 11-2, the updated state of forces $\bar{Q}^{i+1}_{estimated} = \bar{Q}^{i} + \dot{\bar{Q}}$ is beyond the bounding surface, which does not have any physical meaning. Therefore, these forces have to be scaled back to the bounding surface. To avoid numerical issues caused when the forces are exactly located on the bounding surface, an assumed boundary with a very small difference from the original one is defined inside the bounding surface. It is noted that the function f_{BS} results in a value of $-\varepsilon$ (a very small number) instead of 0 for any state of forces that locate on this assumed boundary.

The scaling factor applies to $\dot{\bar{Q}}$ to bring $\bar{Q}^{i+1}_{estimated}$ to this boundary is calculated using a simple geometrical relationship. If it is assumed that $f_{BS}(\bar{Q}^{i}) = f_1$ and $f_{BS}(\bar{Q}^{i+1}_{estimated}) = f_2$, the scaling factor is then calculated:

$$SF = \frac{|f_1| - \varepsilon}{|f_1| + |f_2|} \tag{11.7}$$

Therefore, the actual increment of forces to be used is $SF \times \dot{\bar{Q}}$. Consequently, the normalised tangent plastic stiffness matrix $\bar{\bar{\Re}}^{pl}$ can be defined using the formulation introduced in Section 10.2.5. for the updated state of normalized forces: $\bar{Q}^{i+1} = \bar{Q}^{i} + SF \times \dot{\bar{Q}}$.

11.2 Definition of the Macro-Element in Ruaumoko 3D

The analysis data required in Ruaumoko 3D to define the macro-element is described by the input lines as below:

Basic Element Properties

$JPLAS$	SL	D	N_{max}	K_v	K_h	K_r	$Q_{V,max}$	$Q_{M,max}$	p_1	p_2	WGT

$JPLAS$	$= 0;$	Elastic only
	$= 1;$	Inelastic
SL	$= 0;$	End 1 of member at surface
	$= 1;$	End 2 of member at surface

D	=	Foundation diameter
N_{max}	=	Maximum centred vertical force supported by foundation
K_v	=	Vertical Static stiffness
K_h	=	Horizontal Static stiffness
K_r	=	Rocking Static stiffness
$Q_{V,max}$	=	Maximum normalized horizontal force
$Q_{M,max}$	=	Maximum normalized moment
p_1	=	Numerical parameter for plasticity model
p_2	=	Numerical parameter for plasticity model
WGT	=	Weight of foundation member

Uplift Parameters

α	β	ξ	δ	γ	$Q_M/Q_{M,0}$

α	=	Numerical parameter for uplift initiation limit
β	=	Numerical parameter for uplift initiation limit
ξ	=	Numerical parameter for modifying the coupling stiffness
δ	=	Numerical parameter for modifying the rocking stiffness
γ	=	Numerical parameter for modifying the rocking stiffness
$Q_M/Q_{M,0}$	=	Foundation toppling limit

11.3 Element Test Simulation Results

In this section, the response of the macro-element under different loading scenarios is investigated. The goal is to observe whether the model works as expected under different conditions. This goal was achieved by performing a comprehensive set of numerical force-control simulations summarized in Table 11-1. For each simulation, a

loading time-history was applied on the centre of foundation, and the foundation response in terms of deformation time-history, force-deformation hysteretic loop and the variation of stiffness with time was recorded. In Table 11-1, N_0, V_0 and M_0 represent vertical force, horizontal force and moment applied on the foundation, respectively.

11.3.1 Loading Scenarios

Loading scenario LP1 was selected to present the basic nonlinear behaviour of element by pushing it in vertical direction to the bounding surface. Consequently, the vertical stiffness should gradually become very small and a large vertical displacement should also occur. To observe what happens if the applied load intersects the bounding surface, loading scenario LP2 was selected. Specifically, the element was pushed with a force larger than foundation capacity in vertical direction N_{max}. Theoretically, the foundation failure has to take place. However, the element should be numerically stable, regardless of showing a very large displacement and almost negligible stiffness.

Loading scenario LP3 was selected to present the element response under an increasing and then constant vertical load. This scenario is important as it is the case in many realistic situations. Usually, the foundation is loaded under the weight of structure and when the vertical load is constant, it might be forced to a horizontal force and/or moment. Therefore, a stable response under this loading scenario is expected.

To investigate the behaviour of element under cyclic loading, two loading scenarios in vertical direction, LP4 and Lp5, were used. Specifically, LP4 represents a loading-unloading-reloading case with an increasing pattern approaching to N_{max}. Equally, LP5 shows a loading-unloading-neutral loading-reloading pattern with the maximum load being N_{max}. In both cases, a smooth transition between different loading phases is expected. In addition, the stiffness in unloading phase should be the same as the initial elastic stiffness, and a similar force-displacement trend should be followed in each reloading phase.

The next loading scenarios considered were monotonic rocking under two different vertical force conditions. In this context, LP6 was used to represent a condition when vertical force is small and toppling failure mechanism is dominant. The considered

vertical force on the element was assumed to be $0.2N_{max}$ and the element was pushed by an increasing moment to the corresponding toppling moment. Equally, LP7 was used to represent a condition where vertical force is large and yielding failure mechanism is dominant. In this case, the vertical force was $0.8N_{max}$ and the element was pushed by an increasing moment to a value beyond the yielding moment. Note LP7 is also useful to check the stability of the element after yielding.

In both scenarios, a gradual decrease of rocking stiffness and a continuing increase of rocking are expected. However, for LP7, the stiffness should be very small and the rocking should be very large due to yielding. In addition, the effect of uplift on the rocking stiffness, which is a localised change in the stiffness value, should be observed. When toppling mechanism is dominant, LP6, the vertical displacement is expected to decrease. It means that the centre of foundation intends to move upwards. However, when yielding mechanism governs, LP7, vertical displacement is expected to largely increase similar to rocking.

The element response under cyclic rocking was also investigated by the loading scenario LP8. In this case, only a vertical force corresponding to $N_0 = 0.8N_{max}$ was considered, and a loading-unloading-reloading pattern with an increasing value approaching to the yielding moment. Similar to LP4 and LP5, a smooth transition between different loading phases, a same stiffness for unloading as initial elastic stiffness and a similar force-displacement trend in reloading phases are expected.

LP9 and LP10 were selected to present the element response under monotonic horizontal force and under same vertical force conditions previously introduced. In both cases, the horizontal force was increased to the corresponding yielding force V_{max}. Trends and observations should be similar to that has been explained for LP1 and LP2 when the basic nonlinear behaviour is expected. Equally, to study the element behaviour under cyclic horizontal loading, scenario LP11 was considered. For this loading scenario, the element was pushed vertically to $N_0 = 0.8N_{max}$, and simultaneously forced to a loading-unloading-reloading pattern with an increasing horizontal force approaching to V_{max}. Due to yielding, an increased displacement in both horizontal and

vertical direction is expected. In addition, a smooth transition between different loading phases should be observed.

The element behaviour under the combined vertical, horizontal and rocking forces were next investigated by using the loading scenarios of LP12 and LP13, where LP12 presents a monotonic loading pattern and LP13 shows a cyclic one. It was assumed that the element is pushed vertically to $N_0 = 0.8N_{max}$ and enforced to either an increasing horizontal force to V_{max} (LP12) or a loading-unloading-reloading pattern with an increasing horizontal force approaching to V_{max} (LP13). In addition, the horizontal force was considered to be interrelated to the applied moment, assuming it is located at 10 m high above the foundation level. Thus, the relation between the applied horizontal force and moment is $V_0 = 10M_0$. Trends and behaviours should follow that has been previously explained for individual scenarios.

Finally, the element response to time-history loading was studied considering loading scenarios of LP14 and LP15. The applied vertical force was assumed to be $N_0 = 0.2N_{max}$, and the relation between horizontal force and moment was considered to be the same as that for LP12 and LP13. The maximum horizontal force was selected such that to result in the element yielding. The only difference between LP14 and LP15 is that for LP15 foundation mass, mass moment of inertia and radiation damping were also considered. A stable result is what has to be observed for these two loading scenarios.

Table 11-1. List of the adopted numerical force-controlled simulations.

Loading	**Description**
LP1	Monotonic vertical loading: $N_0 \rightarrow N_{max}$
LP2	Monotonic vertical loading: $N_0 > N_{max}$
LP3	Monotonic vertical loading: $N_0 = 0.8N_{max}$
LP4	Cyclic vertical loading – Type 1: $N_0 \rightarrow N_{max}$
LP5	Cyclic vertical loading – Type 2: $N_0 \rightarrow N_{max}$
LP6	Monotonic rocking: $N_0 = 0.2N_{max}$, $M_0 \rightarrow M_T$
LP7	Monotonic rocking: $N_0 = 0.8N_{max}$, $M_0 > M_{max}$
LP8	Cyclic rocking: $N_0 = 0.8N_{max}$, $M_0 > M_{max}$
LP9	Monotonic horizontal loading: $N_0 = 0.2N_{max}$, $V_0 \rightarrow V_{max}$
LP10	Monotonic horizontal loading: $N_0 = 0.8N_{max}$, $V_0 \rightarrow V_{max}$
LP11	Cyclic horizontal loading: $N_0 = 0.8N_{max}$, $V_0 \rightarrow V_{max}$

Table 11.1. *Continued*.

Loading	Description
LP12	Monotonic horizontal loading with rocking: $N_0 = 0.2N_{max}$, $V_0 \rightarrow V_{max}, M_0 = 10V_0$
LP13	Cyclic horizontal loading with rocking: $N_0 = 0.2N_{max}$, $V_0 \rightarrow V_{max}, M_0 = 10V_0$
LP14	Time-history horizontal loading with rocking: $\mathrm{N_0 = 0.2N_{max}}$, $\mathrm{V_0 \rightarrow V_{max}}, \mathrm{M_0 = 10V_0}$
LP15	Time-history horizontal loading with rocking: $\mathrm{N_0 = 0.2N_{max}}$, $\mathrm{V_0 \rightarrow V_{max}}, \mathrm{M_0 = 10V_0}$

Note. LP 15 is the only loading protocol for which foundation mass, mass moment of inertia and radiation damping are considered.

11.3.2 Properties of the Model

The properties of the soil-foundation interface selected for the purpose of this investigation are presented in Table 6-1. Based on these properties, the parameters of the representative macro-element were then defined, as summarized in

Table 11-3. The corresponding bounding surface of the soil-foundation interface considered is presented in Figure 11-3. Note that the surface is only shown in a 2D space. Specifically, the interaction between the vertical force and moment/horizontal force is shown.

Table 11-2. Properties of the considered soil-foundation interface.

Parameters	Value
Foundation Parameters	
D: Diameter	12 m
M_f: Mass	$5\,E+5$ kg
M_r: Mass moment of inertia	$2.21\,E+7$ kgm^2
Interface Parameters	
Uplift and sliding are allowed	
Soil Parameters	
c_0: Uniform cohesion	$5\,E+4$ Pa
G: Initial shear modulus	$8\,E+7$ Pa
υ: Poisson's ratio	0.5
ρ: Mass density	$2\,E+4$ N/m^3

Table 11-3. Parameters of the considered soil-foundation interface macro-element.

Parameter (*ref.* Table 10-1)	**Value**
Initial Stiffness	
K_v	3838 MN/m
K_h	2558 MN/m
K_r	92103 MN/rad
Plasticity Parameters	
N_{max}	34 MN
p_1	0.1
p_2	5
Radiation Damping	
C_v	99 MNs/m
C_h	46 MNs/m
C_r	889 MNs/rad

The parameters utilized for uplift are:
$\alpha = 6,\ \beta = 2,\ \xi = 0.75,\ \delta = 0.5,\ \gamma = 2$ and $\frac{Q_M}{Q_{M,0}} = 3$.

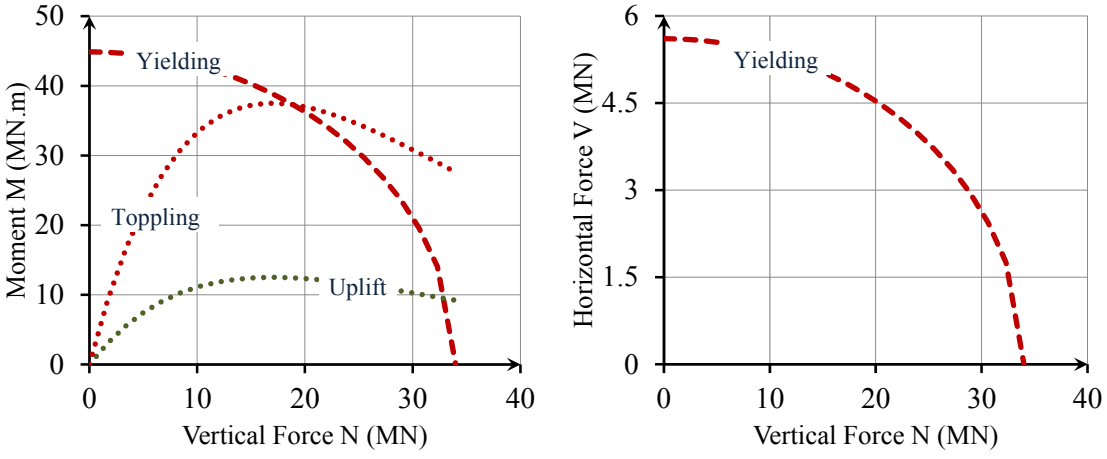

(a) (b)

Figure 11-3. Surface of the ultimate loads for the considered soil-foundation interface model: (a) interaction between moment and vertical force; (b) interaction between horizontal and vertical forces.

11.3.3 Results

From all considered loading scenarios only LP1, LP2, LP4, LP12, LP13, LP14 and LP15 that has more degrees of interest are presented in Figures 11-4 to 11-10. The remaining illustrations are presented in Appendix F. As shown, the implemented macro-element works as expected. Thus, it can be reliably used for any future analysis.

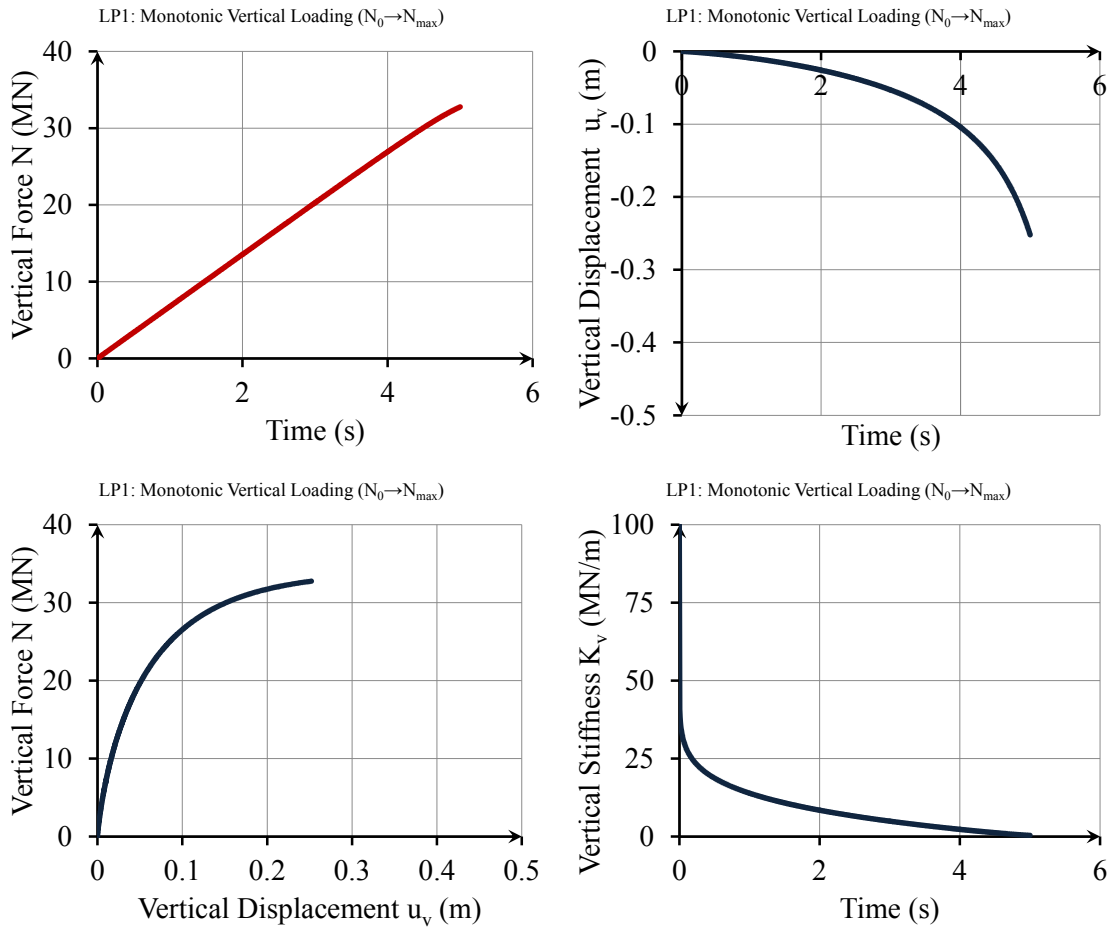

Figure 11-4. The behaviour of macro-element under monotonic vertical loading ($N_0 \rightarrow N_{max}$).

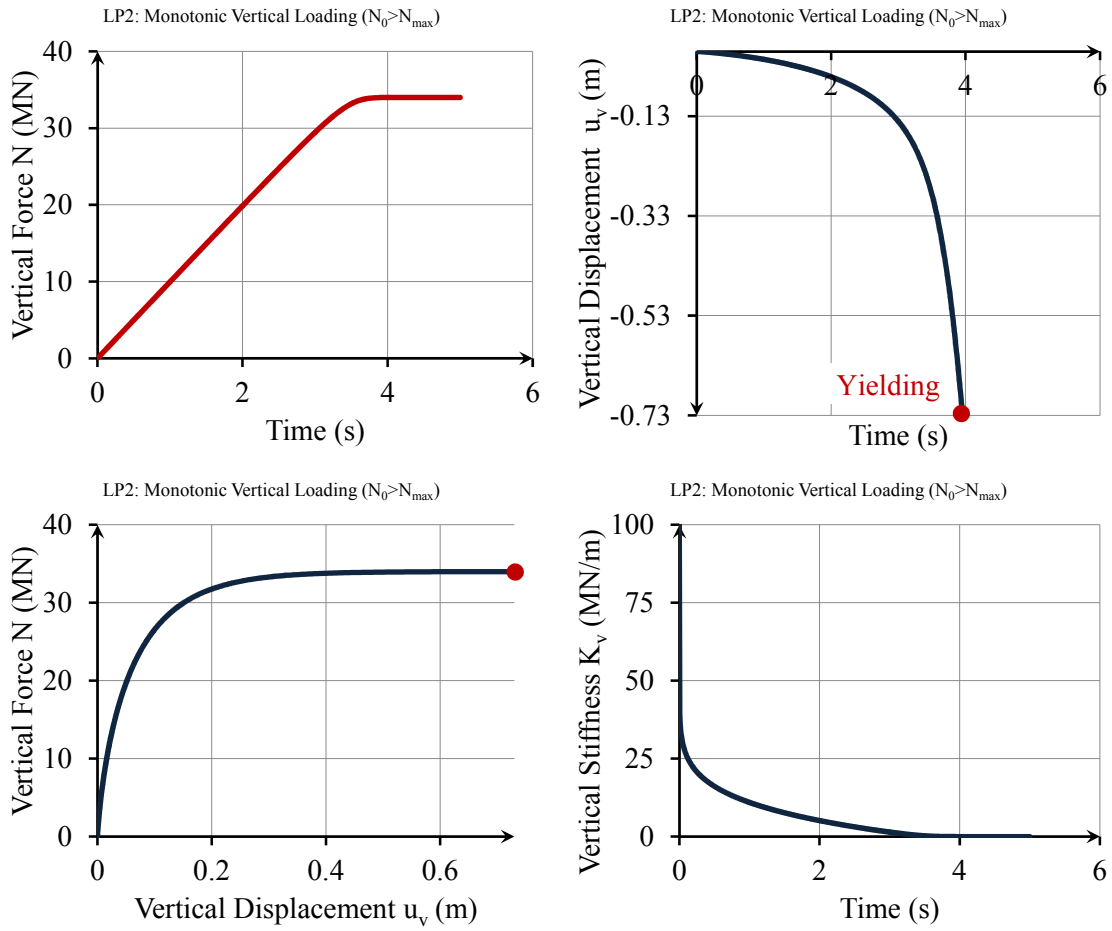

Figure 11-5. The behaviour of macro-element under monotonic vertical loading (N_0>N_{max}).

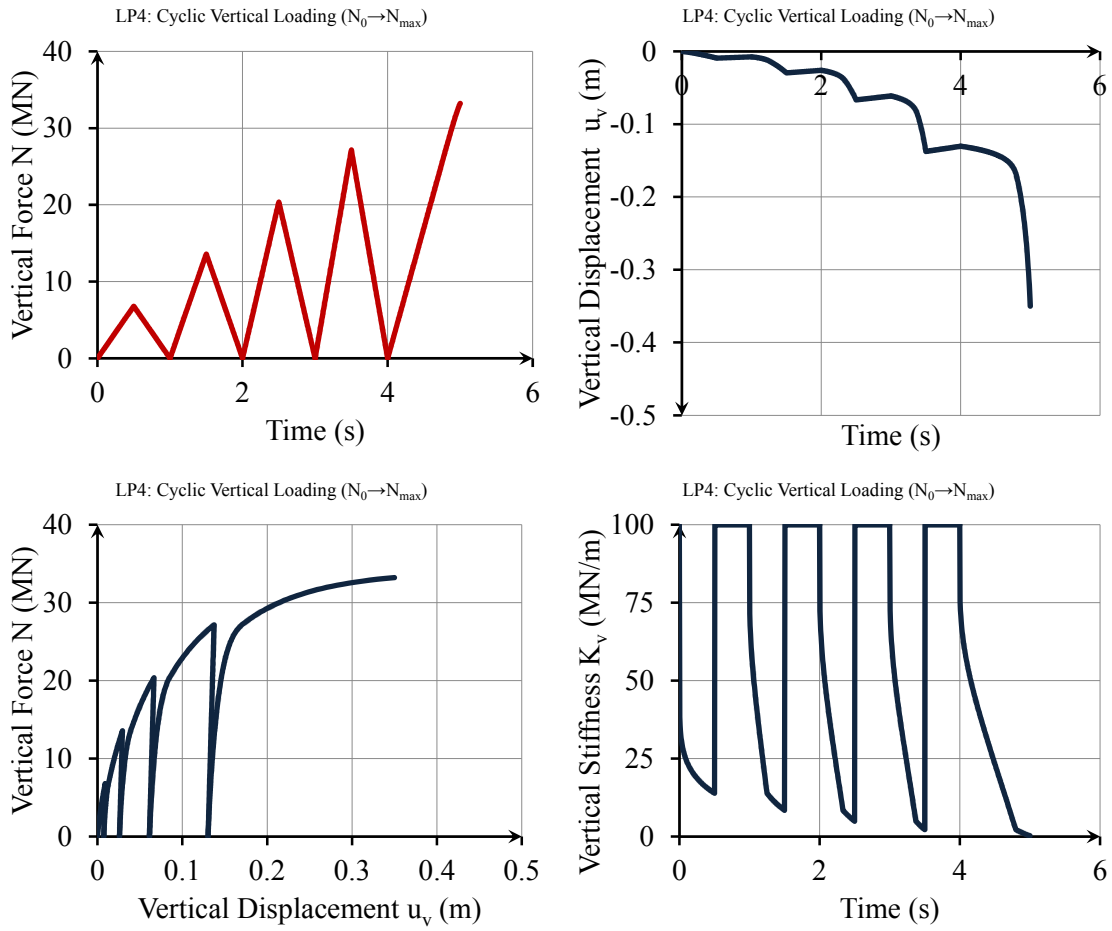

Figure 11-6. The behaviour of macro-element under cyclic vertical loading ($N_0 \rightarrow N_{max}$).

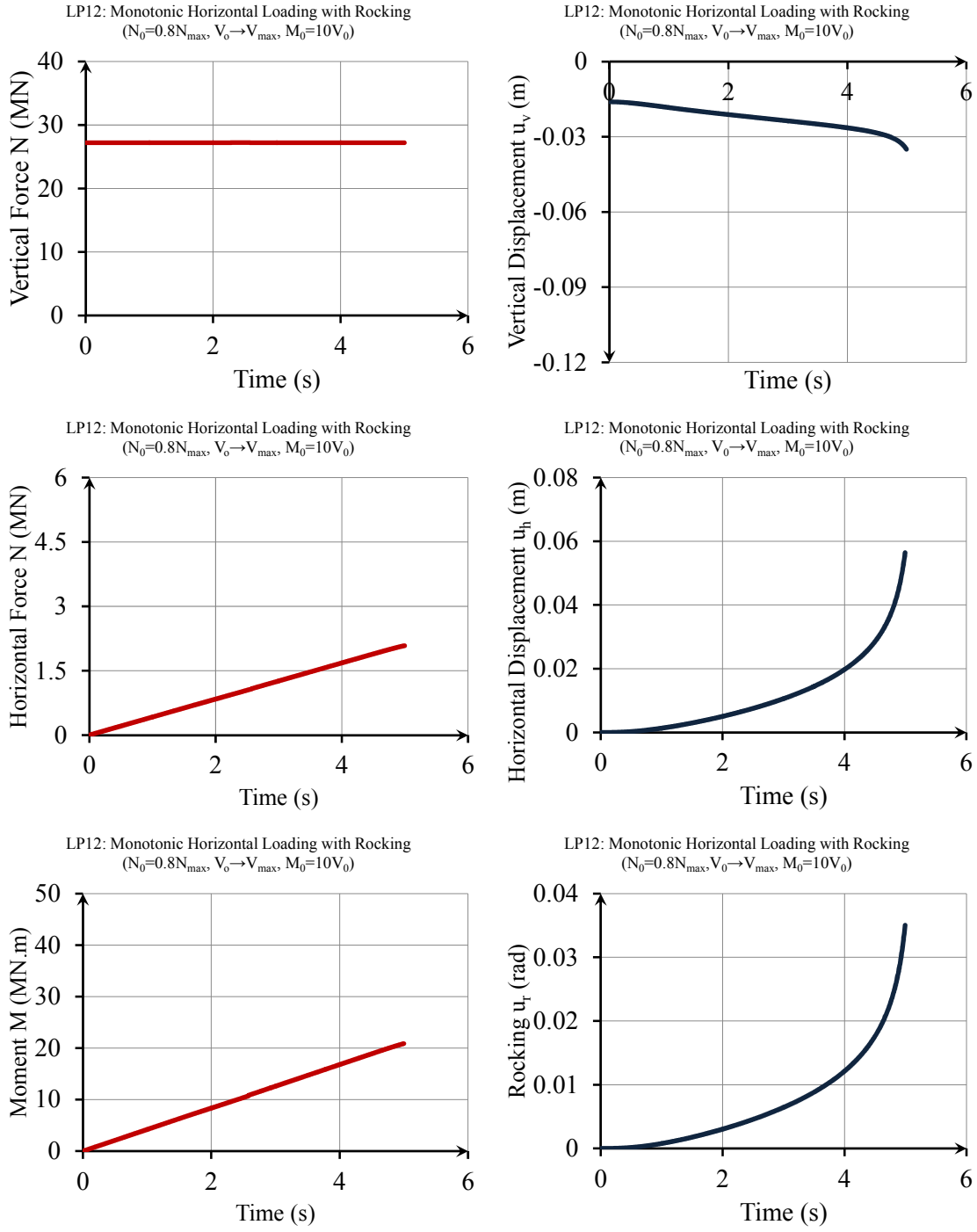

Figure 11-7. The behaviour of macro-element under monotonic horizontal loading with rocking ($N_0=0.8N_{max}$, $V_0 \rightarrow V_{max}$, $M_0=10V_0$).

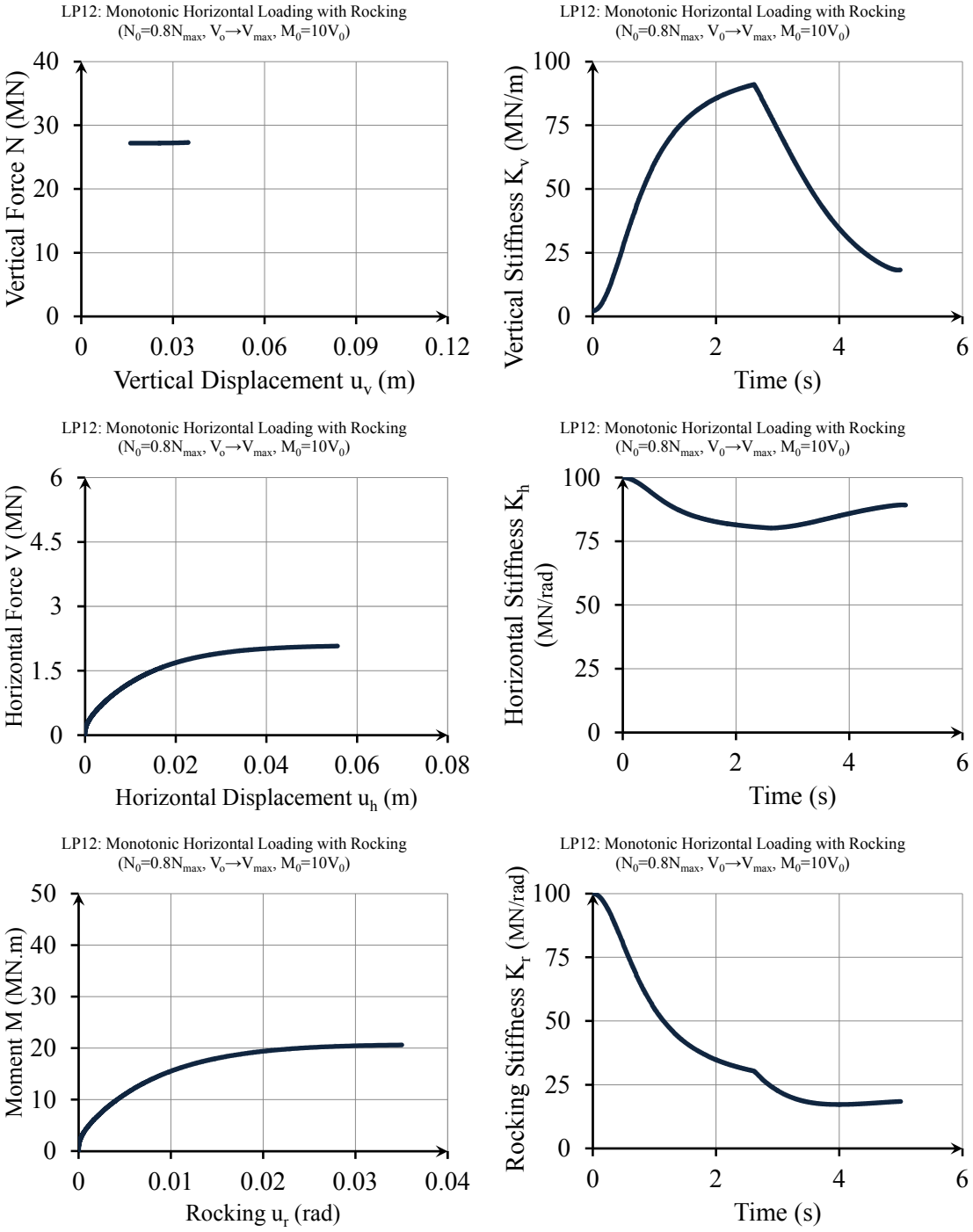

Figure 11-7. *Continued*.

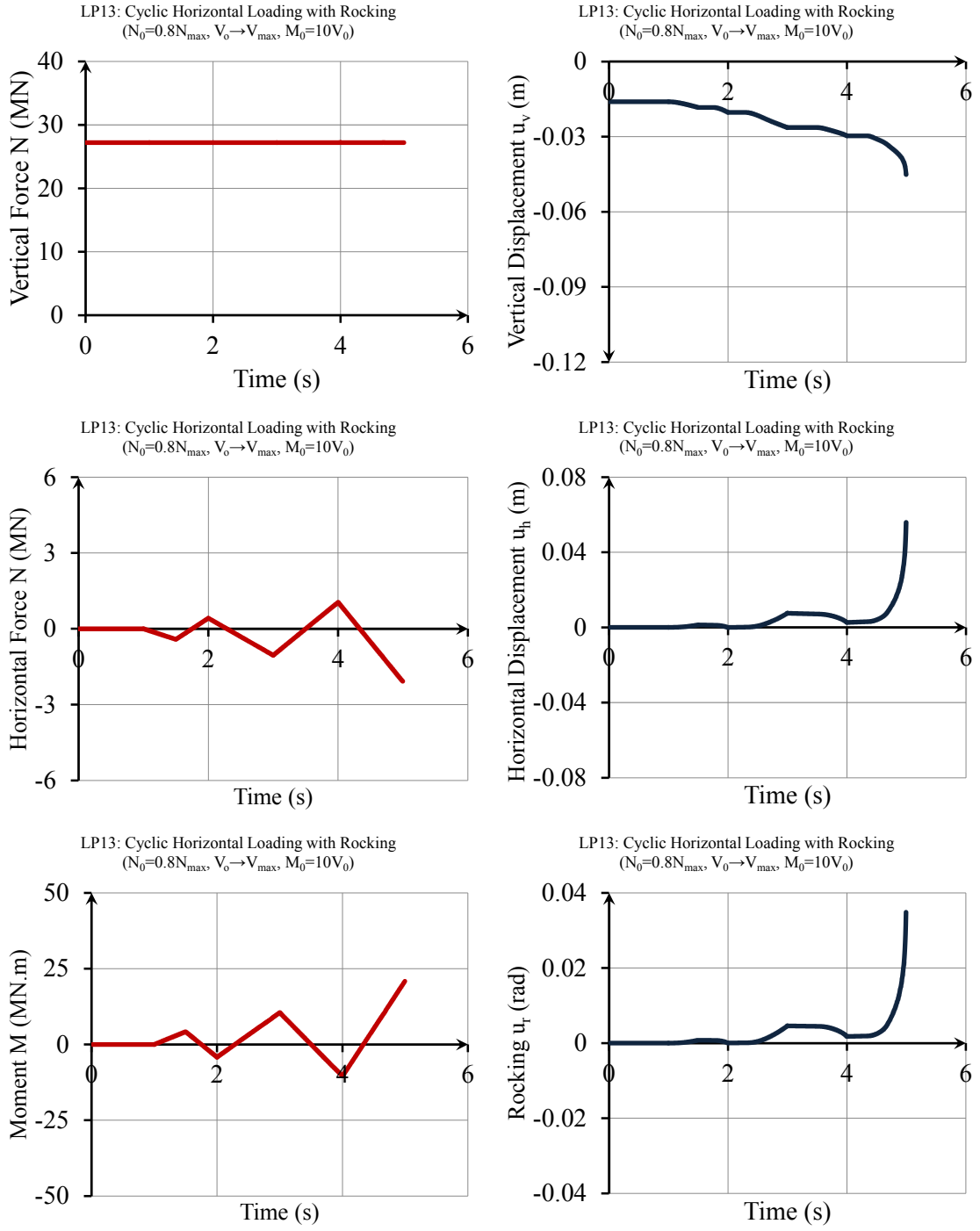

Figure 11-8. The behaviour of macro-element under cyclic horizontal loading with rocking ($N_0=0.8N_{max}$, $V_0 \rightarrow V_{max}$, $M_0=10V_0$).

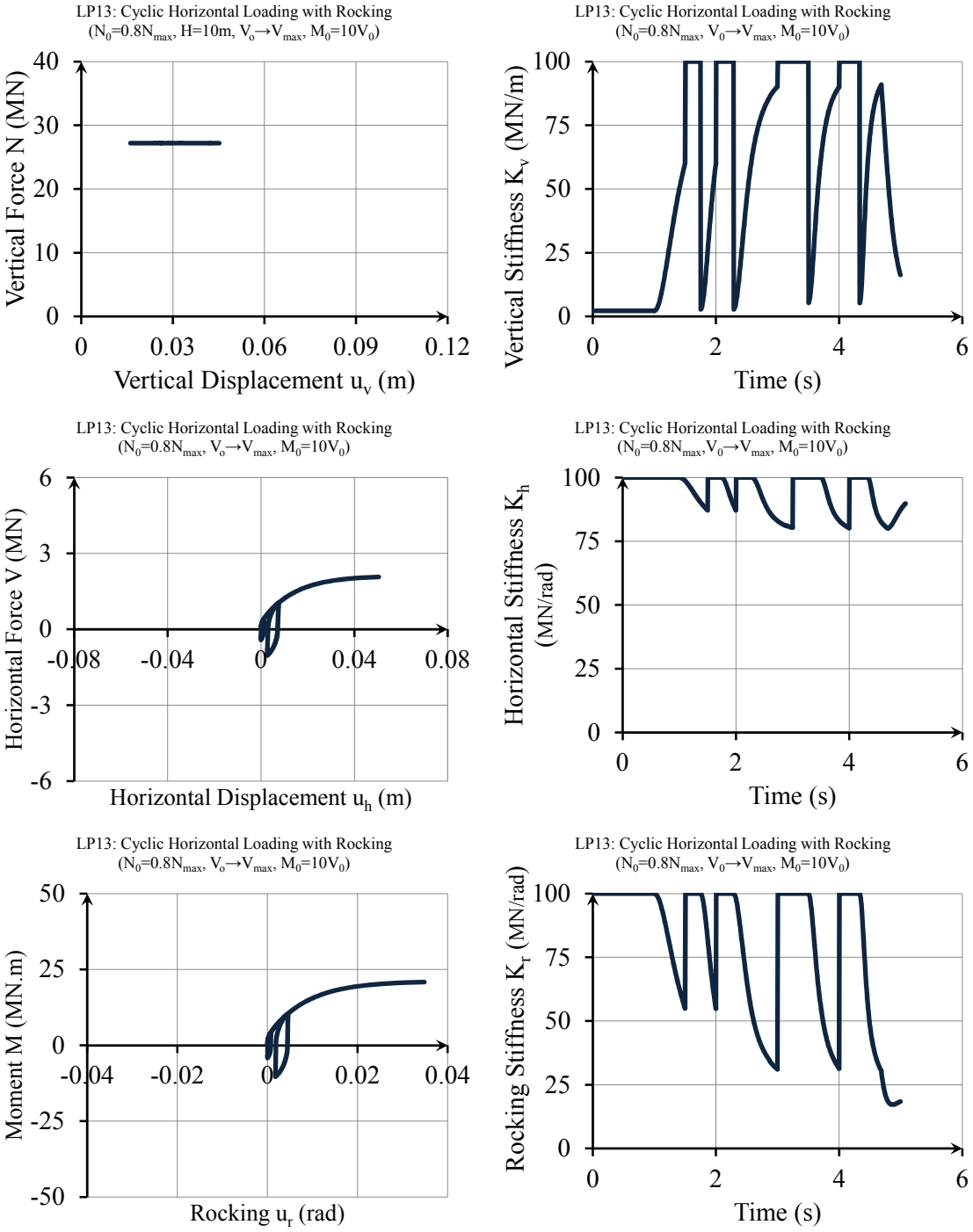

Figure 11-8. *Continued*.

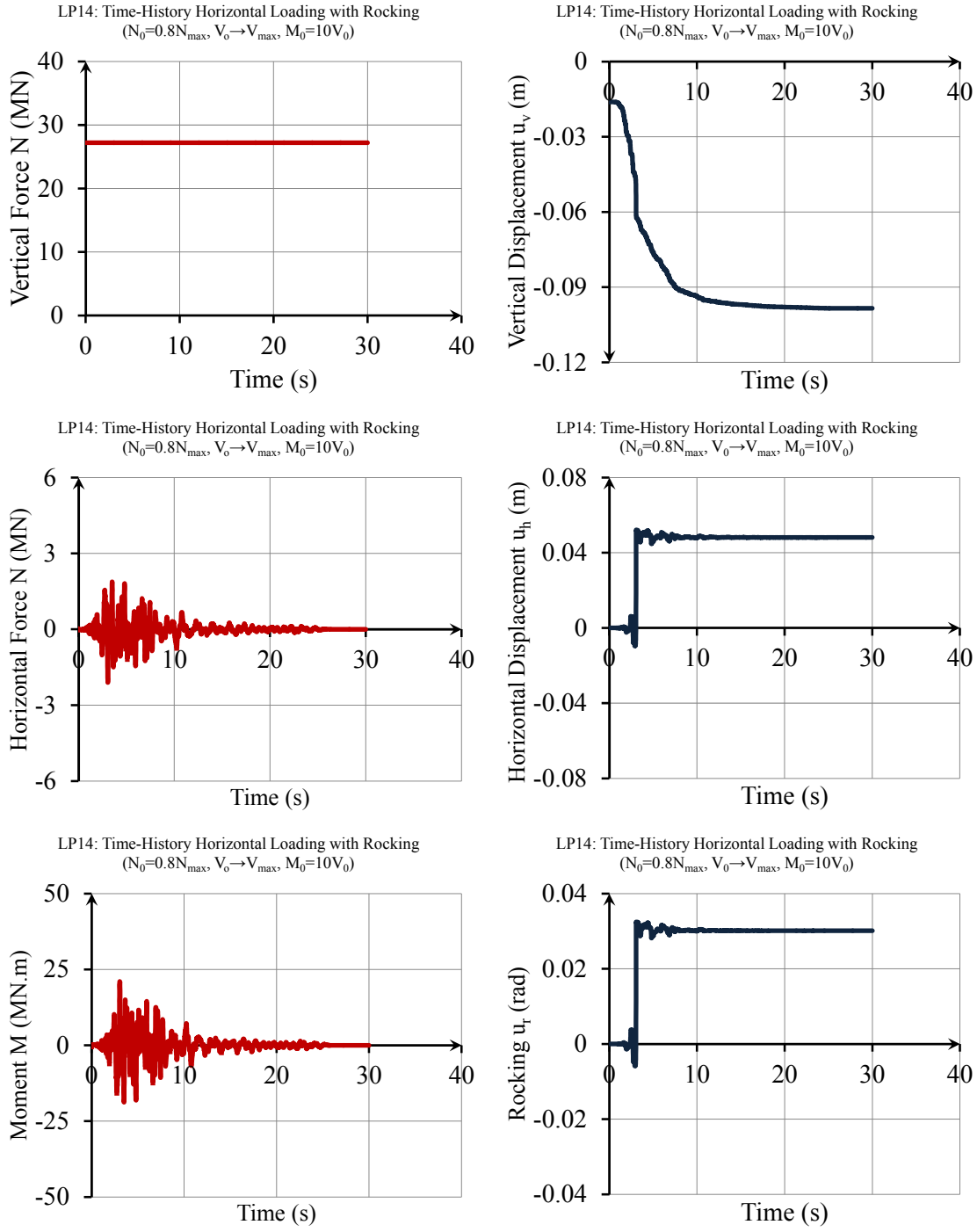

Figure 11-9. The behaviour of macro-element under time-history horizontal loading with rocking ($N_0=0.8N_{max}$, $V_0 \rightarrow V_{max}$, $M_0=10V_0$).

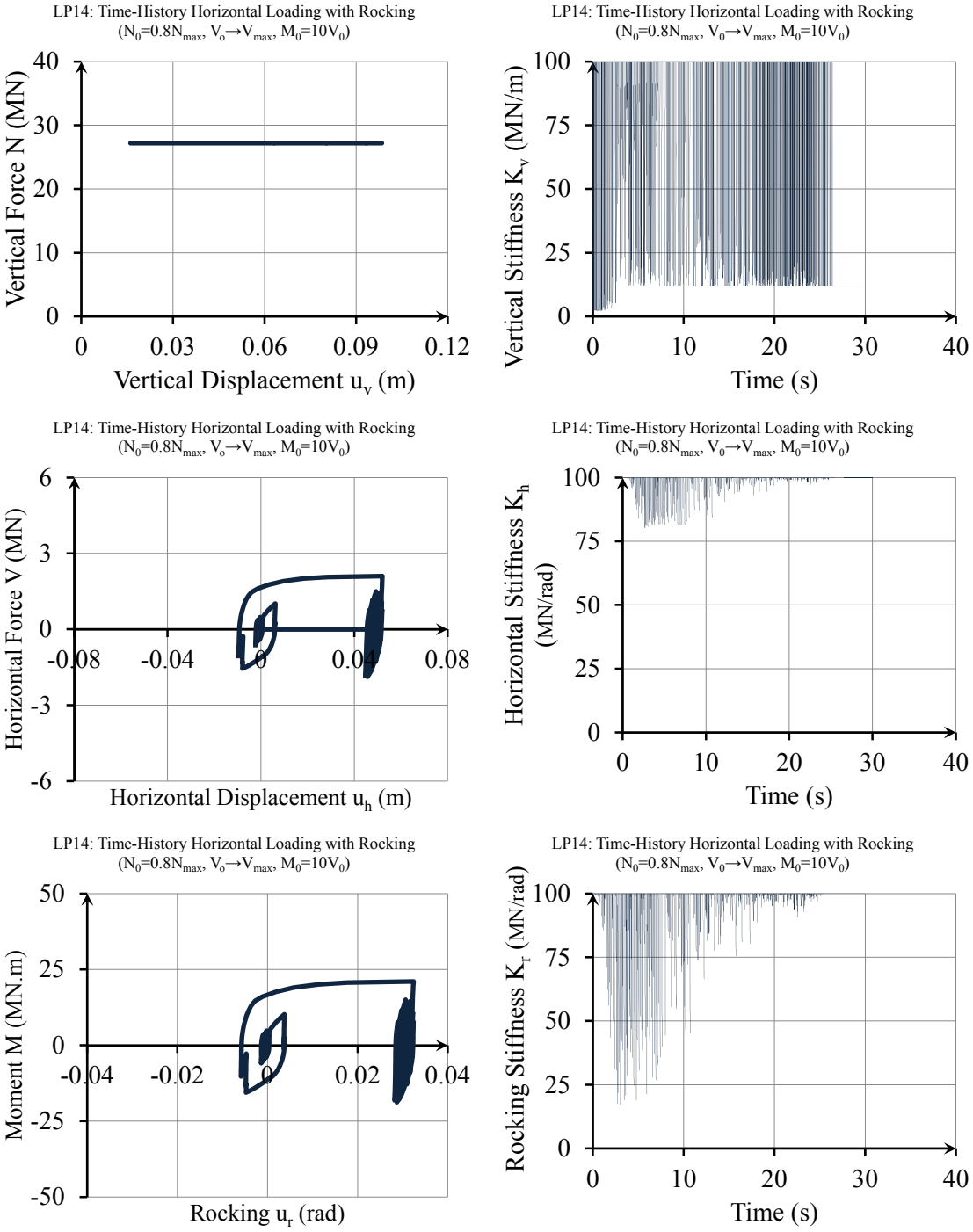

Figure 11-9. *Continued*.

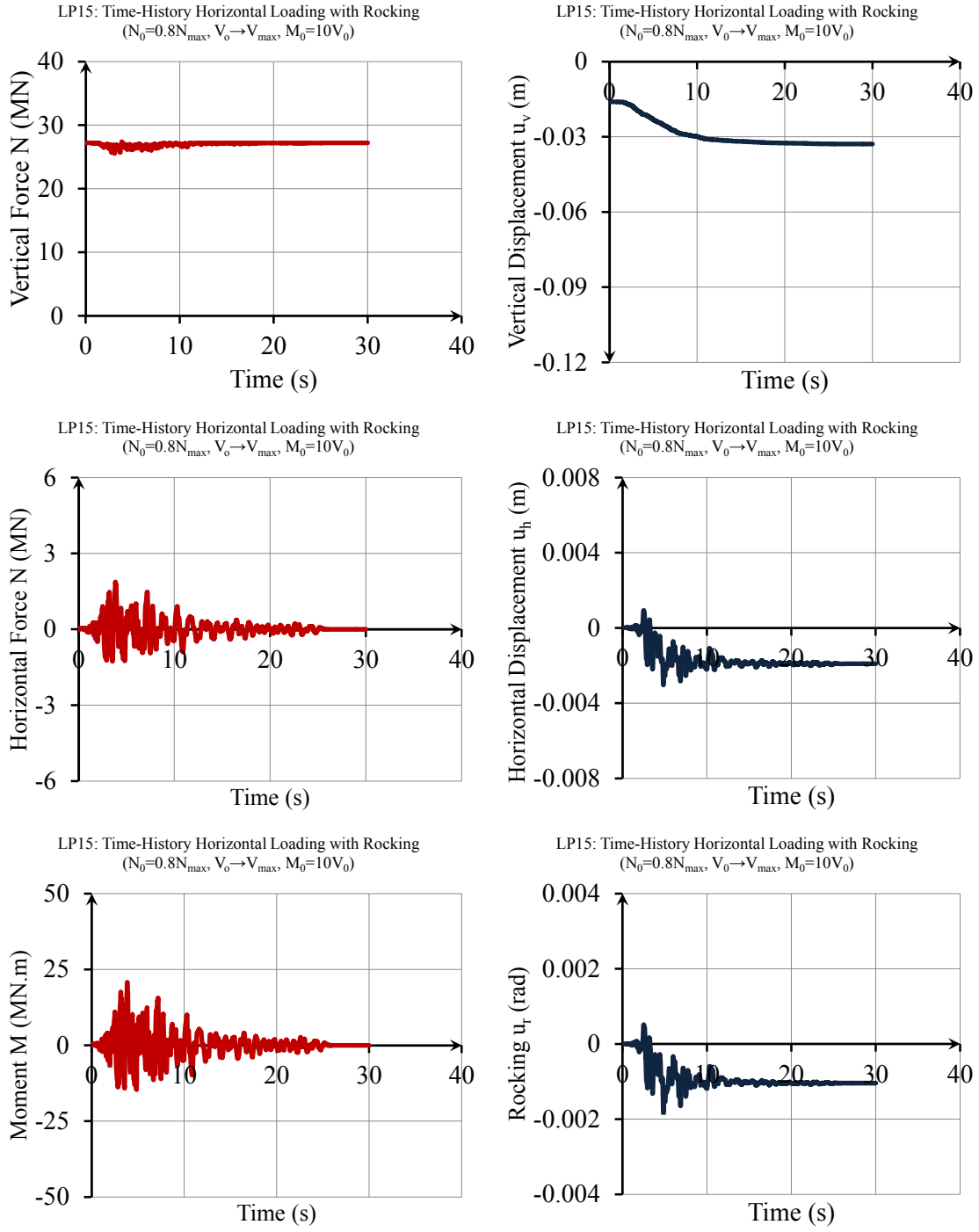

Figure 11-10. The behaviour of macro-element under time-history horizontal loading with rocking ($N_0=0.8N_{max}$, $V_0 \rightarrow V_{max}$, $M_0=10V_0$). Foundation mass and mass moment of inertia is also included and radiation damping is considered.

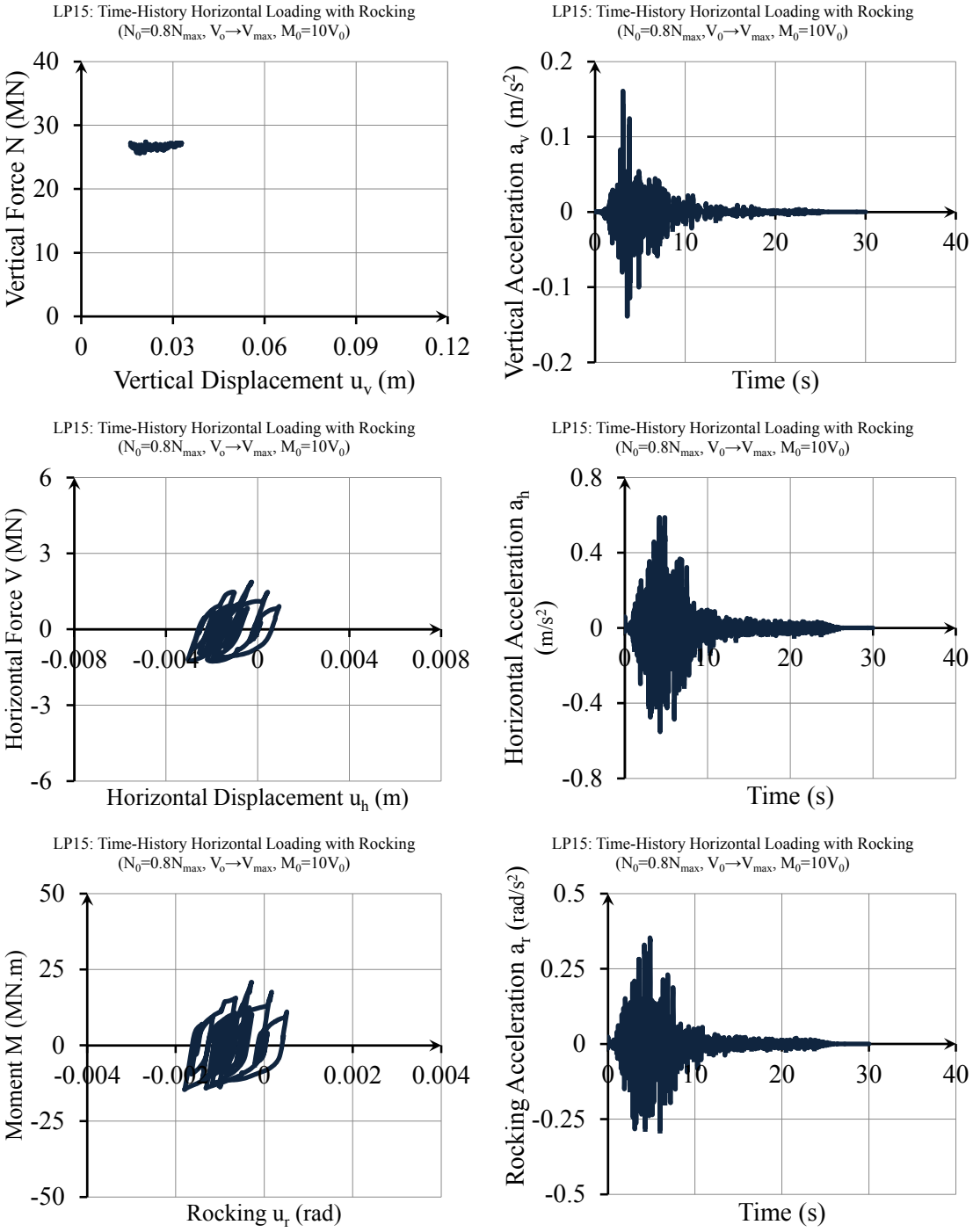

Figure 11-10. *Continued.*

11.4 Summary

In this chapter, the algorithms developed for implementing macro-element in finite-element program Raumoko 3D was explained. Then, the element test simulation results for a comprehensive set of loading scenarios were illustrated. Clearly, the element implemented in Ruaumoko 3D works properly and the observed behaviour is satisfactory.

However, before proceeding to the full investigation of the effects of soil-foundation interface nonlinearity on soil-structure interaction analysis, it is advantageous to first examine these effects on the response of macro-element itself. This approach will obviously enlighten the future analysis and conclusions. Next chapter aims to investigate this matter.

CHAPTER

12. Sensitivity of Foundation Response to Soil-Foundation Interface Parameters

Abstract. A sensitivity analysis on the effects of different parameters defining the degree of nonlinearity at the soil-foundation interface on the response of macro-element is presented in this chapter. In addition, the response of this new element while considered to behave linearly is compared to the response of the previously employed cone model to examine the level of possible differences.

12.1 Introduction

To investigate the effects of soil-foundation interface nonlinearity on the response of macro-element implemented, the soil-foundation interface model introduced in Chapter 11 was used. This model was enforced to two different vertical force conditions, and the foundation response to cyclic and time-history horizontal loading and rocking was examined. In this context, $N_0 = 0.2N_{max}$ was used to represent scenarios with a low level of material nonlinearity in the vertical direction, and $N_0 = 0.8N_{max}$ was used to represent scenarios with a high level of material nonlinearity. The applied forces on the centre of foundation include a horizontal force and a corresponding moment that were set to represent a maximum horizontal force of 1.5 MN acting at the height of 10 m above the foundation level. The applied forces are shown in Figure 12-1.

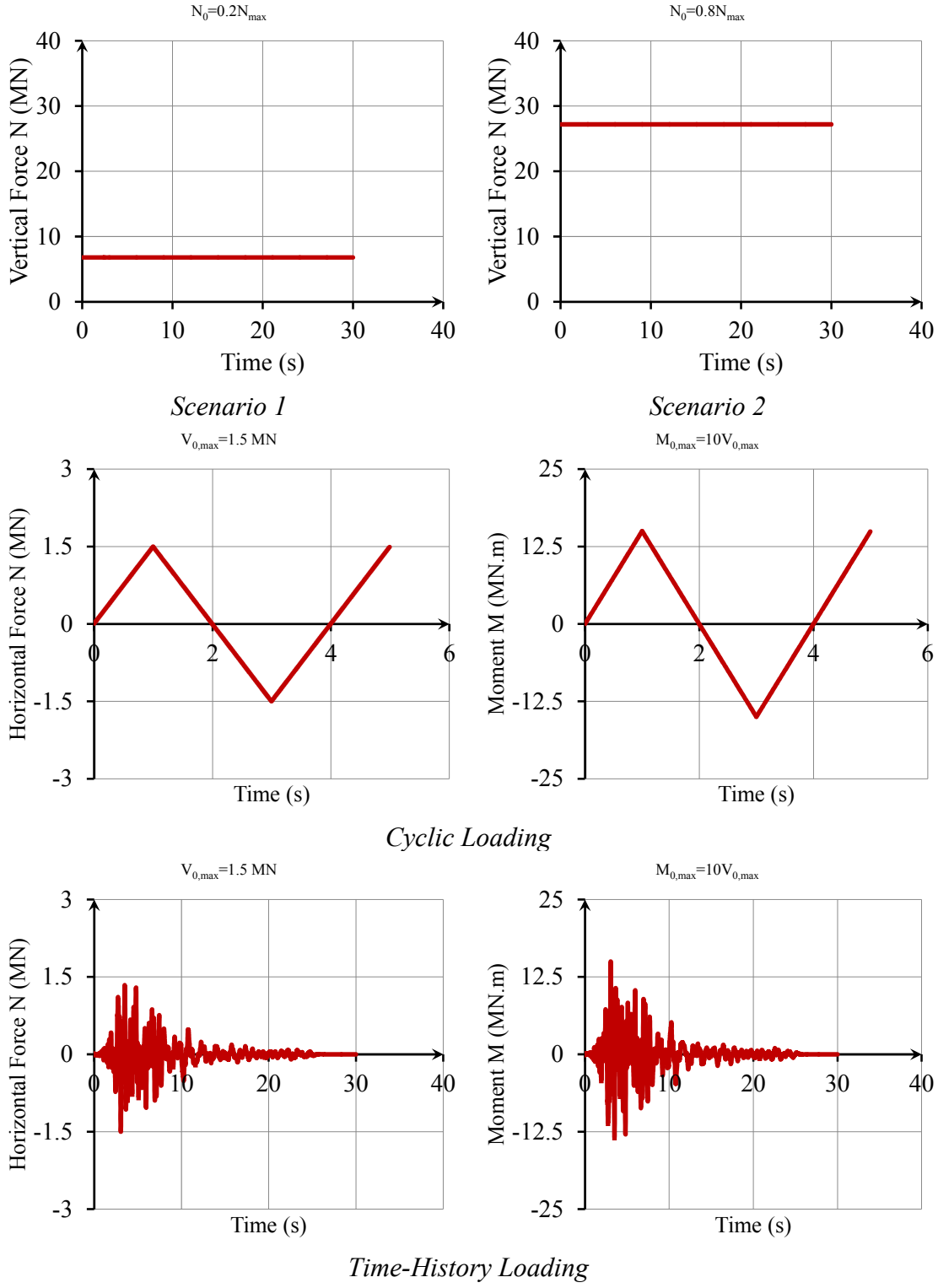

Figure 12-1. Applied forces to considered soil-foundation interface model.

12.2 The Role of Material Nonlinearity

The role of soil material nonlinearity was investigated first, and the response of the nonlinear model was compared with a linear one. Note that for the linear case, the uplift mechanism was also deactivated. To force the macro-element to act as a linear model, a large value of N_{max} was selected. Consequently, the distance between the current state of forces and the bounding surface became so large that the effects of material nonlinearity were negligible.

The results of this comparison are illustrated in Figures 12-2 and 12-3 for cyclic loadings. Equally, Figures 12-4 and 12-5 show the results for time history loadings. In these figures, the response of the model is demonstrated in terms of force-deformation hysteretic loops and also deformation time-histories.

The first conclusion from this comparison is that the model accounting for nonlinearity shows a larger initial settlement, as well as a different and increased final settlement. In contrast, the linear model only is able to present a constant settlement during the loading period. In addition, comparing the results for cycling and time-history loadings shows that the observed deviation in final settlement between the nonlinear and linear models is more significant for time-history loading. Therefore, using a linear model in time-history seismic analysis instead of a proper nonlinear model can be misleading in terms of predicting the foundation settlement.

If horizontal displacement and rocking are considered, it is obvious that the linear model under-predicts the maximum deformation. In addition, it is not able to capture the residual deformation, which in turn can cause extra stress in the structure above. However, due to interface nonlinearity or, more accurately, hysteretic actions, the nonlinear model can impose an additional damping to the soil-structure system that in turn might reduce the structural reactions. This aspect will be investigated in more detail in the next chapter.

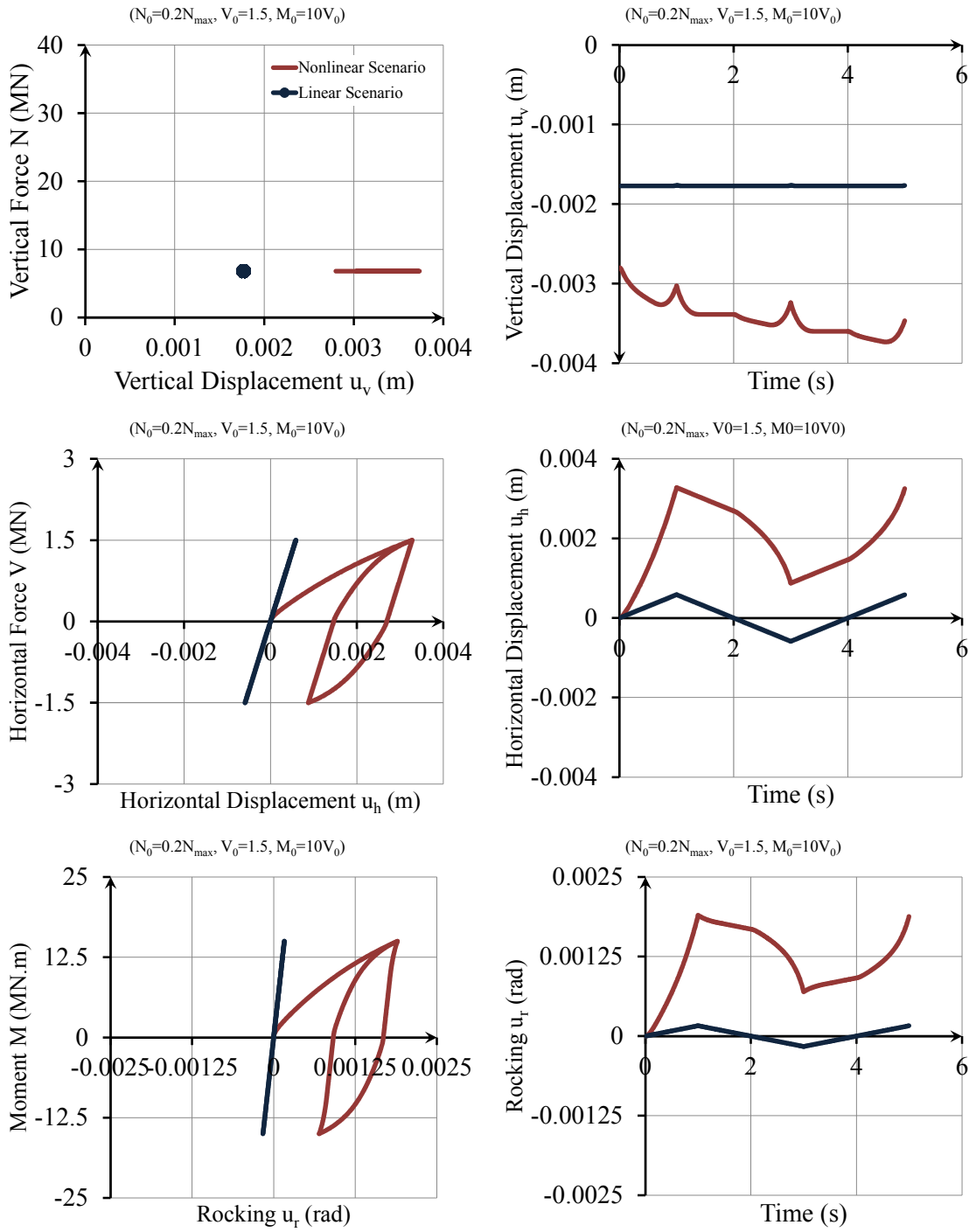

Figure 12-2. The role of material nonlinearity on the response of considered soil-foundation interface model to cyclic loading: (left) nonlinear response; (right) linear response ($N_0=0.2N_{max}$, $V_0=15$ MN, $M_0=10V_0$).

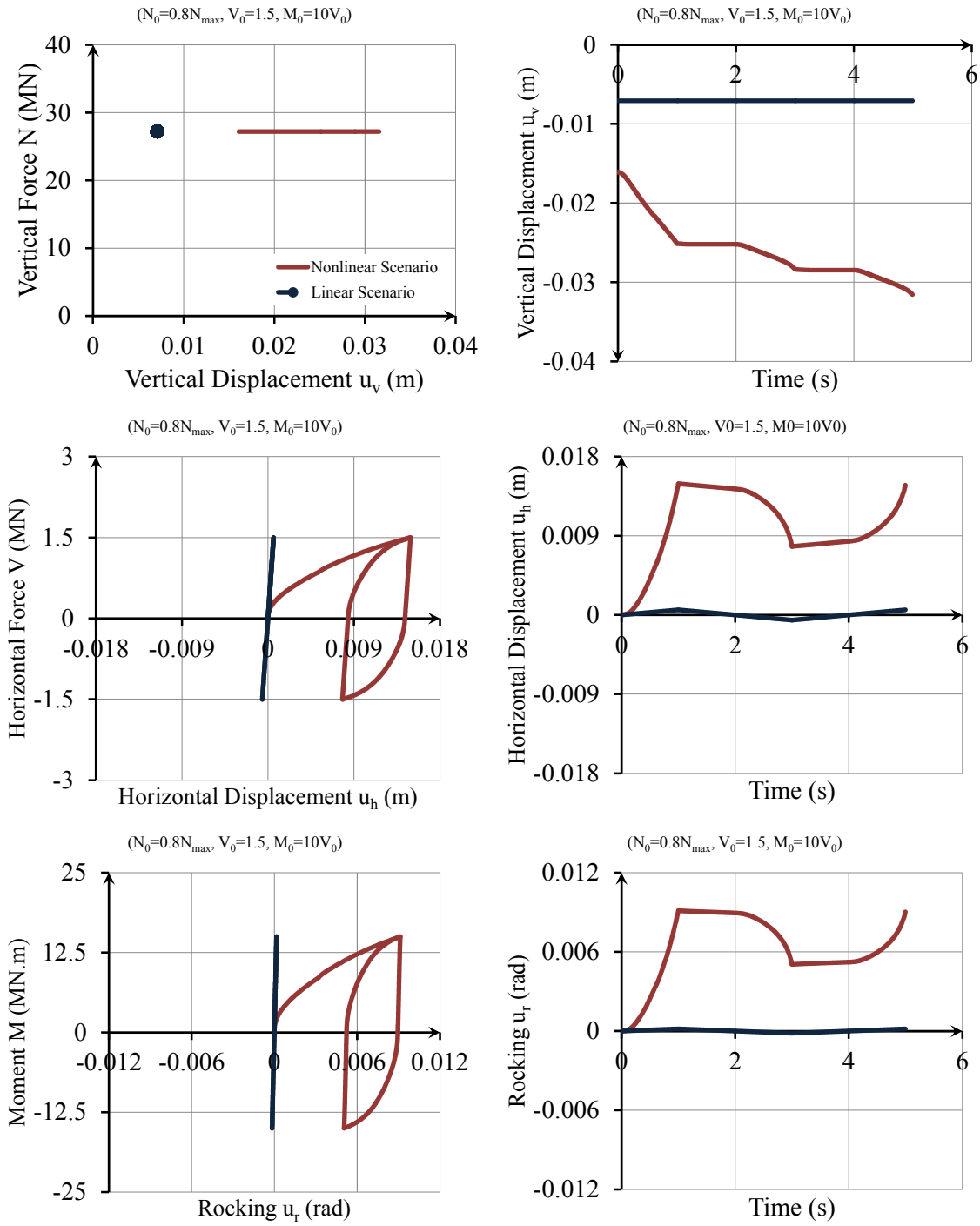

Figure 12-3. The role of material nonlinearity on the response of considered soil-foundation interface model to cyclic loading: (left) nonlinear response; (right) linear response (N_0=0.8N_{max}, V_0=15 MN, M_0=10V_0).

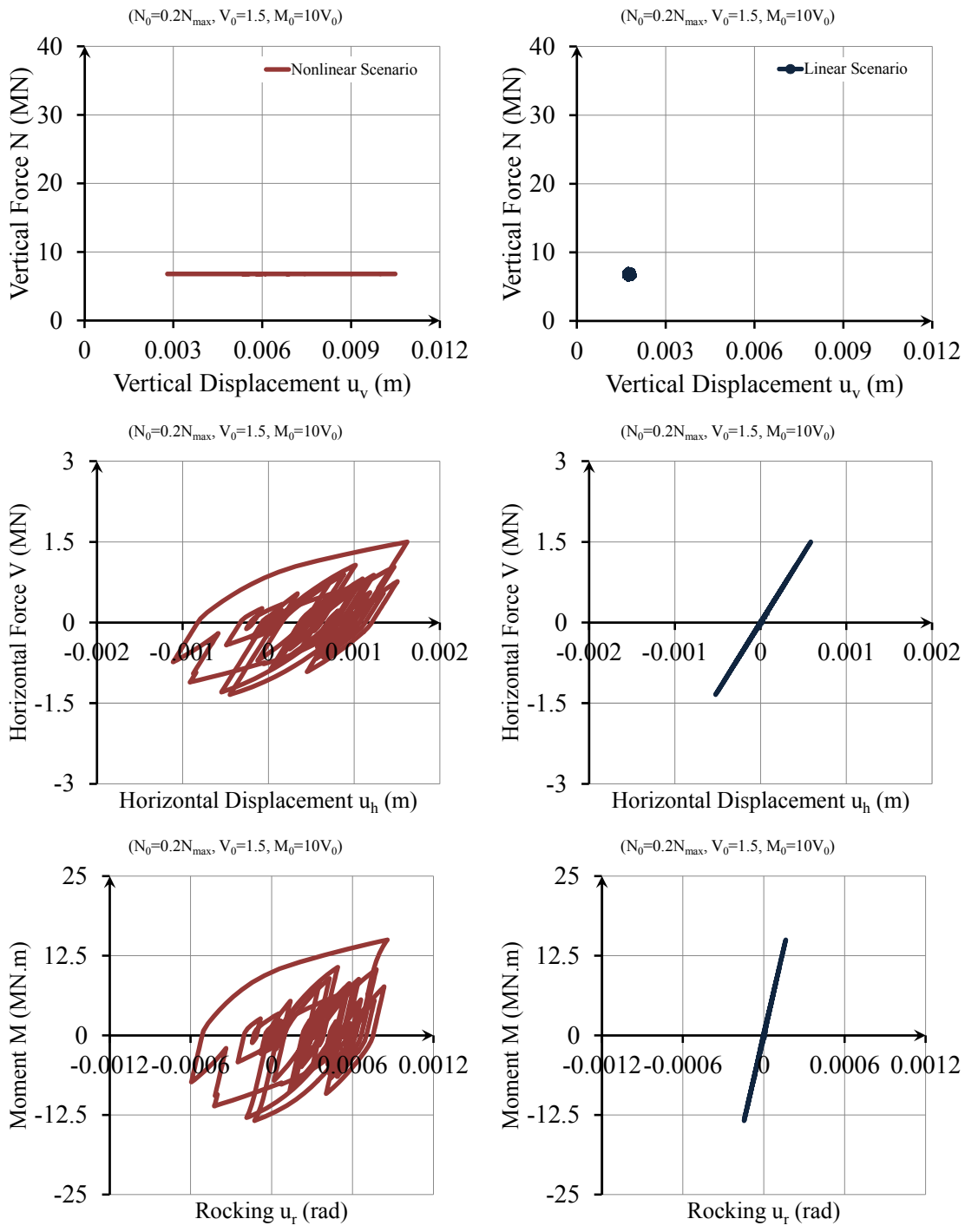

Figure 12-4. The role of material nonlinearity on the response of considered soil-foundation interface model to time-history loading: (left) nonlinear response; (right) linear response (N_0=0.2N_{max}, V_0=15 MN, M_0=10V_0).

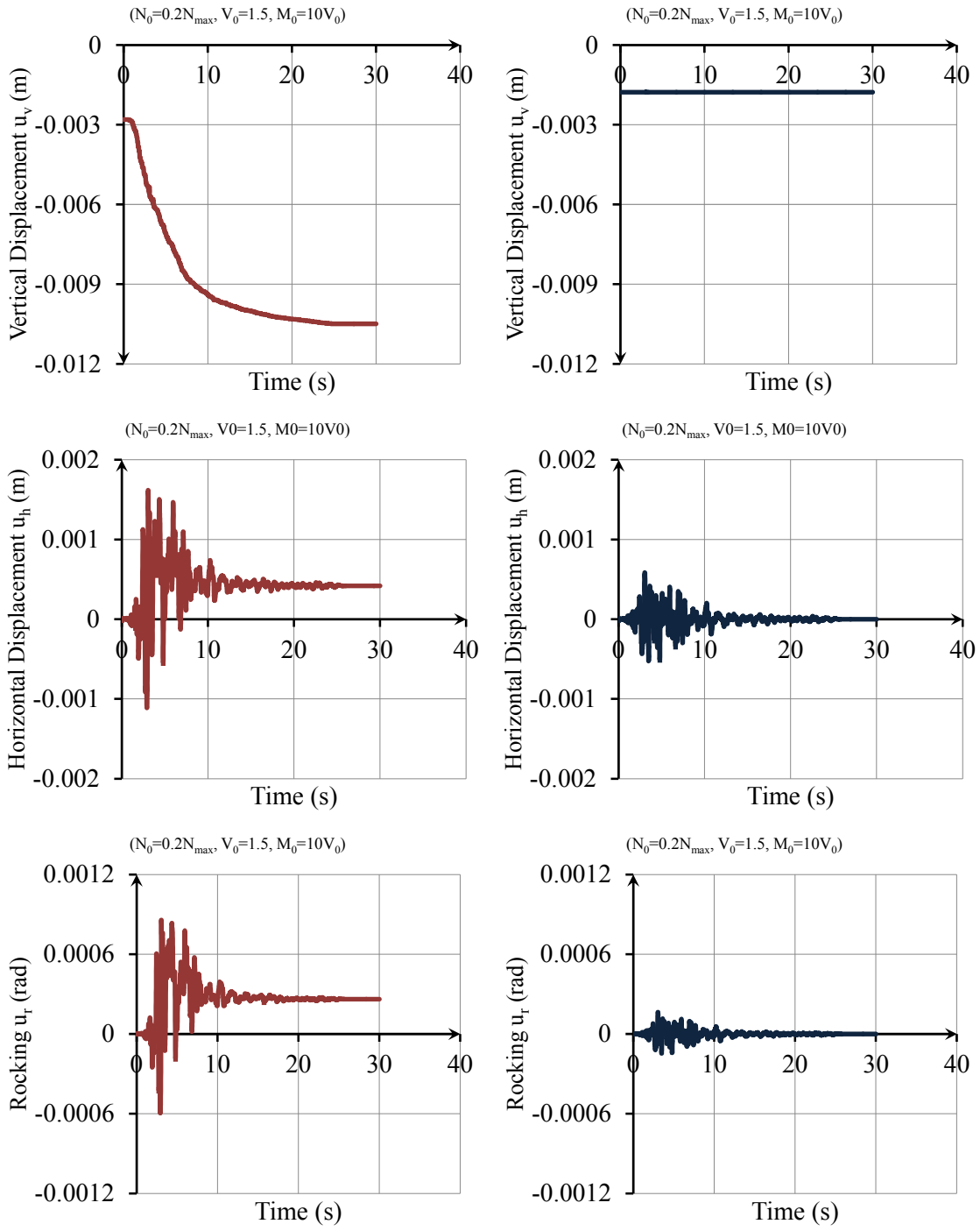

Figure 12-4. *Continued*.

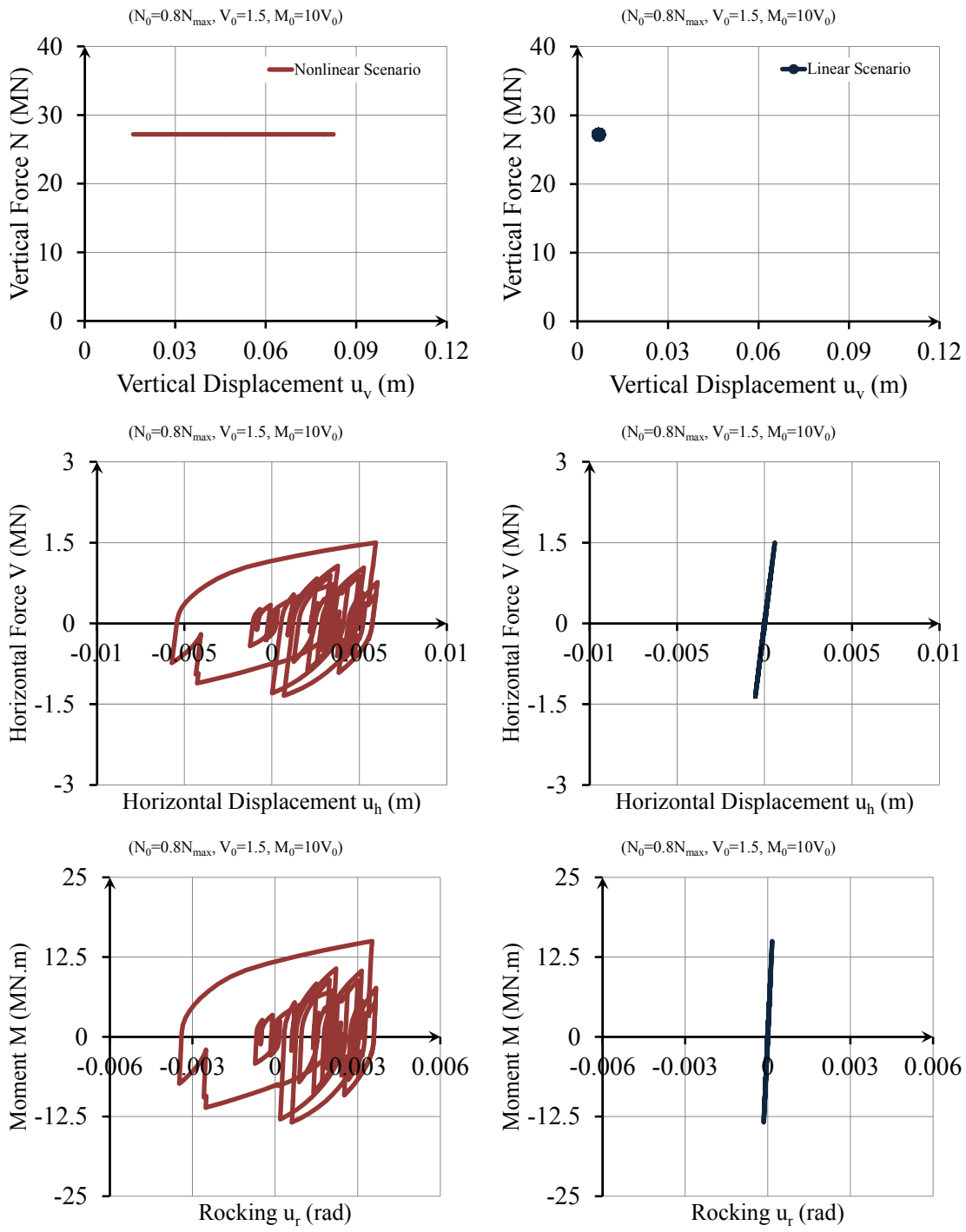

Figure 12-5. The role of material nonlinearity on the response of considered soil-foundation interface model to time-history loading: (left) nonlinear response; (right) linear response (N_0=0.8N_{max}, V_0=15 MN, M_0=10V_0).

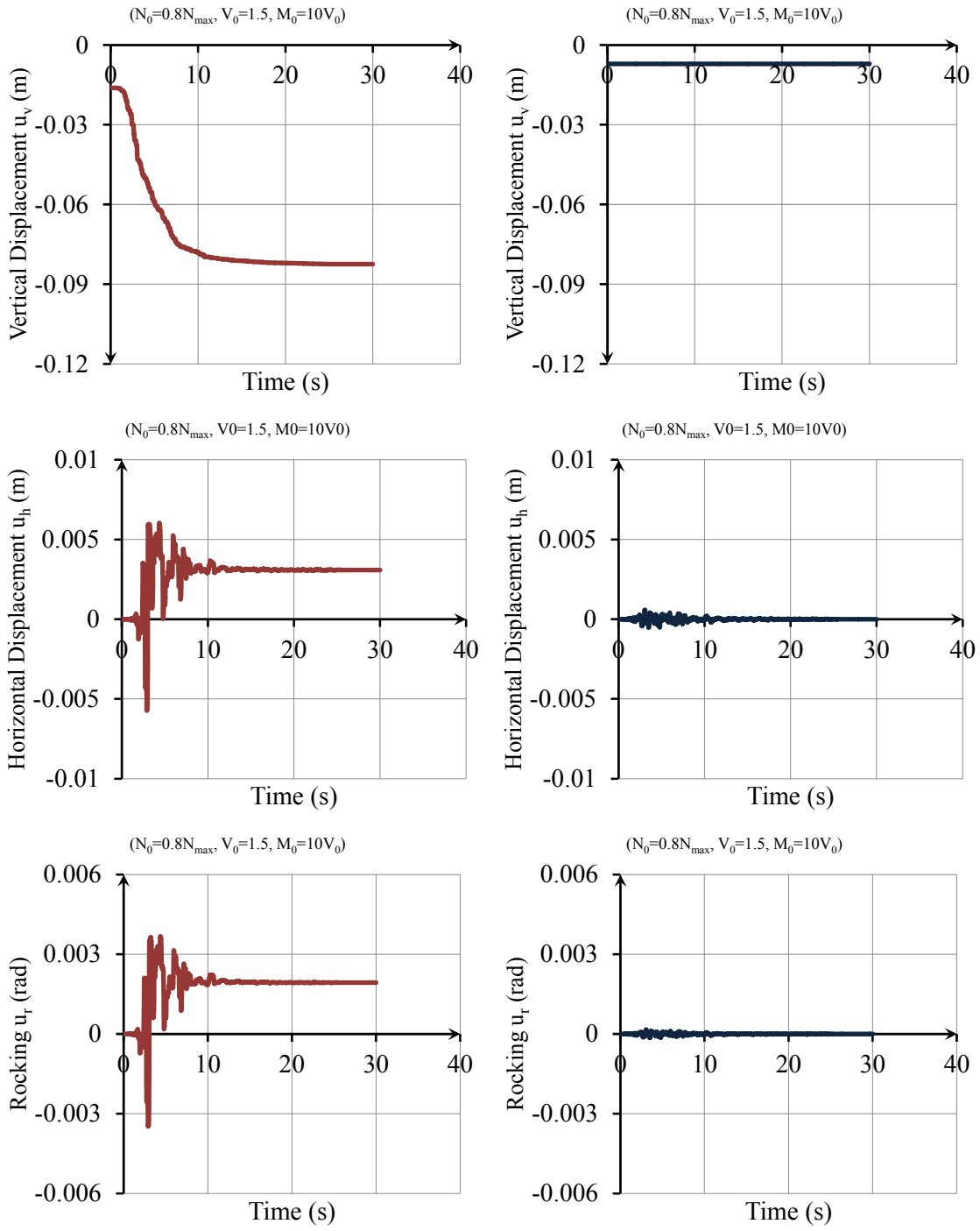

Figure 12-5. *Continued*.

12.3 The Role of Foundation Uplift

The role of foundation uplift on the response of the macro-element is studied next. In this regard, the response of the two models, one with uplift and one without uplift, is compared. To force the macro-element not to show any consequences of uplift, a very small value of numerical parameter α was used. The comparison between the results is shown in Figures 12-6 and 12-7 for cyclic loading. The results for time-history loading are presented in Appendix G.

Clearly, for the example considered and the loading applied, uplift does not play any significant role on the response of macro-element model. Specifically, it does not change the maximum or minimum value of deformation. It also does not modify the hysteretic behaviour either. Finally, it does not vary the residual deformation. The same conclusions can be made when time-history loading is considered as seen in Appendix G. Thus, it can be stated that the effects of uplift on the response of the macro-element itself are effectively negligible, at least for the cases considered.

However, it has to be noted that uplift can play a critical role as a boundary condition. If any state of forces intersects this boundary line, the toppling of the foundation will subsequently occur, which is recognised as a form of foundation failure.

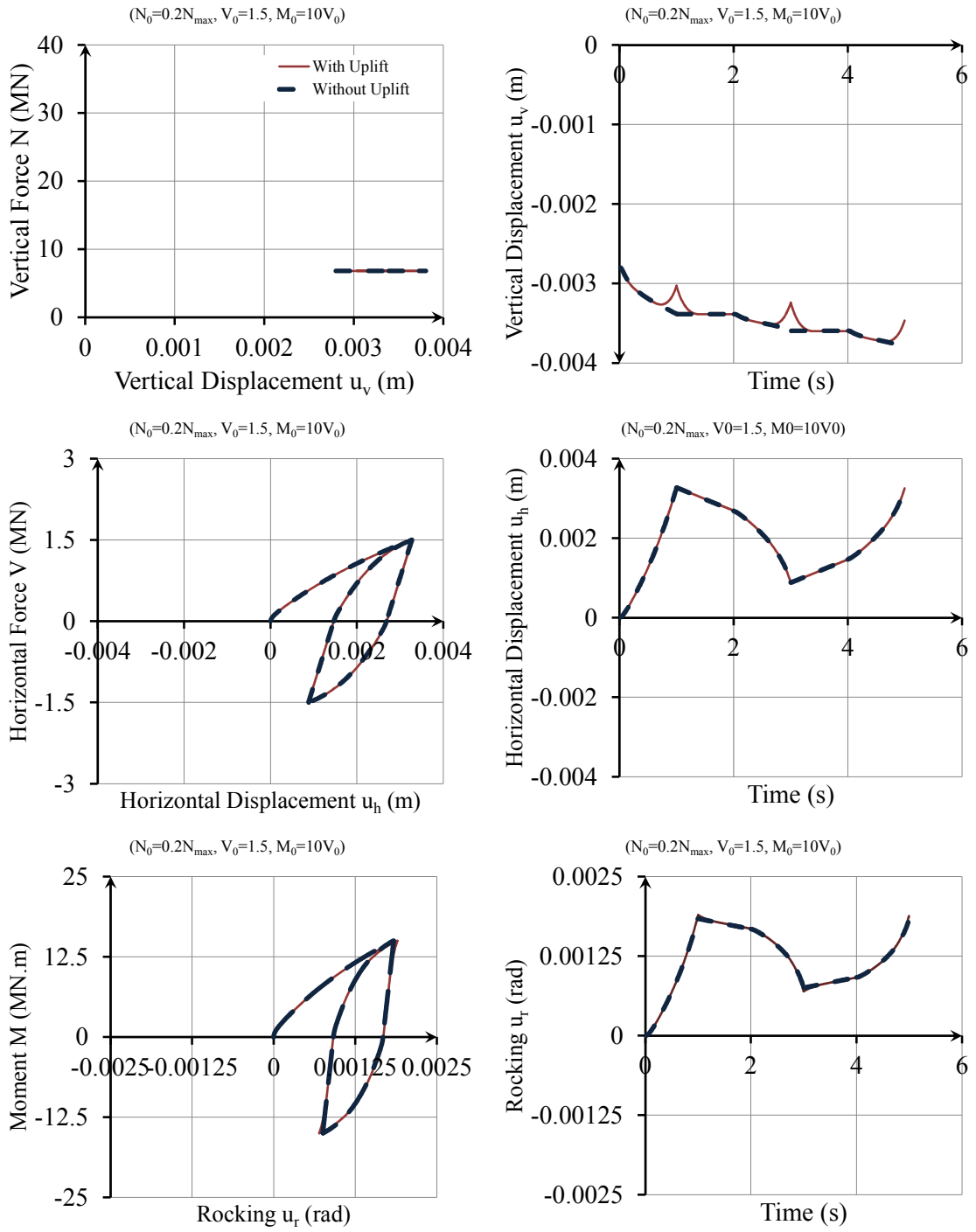

Figure 12-6. The role of foundation uplift on the response of considered soil-foundation interface model to cyclic loading: (left) simulation with uplift; (right) simulation without uplift (N_0=0.2N_{max}, V_0=1.5 MN, M_0=10V_0).

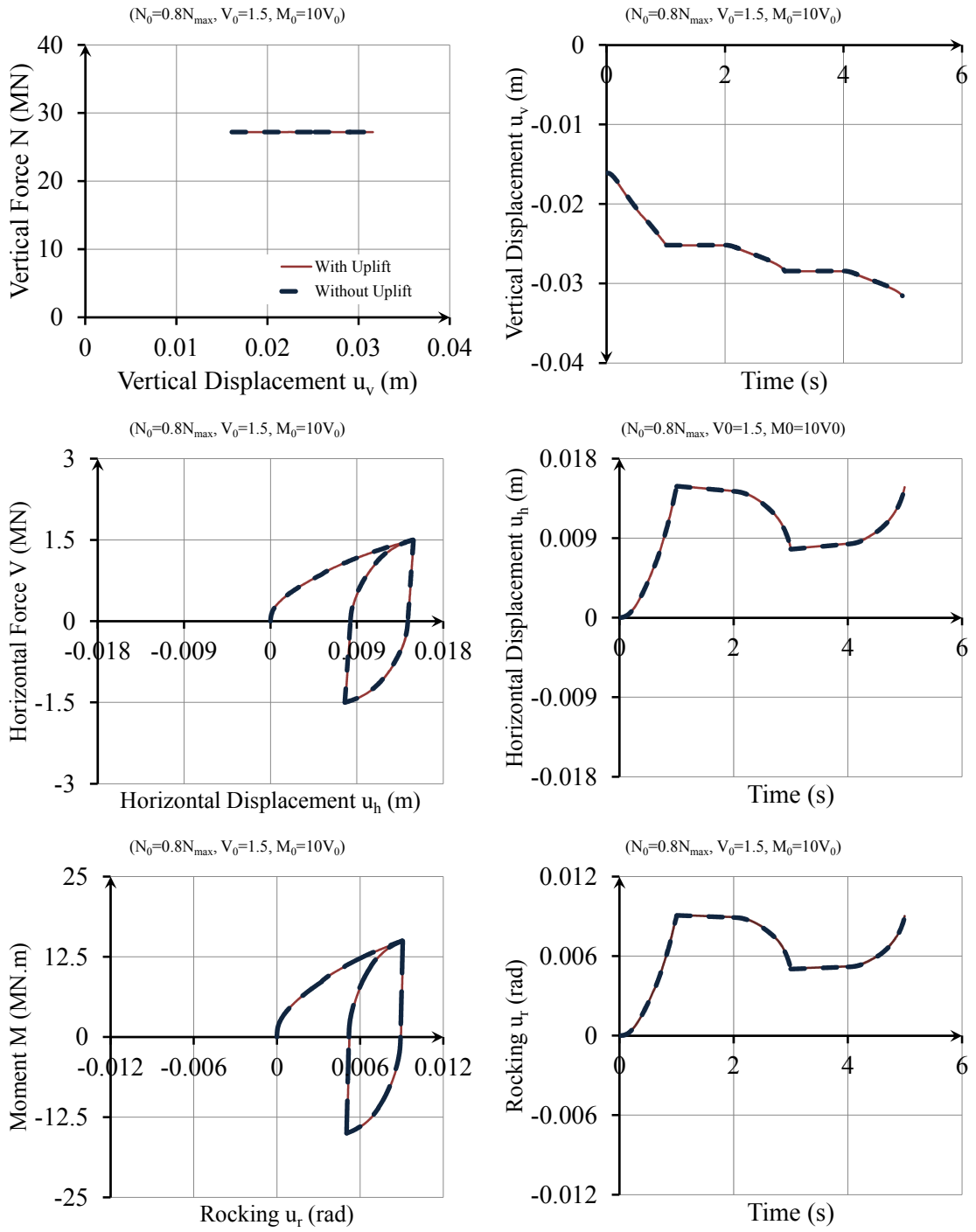

Figure 12-7. The role of foundation uplift to the response of considered soil-foundation interface model to cyclic loading: (left) simulation with uplift; (right) simulation without uplift ($N_0=0.8N_{max}$, $V_0=1.5$ MN, $M_0=10V_0$).

12.4 Sensitivity of Macro-Element Response to Plasticity Parameters

The sensitivity of macro-element response to the plasticity parameters, p_1 and p_2, is investigated next. Specifically, p_1 is a parameter used to define the initial plastic stiffness matrix as a ratio of static stiffness matrix, and p_2 is a parameter used to define the extent of stiffness degradation in reloading conditions.

To investigate the role of p_1, three values of $p_1 = 1$, 0.5 and 0.1 were used. In this context, $p_1 = 1.0$ was chosen to represent the case of initial plastic stiffness matrix being exactly the same as static stiffness matrix. For this condition, not much of soil material nonlinearity is expected. In contrast, $p_1 = 0.1$ represents an initial plastic stiffness matrix that is only $1/10^{th}$ of the static stiffness matrix, and the soil responds in a highly nonlinear fashion. Finally, $p_1 = 0.5$ represents the intermediate condition.

The role of p_2 was studied similarly using three selected values of $p_2 = 1.0$, 5 and 10. It should be noted that a large value of p_2 corresponds to a smaller stiffness in the reloading condition.

The response of the macro-element to cyclic loading for different values of p_1 and p_2 is shown in Figures 12-8 to 12-11. The results for time-history loading are presented in Appendix G. In addition to this graphical presentation, the critical values of the response including the maximum deformation and the residual deformation in vertical, horizontal and rocking directions are summarized in Tables 12-1 to 12-4 for both cyclic and time-history loadings.

12.4.1 The Effect of Variation in p_1

As shown in Figures 12-8 and 12-9, smaller values of p_1 result in an increase in the maximum and residual deformations. This trend is expected, as smaller values of p_1 correspond to higher levels of soil nonlinearity, which in turn means greater deformation. However, it is important to note that the increases in deformation are not a linear function of p_1. In other words, the difference between the maximum and residual deformations for the cases of $p_1 = 0.1$ and 0.5 is much more significant than that for the cases of $p_1 = 0.5$ and 1.0.

This fact can be more clearly recognised from the values presented in Tables 12-1 and 12-2. For example, when cyclic loading with vertical force of $N_0 = 0.2N_{max}$ is considered, the ratio between the maximum rocking of the model with $p_1 = 0.1$ and that for the model with $p_1 = 1$ is 4.9, while this ratio is 1.4 between the response of models with $p_1 = 0.5$ and $p_1 = 1$. In addition, note that the observed difference is more pronounced for rocking than vertical settlement or horizontal displacement, and is more significant for residual than maximum deformation. Therefore, selecting a proper value of p_1 is very important in the accurate prediction of the response of the macro-element.

12.4.2 The Effect of Variation in p_2

Figures 12-10 and 12-11 clearly illustrate that using smaller values of p_2 corresponds to a larger initial settlement followed by a different and increased final settlement. This difference in the final settlement, as summarized in Tables 11-3 and 11-4, is in the order of $30\% - 50\%$, depending on the vertical force, the value of p_2 and the type of loading (cyclic or time-history).

Also shown in Figures 12-10 and 12-11 is that the choice of smaller values of p_2 results in the fatter hysteretic loop for loadings in horizontal and rocking directions. Consequently, larger amount of energy dissipation is expected for models with smaller values of p_2. In addition, the values presented in Table 12-4 for time-history loading shows that the maximum deformation in the horizontal and rocking directions decreases when smaller values of p_2 are used. However, the resulting residual deformations decrease since the hysteretic energy dissipation increases.

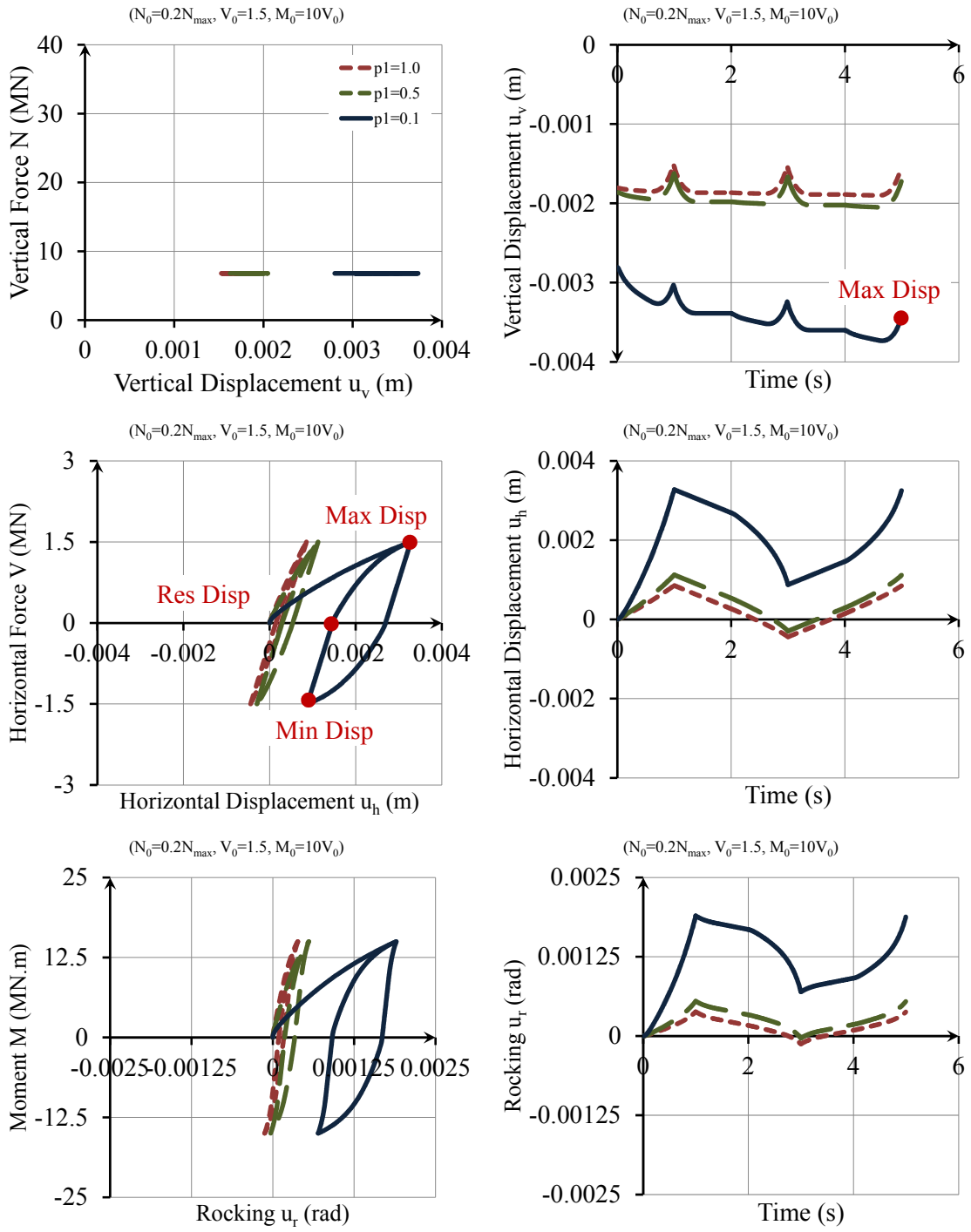

Figure 12-8. The effects of variation in p_1 on the response of considered soil-foundation interface model to cyclic loading ($N_0=0.2N_{max,}$ $V_0=1.5$ MN, $M_0=10V_0$).

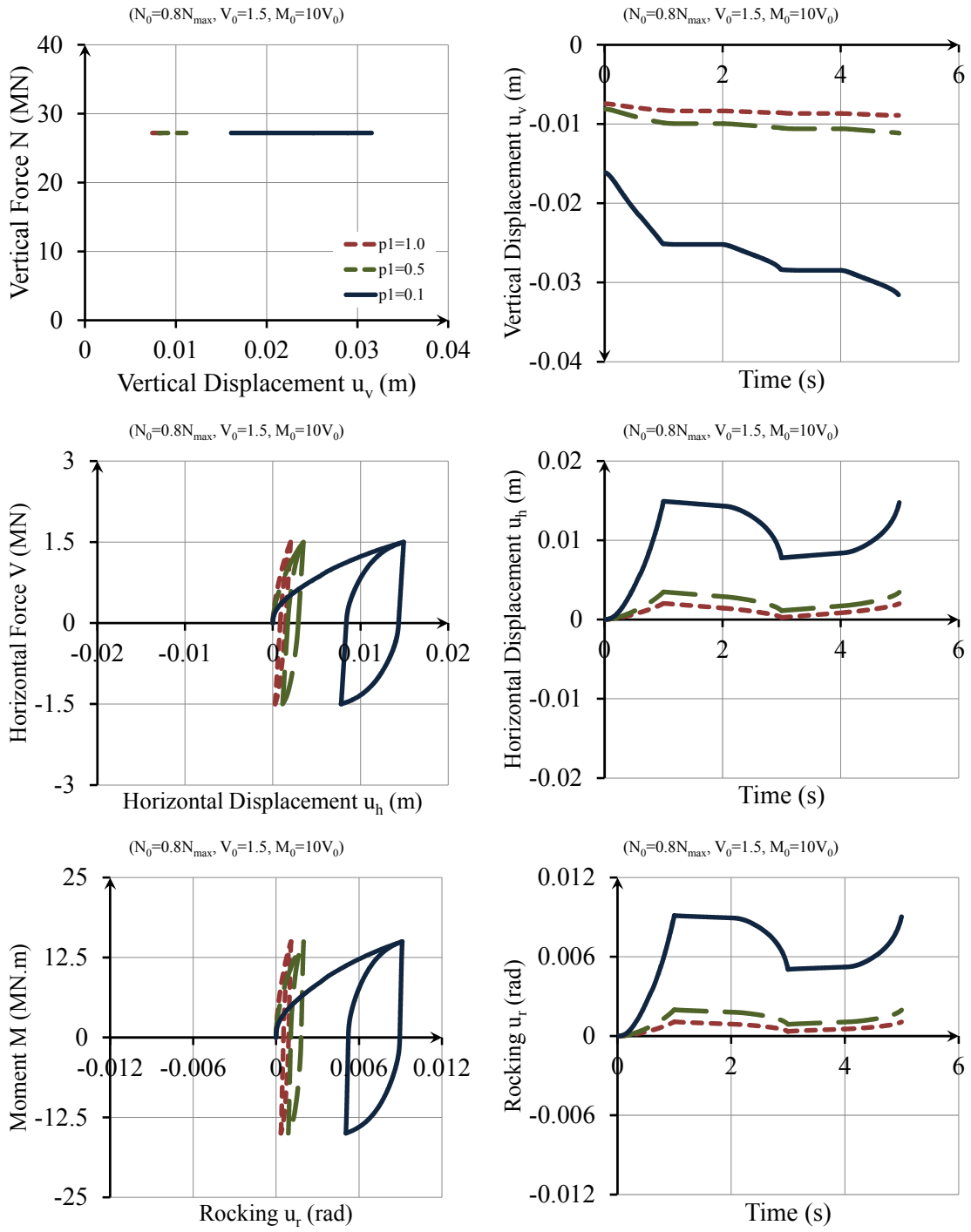

Figure 12-9. The effects of variation in p_1 on the response of considered soil-foundation interface model to cyclic loading ($N_0=0.8N_{max,}$ $V_0=1.5$ MN, $M_0=10V_0$).

Table 12-1. The effects of variation in p_1 on the response of considered soil-foundation interface model to cyclic loading.

Parameter	u_{fv}			u_{fh}				u_{fr}	
	$p_1 = 1.0$	$p_1 = 0.5$	$p_1 = 0.1$	$p_1 = 1.0$	$p_1 = 0.5$	$p_1 = 0.1$	$p_1 = 1.0$	$p_1 = 0.5$	$p_1 = 0.1$
				$N_0 = 0.2N_{max}$					
Max. Disp.	-1.6E-03	-1.7E-03	-3.5E-03	8.6E-04	1.1E-03	3.3E-03	3.8E-04	5.5E-04	1.9E-03
Normalized to the value for $p_1 = 1.0$		**1.1**	**2.2**		**1.3**	**3.8**		**1.4**	**4.9**
Min. Disp.				-4.4E-04	-2.9E-04	8.8E-04	-1.2E-04	-3.3E-05	7.0E-04
Normalized to the value for $p_1 = 1.0$					**0.7**	**2.0**		**0.3**	**5.6**
Res. Disp.[1]				1.5E-04	2.9E-04	1.5E-03	9.1E-05	1.8E-04	9.1E-04
Normalized to the value for $p_1 = 1.0$					**2.0**	**10.0**		**2.0**	**10.0**
				$N_0 = 0.8N_{max}$					
Max. Disp.	-8.9E-03	-1.1E-02	-3.2E-02	2.0E-03	3.5E-03	1.5E-02	1.1E-03	2.0E-03	9.1E-03
Normalized to the value for $p_1 = 1.0$		**1.3**	**3.5**		**1.7**	**7.3**		**1.8**	**8.4**
Min. Disp.				2.7E-04	1.1E-03	7.8E-03	3.5E-04	8.9E-04	5.1E-03
Normalized to the value for $p_1 = 1.0$					**4.2**	**29.2**		**2.5**	**14.3**
Res. Disp.				8.5E-04	1.7E-03	8.4E-03	5.3E-04	1.1E-03	5.2E-03
Normalized to the value for $p_1 = 1.0$					**2.0**	**9.8**		**2.0**	**9.8**

[1]Residual displacement is measured at the end of 2nd unloading.

Table 12-2. The effects of variation in p_1 on the response of considered soil-foundation interface model to time-history loading.

Parameter	u_{fv}			u_{fh}				u_{fr}	
	$p_1 = 1.0$	$p_1 = 0.5$	$p_1 = 0.1$	$p_1 = 1.0$	$p_1 = 0.5$	$p_1 = 0.1$	$p_1 = 1.0$	$p_1 = 0.5$	$p_1 = 0.1$
				$N_0 = 0.2N_{max}$					
Max. Disp.	-1.8E-03	-1.9E-03	-2.8E-03	6.9E-04	7.9E-04	1.6E-03	2.8E-04	3.4E-04	8.6E-04
Normalized to the value for $p_1 = 1.0$		**1.1**	**1.6**		**1.1**	**2.3**		**1.2**	**3.1**
Max. Disp.				-5.2E-04	-5.3E-04	-1.1E-03	-1.7E-04	-1.8E-04	-5.9E-04
Normalized to the value for $p_1 = 1.0$					**1.0**	**2.2**		**1.1**	**3.6**
Res. Disp.				4.2E-05	8.4E-05	4.2E-04	2.7E-05	5.3E-05	2.6E-04
Normalized to the value for $p_1 = 1.0$					**2.0**	**9.9**		**2.0**	**9.8**
				$N_0 = 0.8N_{max}$					
Max. Disp.	-7.4E-03	-8.1E-03	-1.6E-02	1.1E-03	1.7E-03	6.0E-03	5.1E-04	8.5E-04	3.7E-03
Normalized to the value for $p_1 = 1.0$		**1.1**	**2.2**		**1.5**	**5.4**		**1.7**	**7.2**
Max. Disp.				-8.3E-04	-1.4E-03	-5.7E-03	-4.2E-04	-7.6E-04	-3.5E-03
Normalized to the value for $p_1 = 1.0$					**1.7**	**6.9**		**1.8**	**8.3**
Res. Disp.				3.1E-04	6.2E-04	3.1E-03	1.9E-04	3.9E-04	1.9E-03
Normalized to the value for $p_1 = 1.0$					**2.0**	**10.0**		**2.0**	**10.0**

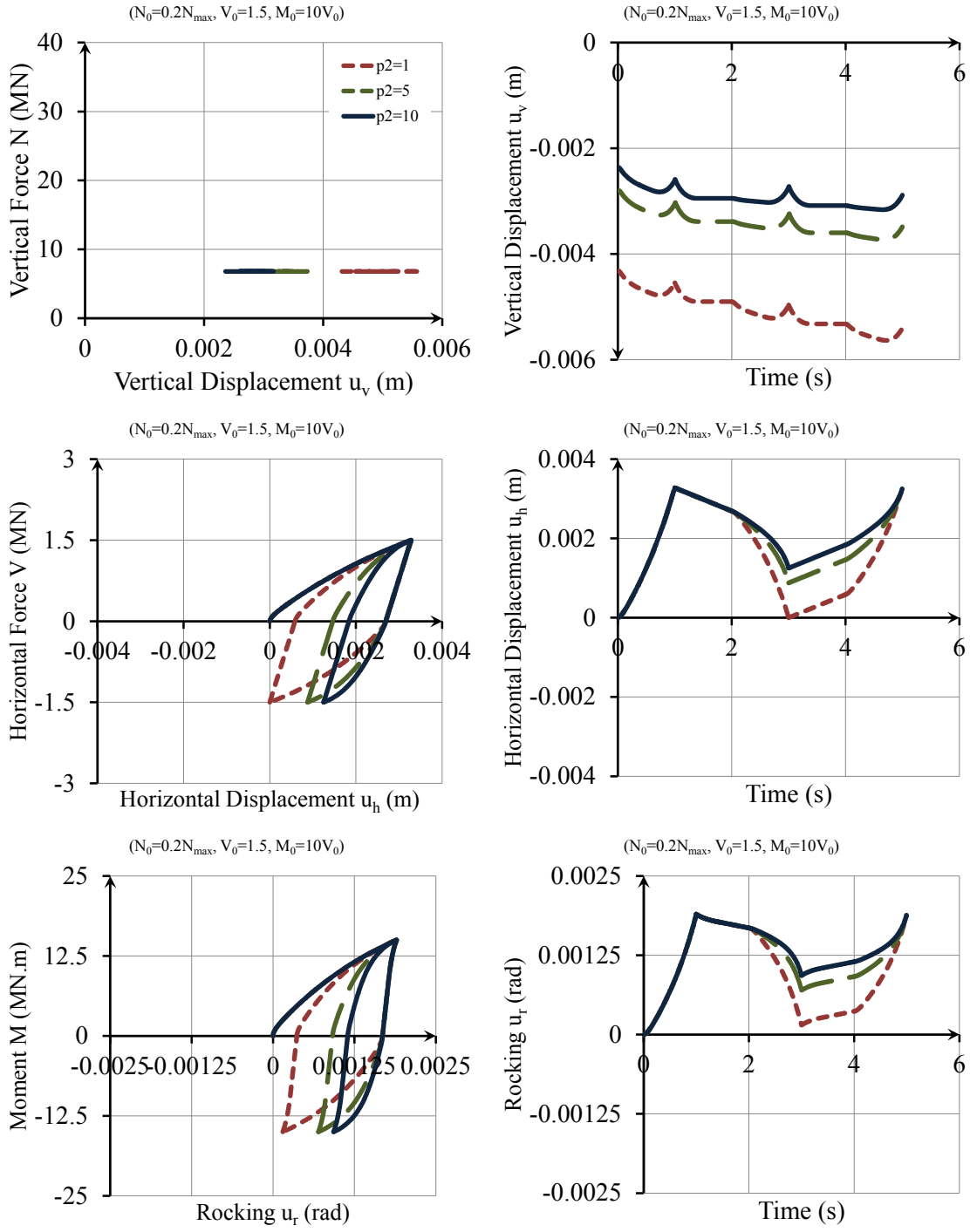

Figure 12-10. The effects of variation in p_2 on the response of considered soil-foundation interface model to cyclic loading ($N_0=0.2N_{max,}$ $V_0=1.5$ MN, $M_0=10V_0$).

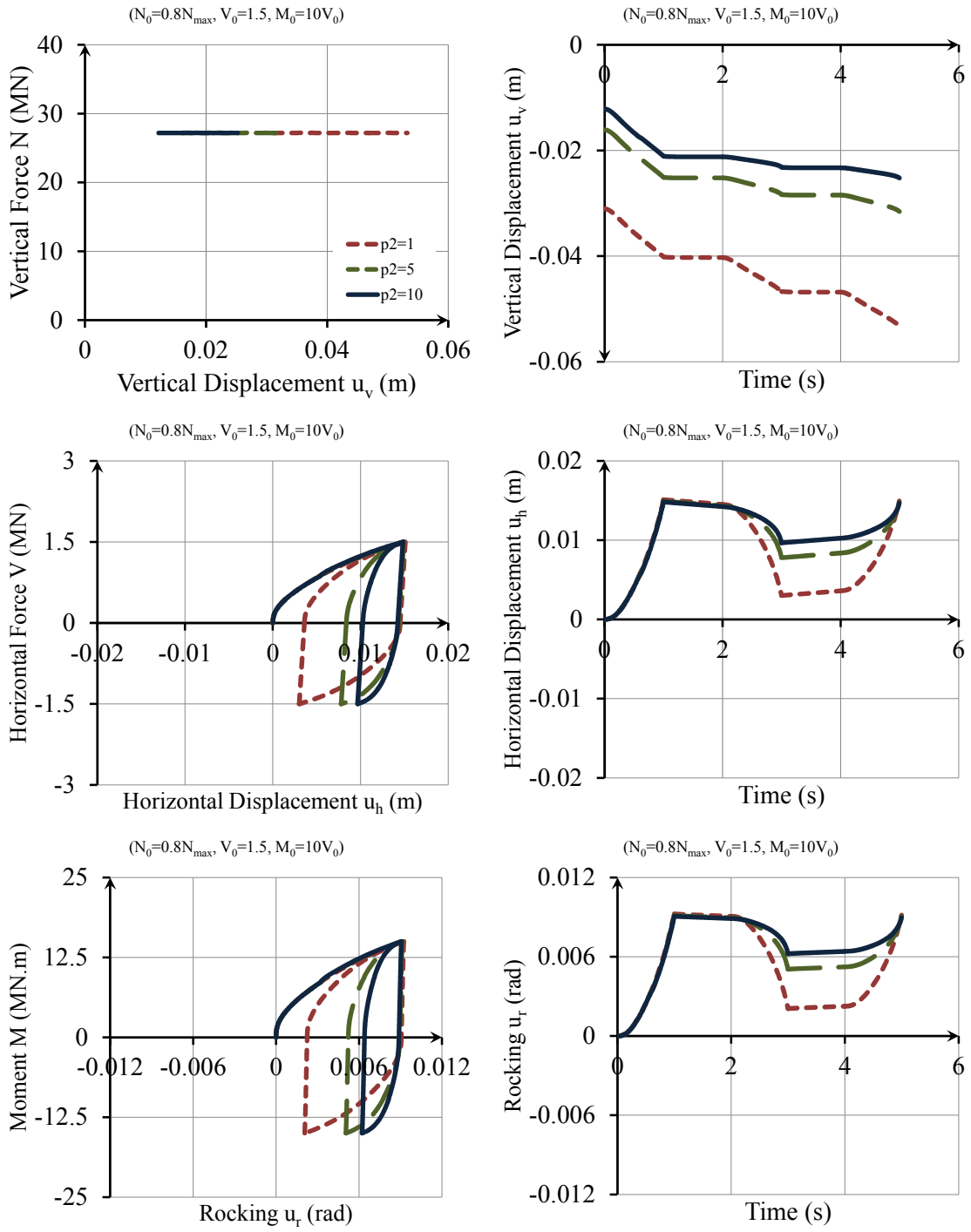

Figure 12-11. The effects of variation in p_2 on the response of considered soil-foundation interface model to cyclic loading ($N_0=0.8N_{max,}$ $V_0=1.5$ MN, $M_0=10V_0$).

Table 12-3. The effects of variation in p_2 on the response of considered soil-foundation interface model to cyclic loading.

Parameter	u_{fv}			u_{fh}			u_{fr}		
	$p_2 = 1$	$p_2 = 5$	$p_2 = 10$	$p_2 = 1$	$p_2 = 5$	$p_2 = 10$	$p_2 = 1$	$p_2 = 5$	$p_2 = 10$
				$N_0 = 0.2N_{max}$					
Max. Disp.	-5.4E-03	-3.5E-03	-2.9E-03	3.3E-03	3.3E-03	3.3E-03	1.9E-03	1.9E-03	1.9E-03
Normalized to the value for $p_2 = 1.0$		**0.6**	**0.5**		**1.0**	**1.0**		**1.0**	**1.0**
Min. Disp.				-9.1E-08	8.8E-04	1.3E-03	1.5E-04	7.0E-04	9.3E-04
Normalized to the value for $p_2 = 1.0$					**NA**	**NA**		**4.6**	**6.2**
Res. Disp.				5.9E-04	1.5E-03	1.8E-03	3.7E-04	9.1E-04	1.1E-03
Normalized to the value for $p_2 = 1.0$					**2.5**	**3.1**		**2.5**	**3.1**
				$N_0 = 0.8N_{max}$					
Max. Disp.	-5.3E-02	-3.2E-02	-2.5E-02	1.5E-02	1.5E-02	1.5E-02	9.2E-03	9.1E-03	9.1E-03
Normalized to the value for $p_2 = 1.0$		**0.6**	**0.5**		**1.0**	**1.0**		**1.0**	**1.0**
Min. Disp.				3.0E-03	7.8E-03	9.7E-03	2.1E-03	5.1E-03	6.2E-03
Normalized to the value for $p_2 = 1.0$					**2.6**	**3.2**		**2.4**	**3.0**
Res. Disp.				3.6E-03	8.4E-03	1.0E-02	2.2E-03	5.2E-03	6.4E-03
Normalized to the value for $p_2 = 1.0$					**2.3**	**2.8**		**2.3**	**2.8**

Table 12-4. The effects of variation in p_2 on the response of considered soil-foundation interface model to time-history loading.

Parameter	u_{fv}			u_{fh}				u_{fr}	
	$p_2 = 1.0$	$p_2 = 0.5$	$p_2 = 0.1$	$p_2 = 1.0$	$p_2 = 0.5$	$p_2 = 0.1$	$p_2 = 1.0$	$p_2 = 0.5$	$p_2 = 0.1$
				$N_0 = 0.2N_{max}$					
Max. Disp.	-4.3E-03	-2.8E-03	-2.4E-03	2.1E-03	1.6E-03	1.5E-03	1.2E-03	8.6E-04	7.9E-04
Normalized to the value for $p_2 = 1.0$		**0.6**	**0.5**		**0.8**	**0.7**		**0.7**	**0.7**
Min. Disp.				-1.5E-03	-1.1E-03	-9.7E-04	-8.2E-04	-5.9E-04	-5.1E-04
Normalized to the value for $p_2 = 1.0$					**0.8**	**0.7**		**0.7**	**0.6**
Res. Disp.				1.5E-04	4.2E-04	5.1E-04	9.1E-05	2.6E-04	3.2E-04
Normalized to the value for $p_2 = 1.0$					**2.9**	**3.5**		**2.9**	**3.5**
				$N_0 = 0.8N_{max}$					
Max. Disp.	-3.1E-02	-1.6E-02	-1.2E-02	7.9E-03	6.0E-03	5.6E-03	4.8E-03	3.7E-03	3.3E-03
Normalized to the value for $p_2 = 1.0$		**0.5**	**0.4**		**0.8**	**0.7**		**0.8**	**0.7**
Min. Disp.				-7.5E-03	-5.7E-03	-4.9E-03	-4.6E-03	-3.5E-03	-2.9E-03
Normalized to the value for $p_2 = 1.0$					**0.8**	**0.7**		**0.8**	**0.6**
Res. Disp.				1.9E-03	3.1E-03	3.6E-03	1.2E-03	1.9E-03	2.2E-03
Normalized to the value for $p_2 = 1.0$					**1.6**	**1.9**		**1.6**	**1.9**

12.5 Comparison between Linear Macro-Element and Cone Model

The response of a linear macro-element is also compared with that of the cone model introduced in Chapters 5. In this regard, the level of difference in deformation and acceleration responses in the horizontal and rocking directions is investigated for a selected time-history loading. There are two main modelling differences between the linear macro-element and the cone model:

1) The way radiation damping is defined

2) The way radiation damping is acting in rocking direction

Radiation damping for the macro-element has been defined using expressions that involve analog velocity V_{La} given by the equation [1]:

$$V_{La} = \frac{3.4}{\pi(1-\upsilon)} V_s \tag{12.1}$$

where V_s is soil shear wave velocity and υ is the Poisson's ratio. In contrast, radiation damping for the cone model is defined using either dilatational wave velocity or two times the shear wave velocity, depending on direction of loading and the value of Poisson's ratio υ [2]. In addition, in the cone model, the dashpot representing radiation damping in the rocking direction is attached between the foundation and an internal mass moment of inertia. In contrast, in the macro-element, the corresponding dashpot is assumed to be attached between the foundation and a fixed-point representing the ground.

These modelling differences are a potential basis for deviations between the response of the macro-element and the cone model. The difference between horizontal and rocking deformation, and acceleration responses of the macro-element and the cone model are presented in Figure 12-12. Clearly, there is not a significant difference for the responses in the horizontal direction. However, an increase in the order of $2-3$ times the rocking

response is expected when the cone model is assumed to represent soil-foundation interface. The observed differences in the foundation rocking responses using these two different models should be taken into account in any future comparison between analyses using cone model and linear macro-element.

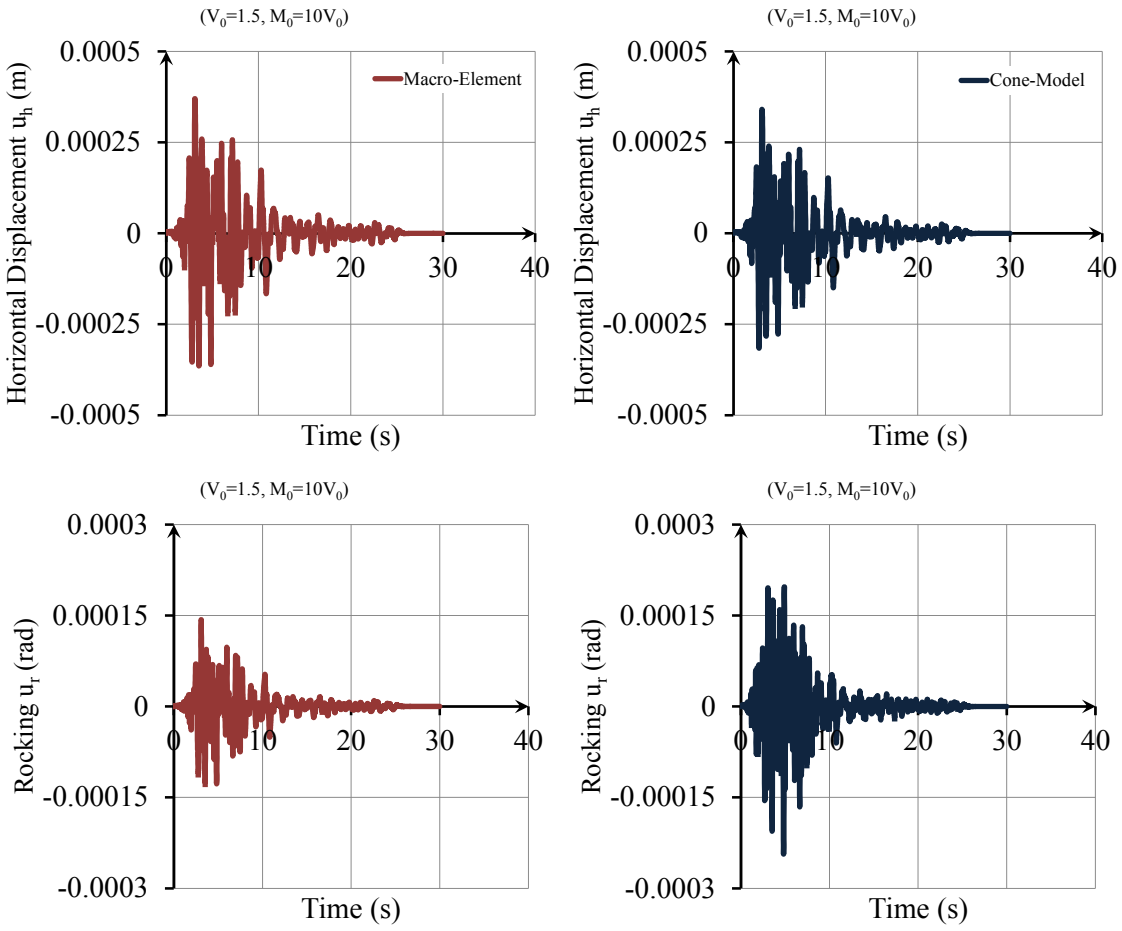

Figure 12-12. Comparison between the response of macro-element and cone model: (left) responses for macro-element; (right) response for cone model.

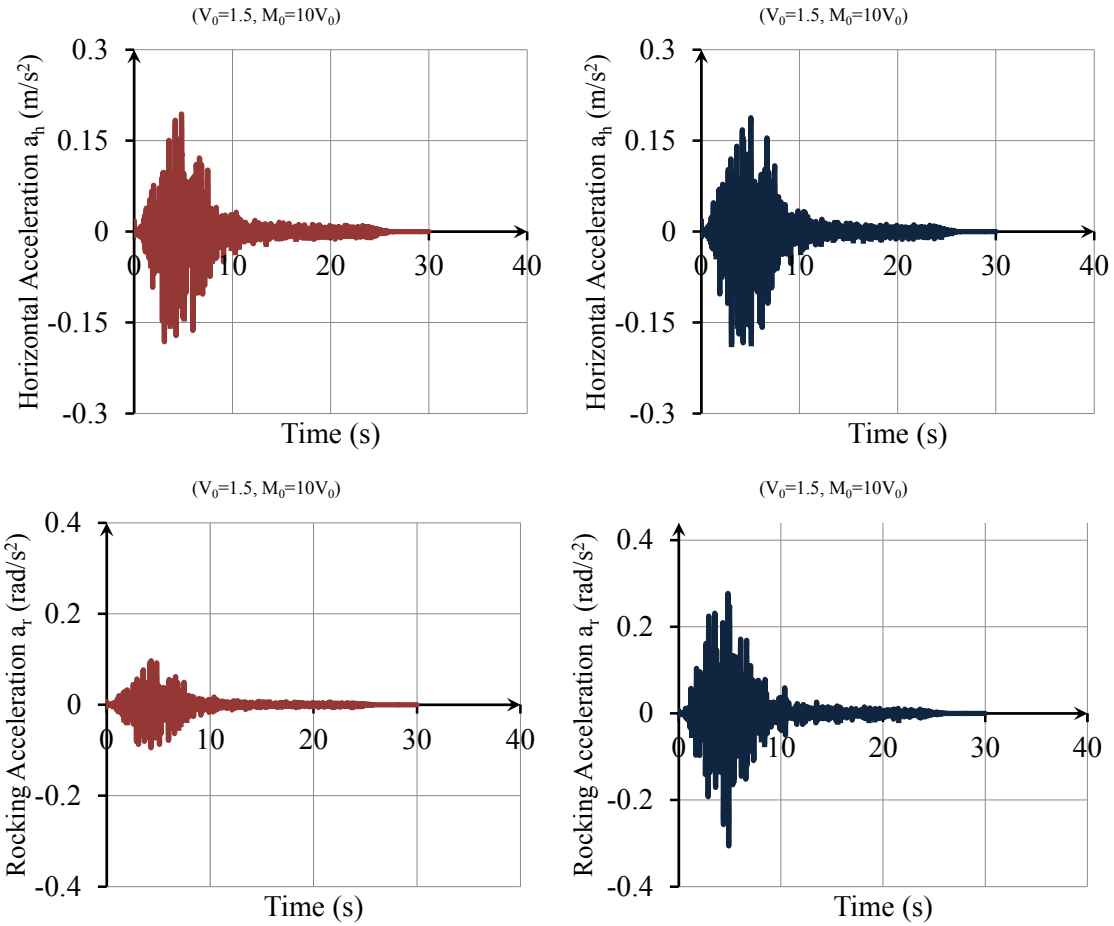

Figure 12-12. *Continued*.

12.6 Summary

The effects of different soil-foundation interface parameters influencing the degree of nonlinearity at the interface level were investigated in this chapter. The first and most important conclusion is that using a linear soil-foundation model instead of a proper nonlinear model can be misleading in the prediction of foundation deformation. In addition, the effects of additional damping to the soil-structure system due to hysteretic actions, which occurs at the soil-foundation interface level, are ignored if the linear soil-foundation model is used. Consequently, different structural reactions might be expected.

It also has been shown that the response of macro-element is highly dependent on its parameters p_1 and p_2. Smaller values of p_1 corresponds to a higher soil nonlinearity

and, consequently, larger deformations. However, smaller values of p_2 results in smaller horizontal displacement and rocking, but, in larger settlement.

Since soil-foundation nonlinearity might change the structural response in a soil-structure system, next chapter aims to investigate these effects in more detail.

References

[1] G. Gazetas and R. Dobry, "Simple radiation damping model for piles and footings," *Journal of Geotechnical Engineeing-ASCE,* vol. 110, pp. 937-56, 1984.

[2] G. Gazetas and R. Dobry, "Horizontal response of piles in layered soils," *Journal of Geotechnical Engineering,* vol. 110, pp. 20-40, 1984.

[3] J. P. Wolf, *Foundation Vibration Analysis Using Simple Physical Models*. Englewood Cliffs, N.J.: Prentice-Hall, 1994.

CHAPTER

13. The Effects of Nonlinear Soil-Structure Interaction on Seismic Response of Structures

Abstract. This chapter presents the impact of base fixity on seismic analysis including soil-structure interaction considering linear and nonlinear soil-foundation interface conditions. A set of inelastic time-history analyses using a yielding single-degree-of-freedom structural system with different fixity conditions at the base are used. The base fixity configurations considered are: (i) fixed-base; (ii) linear flexible-base; (iii) nonlinear flexible-base without uplift; and (iv) nonlinear flexible-base with uplift. A suite of 40 ground motions with large-magnitude and moderate-distance is chosen to ensure robustness of the results across realistic ground motions. The examination of soil-structure interaction effects on the structural response under a design base earthquake (DBE) level, i.e. 500-year return period event, is carried out for all considered scenarios. In addition, the effects of an increase in the seismic intensity up to a maximum credible earthquake (MCE) level, i.e. 2500-year return period event, are also studied for the case of nonlinear flexible-base with uplift.

13.1 Introduction

The effects of soil-structure interaction (SSI) on the structural response investigated in Chapters 7 and 8 were based on the assumption that the soil adjacent to the foundation behaves as a linear or at most an equivalent linear viscoelastic material, similar to most studies on SSI [1-4] and the current design procedures [5-9]. In addition, the foundation is assumed to be fully bonded to the soil underneath. However, geotechnical

investigations after the Northridge 1994, Kobe 1995, Kocaeli 1999 [10] and Christchurch 2010 earthquakes [11] have shown that significant nonlinear action in the soil and soil-foundation interface can be expected due to high levels of seismic excitation and spectral acceleration. Therefore, it is very important to investigate the influence of soil-foundation interface nonlinearity on the effects of SSI [12]. Principally, neglecting such phenomena prohibits the effects and consequences of: (i) energy dissipation due to soil yielding; (ii) large foundation deformation as well as residual settlement and rocking; and (iii) foundation toppling on the structural response.

In this regard, Gandomzadeh et al. [13] carried out a parametric study for an elastic structural system supported on a nonlinear soil stratum. The structure was modelled as a single-bay, single-storey 2D frame having different masses, and the soil was modelled using the Iwan's constitutive nonlinear model. The soil-structure systems considered were then enforced to Ricker wavelet with various amplitudes. They concluded that due to soil nonlinearity and, consequently, an additional energy dissipation to the system, structural response decreases if SSI is considered. This reduction is more pronounced for the systems having a fundamental frequency close to the natural frequency of the soil. In addition, it was stated that soil nonlinearity changes fundamental frequency of the system and this change is significantly affected by the mass of the system.

Saez et al. [14] also studied the effect of elastic and inelastic SSI on seismic demand of single-degree-of-freedom structures. In this study, two inelastic structures, representing low-rise and mid-rise reinforced concrete moment resisting frame buildings, and two soil conditions, representing a dry and a saturated homogenous dense Toyoura sand profile of 30m depth overlaying bedrock, were considered. The soil was modelled using elastic and elasto-plastic constitutive models. The soil-structure systems generated were then excited by a suite of ground motions comprising different earthquake selections and strong-motion parameters. It was concluded that when the soil is in a dry condition, the elastic and inelastic SSI result in a similar effect on structural response. However, when the soil is in a saturated condition, a significant variation exists between elastic and inelastic SSI effect. This variation is obviously due to pore pressure generation that cannot be captured by linear soil models. In addition, it was indicated that the influence of SSI on the structural response when low-rise structural systems on dry soil are

considered, might be either beneficial or detrimental. However, SSI is beneficial for other scenarios considered.

Finally, the effects of SSI on structural response for linear and nonlinear soil-foundation interface conditions were studied by Pecker and Chatzigogos [15] following an incremental dynamic analysis (IDA) approach. The analyses were facilitated using a new dynamic macro-element specifically developed to represent soil-foundation interface nonlinearity [16, 17]. This study covered a typical highway bridge pier excited by a suite of ground motions representing relatively large-magnitude earthquakes with moderate distances and no effects of directivity. In the soil-structure model used, both soil and structure were considered to be nonlinear. It was concluded that nonlinear SSI is always beneficial and significantly reduces the structural ductility demand. However, large displacements and rotations at the foundation are also resulted that might be unaccepted. Therefore, care must be taken into account before moving towards a design philosophy where the ductility demand can be transferred from the structure to the foundation (e.g. [18]).

An attempt was made in this chapter to expand the above mentioned studies and specifically: (i) investigate the effects of linear and nonlinear SSI on structural response; (ii) compare the SSI effects for linear and nonlinear soil-foundation interface conditions; and (iii) examine the effects of soil-foundation nonlinearity at the maximum credible earthquake (MCE) level. In this context, an idealised inelastic single-degree-of-freedom structural system attached to a soil-foundation interface element representing either: (i) a linear condition; (ii) a nonlinear condition without uplift; or (iii) a nonlinear condition with uplift was used. The soil-structure models generated were then enforced to a suite of 40 ground motions scaled to a desired hazard level. Finally, the trends and behaviours were comprehensively quantified and presented.

13.2 Soil-Structure Model Description

The soil-structure system investigated in this research (Figure 13-1) denotes a typical highway bridge pier supported by a rigid circular shallow-foundation and enforced to seismic excitation [15]. It was designed based on a direct displacement-based design

(DDBD) approach specifically introduced to take into account the SSI effects [19]. The design was based on the Eurocode 8 design spectrum-Type 1, considering a firm soil condition and a peak ground acceleration (PGA) of 0.5g. The design performance criteria considered are:

1) System drift limit, $\Delta_d = 0.03h$

2) Maximum foundation rotation, $\theta_{lim} = 0.01\ rad$

3) Maximum structural ductility demand, $\mu = 3$

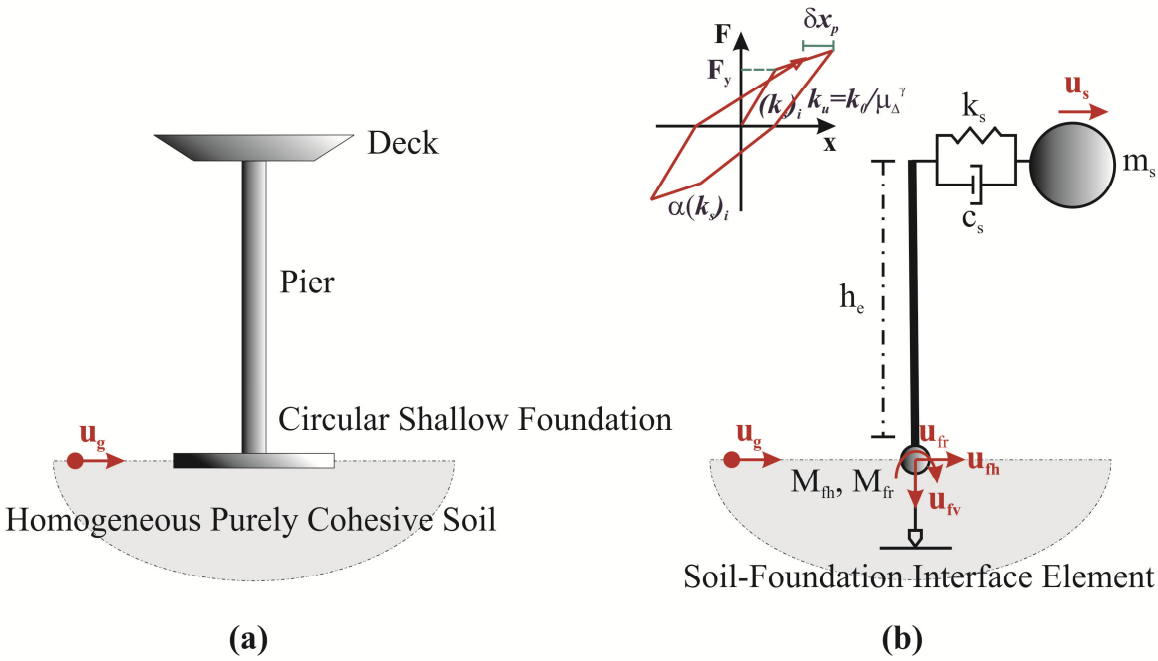

Figure 13-1. Soil-structure system studied: (a) physical; (b) model.

This system was then modelled in the finite-element program Ruaumoko 3D [20] using: (i) a yielding single-degree-of-freedom structure representing the bridge pier; and (ii) a mass-spring-dashpot assembly or a macro-element representing the linear or nonlinear soil-foundation interface condition, respectively. Clearly, this modelling approach follows the substructure technique introduced for SSI analysis.

13.2.1 Structural System

The yielding single-degree-of-freedom structural system used is characterised by its height h_e, mass m_s, lateral stiffness k_s and equivalent structural viscous damping c_s. The damping ratio of 5% was also assumed. In addition, to cover structural nonlinearity, a stiffness-degrading force-deformation hysteresis rule as Takeda (bilinear envelope with strain hardening and stiffness degradation) was considered with 5% post-elastic stiffness and unloading and reloading parameters of $\gamma = 0.3$ and $\delta = 0.2$, respectively (γ and δ are defined in Figure 13-1). This force-deformation behaviour was then assigned to the spring representing the lateral stiffness of the system. The numerical parameters defining the structural system are given in Table 13-1.

13.2.2 Linear Soil-Foundation Interface

To represent the dynamic behaviour of soil-foundation interface assuming a linear response, the commonly used mass-spring-dashpot assembly [21] was attached to the base of the single-degree-of-freedom structural system considered. In this approach, the soil is assumed to behave linearly and the foundation is considered to be fully bonded to the soil. The springs in this assembly represent the static stiffness of the soil-foundation system and the dashpots represent the radiation damping. The formulations and the corresponding numerical parameters used to define this element are given in Table 13-1.

13.2.3 Nonlinear Soil-Foundation Interface

The dynamic behaviour of the soil-foundation interface with nonlinear condition was included in the model by a link element, denoted as macro-element, introduced by Chatzigogos et al. [16, 17]. This macro-element is specifically formulated to reproduce all nonlinearity expected at the foundation level including: (i) soil material nonlinearity (yielding); and (ii) interface nonlinearity (uplift). It principally uses a nonlinear constitutive law linking force parameters to displacement parameters. These parameters are selected such that to be directly linked to those related to the structure supported by the foundation. The details about macro-element adopted can be found in Chapter 10 or the original work by Chatzigogos et al. [16, 17].

In addition, the macro-element is coupled with the same dashpot as for the linear soil-foundation model to cover radiation damping. The formulations and the corresponding numerical parameters used to define macro-element are given in Table 13-1.

Table 13-1. Properties of the soil-structure model.

Parameter	**Formulation/Description**	**Value**
Structural Parameter:		
1. height, h_e	effective height to centre of the mass	20 m
2. mass, m_s	including the mass of the deck and pier	1.22 kt
3. initial lateral stiffness, $(k_s)_i$	-	25 MN/m
4. coefficient of viscous damping, c_s	$c_s = 2(5\%)\sqrt{m_s(k_s)_i}$	0.55 MN.s/m
5. yield strength, f_y	-	1.27 MN
6. yield displacement, δ_y	$\delta_y = f_y/(k_s)_i$	0.051 m
Soil-Foundation Interface Parameters:		
• Soil and Foundation		
1. soil mass density, ρ	-	1.6 t/m^3
2. Poisson's ratio, υ	-	0.3
3. soil shear wave velocity, V_s	-	255 m/s
4. soil shear modulus, G	-	104 MPa
5. soil cohesion, c_0	-	0.15 MPa
6. foundation radius, r	-	3.75 m
7. foundation mass, M_{fh}		0.22 kt
8. foundation mass moment of inertia, M_{fr}		0.78 kt.m^2
• Mass-Spring Dashpot Assembly		
1. Vertical stiffness, K_v	$K_v = \frac{4Gr}{1-\upsilon}$	2229 MN/m
2. Horizontal stiffness, K_h	$K_h = \frac{8Gr}{2-\upsilon}$	1835 MN/m
3. Rocking stiffness, K_r	$K_v = \frac{8Gr^3}{3(1-\upsilon)}$	20893 MN.m

Table 12-1. *Continued.*

• Macro-Element		
a) Plasticity Parameters		
1. Maximum cantered vertical force, N_{max}	$N_{max} = 6.06c_0A$	40 MN
2. Maximum normalized horizontal force, $Q_{V,max}$	$Q_{V,max} = \frac{c_0A}{N_{max}}$	0.165
3. Maximum normalized moment, $Q_{M,max}$	$Q_{M,max} = \frac{0.67c_0AD}{DN_{max}}$	0.11
4. Numerical parameter expressing the extent of initial plastic stiffness, p_1	-	0.5
5. Numerical parameter expressing the extent of stiffness degradation in reloading, p_2	-	4
b) Uplift Parameters		
1. α	$Q_{M,0} = \pm\frac{Q_N}{\alpha}\exp(-\beta Q_N)$	6
2. β		1.5
3. ξ	$\Re_{vr}^{el} = \Re_{rv}^{el} = \begin{cases} 0, & \lvert q_M^{el}\rvert \le \lvert q_{M,o}^{el}\rvert \\ \xi(1-\frac{q_{M,o}^{el}}{q_M^{el}})\Re_v^{st}, & q_M^{el}\rvert > \lvert q_{M,o}^{el}\rvert \end{cases}$	0.75
4. δ	$\Re_r^{el} = \begin{cases} K_r, & \lvert q_M^{el}\rvert \le \lvert q_{M,o}^{el}\rvert \\ \gamma\delta\left(\frac{q_{M,0}^{el}}{q_M^{el}}\right)^{1+\delta}\Re_r^{st} + \xi^2(1-\frac{q_{M,o}^{el}}{q_M^{el}})^2\Re_v^{st}, & q_M^{el}\rvert > \lvert q_{M,o}^{el}\rvert \end{cases}$	0.5
5. γ		2.0
6. $Q_M/Q_{M,0}$	$\frac{Q_M}{Q_{M,0}} = 3 - 2(\frac{q_{M,0}^{el}}{q_M^{el}})$	3
• Radiation Damping		
1. Vertical damping, C_v	$C_v = \rho[\frac{3.4}{\pi(1-\upsilon)}V_s]A$	28 MN.s/m
2. Horizontal damping, C_h	$C_h = \rho V_sA$	18 MN.s/m
3. Rocking damping, C_r	$C_r = \rho[\frac{3.4}{\pi(1-\upsilon)}V_s]I_r$	98 MN.s/m

13.3 Ground Motions and Scaling Scheme

To cover the uncertainties resulting from record-to-record variability, the generated soil-structure model was subjected to a large number of ground motions with different characteristics. An ensemble of 40 earthquake ground motions recorded on stiff/soft soil (soil type C with $V_s = 180 - 360$ m/s and soil type D with $V_s < 180$ m/s to a depth of 30 m based on USGS soil geomatrix classification) was used in the analyses. All

selected records are from earthquakes with magnitude of 6.5-7.5 and have source-to-site distance (closest distance to fault rupture) in the range of 15-40 km. Detailed information about the selected suite of ground motions can be found in Chapter 6.

The selected ground motions were then scaled using the method introduced in New Zealand Standard [22] to match the target spectrum over the period range of interest. The target spectrum chosen represents a 5% damped elastic acceleration response spectrum for: (i) soil class C; (ii) hazard factor (Z=PGA) of 0.4g; (iii) return period factor of 1.0 corresponding to a design based earthquake (DBE) level. The period range of interest considered is 0.5-2.2 s covering periods between $0.4T_{FB}$ and $1.3T_{SSI}$, where T_{FB} is the fundamental period of the fixed-base system and T_{SSI} is the fundamental period of the corresponding soil-structure system. Scaled acceleration response spectra are presented in Figure 13-2.

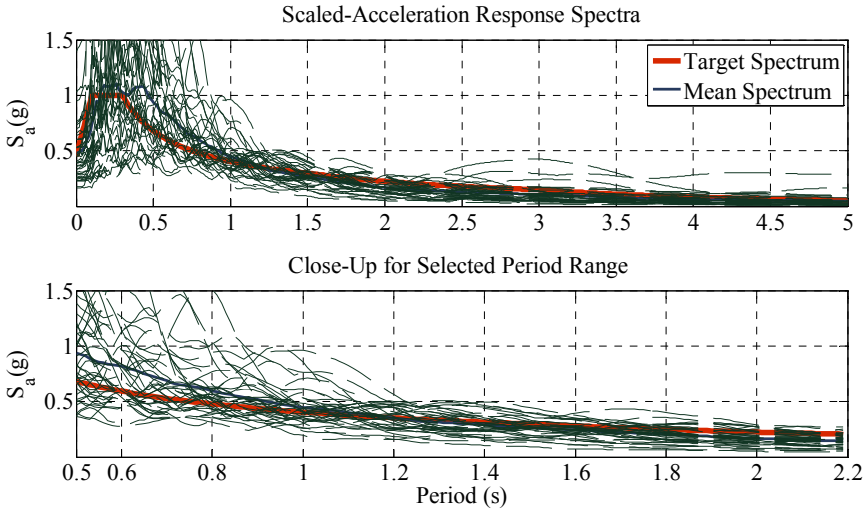

Figure 13-2. Scaled acceleration response spectra for the ground motions selected.

In addition, to investigate the effects of soil-foundation nonlinearity on the response of soil-structure systems when the maximum credible earthquake (MCE) level is considered, the ground motions selected were also scaled for the return period of 2500 years. It should be noted that these scaled records were only used for the results presented in Section 12.4.4.

13.4 Soil-Structure Interaction Effects on Structural Response

13.4.1 Typical Result of a Dynamic Analysis

A typical dynamic response of the fixed-base model and the corresponding nonlinear flexible-base model with uplift is shown in Figures 12-3 and 12-4, respectively. The quantities depicted are: (i) structural acceleration a_s, that is the total acceleration of the structural mass representing the base shear; (ii) total displacement u_{tot}, that is a measure of the displacement at the roof level including lateral displacement resulted from foundation motion and structural distortion, which can cause the pounding between adjacent structures; and (iii) structural force-deformation hysteretic behaviour $F_{s,el}\ vs.\ u_s$ that shows the maximum structural force and distortion in addition to the degree of structural nonlinearity experienced.

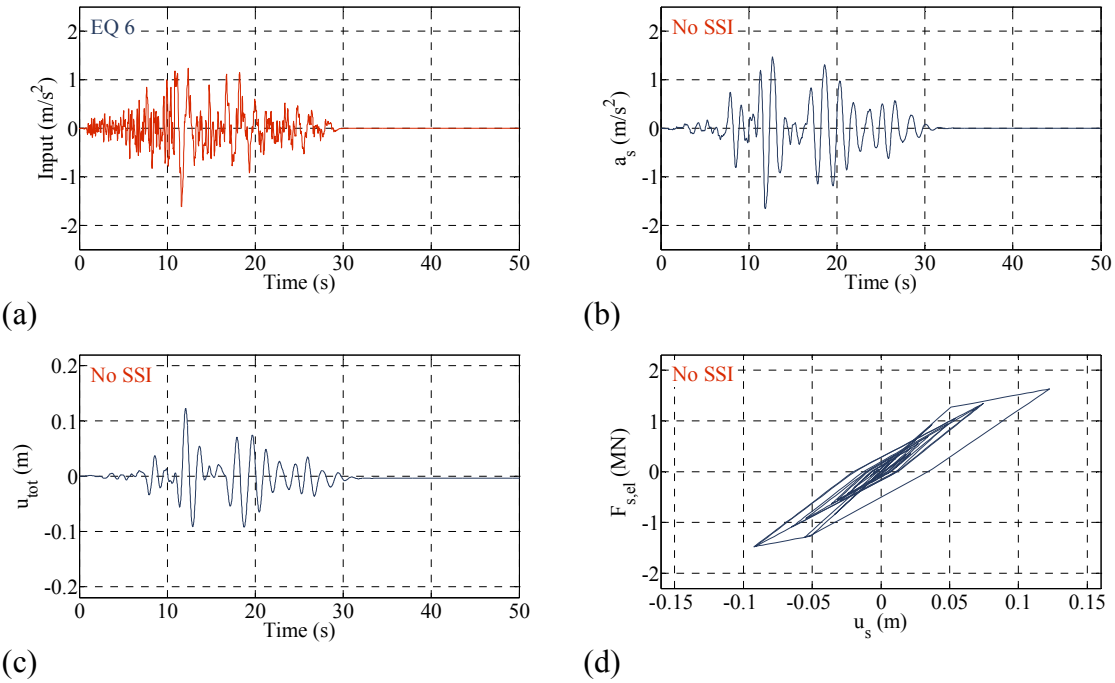

Figure 13-3. Example of a dynamic structural response of the fixed-base model subjected to EQ 6: (a) input ground motion; (b) structural acceleration; (c) total displacement; (d) structural force-deformation hysteretic behaviour.

The other quantities only considered for the flexible-base mode are: (iv) horizontal foundation displacement u_{fh}; (v) foundation rocking u_{fr}; and (vi) vertical foundation displacement u_{fv}. These parameters are all defined at the foundation centre. It should be noted that when $u_{fv} < 0$, the foundation centre moves downwards (settles), and when $u_{fv} > 0$, a separation between the foundation centre and the ground surface occurs. However, this separation does not mean toppling.

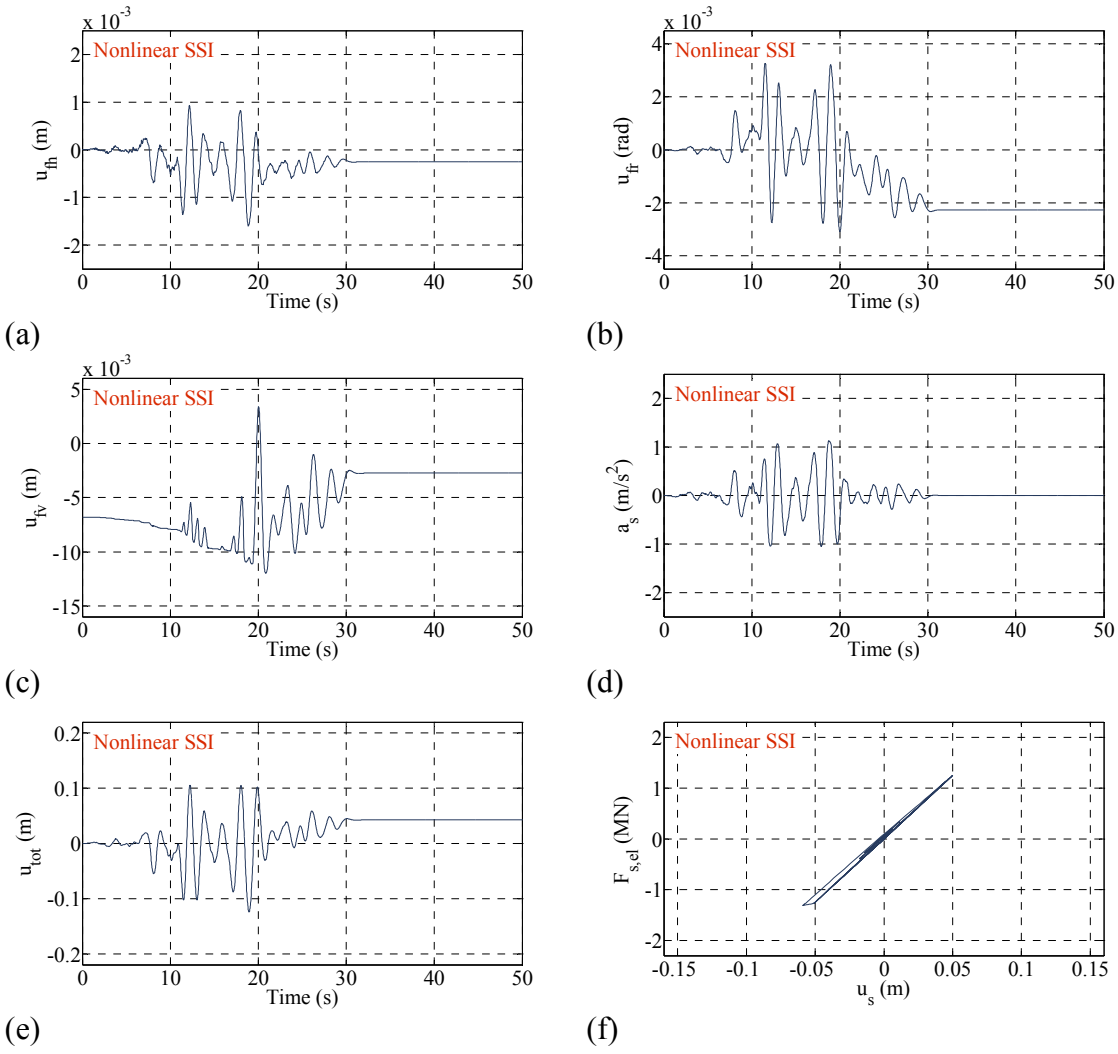

Figure 13-4. Example of a dynamic structural response of the nonlinear flexible-base model subjected to EQ 6: (a) horizontal foundation displacement; (b) foundation rocking; (c) vertical foundation displacement; (d) input ground motion; (e) structural acceleration; (f) total displacement; (g) structural force-deformation hysteretic behaviour.

As illustrated in these figures, the inclusion of nonlinear SSI in dynamic analysis results in a residual foundation deformation that, in turn, causes a more significant residual total displacement compared to that for the fixed-base model. In addition, foundation settlement exists as a result of this integration that cannot be captured in a traditional fixed-base model. Finally, the nonlinear behaviour of the foundation most probably makes the system to show a smaller structural acceleration and less degree of nonlinearity.

13.4.2 Soil-Structure Interaction Effects Presentation

To illustrate SSI effects on structural response for the different soil-foundation interface conditions examined, the maximum values of: (i) structural acceleration a_s; (ii) total displacement u_{tot}; and (iii) normalized structural distortion by the yield displacement u_s/δ_y are compared for the fixed-base (FB) and flexible-base (SSI) models. In addition, the residual foundation settlement $(u_{fv})_{res}$ and rocking $(u_{fr})_{res}$ are also illustrated for flexible-base models.

13.4.3 Linear Soil-Structure Interaction Effects

The results of the numerical simulations using models with linear soil-foundation interface are presented in Figure 13-5. Clearly, as the foundation behaves linearly and the vertical and rocking foundation responses are independent, the foundation settlement under the total weight of the system is constant for all ground motions considered, and no residual foundation rocking is observed. Furthermore, in terms of structural acceleration, in contrast to the current design provisions, SSI can either decrease or increase the response. In this context, the probability of amplification is 25%, a percentage value that cannot be simply neglected.

However, it should be noted that the degree of reduction is higher than the degree of amplification. The maximum reduction in the structural acceleration due to SSI is about 40%, while the maximum amplification is about 20%. In addition, at the 84^{th} percentile level, a linear soil-structure model appears to reduce the structural acceleration by about 10%.

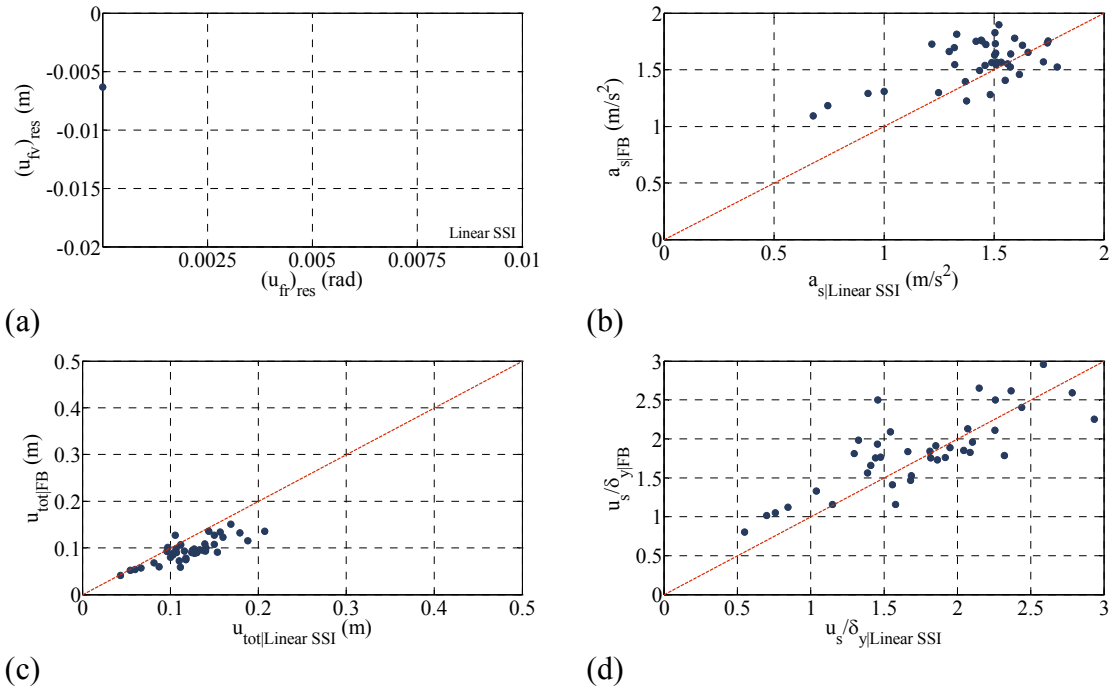

Figure 13-5. SSI effects on structural response for models with linear soil-foundation interface: (a) vertical foundation displacement vs. foundation rocking; (b) structural acceleration; (c) total displacement; (d) normalized structural distortion by the yield displacement.

The response amplification effects of SSI are more pronounced when total displacement is considered. Specifically, for almost 95% of the cases, SSI results in an amplified total displacement, with a maximum amplification of about 90%. Moreover, at the 84^{th} percentile level, SSI increases the total displacement by almost 20%. The risk of such non-negligible level of amplification emphasizes that SSI should be always considered in studies where pounding effects are of concern.

Finally, if structural distortion is considered, SSI can also result in either a reduction or an amplification in the response. In this case, the probability of amplification is about 45% with the maximum reduction and amplification being in the order of 40%. Note that the structural distortion is reduced at the 84^{th} percentile level by about 10% when a linear soil-structure model is used.

The SSI effects on structural response presented above for soil-structure systems with linear soil-foundation interface are in complete agreement with the results that has been previously presented in Chapter 8. Explicitly, the effects of linear SSI may not be always as beneficial as considered in practice. However, it should be noted that the

assumption of having linear soil-foundation interface might not be appropriate for some soil-structure-earthquake scenarios.

13.4.4 Nonlinear Soil-Structure Interaction Effects Considering Only Material Nonlinearity

The role of soil material nonlinearity (yielding) on SSI effects is discussed next. In this regard, the macro-element was used in the dynamic analyses adopted to represent soil-foundation interface. The uplift was at this stage deactivated in the element to avoid the effects of geometrical nonlinearity being included. The results of the corresponding analyses are presented in Figure 13-6.

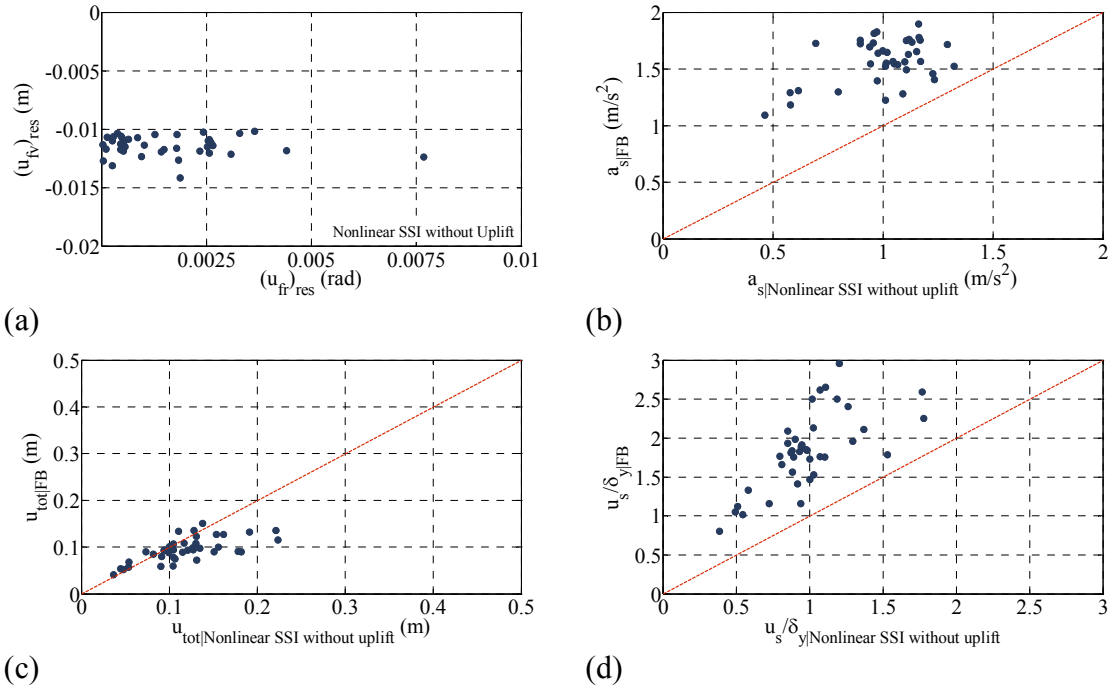

Figure 13-6. SSI effects on structural response for models with nonlinear soil-foundation interface without uplift: (a) vertical foundation displacement vs. foundation rocking; (b) structural acceleration; (c) total displacement; (d) normalized structural distortion by the yield displacement.

As expected, the foundation element responds nonlinearly and, as a consequence, the soil-structure system considered experiences residual settlement and rocking at the foundation level. It is interesting to note that although the vertical force on the foundation is constant, the residual settlement will have different values. The reason is that in the macro-element formulation, the vertical force and displacement are

interconnected with the applied moment and corresponding rocking. Therefore, depending on the input excitation characteristics and foundation rocking behaviour, different residual settlement might result. In addition, note that for all cases examined, residual displacement is a negative value representing a settlement condition compared to the separation from the ground surface.

Furthermore, in contrast to what observed in the case of linear SSI, structural acceleration and structural distortion always decrease due to SSI consideration. The maximum reduction in the response is 60% for structural acceleration and similarly for structural distortion. This high degree of reduction in the response is obviously due to a large amount of energy dissipation occurring at the soil-foundation interface level. In addition, consideration of soil material nonlinearity can reduce structural acceleration and structural distortion at the 84^{th} percentile level by almost 30% and 50%, respectively. It is also interesting to note that although foundation yielding decreases structural ductility level, it cannot totally prevent the structure from yielding.

However, when total displacement is considered, different trends and conclusions are observed. SSI increases total displacement for almost 70% of the cases compared to fixed-base conditions. In addition, the amplification in the response at the 84^{th} percentile level is about 20% with the possibility of an increase up to 100%. It highlights that the beneficial role of SSI in decreasing structural acceleration and ductility demand is compensated by large foundation displacement and rocking that might become totally unacceptable.

13.4.5 Nonlinear Soil-Structure Interaction Effects Considering Material and Geometrical Nonlinearity

Obviously, material and geometrical soil-foundation interface nonlinearity are two inseparable phenomena. Thus, their combined role on SSI effects should be investigated when soil-foundation interface nonlinearity is included in the SSI analysis. In this regard, the macro-element with an activated uplift option was used in the simulations adopted. Note that when foundation uplift is considered, an extra type of foundation failure, referred to as toppling, is introduced. Principally, foundation toppling occurs when the separation between the soil and foundation exceeds a predefined limit. The

results of the numerical analyses considering both material and geometrical nonlinearity are presented in Figure 13-7.

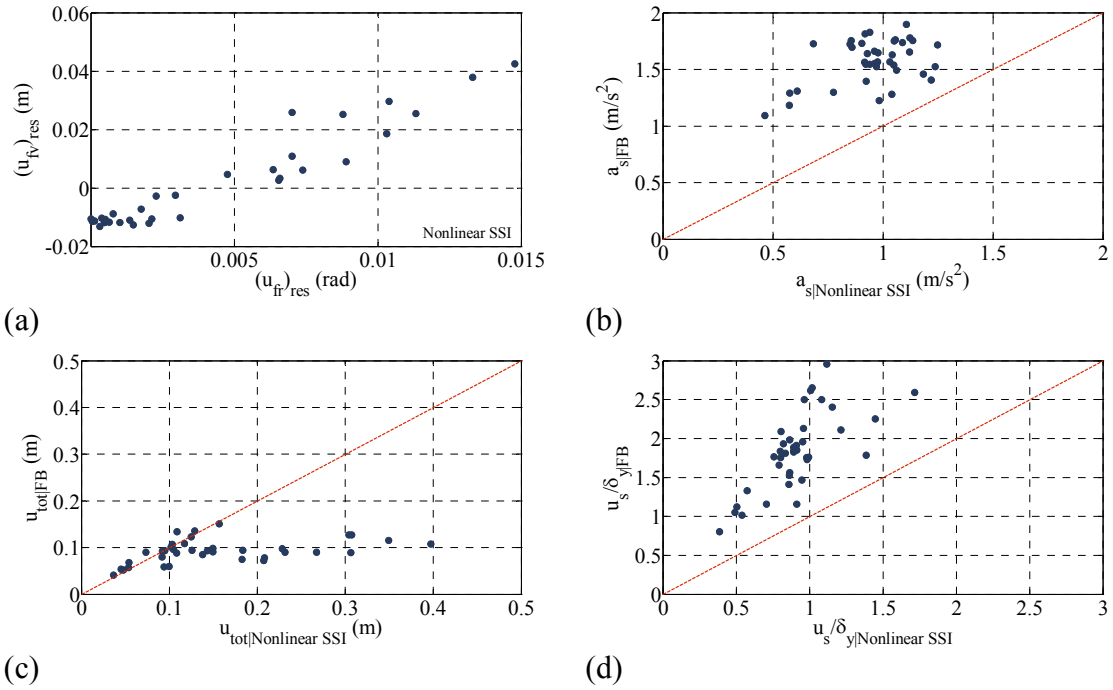

Figure 13-7. SSI effects on structural response for models with nonlinear soil-foundation interface: (a) vertical foundation displacement vs. foundation rocking; (b) structural acceleration; (c) total displacement; (d) normalized structural distortion by the yield displacement.

As foundation uplift is included in the dynamic analysis, the soil-structure system considered experiences a larger degree of nonlinearity at the foundation level. Specifically, foundation failure due to soil yielding occurs in 6 cases, where the foundation motion is getting very large without being stabilized. Having larger degree of nonlinearity also can be distinguished in terms of residual settlement and rocking at the foundation level.

As shown in Figure 13-7, residual foundation rocking can increase up to 0.015 rad compared to 0.005 rad when foundation uplift has been neglected. Due to this large foundation rocking, the centre of foundation even may experience a residual separation from the ground level. In addition to the cases of failure due to soil yielding, 1 toppling failure was also observed. Therefore, 7 cases out of 40 scenarios investigated

experienced foundation failure. These failure cases are not shown in the graph presenting $(u_{fv})_{res}\ vs.\ (u_{fr})_{res}$.

Similar trends and conclusions to those described for the case of nonlinear SSI without uplift are valid in the case of nonlinear SSI with both material and geometric nonlinearity. More specifically, nonlinear SSI with uplift also always decreases structural acceleration and normalized structural distortion. The maximum reduction in the response is also 60% with the reduction at the 84^{th} percentile level being 40% and 60% for structural acceleration and structural distortion, respectively. It implicitly concludes that foundation uplift does not have a significant effect on the original structural response.

However, when total displacement is considered, the effect of foundation uplift is notable. This is due to the fact that the total displacement includes foundation motion as a rigid body that, in turn, is significantly affected by foundation uplift. Nonlinear SSI with uplift increases the total displacement for almost 75% of the cases, and the maximum amplification in the response can be up to 200%, even before showing foundation failure due to soil yielding. Note that the cases with the largest values of total displacement (6 in total) correspond to the cases where the foundation failure is due to soil yielding. Nonlinear SSI with uplift at 84^{th} percentile level increases the total displacement by about 180%.

13.4.6 Comparison of Soil-Structure Interaction Effects for Different Soil-Foundation Interface Conditions

An attempt is also made to better illustrate and compare SSI effects when different soil-foundation interface conditions are considered. In this regard, Figures 13-8 and 13-9 compare the previously defined response parameters for the cases of nonlinear SSI vs. linear SSI and nonlinear SSI vs. nonlinear SSI without uplift, respectively.

When nonlinear SSI effects on soil-structure system response are compared with the linear SSI effects (Figure 13-8), it is clear that residual foundation displacement/rocking, which might have a significant consequence in terms of design and recovery after earthquake event, is not taken into account in linear SSI. In addition, it can be concluded that linear SSI gives a larger structural acceleration and structural

distortion. This increase is in the range of 30% − 80% for structural acceleration and in the range of 30% − 150% for normalized structural distortion. Therefore, using a linear SSI analysis to define structural reactions and deformations when soil-foundation interface nonlinearity is probable to occur, can lead to misleading results and conclusions. On the other hand, if total displacement is considered, soil-foundation interface nonlinearity can result in either reduction or amplification in the response compared to the case when linear SSI is considered. For almost 50% of the cases considered, soil-foundation interface nonlinearity results in larger total displacement. The maximum amplification in the response, ignoring failed scenarios due to soil yielding, is about 120%, while the maximum reduction is about 40%. It clearly demonstrates that soil-foundation interface nonlinearity also plays an important role in terms of total displacement.

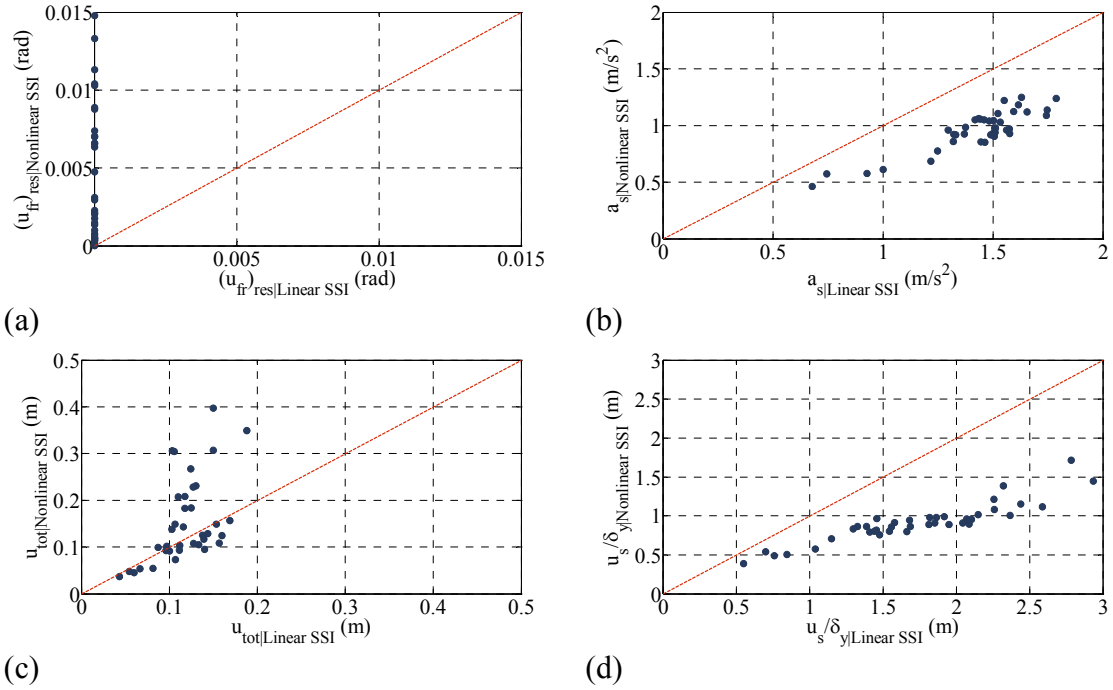

Figure 13-8.Comparison of dynamic structural response between models with nonlinear and linear soil-foundation interfaces: (a) vertical foundation displacement vs. foundation rocking; (b) structural acceleration; (c) total displacement; (d) normalized structural distortion by the yield displacement.

If the results from nonlinear SSI analyses are compared with those from nonlinear SSI without uplift, as shown in Figure 13-9, it is noticeable that foundation uplift has a significant effect on the foundation rocking and, consequently, total displacement. For

almost all the cases considered foundation uplift result in an equal or a larger residual foundation rocking and total displacement. However, at least for the example considered and the loading applied, the effects of foundation uplift on structural acceleration and structural distortion is not significant. Principally, considering both material and geometrical nonlinearity only slightly reduces structural acceleration and structural distortion as compared to the case when foundation uplift is ignored.

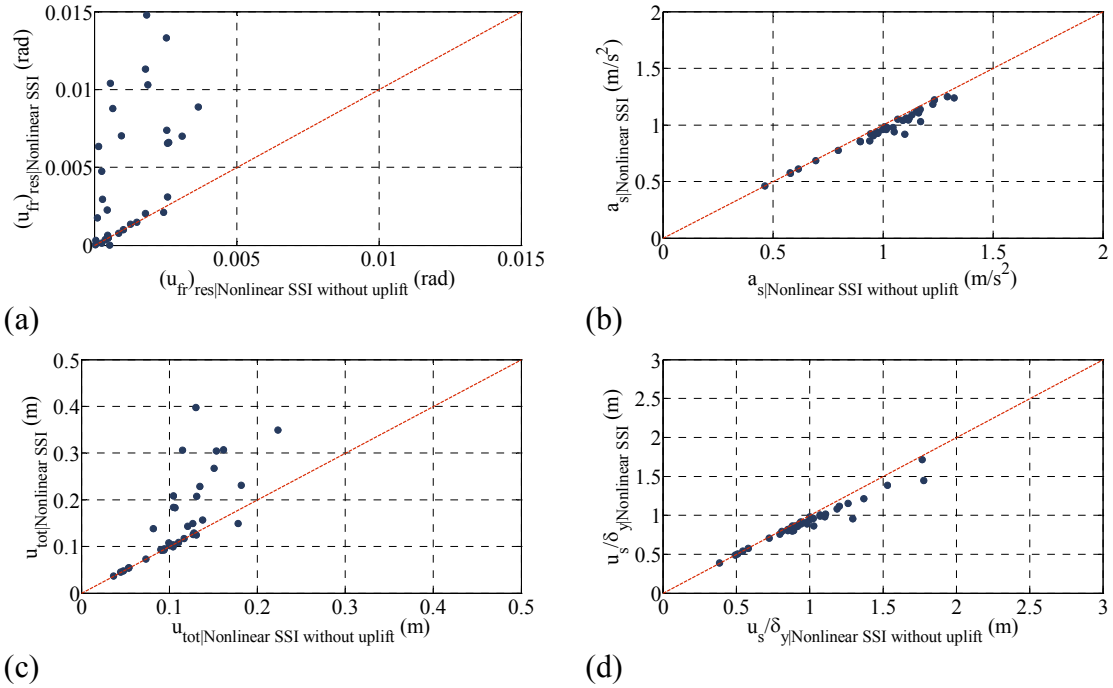

Figure 13-9.Comparison of dynamic structural response between models with nonlinear and nonlinear without uplift soil-foundation interfaces: (a) vertical foundation displacement vs. foundation rocking; (b) structural acceleration; (c) total displacement; (d) normalized structural distortion by the yield displacement.

13.4.7 The Role of Earthquake Design Level

As shown in the Christchurch earthquake sequence in 2010-2011, structures designed for the DBE level might be subjected to extreme events during their life time. Therefore, from a design point of view, it is important to assure that structures can resist the higher seismic demand without collapsing or, where possible, without being damaged beyond reparability level. In this regard, to investigate the role of earthquake design level on the response of soil-structure systems with nonlinear soil-foundation interface, the suite of ground motions selected were scaled up to the maximum credible earthquake (MCE) level, i.e. with a 2500-year return period,

and the dynamic simulations previously described were repeated with the records scaled to MCE. The results of these simulations are summarised in Figure 13-10.

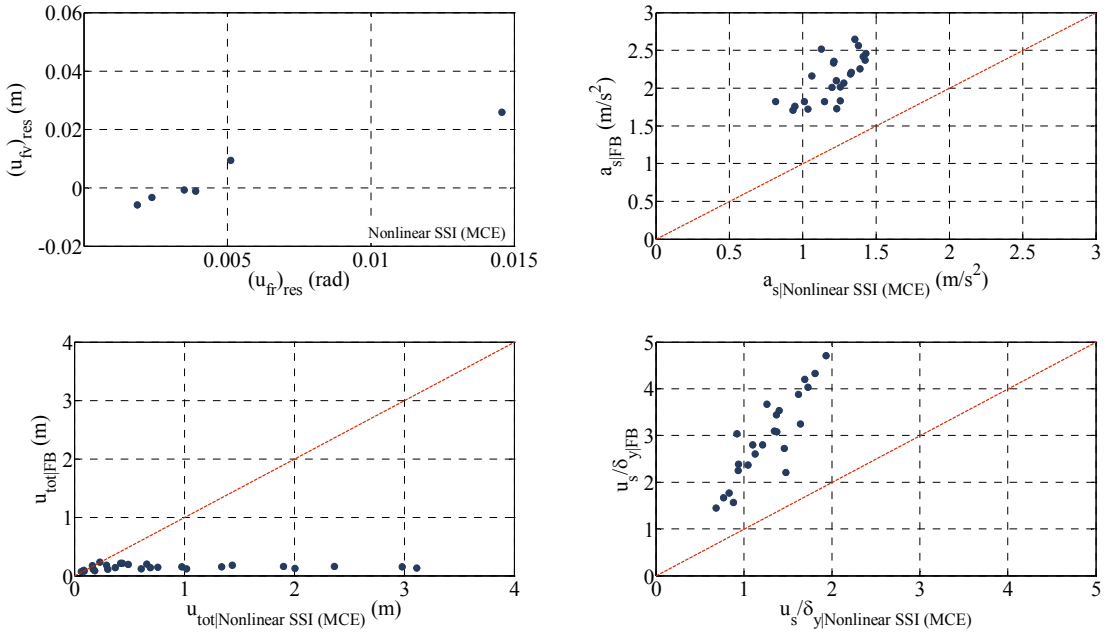

Figure 13-10. SSI effects on structural response for models with nonlinear soil-foundation interface considering MCE hazard level.

As expected, pushing foundation with larger forces will result in a larger number of failure cases. In this regard, 16 cases failed due to foundation toppling, 18 cases failed due to soil yielding, and only 6 cases avoided any foundation failure. Large foundation motion obviously results in a very large total and residual displacement that is further out of the acceptable range. However, large soil-foundation interface nonlinearity was in favour of structural response in terms of structural acceleration and structural distortion. Specifically, nonlinear SSI, in general, reduced structural acceleration by a factor of 2 and structural distortion by a factor of 2.5. It implicitly means that soil-foundation nonlinearity can act as an isolation mechanism preventing the damage to be transferred to the structure.

The statistics presented gives the crude impression that, using nonlinear SSI as an isolation mechanism in extreme events can result in system collapse due to foundation toppling with 40% probability, structural protection but with large foundation movement with 45% probability and full structural protection with 15% probability.

13.5 Summary

This chapter aimed to investigate the role of soil-foundation interface nonlinearity on the seismic SSI analysis. With this purpose, a comparative analysis was performed between soil-structure models with four different base fixity conditions, including: (i) fixed-base; (ii) linear flexible-base; (iii) nonlinear flexible-base without uplift; and (iv) nonlinear flexible-base with uplift. In this context, the structure was modelled as a yielding single-degree-of-freedom system with Takeda type force-deformation behaviour, and the soil-foundation interface was modelled either with a spring-mass-dashpot assembly (for linear case) or macro-element (for nonlinear cases). The generated models were then subjected to a suite of recorded ground motions representing large-magnitude, moderate-distance earthquake events. The results of the simulations adopted can be summarised as:

1) In contrast to what typically believed in practice, linear SSI can result in beneficial or detrimental effects on the structural response depending on the soil-structure-earthquake scenario considered.

2) The role of soil material nonlinearity on the SSI effects is significant. Specifically, this role is favourable in reducing the structural response compared to that of the fixed-base condition. However, this beneficial role might be compensated with large foundation displacement and rocking that might be totally unacceptable.

3) Foundation uplift increases the degree of nonlinearity on the foundation behaviour and, consequently, causes larger foundation displacement and rocking. In this context, foundation might fail due to excessive soil material nonlinearity or toppling, while it would not be captured if the uplift was not considered. However, at least for the example considered and the loading applied, the effects of foundation uplift on the structural response are negligible compared to the effects of soil material nonlinearity.

4) Soil-foundation interface nonlinearity in the extreme events can be used as a damage prevention mechanism if the toppling and large rigid body deformation can be appropriately treated.

5) Finally, it should be noted that this study only covered a simplified SDOF system. Thus, the differential movement of the individual foundations was not taken into account. These individual foundation movements, and possibly failures, might introduce large deformations/stresses in the structure above and, consequently, cause greater damage than that predicted in fixed-base analysis. Therefore, a further study is required to investigate these effects in more detail.

References

[1] A. S. Veletsos and J. W. Meek, "Dynamic behaviour of building-foundation systems," *Earthquake Engineering and Structural Dynamics,* vol. 3, pp. 121-138, 1974.

[2] M. Ciampoli and P. E. Pinto, "Effects of soil-structure interaction on inelastic seismic response of bridge piers," *Journal of Structural Engineering,* vol. 121, pp. 806-814, 1995.

[3] J. P. Stewart*, et al.*, "Seismic soil-structure interaction in buildings. I: analytical methods," *Journal of Geotechnical and Geoenvironmental Engineering,* vol. 125, pp. 26-37, Jan 1999.

[4] J. P. Stewart*, et al.*, "Revisions to soil-structure interaction procedures in NEHRP design provisions," *Earthquake Spectra,* vol. 19, pp. 677-696, 2003.

[5] ATC-40, "Seismic evaluation and retrofit of concrete buildings," ed: Applied Technology Concil, 1996.

[6] ASCE-7, "Minimum design loads for buildings and other structures," ed: Amarican Society of Civil Engineers, 1998.

[7] FEMA-356, "Prestandard and Commentary for the Seismic Rehabilitation of Buildings," ed. Washington, D.C.: Federal Emergency Management Agency, 2000.

[8] FEMA-450, "NEHRP recommended provisions for seismic regulations for new buildings and other structures," ed. Washington, D.C.: Building Seismic Safety Council, 2003.

[9] FEMA-440, "Improvement of nonlinear static seismic analysis procedures," ed. Redwood City, California: Applied Technology Council, 2005.

[10] E. E. R. Institute, "1999 Kocaeli, Turkey," *Earthquake Reconnaissance Report,* vol. Special Issue of Earthquake Spectra, 2001.

[11] M. Cubrinovski*, et al.*, "Geotechnical aspects of the 22 February 2011 Christchurch earthquake," *Bulletin of the New Zealand Society of Earthquake Engineering,* vol. 44, pp. 205-226, 2011.

[12] G. Gazetas and M. Apostolou, "Nonlinear soil-structure interaction: foundation uplifting and soil yielding," presented at the Proceedings Third UJNR Workshop on Soil-Structure Interaction, Menlo Park, California, USA, 2004.

[13] A. Gandomzadeh*, et al.*, "Influence of soil nonlinearities on dynamic soil-structure interaction," presented at the Fifth International Conference on Recent Advances in Geotechnical Earthquake Engineering and Soil Dynamics, San Diego, California, USA, 2010.

[14] E. Saez*, et al.*, "Effect of elastic and inelastic DSSI on seismic demands of SDOFS structures," presented at the Fifth International Conference on Recent Advances in Geotechnical Earthquake Engineering and Soil Dynamics, San Diego, California, USA, 2010.

[15] A. Pecker and C. T. Chatzigogos, "Non linear soil structure interaction: impact on the seismic response of structures," presented at the 14th European Conference on Earthquake Engineering, Ohrid, Republic of Macedonia, 2010.

[16] C. T. Chatzigogos, "Macroelement modeling of shallow foundations," vol. 29, ed, 2009, pp. 765-781.

[17] C. T. Chatzigogos*, et al.*, "A macroelement formulation for shallow foundations on cohesive and frictional soils," *International Journal for Numerical and Analytical Methods in Geomechanics,* 2010.

[18] I. Anastasopoulos*, et al.*, "Soil failure can be used for seismic protection of structures," *Bulletin of Earthquake Engineering,* vol. 7, 2009.

[19] R. Figini, "Nonlinear dynamic soil-structure interaction: application to seismic analysis and design of structures on shallow foundations," PhD Thesis, Politecnico di Milano, 2010.

[20] A. Carr, "Ruaumoko 3D, Nonlinear FEM Computer Program," ed. New Zealand: University of Canterbury, 2011.

[21] G. Gazetas, "Formulas and charts for impedances of surface and embedded foundations," *Journal of geotechnical engineering,* vol. 117, pp. 1363-1381, 1991.

[22] NZS1170.5, "Structural design actions, part 5: earthquake actions," ed. New Zealand, 2004.

CHAPTER

14. Soil-Structure Interaction Effects and Design Procedures

Abstract. This chapter reviews current design guidelines with regard to the incorporation of soil-structure interaction in design procedures. It is followed by a discussion on the inadequacies of current procedures based on the results in this research.

14.1 Soil-Structure Interaction in Design Codes

14.1.1 ATC 40: 1996

It has been stated in the ATC 40 Standard [1] that deformation and movement of the foundation can significantly affect the seismic response and performance of structures. It was then suggested to directly include foundation flexibility into the structural model and follow the same methodology introduced for structural analysis with fixed-base conditions. A general discussion was also presented to provide guidance regarding how to model the foundation. However, this guideline has typically been overlooked.

14.1.2 ASCE 7: 1998

Soil-structure interaction effects on design earthquake forces and the corresponding displacements of the structure have also been addressed in ASCE 7 [2]. Provisions were introduced for use with the equivalent lateral force procedure and for use with the modal analysis procedure. These two provisions cover the main design approaches.

14.1.2.1 Soil-structure interaction effects in ASCE 7: equivalent lateral force procedure

To account for the effects of soil-structure interaction in the equivalent lateral force procedure, the base shear calculated for fixed-base assumption is reduced:

$$\tilde{V} = V - \Delta V \tag{14.1}$$

This reduction ΔV is due to the change in the building period and damping factor and is defined:

$$\Delta V = [C_s - \tilde{C}_s(\frac{0.05}{\tilde{\xi}})^{0.4}]W_e \tag{14.2}$$

where:

C_s = the seismic design coefficient computed for the fundamental period of the structure when fixed at the base

$\tilde{C}_s$ = the seismic design coefficient computed for the effective period of the soil-structure system

$\tilde{\xi}$ = the effective damping ratio of the soil-structure system

W_e = the effective seismic weight of the structure which shall be taken as 0.7 times the total seismic weight

In this standard, the maximum reduction is limited to 0.3V.

To compute the expected reduction in base shear using Equation (14.2), the effective period $\tilde{T}$ and the effective damping ratio of the soil-structure interacting system $\tilde{\xi}$ has to be determined. ASCE 7 also presents simplified formulas for this purpose.

Effective period of the soil-structure system $\tilde{T}$: this value is determined:

$$\tilde{T} = T\sqrt{1 + \frac{k_s}{K_h} + \frac{k_s h_e^2}{K_r}}) \tag{14.3}$$

where:

T = the fundamental period of the structure when fixed at the base

k_s = the stiffness of the structure when fixed at the base, defined as $k_s = 4\pi^2(\frac{W_e}{gT^2})$

h_e = the effective height of the structure which shall be taken as 0.7 times the total height h_n

K_h = the horizontal stiffness of the foundation

K_r = the rocking stiffness of the foundation

The stiffness properties of the foundation, K_h and K_r have to be computed from established formulas and charts that are available in the literature, such as those presented by Gazetas [3]. In this computation, it is important to use soil properties that are compatible with soil strain levels associated with the design earthquake. This requirement is necessary because in most earthquake events the soil behaves nonlinearly. Thus shear modulus and shear wave velocity decrease with increasing shear strain. The effective (degraded) shear modulus G_{sec} and the large strain shear wave velocity $(V_s)_{sec}$ can be estimated on the basis of the anticipated maximum ground acceleration in accordance with Table 14-1.

Table 14-1. Effective shear modulus and shear wave velocity as determined by shaking intensity [2].

Value	**Anticipated Maximum Ground Acceleration (g)**			
	≤ 0.10	≤ 0.15	≤ 0.2	≥ 0.3
G_{sec}/G_{max}	0.81	0.64	0.49	0.42
$(V_s)_{sec}/(V_s)_0$	0.9	0.8	0.7	0.65

where, in Table 14-1:

$(V_s)_0$ = the average shear wave velocity for the soils beneath the foundation at small strain levels (10^{-3}% or less)

$G_{max} = \rho(V_s)^2_{sec}$ = the average shear modulus for the soils beneath the foundation at small strain levels

ρ = the average mass density of the soils

Effective damping ratio for the soil-structure interacting system $\tilde{\xi}$: this value is defined:

$$\tilde{\xi} = \xi_f + \frac{0.05}{(\tilde{T}/T)^3} \tag{14.4}$$

where:

ξ_f = the foundation damping factor as specified in Figure 14-1.

In Figure 14-1, two marginal lines, the solid and dashed lines, are used, which correspond to maximum ground accelerations $0.2g$ and $0.1g$, respectively. Any maximum ground acceleration between these two marginal lines is determined by averaging the results obtained from the solid and the dashed lines.

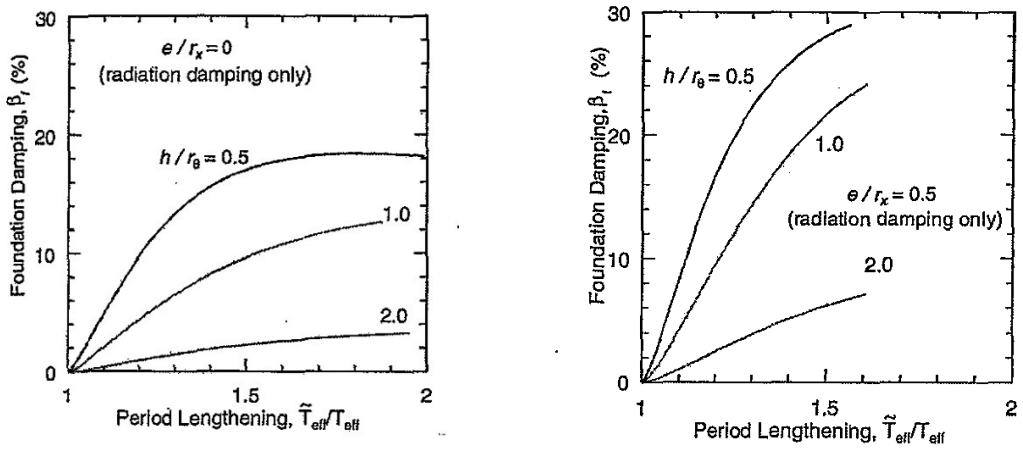

Figure 14-1. Foundation damping factor [2].

The quantity r in Figure 14-1 is the equivalent foundation radius, defined:

for $h_e/L \leq 0.5$:

$$r = r_h = \sqrt{\frac{A}{\pi}} \tag{14.5}$$

for $h_e/L \geq 1$:

$$r = r_r = \sqrt[4]{\frac{4I}{\pi}} \tag{14.6}$$

where:

L = the overall length of the side of the foundation in the direction being analysed

A = the area of the load-carrying foundation (the area of the foundation footprint if the foundation components are inter connected)

I = the static moment of inertia of the load-carrying foundation about a horizontal centroidal axis normal to the direction in which the structure is analysed

For intermediate values of h_e/L, the value of r has to be determined by linear interpolation.

Foundation damping ratio ξ_f has to be modified if the structures are supported on point bearing piles or if the soil beneath the foundation consists of a soft stratum of reasonably uniform properties under-laid by a much stiffer deposit. The modified damping factor ξ_{fm} is then defined:

$$\xi_{fm} = \left(\frac{4D_s}{(V_s)_{sec}\bar{T}}\right)^2 \xi_f \tag{14.7}$$

where D_s is the total depth of the stratum. Regardless of adjusting ξ_f or not, ASCE-7 does not allow any value less than 5% to be considered for $\bar{\xi}$.

Soil-structure interaction also modifies the deflection of the fixed-base structure δ_x. To account for this modification, ASCE-7 uses a simple formula defined:

$$\tilde{\delta}_x = \frac{\tilde{V}}{V}\left[\frac{M_0 h_x}{K_r} + \delta_x\right] \tag{14.8}$$

where:

$\tilde{\delta}_x$ = the modified deflection

M_0 = the overturning moment at the base determined using the unmodified seismic forces

h_x = the height above the base to the level under consideration

14.1.2.2 Soil-structure interaction effects in ASCE 7: modal analysis procedure

Based on what has been presented in ASCE 7, soil-structure interaction only affects the first mode of vibration. Thus, no modification has to be made in the forces or deflections contributed from the higher modes. The effect of soil-structure interaction on the base shear corresponding to the fundamental mode of vibration V_1 is represented by a reduction in the base shear defined:

$$\tilde{V}_1 = V_1 - \Delta V_1 \tag{14.9}$$

where ΔV_1 in this equation is computed according to Equation (14.2), with W_e taken as the seismic mass contributing to the fundamental mode W_{e1}, C_s is computed for the fundamental period of the structure when fixed at the base T_1, and $\tilde{C}_s$ is computed for the fundamental effective period of the soil-structure interacting system $\tilde{T}_1$. Once again, note that the maximum reduction in $\tilde{V}_1$ is limited to $0.3\tilde{V}_1$.

For this calculation, the period $\tilde{T}_1$ is determined from Equation (14.3) while T is replaced by T_1, k_s is calculated using W_{e1}, and h_e is defined:

$$h_e = \frac{\sum_{i=1}^{n} W_i \varphi_{i1} h_i}{\sum_{i=1}^{n} W_i \varphi_{i1}} \tag{14.10}$$

The modified deflection for the fundamental mode of vibration $\tilde{\delta}_{x1}$ is also defined:

$$\tilde{\delta}_{x1} = \frac{\tilde{V}_1}{V} \left[\frac{M_{01} h_x}{K_r} + \delta_{x1} \right] \tag{14.11}$$

where:

M_{01} = the overturning moment at the base for the fundamental mode of the fixed-base structure

δ_{x1} = the fundamental mode deflections at level x of the fixed-base structure

14.1.3 FEMA 356: 2000

FEMA 356 also acknowledged the effects of soil-structure interaction on the structural response. However, it did not introduce any special procedure to account for these effects, and users were asked to follow the simplified procedure covered in ASCE 7. However, FEMA 356 introduces an interesting modification to ASCE 7, the effective shear modulus and shear wave velocity are computed considering soil condition, as well as maximum ground acceleration. This change is shown in
Table 14-2. In Table 9-2, the following definitions are employed:

1) Site class A represents hard rock with average shear wave velocity $V_s > 1500$ m/s

2) Site class B represents rock with average shear wave velocity $750 < V_s < 1500$ m/s

3) Site class C represents very dense soil and soft rock with average shear wave velocity $360 < V_s < 750$ m/s or with either standard blow count $\bar{N} > 50$ or undrained shear strength $\bar{s}_u > 100$ kPa

4) Site class D represents stiff soil with average shear wave velocity $180 < V_s < 360$ m/s or with either $15 < \bar{N} < 50$ or $50 < \bar{s}_u < 100$ kPa

5) Site class E represents any profile with more than 3 m of soft clay defined as soil with plasticity index $PI > 20$ or water content $w > 40$ percent and $\bar{s}_u < 20$ kPa or a soil profile with $V_s < 180$ m/s

6) Site class F represents soils requiring specific geotechnical investigation

Table 14-2. Effective shear modulus ratio as determined by shaking intensity and site class [4].

Site Class	**Anticipated Maximum Ground Acceleration (g)**			
	$= 0$	$= 0.1$	$= 0.4$	$= 0.8$
A	1	1	1	1
B	1	1	0.95	0.9
C	1	0.95	0.75	0.6
D	1	0.9	0.5	0.1
E	1	0.6	0.05	*
F	*	*	*	*

*Site specific geotechnical investigation and dynamic site response analyses shall be performed.

14.1.4 FEMA 450: 2003

This standard uses the same procedure introduced in ASCE 7 [5].

14.1.5 FEMA 440: 2005

To improve the analysis procedures introduced in ASCE 7, a modified methodology has been introduced in FEMA 440 [6] to more realistically represent the dissipation of energy from the soil-structure interacting system. It considered both radiation and hysteretic soil damping. The difference between this method and ASCE 7 is that it includes procedures that can be incorporated into nonlinear static seismic analysis instead of being only applicable for linear analysis. Following this methodology, the

elastic and inelastic deformations in the structural and geotechnical parts of the overall system will be taken into account in the evaluation of foundation damping.

In this simplified procedure, foundation damping is linked to the ratio of the effective period of the soil-structure system to that of a fixed-base model. In addition, foundation size and foundation embedment are the other factors affecting foundation damping. The procedure for evaluating foundation damping is summarized:

1) Evaluate the fundamental period of the structure when fixed at the base T and the effective period of the soil-structure system $\tilde{T}$ using appropriate foundation modelling assumptions.

2) Calculate the effective stiffness of the structure when fixed at the base k_s:

$$k_s = 4\pi^2(\frac{W_e}{gT^2}) \tag{14.12}$$

where W_e is the effective seismic weight of the structure which can be taken as 0.7 times the total seismic weight.

3) Calculate the equivalent foundation radius for translation r_h:

$$r_h = \sqrt{\frac{A}{\pi}} \tag{14.13}$$

where A is the area of the load-carrying foundation.

4) Calculate the horizontal stiffness of the foundation K_h. This value can be estimated:

$$K_h = \frac{8}{2-\upsilon} G_{sec} r_h \tag{14.14}$$

where G_{sec} is the effective (strain-degraded) shear modulus and υ is the soil Poisson's ratio ($\sim$0.3 for sand and $\sim$0.4 for clay).

5) Calculate the rocking stiffness of the foundation K_r:

$$K_r = \frac{k_s h_e^2}{(\frac{\tilde{T}}{T})^2 - 1 - \frac{k_s}{K_h}} \tag{14.15}$$

where h_e is the effective height of the structure.

6) Calculate the equivalent foundation radius for rocking r_r:

$$r_r = (\frac{3(1-\upsilon)K_r}{8G_{sec}})^{\frac{1}{3}} \tag{14.16}$$

7) Determine the basement embedment e, if applicable.

8) Estimate the effective period-lengthening ratio $\tilde{T}_e/T_e$:

$$\frac{\tilde{T}_e}{T_e} = \{1 + \frac{1}{\tilde{\mu}}[\left(\frac{\tilde{T}}{T}\right)^2 - 1]\}^{0.5} \tag{14.17}$$

where $\tilde{\mu}$ is the expected ductility demand for the system including soil and structure effects. It is important to note that the ratio of $\tilde{T}_e/T_e$ is calculated for the structure in its degraded state accounting for structural ductility.

9) Determine the foundation damping ξ_f based on $\tilde{T}_e/T_e$, e/r_x and h_e/r_r using Figure 14-1.

The computed foundation damping is combined with conventional initial structural damping ξ_s to generate a revised damping ratio for the soil-structure system. The effective damping factor $\tilde{\xi}$ is calculated:

$$\tilde{\xi} = \xi_f + \frac{\xi_s}{(\tilde{T}_e/T_e)^3} \tag{14.18}$$

This system damping ratio modifies the foundation input motion imparted to the system model, as introduced in Section 14.1.2.1.

14.2 Inadequacies of Current Design Procedures

Modification in structural acceleration a_s and structural drift dr due to soil-structure interaction effects is compared between the outcomes of this research and the recommendations made by: (i) ASCE 7 for structures with linear behaviour; and (ii) FEMA 440 for structures with nonlinear behaviour. In this comparison, the response modification spectra presented for structures with linear behaviour in Chapter 7 is compared with the response modification spectra generated for all considered soil-structure models using the equations introduced in ASCE 7, i.e. Equations (14.2), (14.4) and (14.8). In addition, the response modification spectra presented for structures with nonlinear behaviour in Chapter 8 is compared with the response modification spectra generated based on the equations introduced in FEMA 440, i.e. Equations (14.2), (14.17), (14.8) and (14.8).

To develop response modification spectra based on design codes, the design spectra introduced in New Zealand Standard, NZS1170.5: 2004 [7] corresponding to three soil types E, D and C are considered. The choice of selecting three soil types is because: (i) the input ground motions used in the previous simulations to develop the response modification spectra were not scaled to any specific design spectrum of a certain soil type. Therefore, the results presented previously cover a wide range of soil types and, consequently, cannot be specifically assigned to a soil type or the other; and (ii) the similarities and differences between soil-structure interaction effects when different soil types are taken into account is also aimed to be investigated.

Figure 14-2 illustrates the design spectra for soil types considered, as well as the normalized ground motion spectra used in the previous simulations. It should also be noted that the design spectra presented does not include the hazard factor and the return period factor.

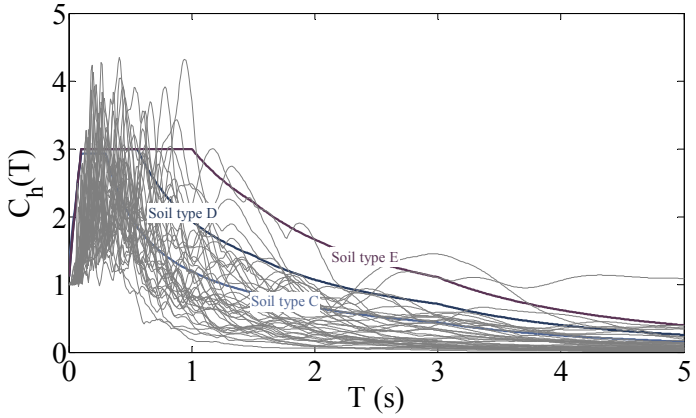

Figure 14-2. Design spectra for soil types E, D and C based on NZS1170.5: 2004, and the normalized ground motion spectra used in the previous Monte Carlo simulations.

The comparison between response modification spectra is presented in Figure 14-3 for structural acceleration and in Figure 14-4 for structural drift. If structural acceleration is considered, apart from the difference in degrees of variation in the results, design codes clearly result in much more reduction in the structural acceleration than that is obtained from time-history analyses. Note that the difference in reduction level is more significant when structures with nonlinear behaviour are taken into account. Furthermore, results from design codes never show the possibility of amplification in the structural acceleration. It is a matter that cannot be simply neglected. It thus can be concluded that the method introduced in design codes to include soil-structure interaction effects on structural acceleration is non-conservative and needs to be re-examined.

If structural drift is considered, similar conclusions can be made. Design codes are non-conservative about addressing soil-structure interaction effects on structural drift. In addition, this non-conservatism is more critical in case of structural drift noting the high values of probability and the possible level of amplification.

It is also insightful to note that, in general, soil-structure interaction effects for different soil types are not very different if the code approach is followed. This assumption might not be always true considering the real situations. However, more investigations are required to confirm the point.

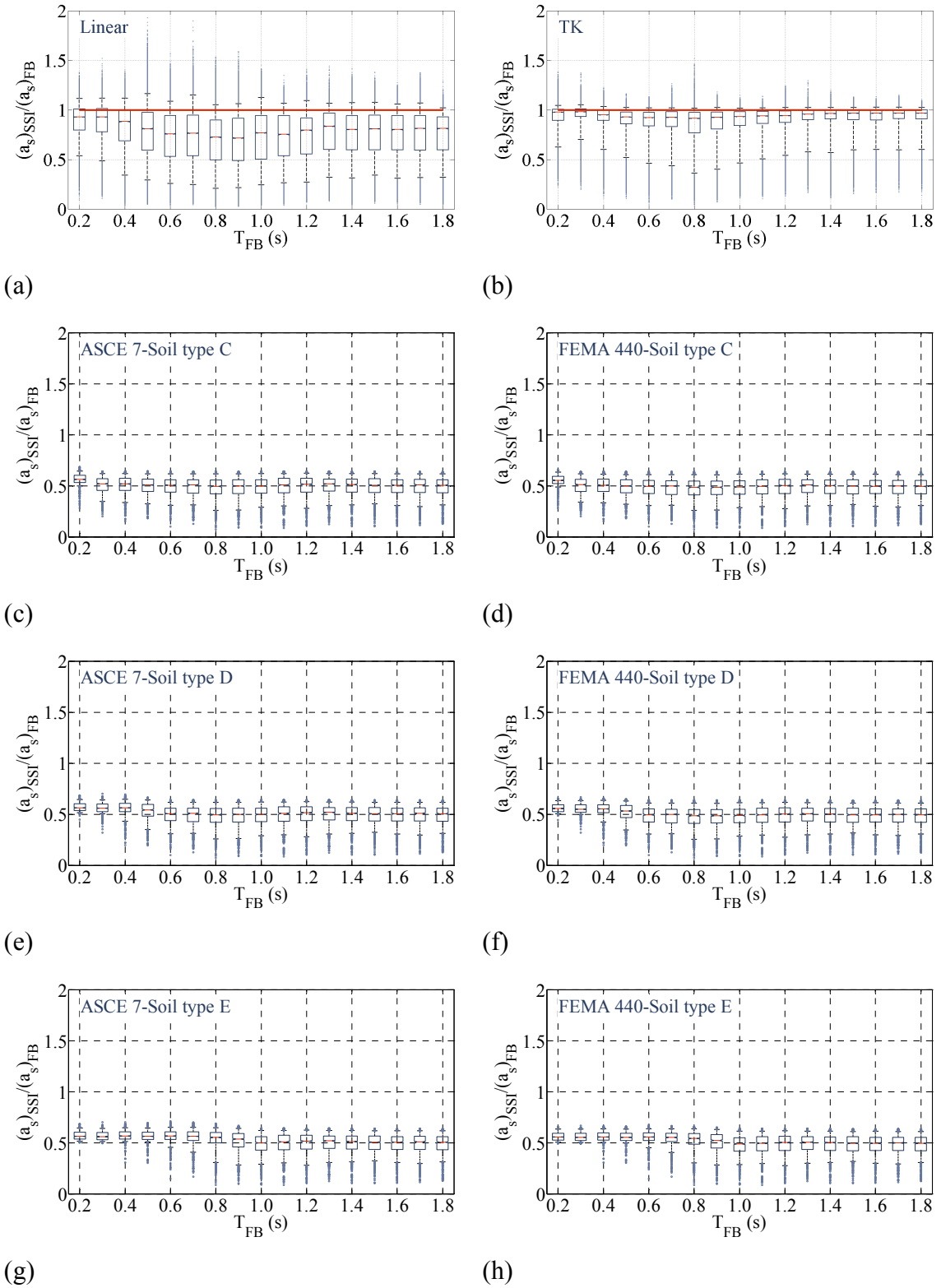

Figure 14-3. Modification spectra for structural acceleration: (a-b) based on outcomes of this research; (c, e and g) based on ASCE 7; and (d, f and h) based on FEMA 440.

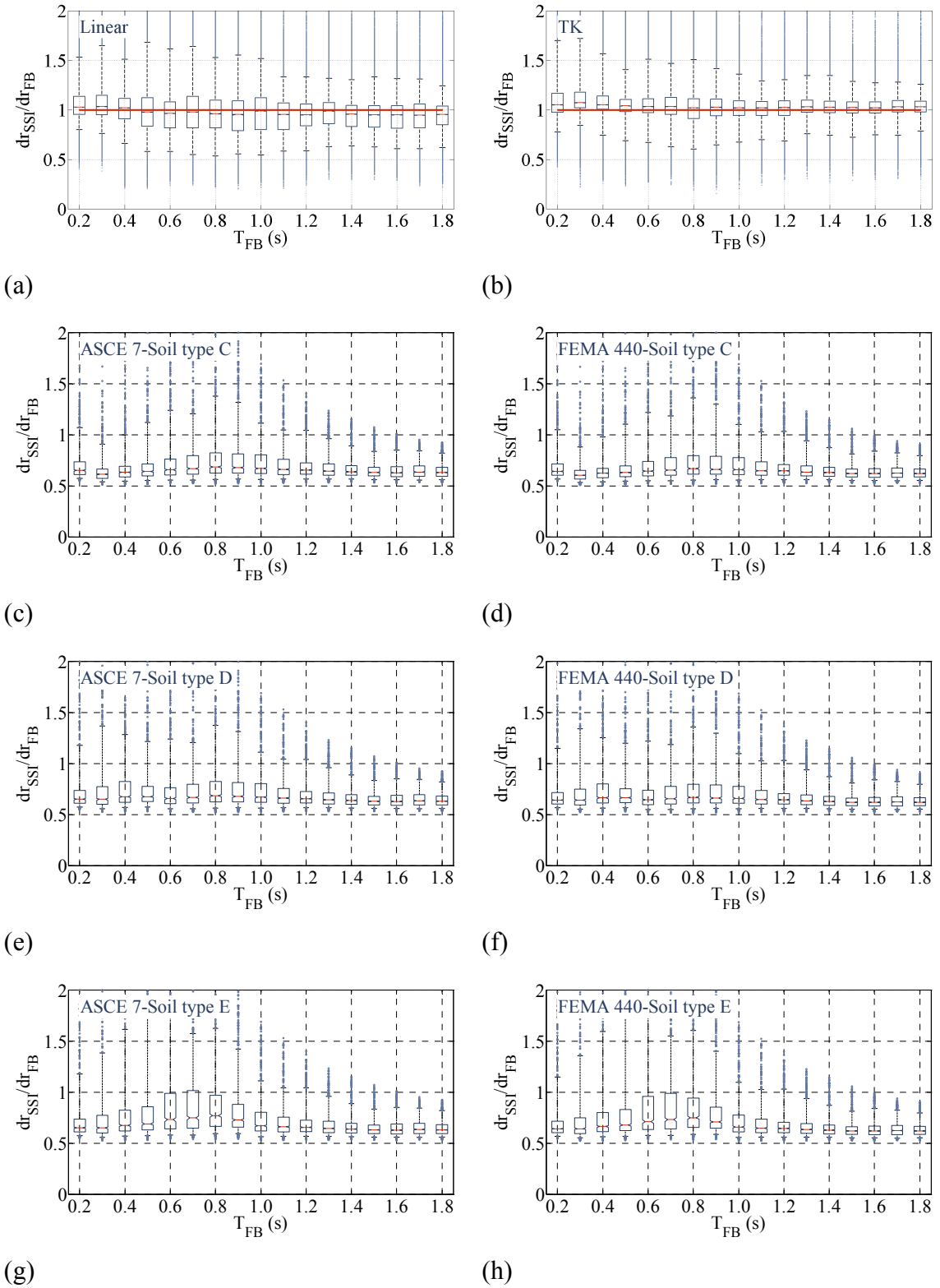

Figure 14-4. Modification spectra for structural drift: (a-b) based on outcomes of this research; (c, e and g) based on ASCE 7; and (d, f and h) based on FEMA 440.

The other inadequacy in code design provisions is that they do not discuss the effects of soil-structure interaction on the total displacement. Total displacement is the displacement measured at the roof level including lateral displacement resulted from foundation response and structural distortion that causes pounding between adjacent structures. As shown in Chapters 7 and 8, soil-structure interaction amplification effects on total displacement are significant and cannot be simply neglected.

Furthermore, except from FEMA 440, design codes do not distinguish between the soil-structure interaction effects on structural response when structures with linear or nonlinear behaviour are considered. As discussed in Chapter 8, this assumption is non-conservative and should be reconsidered. Specifically, structural nonlinearity increases the modification in the structural acceleration due to soil-structure interaction effects and depending on the situation, this increase can be significant.

The current design codes also do not have any solutions for the cases when earthquake events with enhanced spectral ordinates at longer periods occur. These events are more likely to have amplification in the structural response due to period elongation instead of having a reduction. Therefore, the procedure introduced in the current codes might result in incorrect structural forces and deformations.

Finally, the effects of soil-foundation interface nonlinearity are not considered in the current design code provisions. As shown in Chapter 13, foundation nonlinearity reduces the force and deformation demand on the structure, while might increase the total displacement. In addition, foundation nonlinearity causes residual settlement and tilting of the foundation that, in turn, can have a significant effect on the global structural behaviour.

14.3 Implementation of the Computed Probabilistic Results into a Design Framework

The probabilistic results explained in the preceding chapters can also be used in establishing a design framework for soil-structure systems which can be simply used by practicing engineers. In this framework, two design aspects including the expected foundation movement and the potential modification in response of soil-structure system have to be considered and appropriately dealt with.

To take account of foundation movement, the concept of foundation design spectra briefly introduced in Chapters 7 and 8 can be used. Foundation design spectra, principally, define the maximum foundation movement expected along a range of fundamental structural periods. As clearly shown in Figures 7-3 and 8-2, foundation movement in horizontal and rocking directions, u_{fh} and u_{fr}, follow the same logic applies to the displacement response of the fixed-base structures to the enforced ground motions. In other words, foundation movement will increase up to a certain level as the structural period increases and keep constant (or slightly reduced) afterwards. The outcomes from those figures are summarised in a schematic illustration shown in Figure 14-5.

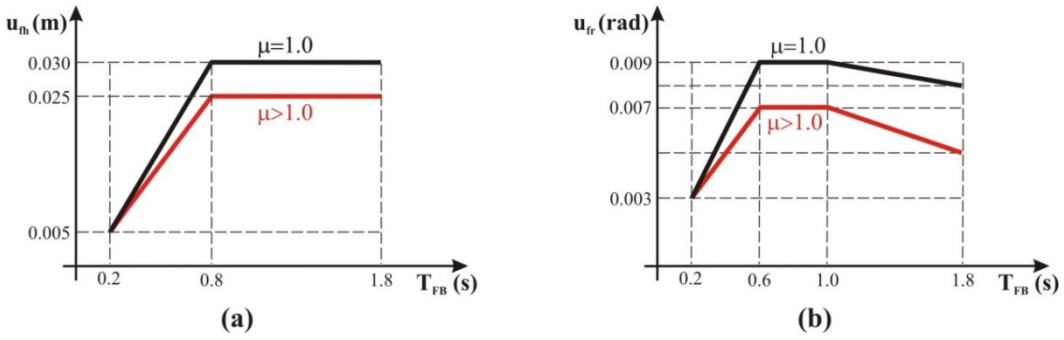

Figure 14-5. Schematic illustration of foundation spectra: (a) horizontal displacement spectrum; (b) rocking spectrum.

Knowing the fundamental period of the fixed based structure, T_{FB}, a design engineer can then use these spectra to estimate the extent of maximum foundation movement to be

expected. These defined values then can be used in design of the foundation or overlaying structure.

The potential modification in structural response due to soil-structure interaction effects can be incorporated into a design framework noting that soil-structure interaction may result in either amplification or reduction in the structural response. This point has been discussed with details in Chapters 7 and 8, and clearly illustrated in Figures 7-5 and 8-7. Taking into consideration the increasing and decreasing soil-structure interaction effects on structural response, two different approaches then have to be adopted while each addresses one aspect of the phenomenon.

If a design engineer is concerned about the potential amplification in the structural response due to soil-structure interaction effects, risk spectra along with the response amplification spectra can be used. On the other hand, if a design engineer is investigating the potential advantages of the decreasing effect of soil-structure interaction, response reduction spectra can be utilized.

Let us assume that the amplification effects of soil-structure interaction are needed to be investigated. In this regard, the concept of risk spectra introduced in Chapters 7 and 8, and shown in Figures 7-8 and 8-11 has to be first used. Figure 4-6 schematically summarises the outcomes from these figures. If for the known fundamental period of the structure, the likelihood of the amplification in the response is higher than an acceptable level, then the designer need to be concerned about the increasing (detrimental) effects of soil-structure interaction. Having unacceptable amplification likelihood, the response amplification spectra have to be used consequently. The values of the response amplification spectra correspond to the maximum amplification expected in the structural response at a predefined percentile. If, for example, 95^{th} percentile values were taken into consideration (allowing for 5% likelihood of discrepancy), the response amplification spectra would be shown in Figure 8-8. The outcomes from this figure are summarised in a schematic illustration shown in Figure 14-6.

Knowing the fundamental period of the structure, the design engineer can then use these response amplification spectra to estimate the extent of amplification expected in

structural response. If this amplification is within an acceptable range, the detrimental (increasing) effects of soil-structure interaction can be safely ignored. However, if the amplification level is not negligible, the response of the fixed-base structure has to be modified accordingly by using the amplification factor resulted from the response amplification spectra to emulate soil-structure interaction effects.

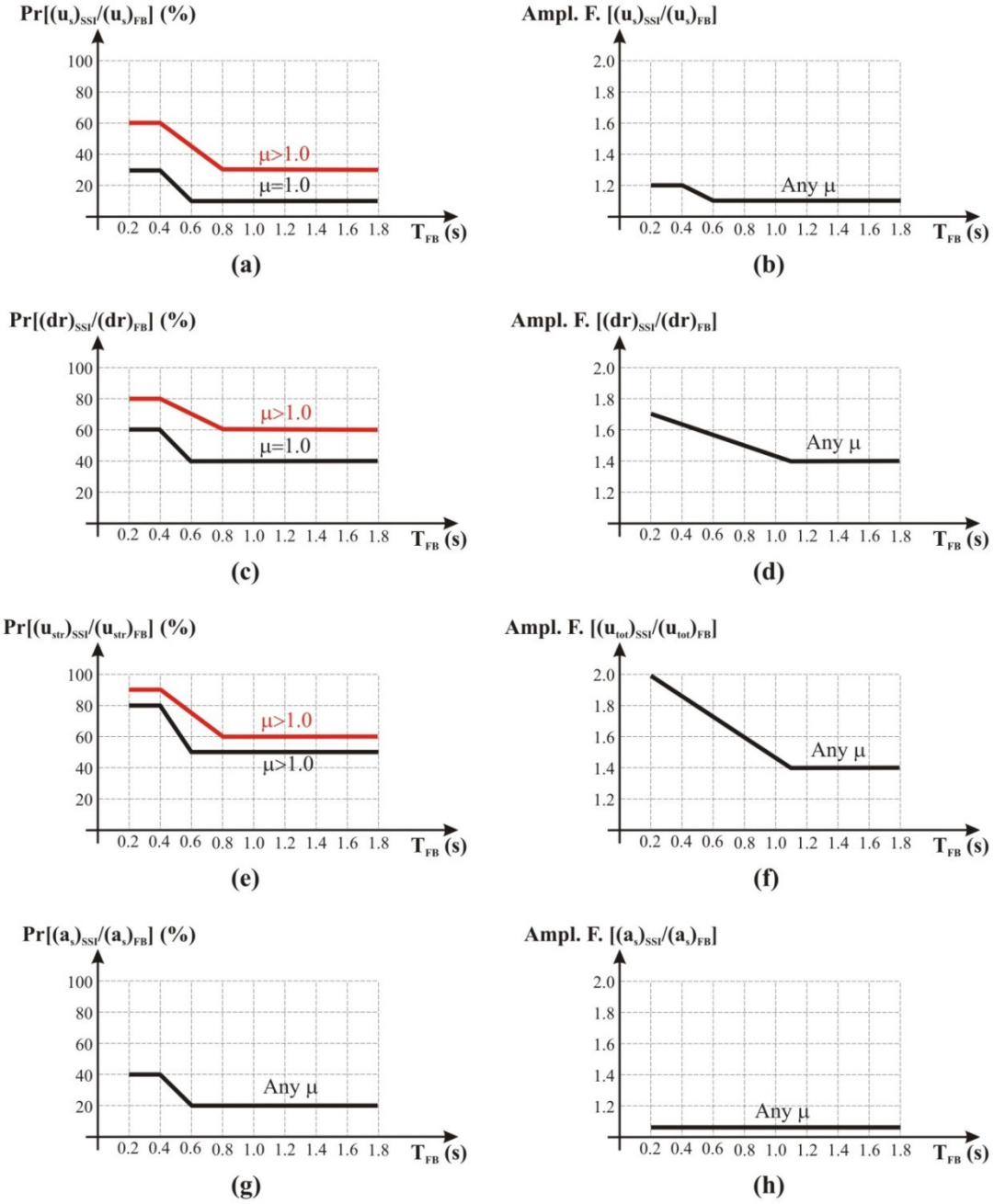

Figure 14-6. Schematic illustration of: (left) risk spectra; (right) response amplification spectra for: (a,b) structural distortion; (c,d) structural drift; (e,f) total displacement; and (g,h) structural acceleration.

On the other hand, if the design engineer is interested to investigate the advantage of reducing soil-structure interaction effects, the response reduction spectra has to be used to justify the application of the further complex analysis incorporating soil-structure interaction effects. Response reduction spectra represent the likelihood of a reduction greater than a specific level that might occur in structural response due to soil-structure interaction effects. If 5th percentile values (representing 5% likelihood of occurrence) are considered, the response reduction spectra are shown in Figure 8-8. The schematic representation of the results presented in Figure 8-8 is shown in Figure 14-7.

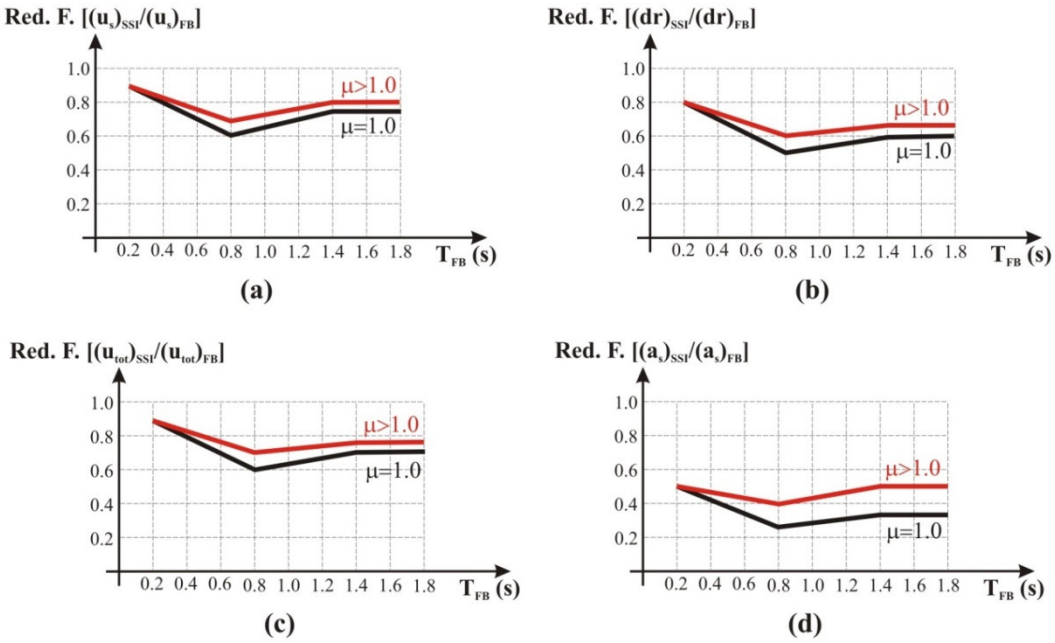

Figure 14-7. Schematic illustration of response reduction spectra for: (a) structural distortion; (b) structural drift; (c) total displacement; and (d) structural acceleration.

Knowing the fundamental structural period, the designer can then use the response reduction spectra to find out how much reduction might be occur due to soil-structure interaction effects and if it is worth to run any further complex analysis to identify the potential soil-structure interaction effects. However, if a further analysis is decided to be run, it is important to model the foundation flexibility in a most appropriate way to minimize any misinterpretation of results.

14.4 Summary

Inclusion of soil-structure interaction effects in design procedures introduced in the current codes has been reviewed in this chapter. In addition, considering the results have been presented in the previous chapters, a discussion on the inadequacies of current practice was presented. Finally, the conceptual design framework for soil-structure systems developed based on the probabilistic results presented was explained and discussed.

References

[1] ATC-40, "Seismic evaluation and retrofit of concrete buildings," ed: Applied Technology Concil, 1996.

[2] ASCE-7, "Minimum design loads for buildings and other structures," ed: Amarican Society of Civil Engineers, 1998.

[3] G. Gazetas, "Formulas and charts for impedances of surface and embedded foundations," *Journal of geotechnical engineering,* vol. 117, pp. 1363-1381, 1991.

[4] FEMA-356, "Prestandard and Commentary for the Seismic Rehabilitation of Buildings," ed. Washington, D.C.: Federal Emergency Management Agency, 2000.

[5] FEMA-450, "NEHRP recommended provisions for seismic regulations for new buildings and other structures," ed. Washington, D.C.: Building Seismic Safety Council, 2003.

[6] FEMA-440, "Improvement of nonlinear static seismic analysis procedures," ed. Redwood City, California: Applied Technology Council, 2005.

[7] NZS1170.5, "Structural design actions, part 5: earthquake actions," ed. New Zealand, 2004.

CHAPTER 15. Conclusions

The effects of soil-shallow foundation-structure on the seismic response of structures have been investigated using a robust and systematic probabilistic approach. A large number of analyses were carried out using a wide range of models and input ground motions to cover the uncertainty in model parameters and variability in the spectral characteristics of input ground motions. In the analyses, the structure was represented by an either elastic (Chapter 7) or nonlinear (Chapters 8 and 9) viscously damped single-degree-of-freedom system. In addition, the soil-foundation interface was presented by an either equivalent linear cone model (Chapters 7, 8 and 9) or nonlinear macro-element (Chapter 13). Based on the statistical analyses of the results, the following conclusions can be made:

The Effects of Soil-Structure Interaction on Seismic Structural Response:

1) The existing uncertainty in input ground motion and variability in model parameters cause significant variation in foundation response. Considering the observed median values and associated dispersion of results shows that foundations will experience larger horizontal displacement and rocking when structures with longer periods are considered. In this context, foundation response spectra can be established.

2) The contribution of foundation rocking to the total structural displacement is more significant compared to the contribution of horizontal foundation displacement. Furthermore, it has been shown that horizontal foundation displacement is more important for the case of stiffer structures ($T_{FB} < 0.6$ s),

while foundation rocking plays a more significant role for structures with periods in the range of $0.6 - 1.2$ s.

3) When structural nonlinearity is considered, foundation responses decrease and this reduction is more pronounced for foundation rocking.

4) Consideration of soil-structure interaction in dynamic analysis with linear structural behaviour may increase the structural distortion up to 20%, even though a reduction is expected for the 50^{th} percentile case. Taking into account the probability of having amplification in the structural distortion ($10\% - 30\%$) along with the median percentage increase in values ($5\% - 10\%$) implies the risk of amplification in the structural distortion is relatively low. Since the structure behaves linearly, similar trends and conclusions can be also made if structural acceleration is considered.

5) The likelihood of having amplification in structural drift rises to $40\% - 60\%$, while the likely maximum amplification might be up to 70%. The corresponding values are more significant for total displacement. Specifically, the probability of having amplification is $45\% - 80\%$, and the maximum amplification compared to a fixed-base assumption is 100%. Considering the substantial probability of amplification and expected maximum response in terms of structural drift and total displacement, it is suggested that the soil-structure interaction effects must be considered in second-order ($P - \Delta$) and pounding studies.

6) Based on median structural response and probability of amplification in the response, soil-structure interaction with detrimental effects is more pronounced for structures with nonlinear behaviour. This outcome implies that the evaluation of soil-structure interaction effects based on systems with linear behaviour is not conservative and needs to be reconsidered in design codes.

7) In general, the probability of having amplification in response is higher for stiffer structures ($T_{FB} < 0.6\,sec$), indicating that stiff structures are more likely to exhibit detrimental soil-structure interaction effects. However, the median amplification level is effectively similar for all period ranges,

illustrating differences in dispersion of results across different periods that should be considered.

8) The specific nonlinear force-displacement behaviour of the structures does not have a significant effect on any structural response modification factors due to soil-structure interaction effects.

9) There is a clear link between the increase in the structural strength demand due to soil-structure interaction effects and the response spectrum characteristics of the ground motion. Detrimental soil-structure interaction effects or amplification in the structural strength demand occur for ground motions having an ascending branch in the response spectrum in the range of periods slightly greater than fundamental structural period.

10) If input ground motions with enhanced spectral ordinates at large periods are considered, the probability of having amplification in structural response due to soil-structure interaction effects will increase. However, in terms of the median percentage increase, no significant change is expected. Note that this latter point implies a significant shift in the level of excedance and its contribution.

Soil, Structural and System Parameters and the Degree of Soil-Structure Interaction Effects on Structural Response:

1) From all considered soil, structural, and soil-structure system parameters only initial soil shear wave velocity $(V_s)_0$, shear wave velocity degradation ratio $(V_s)_{sec}/(V_s)_0$, $\sigma = (V_s)_{sec}T_{FB}/h_e$ and $\varphi = \frac{h_e}{(V_s)_{sec}T_{FB}}(h_e/r)^{0.25}$ have a pronounced correlation with structural response modification factors due to soil-structure interaction effects.

2) An increase in $(V_s)_0$, $(V_s)_{sec}/(V_s)_0$ and σ cause a less variation in the resulted structural response modification factors. In addition, as these parameters increase, the response modification factors approach 1.0, indicating the

behaviour of the soil-structure systems are more similar to the behaviour of the corresponding fixed-base system.

3) Considering the median values (50^{th} percentiles), an increase in $(V_s)_0$, $(V_s)_{sec}/(V_s)_0$ and σ results in an increase in the structural distortion modification factors, while dr, u_{tot} and a_s are only weakly sensitive to the parameters considered.

4) The likely maximum modifications in structural distortion and structural acceleration are independent from the variation of $(V_s)_0$, $(V_s)_{sec}/(V_s)_0$ and σ. However, if structural drift or total displacement is considered, a sharp reduction in the maximum modification factors is observed due to an increase in $(V_s)_0$, $(V_s)_{sec}/(V_s)_0$ and σ.

5) When φ increases, the median structural distortion modification factors and the median structural acceleration modification factors reduce very sharply. Maximum values likely follow similar trends. In contrast, the variation in structural drift modification factors and total displacement modification factors gets more significant as φ increases. This variation is more likely to result in amplification in structural drift and total displacement, than in a reduction.

6) In terms of quantification of risk, the probability of amplification in the response is very small for structural distortion and is almost negligible for structural acceleration. In contrast, the probability of amplification in structural drift and total displacement is a risk that cannot be neglected.

7) An increase in $(V_s)_0$, $(V_s)_{sec}/(V_s)_0$ and σ results in a reduction in the probability of amplification in the structural response modification factors, as well as a reduction in the values of median percentage increase. Specifically, when $\sigma > 20$, detrimental soil-structure interaction effects on the structural response can be practically ignored.

8) An increase in φ reduces the probability of amplification in structural distortion such that the amplification can be practically ignored when $\varphi > 1.0$. However, the probabilities of amplification and the corresponding values of

median percentage increase for structural drift and total displacement rise when φ increases.

Impact of Soil-Foundation Interface Nonlinearity on Soil-Structure Interaction Analysis:

1) The role of soil material nonlinearity on the soil-structure interaction effects is significant. Specifically, this role is favourable in reducing the structural response compared to that of the fixed-base condition. However, this beneficial role might be accompanied with large foundation displacement and rocking that can be very unacceptable.

2) Foundation uplift increases the degree of nonlinearity on the foundation behaviour and, consequently, causes larger foundation displacement and rocking. In this context, foundations may fail due to excessive soil material nonlinearity or toppling, while it would not be captured if the uplift was not considered. However, the effects of foundation uplift on the structural response are negligible compared to the effects of soil material nonlinearity.

3) Soil-foundation interface nonlinearity in extreme events can be used as a damage prevention mechanism if toppling and large rigid body deformation can be appropriately treated.

In summary, soil-structure interaction effects are quantified, and it has been shown that soil-structure interaction can be *both beneficial and detrimental*. The exact risk is also quantified across linear and nonlinear cases. The analyses and results present and create *a rigorous framework an approach* for considering these types of problems. This approach can be replicated, and the outcomes of which can be used to add probabilistic risk directly into design. Hence, given the impact of soil-structure interaction, *these results are critical to better design* and should significantly inform design codes and practice in structural engineering in seismic zones.

CHAPTER 16. Recommended Future Studies

The framework presented and comprehensive analyses carried out in this study only covered single-degree-of-freedom systems. Thus, it is suggested to replicate the methodology introduced for general multi-degree-of-freedom systems to investigate the effects of soil-structure interaction on structural response when higher modes of vibration are included. Specifically, the response modification for each degree of freedom should be identified as well as the modification on the global structural behaviour. It may also be insightful to investigate the degree of soil-structure interaction effects on each of the different modes of vibration.

Performing a more general probabilistic analysis for soil-structure interaction scenarios with nonlinear soil-foundation interface, varying the soil and structural parameters, and covering a wide range of realistic systems is also useful. In more detail, the probabilistic methodology introduced in Chapter 6 should be modified and replicated for soil-structure models presented in Chapter 13. In this context, the effects of soil-foundation interface nonlinearity can be quantified through a wide range of periods.

It should also be noted that, in this study, the differential movement of the individual foundations of a structural model was not taken into account. These individual foundation movements, and possibly failures, might introduce large deformations/stresses in the structure above and, consequently, cause greater damage than that predicted in fixed-base analysis. Therefore, a further study is required to investigate these effects in more detail.

Finally, it is important to use the insights gained from and the results provided by this study to develop a new design procedure taking into account the effects of soil-structure interaction on structural response in a more robust fashion.

APPENDICES

APPENDIX

A. Results for Seismic Soil-Structure Interaction Effects on Structures with Linear Behaviour

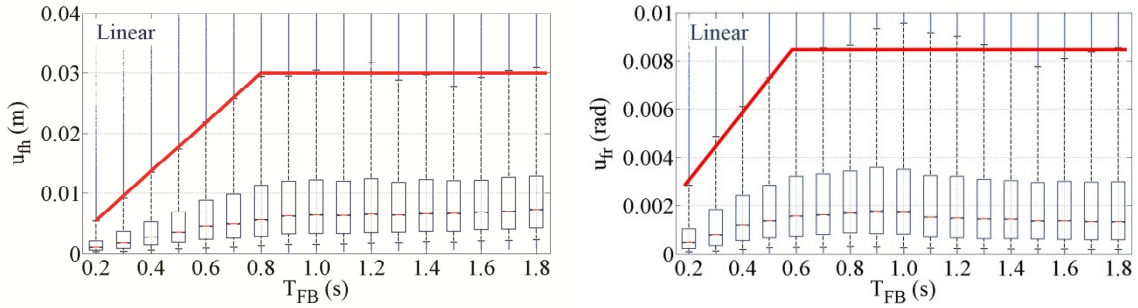

Figure A-1. Foundation response spectra in horizontal and rocking directions.

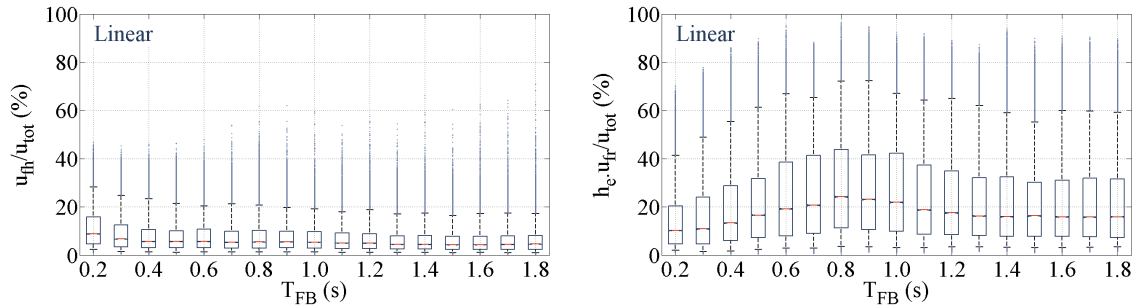

Figure A-2. Contribution of horizontal foundation motion and foundation rocking on total displacement.

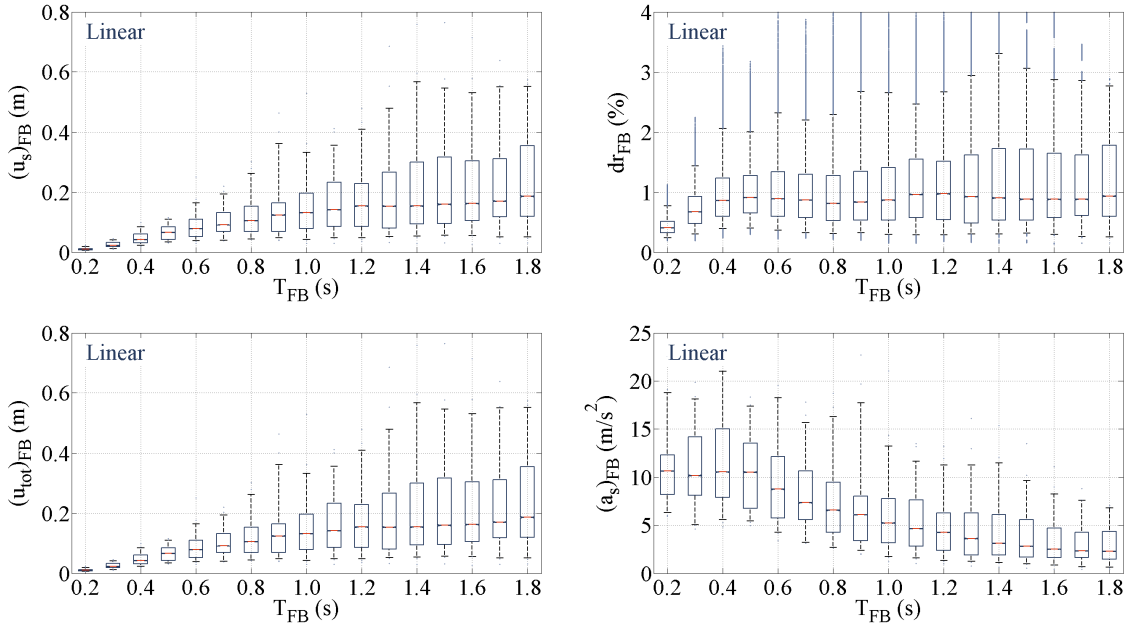

Figure A-3. Response spectra for fixed-base structures with linear behaviour.

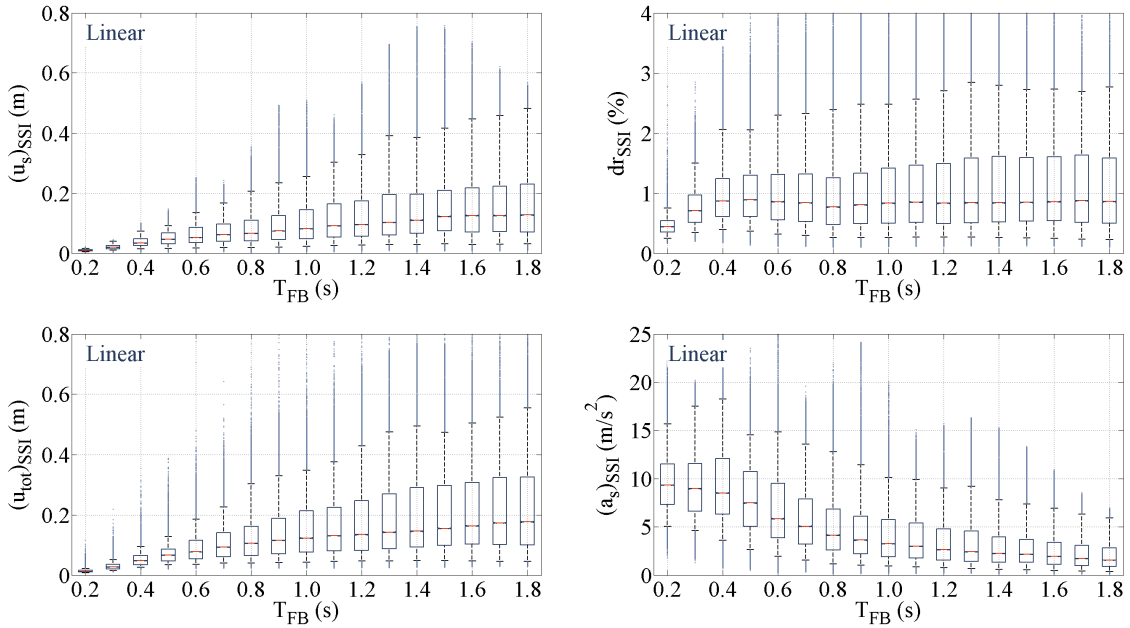

Figure A-4. Response spectra for flexible-base structures with linear behaviour.

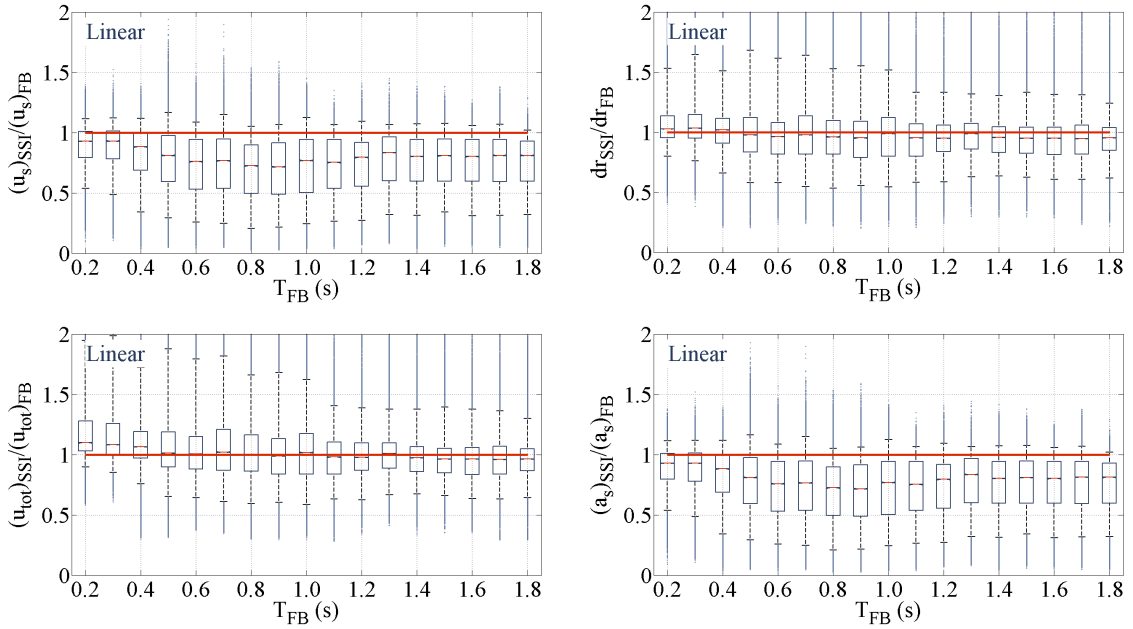

Figure A-5. Response modification spectra for structures with linear behaviour.

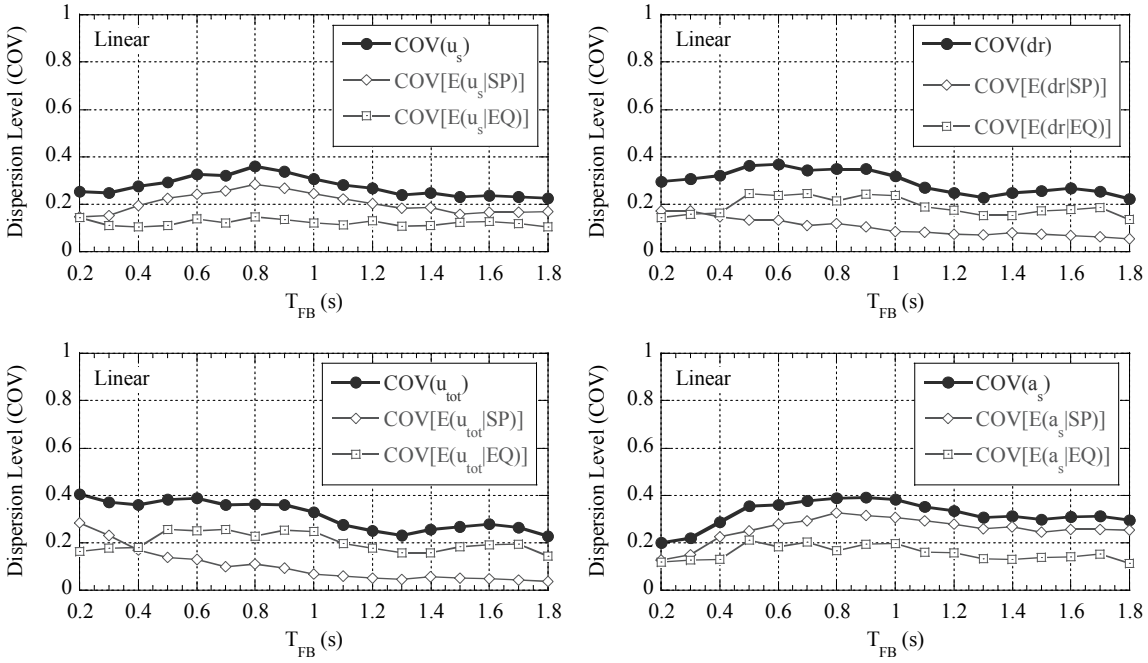

Figure A-6. Dispersion spectra for structures with linear behaviour.

APPENDIX

B. Results for Seismic Soil-Structure Interaction Effects on Structures with Nonlinear Behaviour

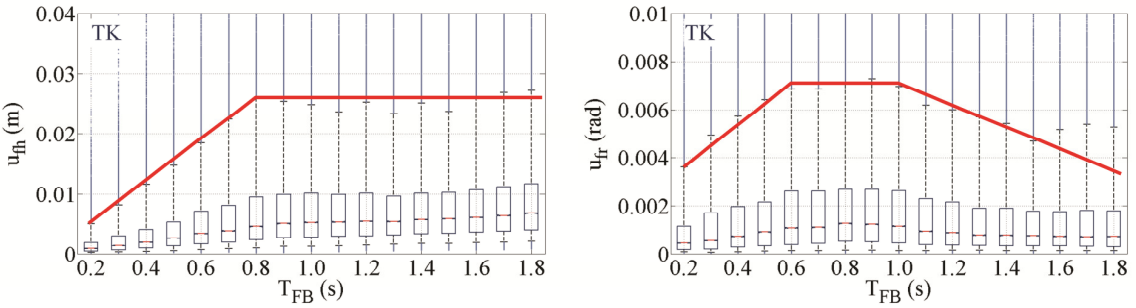

Figure B-1. Foundation response spectra in horizontal and rocking directions.

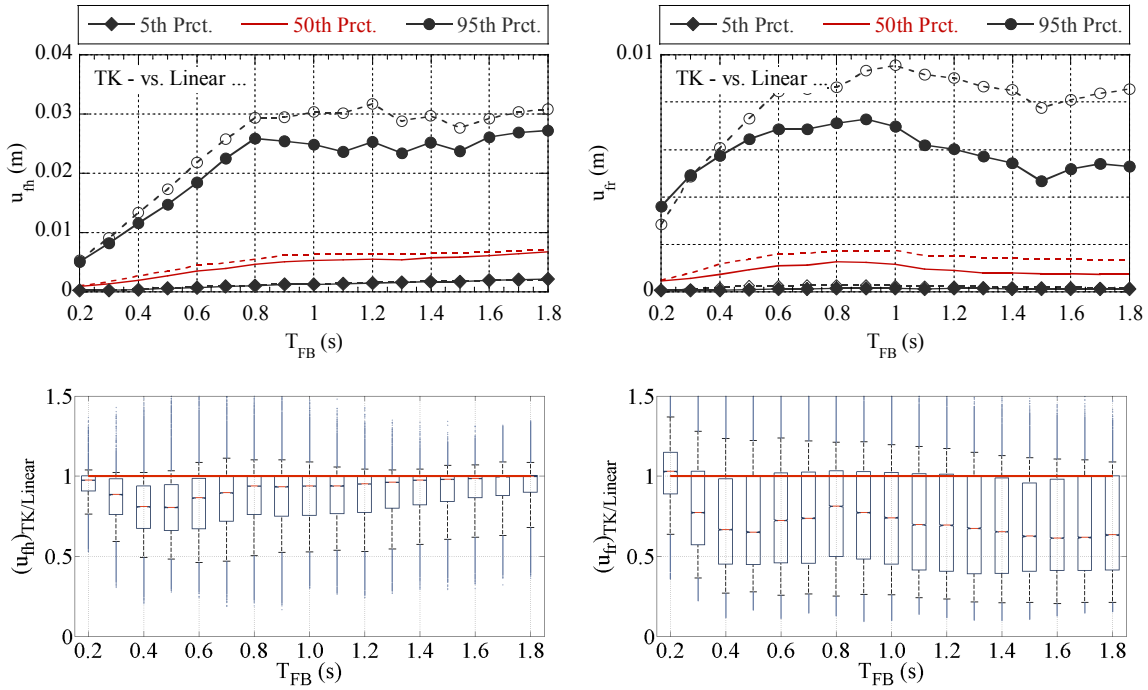

Figure B-2. The effects of structural nonlinearity on horizontal foundation motion and foundation rocking.

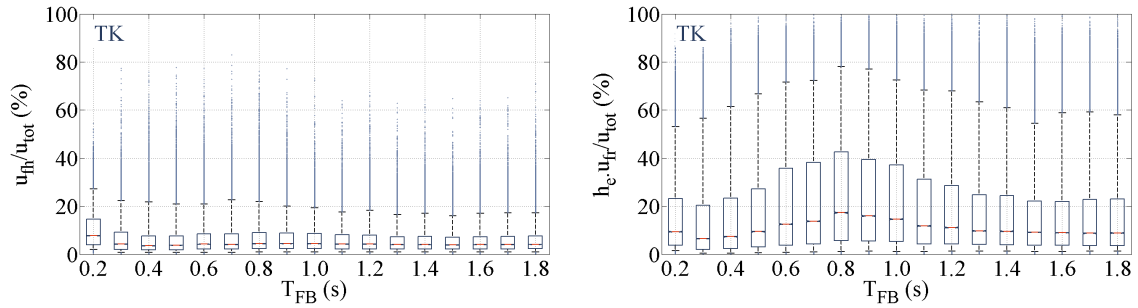

Figure B-3. Contribution of horizontal foundation motion and foundation rocking on total displacement.

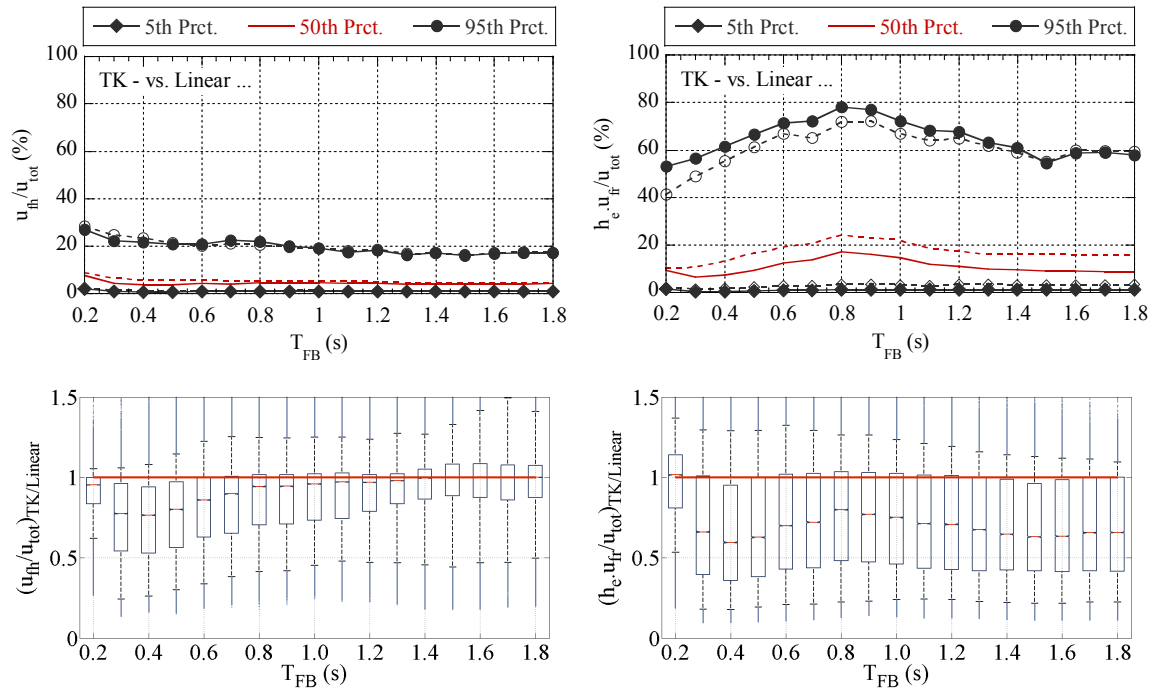

Figure B-4. The effects of structural nonlinearity on the contribution of horizontal foundation motion and foundation rocking on total displacement.

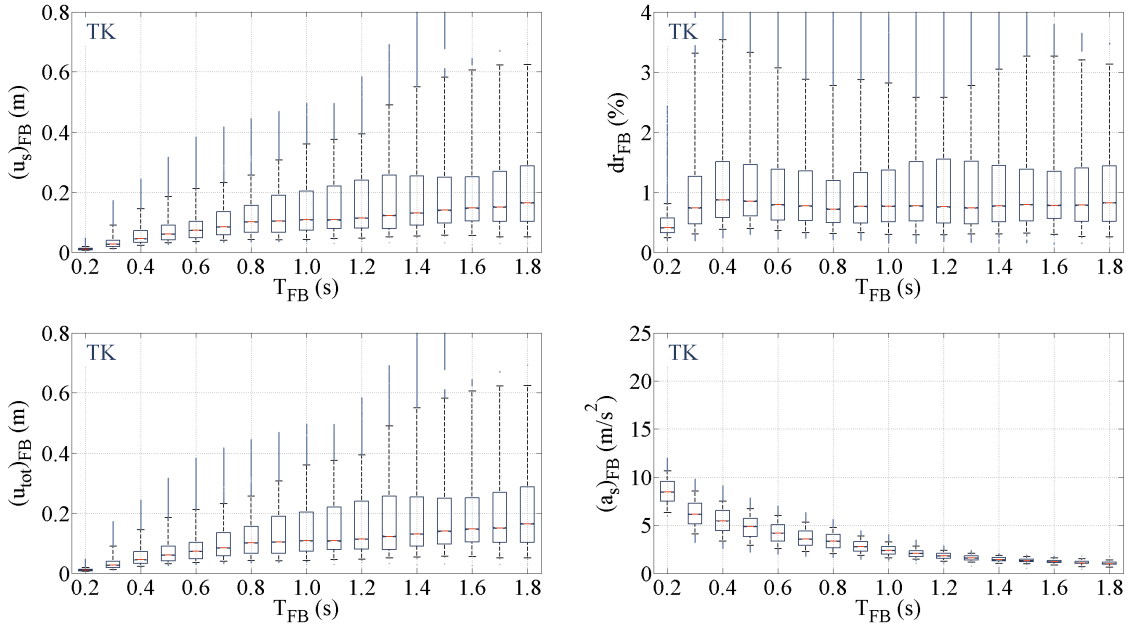

Figure B-5. Response spectra for fixed-base structures with TK hysteretic behaviour.

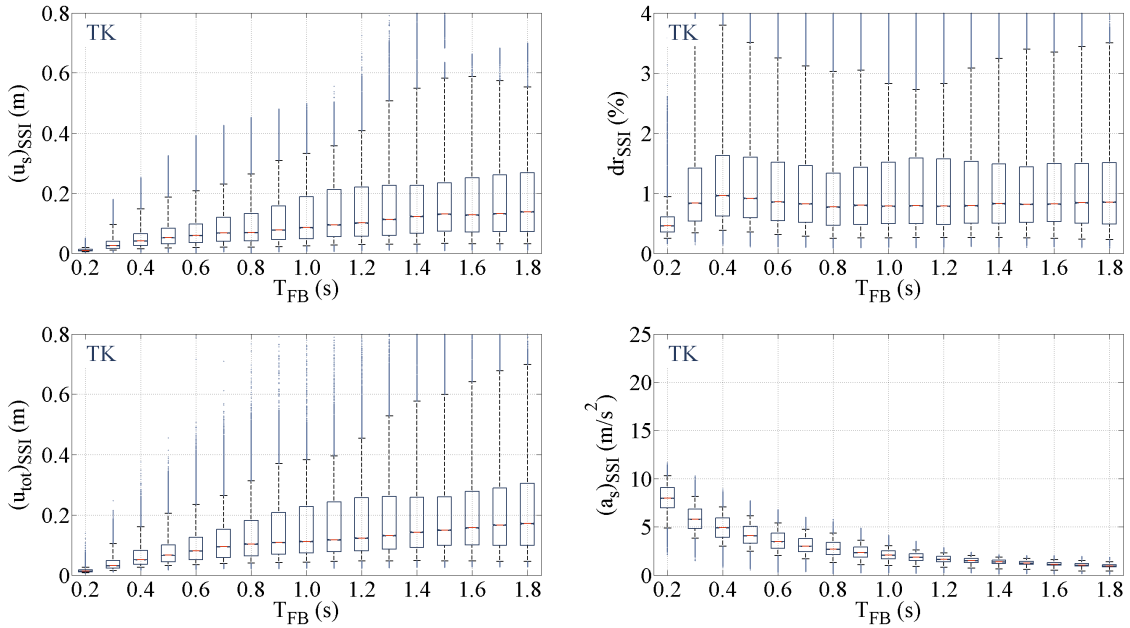

Figure B-6. Response spectra for flexible-base structures with TK hysteretic behaviour.

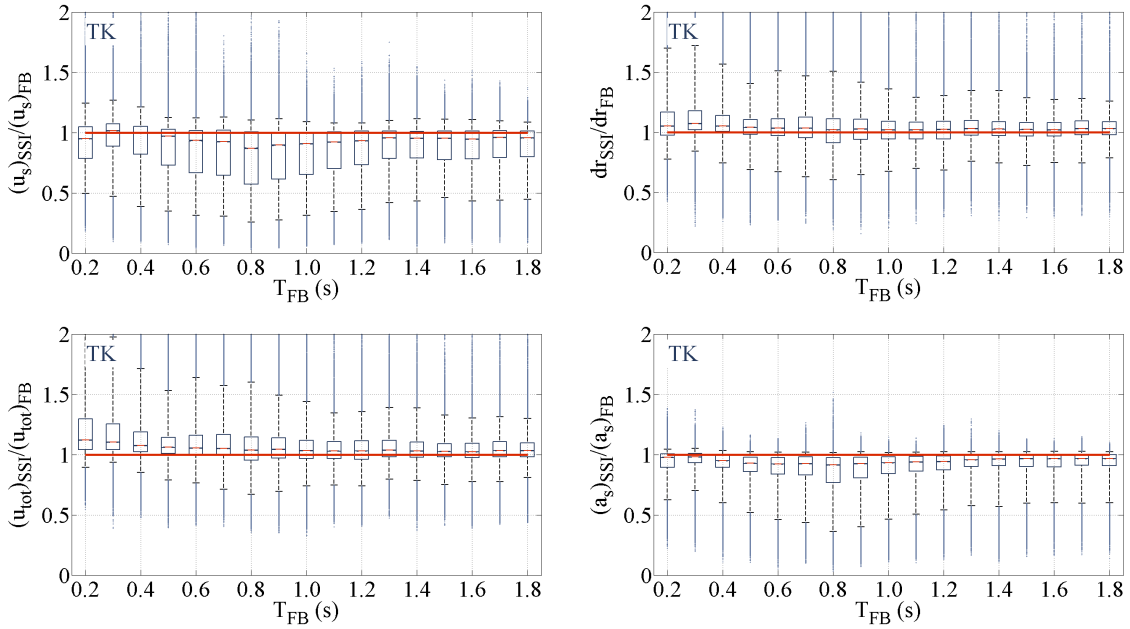

Figure B-7. Response modification spectra for structures with TK hysteretic behaviour.

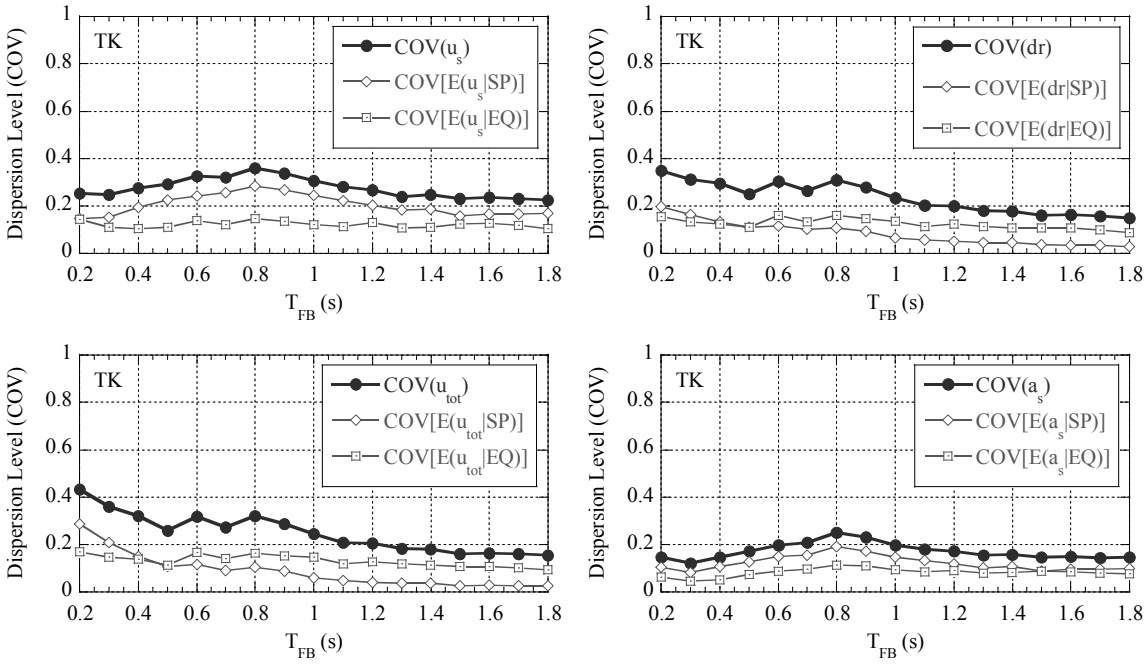

Figure B-8. Dispersion spectra for structures with TK hysteretic behaviour.

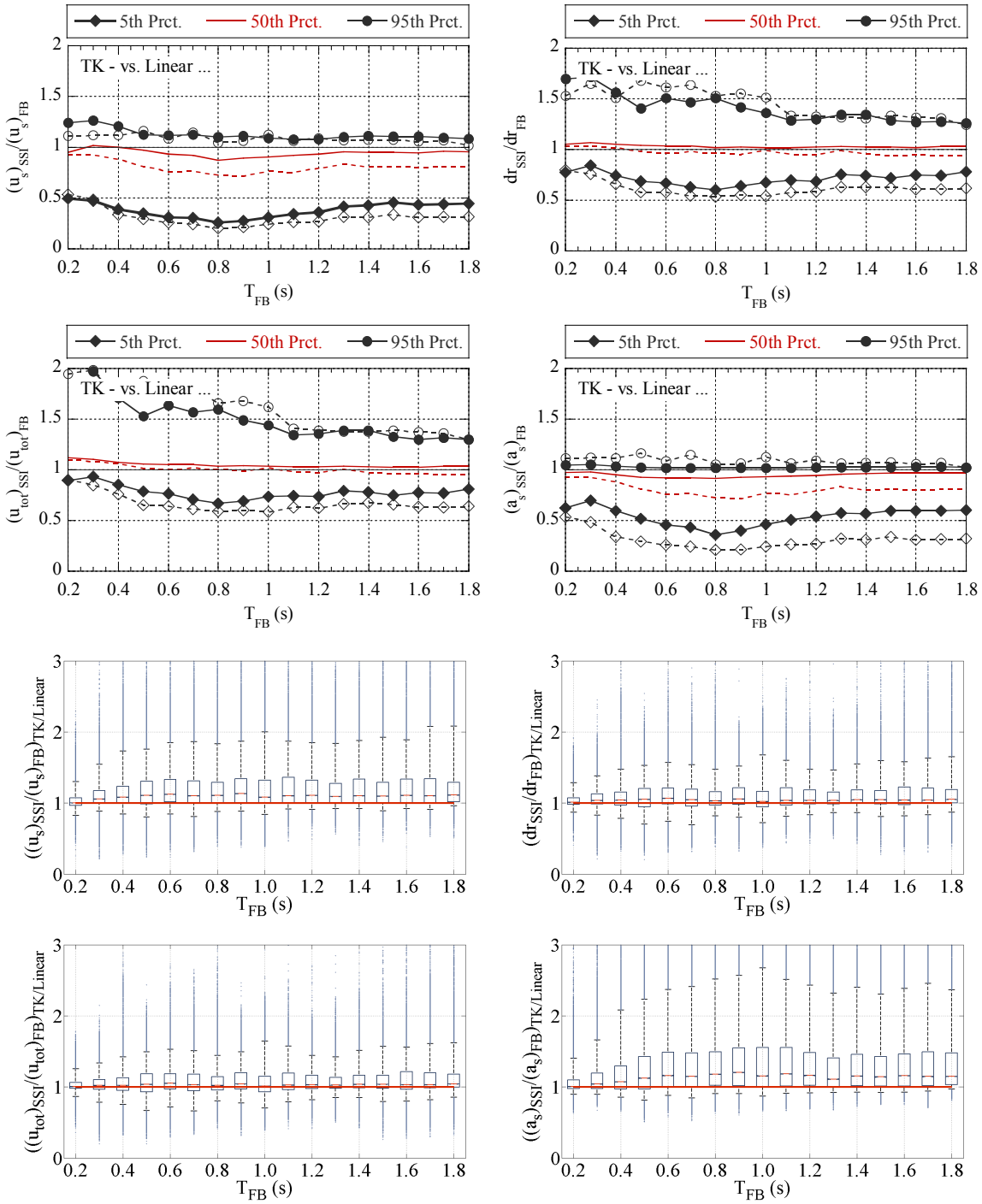

Figure B-9. The effects of structural nonlinearity on structural response modification spectra.

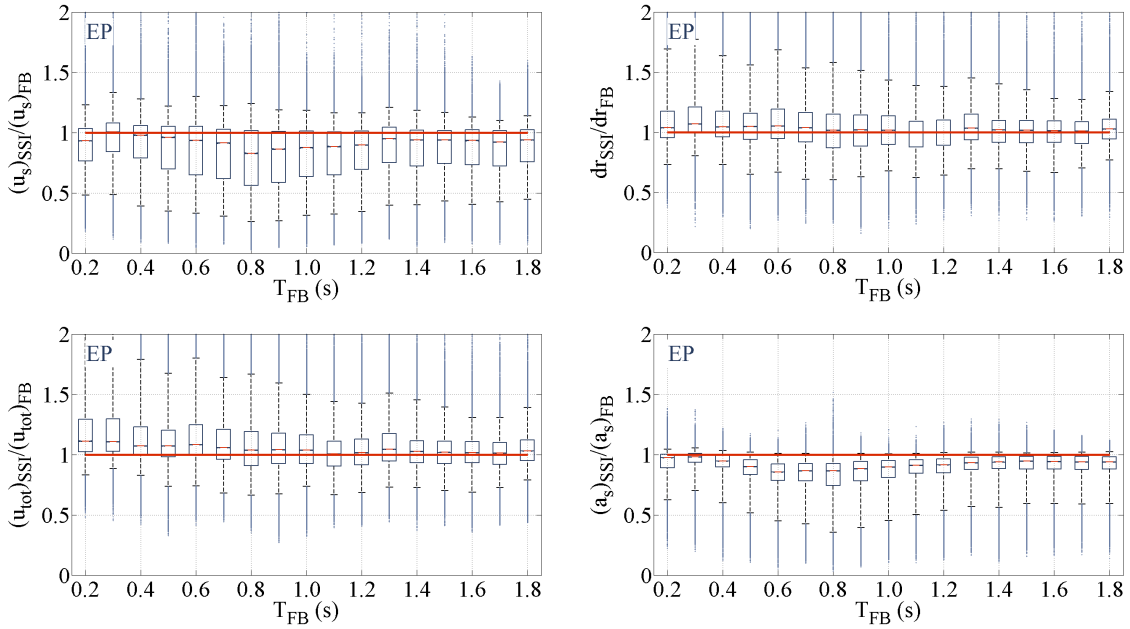

Figure B-10. Response modification spectra for structures with EP hysteretic behaviour.

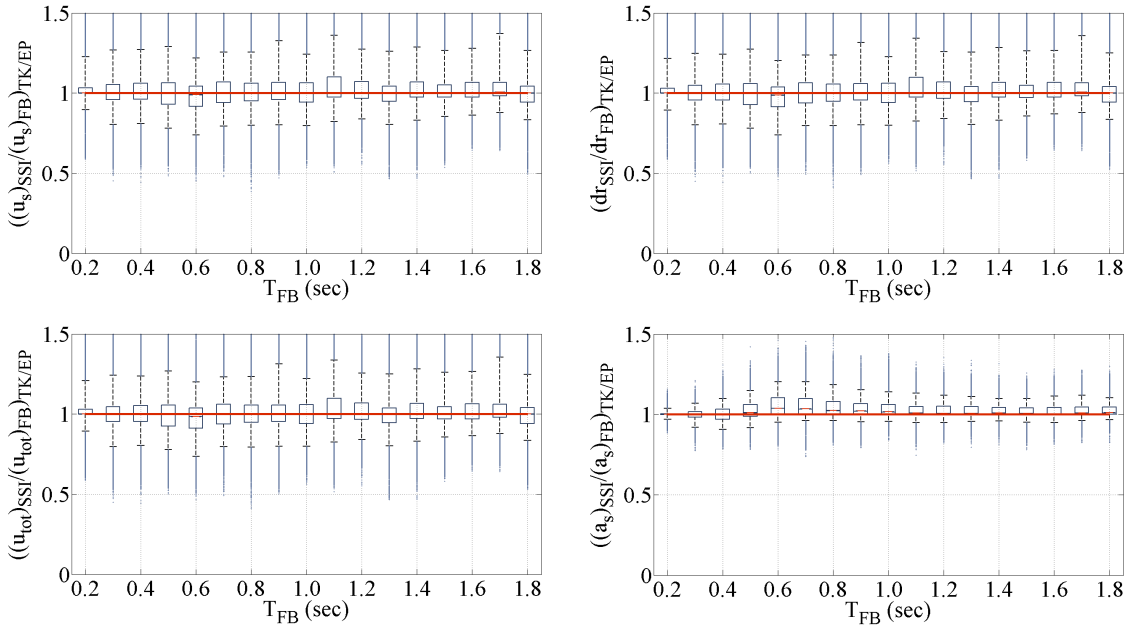

Figure B-11. The effects of structural force-deflection behaviour on response modification spectra (TK vs. EP).

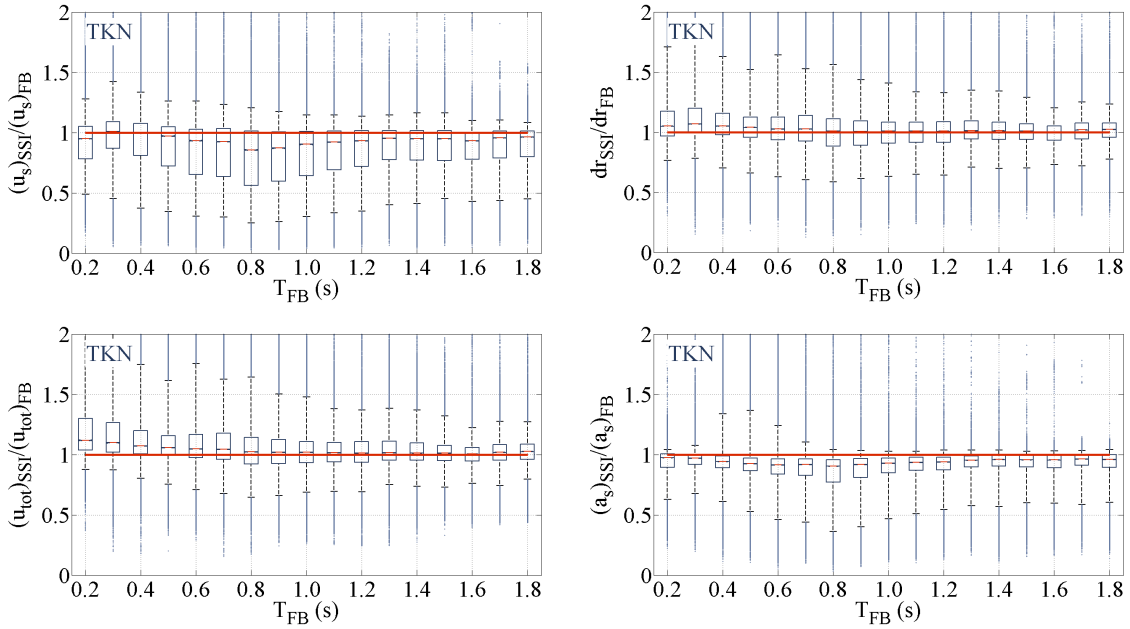

Figure B-12. Response modification spectra for structures with TKN hysteretic behaviour.

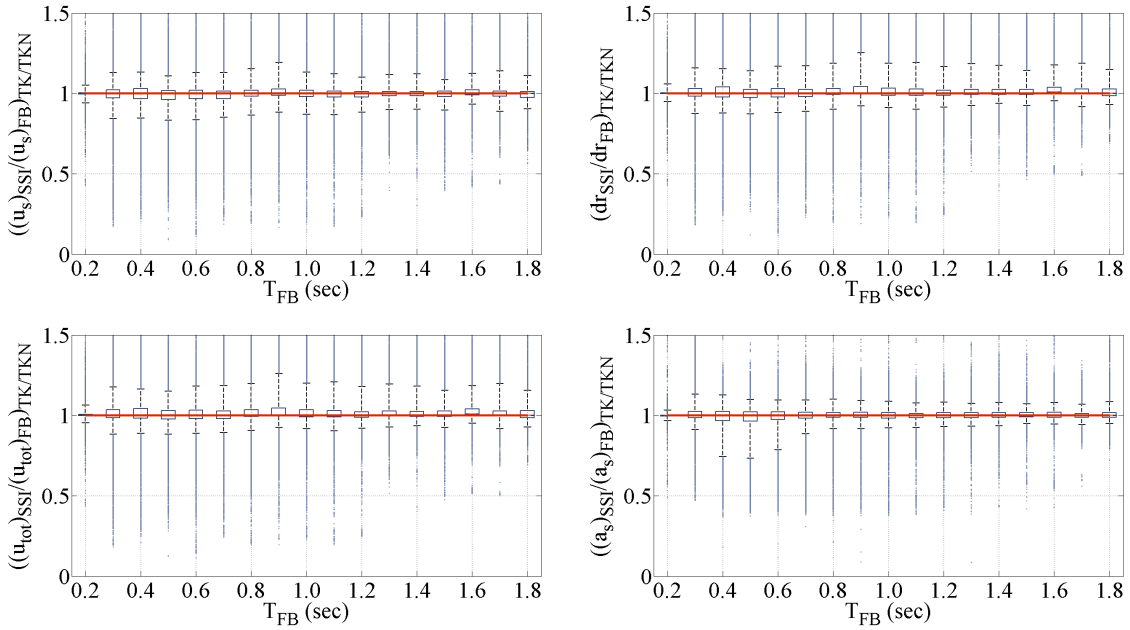

Figure B-13. The effects of structural force-deflection behaviour on response modification spectra (TK vs. TKN).

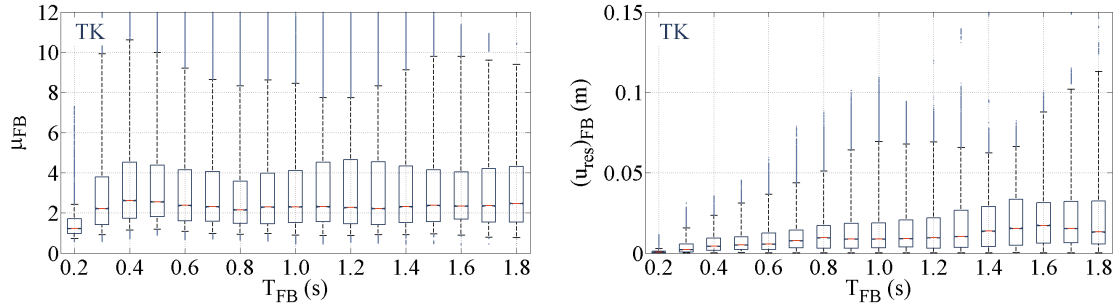

Figure B-14. Displacement ductility and residual displacement spectra for fixed-base structures with TK hysteretic behaviour.

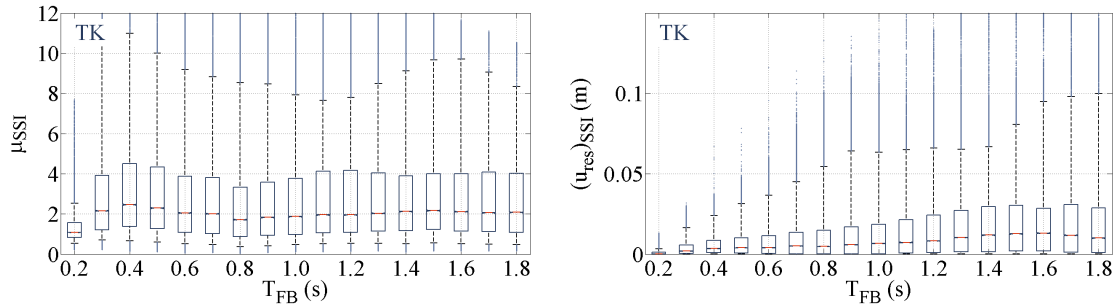

Figure B-15. Displacement ductility and residual displacement spectra for fixed-base structures with TK hysteretic behaviour.

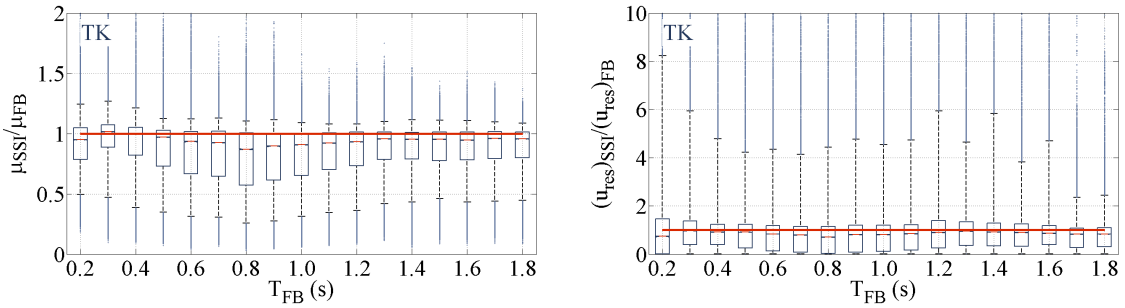

Figure B-16. Displacement ductility and residual displacement modification spectra for structures with TK hysteretic behaviour.

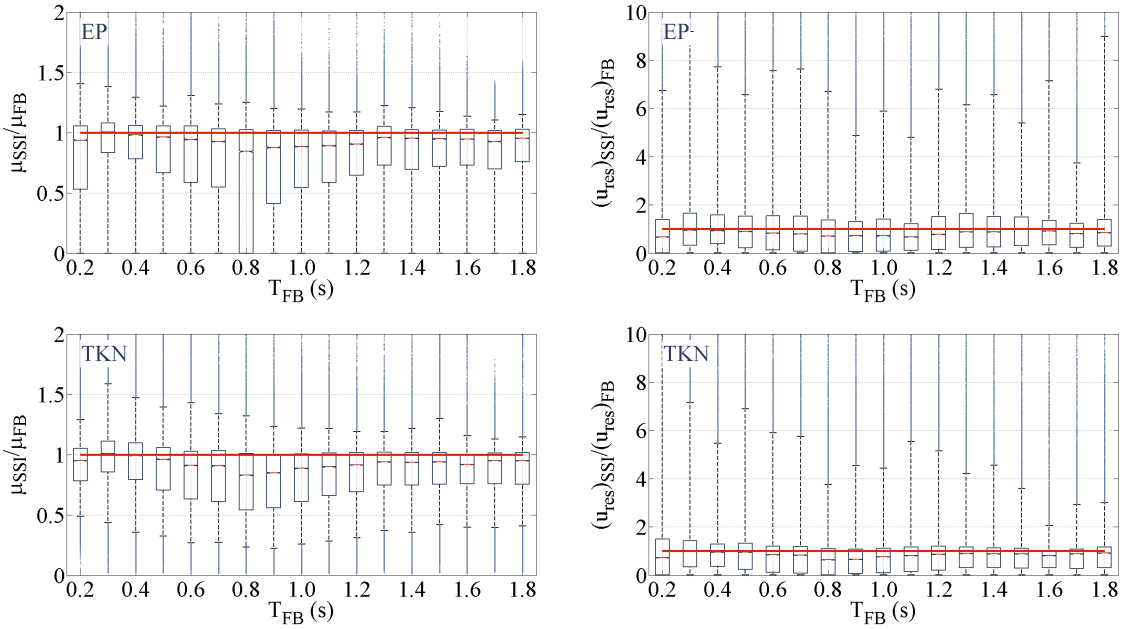

Figure B-17. Displacement ductility and residual displacement modification spectra for structures with EP, TKN hysteretic behaviour.

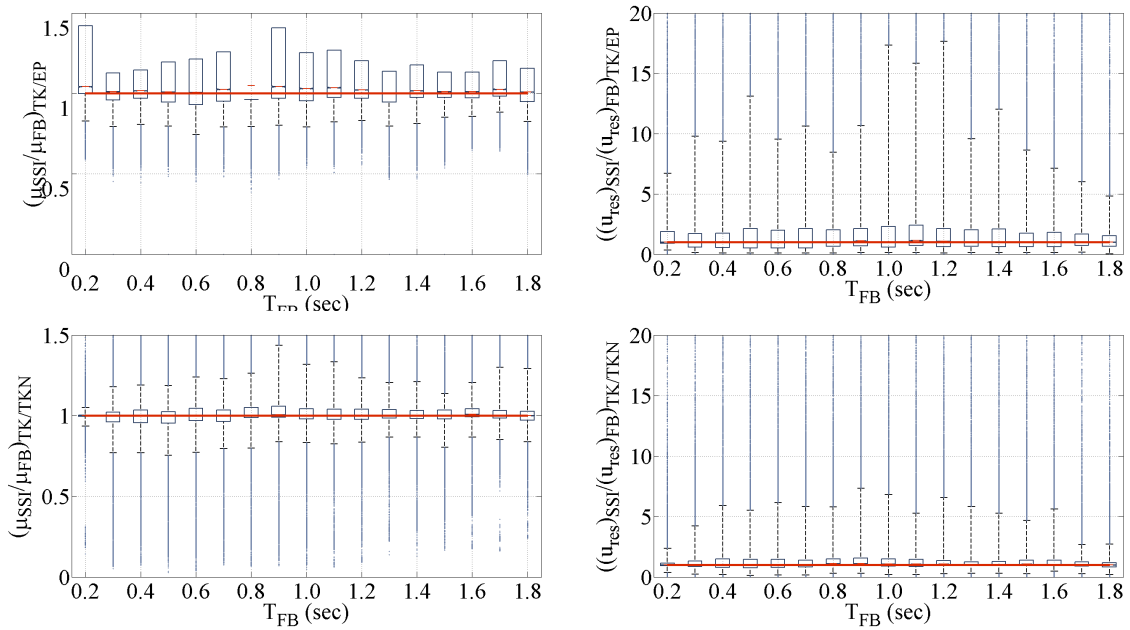

Figure B-18. The effects of structural force-deflection behaviour on displacement ductility and residual displacement modification spectra (TK vs. EP and TK vs. TKN).

APPENDIX

C. Results for Risk Analysis of Soil-Structure Interaction Phenomena with Detrimental Effects

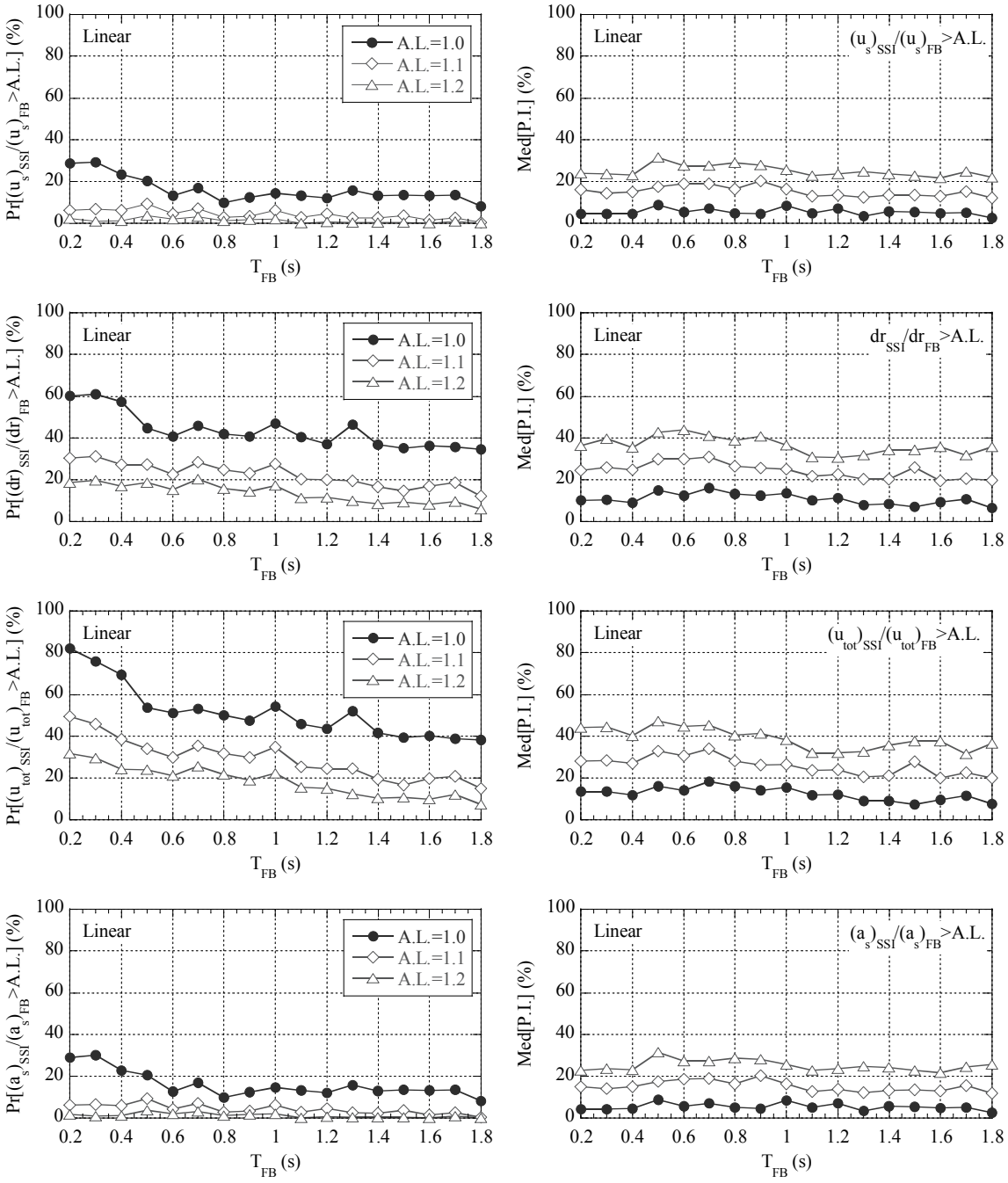

Figure C-1. Risk spectra for structures with linear behaviour: (left) probability of amplification in the response; (right) level of increase in the demand.

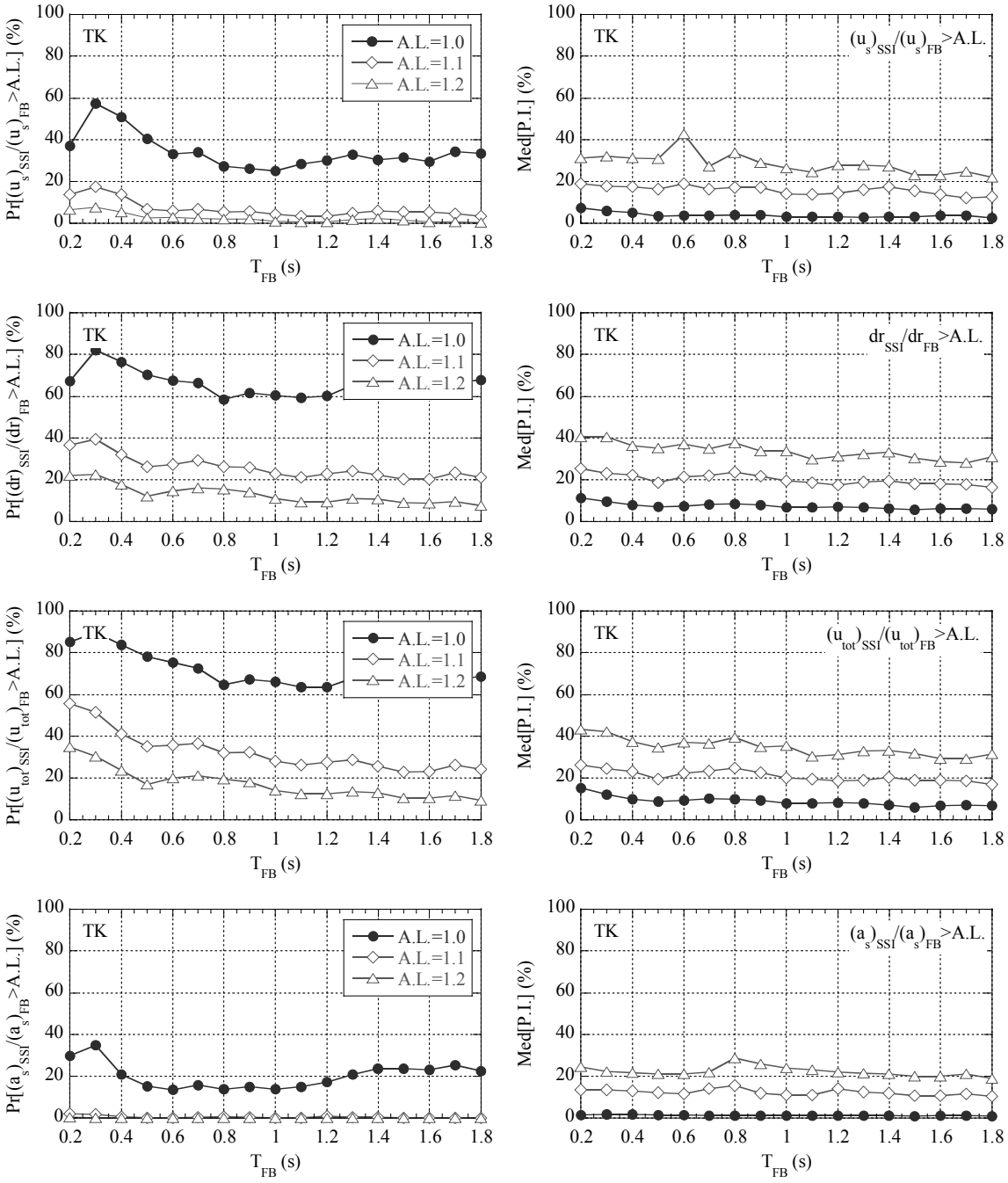

Figure C-2. Risk spectra for structures with TK hysteretic behaviour: (left) probability of amplification in the response; (right) level of increase in the demand.

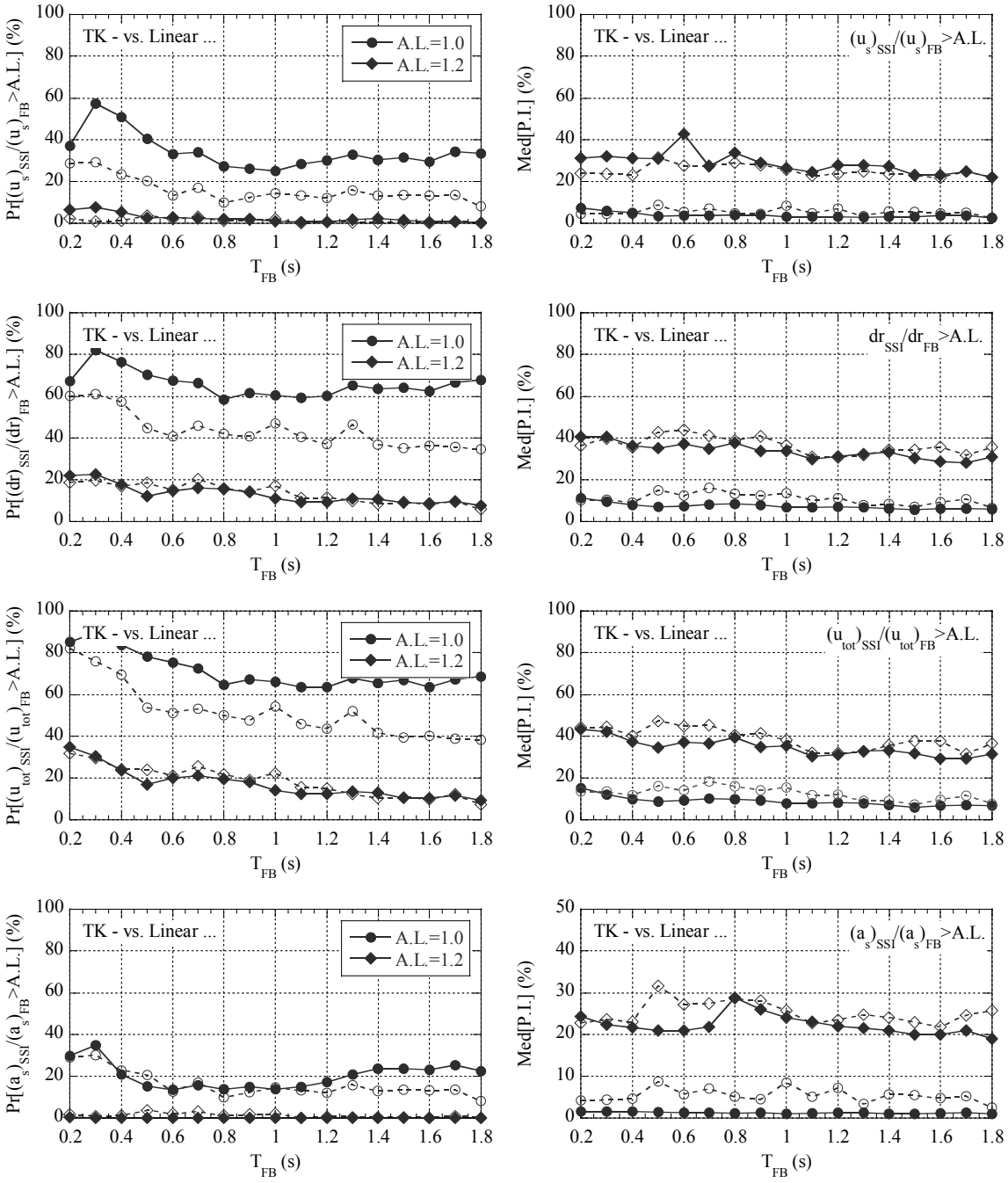

Figure C-3. The effects of structural nonlinearity on risk spectra: (left) probability of amplification in the response; (right) level of increase in the demand.

APPENDIX

D. Results for Risk Analysis Considering Special Ground Motions

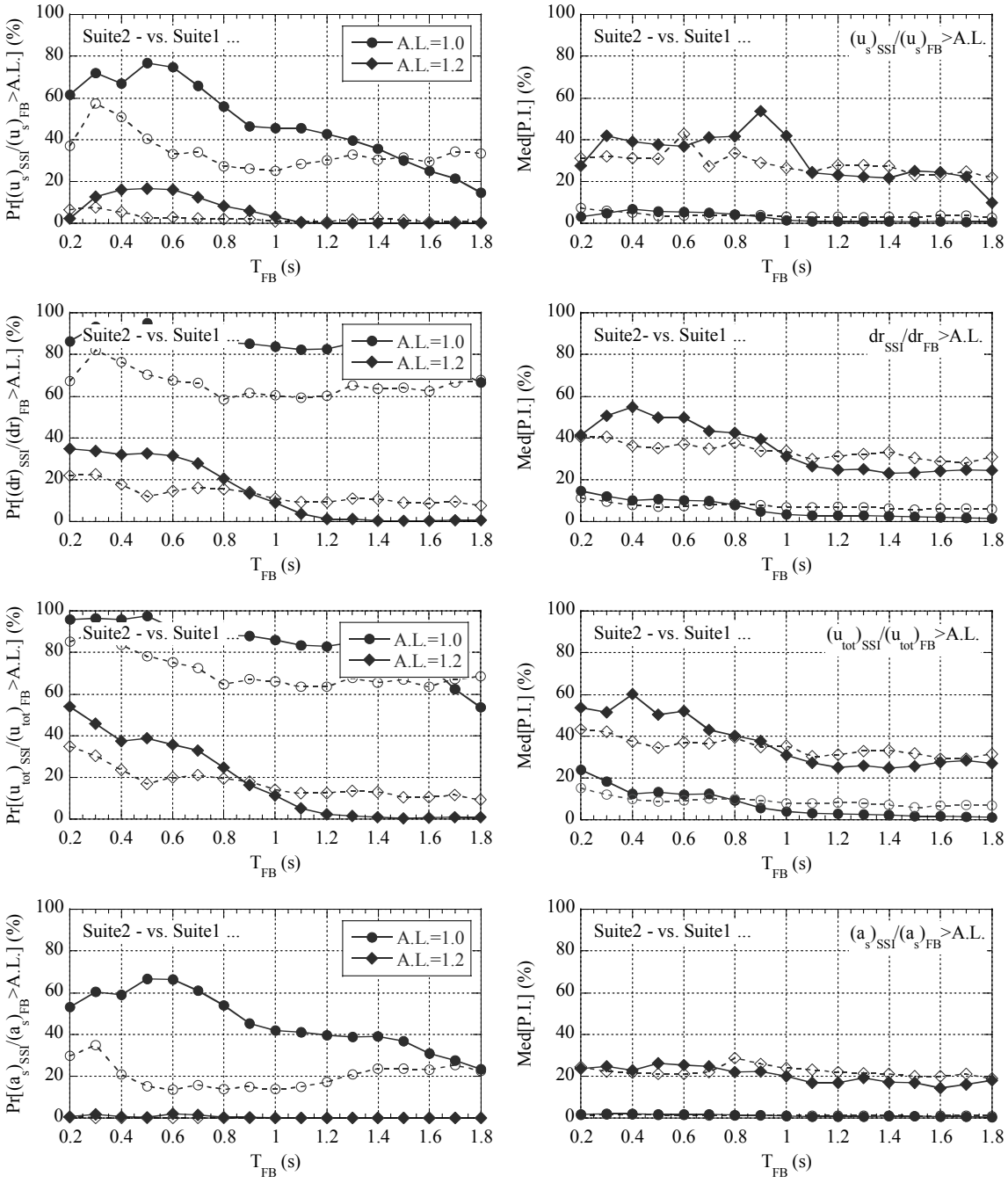

Figure D-1. Risk spectra for structures with TK hysteretic behaviour considering the ground motions of suite2: (left) probability of amplification in the response; (right) level of increase in the demand.

APPENDIX

E. Results for Sensitivity Analysis Considering the Effects of Model Parameters

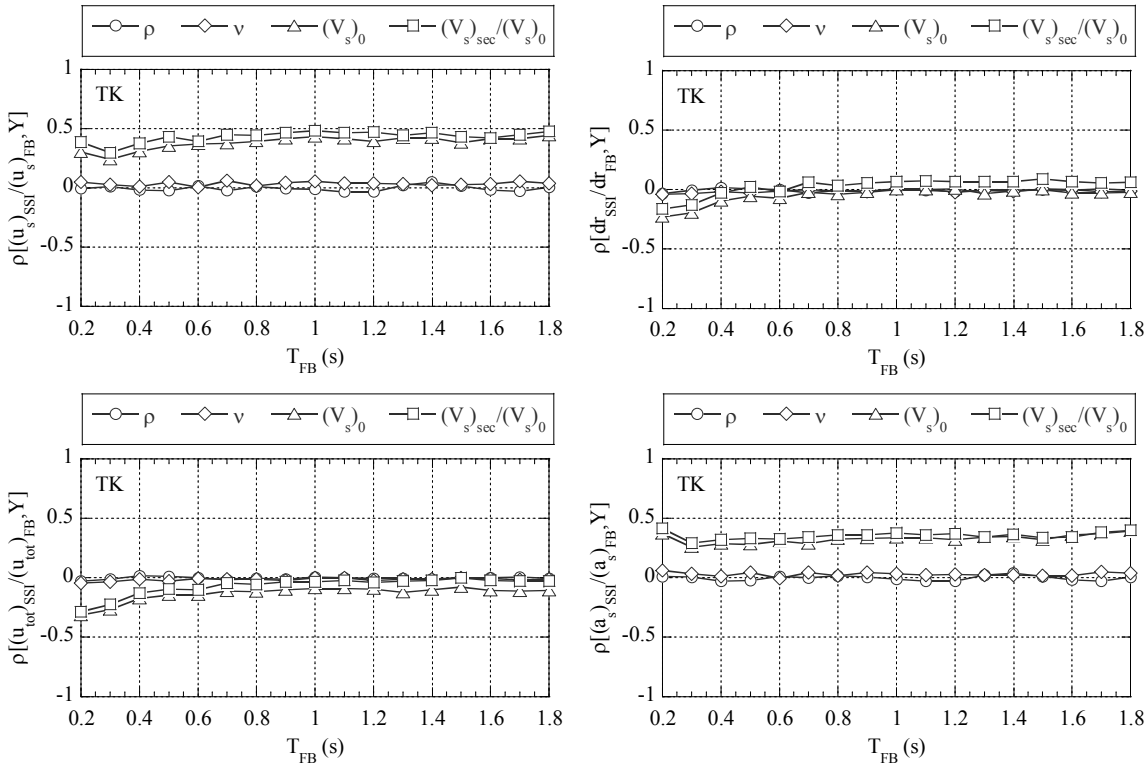

Figure E-1. Pearson correlation coefficient spectra representing the correlation between structural response modification factors and soil parameters.

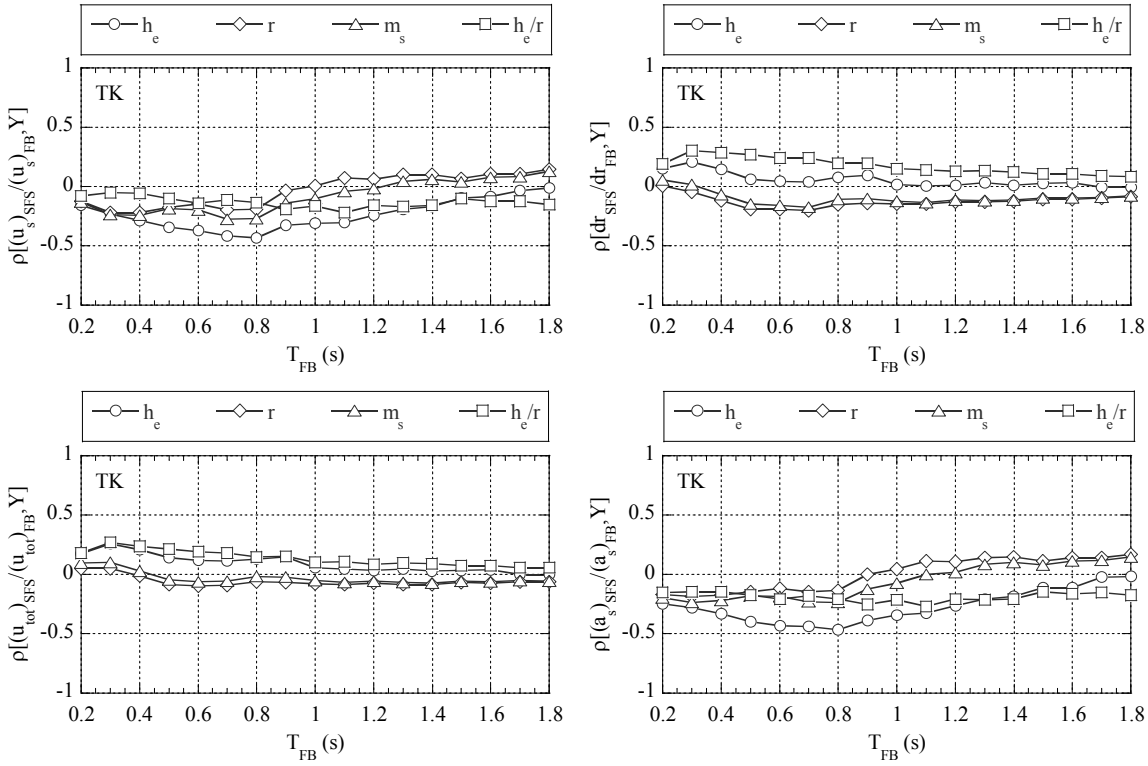

Figure E-2. Pearson correlation coefficient spectra representing the correlation between structural response modification factors and structural parameters.

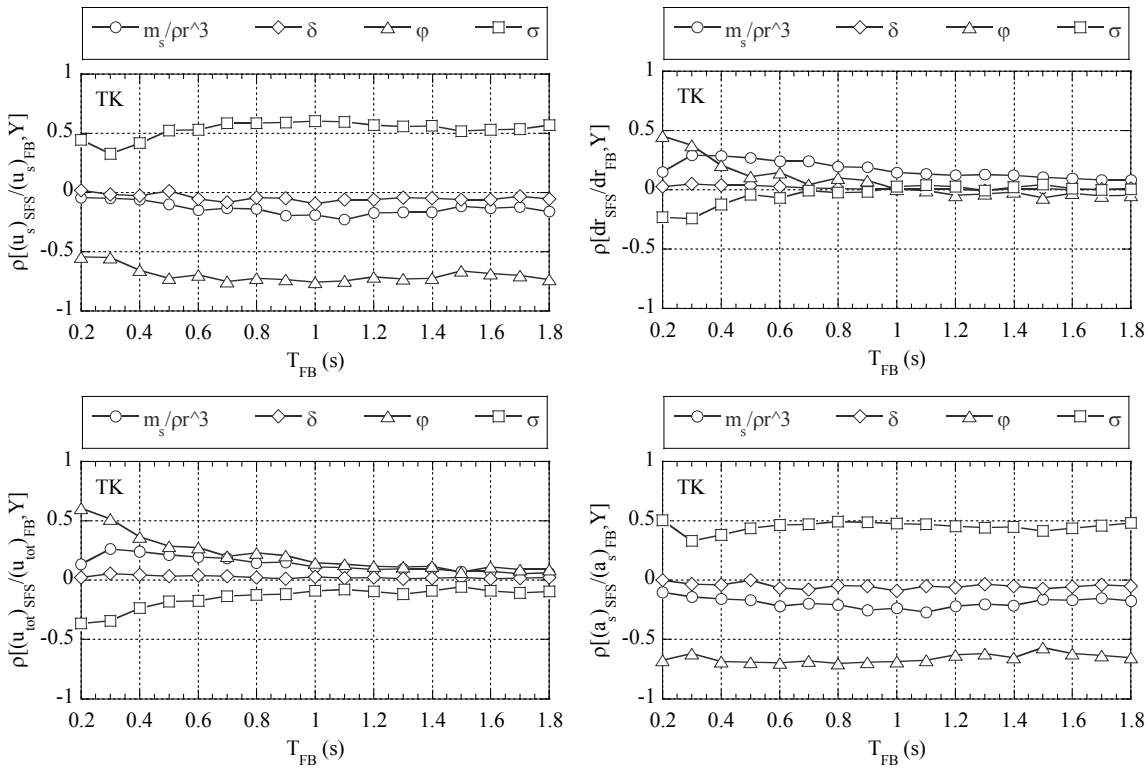

Figure E-3. Pearson correlation coefficient spectra representing the correlation between structural response modification factors and soil-structure system parameters.

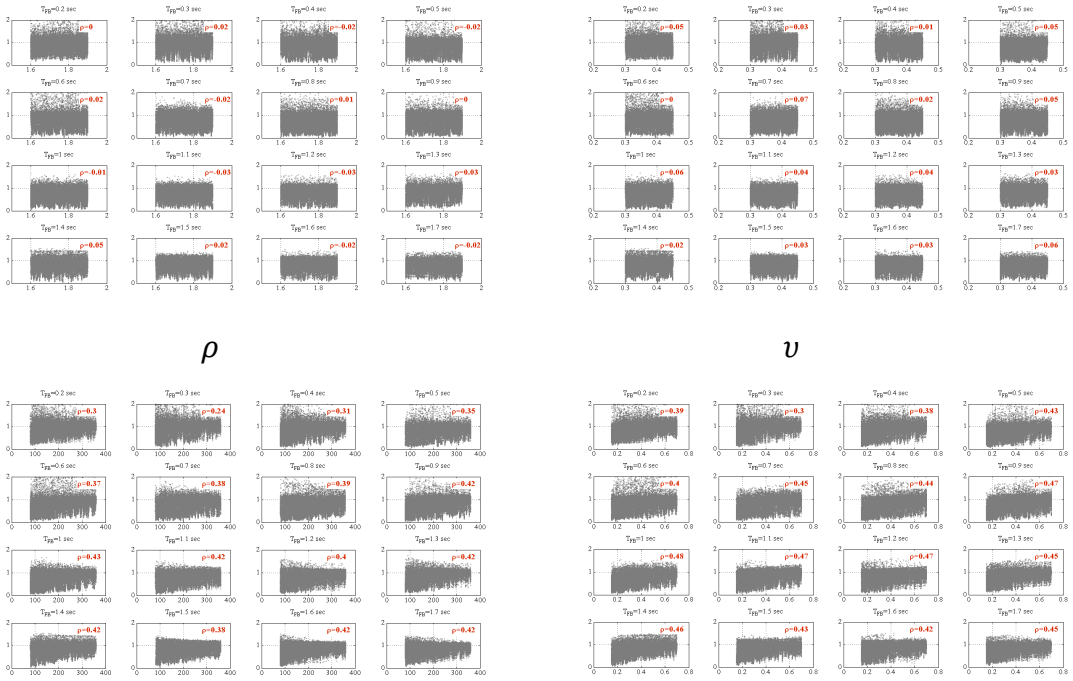

Figure E-4. Correlation and dependency between structural distortion modification factors and soil parameters.

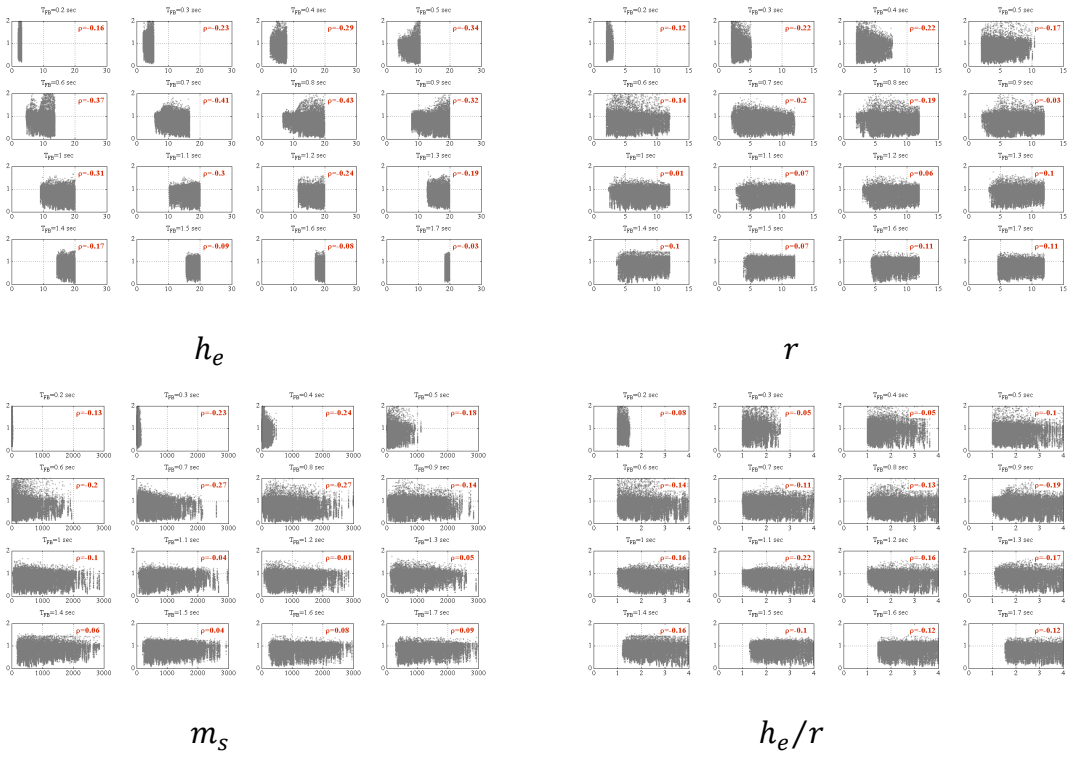

Figure E-5. Correlation and dependency between structural distortion modification factors and structural parameters.

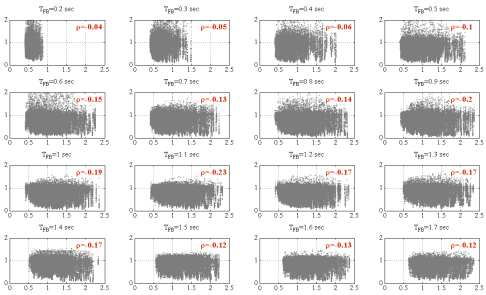

$m_s/\rho r^3$

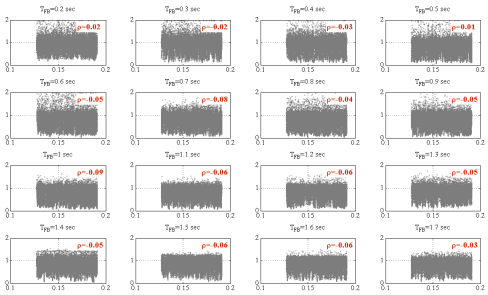

$\delta = m_s/\rho\pi r^2 h_e$

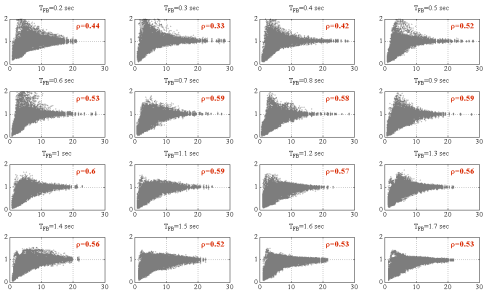

$\sigma = (V_s)_{sec} T_{FB}/h_e$

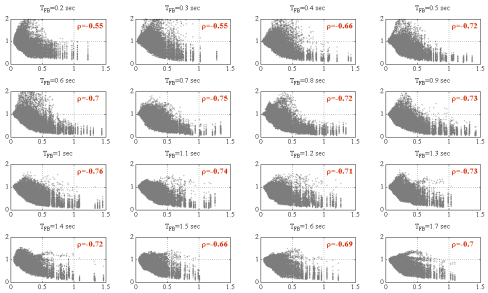

$\varphi = \dfrac{h_e}{(V_s)_{sec} T_{FB}} (h_e/r)^{0.25}$

Figure E-6. Correlation and dependency between structural distortion modification factors and soil-structure system parameters.

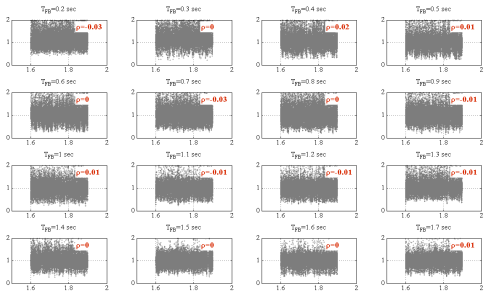

ρ

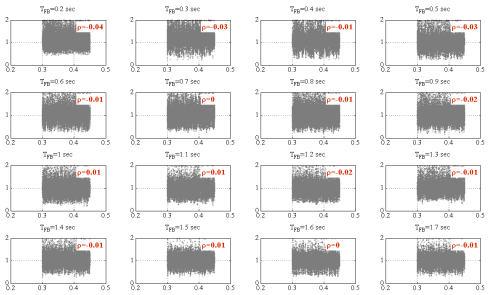

υ

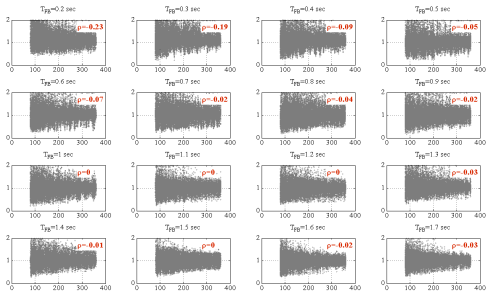

$(V_s)_0$

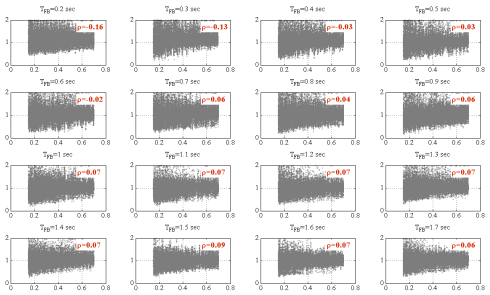

$(V_s)_{sec}/(V_s)_0$

Figure E-7. Correlation and dependency between structural drift modification factors and soil parameters.

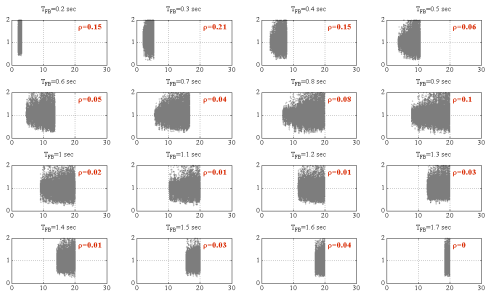

h_e

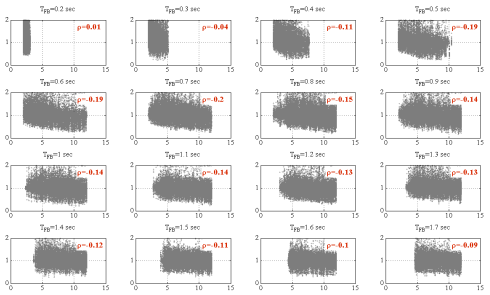

r

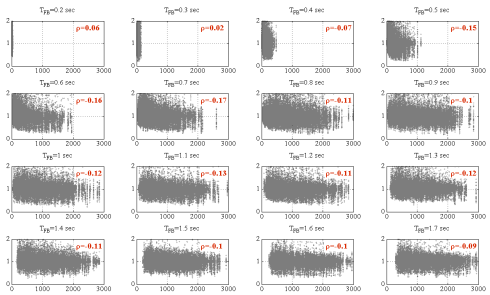

m_s

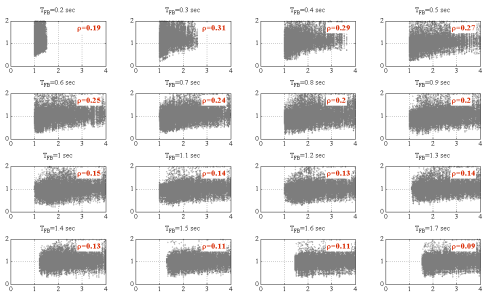

h_e/r

Figure E-8. Correlation and dependency between structural drift modification factors and structural parameters.

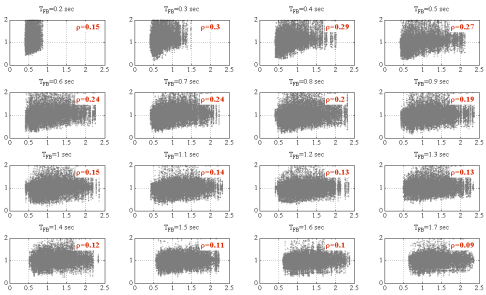

$m_s/\rho r^3$

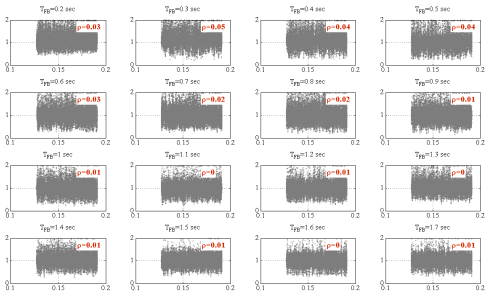

$\delta = m_s/\rho\pi r^2 h_e$

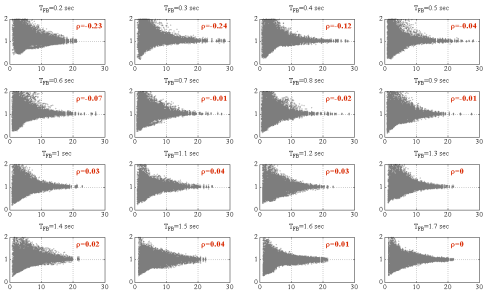

$\sigma = (V_s)_{sec} T_{FB}/h_e$

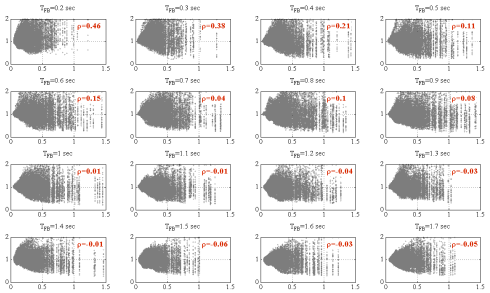

$\varphi = \dfrac{h_e}{(V_s)_{sec} T_{FB}} (h_e/r)^{0.25}$

Figure E-9. Correlation and dependency between structural drift modification factors and soil-structure system parameters.

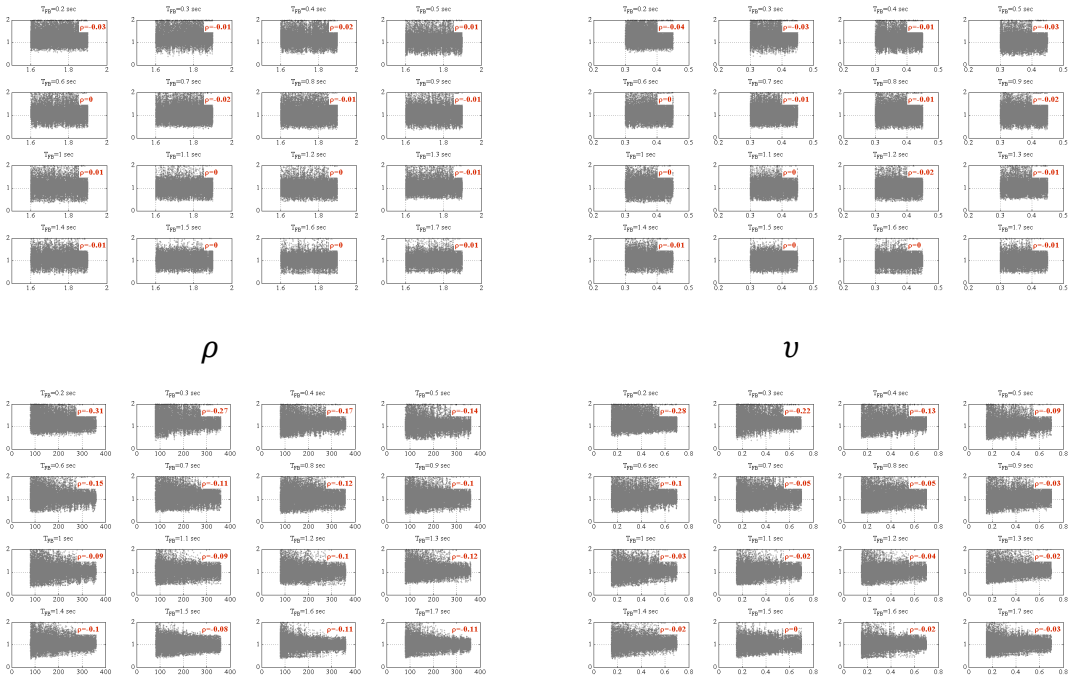

ρ υ

$(V_s)_0$ $(V_s)_{sec}/(V_s)_0$

Figure E-10. Correlation and dependency between total displacement modification factors and soil parameters.

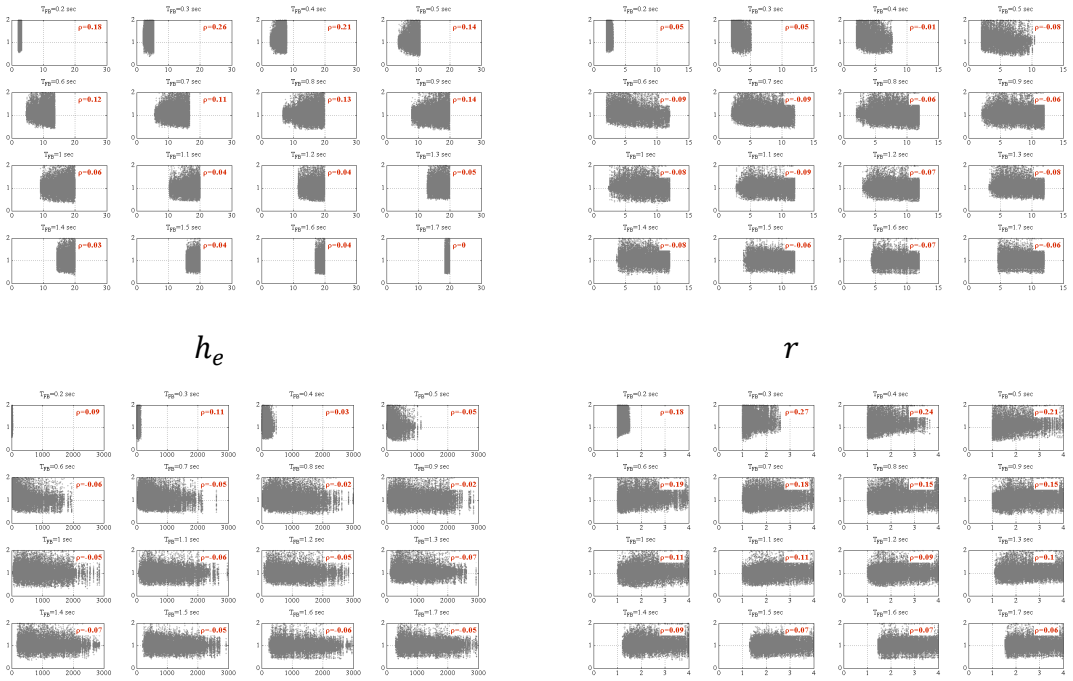

h_e r

m_s h_e/r

Figure E-11. Correlation and dependency between total displacement modification factors and structural parameters.

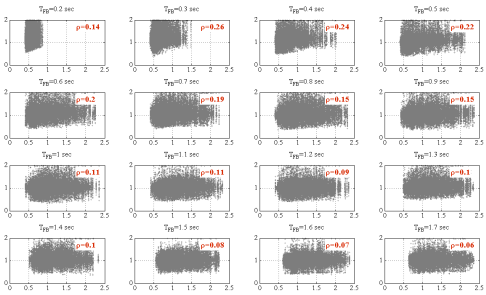

$m_s/\rho r^3$

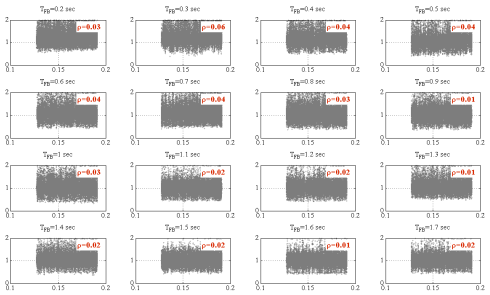

$\delta = m_s/\rho\pi r^2 h_e$

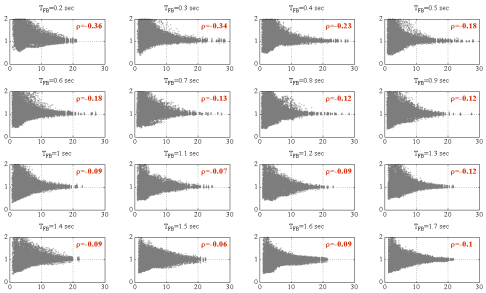

$\sigma = (V_s)_{sec} T_{FB}/h_e$

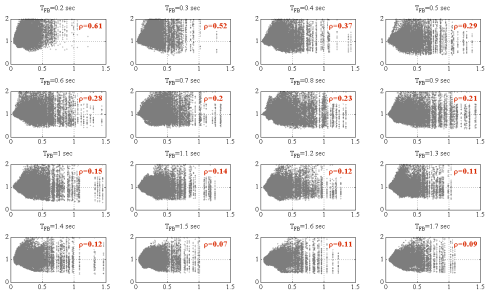

$\varphi = \dfrac{h_e}{(V_s)_{sec} T_{FB}} (h_e/r)^{0.25}$

Figure E-12. Correlation and dependency between total displacement modification factors and soil-structure system parameters.

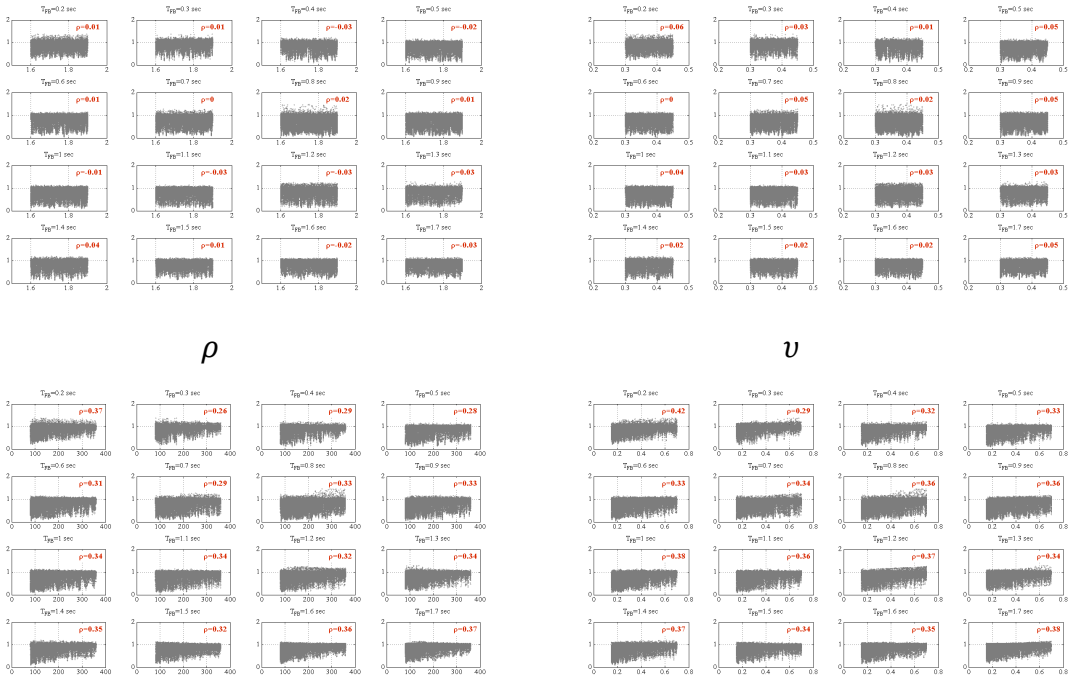

ρ υ

$(V_s)_0$ $(V_s)_{sec}/(V_s)_0$

Figure E-13. Correlation and dependency between structural acceleration modification factors and soil parameters.

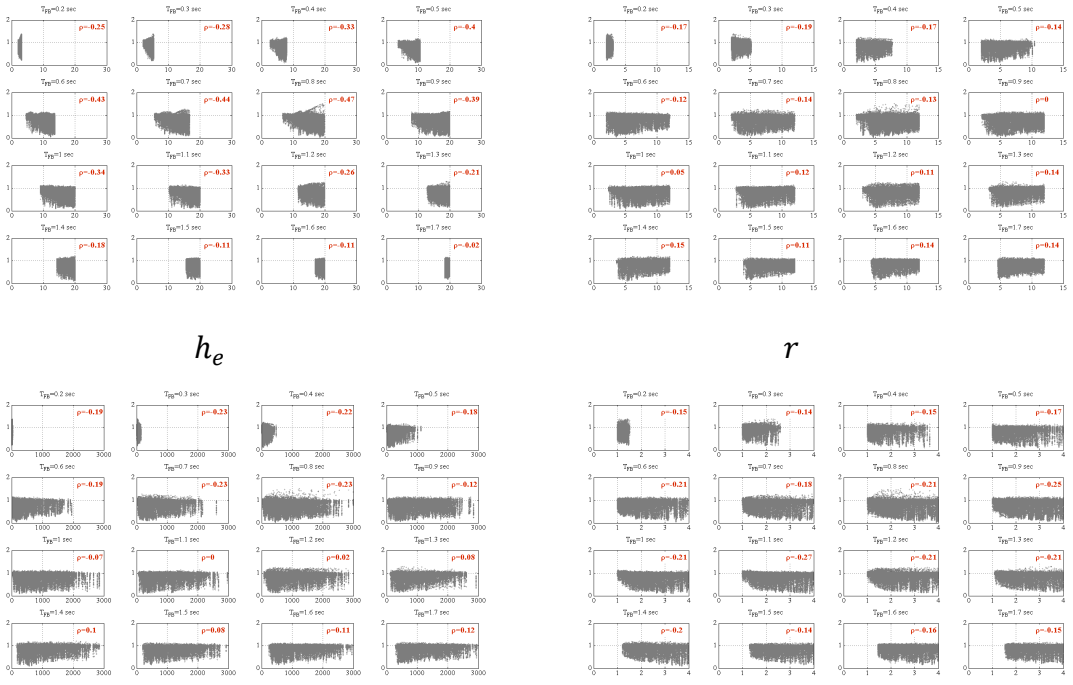

h_e r

m_s h_e/r

Figure E-14. Correlation and dependency between structural acceleration modification factors and structural parameters.

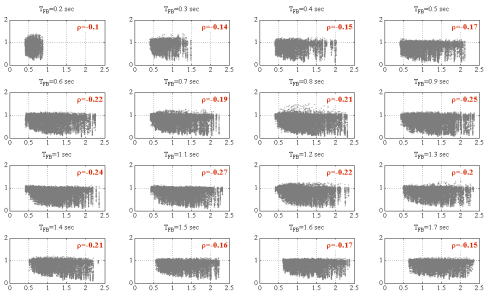

$m_s/\rho r^3$

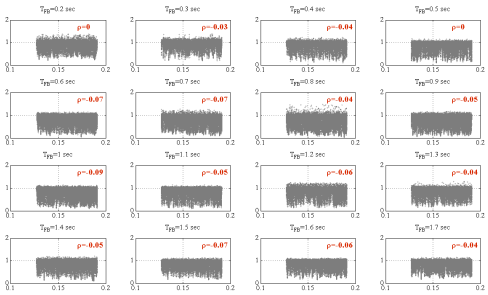

$\delta = m_s/\rho\pi r^2 h_e$

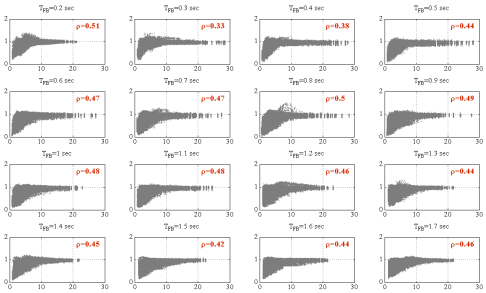

$\sigma = (V_s)_{sec} T_{FB}/h_e$

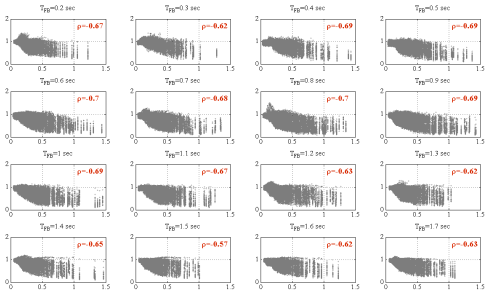

$\varphi = \dfrac{h_e}{(V_s)_{sec} T_{FB}} (h_e/r)^{0.25}$

Figure E-15. Correlation and dependency between structural acceleration modification factors and soil-structure system parameters.

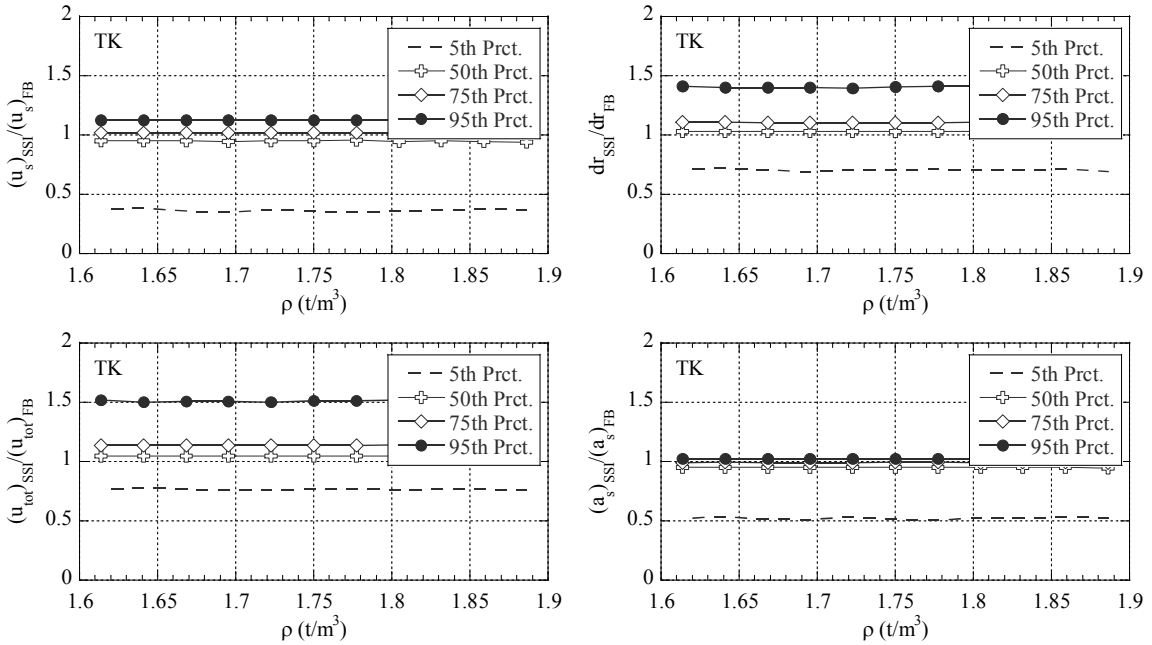

Figure E-16. The effects of soil density on structural response modification factors.

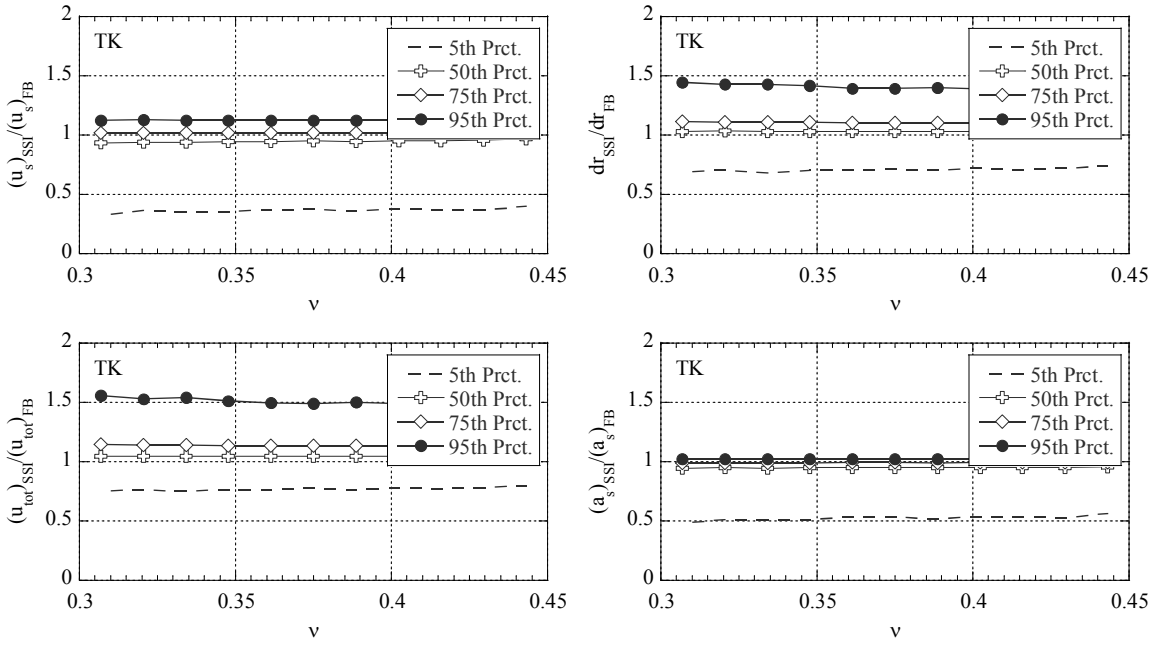

Figure E-17. The effects of Poison's ratio on structural response modification factors.

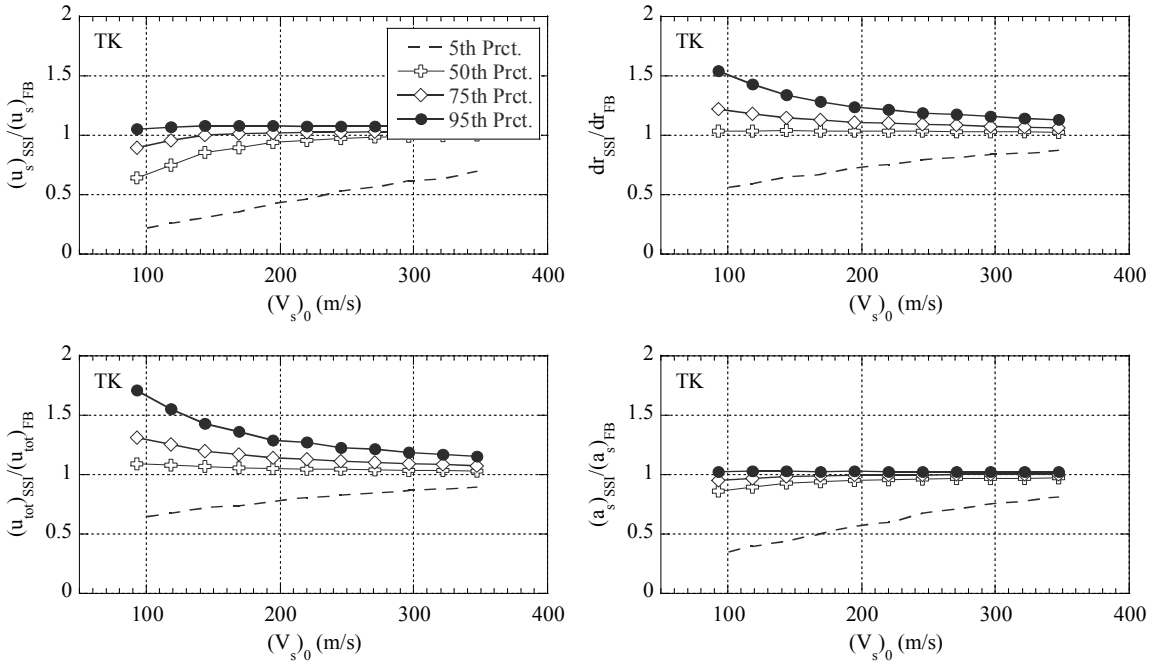

Figure E-18. The effects of soil shear wave velocity on structural response modification factors.

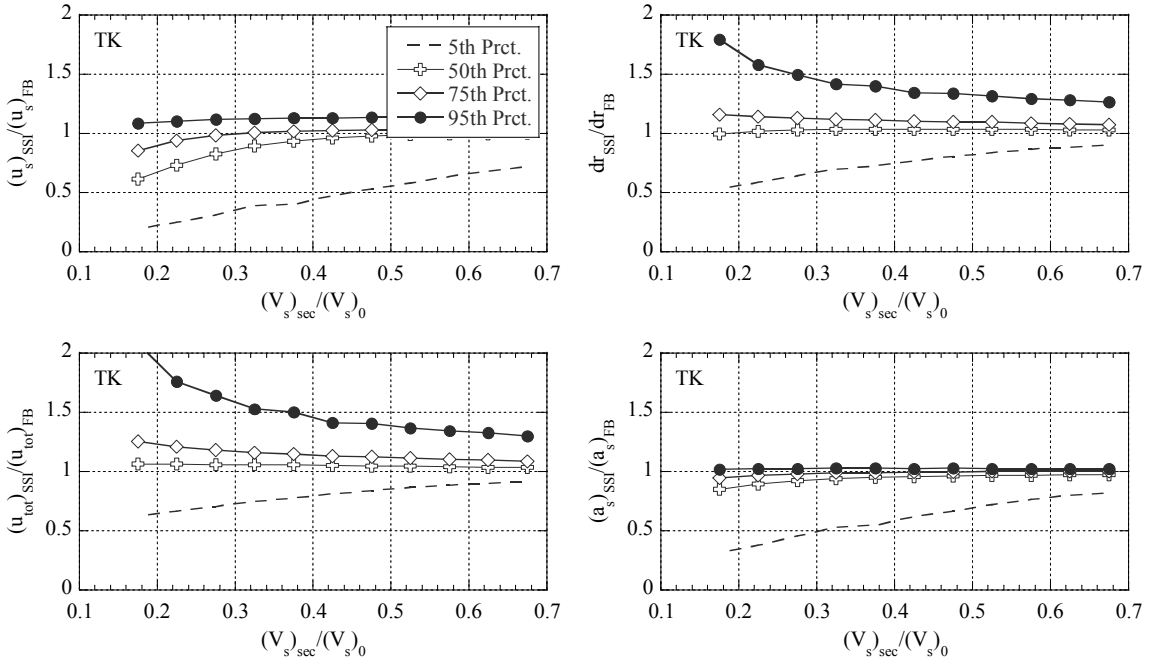

Figure E-19. The effects of shear wave velocity degradation ratio on structural response modification factors.

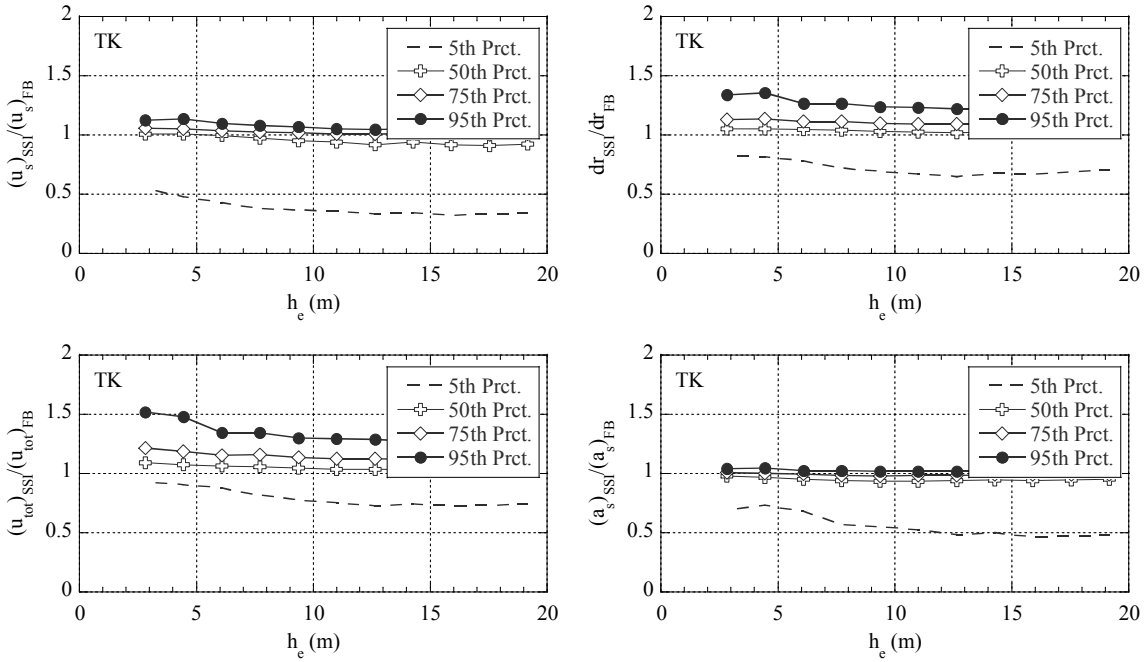

Figure E-20. The effects of effective structural height on structural response modification factors.

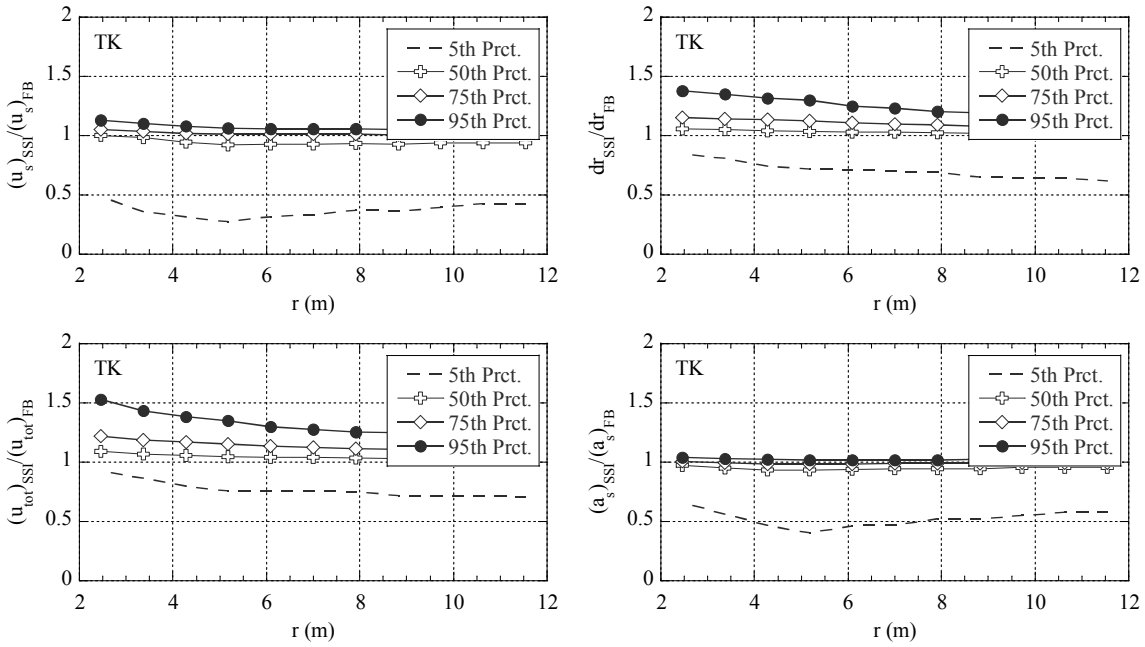

Figure E-21. The effects of foundation radius on structural response modification factors.

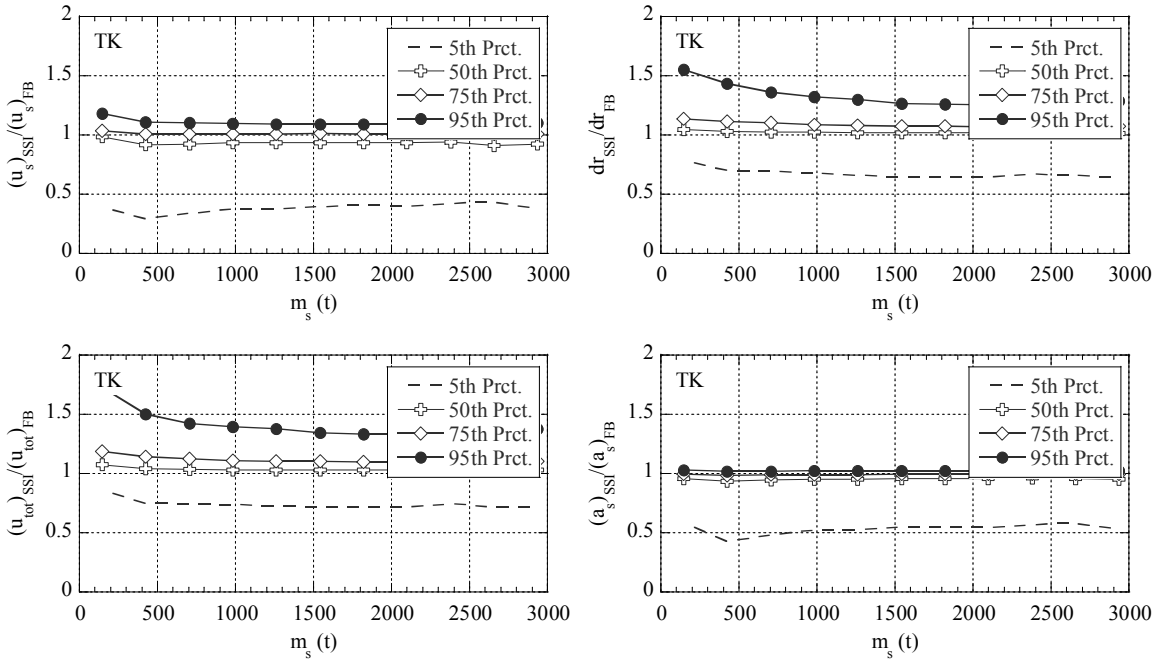

Figure E-22. The effects of structural mass on structural response modification factors.

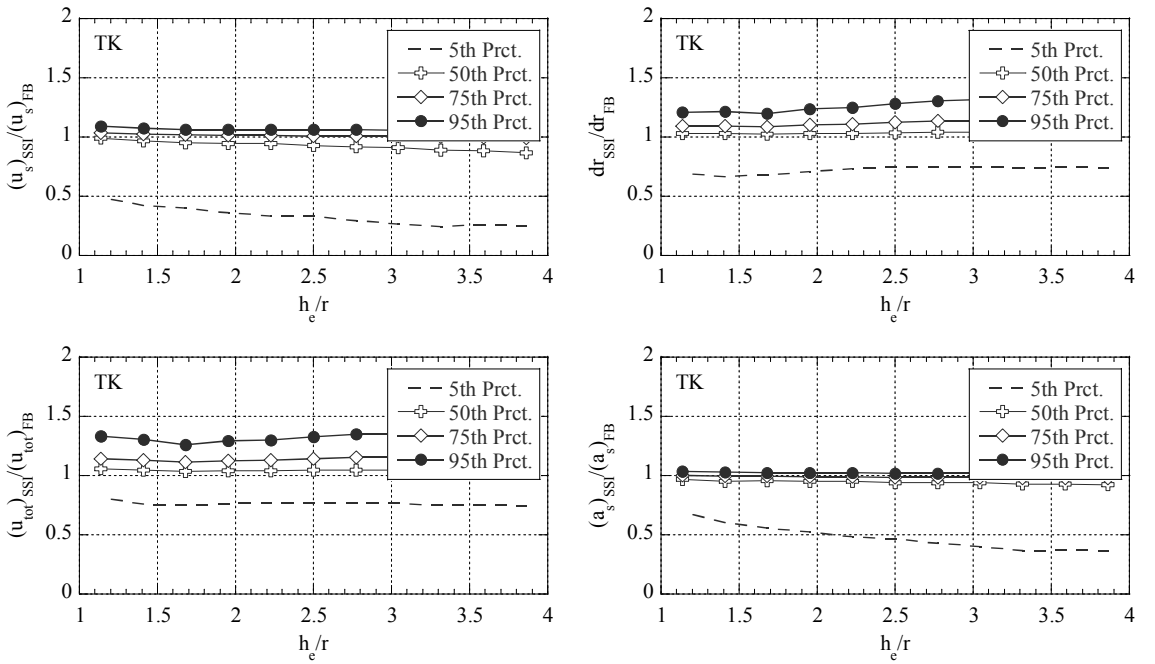

Figure E-23. The effects of structural aspect ratio on structural response modification factors.

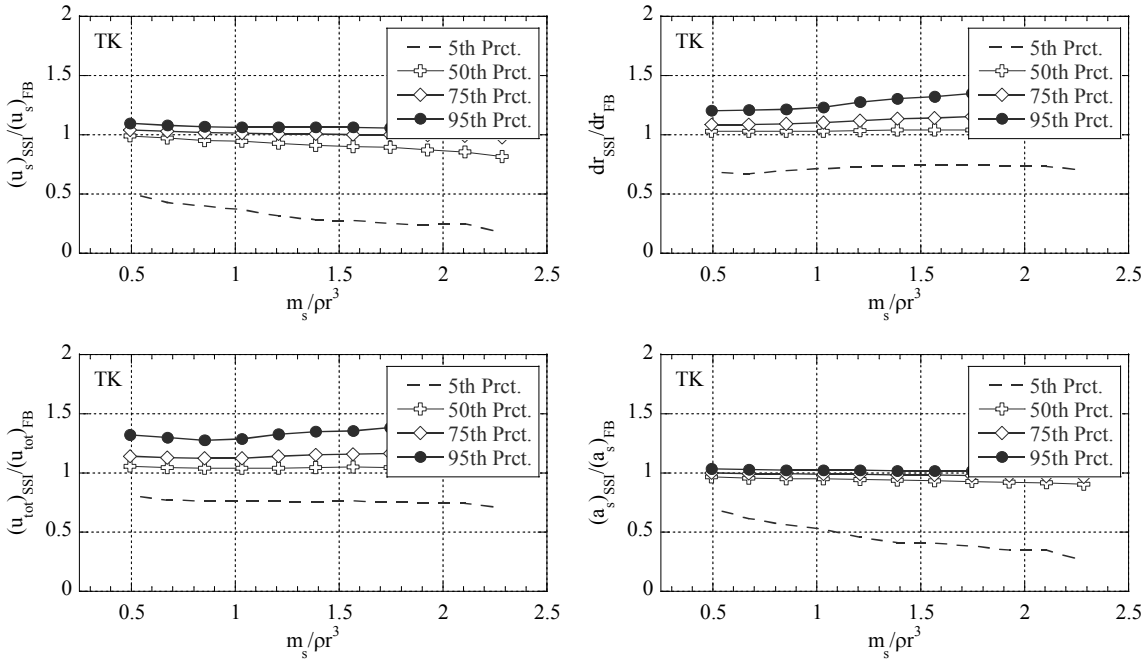

Figure E-24. The effects of $m_s/\rho r^3$ on structural response modification factors.

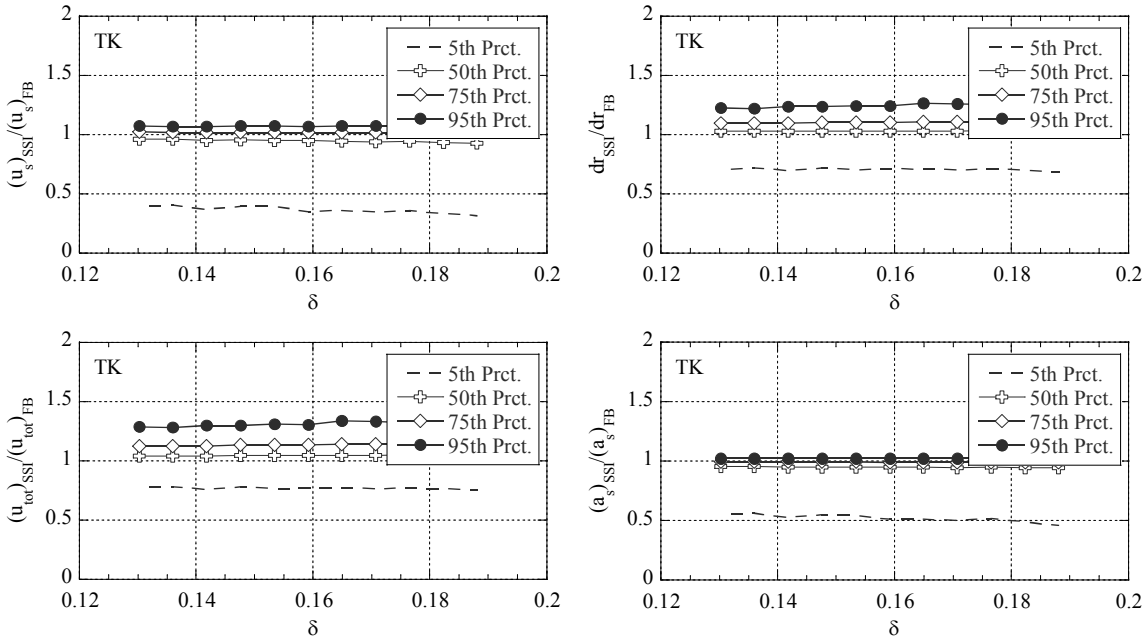

Figure E-25. The effects of $\delta = m_s/(\rho\pi r^2 h_e)$ on structural response modification factors.

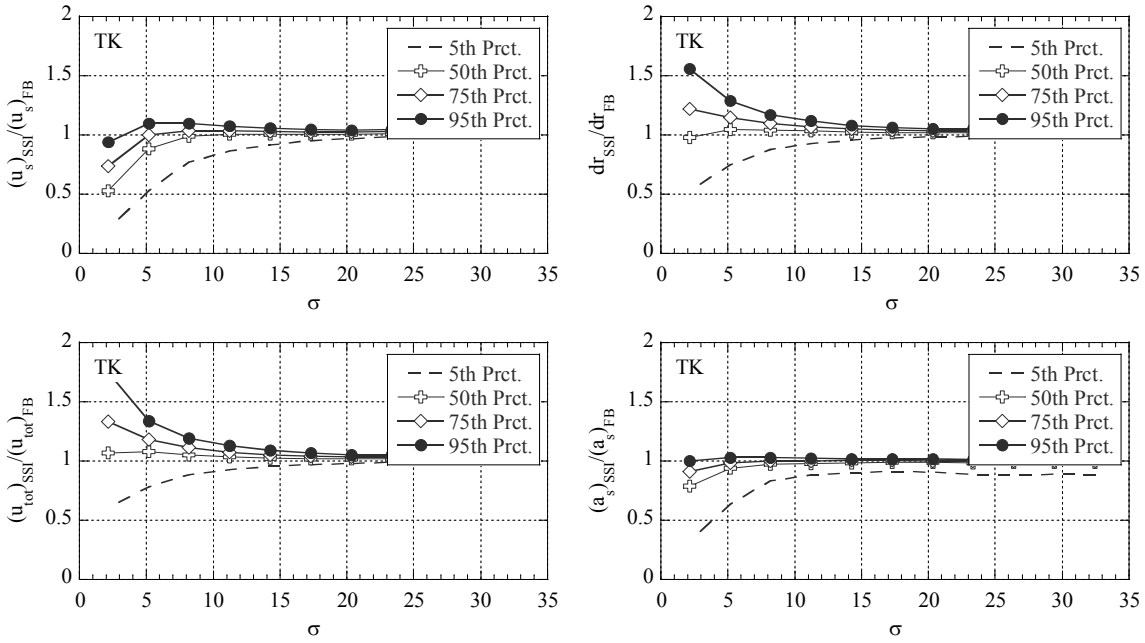

Figure E-26. The effects of $\sigma = (V_s)_{sec}T_{FB}/h_e$ on structural response modification factors.

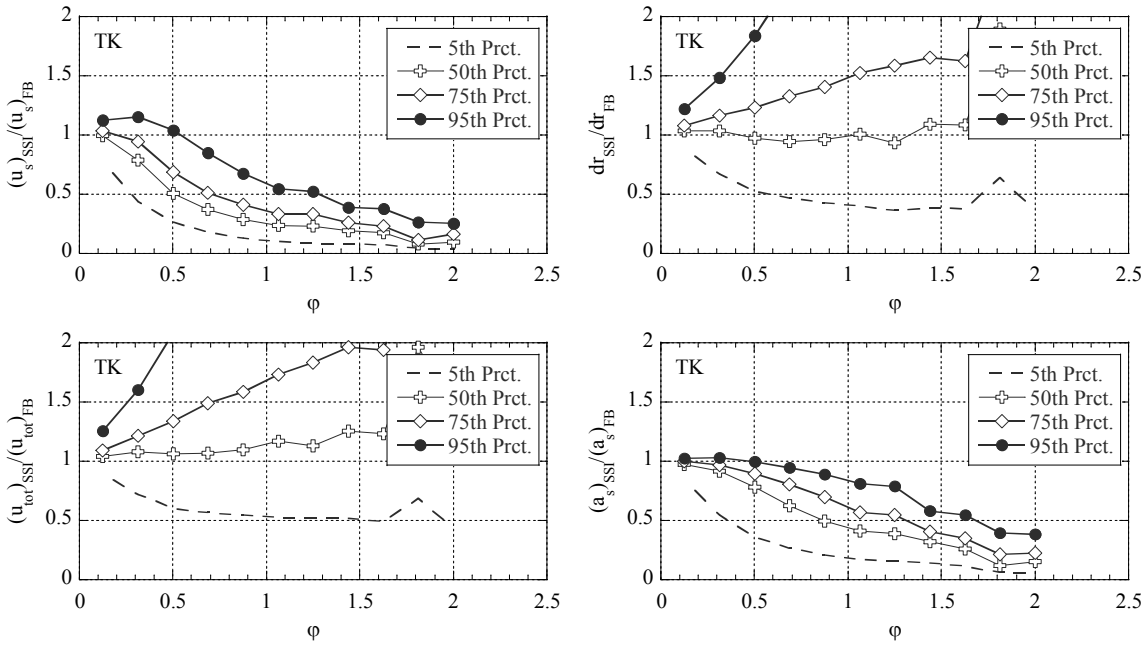

Figure E-27. The effects of $\varphi = \frac{h_e}{(V_s)_{sec}T_{FB}}(h_e/r)^{0.25}$ on structural response modification factors.

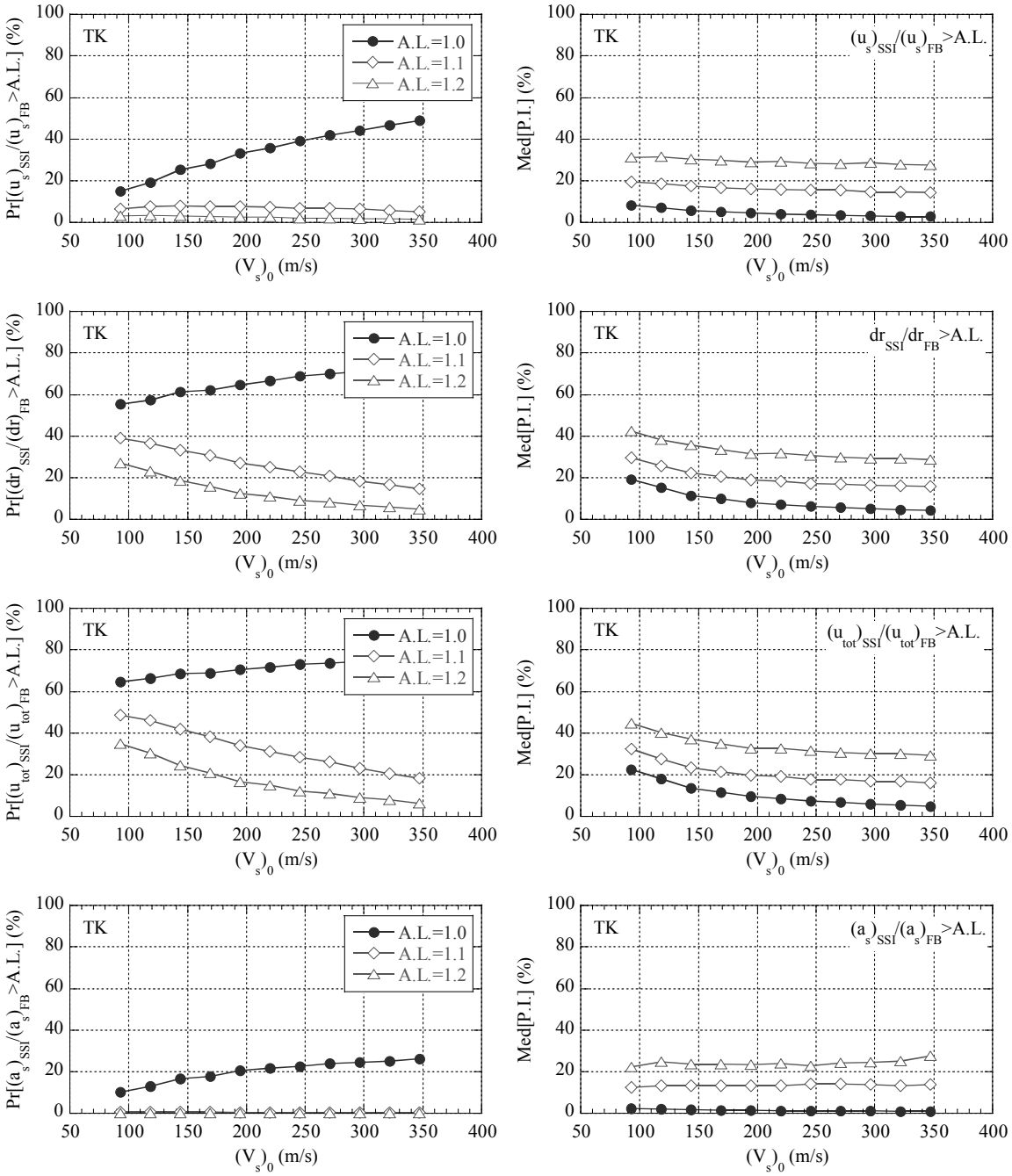

Figure E-28. Risk of detrimental SSI effects based on variation in initial soil shear wave velocity: (left) probability of amplification in the response; (right) level of increase in the demand.

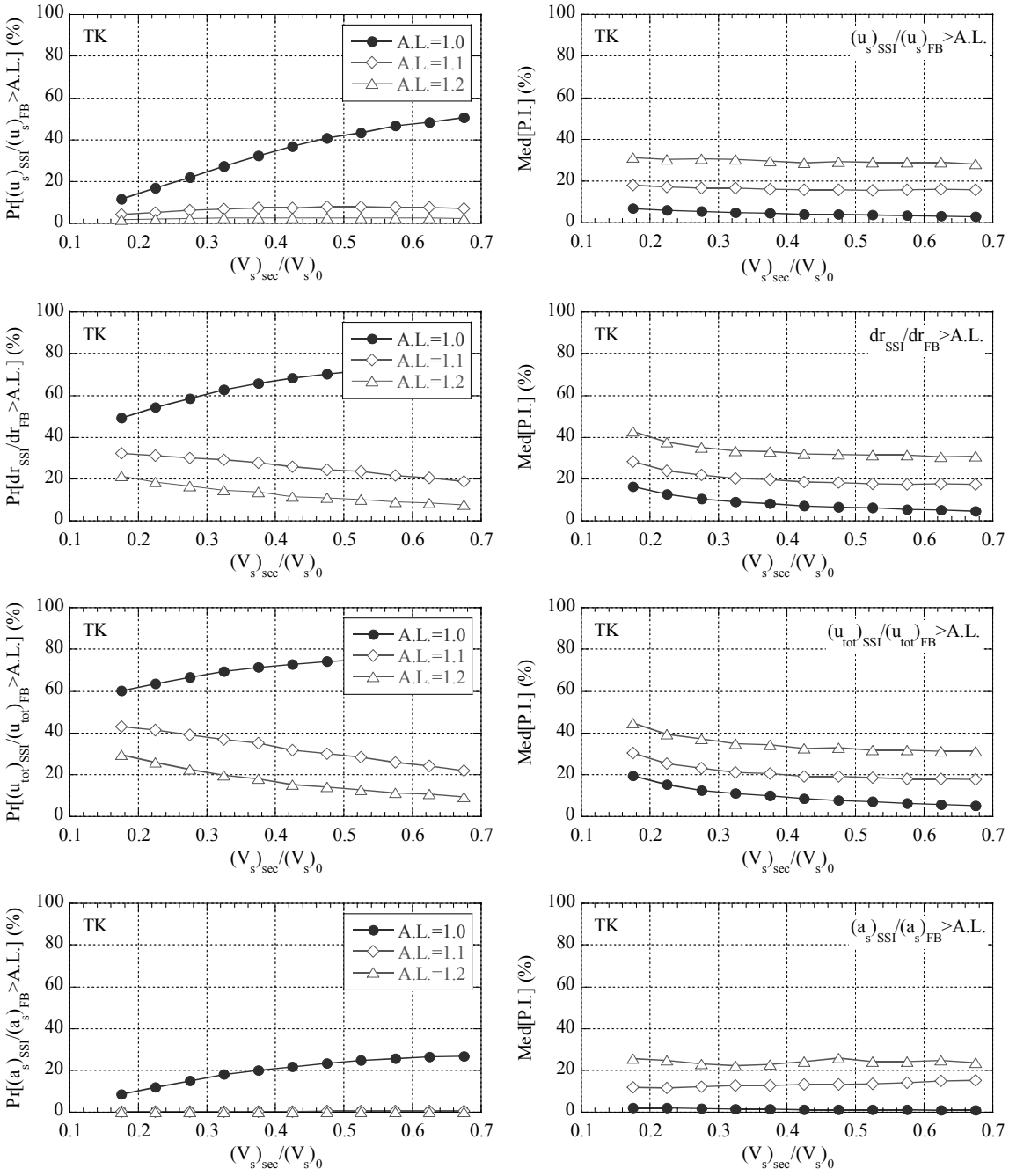

Figure E-29. Risk of detrimental SSI effects based on variation in shear wave velocity degradation.

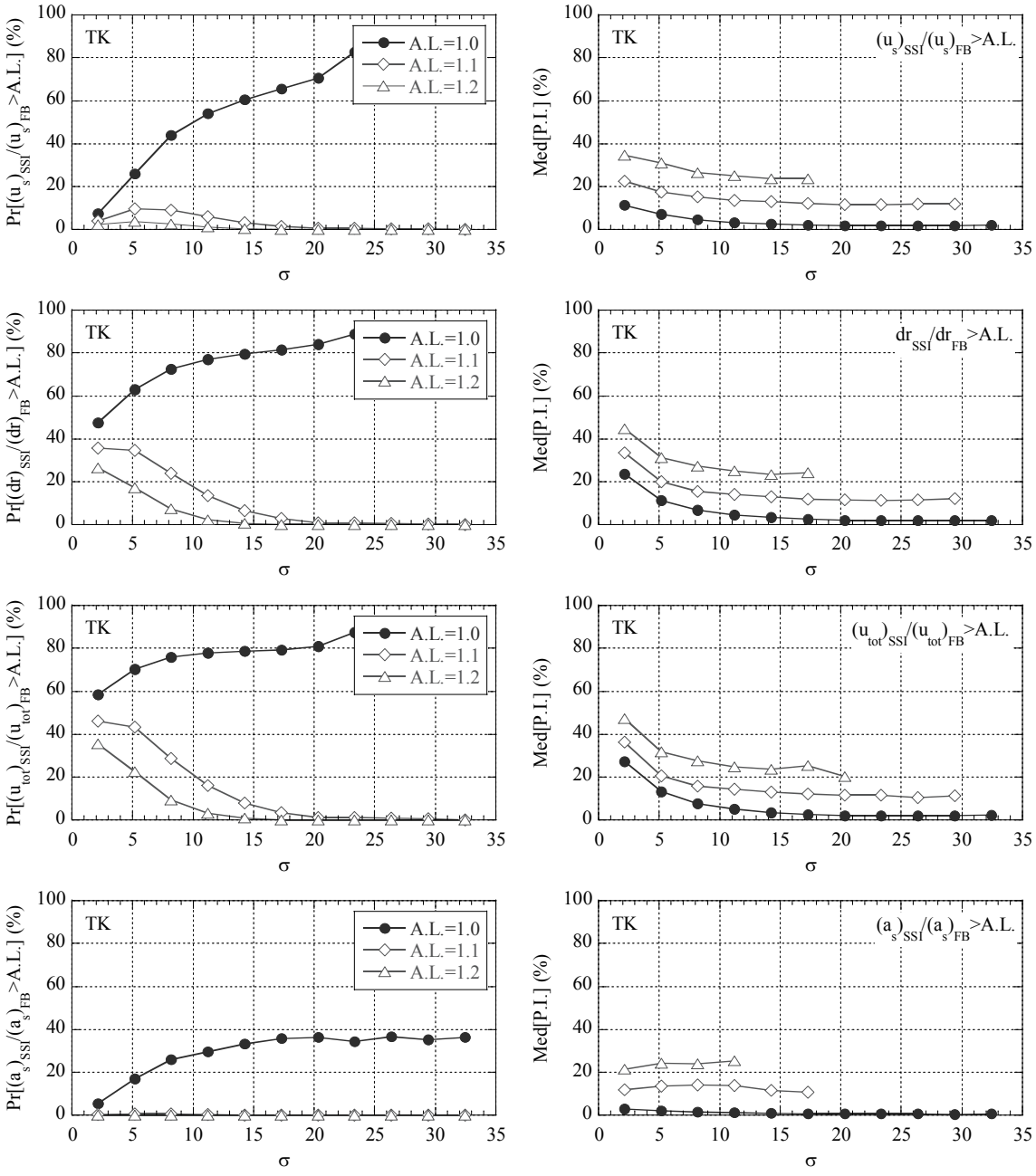

Figure E-30. Risk of detrimental SSI effects based on variation in of $\sigma = (V_s)_{sec}T_{FB})/h_e$.

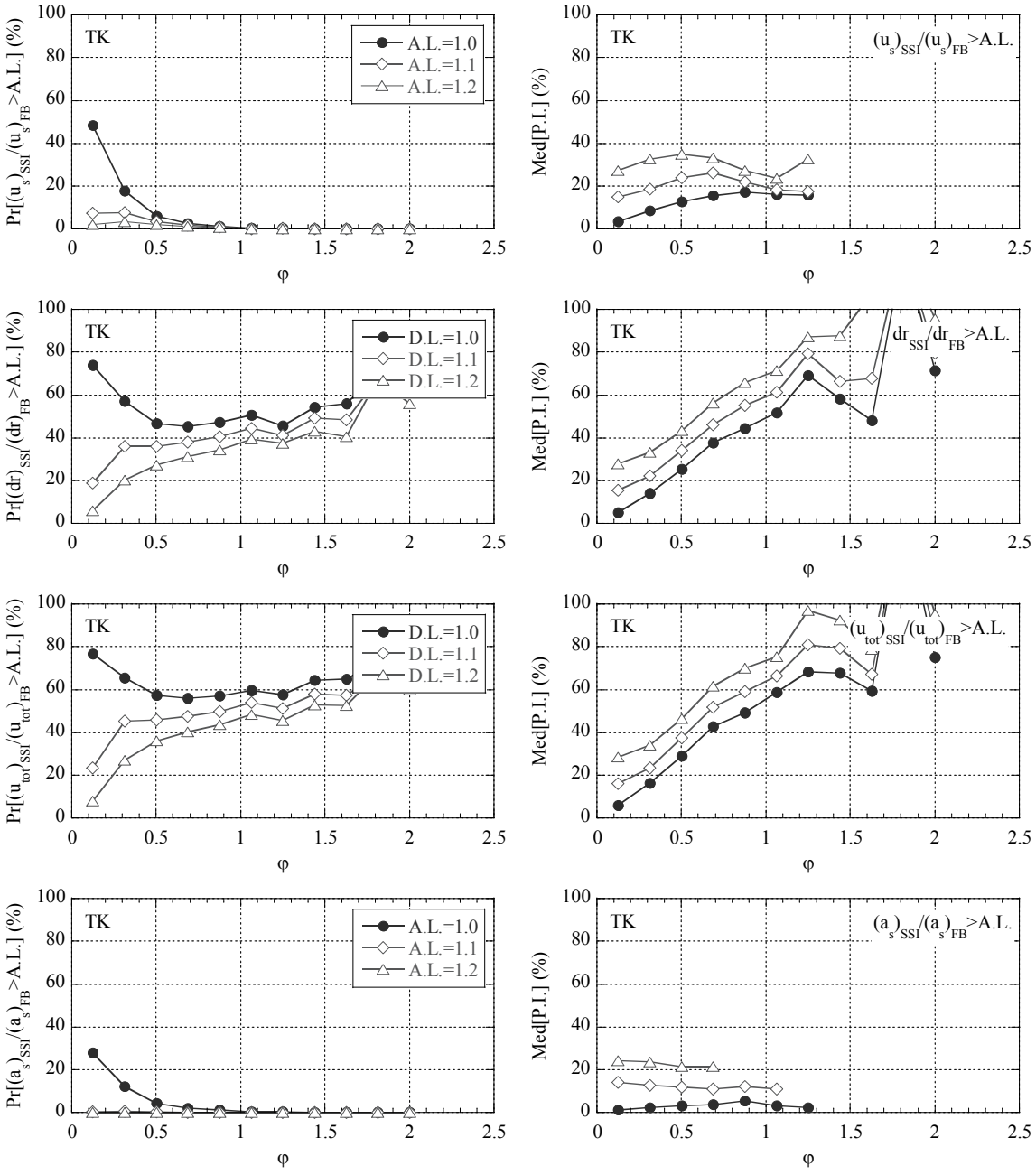

Figure E-31. Risk of detrimental SSI effects based on variation in of $\varphi = \frac{h_e}{(V_s)_{sec} T_{FB}} (h_e/r)^{0.25}$.

APPENDIX

F. Results for Behaviour of Macro-Element under Different Loading Scenarios

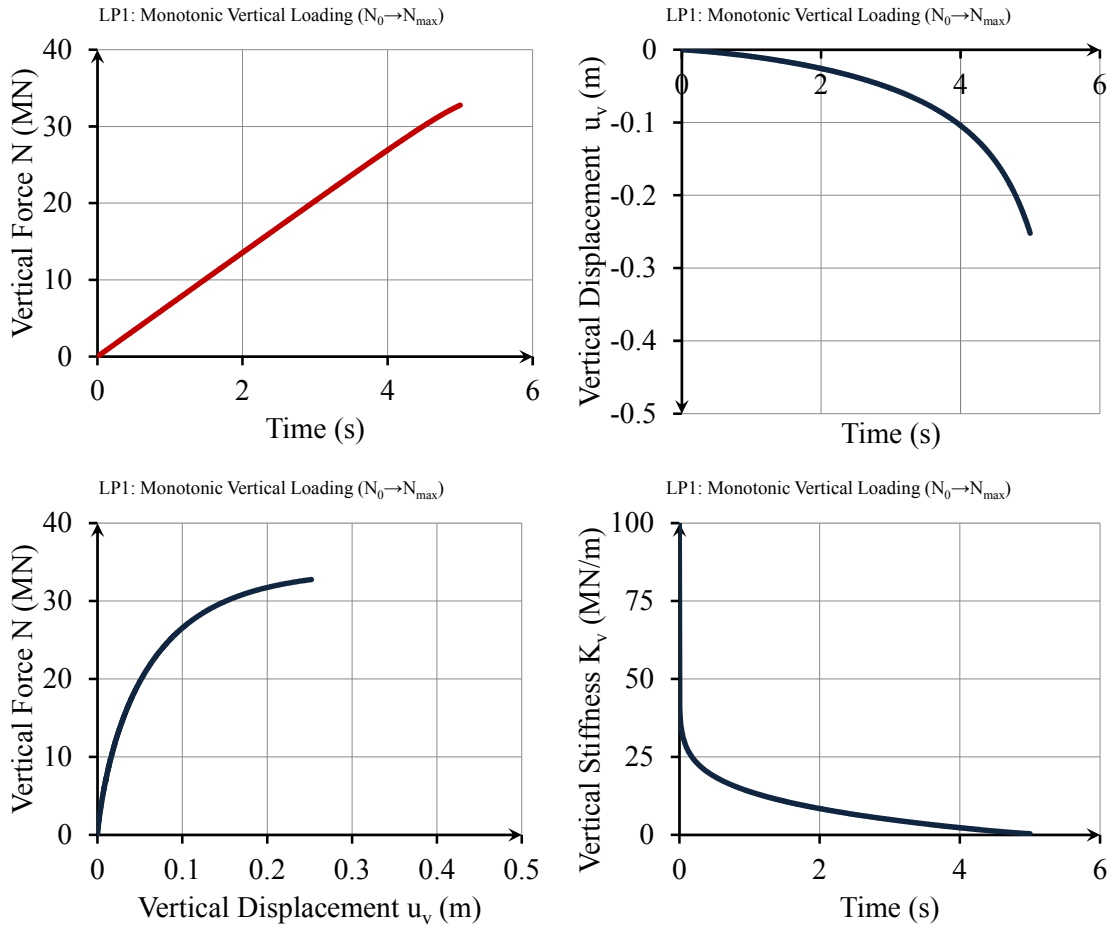

Figure F-1. The behaviour of macro-element under monotonic vertical loading ($N_0 \rightarrow N_{max}$).

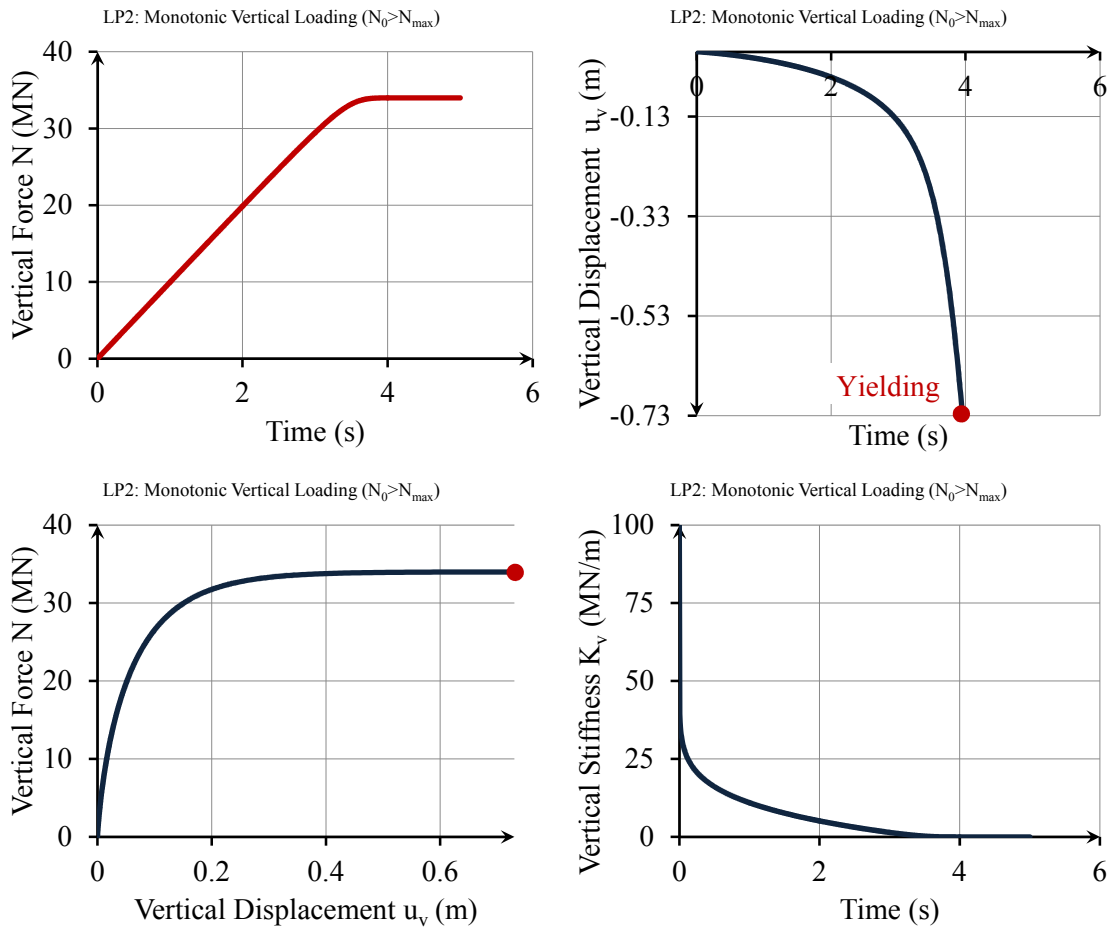

Figure F-2. The behaviour of macro-element under monotonic vertical loading (N_0>N_{max}).

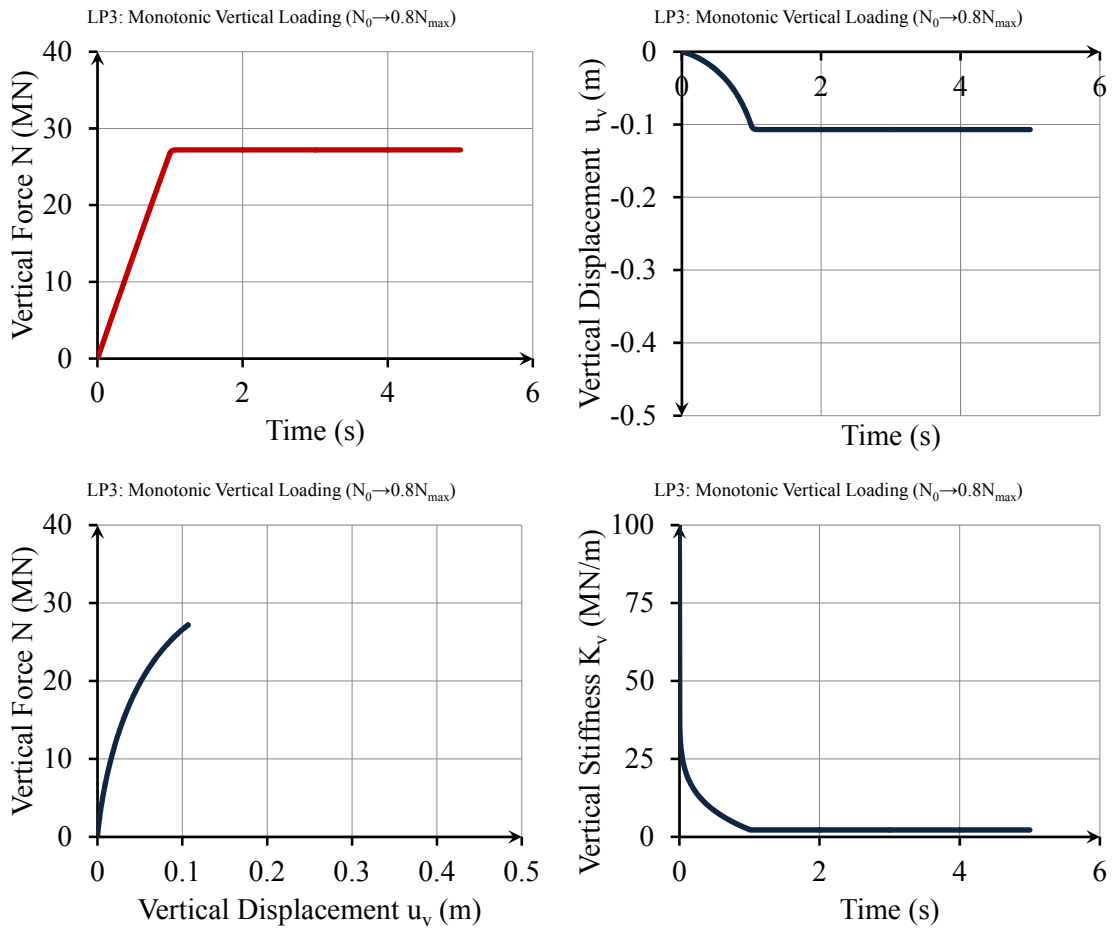

Figure F-3. The behaviour of macro-element under monotonic vertical loading (N_0→0.8N_{max}).

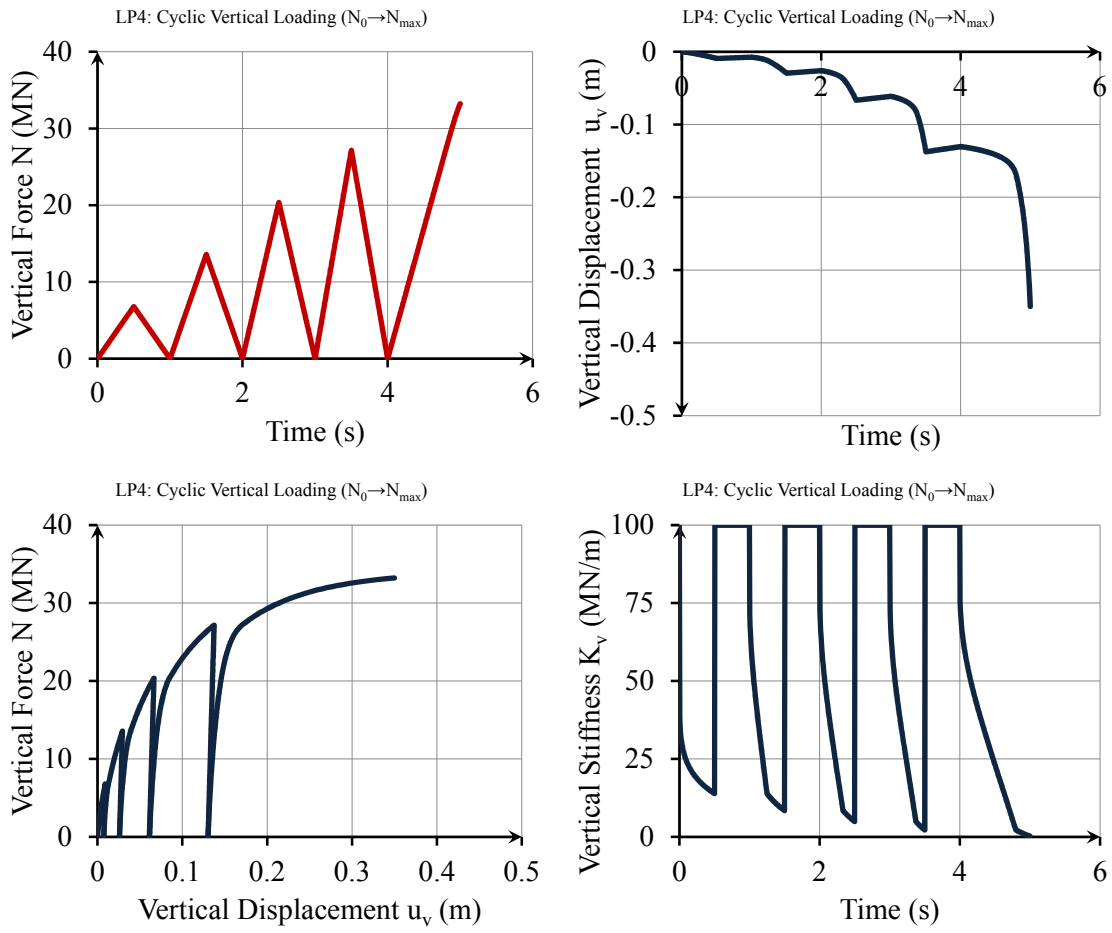

Figure F-4. The behaviour of macro-element under monotonic vertical loading ($N_0 \rightarrow N_{max}$).

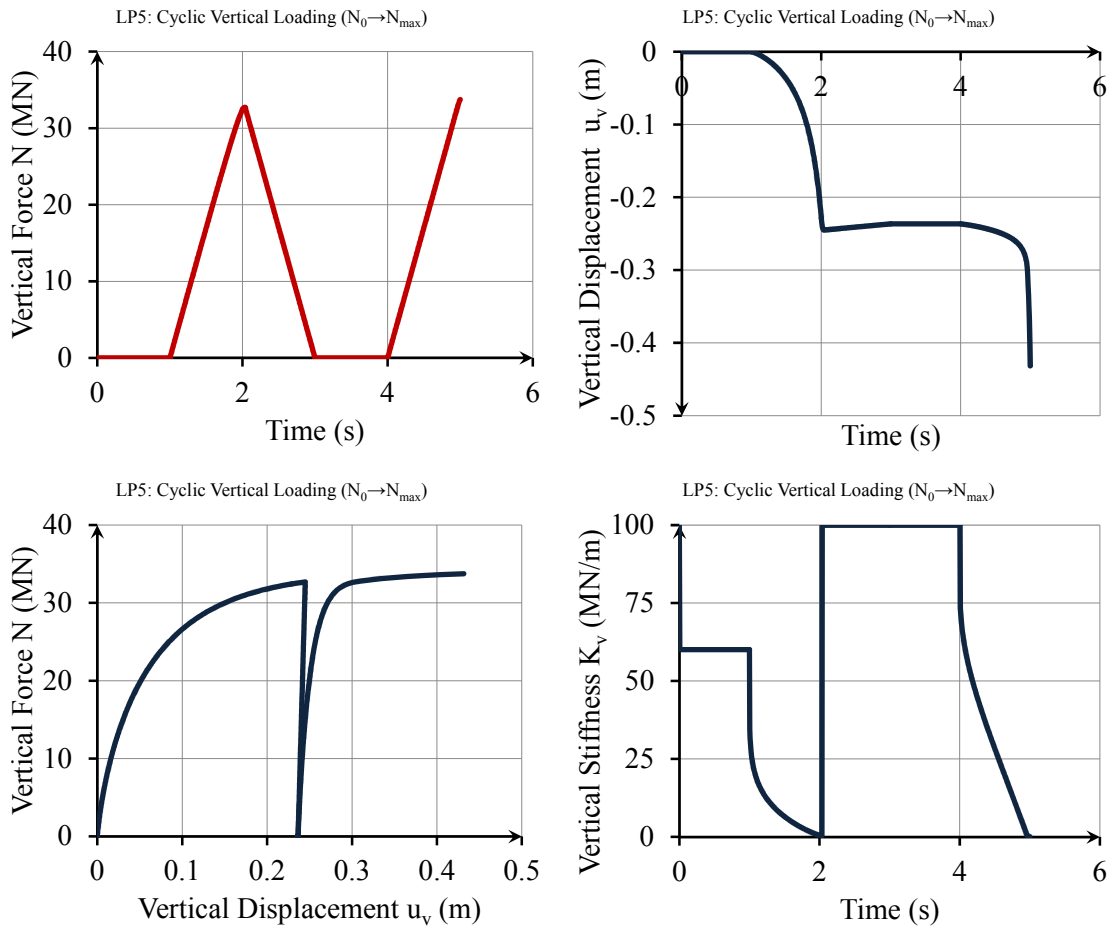

Figure F-5. The behaviour of macro-element under monotonic vertical loading ($N_0 \rightarrow N_{max}$).

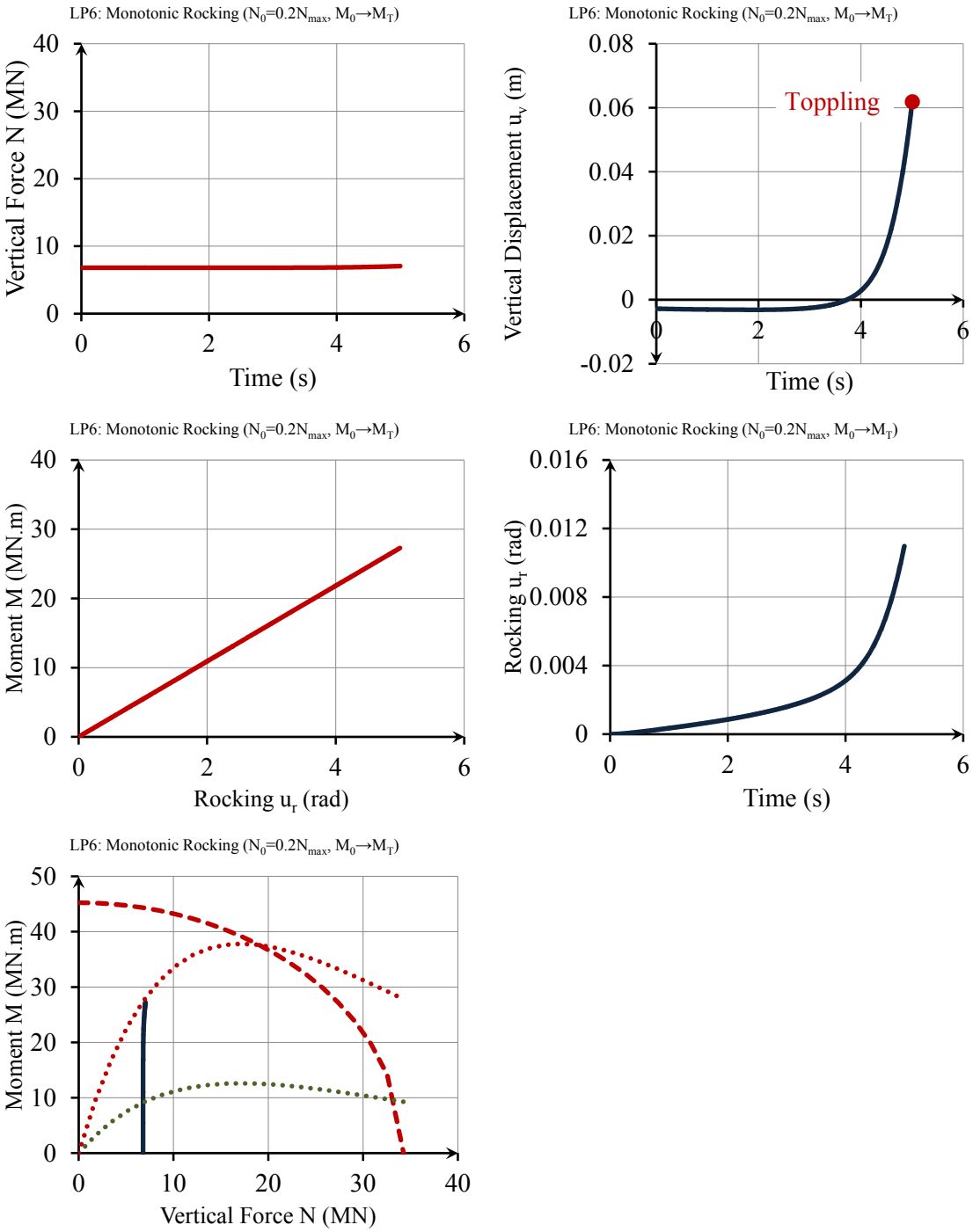

Figure F-6. The behaviour of macro-element under monotonic rocking (N_0=0.2N_{max}, M_0→M_T).

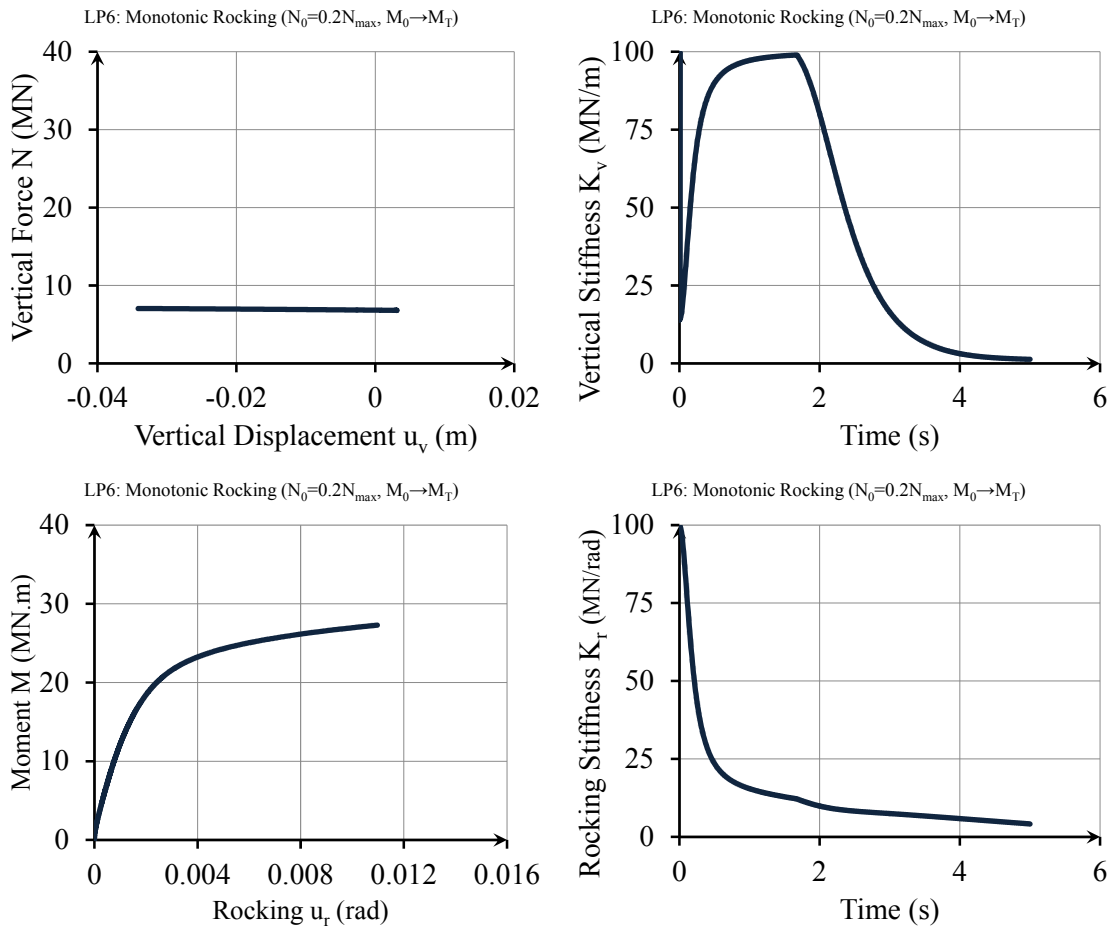

Figure F-6. *Continued*.

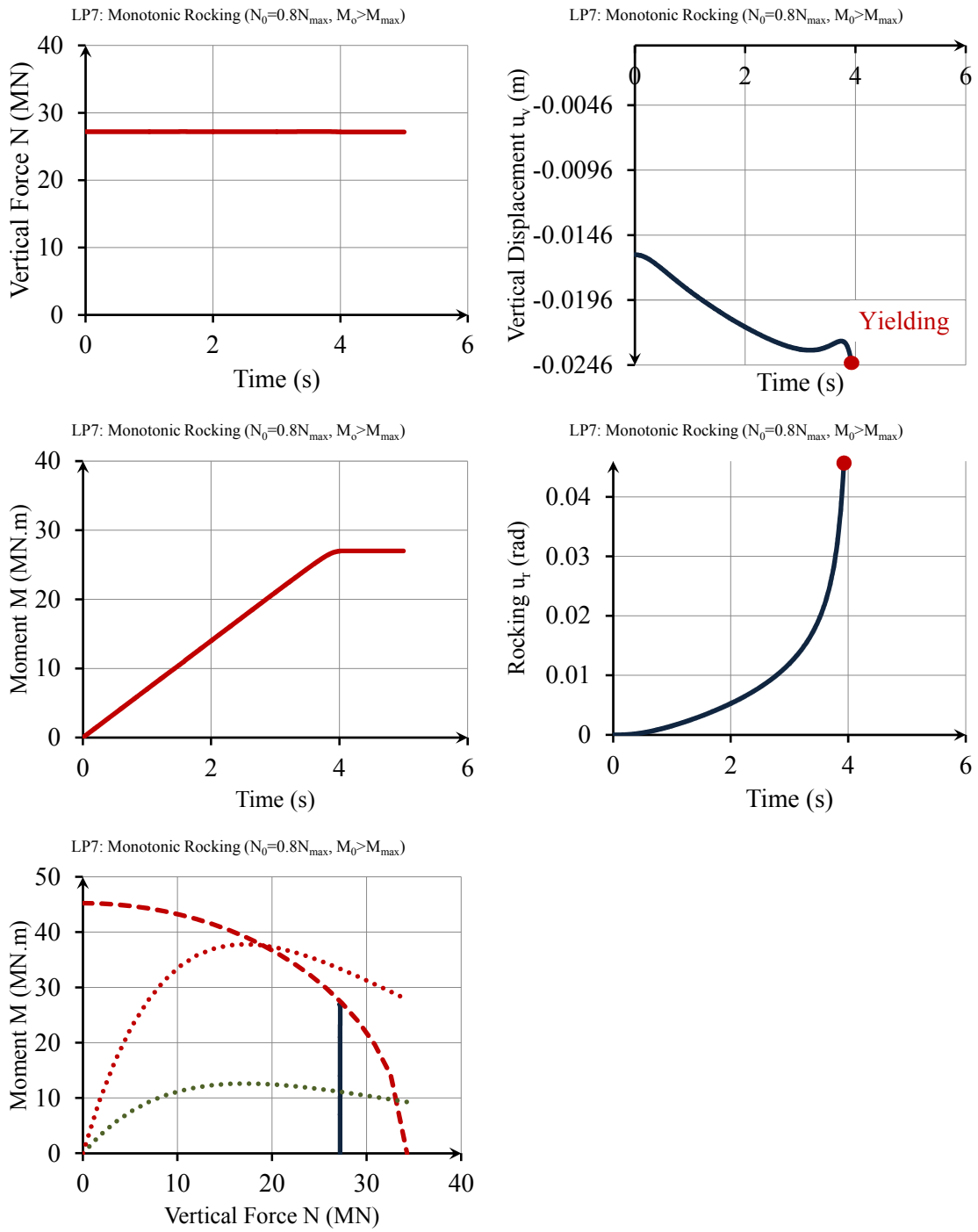

Figure F-7. The behaviour of macro-element under monotonic rocking (N_0=0.8N_{max}, M_0>M_{max}).

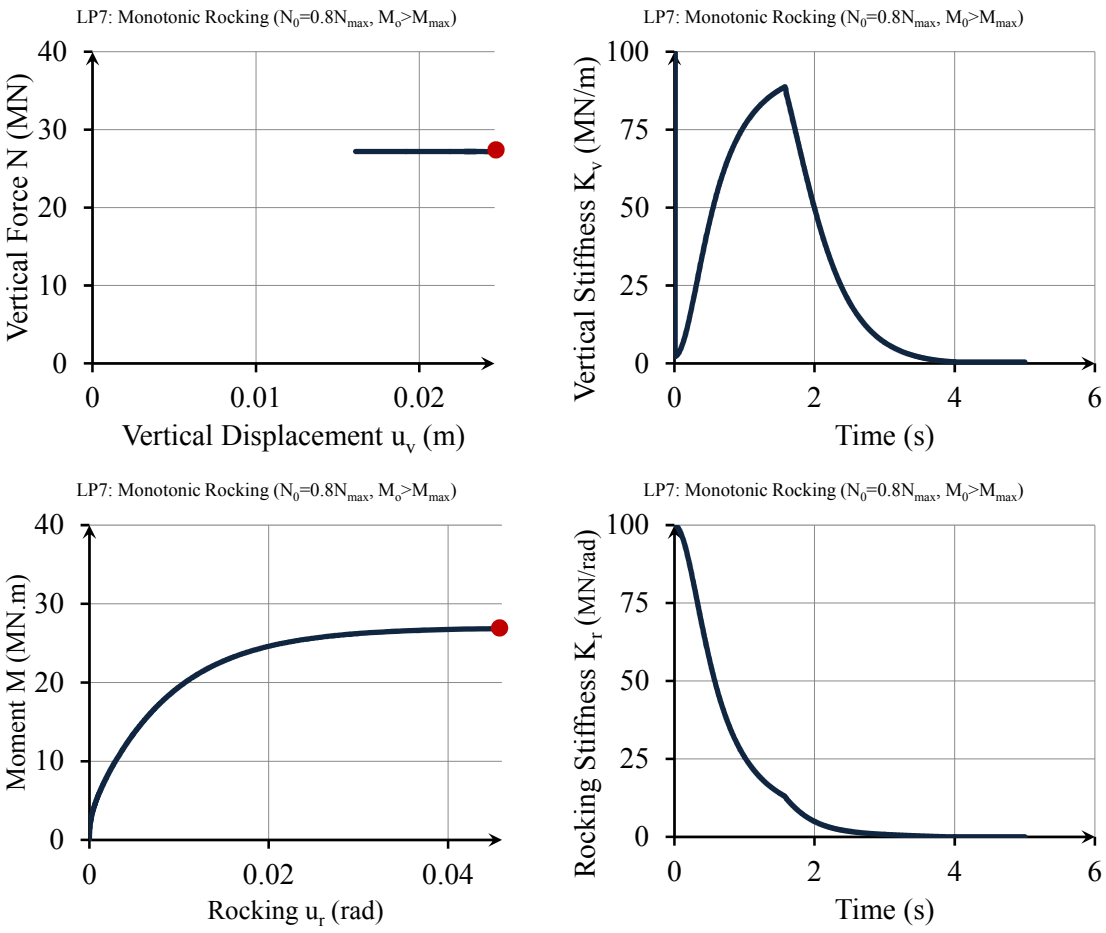

Figure F-7. *Continued*.

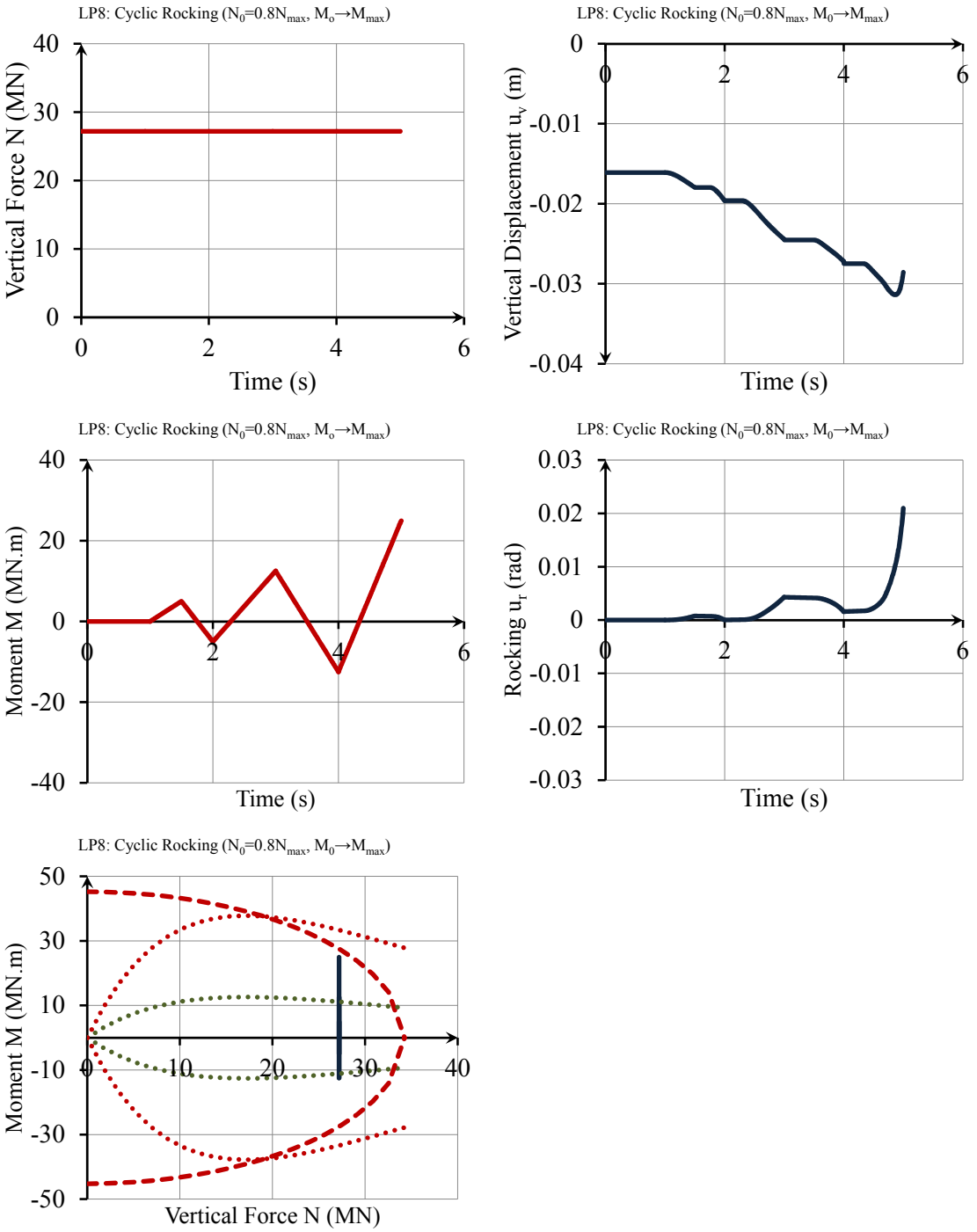

Figure F-8. The behaviour of macro-element under cyclic rocking (N_0=0.8N_{max}, M_0→M_{max}).

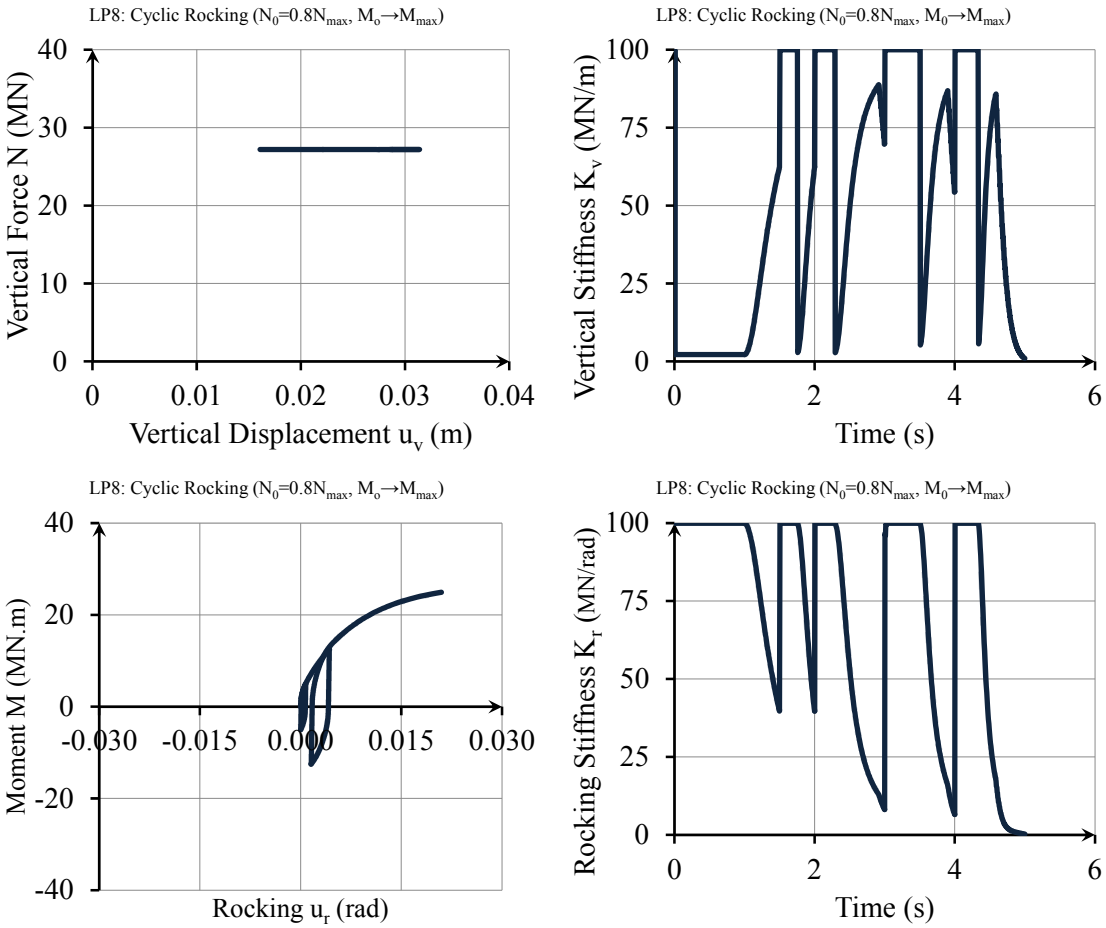

Figure F-8. *Continued*.

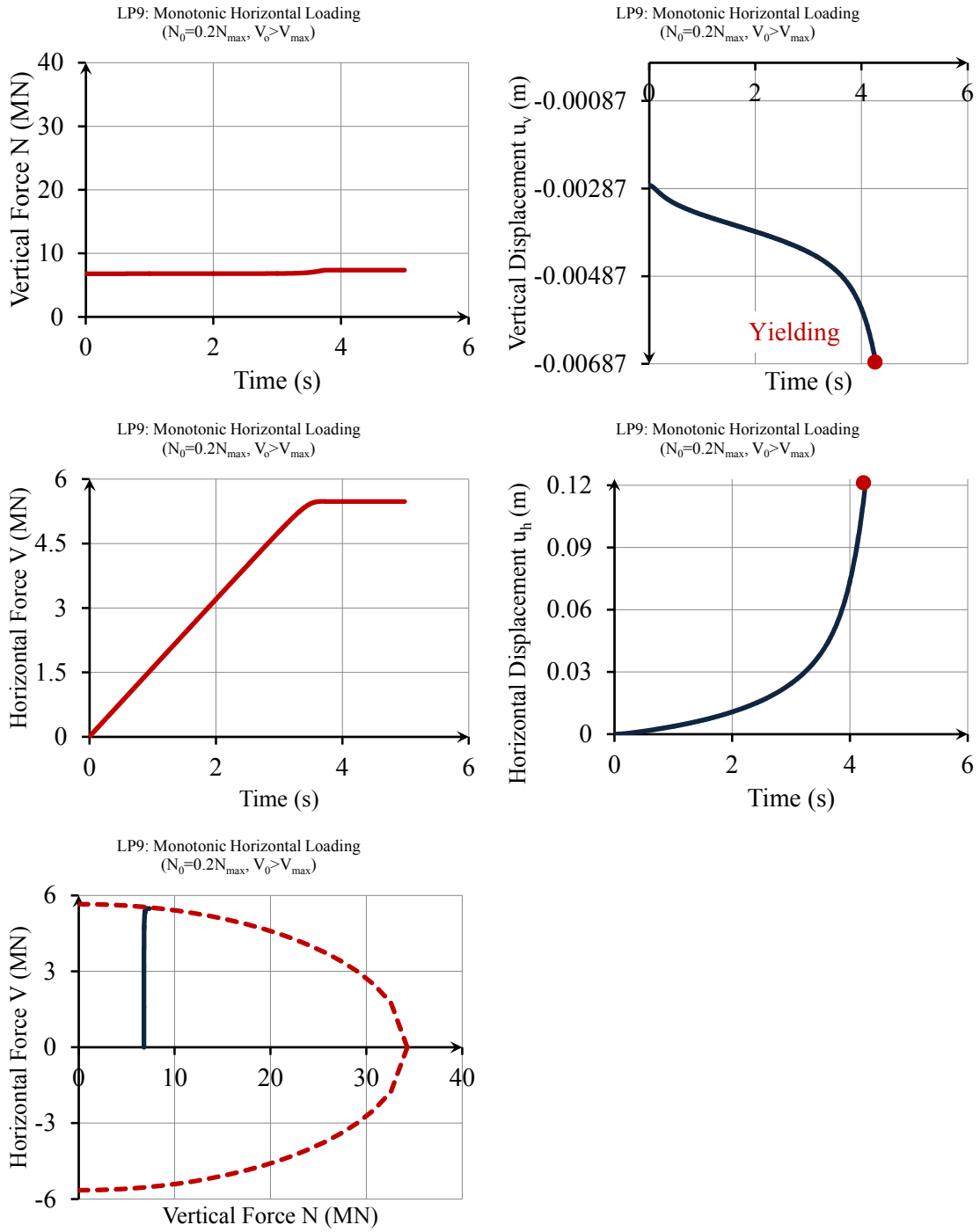

Figure F-9. The behaviour of macro-element under monotonic horizontal loading (N_0=0.2N_{max}, V_0>V_{max}).

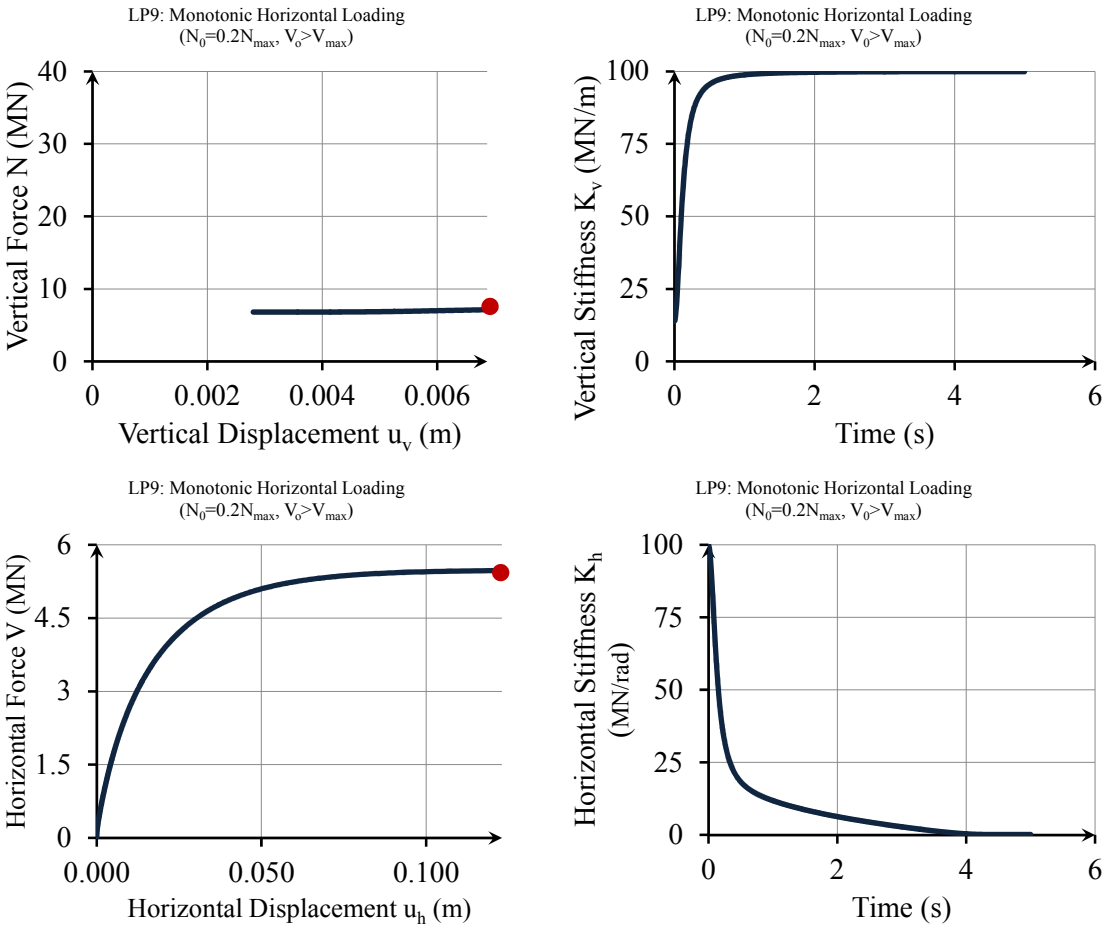

Figure F-9. *Continued*.

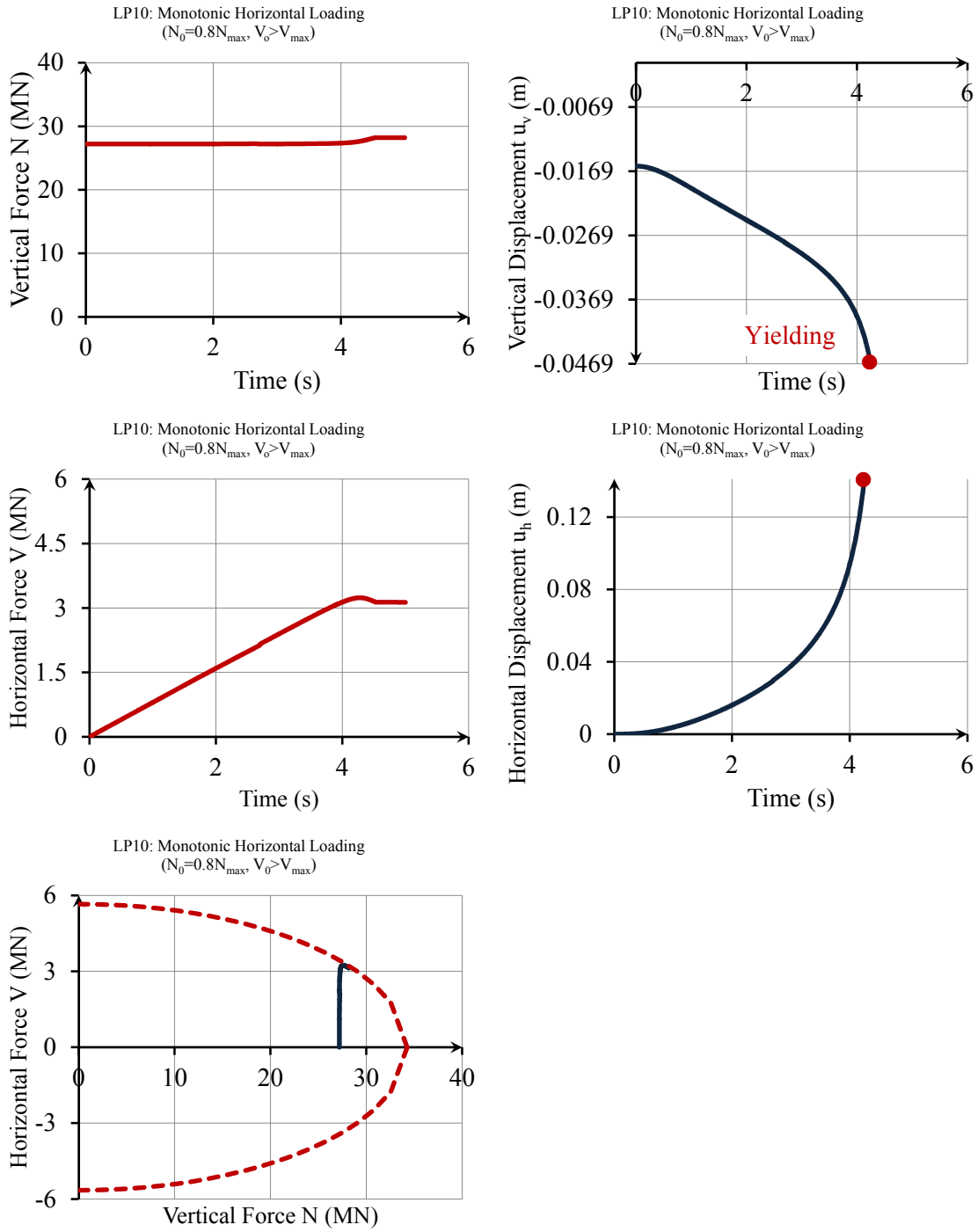

Figure F-10. The behaviour of macro-element under monotonic horizontal loading ($N_0=0.8N_{max}$, $V_0>V_{max}$).

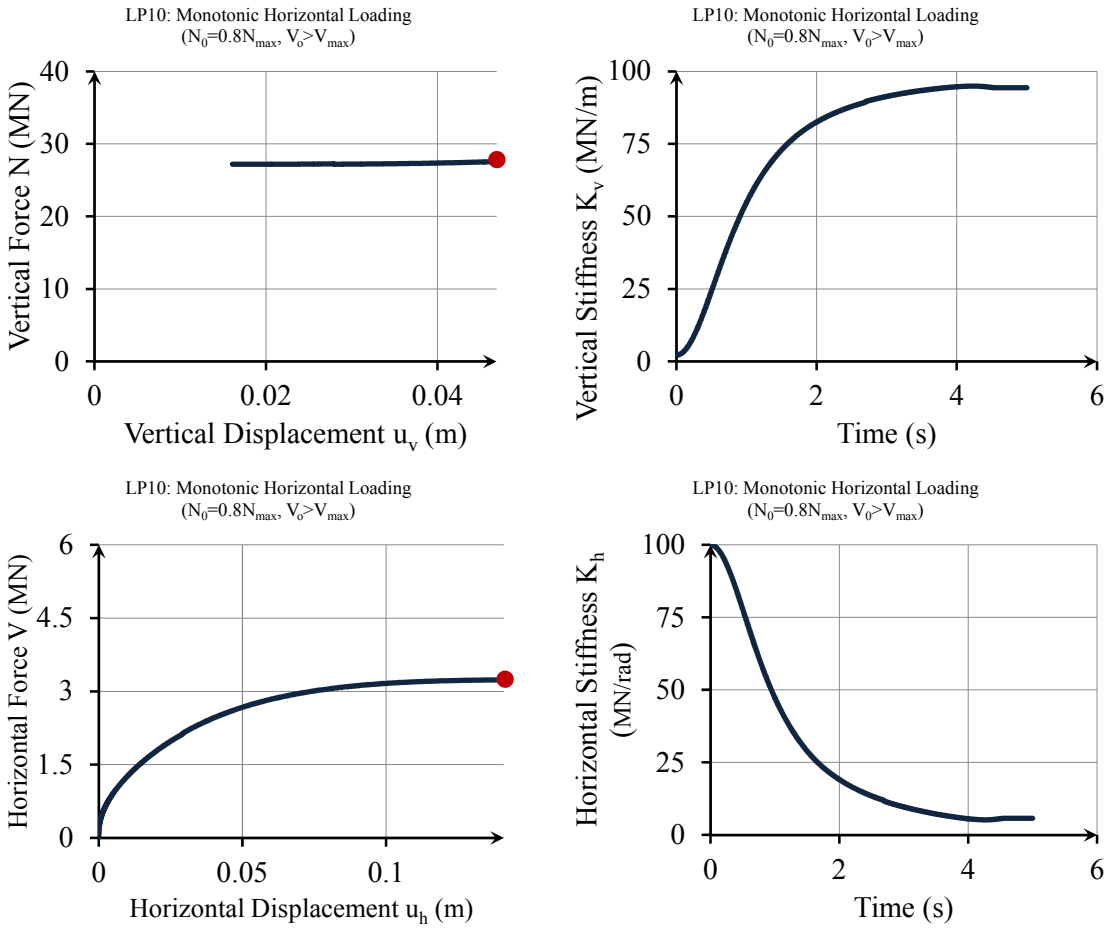

Figure F-10. *Continued*.

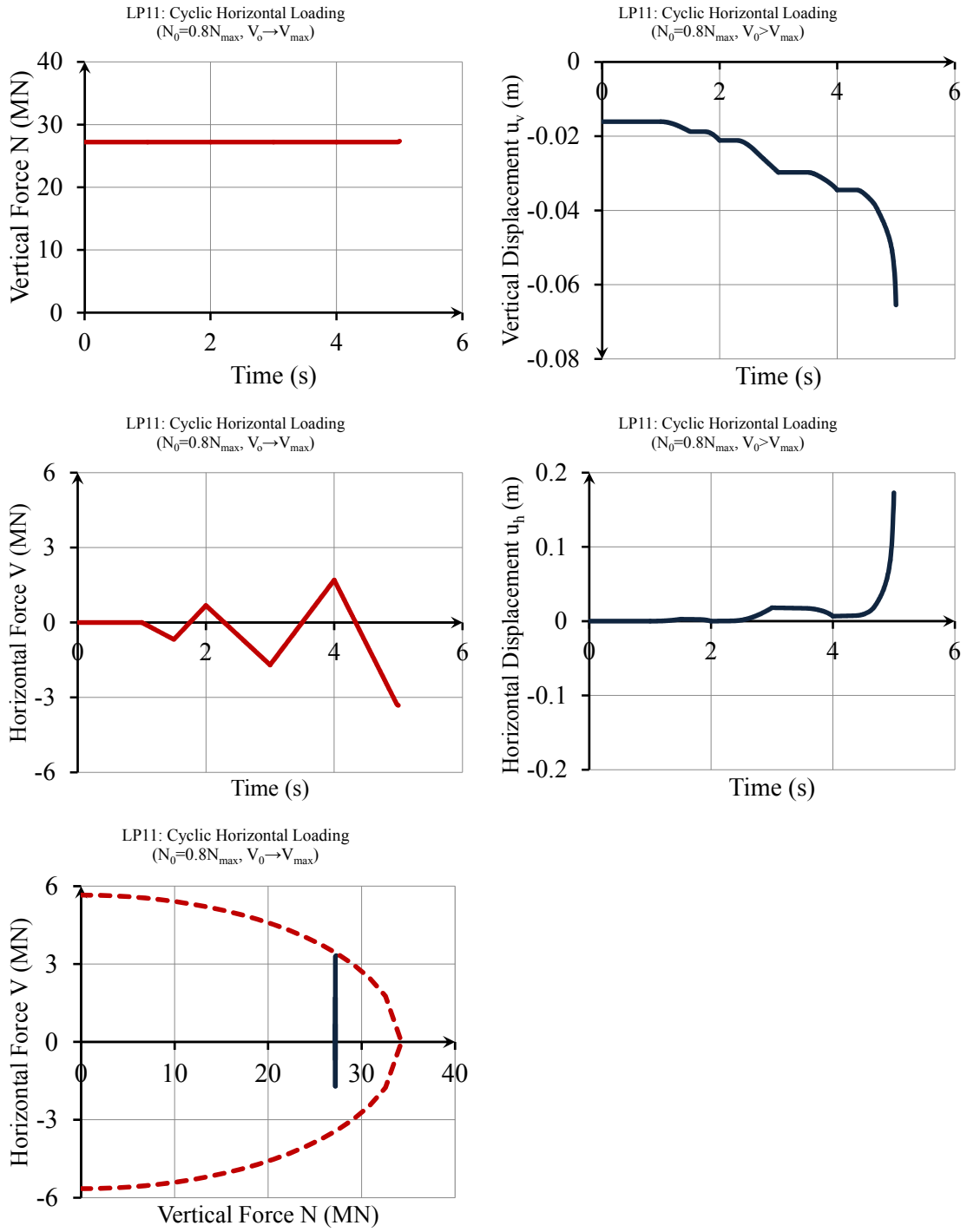

Figure F-11. The behaviour of macro-element under cyclic horizontal loading (N_0=0.8N_{max}, $V_0 \rightarrow V_{max}$).

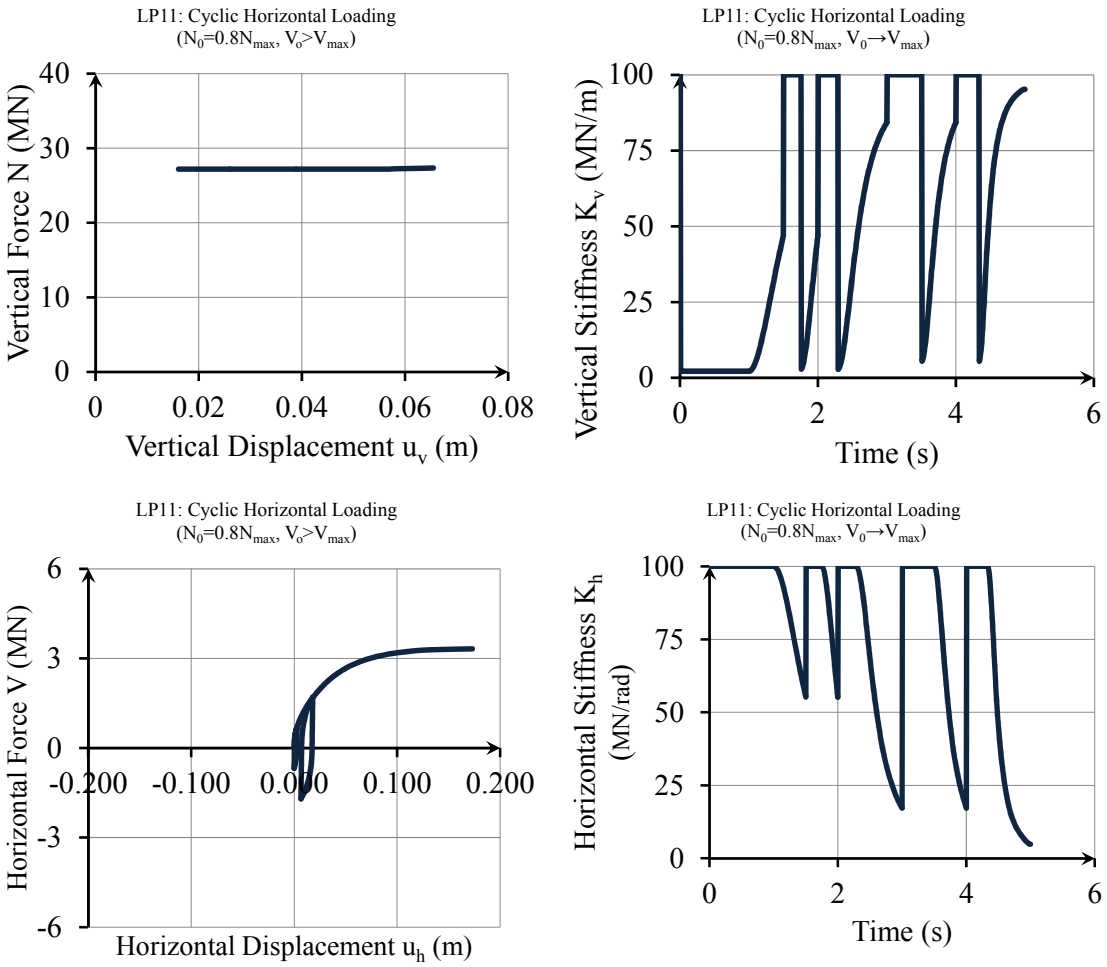

Figure F-11. *Continued*.

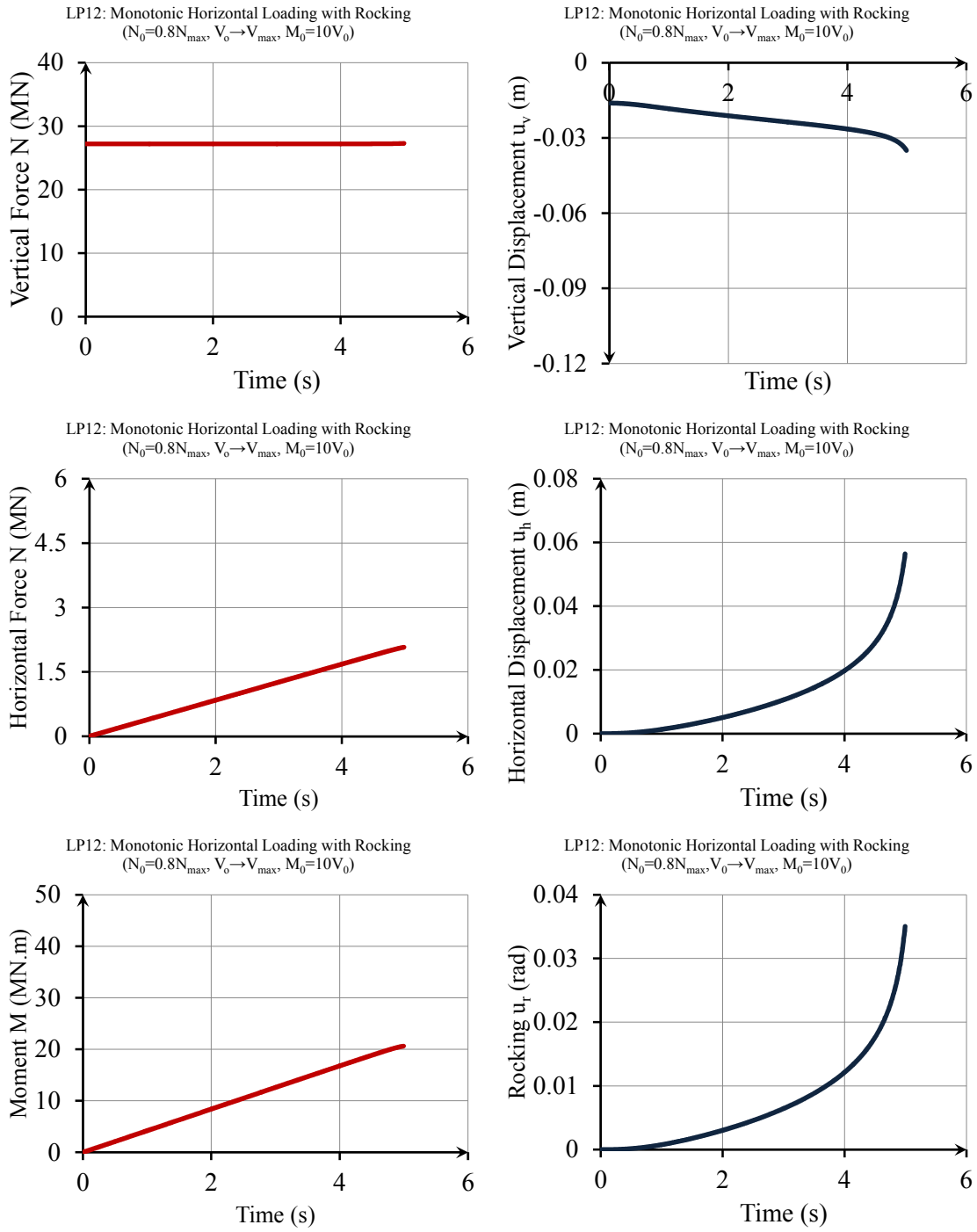

Figure F-12. The behaviour of macro-element under monotonic horizontal loading with rocking ($N_0=0.8N_{max}$, $V_0 \rightarrow V_{max}$, $M_0=10M_{max}$).

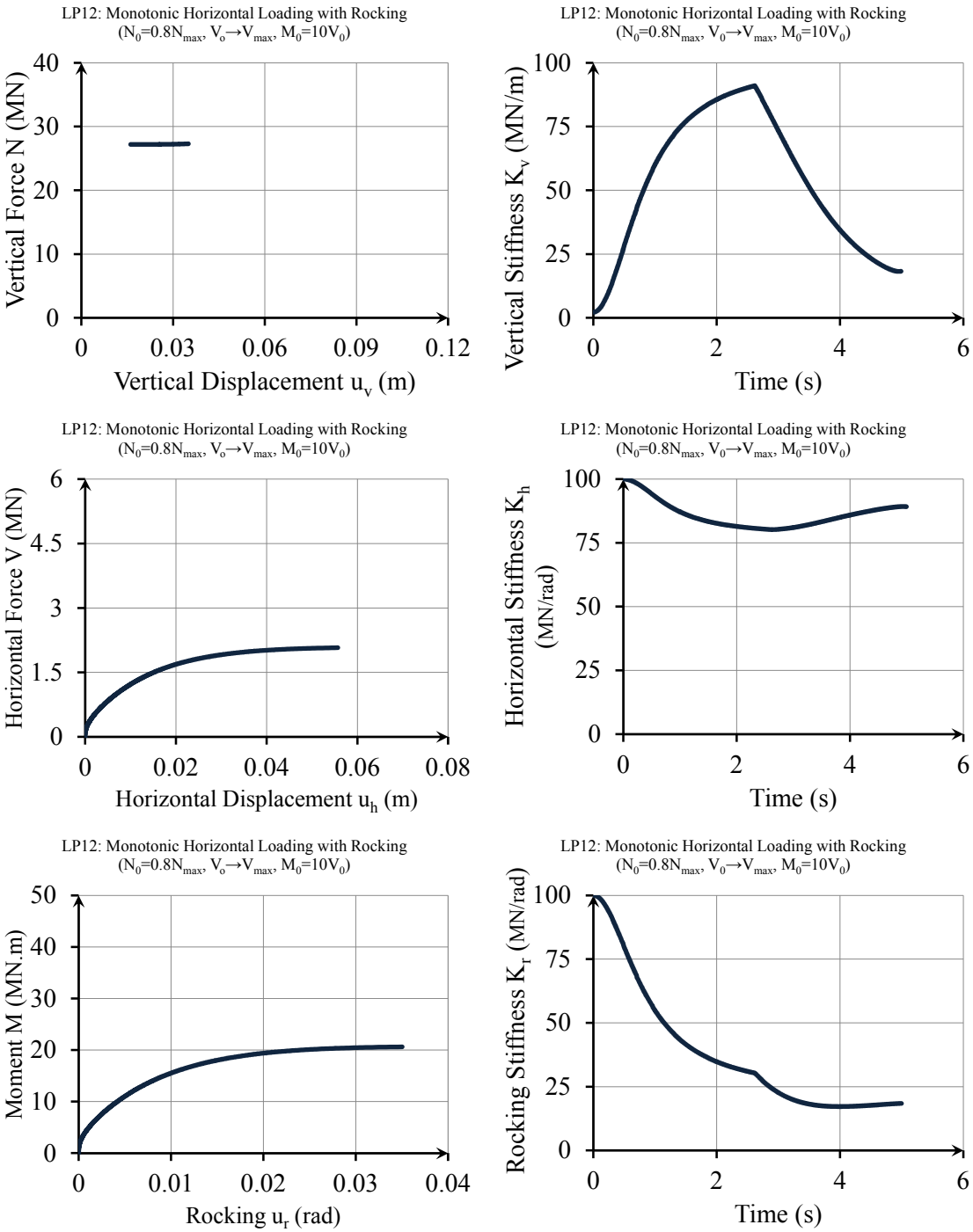

Figure F-12. *Continued*.

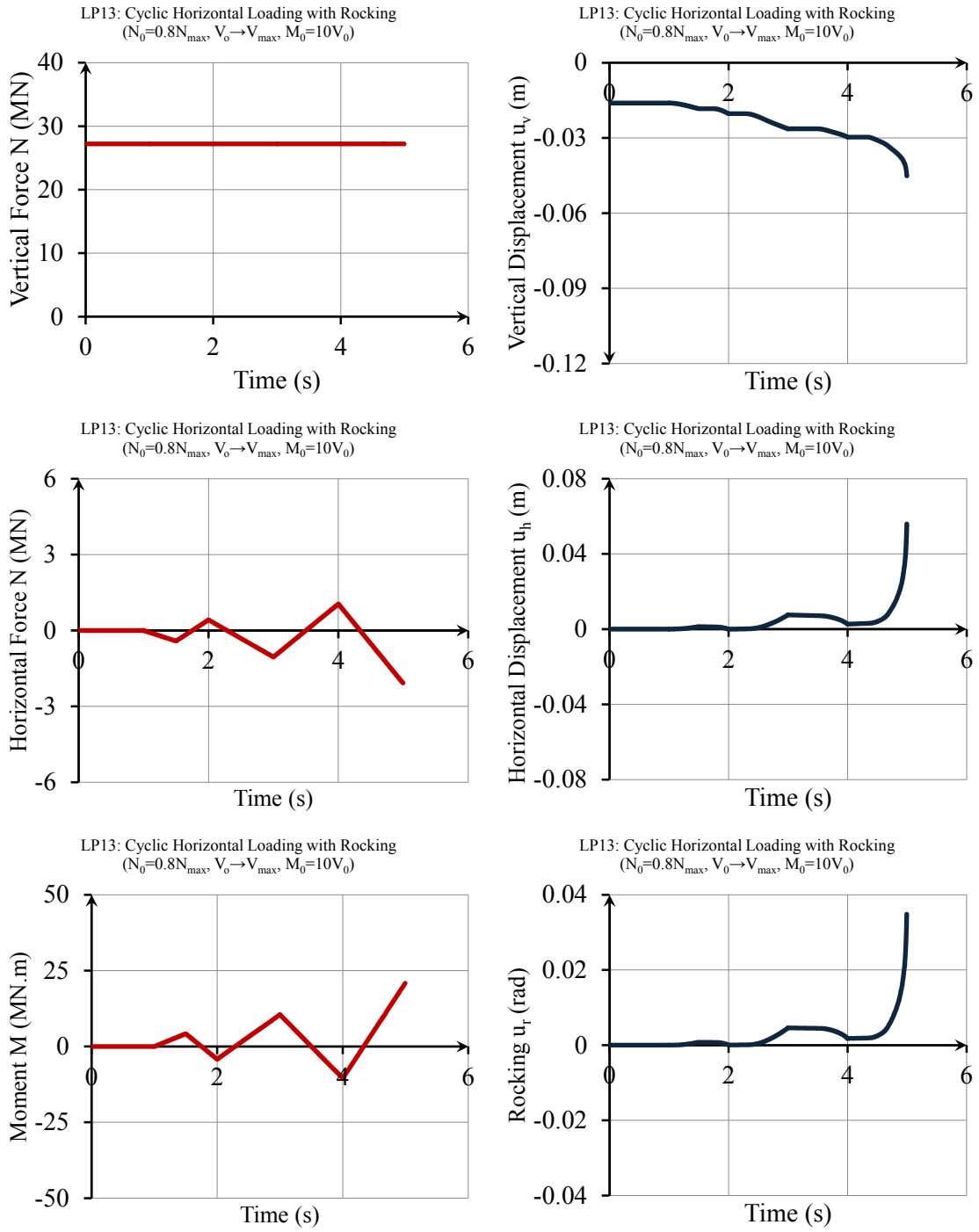

Figure F-13. The behaviour of macro-element under cyclic horizontal loading with rocking ($N_0=0.8N_{max}$, $V_0 \rightarrow V_{max}$, $M_0=10M_{max}$).

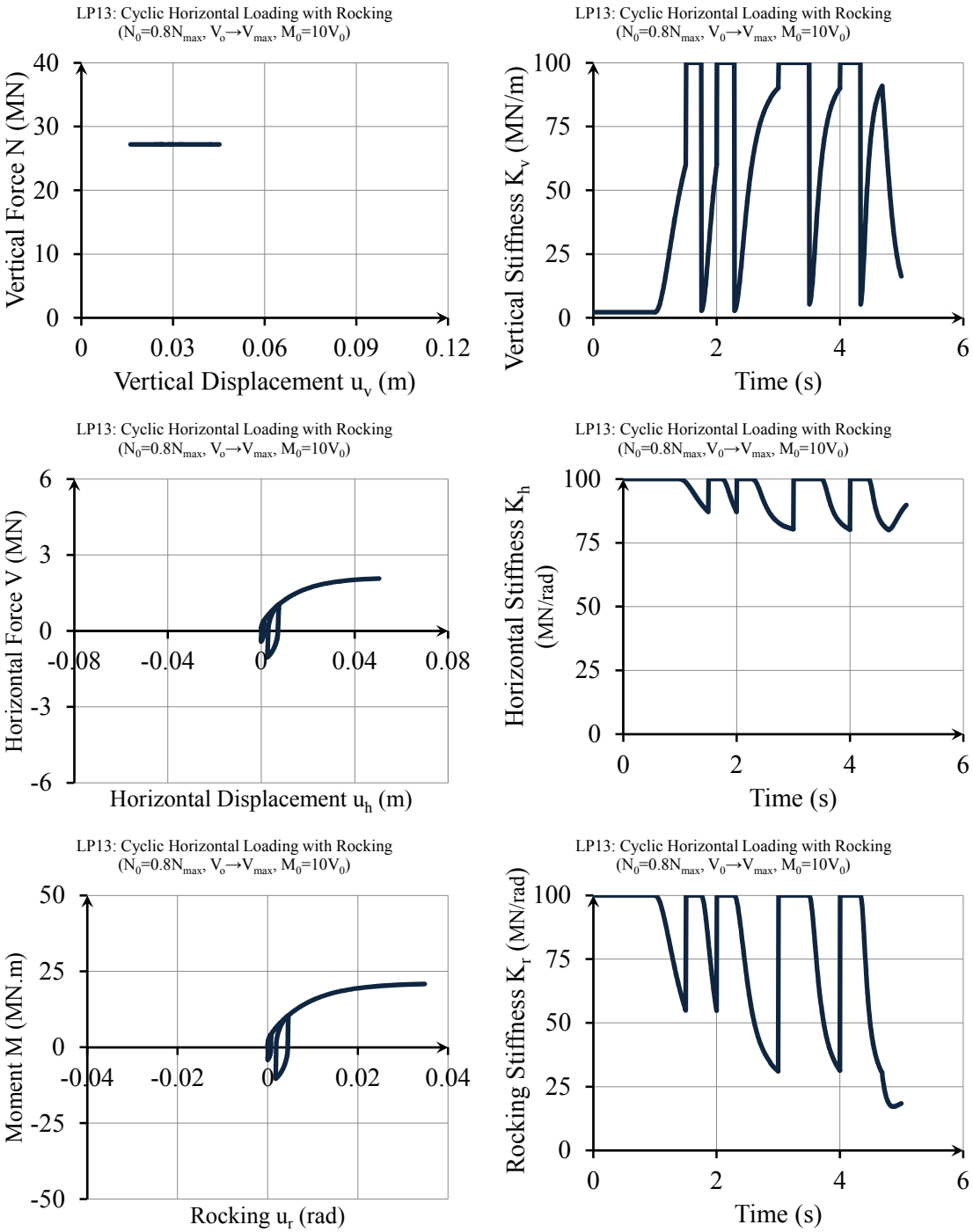

Figure F-13. *Continued*.

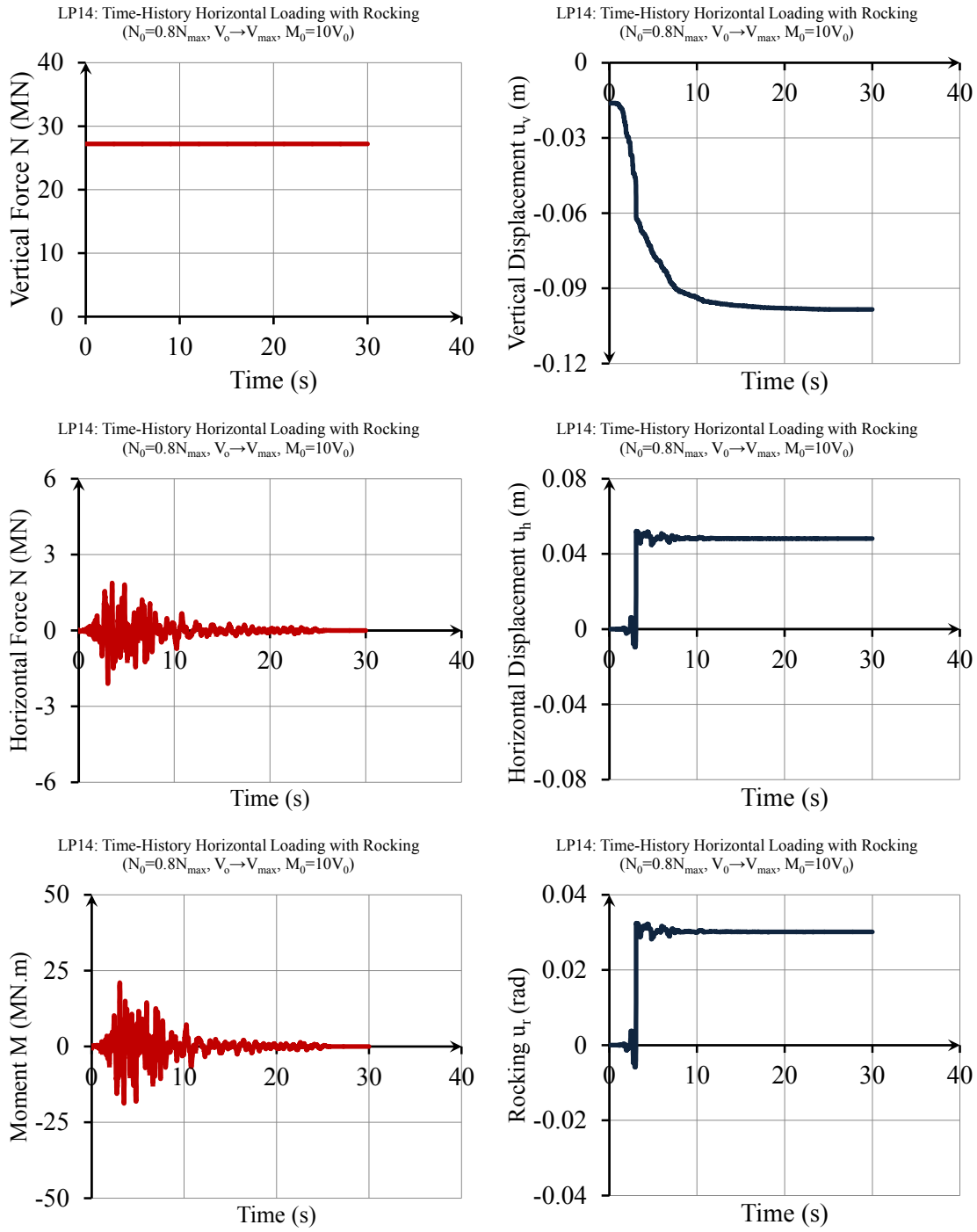

Figure F-14. The behaviour of macro-element under time-history horizontal loading with rocking (N_0=0.8N_{max}, V_0→V_{max}, M_0=10M_{max}).

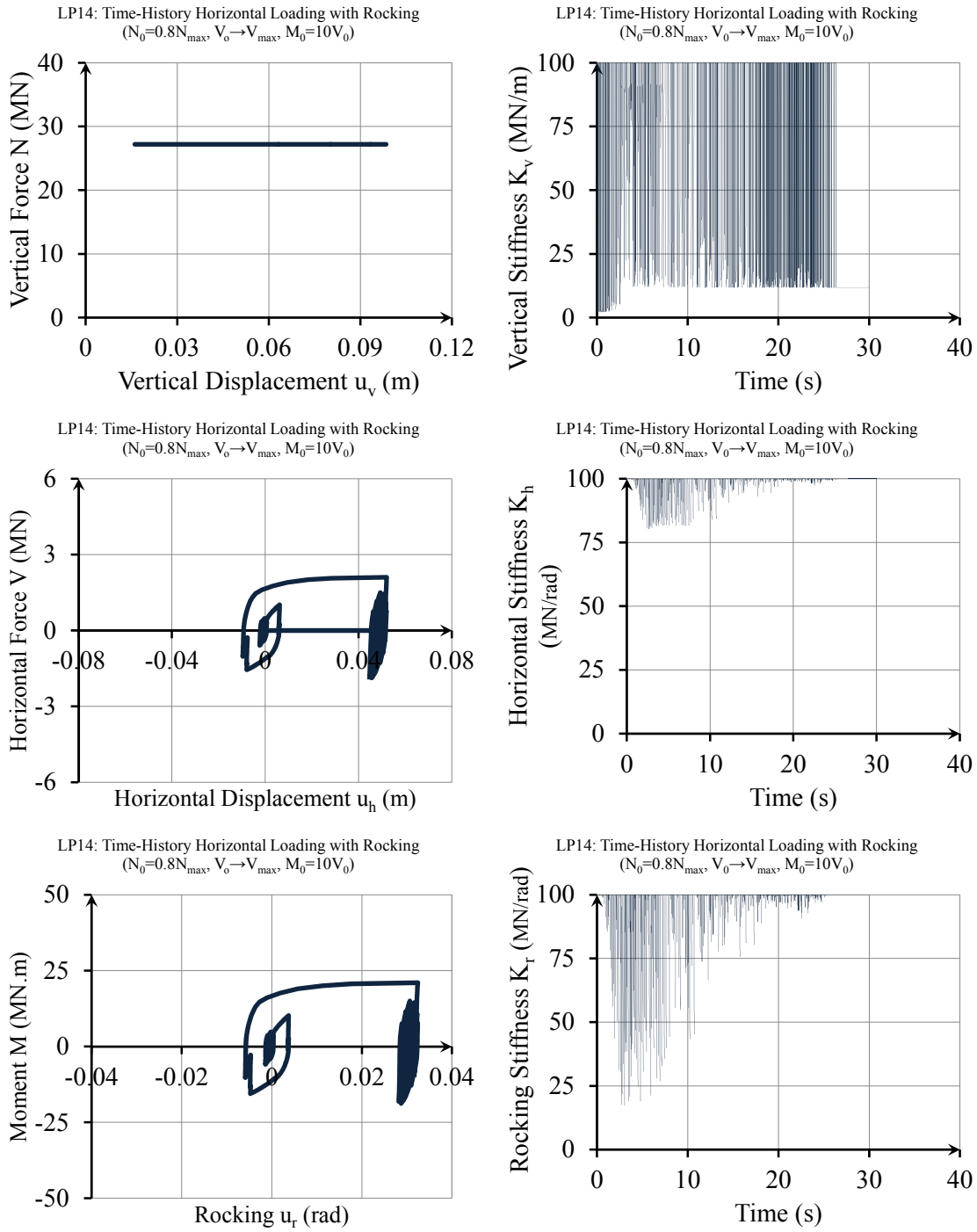

Figure F-14. *Continued*.

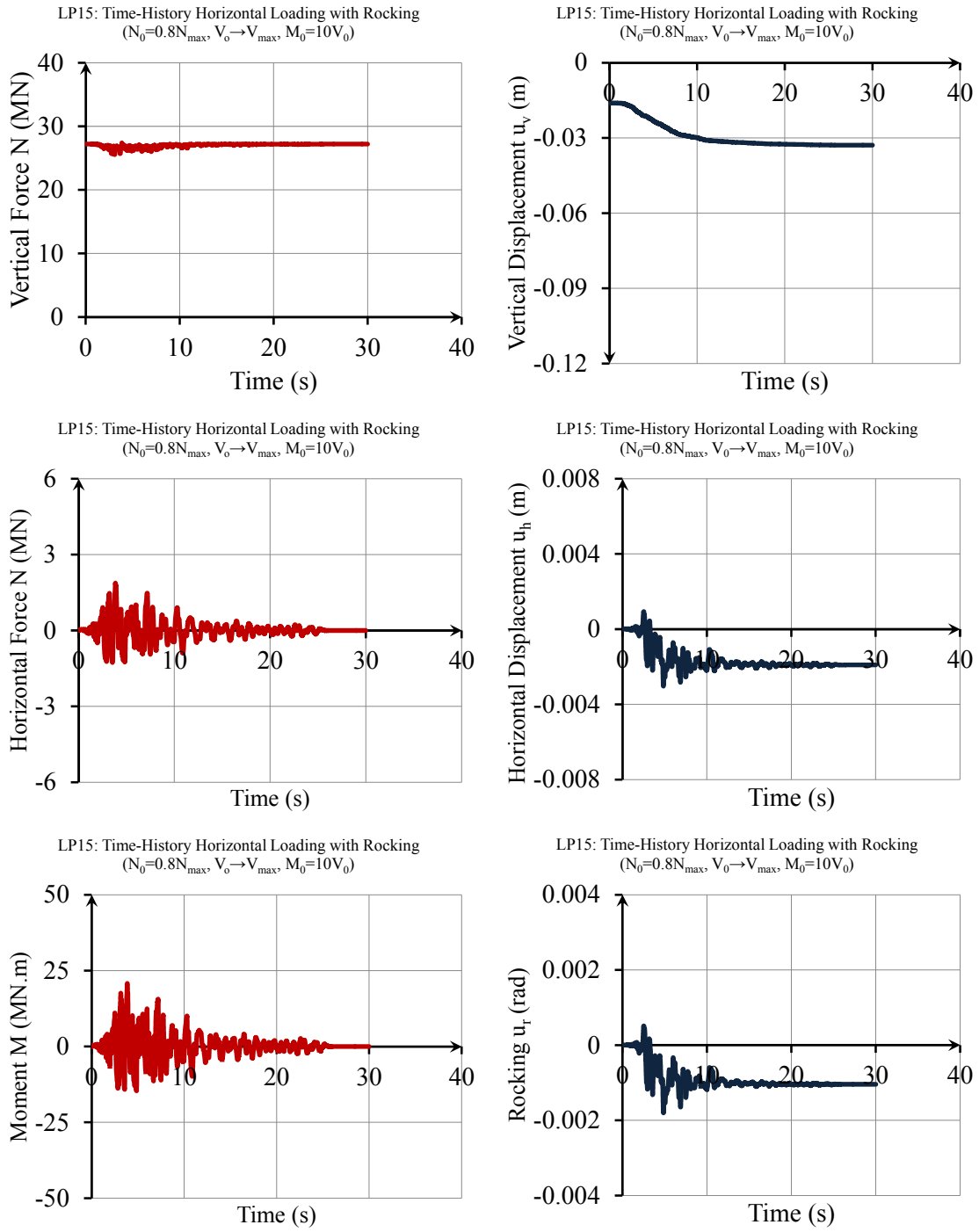

Figure F-15. The behaviour of macro-element under time-history horizontal loading with rocking (N_0=0.8N_{max}, V_0→V_{max}, M_0=10M_{max}). Foundation mass and mass moment of inertia is also included and radiation damping is considered.

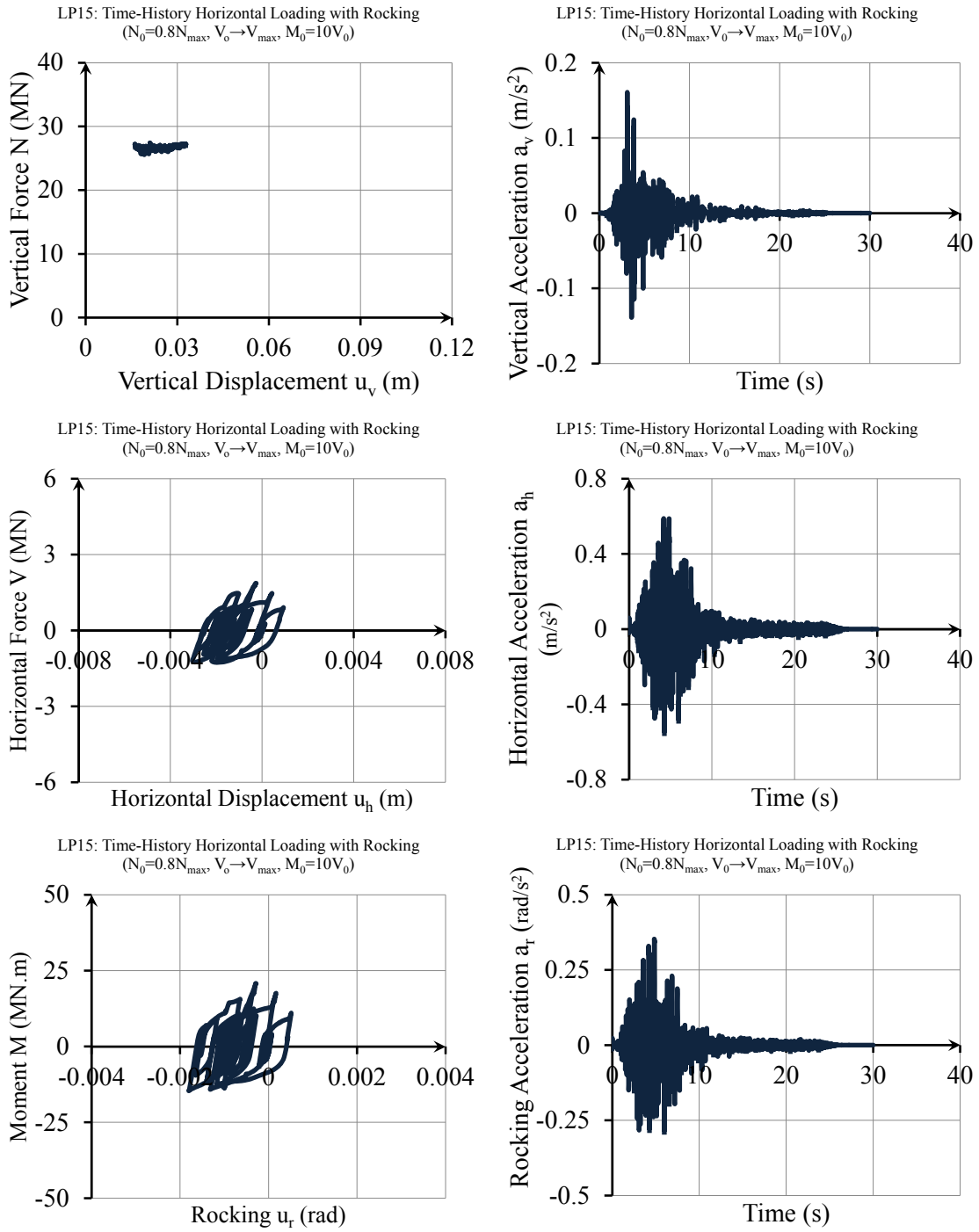

Figure F-15. *Continued.*

APPENDIX

G. Results for Sensitivity of Foundation Response to Soil-Foundation Interface Parameters

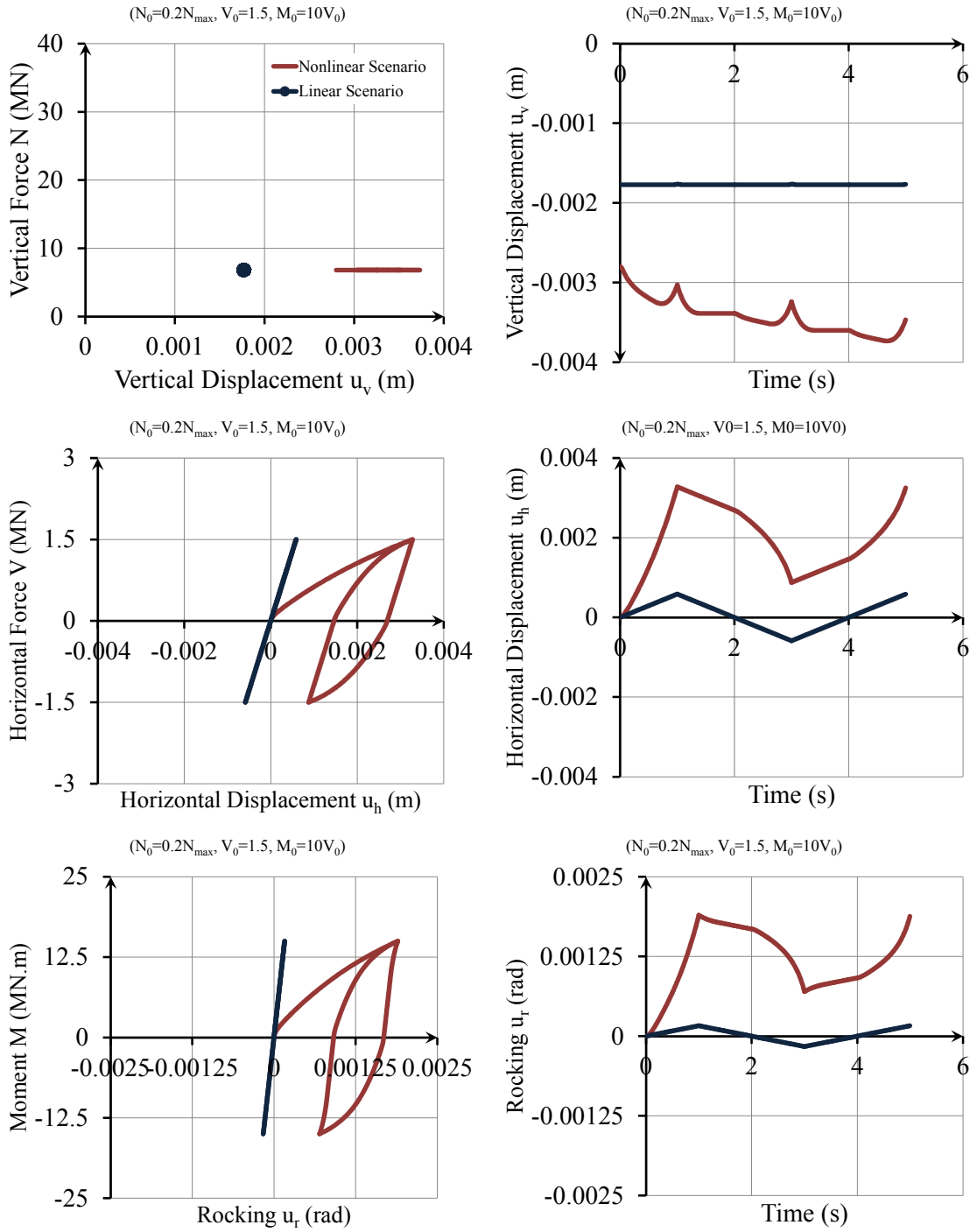

Figure G-1. The role of material nonlinearity on the response of considered soil-foundation interface model to cyclic loading: (left) nonlinear response; (right) linear response (N_0=0.2N_{max}, V_0=15 MN, M_0=10V_0).

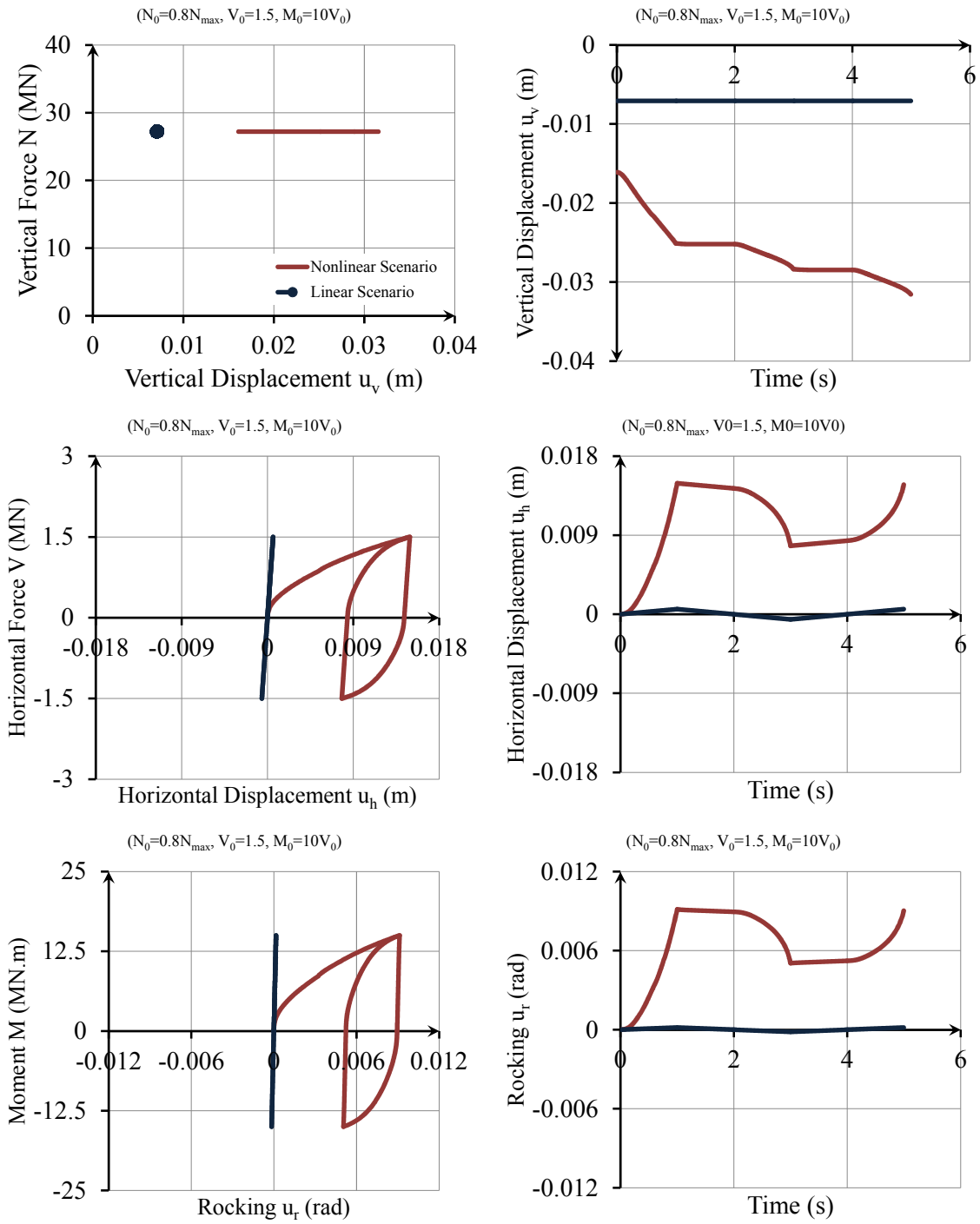

Figure G-2. The role of material nonlinearity on the response of considered soil-foundation interface model to cyclic loading: (left) nonlinear response; (right) linear response (N_0=0.8N_{max}, V_0=15 MN, M_0=10V_0).

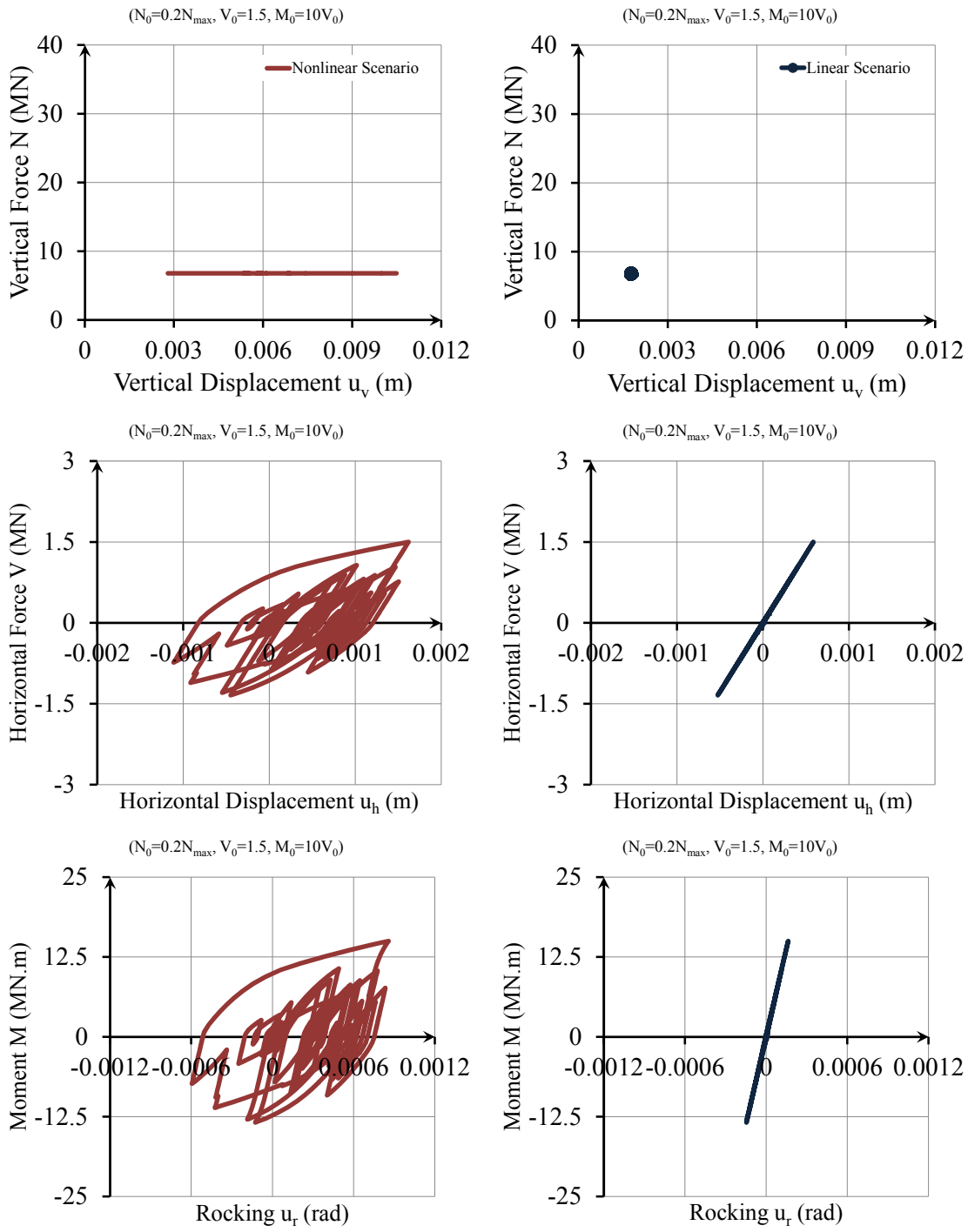

Figure G-3. The role of material nonlinearity on the response of considered soil-foundation interface model to time-history loading: (left) nonlinear response; (right) linear response (N_0=0.2N_{max}, V_0=15 MN, M_0=10V_0).

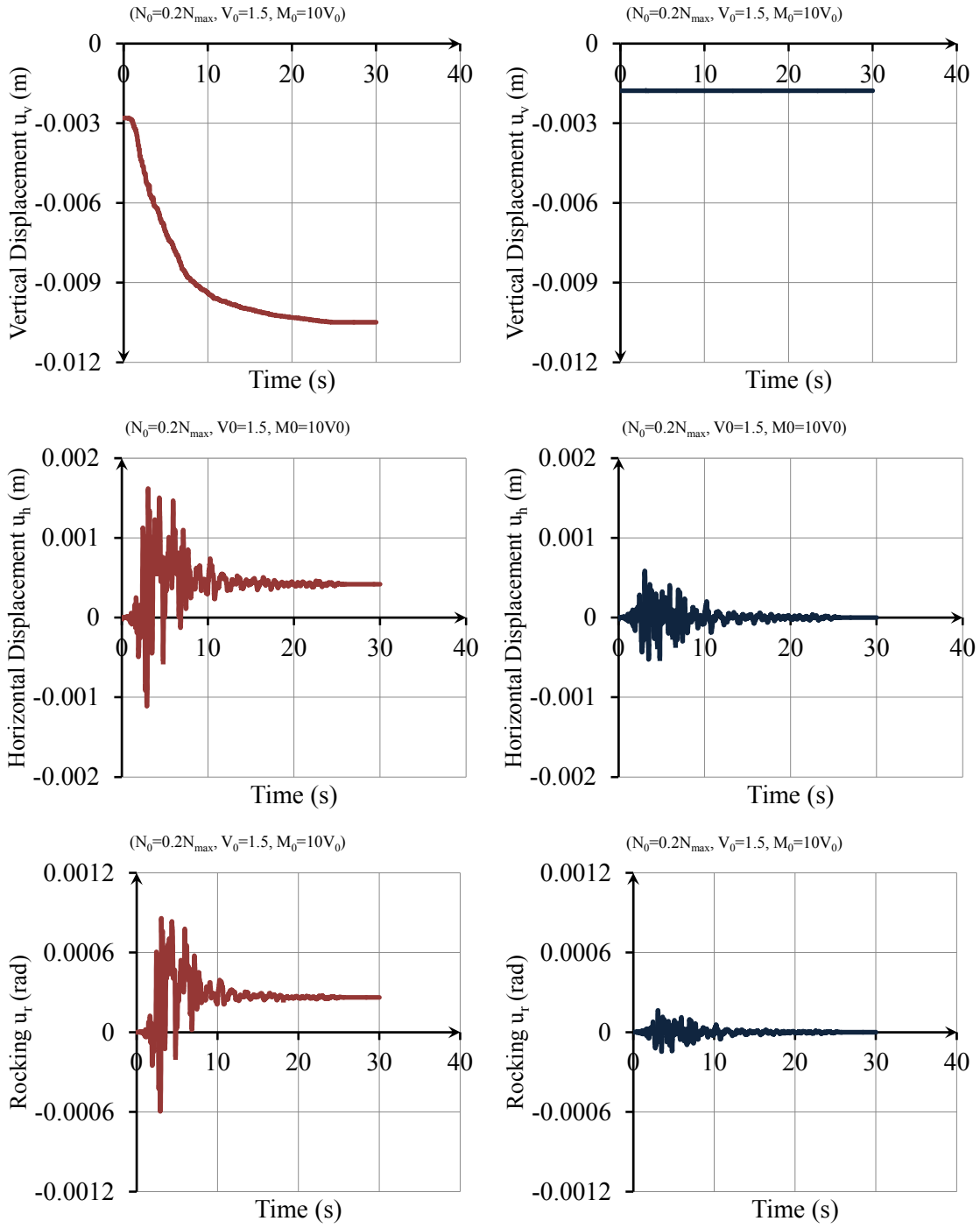

Figure G-3. *Continued.*

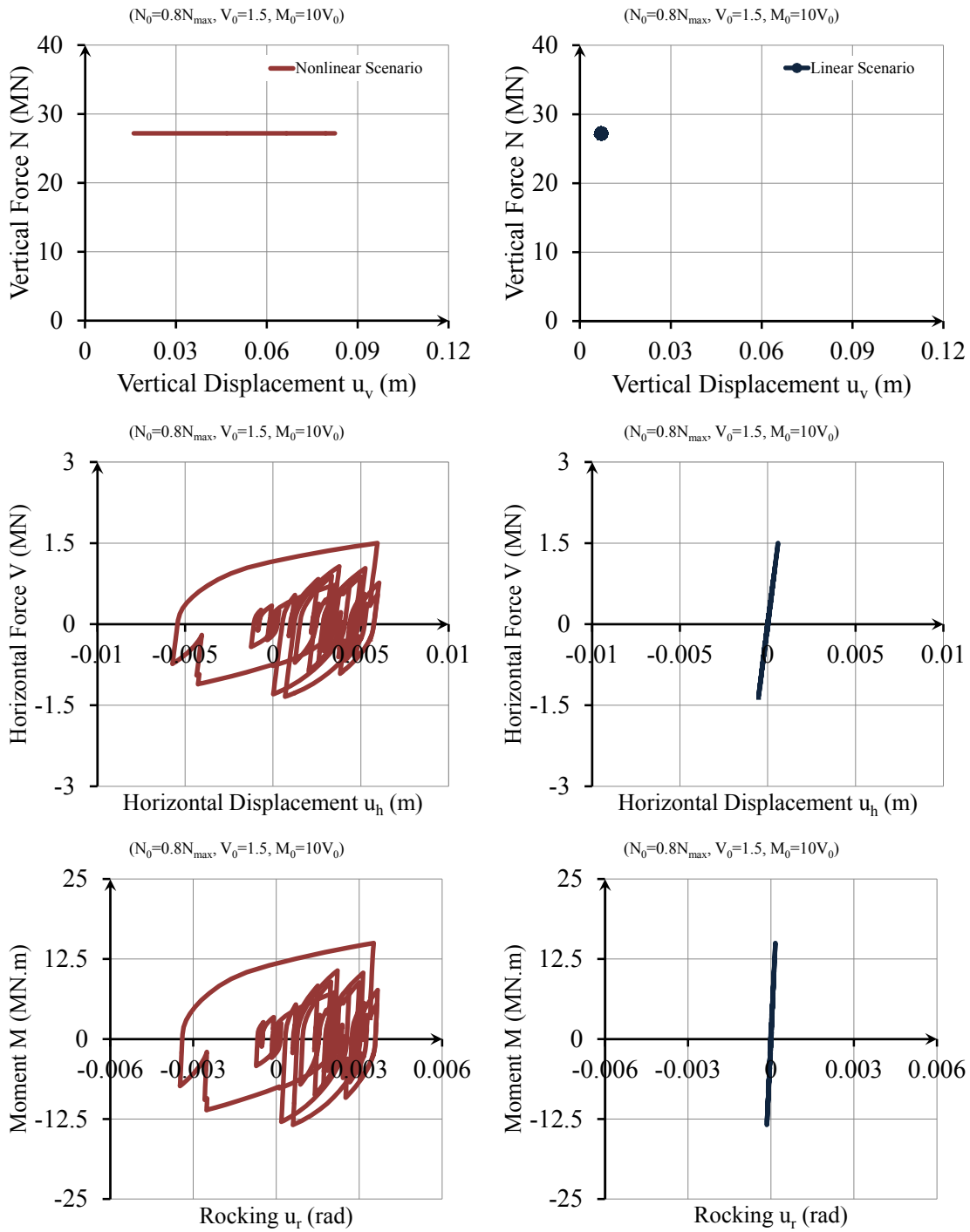

Figure G-4. The role of material nonlinearity on the response of considered soil-foundation interface model to time-history loading: (left) nonlinear response; (right) linear response (N_0=0.8N_{max}, V_0=15 MN, M_0=10V_0).

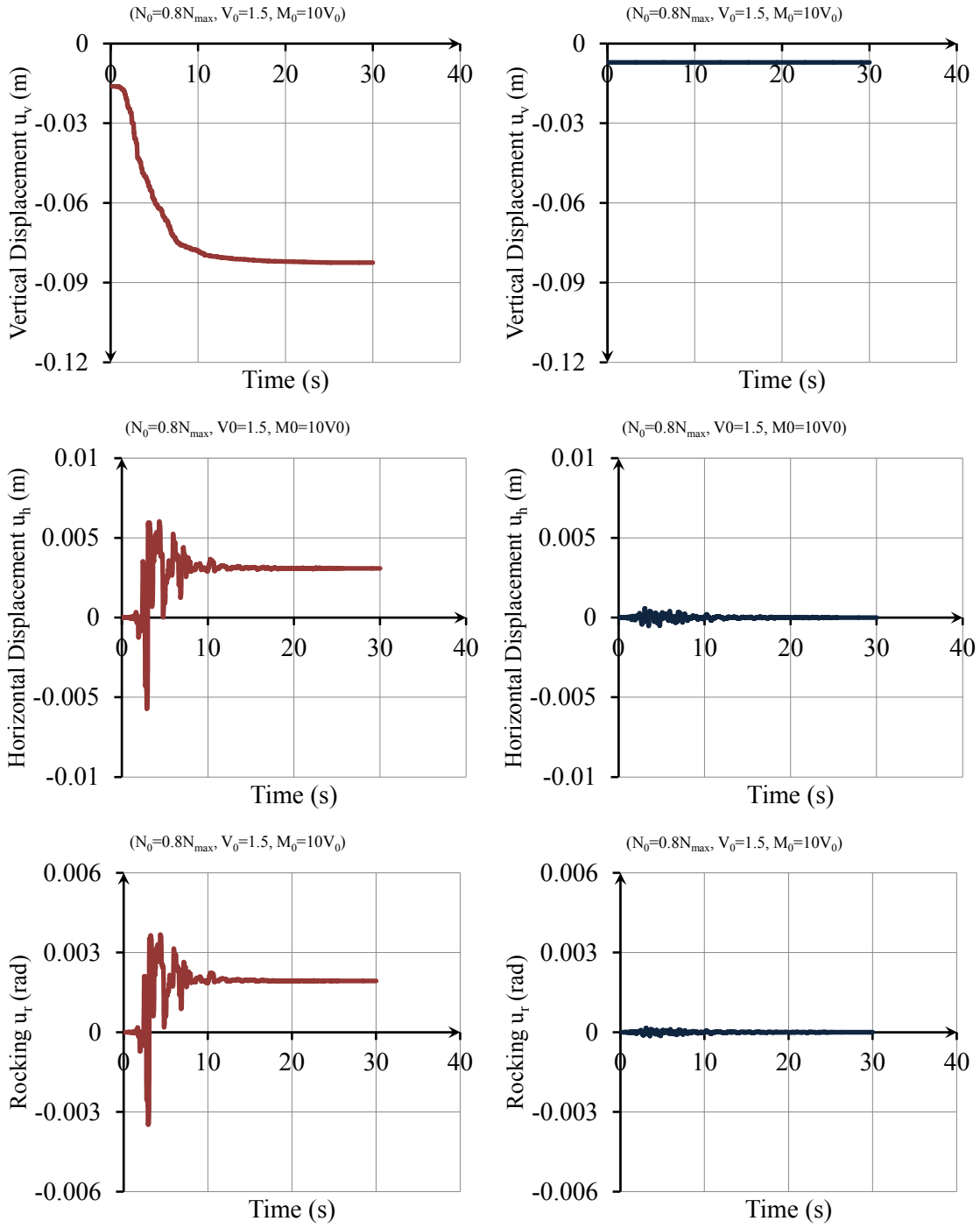

Figure G-4. *Continued.*

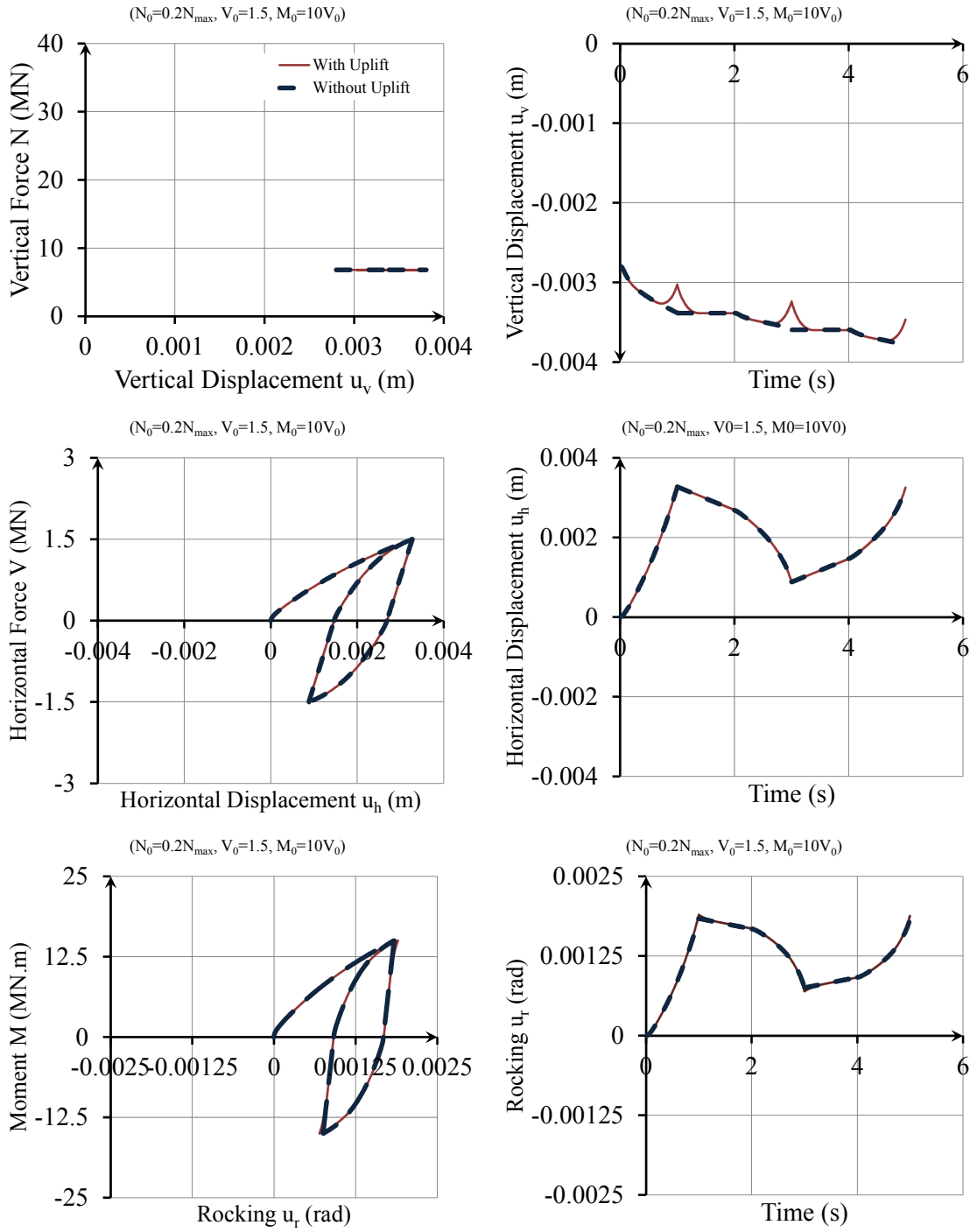

Figure G-5. The role of foundation uplift on the response of considered soil-foundation interface model to cyclic loading: (left) simulation with uplift; (right) simulation without uplift (N_0=0.2N_{max}, V_0=1.5 MN, M_0=10V_0).

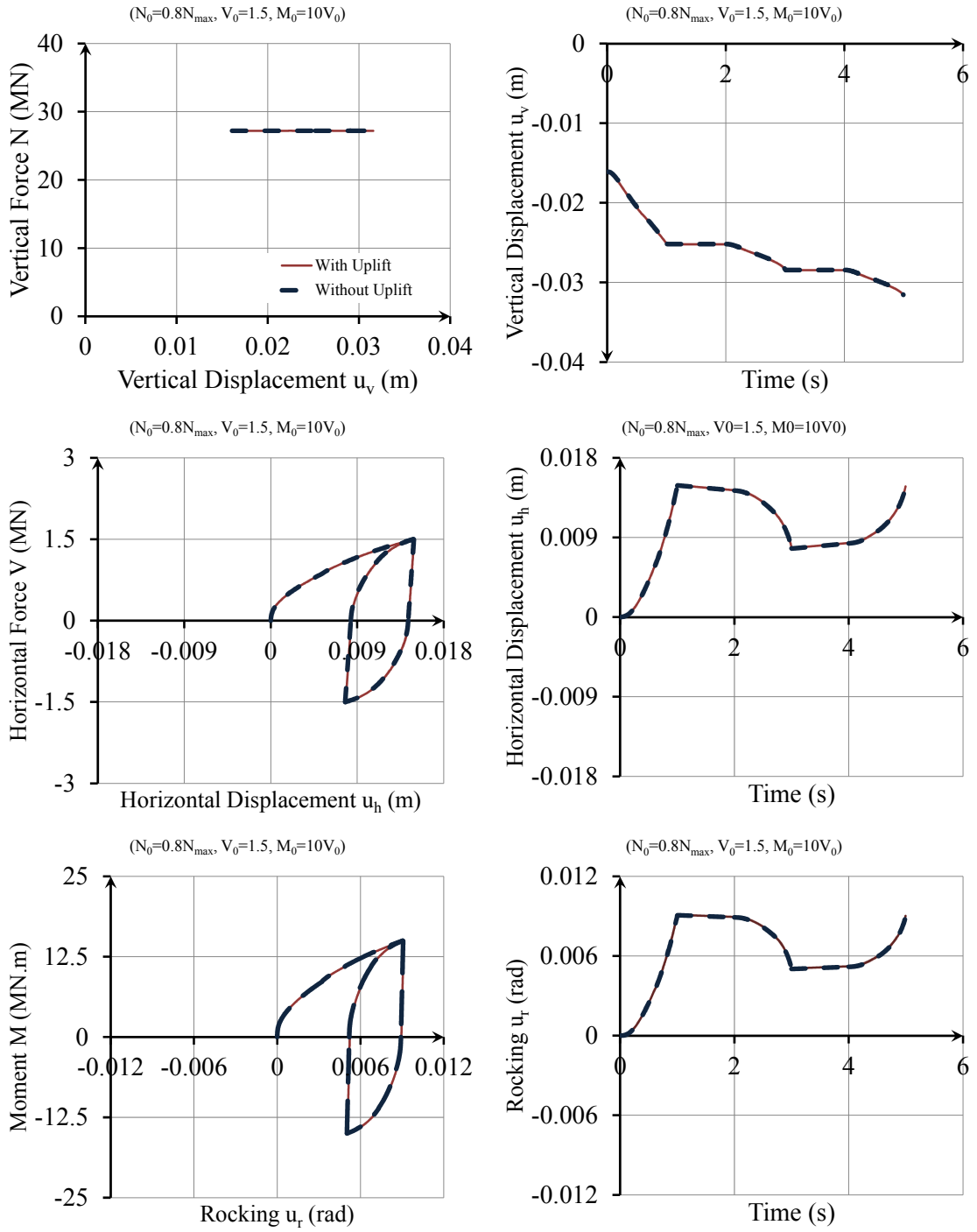

Figure G-6. The role of foundation uplift to the response of considered soil-foundation interface model to cyclic loading: (left) simulation with uplift; (right) simulation without uplift ($N_0=0.8N_{max}$, $V_0=1.5$ MN, $M_0=10V_0$).

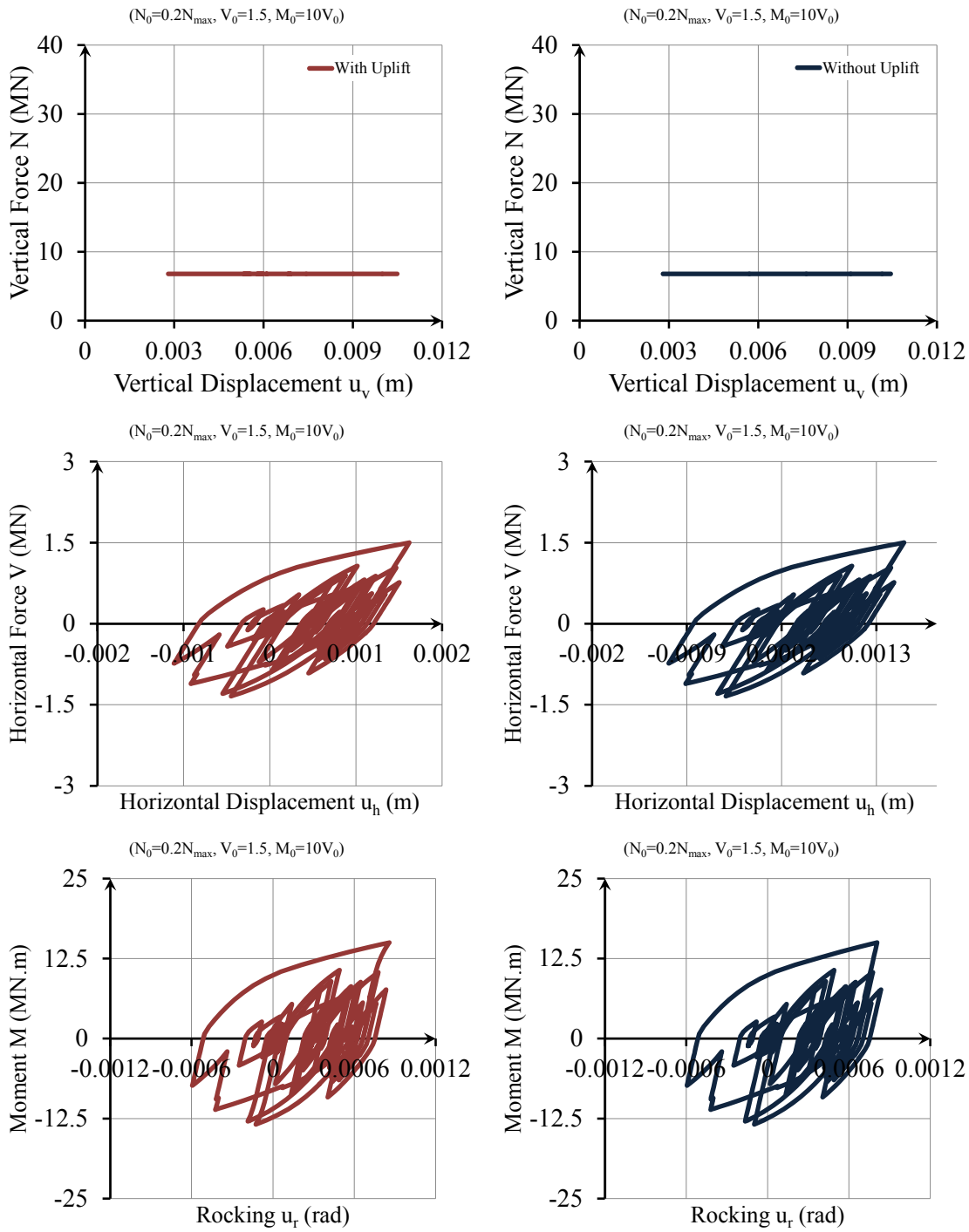

Figure G-7. The role of foundation uplift to the response of considered soil-foundation interface model to time-history loading: (left) simulation with uplift; (right) simulation without uplift (N_0=0.2N_{max}, V_0=1.5 MN, M_0=10V_0).

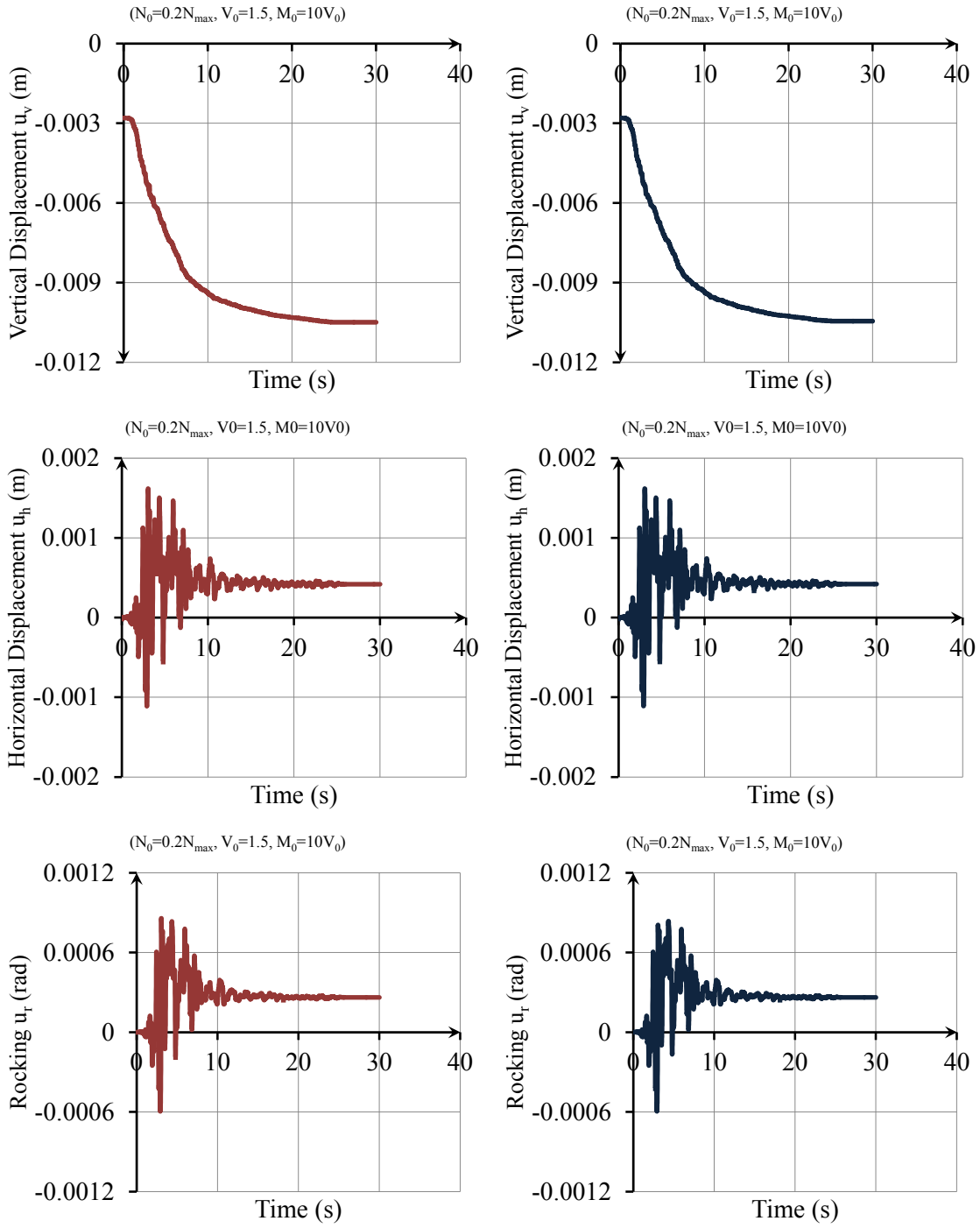

Figure G-7. *Continued.*

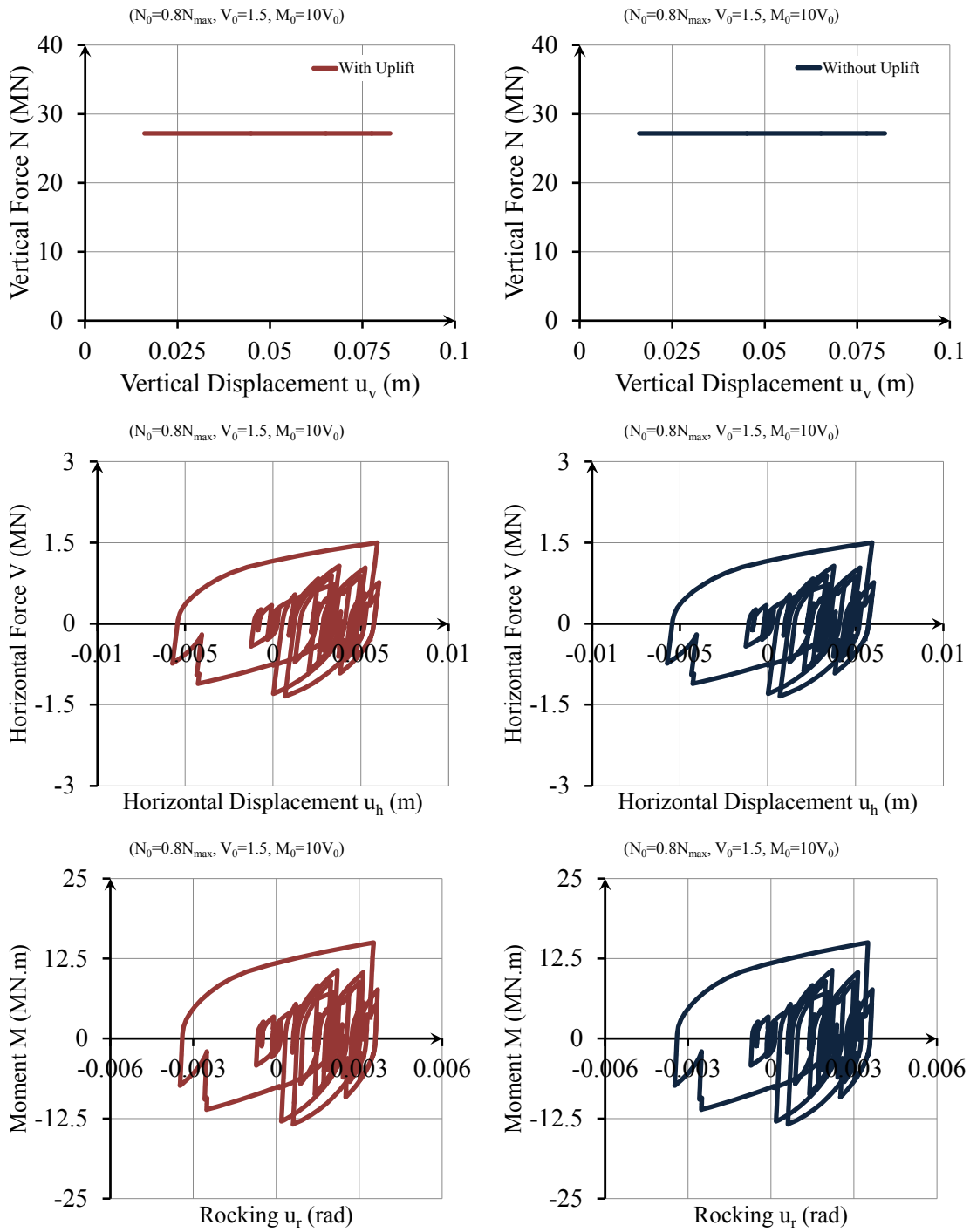

Figure G-8. The role of foundation uplift to the response of considered soil-foundation interface model to time-history loading: (left) simulation with uplift; (right) simulation without uplift (N_0=0.8N_{max}, V_0=1.5 MN, M_0=10V_0).

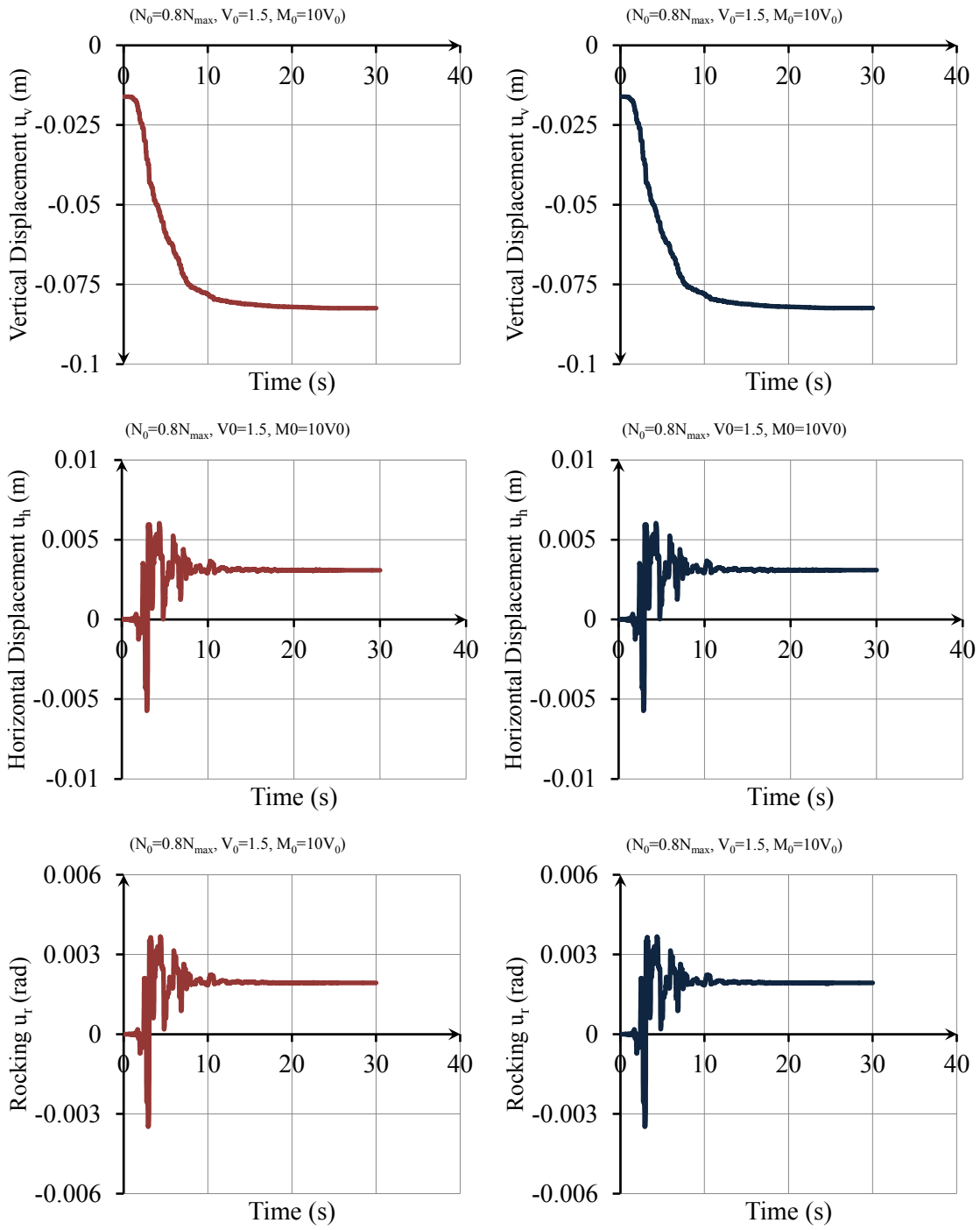

Figure G-8. *Continued.*

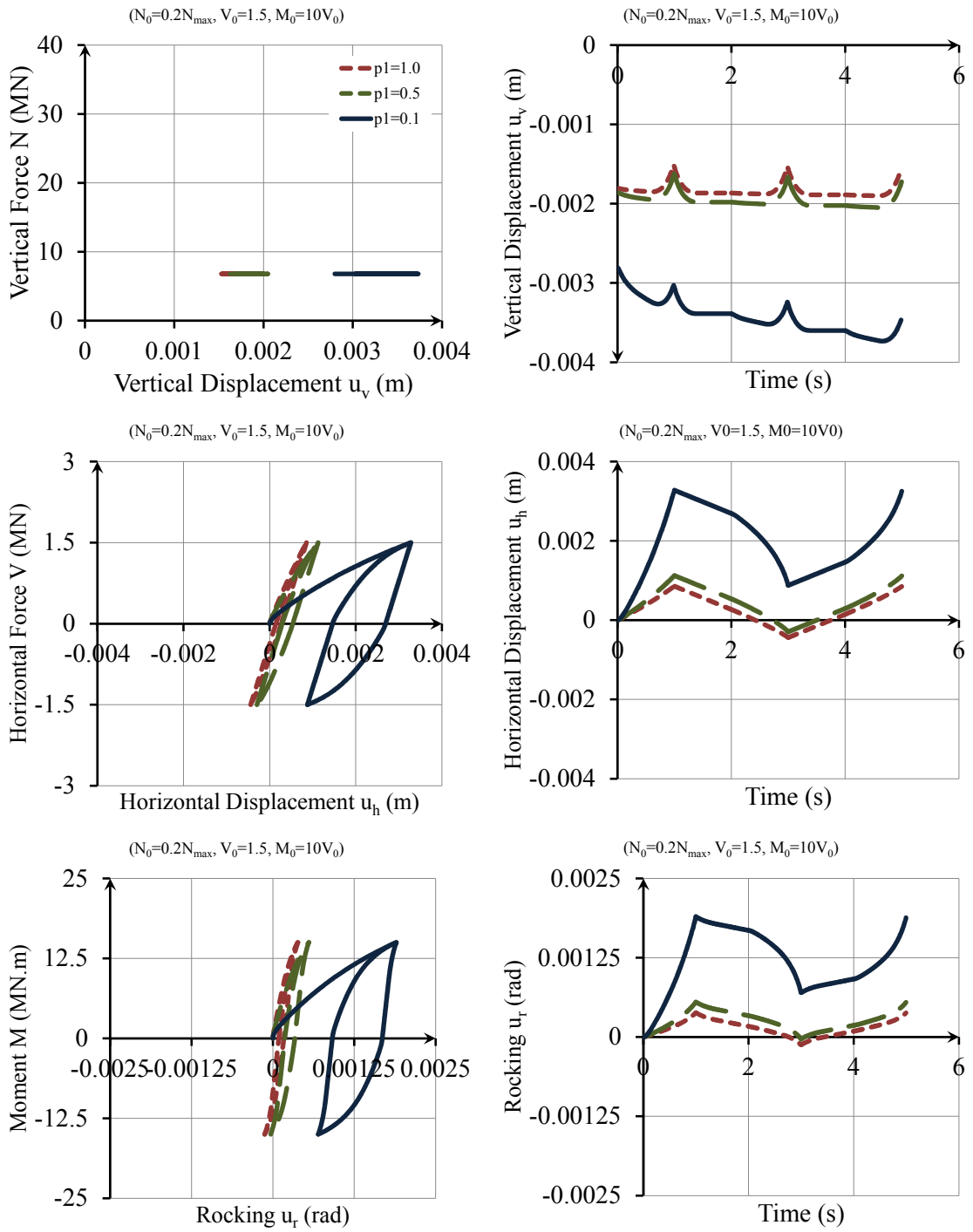

Figure G-9. The effects of variation in p_1 on the response of considered soil-foundation interface model to cyclic loading (N_0=0.2$N_{max,}$ V_0=1.5 MN, M_0=10V_0).

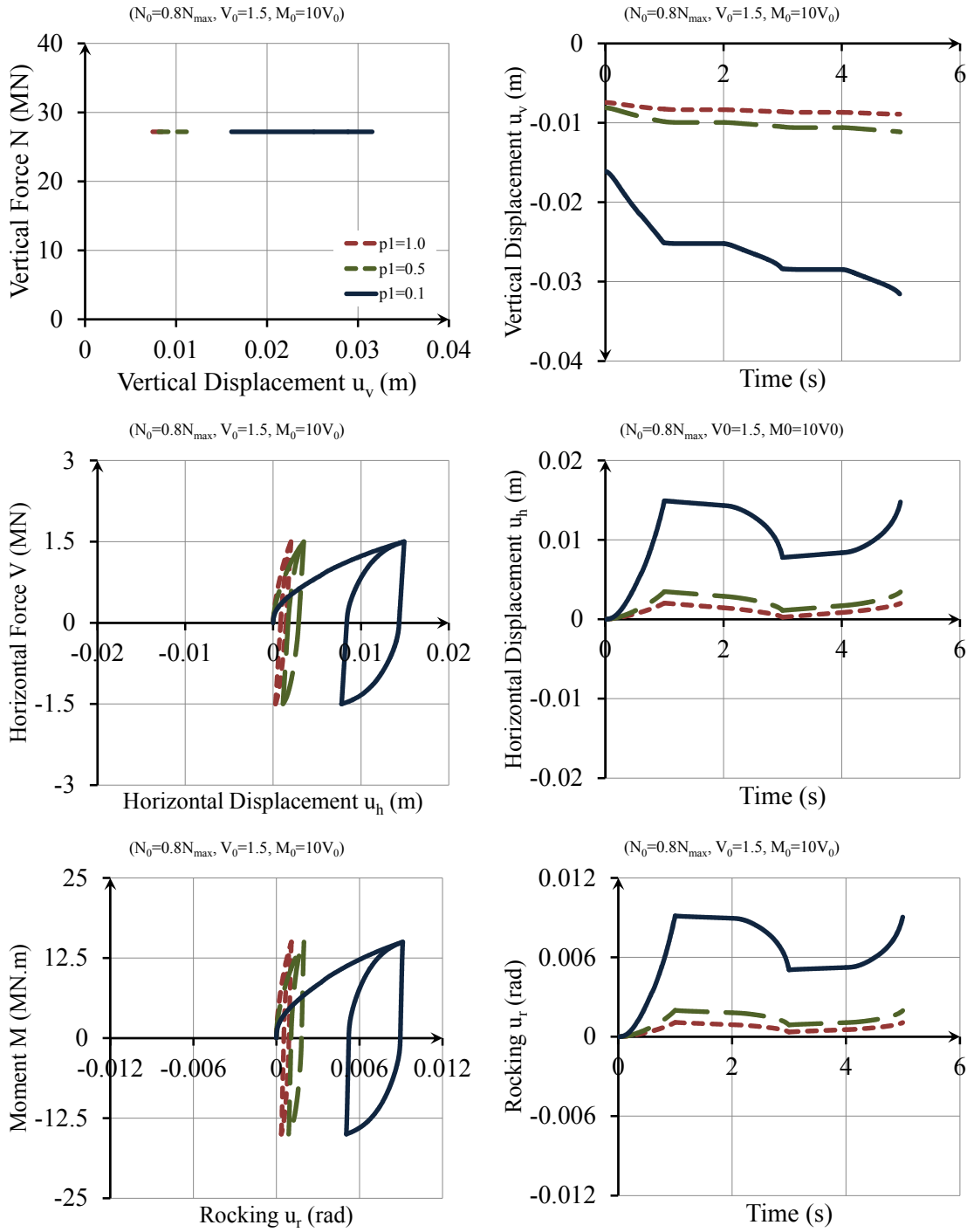

Figure G-10. The effects of variation in p_1 on the response of considered soil-foundation interface model to cyclic loading (N_0=0.8$N_{max,}$ V_0=1.5 MN, M_0=10V_0).

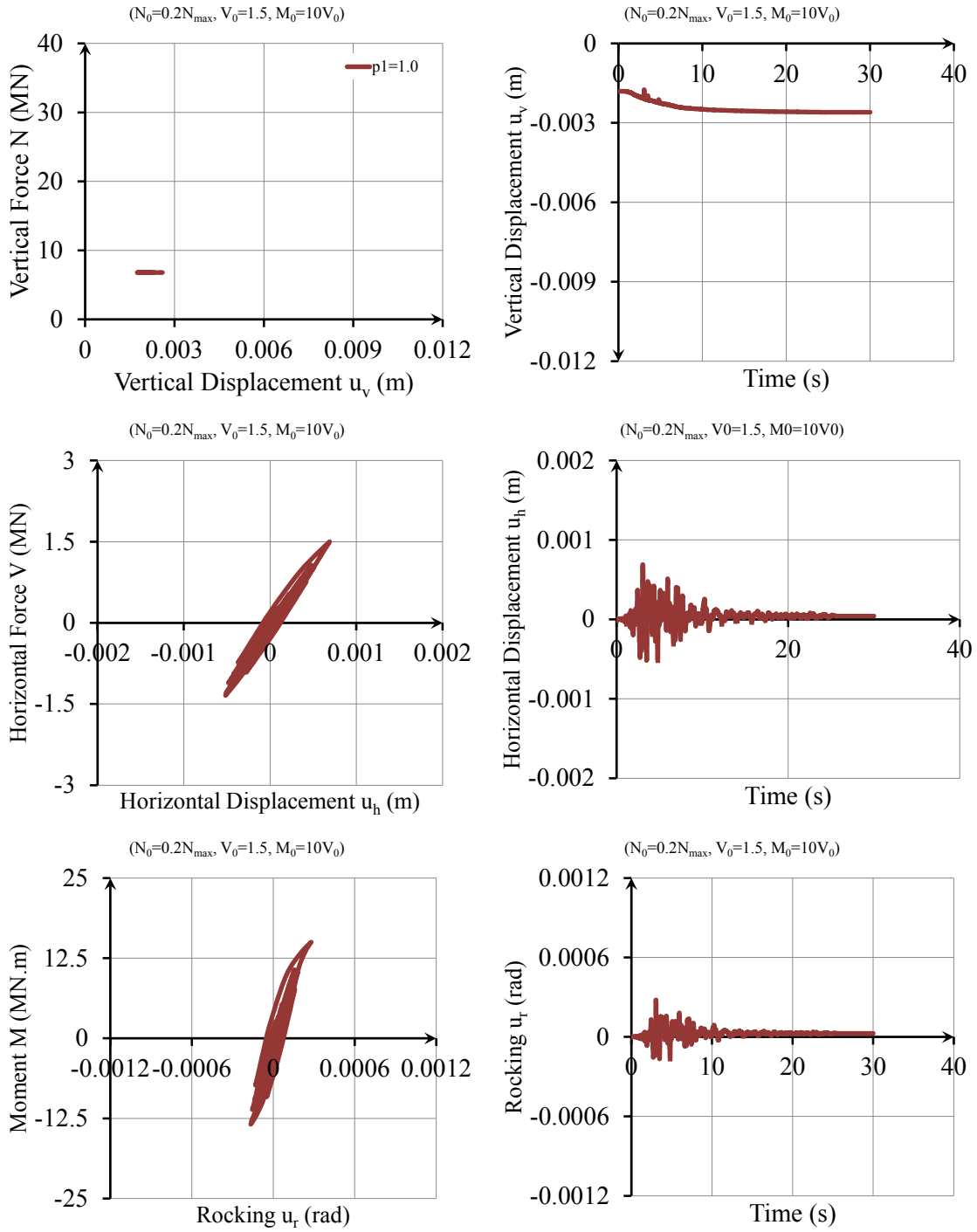

Figure G-11. The effects of variation in p_1 on the response of considered soil-foundation interface model to time-history loading (N_0=0.2N_{max}, V_0=1.5 MN, M_0=10V_0).

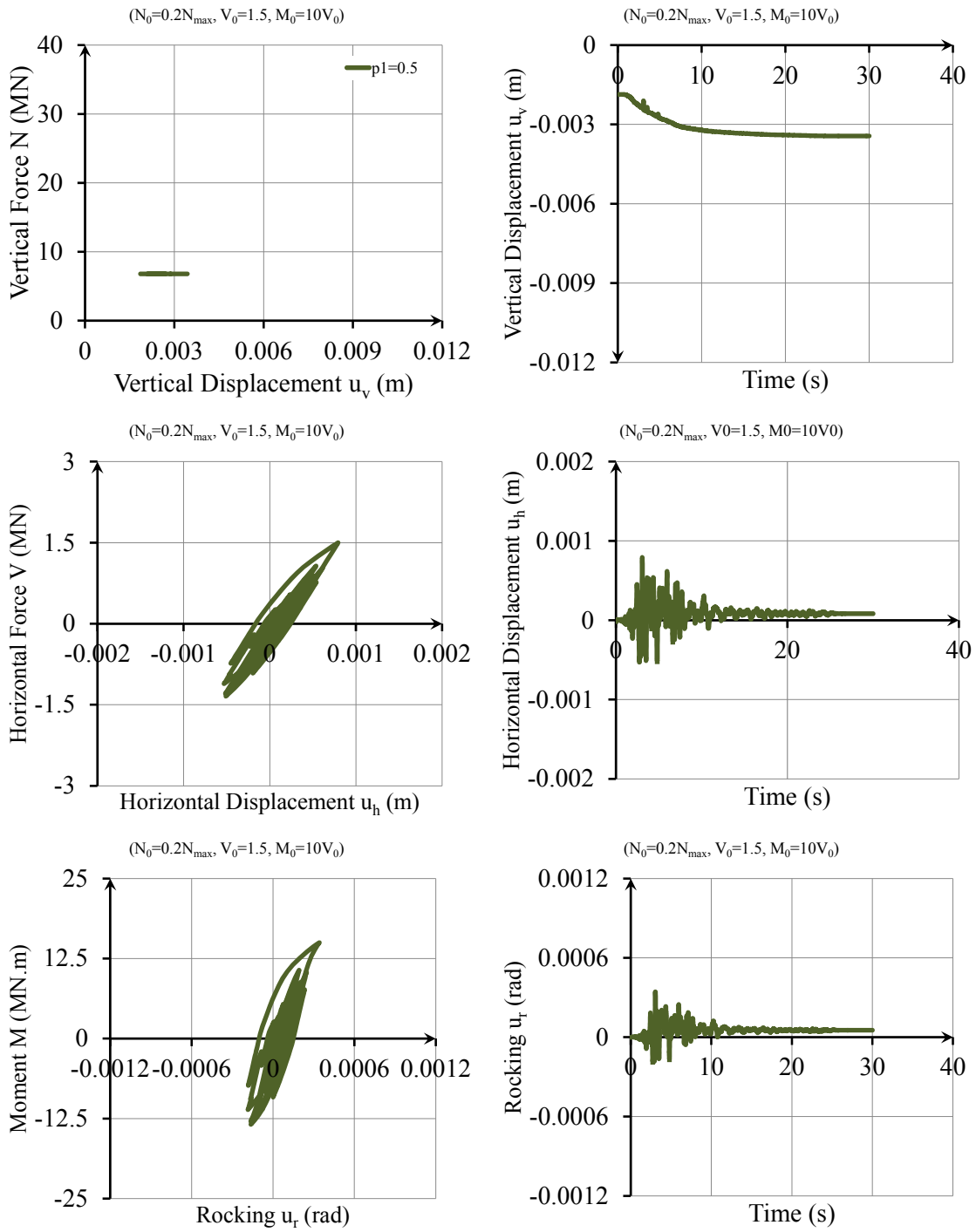

Figure G-11. *Continued*.

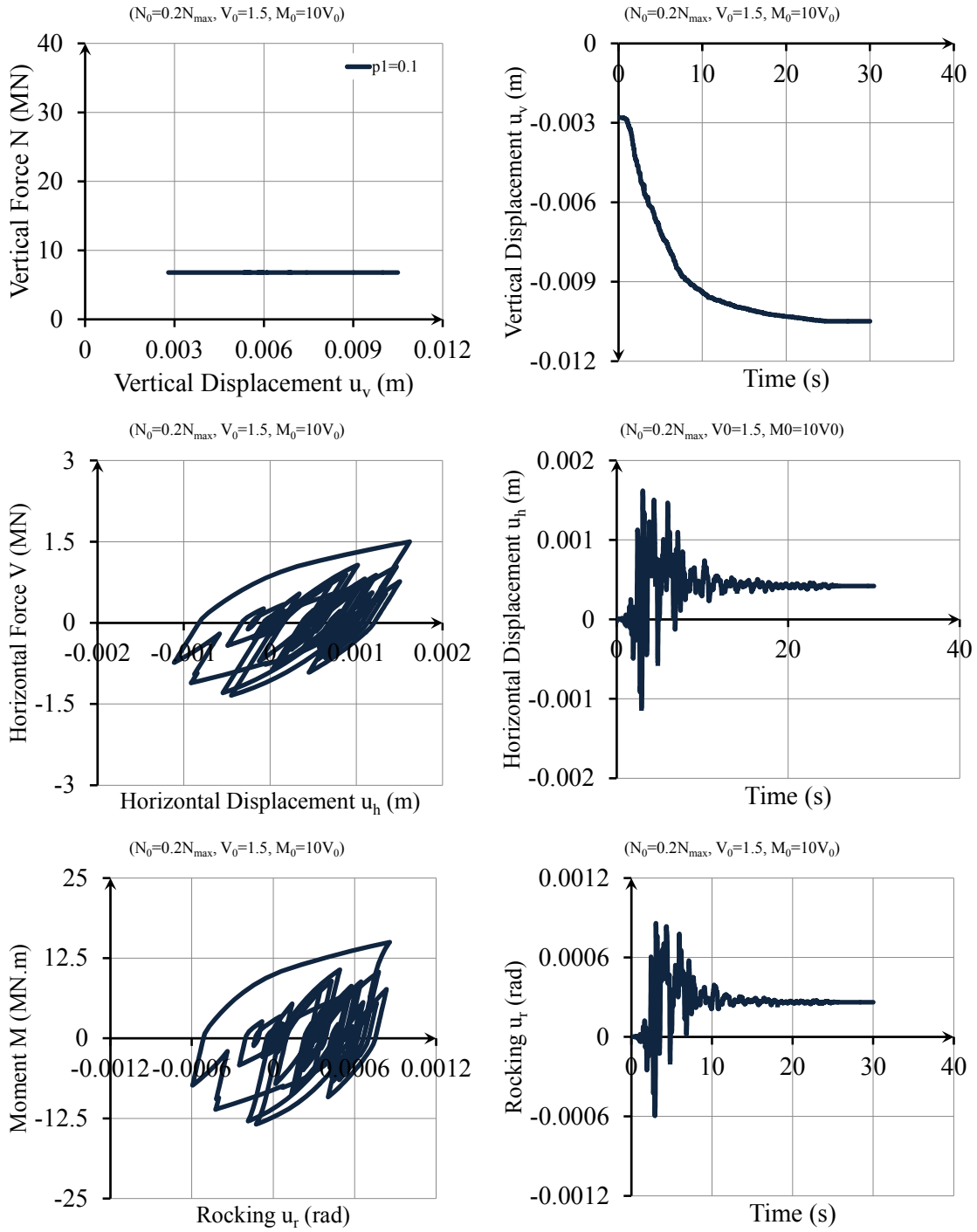

Figure G-11. *Continued*.

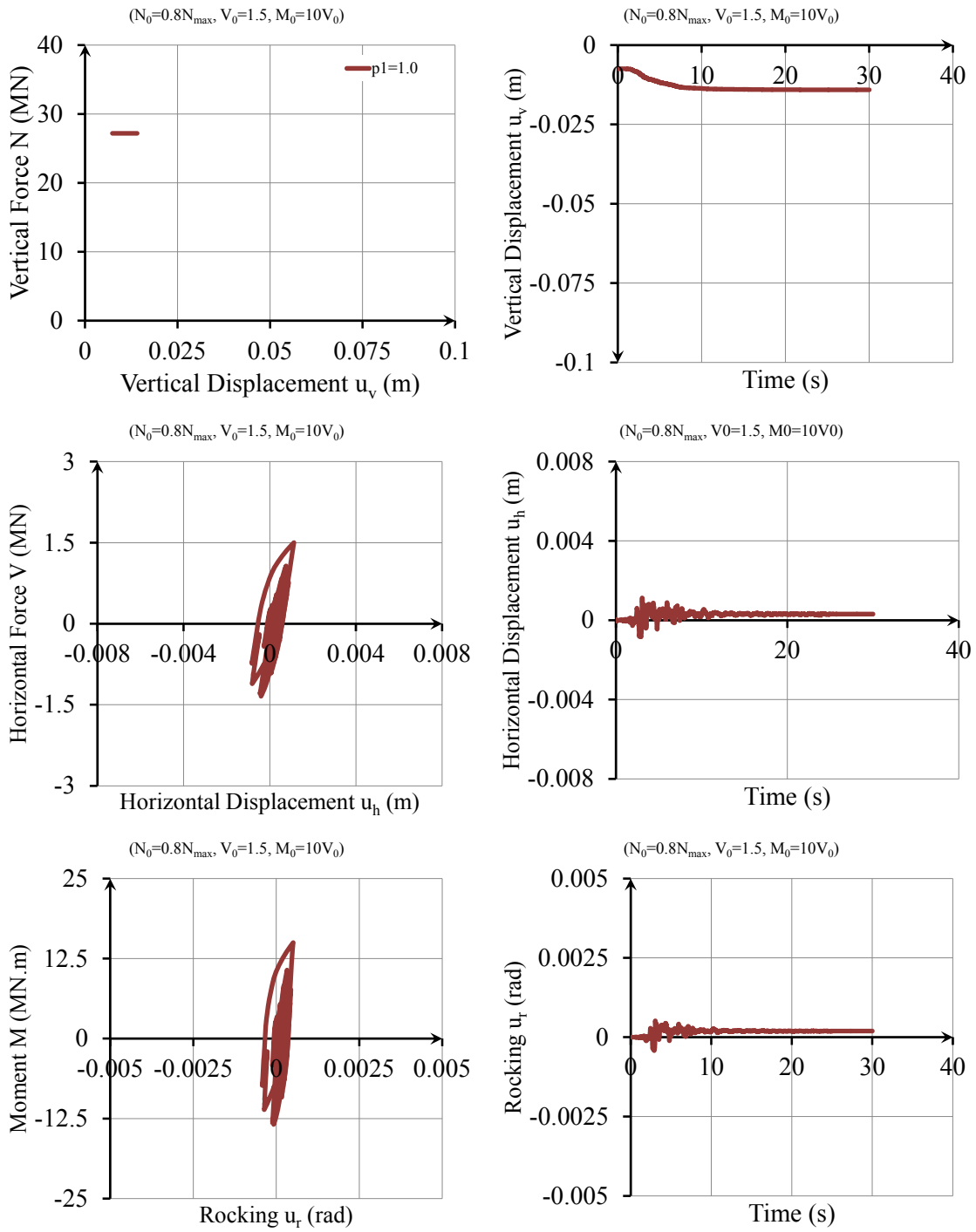

Figure G-12. The effects of variation in p_1 on the response of considered soil-foundation interface model to time-history loading (N_0=0.8$N_{max,}$ V_0=1.5 MN, M_0=10V_0).

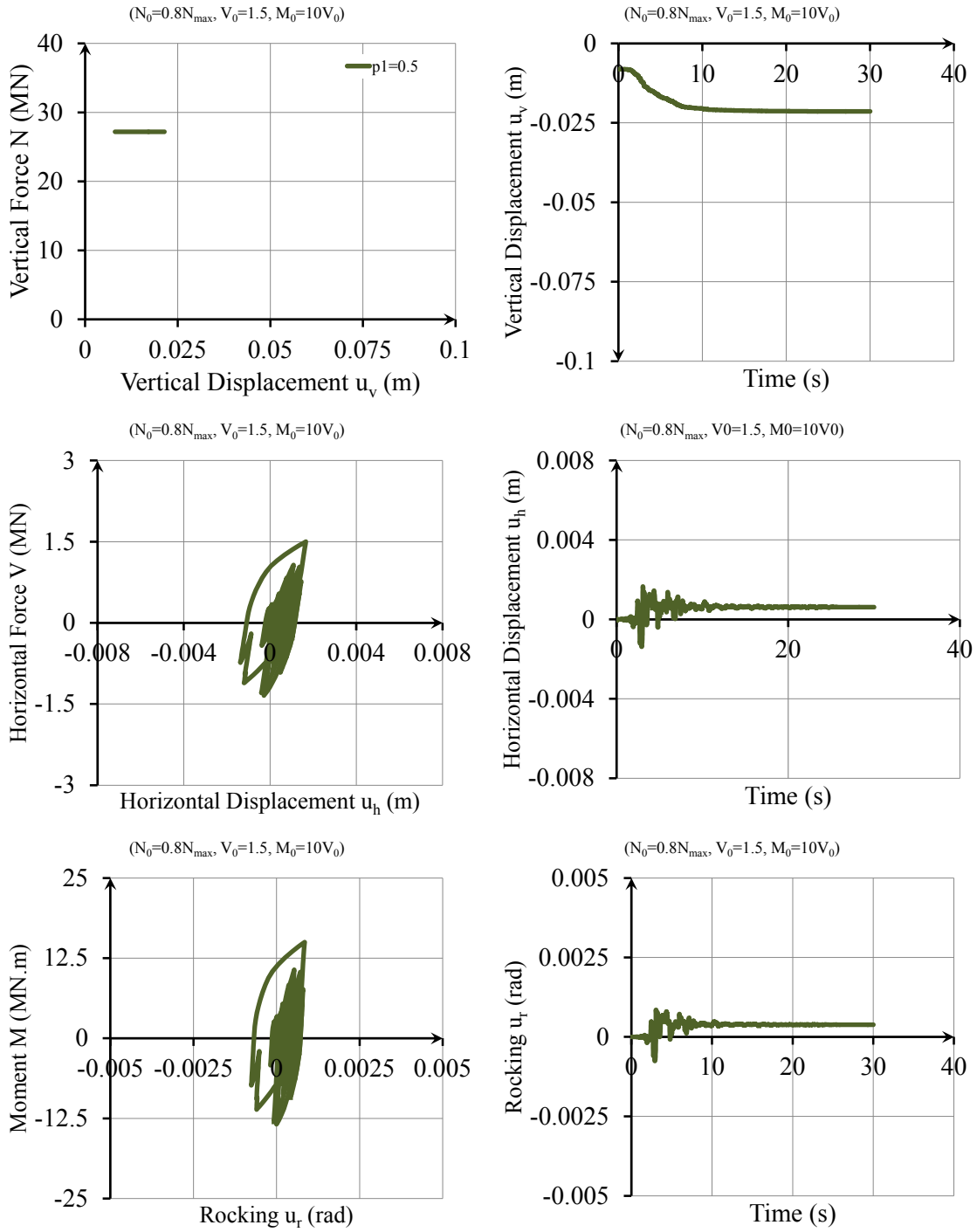

Figure G-12. *Continued*.

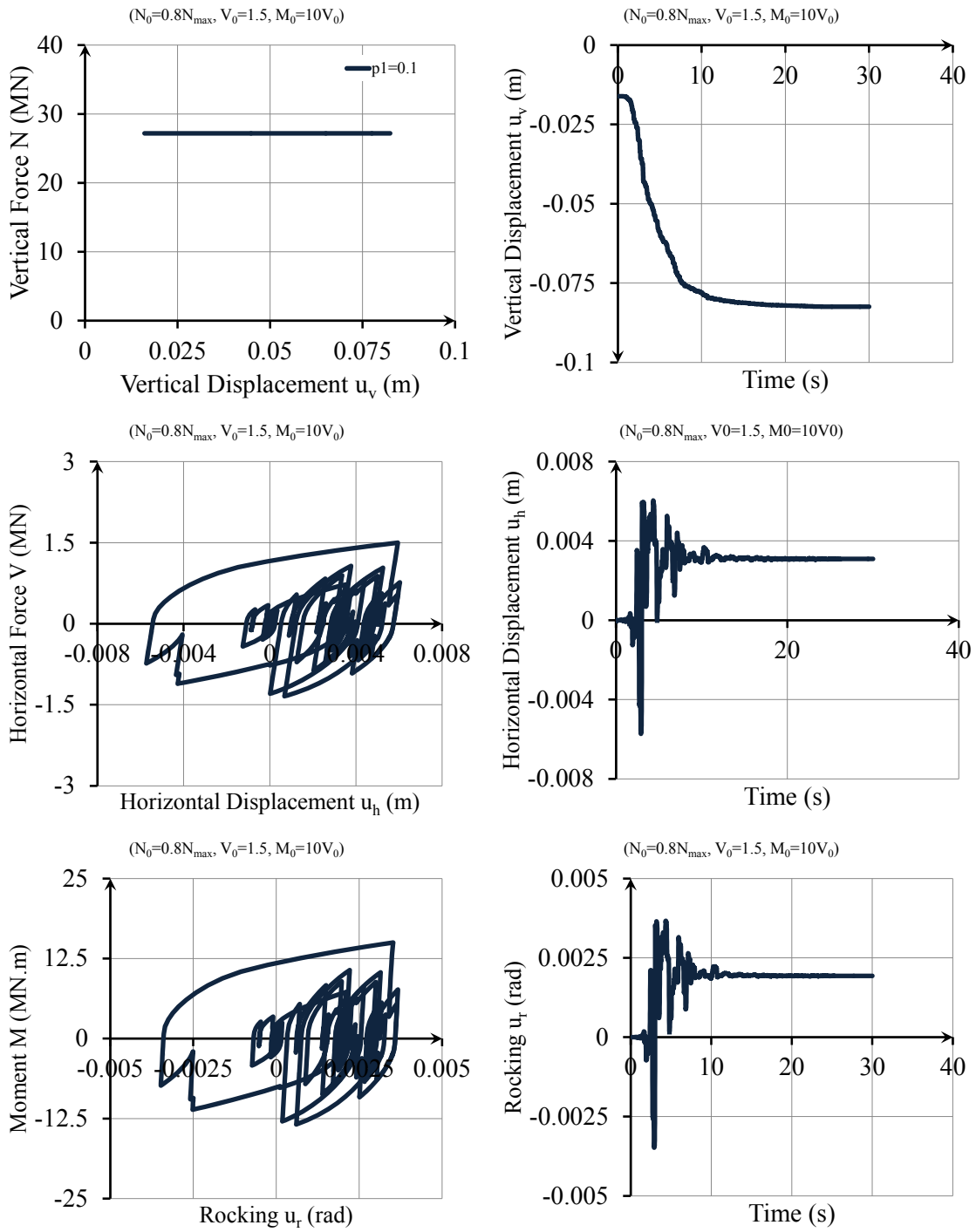

Figure G-12. *Continued*.

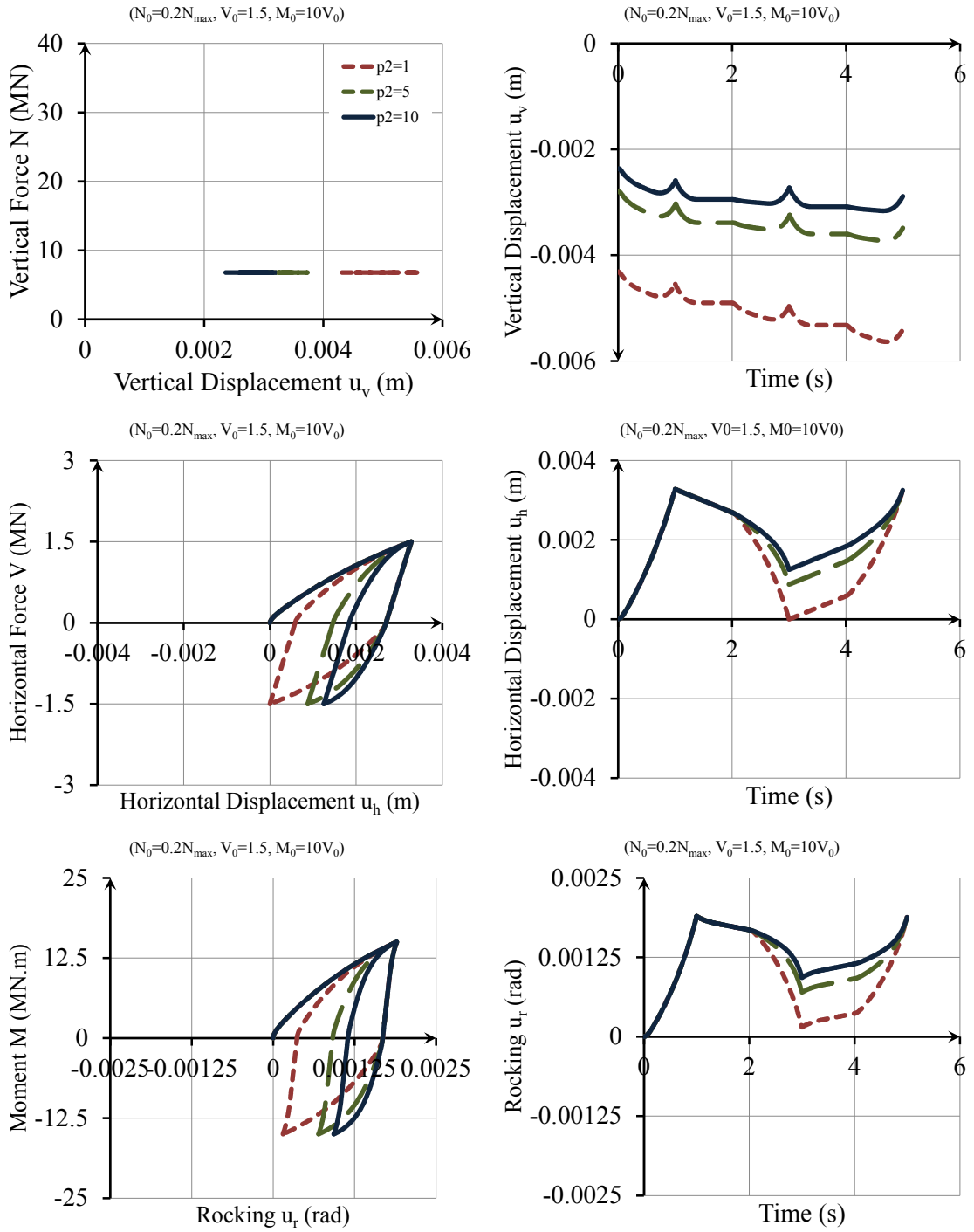

Figure G-13. The effects of variation in p_2 on the response of considered soil-foundation interface model to cyclic loading (N_0=0.2$N_{max,}$ V_0=1.5 MN, M_0=10V_0).

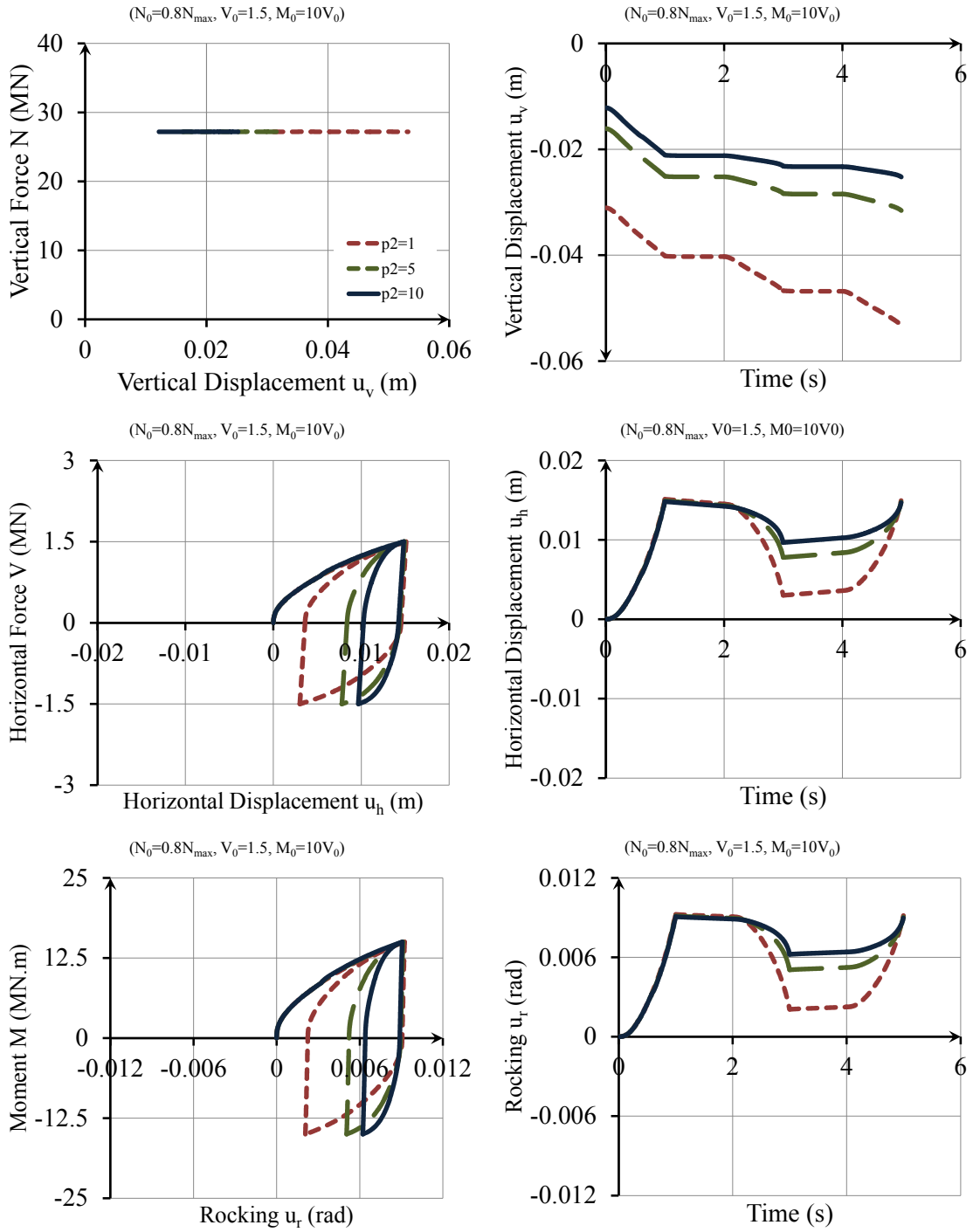

Figure G-14. The effects of variation in p_2 on the response of considered soil-foundation interface model to cyclic loading (N_0=0.8$N_{max,}$ V_0=1.5 MN, M_0=10V_0).

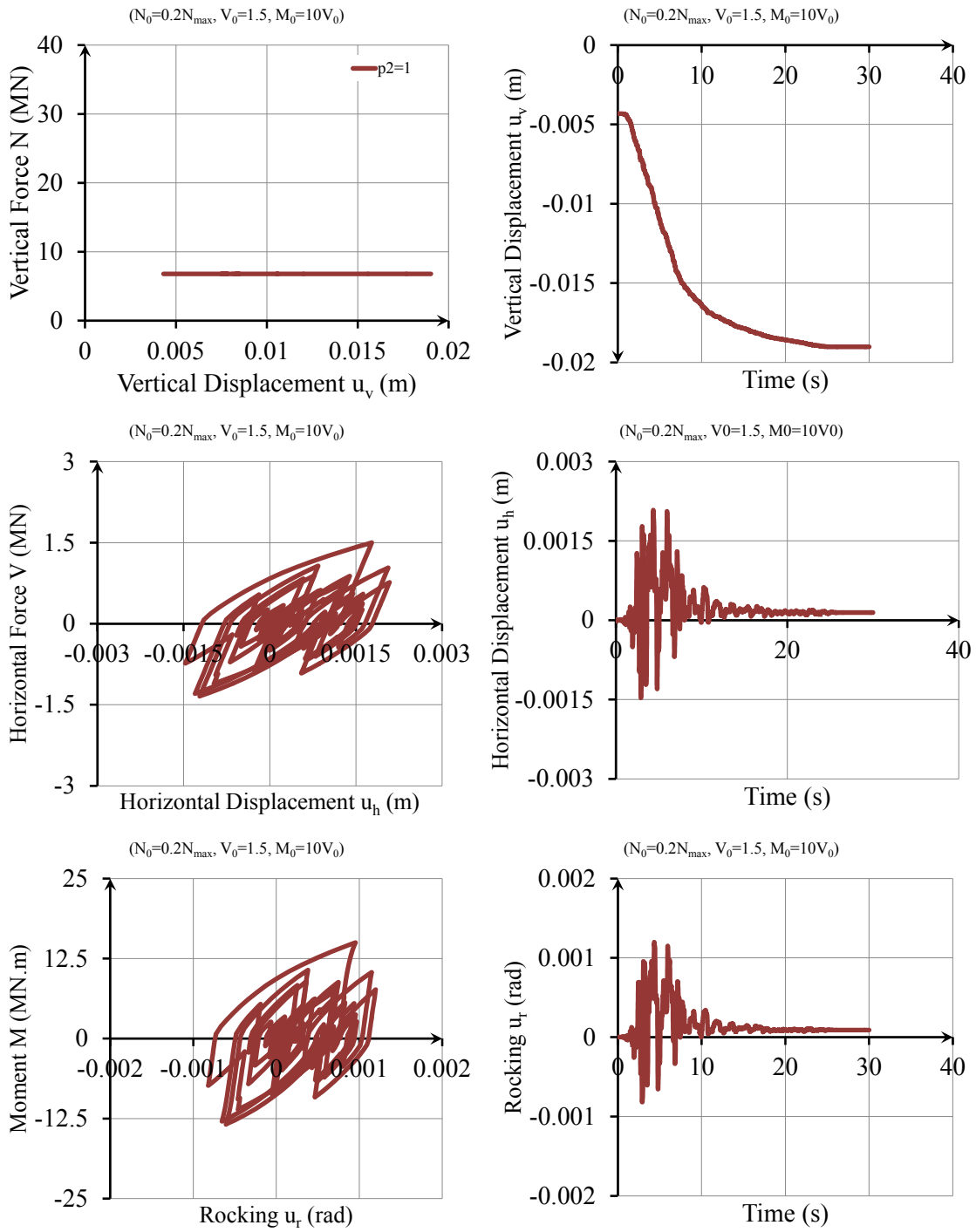

Figure G-15. The effects of variation in p_2 on the response of considered soil-foundation interface model to time-history loading (N_0=0.2$N_{max,}$ V_0=1.5 MN, M_0=10V_0).

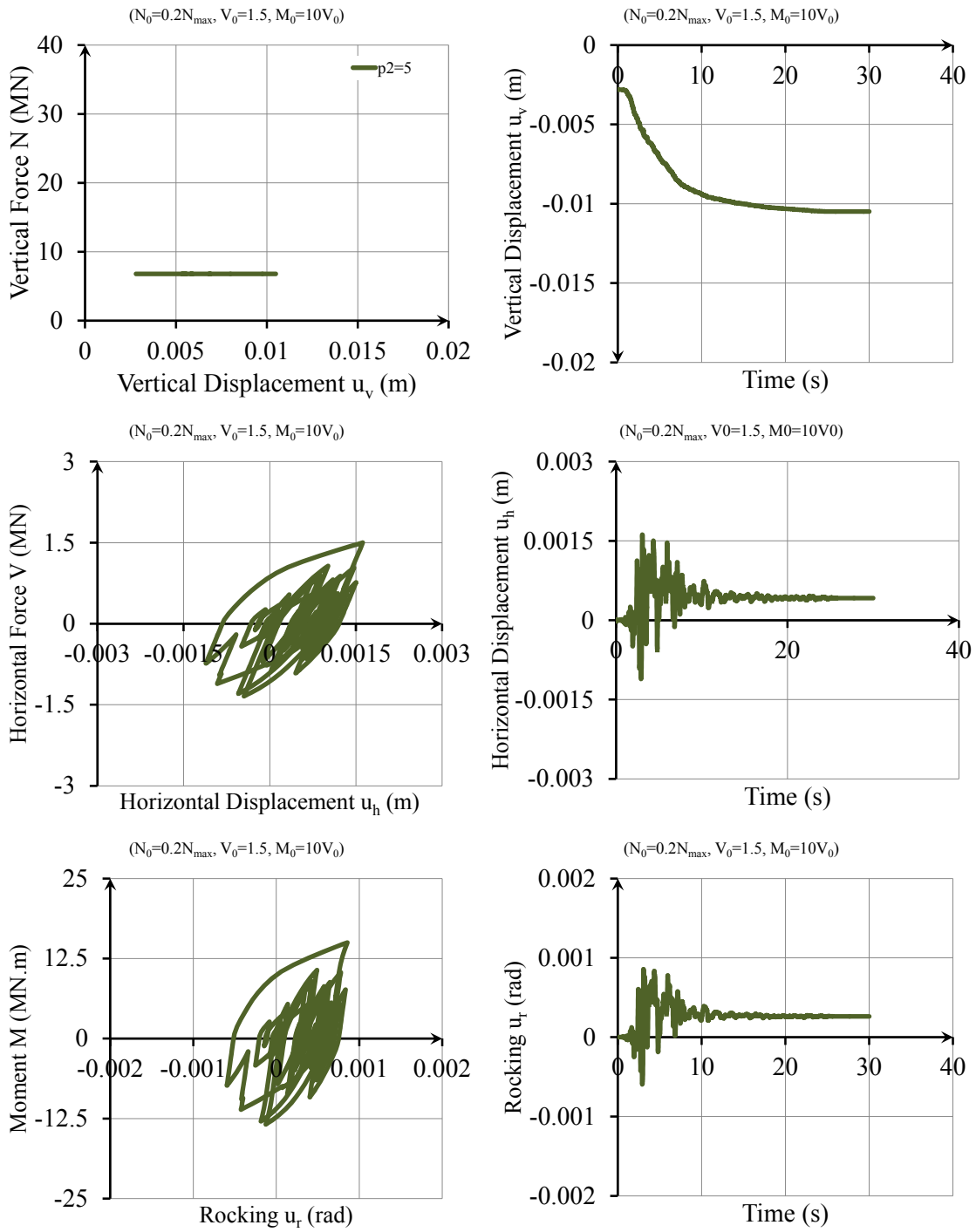

Figure G-15. *Continued*.

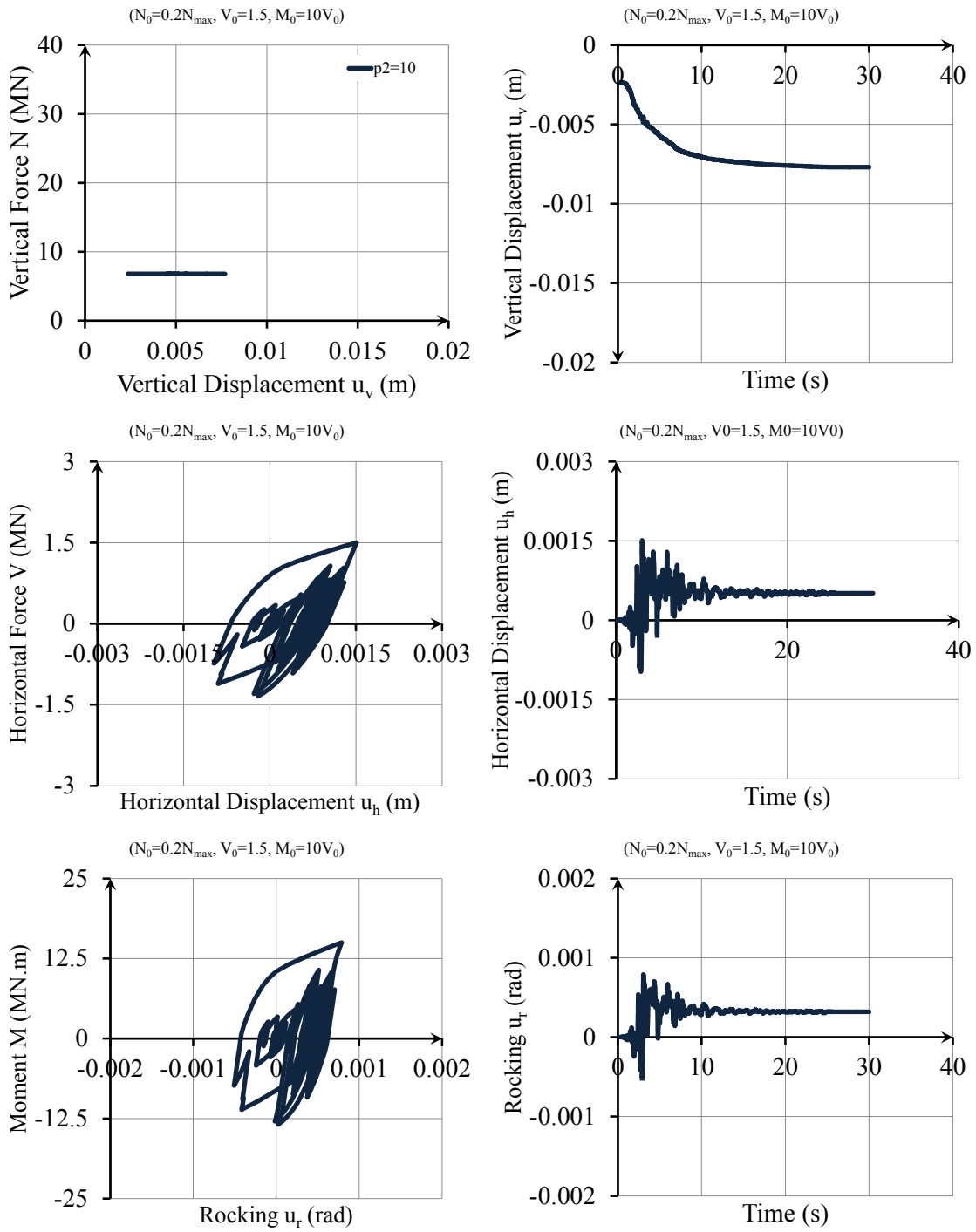

Figure G-15. *Continued*.

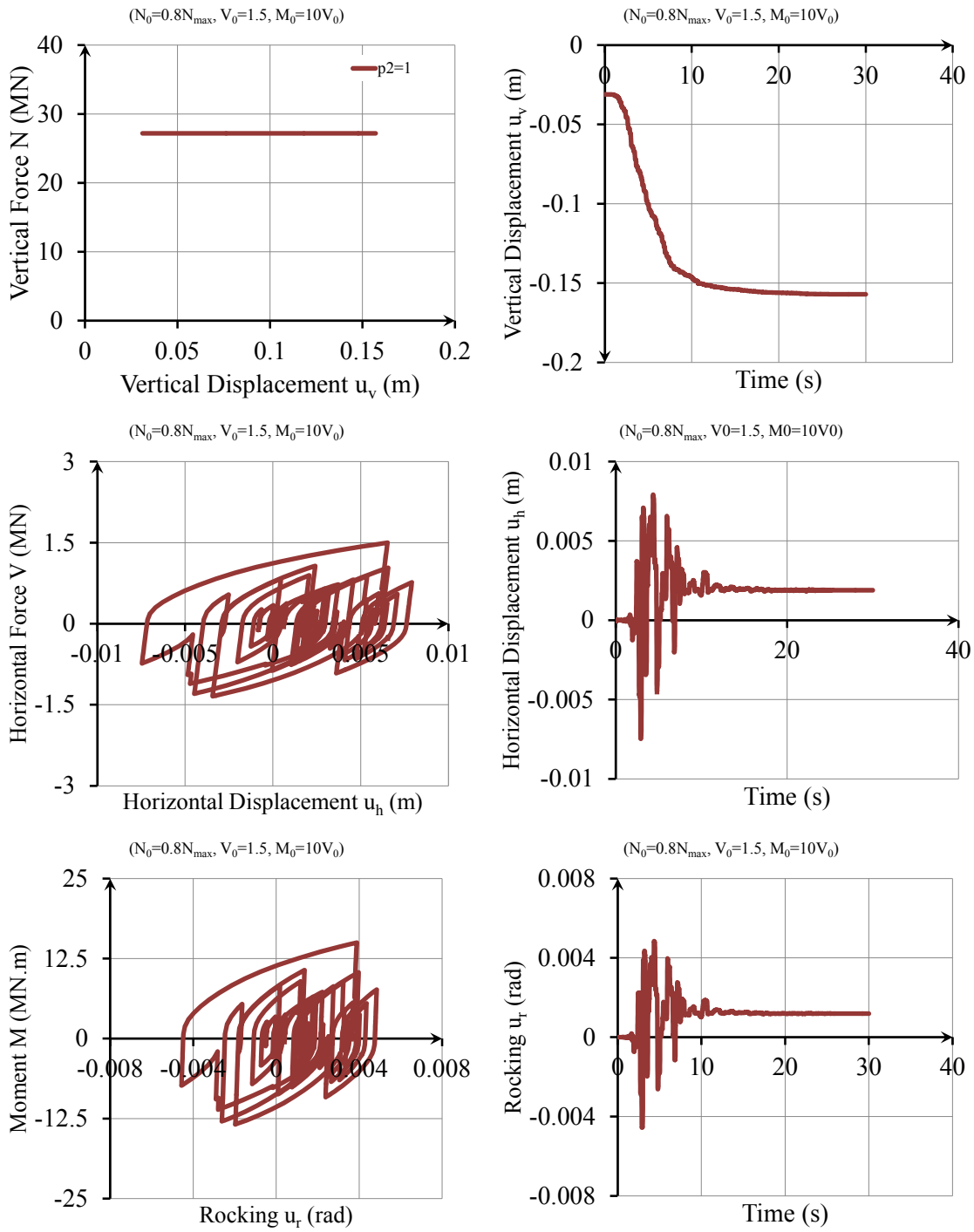

Figure G-16. The effects of variation in p_2 on the response of considered soil-foundation interface model to time-history loading (N_0=0.8$N_{max,}$ V_0=1.5 MN, M_0=10V_0).

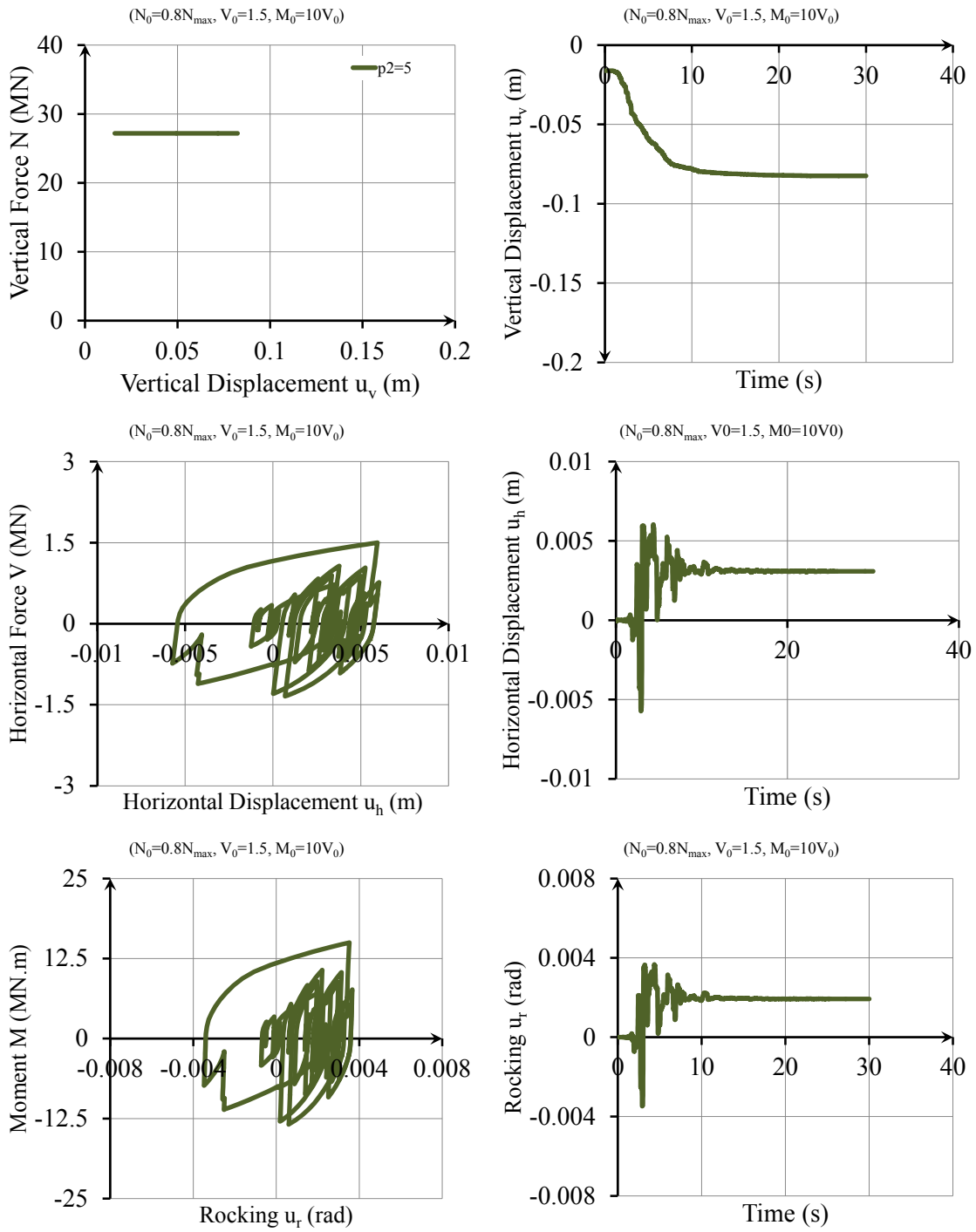

Figure G-16. *Continued*.

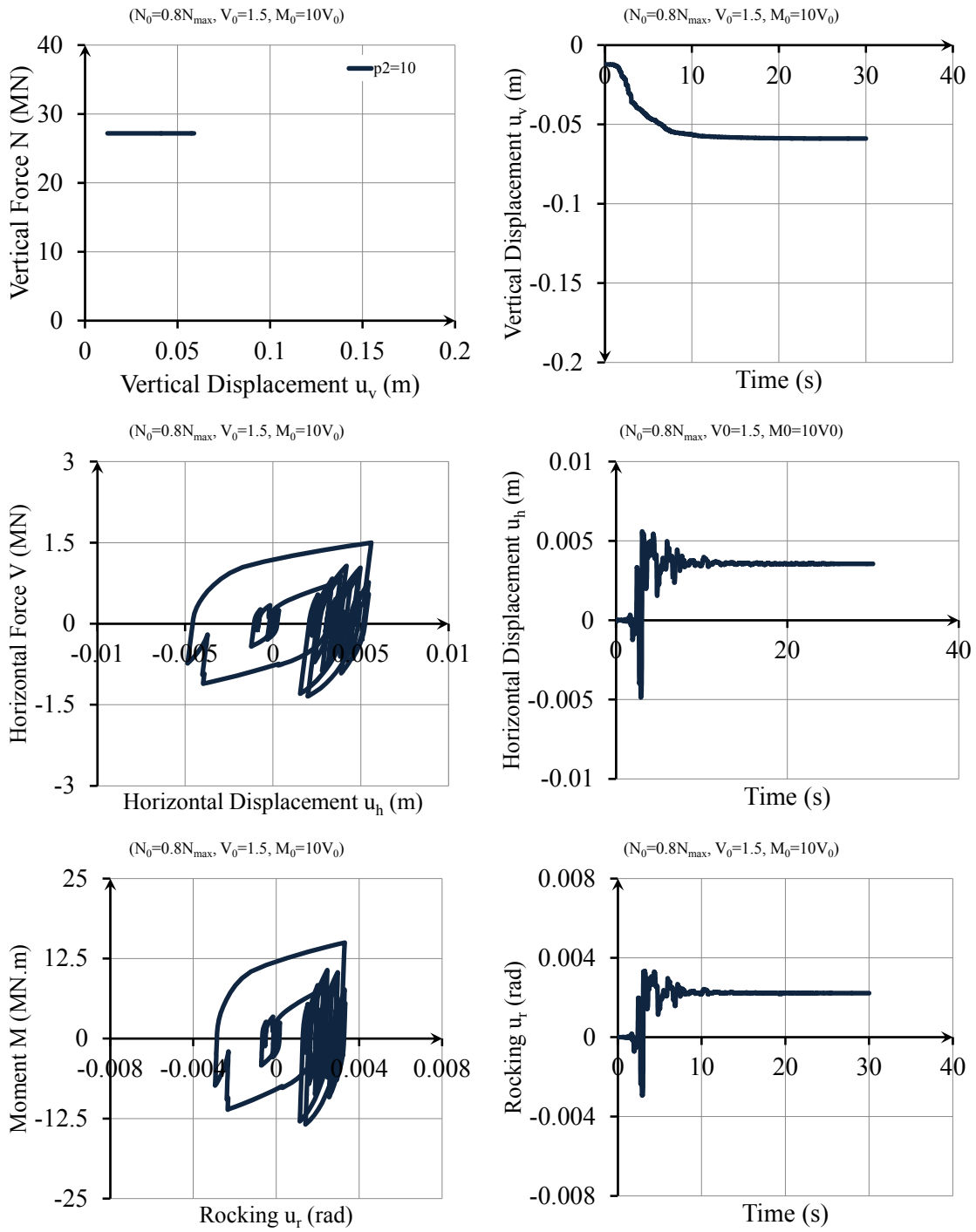

Figure G-16. *Continued*.

APPENDIX

H. Results for Soil-Structure Interaction Analysis Considering Soil-Foundation Interface Nonlinearity

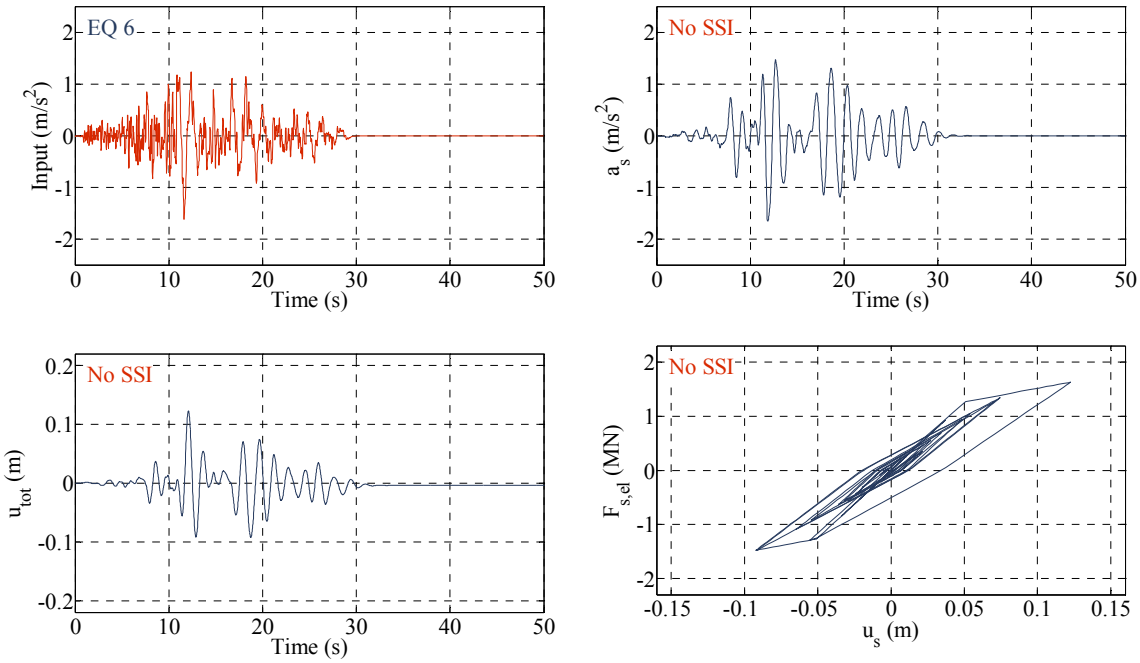

Figure H-1. Example of dynamic structural response of a fixed-base model.

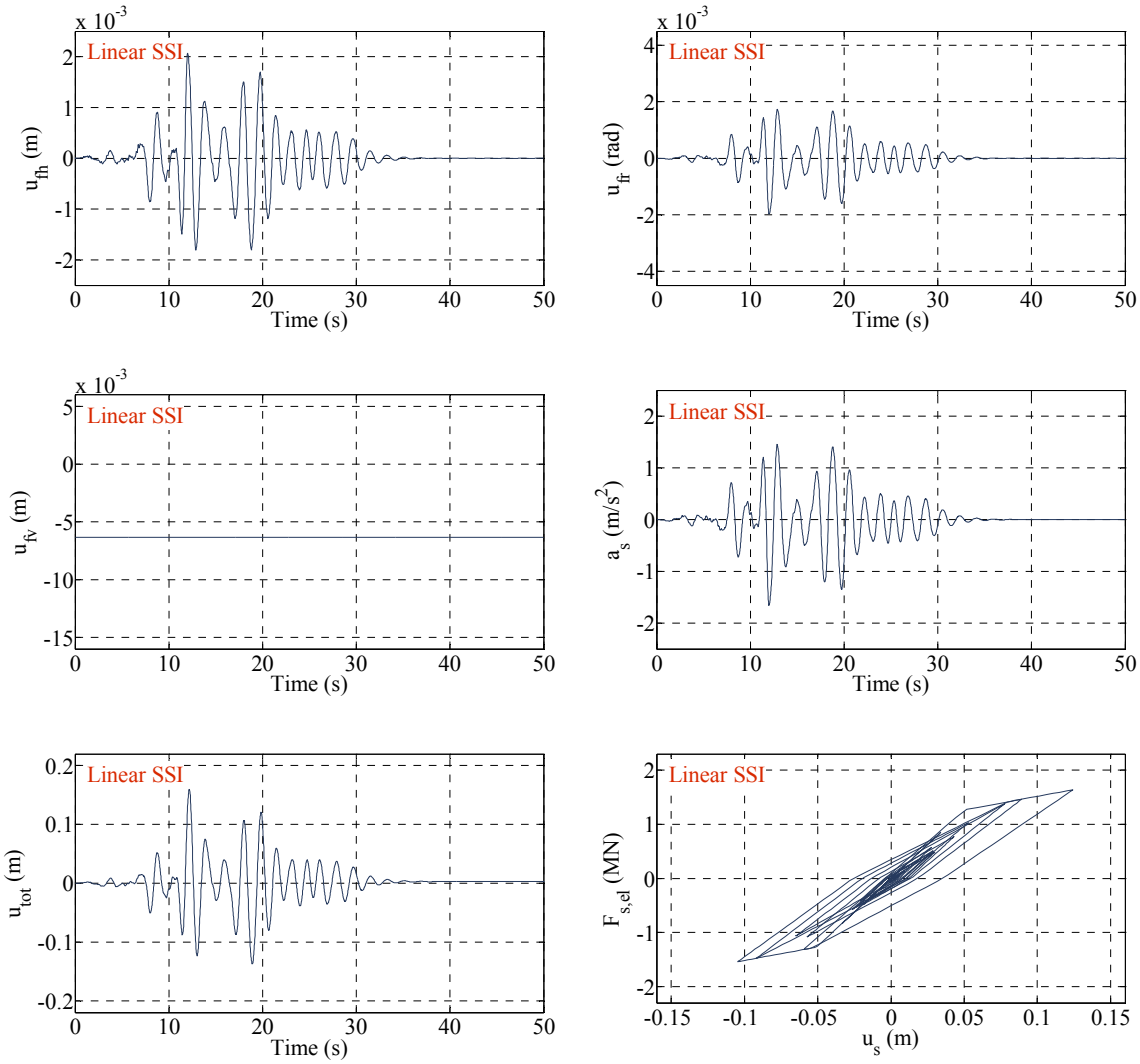

Figure H-2. Example of dynamic structural response of a linear flexible-base model.

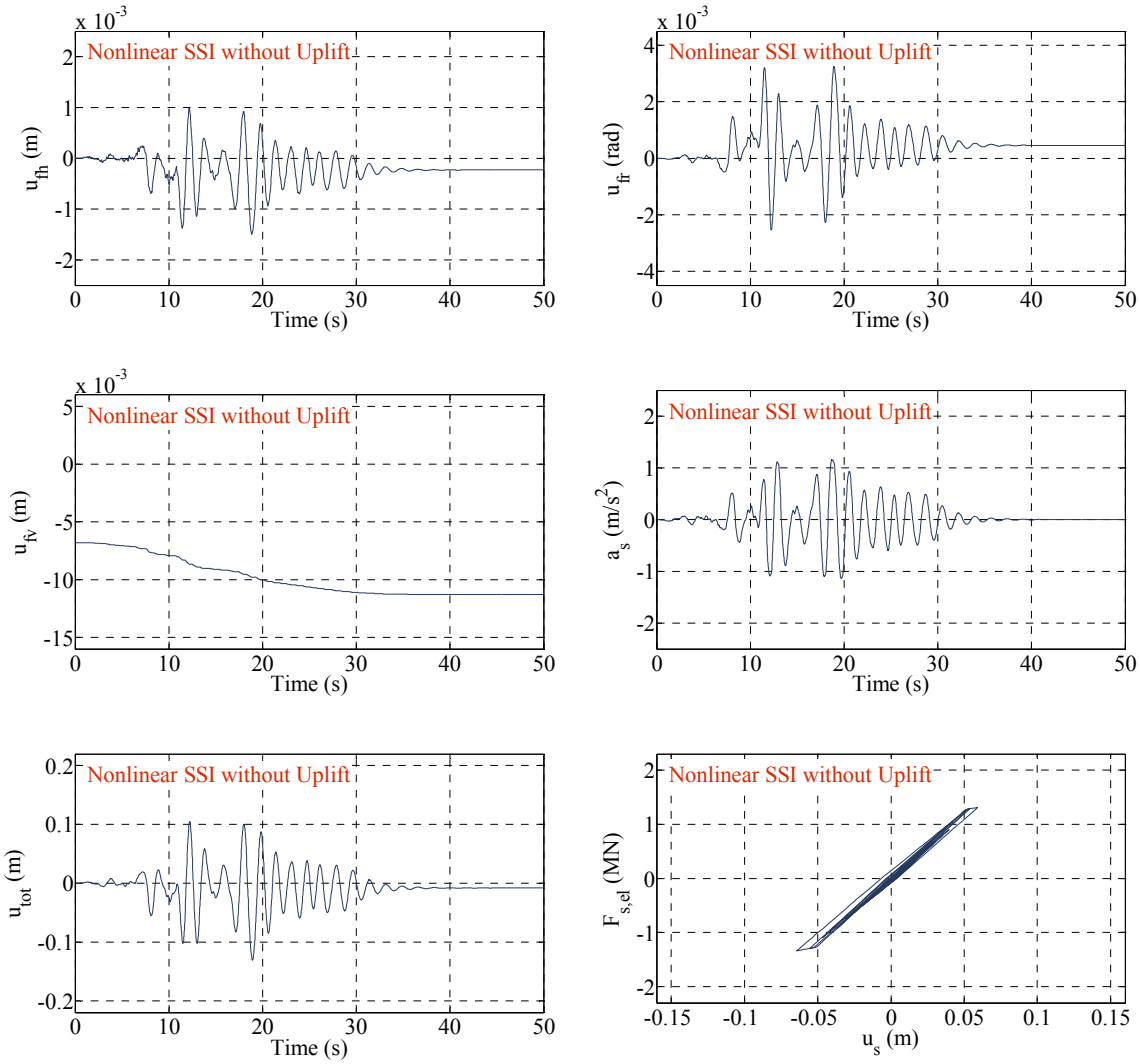

Figure H-3. Example of dynamic structural response of a nonlinear flexible-base model without uplift.

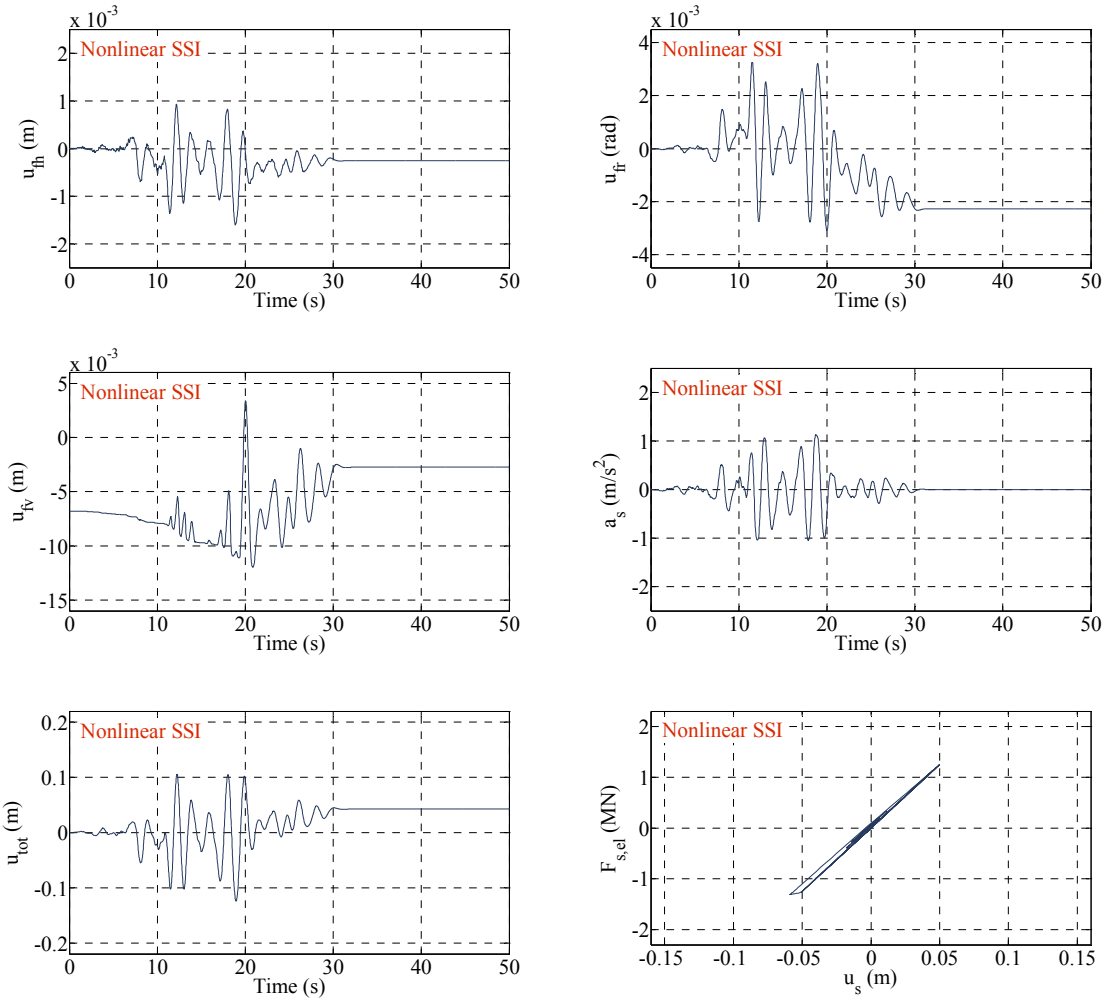

Figure H-4. Example of dynamic structural response of a nonlinear flexible-base model with uplift.

Author's Other Publications

Journal Papers

1) M. Moghaddasi, et al., "Effects of Soil-Foundation-Structure Interaction on Seismic Structural Response via Robust Monte Carlo Simulation," *Engineering Structures,* vol. 33, pp. 1338-1347, 2011.

2) M. Moghaddasi, et al., "Probabilistic evaluation of soil-foundation-structure interaction effects on seismic structure response," *Earthquake Engineering & Structural Dynamics*, vol. 40, pp. 135-154, 2010.

3) M. Moghaddasi, et al., "Stochastic quantification of soil-shallow foundation-structure interaction," *Journal of Earthquake Engineering*, vol. Paper accepted for publication, 2012.

4) M. Moghaddasi, et al., "Sensitivity analysis for soil-structure interaction phenomenon using stochastic approach," *Journal of Earthquake Engineering*, vol. Paper accepted for publication, 2012.

Conference Papers

5) M. Moghaddasi, et al., "Monte Carlo simulation of SSI effects using simple rheological soil model" presented at the *2009 NZSEE Conference*, Christchurch, New Zealand, 2009.

6) M. Moghaddasi, et al., "A robust probabilistic evaluation of soil-foundation-structure interaction effects on structural response," in *SFSI Workshop 09*, University of Auckland, New Zealand, 2009.

7) M. Moghaddasi, et al., "Soil-foundation-structure interaction effects on nonlinear seismic demand of structures," presented at the *2010 NZSEE Conference*, Wellington, New Zealand, 2010.

8) M. Moghaddasi, et al., "Development of a probabilistic seismic design framework for soil-shallow foundation-structure systems," presented at the *14th European Conference on Earthquake Engineering*, Ohrid, 2010.

9) M. Moghaddasi, et al., "The effects of soil-foundation nonlinearity on seismic soil-structure interaction analysis," presented at the *2012 NZSEE Conference, Christchurch*, New Zealand, 2012.